M.A. Hayat
Editor

Tumors of the Central Nervous System

Volume 4
Brain Tumors (Part 2)

Springer

Tumors of the Central Nervous System

Tumors of the Central Nervous System
Volume 4

For other titles published in this series, go to
www.springer.com/series/8812

Tumors of the Central Nervous System
Volume 4

Tumors of the Central Nervous System

Brain Tumors (Part 2)

Edited by

M.A. Hayat
Distinguished Professor
Department of Biological Sciences,
Kean University, Union, NJ, USA

Springer

Editor
M.A. Hayat
Department of Biological Sciences
Kean University
Union, NJ, USA
ehayat@kean.edu

ISBN 978-94-007-1705-3 e-ISBN 978-94-007-1706-0
DOI 10.1007/978-94-007-1706-0
Springer Dordrecht Heidelberg London New York

Library of Congress Control Number: 2011923069

"Although touched by technology, surgical pathology always has been, and remains, an art. Surgical pathologists, like all artists, depict in their artwork (surgical pathology reports) their interactions with nature: emotions, observations, and knowledge are all integrated. The resulting artwork is a poor record of complex phenomena."

Richard J. Reed MD

Preface

It is recognized that scientific journals and books not only provide current information but also facilitate exchange of information, resulting in rapid progress in the medical field. In this endeavor, the main role of scientific books is to present current information in more details after careful additional evaluation of the investigational results, especially those of new or relatively new therapeutic methods and their potential toxic side- effects.

Although subjects of diagnosis, drug development, therapy and its assessment, and prognosis of tumors of the central nervous system, cancer recurrence, and resistance to chemotherapy are scattered in a vast number of journals and books, there is need of combining these subjects in single volumes. An attempt will be made to accomplish this goal in the projected ten-volume series of handbooks.

In the era of cost-effectiveness, my opinion may be minority perspective, but it needs to be recognized that the potential for false-positive or false-negative interpretation on the basis of a single laboratory test in clinical pathology does exist. Interobservor or intraobservor variability in the interpretation of results in pathology is not uncommon. Interpretative differences often are related to the relative importance of the criteria being used.

Generally, no test always performs perfectly. Although there is no perfect remedy to this problem, standardized classifications with written definitions and guidelines will help. Standardization of methods to achieve objectivity is imperative in this effort. The validity of a test should be based on the careful, objective interpretation of the tomographic images, photo-micrographs, and other tests. The interpretation of the results should be explicit rather than implicit. To achieve accurate diagnosis and correct prognosis, the use of molecular criteria and targeted medicine is important. Equally important are the translation of molecular genetics into clinical practice and evidence-based therapy. Translation of medicine from the laboratory to clinical application needs to be carefully expedited. Indeed, molecular medicine has arrived.

This is the fourth volume in the series, Tumors of the Central Nervous System. As in the case of the three previously published volumes, this volume mainly contains information on the diagnosis, therapy, and prognosis of brain tumors. Insights on the understanding of molecular pathways involved in tumor biology are explained, which lead to the development of effective drugs. Information on pathways (e.g., hedgehog) facilitates targeted therapies in cancer. Tumor models are also presented, which utilize expression data, pathway sensitivity, and genetic abnormalities, representing targets in cancer. For example, rat model of malignant brain tumors using implantation of

doxorubicin with drug eluting beads for delivery is explained. The future of pathway-driven therapies for tumors is summarized.

The importance of personalizing cancer care is emphasized. The need for supportive measures for survivors of brain cancer is pointed out, so is the quality of life monitoring. The need of rehabilitation therapy for patients with primary and metastatic brain tumors is also emphasized.

Role of MicroRNA in distinguishing primary tumors from metastatic tumors is discussed. Advantages and limitations of chemotherapy (e.g., temozolomide and doxorubicin) are discussed. The complexity of tumor to tumor transfer is explained; examples discussed are: brain metastases from breast cancer and brain metastases from melanoma. Identification and characterization of biomarkers, including those for metastatic brain tumors, are presented. Genomic analysis for identifying clinically relevant subtypes of glioblastoma is included.

A large number of imaging modalities, including Fourier transform infrared imaging, elastic light single-scattering spectroscopy, diffusion tensor imaging, quantitative FDG-PET, intraoperative magnetic resonance imaging, functional magnetic resonance imaging, and ultrasound, are detailed to study progression and invasion of gliomas, intraoperative brain tumor detection, quantitative analysis of pyramidal tracts in brain tumor patients, diagnoses of peripheral nerve sheath tumors, targeted cancer chemotherapy, skull base tumors, growth of malignant gliomas, trigeminal neuralgia, and disappearing brain lesions.

Introduction to new technologies and their applications to tumor diagnosis, treatment, and therapy assessment are explained. Molecular profiling of brain tumors to select therapy in clinical trials of glioblastoma is included. Several surgical treatments, including resection, Gamma knife surgery, and radiosurgery, are discussed. The remaining six volumes in this series will provide additional recent information on this and other aspects of other types of CNS malignancies.

By bringing together a large number of experts (oncologists, neurosurgeons, physicians, research scientists, and pathologists) in various aspects of this medical field, it is my hope that substantial progress will be made against this terrible disease. It would be difficult for a single author to discuss effectively the complexity of diagnosis, therapy, and prognosis of any type of tumor in one volume. Another advantage of involving more than one author is to present different points of view on a specific controversial aspect of the CNS cancer. I hope these goals will be fulfilled in this and other volumes of this series. This volume was written by 103 contributors representing 15 countries. I am grateful to them for their promptness in accepting my suggestions. Their practical experience highlights their writings, which should build and further the endeavors of the reader in this important area of disease. I respect and appreciate the hard work and exceptional insight into the nature of cancer provided by these contributors. The contents of the volume are divided into seven subheadings: Introduction, Diagnosis and Biomarkers, Therapy, Tumor to tumor cancer, Imaging methods, Prognosis, and Quality of life for the convenience of the reader.

It is my hope that the current volume will join the preceding volumes of the series for assisting in the more complete understanding of globally relevant cancer syndromes. There exists a tremendous, urgent demand by the public and the scientific community to address to cancer diagnosis, treatment, cure, and hopefully prevention. In the light of existing cancer calamity, government funding must give priority to eradicating this deadly malignancy over military superiority.

I am thankful to Dr. Dawood Farahi and Dr. Kristie Reilly for recognizing the importance of medical research and publishing through an institution of higher education.

Union, New Jersey M.A. Hayat
April 2011

Contents

Contents of Volume 1

Contents of Volume 2

Contents of Volume 3

Contributors

Anette Abschütz Program Infection and Cancer, Deutsches Krebsforschungszentrum, D-69120 Heidelberg, Germany

Abedelnasser Abulrob Institute for Biological Sciences, National Research Council of Canada, Ottawa, ON, Canada, Abedelnasser.abulrob@nrc-cnrc.gc.ca

Ryojo Akagami Division of Neurosurgery, Gordon and Leslie Diamond Health Care Center, Vancouver General Hospital, Vancouver, BC V521M9, Canada, Ryojo.akagami@vch.ca

Luciana Oliveira de Almeida Oncogenetic Laboratory, Department of Medical Genetics, Rebeirao Preto Medical School, University of Sao Paulo, 14049-900 Ribeirao Preto, SP, Brazil, lu_olive@yahoo.com

Filippo Alongi IRCCS Humanitas, Via Manzoni 56, 20089, Rozzano, Italy, Filippo.alongi@humanitas.it

Beng Ti Ang Department of Neurosurgery, National Neuroscience Institute, Singapore 308433, Singapore; Singapore Institute for Clinical Sciences, A*STAR, Singapore 117609, Singapore

Daniel Argibay-Quiñones Laboratory of Image Processing, University of Valladolid, Valladolid, Spain, dargqui@lpi.tel.uva.es

Ayçe Atalay Department of Physical Medicine and Rehabilitation, Acibadem University, Faculty of Medicine, Istanbul, Turkey, ayce.atalay@acibadem.edu.tr

Isabelle Baldi Laboratoire Sante Travail Environnement, ISPED, University Victor Segalen Bordeaux 2, Bordeaux Cedex, France, Isabelle.baldi@isped.u-bordeaux.fr

Erik Magnus Berntsen Department of Radiology, St. Olavs Hospital, University Hospital of Trondheim, N-7006, Trondheim, Norway; MI Lab and Department of Circulation and Medical Imaging, Norwegian University of Science and Technology, Trondheim, Norway, erik.berntsen@stolav.no; erik.berntsen@gmail.com

Thomas Brinker International Neuroscience Institute GmbH, D-30625 Hannover, Germany, thbrinker@gmail.com

Virginie Callot Centre de Résonance Magnétique Biologique et Médicale (CRMBM), UMR 6612, CNRS, Université de la Méditerranée, Faculté de Médecine, 27 boulevard Jean Moulin, 13385 Marseille cedex 05, France

Rubén Cárdenes Laboratory of Image Processing, University of Valladolid, Valladolid, Spain, ruben@lpi.tel.uva.es

Eleanor B. Carson-Walter Department of Neurosurgery, University of Rochester, Rochester, NY 14642, USA, Eleanor_carson-walter@urmc.rochester.edu

Arturo Chiti IRCCS Humanitas, Via Manzoni 56, 20089, Rozzano, Italy

Yuk Kien Chong Department of Research, Singapore Institute for Clinical Sciences, A*STAR, Singapore 117609, Singapore

Mark Cohen Department of Surgery and Pharmacology, University of Kansas Medical Center, Kansas, KS 66160, USA, mcohen@kumc.edu

Alessandro Consales Department of Neurosciences, Gaslini Children's Hospital, 16147 Genoa, Italy

Patrick J. Cozzone Centre de Résonance Magnétique Biologique et Médicale (CRMBM), UMR 6612, CNRS, Université de la Méditerranée, Faculté de Médecine, 27 boulevard Jean Moulin, 13385 Marseille cedex 05, France, Patrick.cozzone@univmed.fr

Kathya Daigle Department of Neurosurgery and Neuro-Oncology, Faculty of Medicine, Sherbrooke University, Sherbrooke, QC, Canada

Matthew L. Dashnaw Department of Neurosurgery, University of Rochester, Rochester, NY 14642, USA

Isao Date Department of Neurological Surgery, Okayama University Graduate School of Medicine, Dentistry and Pharmaceutical Sciences, Okayama, Okayama, Japan

Ivana Dokic Program Infection and Cancer, Deutsches Krebsforschungszentrum, D-69120 Heidelberg, Germany

Charles Dong Division of Neurosurgery, Gordon and Leslie Diamond Health Care Center, Vancouver General Hospital, Vancouver, BC V521M9, Canada

Fritz C. Eilber Division of Surgical Oncology, UCLA, Los Angeles, CA 90095-1782, USA, fceilber@mednet.ucla.edu

Rudolf Fahlbusch International Neuroscience Institute, Hannover, Germany

Francesca Fazzini Department of Neurosciences, Gaslini Children's Hospital, 16147 Genoa, Italy

John C. Flickinger Department of Neurological Surgery, University of Pittsburgh, Pittsburgh, PA 15213, USA

David Fortin Department of Neurosurgery and Neuro-Oncology, Faculty of Medicine, Sherbrooke University, Sherbrooke, QC, Canada, David.fortin@usherbrooke.ca

Zhen Fu Department of Neurosurgery, The First Affiliated Hospital of Nanjing Medical University, Nanjing 210029, China

Takamitsu Fujimaki Department of Neurosurgery, Saitama Medical University, Moroyama 350-0495, Japan, tfujimak@saitama-med.ac.jp

Roberto Gaggero Department of Neurosciences, Gaslini Children's Hospital, 16147 Genoa, Italy, garob@iol.it

Damien Galanaud Centre de Résonance Magnétique Biologique et Médicale (CRMBM), UMR 6612, CNRS, Université de la Méditerranée, Faculté de Médecine, 27 boulevard Jean Moulin, 13385 Marseille cedex 05, France

Maria Luisa Garrè Department of Neurosciences, Gaslini Children's Hospital, 16147 Genoa, Italy

Venelin M. Gerganov International Neuroscience Institute, Hannover, Germany, vgerganov@gmail.com

Mario Giordano International Neuroscience Institute, Hannover, Germany

Philippe Goffaux Department of Neurosurgery and Neuro-Oncology, Faculty of Medicine, Sherbrooke University, Sherbrooke, QC, Canada, Philippe.goffaux@usherbrooke.ca

Asta Kristine Håberg Department of Neuroscience, Faculty of Medicine, Norwegian University of Science and Technology, N-7489, Trondheim, Norway; MI Lab and Department of Circulation and Medical Imaging, Norwegian University of Science and Technology, Trondheim, Norway, asta.haberg@ntnu.no

Amanda Hambrecht Department of Biology, University of Southern California, CA, USA; Department of Neurosurgery, Beckman Research Institute, City of Hope National Cancer Center, CA, USA

Caroline Hayhurst Department of Neurosurgery, University Hospital of Wales, Heath Park, Cardiff CF14 4XW, UK, carolinehayhurst@hotmail.com

Juliette Hukin Neurology Division ACB, K3-145, British Columbia Children's Hospital, Vancouver, BC V6H3V4, Canada, jhukin@cw.bc.ca

Henrik Huttunen Division of Neurosurgery, Gordon and Leslie Diamond Health Care Center, Vancouver General Hospital, Vancouver, BC V521M9, Canada

Nuhad K. Ibrahim Department of Breast Medical Oncology, The University of Texas M.D. Anderson Cancer Center, Houston, TX 77030, USA, nibrahim@mdanderson.org

Umar Iqbal Institute for Biological Sciences, National Research Council of Canada, Ottawa, ON, Canada

Rahul Jandial Department of Neurosurgery, Beckman Research Institute, City of Hope National Cancer Center, CA, USA

Chunsheng Kang Department of Neurosurgery, The First Affiliated Hospital of Nanjing Medical University, Nanjing 210029, China

Hideyuki Kano Department of Neurological Surgery, University of Pittsburgh, Pittsburgh, PA 15213, USA, kanoh@upmc.edu

Tim Kees Program Infection and Cancer, Deutsches Krebsforschungszentrum, D-69120 Heidelberg, Germany

Lucyna Kepka Maria Sklodowska-Curie Memorial Cancer Center and Institute of Oncology, Department of Radiation Oncology, ul. Roentgena 5, 02-781 Warsaw, Poland, lucynak@coi.waw.pl

Raimund Kleiser Institute of Radiology, Landes-Nervenklinik Wagner-Jauregg, 4020 Linz, Austria, raimund.kleiser@gespag.at

Milena Kolodziejczyk Maria Sklodowska-Curie Memorial Cancer Center and Institute of Oncology, Department of Radiation Oncology, ul. Roentgena 5, 02-781 Warsaw, Poland

Douglas Kondziolka Department of Neurological Surgery, University of Pittsburgh, Pittsburgh, PA 15213, USA

Andrew Lewis International Neuroscience Institute GmbH, D-30625 Hannover, Germany

Ning Liu Department of Neurosurgery, The First Affiliated Hospital of Nanjing Medical University, 210029 Nanjing, China

Hugues Loiseau Laboratoire Sante Travail Environnement, ISPED, University Victor Segalen Bordeaux 2, Bordeaux Cedex, France

L. Dade Lunsford Department of Neurological Surgery, University of Pittsburgh, Pittsburgh, PA 15213, USA

Marcos Martín-Fernández Laboratory of Image Processing, University of Valladolid, Valladolid, Spain, marcma@tel.uva.es

Marc R. Matrana Department of Breast Medical Oncology, The University of Texas M.D. Anderson Cancer Center, Houston, TX 77030, USA

Anthony P. McHale School of Pharmacy, University of Ulster, Coleraine, Co. Derry BT51 1SA, UK, ap.mchale@ulster.ac.uk

Rodrigo Mora Program Infection and Cancer, Deutsches Krebsforschungszentrum, D-69120 Heidelberg, Germany

Emma Muñoz-Moreno Laboratory of Image Processing, University of Valladolid, Valladolid, Spain, emunmor@lpi.tel.uva.es

Pierina Navarria IRCCS Humanitas, Via Manzoni 56, 20089, Rozzano, Italy

Josh Neman Department of Neurosurgery, Beckman Research Institute, City of Hope National Cancer Center, CA, USA, jneman@coh.org

Janpeter Nickel Institute of Neurology, Heinrich-Heine-University, 40225 Düsseldorf, Germany

Ajay Niranjan Department of Neurological Surgery, University of Pittsburgh, Pittsburgh, PA 15213, USA

Johannes Noack Program Infection and Cancer, Deutsches Krebsforschungszentrum, D-69120 Heidelberg, Germany

Nikolitsa Nomikou Research and Development, Sonidel Ltd., Dublin 5, Ireland, n.nomikou@sonidel.com

Keisuke Onoda Department of Neurological Surgery, Okayama Red Cross General Hospital, Okayama, Okayama, Japan

Antonio Palmieri Neurology Unit, San Tommaso Dei Battuti Hospital, 30026 Portogruaro, Italy

Robert Pichler Transportation Research Institute, The University of Michigan, Ann Arbor, MI 481 09-2150, USA, Robert.pichler@gespag.at

Thomas Picht Department of Neurosurgery, Charité - Universitaetsmedizin Berlin, Berlin, Germany, Thomas.picht@charite.de

Peiyu Pu Department of Neurosurgery, The first Affiliated Hospital of Nanjing Medical University, Nanjing 210029, China

Anne Regnier-Vigouroux Program Infection and Cancer, Deutsches Krebsforschungszentrum, D-69120 Heidelberg, Germany, regnier@dkfz-heidelberg.de

David Roberge Department of Radiation Oncology, McGill University Health, Center/Montreal General Hospital, Montreal, QC H3G 1A4, Canada, David.roberge@mcgill.ca

Joshua B. Rubin Division of Pediatric Hematology/Oncology, Department of Pediatrics, Washington University School of Medicine, St. Louis, MO 63110, USA, Rubin_J@kids.wustl.edu

Amir Samii International Neuroscience Institute, Hannover, Germany

Madjid Samii International Neuroscience Institute, Hannover, Germany

Rosario Sarabia-Herrero Neurosurgery Service, Hospital Universitario Río Hortega, Valladolid, Spain, rsarabia@saludcastillayleon.es

Toru Satoh Department of Neurological Surgery, Ryofukai Satoh Neurosurgical Hospital, 5-23-23 Matsunaga, Fukuyama, Hiroshima 729-0104, Japan, ucsfbtrc@urban.ne.jp

Marta Scorsetti IRCCS Humanitas, Via Manzoni 56, 20089, Rozzano, Italy

Rüdiger J. Seitz Institute of Neurology, Heinrich-Heine-University, 40225 Düsseldorf, Germany

Elizabeth Shurell Division of Surgical Oncology, UCLA, Los Angeles, CA 90095-1782, USA

Mohit Singh Neurology Division ACB, K3-145, British Columbia Children's Hospital, Vancouver, BC V6H3V4, Canada

Luis Souhami Department of Radiation Oncology, McGill University Health, Center/Montreal General Hospital, Montreal, QC H3G 1A4, Canada

Sabine Spiegl-Kreinecker Transportation Research Institute, The University of Michigan, Ann Arbor, MI 481 09-2150, USA

Danica Stanimirovic Institute for Biological Sciences, National Research Council of Canada, Ottawa, ON, Canada

Pasquale Striano Department of Neurosciences, Gaslini Children's Hospital, 16147 Genoa, Italy

Carol Tang Department of Research, National Neuroscience Institute, Singapore 308433, Singapore, carol_tang@nni.com.sg

Tan Boon Toh Department of Physiology, National University of Singapore, Singapore 117597, Singapore

Boguslaw Tomanek Institute for Biological Sciences, National Research Council of Canada, Ottawa, ON, Canada

Johannes Trenkler Institute of Radiology, Landes-Nervenklinik Wagner-Jauregg, Wagner-Jauregg-Weg 15, 4020 Linz, Austria

Horst Urbach Radiologische Klinik, Neuroradiologie, Universitatsklinikum Bonn, 53105 Bonn, Germany, Horst.urbach@ukb.uni-bonn.de

Luca Valentinis Neurology Unit, San Tommaso Dei Battuti Hospital, 30026 Portogruaro, Italy, luca.valentinis@tin.it

Kevin A. Walter Department of Neurosurgery, University of Rochester, Rochester, NY 14642, USA

B. Mark Woerner Division of Pediatric Hematology/Oncology, Department of Pediatrics, Washington University School of Medicine, St. Louis, MO 63110, USA

Gabriele Wurm Institute of Neurosurgery, Landes-Nervenklinik Wagner-Jauregg, 4020 Linz, Austria

Xinmai Yang Department of Mechanical Engineering, The KU Bioengineering Research Center, University of Kansas, Lawrence, KS 66045, USA, xmyang@ku.edu

Yongping You Department of Neurosurgery, The First Affiliated Hospital of Nanjing Medical University, Nanjing 210029, China, Yypl9@njmu.edu.cn

Jinyuan Zhou Johns Hopkins School of Medicine, Department of Radiology, 600 N. Wolfe Street, Park 336, Baltimore, MD 21287, USA, jzhou@mri.jhu.edu

Part I
Introduction

Chapter 1

Epidemiology of Primary Brain Tumors

Isabelle Baldi and Hugues Loiseau

Abstract Epidemiology of primary brain tumors includes a descriptive approach (determination of prevalence and incidence) and an analytical approach (identification of risk factors). Among risk factors, some are intrinsic to the person and others are external causes that are more easily preventable. Descriptive epidemiological data have concluded an increase of annual incidence of primary brain tumor in most industrialized countries. Main explanations for this increase are the ageing of the population and a better access to the diagnostic imaging, albeit it is not possible to exclude changes in risks factors. Comparing incidences between registries is difficult. Spatial and temporal variations constitute one explanation for the discrepancies and evolutions of coding methods another one. Intrinsic factors likely to modify the risk are age, genetic predisposition and susceptibility, gender, race, birth weight, and allergy. Extrinsic factors likely to modify the risk are mainly radiation exposures. Many studies concerning, among others, electro magnetic fields, and especially cellular phones, pesticides, substitutive hormonal therapy, and diet have been published. Until now, results remain globally inconclusive. Weak incidence of primary brain tumors constitutes a huge limiting factor in the progress of knowledge, both on incidence and risk factors. Important mobilization of the neuro-oncological community is mandatory to obtain consistent and valuable data that will lead to a significant improvement in our knowledge of brain tumor epidemiology.

I. Baldi (✉)
Laboratoire Sante Travail Environnement, ISPED, University Victor Segalen Bordeaux 2, Bordeaux Cedex, France
e-mail: Isabelle.baldi@isped.u-bordeaux.fr

Keywords Brain tumor · Medulloblastoma · Hematopoietic neoplasms · Li-Fraumeni syndrome · Turcot's syndrome · Ependymoma

Introduction

Considering that principles of epidemiology began to form in the second half of the 20th century, it is a relatively new scientific approach to health problems. Nevertheless, the oldest population-based tumor registry in the world started in Connecticut as early as 1941 with a retrospective registration from 1935, followed by the Danish Cancer Registry in 1942. This demonstrates the foremost concern of improving knowledge in the field of cancer and the early and dynamic role of cancer physicians in this research area. Subsequently, several hundreds of cancer registries were established worldwide, and the International Agency for Research on Cancer was established in 1965 as a specialized research center of the World Health Organization (http://www.iarc.fr/). Epidemiology makes it possible to describe the incidence and mortality due to cancer (descriptive epidemiology), and to identify risk factors for cancer, the strength of their association with the disease, and the potential causal relation (analytical epidemiology), with the underlying purpose of improving cancer prevention.

Some common difficulties are encountered with registries for different tumor sites. One of them is the need for a multidisciplinary approach for registering cases, because views and coding systems change with time. Considering brain tumors, two classifications are used: the International Classification of Disease for

M.A. Hayat (ed.), *Tumors of the Central Nervous System, Volume 4*,
DOI 10.1007/978-94-007-1706-0_1,

Oncology (ICD-O) with the morphology codes and the site codes (Fritz et al. 2000), and the World Health Organization's histological classification of primary brain tumors (Louis et al. 2007). According to these classifications, worldwide registries do not necessarily include exactly the same subtypes of brain tumors, which may explain some differences in the incidence rates. The evolution of coding systems with time and the poor reproducibility for histological assessment of some tumors, such as gliomas, also make comparisons difficult. Many published data have included different tumor types which could have a similar origin. That could explain some discrepancies in the results.

Descriptive Epidemiology of Primary Brain Tumors

Methodological Endpoints

Various parameters can be used to describe the burden of brain tumors in human populations and to help in medical care planning. The most common ones are the prevalence and the incidence of these diseases. Data concerning prevalence rates of brain tumors (proportion of people alive on a certain date in a population who previously had a diagnosis of brain tumor) are scarce and controversial. Some estimations have been given by the International Agency for Research on Cancer, based on incidence and survival data (Pisani et al. 2002), but they appear lower than those calculated in the United States from the Central Brain Tumor Registry of the United States, which are about 130/100,000 for benign and malignant tumors (Davis et al. 2001).

The main indicator allowing spatial and time-related comparison is annual incidence (i.e., number of new brain tumors in 1 year and in a given population, usually per 100,000 inhabitants).

Annual incidence rates reported by some of the main registries worldwide are summarized in Table 1.1 according to histological subtypes. Incidence rates vary in the published studies, mainly due to differences in study methodology. The global rate ranges from 8.5 to 19.25/100,000. Primary brain tumor incidence in children is 4.9/100,000 in Sweden (Dreifaldt et al. 2004) and 2.5/100,000 in Germany (Kaatsch et al. 2001), but studies do not consider the same age limit for childhood.

Neuroepithelial tissue tumors, tumors of the meninges and those of the cranial and spinal nerves represent the main histological subtypes, and account for ~85% of the primary brain tumors in adults. In adults, the main histological types are the neuroepithelial tumors (mainly represented by gliomas), tumors of the meninges, tumors of the cranial and spinal nerves, lymphomas and hematopoietic neoplasms, and germ cell tumors. In adults, the incidence of neuroepithelial tumors ranges from 2.2 (Kuratsu et al. 2001) to 7.8/100,000. The incidence of glioblastomas, the most malignant type of gliomas, ranges from 1.6 (Liigant et al. 2000) to 4.5/100,000. The incidence of meningioma presents the widest variations, ranging from 1.3 (Arora et al. 2009) to 7.8/100,000 (www.cbtrus.org). The annual incidence of schwannoma is 1.1/100,000 and the incidence of vestibular schwannoma is 0.55/100,000 (Schellinger et al. 2008). In children, neuroepithelial tissue tumors alone account for ~75% of primary brain tumors. Histological subtypes differ in children, astrocytoma predominating (pilocytic astrocytoma) together with embryonal medulloblastoma and followed by ependymoma.

Even when caution is used when comparing incidence due to variations in the period of recording and in diagnostic tools (radiology, histology, autopsy), it may be assumed that the burden of primary brain tumor in health care systems is likely to be underestimated for several reasons. First, some cancer registries do not record benign tumors, a situation although more frequent in the past decades, slowly changing since the recent recommendations (McCarthy et al. 2002). Secondly, some registries only collect histologically confirmed cases, while the proportion of cases without histological confirmation has been shown to reach up to 31%. Third, some specific cases, such as malignant transformation, secondary localization, and occurrence of tumors at different sites observed in inherited genetic syndromes, are not systematically recorded in registries. Yet, these tumors have an impact in terms of public health and health-care planning.

Primary brain tumors are topographically distributed according to a volumetric gradient (i.e. supratentorial tumors are more frequent than infratentorial tumors, which are more frequently observed than spinal tumors).

Table 1.1 Incidence data from the main registries of central nervous system tumors around the world

Country	Rochester	Greece	Kumamoto	Cbtrus	Austria	California	Estonie	Finland	Israel	England	France
Authors	Radhakrishnan et al. (1995)	Gousias et al. (2009)	Kuratsu et al. (2001)	www.cbtrus.org	Wöhrer et al. (2009)	Brown et al. (2009)	Liigant et al. (2000)	Larjavaara et al. (2008)	Sadetzki et al. (2008)	Arora et al. (2009)	RSTNC
Age-adjusted population	**local**	**Greek population**	**Japanese population**	**US**	**US**	**US**	**World**	**World population**	**World population**	**World**	
Period of recruitment	1950–1989	2005–2007	1989–1998	2002–2006	2005	2001–2005	1986–1996	2000–2002	2001–2003	1995–2003	2000–2007
Number of cases	**339**	**56**	**2129**	**85,670**	**1688**	**24,293**	**1665**	**331**	**548**	**54, 336**	**1983**
Population	**70,000**	**488,435**	**1,850,000**		**8,200,000**	**36,500,000**	**1,500,000**				**1,300,000**
Histological confirmation (%)	**63.1**	**91**	**70.9**		**80.9**		**80.8**	**99**	**95**		**77.9**
Histological classification	**WHO (1993)**		**WHO (1993)**	**WHO**	**ICDO-3**	**WHO (1993)**	**WHO (1993)**	**ICDO-3**	**WHO (2002)**	**WHO (2000)**	**WHO (2000)**
Ages	**All**	**>20**	**All**	**All**	**All**	**All**	**All**	**20–69**	**>18**	**<85**	**All**
Age-adjusted incidence	**19.1**		**10.97**	**18.28**	**18.1**	**14.3**	**8.46**			**9.21**	**19.25**
Tumours of neuroepithelial tissue	**6.14**	**5.73**		**6.49**	**7.26**		**3.72**	**4.7**		**5.24**	**7.83**
Pilocytic astrocytoma				0.34	0.57	0.3		0.3		0.31	0.26
Diffuse astrocytoma	1.30			0.10	0.75		1.27	0.7		0.08	0.32
Anaplastic astrocytoma				0.41	0.44	0.4	0.46	0.5		0.18	0.39
Unique astrocytoma variants				0.10						0.02	0.06
Astrocytoma, NOS			0.57	0.44		0.3		0.03		0.75	0.12
Glioblastoma	3.60	3.69		3.11	3.40	2.6	1.58	2.0	3.26	1.89	5.22
Oligodendroglioma	0.60			0.31	0.70	0.3	0.22	0.5		0.07	0.14
Anaplastic oligodendroglioma				0.14		0.1				0.21	0.09
Ependymoma/ anaplastic ependymoma	0.20			0.28	0.57	0.2	0.22	0.2		0.25	0.30
Ependymoma variants				0.09							0.08
Mixed glioma	0.10			0.19		0.2	0.11	0.5		0.08	0.51
Glioma malignant, NOS			1.56	0.42		0.3		0.02			0.25
Choroid plexus				0.04	0.05			0.01		0.03	0.04
Neuroepithelial				0.02						0.09	0.05

Table 1.1 (continued)

Country	Rochester	Greece	Kumamoto	Cbtrus	Austria	California	Estonie	Finland	Israel	England	France
Benign and malignant neuronal/glial neuronal and mixed				0.27	0.29					0.01	0.29
Pineal parenchyma	0.04			0.03	0.07					0.05	0.01
Embryonal/ primitive/ medulloblastoma	0.30		0.07	0.20	0.25	0.2	0.32			0.28	0.23
Tumors of cranial and spinal nerves			**1.08**	**1.66**	**1.36**		**0.40**				**2.27**
Nerve sheath, benign and malignant	0.90			1.66	1.24	1.5				0.66	
Tumors of meninges				**6.40**	**5.31**	**4.5**				**1.38**	**6.07**
Meningioma	7.80		3.40	6.17	5.23		1.63			1.28	5.92
Other mesenchymal, benign and malignant				0.07	0.08						0.15
Hemangioma	0.20			0.14							0.00
Lymphoma and hematopoietic neoplasms				**0.47**	**0.57**						
Lymphoma	0.20		0.29	0.47	0.48	0.4					0.61
Germ cell tumors and cysts				**0.08**	**0.09**						
Germ cell tumors, cysts and heterotopias			0.20	0.08						0.06	0.10
Tumors of sellar region				**2.08**	**1.81**						
Pituitary	2.80		2.06	1.95	1.63	2	0.36			0.82	
Craniopharyngioma	0.30		0.17	0.13						0.12	0.21
Local extension from regional tumors				**0.02**							
Chordoma/ chondrosarcoma				0.02						0.01	0.05
Unclassified tumors				**1.10**							
Hemangioblastoma	0.20			0.15						0.10	0.26
Neoplasm, unspecified	0.80			0.95			1.63				0.59
All other				0.01	1.78		0.96			0.91	0.73

Whatever the registry, variations in incidence rates according to age appear triphasic. A first moderate peak is observed between 0 and 15 years of age, corresponding to the childhood brain tumors. The incidence is low between 15 and 35 years of age, but an increase is observed thereafter until 70 or 75 years of age. Beyond this age, decreasing incidence is usually observed. Some variations have been reported both in the incidence rates and in the peak age of incidence (i.e., 65, 70 or 75 years of age). Countries differ in public health resources and the age pyramid, which may explain such differences. However, variations in age adjustment within studies may also partly explain the differences: some incidence rates are crude while others are standardized in the US or world population.

Increasing incidence rates were reported from the 1970s worldwide, a trend that appeared more pronounced in subgroups such as the elderly and children. The annual increase was ∼1% per year in adults and from 1 to 2% in children with some variations according to the histological subtypes. Since the 1990s, some data tend to report a plateau. Some authors have considered the increase in the rates to be artefactual with three main explanations for this: (1) ageing of the populations, (2) improvement in health access and in diagnostic procedures, corresponding to the introduction of CT-scan during the 1970s and then MRI during the 1980s; (3) adjustment of neurosurgical procedures despite aging, leading to an increase in the rate of histological confirmation of gliomas, even in the elderly (up to 98% in some cancer registries).

However, these arguments are not consistent with some other findings such as the continuous increase in some histological types such as meningiomas or in some population groups such as children.

Most of the histological subtypes have increased except the primary brain lymphomas, that have a stable or decreasing incidence. This situation is explained by important changes in the therapeutic armamentarium with the introduction of highly active anti-retroviral therapy (HAART), which has led to the end of lymphoma in AIDS patients. The incidence of grade 2 and 3 astrocytomas also appears to be decreasing, but this is explained by changes in histological classification in favor of oligodendroglioma and mixed tumors.

Analytical Epidemiology of Primary Brain Tumors

The descriptive epidemiology of brain tumors highlights geographical and temporal variations, which suggest the possible role of both intrinsic and extrinsic factors. We present here the main hypotheses studied to date.

Endogenous Risk Factors

The most important factor associated with an increase in the risk of brain tumour is age, albeit some specific types (medulloblastoma and pilocytic astrocytoma) occur rather specifically in children. Incidence rates are below 10/100,000 before the age of 35, and exceeds 40/100,000 after the age of 65.

Even if between-country or between-continent comparisons are biased by methodological registration differences, data from within-country comparisons suggest consistent differences in brain tumor incidence between ethnic groups (Darefsky and Dubrow, 2009; Sadetzki et al. 2008). White populations (Northern America, Australia, and Europe) present the highest rates, approximately two-fold the rates of black people or Asians. These differences concern most of the histological subtypes and tumor types. They might result from genetic, nutritional or environmental factors, but also possibly from greater access to diagnostic facilities and medical care in some ethnic groups.

Incidence of brain tumors is clearly related to sex, with opposite patterns for meningiomas and gliomas. Higher rates of meningiomas in women, specifically during reproductive period, were identified as early as 1930 by Harvey Cushing (McKinley et al. 2000) and are constantly observed in all countries. The opposite pattern is observed for gliomas with higher rates in men. The differences in incidence between sexes suggest that sex hormones and/or genetic differences between males and females may play a role in the occurrence of these tumors.

Birth weight and height are objective measures that have been suggested to be crude markers in children of prenatal conditions and exposures (as indicators of maternal nutritional status, diseases and exposures). It has also been hypothesized that the insulin-like

growth factor system could play a role both in stimulating body weight and growth and in stimulating the proliferation of malignant cells. Thus, in the past 20 years, body measures at birth have been studied in relation to some childhood tumors, including brain tumors. In 2008, a meta-analysis was performed on this controversial question, including two cohorts and six case-control studies (Harder et al. 2008) and concluded that high birth weight was followed by a significant increase in medulloblastoma and astrocytoma risk in childhood. However, the results remained inconclusive for ependymoma. More recently, tallness and body mass index have also been identified as possible risk factors for adult-onset gliomas, with the additional hypothesis that energy balance could also play a role in brain tumor occurrence (Moore et al. 2009).

The role of allergy in cancer in general is controversial: on one hand, those with a history of allergy may possess an enhanced capacity for immune surveillance and limit abnormal cell proliferation, and on the other hand the immune response may be related to cancer development. However, studies on brain tumors have consistently reported an inverse association between a history of allergy (atopic diseases such as asthma, eczema. . .) and the occurrence of glioma. The association with meningioma is less consistent but was also found in some studies. A meta-analysis identified 12 studies of glioma and atopic disease and pooled analysis assessed a 40% significant decrease in the risk of glioma for subjects with a history of allergy and a 30% decrease in subjects with a history of asthma or eczema (Linos et al. 2007). In the same meta-analysis, no clear association was noted for allergy and meningioma in six studies.

Some inherited genetic syndromes are well-described in gliomas and they lead to brain tumors more or less early in life: neurofibromatosis type 1 and 2, tuberous sclerosis, Li-Fraumeni syndrome, Turcot's syndrome. However, these syndromes account for fewer than 1% of gliomas, a proportion slightly higher in children around 2–3% (Bondy et al. 2008). High-penetrant genes explain a part of these specific syndromes: 70% of Li Fraumeni syndrome families are explained by p53 germ-line mutations. Outside the context of the rare cancer-prone families, an increase in risk for primary brain tumors among relatives of brain tumor patients, especially gliomas, was suggested by Margareth Wrensch more than 10 years ago (Wrensch et al. 1997) and has since been proven statistically significant. The familial forms could account for 5% of the cases (Malmer et al. 2007). Thus, international efforts are currently in progress to investigate brain tumors and try to identify susceptibility alleles and explain familial aggregation and early-onset pediatric cases. Genetic polymorphisms could play a role in several pathways such as DNA repair, cell cycle, inflammation, angiogenesis and subsequently in malignant transformation. Several genes implicated in DNA repair provide interesting hypotheses (ERCC1, ERCC2, MGMT) (Gu et al. 2009). Results concerning cell cycle genes and metabolism genes (Glutathione S transferase variants) remain controversial and inconclusive to date (Lai et al. 2005). Candidate genes in the field of immune function (IL-4, IL-4RA, IL13) are suspected to play a role in the initiation of glioma, a hypothesis consistent with the epidemiological finding of an inverse relationship between allergic diseases and gliomas. Yet it is not possible to rule out the possibility that gliomas are themselves responsible for inhibiting allergies. Although many genes have been investigated in isolated studies, there is a clear need for replication of the results. Only results for CDK2B and RTEL1 polymorphisms have been replicated (Shete et al. 2009; Wrensch et al. 2009). There is also a need for studies consistent with epidemiological hypotheses and exploring relevant genes in relation with suspected risk factors.

Exogenous Risk Factors

Ionizing Radiations

At the beginning of the 1900s, the invention of ray machines to image body structures and treat health conditions was rapidly followed by the finding that they could harm the tissue by breaking and rearranging the genes, a process potentially inducing cancer. However, neurological tissue was long considered resistant to such damage.

Evidence that exposure to low-dose rays also damages neural tissue was found first in individuals treated with radiotherapy for childhood *tinea capitis* in the 1950s in Israel. A retrospective cohort of 11,000 adults showed that 1–2 Gy administered during childhood led to a 9.5-fold increase in meningioma incidence, with a mean latency of ∼36 years. In the 1980s a

higher incidence of meningioma was also observed in women with a history of full-mouth dental rays, especially for radiographies performed during childhood or before 1945 when doses were higher. In the 1990s it was additionally demonstrated that a significant dose-related excess of brain tumors occurred in Hiroshima and Nagasaki atomic bomb survivors, especially for schwannoma, but also for meningioma, glioma, and other types of brain tumors, with higher risks for those exposed during childhood. This result has not been demonstrated for other diagnostic radiographies.

Doses of radiation used in radiotherapies (i.e., >10 Gy) have been shown to significantly increase the risk of meningioma in a survey of cohorts of patients treated for brain tumors or other health conditions, with a mean latency ~20 years (Umansky et al. 2008). Even if they are less frequent, radiation-induced gliomas have been described, especially in cohorts of children treated for brain tumors or leukemia. Data in adults are more limited but show a heightened risk in certain groups (Prasad and Haas-Kogan, 2009).

Electromagnetic Fields

The universal use of electricity and the rapid development of associated technologies in the past decades have raised questions regarding the potential contribution of electromagnetic fields in the development of some cancers, including brain tumors. Differences in exposure have been considered according to the context of use and to the characteristics of the fields. Levels of occupational exposures have been found greater than levels in the home environment. Extremely low frequency fields resulting from power lines have been differentiated from radiofrequencies, as effects on cells, if any, could be subtended by different mechanisms. Extremely low frequency fields have been classified as possibly carcinogenic to humans by the International Agency for Research on Cancer, mainly because of epidemiological evidence for childhood leukemia, but with insufficient evidence concerning brain cancer risk (IARC 2002). A recent review confirmed that the available data remain inconclusive concerning the role of ELF in brain tumors (Kheifets et al. 2009). Moreover, the recent and rapid increase in the use of cell phones in the 1990s has also stimulated epidemiological research on the contribution of radiofrequencies to the development of brain tumors. Several meta-analyses have been performed, the most recent ones focusing on studies with long-term cell phone use (>10 years) (Khurana et al. 2009; Ahlbom et al. 2009). Two streams of data have been identified: the "Hardell group" studies and the "INTERPHONE group" studies. While the first concluded in elevated risks of developing ipsilateral astrocytoma and acoustic schwannoma, but the data from the second group (INTERPHONE Study Group, 2010) do not support the same conclusion. This has led to the present dual conclusion that (1) no causal association is demonstrated, but that (2) the absence of association might result from an observation period too short for assessing the effects of long-term use. As young children now use these devices, and user exposure has become more intensive, the present conclusions might be revised with time.

Nutrition and Nitroso-Compounds

The nitroso-compounds (NOC) (mainly represented in food by *N*-nitrosamines and *N*-nitrosamides) hypothesis has been the most prominent in the research of nutritional risk factors for brain tumors (Dietrich et al. 2005). This hypothesis relies on experimental results showing that a subgroup of *N*-nitrosamides, the *N*-nitrosoureas, can lead to the formation of ethylnitrosoureas in the presence of nitrite and subsequently induce brain tumors in animals. The nitrosation of amides is accelerated by citrate and organic acids, and inhibited by Vitamins C and E. Human nutritional exposure to *N*-nitrosamides has been found to result from consumption of food containing NOC (cured meat, beer, etc.) and from endogenous formation in the stomach during the digestive process. These experimental data have encouraged epidemiological studies to focus on the potential role of cured meat, a known source of nitroso-compounds and precursors, and on fruit, vegetable, and vitamin supplements as inhibitors of nitrosation. Positive associations have been repeatedly found between maternal intake of cured meat and pediatric brain tumors (Huncharek and Kupelnick, 2004). However, results in adults are less conclusive (Terry et al. 2009). The inconsistency in the findings suggests the need for studies with an accurate methodology for NOC exposure assessment, analysis by histological types, and consideration for other potential sources of NOC compounds (especially

smoking, but also cosmetics, drugs, other chemicals, some occupational settings such as rubber, leather and metal industries).

Speculation on the role of aspartame in brain cancer was derived from a few experimental results in rats on the carcinogenic risk of this substance. However, to date, no epidemiological study has demonstrated a risk for humans (Lim et al. 2006). Some other miscellaneous nutritional exposures have been explored (zinc, caffeine, acrylamide, etc.) in a few studies, but the results remain too scarce for any conclusion.

Smoking Habits

The hypothesis of the potential role of smoking in brain tumor is supported by the presence of several well-known carcinogenic substances in tobacco smoke, with a specific attention for *N*-nitrosocompounds. It has also been suggested that tobacco smoke could enhance the blood–brain barrier permeability and could therefore facilitate the effect of other toxics. However, well-designed studies that have explored the role of smoking on brain neoplasm in humans are very few compared to other cancer sites, and most of them have only considered gliomas. Only case-control studies were published until 2004, after which results from 4 cohorts provided new data. The meta-analysis by Mandelzweig et al. (2009) included 17 studies regarding smoking (ever versus never) and gliomas and showed a moderate but not statistically significant increase in risk (10%). Nevertheless, a significant increase in risk was seen when considering cohort studies separately. (OR: 1.16; $p = 0.007$).

Infectious Agents: Birth Season

As infectious agents have been found to cause brain tumors in experiment animals, these agents have also been suggested as potential risk factors in human brain tumors. Viruses have been the most studied, and among them are retroviruses, papovaviruses, and adenoviruses. Special attention has been paid to SV40 because of specific exposure conditions when polio vaccines were inadvertently contaminated with this oncovirus between 1955 and 1963, resulting in 10–30 million people being contaminated through vaccine administration. However, a recent review of existing studies on the risk of cancer from SV40 contaminated vaccines did not support the hypothesis that SV40 plays a role in brain cancer occurrence (Shah 2007). Controversial data have also been published on Varicella Zoster Virus and other Herpes Viruses, and on influenza virus, with a specific consideration of infection during pregnancy or just after birth. However, the difficulty to ascertain the history of infection is a limitation of these studies. Thus, while some studies have tried to document this hypothesis taking into account the winter season as a surrogate for infection, inconsistent results have been obtained concerning seasonality of birth in children with brain tumors. Larger-scale studies are needed to further explore this hypothesis. Briefly, the only certain association to date between infection and brain tumors concerns the HIV-related brain lymphomas.

Hormonal Factors

Some descriptive data point to the possible role of hormones: (1) the incidence of meningioma is twice as high in women as in men, especially during the reproductive life period, (2) the incidence of gliomas is two-fold higher in men. As these two opposite trends start during adolescence, increase until 50–54 years old and decrease thereafter, they suggest an inverse role of hormonal factors in these two types of tumors. Epidemiological studies have also shown an association between meningioma and breast cancer, a pathology for which the role of hormones is clearly demonstrated. Thus, several epidemiological studies have been conducted in recent years to search for an association between sex hormones and the occurrence of glioma or meningioma. Across studies, a reduced risk with hormone replacement therapy use and an increased risk with later age at menarche appeared consistent for gliomas, while meningioma risk seems to increase with menopause. No clear association was found with contraceptive use, pregnancy, and breastfeeding (Cowppli-Bony et al. 2011). The hypothesis of the role of sex hormones has also been suggested on the basis of clinical and experimental observations. Case reports have shown exacerbation of symptoms due to the progression of meningioma after the placement of a contraceptive implant, during the luteal phase of the menstrual cycle and during pregnancy. In vitro studies have shown a proliferation of

meningioma cells when exposed to progesterone or estrogens together and inhibition of glioma cell growth and induction of their apoptosis when exposed to estrogens. Some animal experiments reinforce these data. Thus, after transplantation of glioblastoma lines, tumor growth appears quicker and survival shorter in male rats and mice compared to females. The role of hormones has been reinforced by the identification of hormonal receptors in tumor tissues: ~80% of meningiomas have progesterone receptors, 40% estrogen receptors and 40% androgen receptors, and many other tumor types also present hormonal receptors (chordoma, craniopharyngioma, insulinoma, etc.).Yet, the role of these receptors is controversial as their functionality is not proven, and hormonal therapies have proven inefficient.

Pesticides

The role of pesticides in the risk of CNS tumors was first suggested by studies on the mortality of farmers in the United States and in Scandinavian countries. Indeed, farmers globally present a lower risk of cancer than the general population, but a higher risk for some specific cancer sites, including the CNS. This result was consistent between studies and was confirmed in a meta-analysis (Acquavella et al. 1998). Based on 33 studies, a meta-analysis (Khuder et al. 1998) calculated a 30% statistically significant increase in the risk of brain tumors in farmers (OR = 1.3; IC = 1.09–1.56). Several factors could explain this increase: pesticides but also viruses, solvents, and fertilizers. The use of insecticides in agriculture has been classified by the International Agency for Cancer Research as probably carcinogenic (2A) in humans, and some of them have been proven as carcinogens in animals. This constitutes an important hypothesis to explain the epidemiological findings in farmers, but there is a lack of data, considering the registration as pesticides of >1000 substances in recent decades. In epidemiological studies on pesticides and brain tumors, the strength of the association was generally between 1.5 and 2, and did not always reach statistical significance. In most studies, pesticide exposure was roughly assessed on the basis of job titles. Most recent studies have developed efforts for more accurate exposure assessment. For instance, in the Upper Midwest Health Study, lists of pesticides were priorly-established, proposed to participants, and pesticides were then grouped into categories corresponding to their chemical properties (Ruder et al. 2006). Analysis found tendencies for carbamate herbicides and for arsenicals, even if non-statistically significant because of the small numbers involved. Another study used a job-exposure matrix and provided results for classes of pesticides with life-long cumulative scores (Samanic et al. 2008). In this study, women who reported ever using herbicides had a significant increase in risk of meningioma, with a dose-effect relationship. The role of pesticide exposure is also suspected in children where exposure during pregnancy or in early life could play a role, through parental occupational exposure or home pesticide exposure.

Other Potential Exogenous Risk Factors

Various other hypotheses have been explored, such as effects of specific chemicals, including dyes, solvents, acrylonitrile, and heavy metals. Some drugs have also been investigated, with a specific interest in an apparent decrease in risk for patients treated with Non Steroidal Anti-inflammatory drugs, nitrosephedrin or antiepileptic. Other medical conditions such as hypertension, a history of head trauma, and a history of epilepsy have also been tested as risk factors but with inconclusive results to date.

In conclusion, numerous hypotheses on exogenous risk factors have been made to find clues for the etiology of brain tumors. They sometimes stem from experimental data proving the role of genotoxic or carcinogenic substances in animals (nitrosoureas, etc.), and sometimes from epidemiological evidence showing variations in incidence according to individual characteristics (age, sex). Some others are flawed by inaccurate assessment of exposure to the risk factors. Interactions between several factors might also be an explanation for the complexity of the situation. Brain tumors may occur from the combination of several exogenous factors, or from endogenous factors such as individual susceptibility (possibly explained by genetic polymorphisms) and environmental factors.

References

Acquavella J, Olsen G, Cole P, Ireland B, Kaneene J, Schuman S, Holden L (1998) Cancer among farmers: a meta-analysis. Ann Epidemiol 8:64–74

Ahlbom A, Feychting M, Green A, Kheifets L, Savitz DA, Swerdlow AJ (2009) Epidemiologic evidence on mobile phones and tumor risk: a review. Epidemiology 20:639–652

Arora RS, Alston RD, Eden TOB, Estlin EJ, Moran A, Birch JM (2009) Age-incidence patterns of primary CNS tumors in children, adolescents, and adults in England. Neuro-oncology 11:403–413

Bondy ML, Scheurer ME, Malmer B, Barnholtz-Sloan JS, Davis FG, Il′yasova D, Kruchko C, McCarthy BJ, Rajaraman P, Schwartzbaum JA, Sadetzki S, Schlehofer B, Tihan T, Wiemels JL, Wrensch M, Buffler PA (2008) Brain Tumor Epidemiology Consortium. Brain tumor epidemiology: consensus from the Brain Tumor Epidemiology Consortium. Cancer 113:1953–1968

Brown M, Schrot R, Bauer K, Letendre D (2009) Incidence of first primary central nervous system tumors in California, 2001–2005. J Neurooncol 94:249–261

Cowppli-Bony A, Bouvier G, Rué M, Loiseau H, Vital A, Lebailly P, Fabbro-Peray P, Baldi I (2011) Brain tumors and hormonal factors: review of the Aepidemiological literature. Cancer Causes Control 22:697–714

Darefsky AS, Dubrow R (2009) International variation in the incidence of adult primary malignant neoplasms of the brain and central nervous system. Cancer Causes Control 20: 1593–1604

Davis FG, Kupelian V, Freels S, McCarthy B, Surawicz T (2001) Prevalence estimates for primary brain tumors in the United States by behavior and major histology groups. Neuro-oncology 3:152–158

Dietrich M, Block G, Pogoda JM, Buffler P, Hecht S, Preston-Martin S (2005) A review: dietary and endogenously formed *N*-nitroso compounds and risk of childhood brain tumors. Cancer Causes Control 16:619–635

Dreifaldt AC, Carlberg M, Hardell L (2004) Increasing incidence rates of childhood malignant diseases in Sweden during the period 1960–1998. Eur J Cancer 40:1351–1360

Fritz A, Percy C, Jack A, Shanmugaratnam K, Sobin L, Parkin M Whelan SL (2000) International classification of diseases for oncology, 3rd edn. World Health Organization, Geneva

Gousias K, Markou M, Voulgaris S, Goussia A, Voulgari P, Bai M, Polyzoidis K, Kyritsis A, Alamanos Y (2009) Descriptive epidemiology of cerebral gliomas in northwest Greece and study of potential predisposing factors, 2005–2007. Neuroepidemiology 33:89–95

Gu J, Liu Y, Kyritsis AP, Bondy ML (2009) Molecular epidemiology of primary brain tumors. Neurotherapy 6:427–435

Harder T, Plagemann A, Harder A (2008) Birth weight and subsequent risk of childhood primary brain tumors: a meta-analysis. Am J Epidemiol 168:366–373

Huncharek M, Kupelnick B (2004) A meta-analysis of maternal cured meat consumption during pregnancy and the risk of childhood brain tumors. Neuroepidemiology 23:78–84

INTERPHONE Study Group (2010) Brain tumour risk in relation to mobile telephone use: results of the INTERPHONE international case-control study. Int J Epidemiol 39: 675–694

Kaatsch P, Rickert CH, Kühl J, Schüz J, Michaelis J (2001) Population-based epidemiologic data on brain tumors in German children. Cancer 15:3155–3164

Kheifets L, Bowman JD, Checkoway H, Feychting M, Harrington JM, Kavet R, Marsh G, Mezei G, Renew DC, van Wijngaarden E (2009) Future needs of occupational epidemiology of extremely low frequency electric and magnetic fields: review and recommendations. Occup Environ Med 66:72–80

Khuder SA, Mutgi AB, Schaub EA (1998) Meta-analyses of brain cancer and farming. Am J Indus Med 34: 252–260

Khurana VG, Teo C, Kundi M, Hardell L, Carlberg M (2009) Cell phones and brain tumors: a review including the long-term epidemiologic data. Surg Neurol 72:205–214

Kuratsu J, Takeshima H, Ushio Y (2001) Trends in the incidence of primary intracranial tumors in Kumamoto, Japan. Int J Clin Oncol 6:183–191

Lai R, Crevier L, Thabane L (2005) Genetic polymorphisms of glutathione S-transferases and the risk of adult brain tumors: a meta-analysis. Cancer Epidemiol Biomarkers Prev 14:1784–1790

Larjavaara S, Haapasalo H, Sankila R, Helén P, Auvinen A (2008) Is the incidence of meningiomas underestimated? A regional survey. Br J Cancer 99:182–184

Liigant A, Asser T, Kulla A, Kaasik AE (2000) Epidemiology of primary central nervous system tumors in Estonia. Neuroepidemiology 19:300–311

Lim U, Subar AF, Mouw T, Hartge P, Morton LM, Stolzenberg-Solomon R, Campbell D, Hollenbeck AR, Schatzkin A (2006) Consumption of aspartame-containing beverages and incidence of hematopoietic and brain malignancies. Cancer Epidemiol Biomarkers Prev 15:1654–1659

Linos E, Raine T, Alonso A, Michaud D (2007) Atopy and risk of brain tumors: a meta-analysis. J Natl Cancer Inst 99: 1544–1550

Louis DN, Ohgaki H, Wiestler D, Cavanee WK (2007) WHO classification of tumours of the central nervous system, 4th edn. IARC, Lyons

Malmer B, Adatto P, Armstrong G, Barnholtz-Sloan J, Bernstein JL, Claus E, Davis F, Houlston R, Il′yasova D, Jenkins R, Johansen C, Lai R, Lau C, McCarthy B, Nielsen H, Olson SH, Sadetzki S, Shete S, Wiklund F, Wrensch M, Yang P, Bondy M (2007) GLIOGENE—an international consortium to understand familial glioma. Cancer Epidemiol Biomarkers Prev 16:1730–1734

Mandelzweig L, Novikov I, Sadetzki S (2009) Smoking and risk of glioma: a meta-analysis. Cancer Causes Control 20: 1927–1938

McCarthy BJ, Surawicz T, Bruner JM, Kruchko C, Davis F (2002) Consensus conference on brain tumor definition for registration, November 10, 2000. Neuro-oncology 4: 134–145

McKinley BP, Michalek AM, Fenstermaker FA, Plunkett RJ (2000) The impact of age and sex on the incidence of glial tumors in New York state from 1976 to 1995. J Neurosurg 93:932–939

Moore SC, Rajaraman P, Dubrow R, Darefsky AS, Koebnick C, Hollenbeck A, Schatzkin A, Leitzmann MF (2009) Height, body mass index, and physical activity in relation to glioma risk. Cancer Res 69:8349–8355

Pisani P, Bray F, Parkin DM (2002) Estimates of the world-wide prevalence of cancer for 25 sites in the adult population. Int J Cancer 97:72–81

Prasad G, Haas-Kogan DA (2009) Radiation-induced gliomas. Exp Rev Neurother 9:1511–1517

Radhakrishnan K, Mokri B, Parisi JE, O'Fallon WM, Sunku J, Kurland LT (1995) The trends in incidence of primary brain tumors in the population of Rochester, Minnesota. Ann Neurol 37:67–73

RSTNC. Registre des Tumeurs du Système Nerveux Central de Gironde. http://etudes.isped.u-bordeaux2.fr/registres-cancers-aquitaine/Snc/S_Accueil.aspx

Ruder AM, Waters MA, Carreón T, Butler MA, Davis-King KE, Calvert GM, Schulte PA, Ward EM, Connally LB, Lu J, Wall D, Zivkovich Z, Heineman EF, Mandel JS, Morton RF, Reding DJ, Rosenman KD, Brain Cancer Collaborative Study Group (2006) The Upper Midwest Health Study: a case-control study of primary intracranial gliomas in farm and rural residents. J Agric Saf Health 12:255–274

Sadetzki S, Zach L, Chetrit A, Nass D, Hoffmann C, Ram Z, Zaaroor M, Umansky F, Rappaport ZH, Cohen A, Wald U, Rothman S, Hadani M (2008) Epidemiology of gliomas in Israel: a nationwide study. Neuroepidemiology 31: 264–269

Samanic CM, De Roos AJ, Stewart PA, Rajaraman P, Waters MA, Inskip PD (2008) Occupational exposure to pesticides and risk of adult brain tumors. Am J Epidemiol 167:976–985

Schellinger KA, Propp JM, Villano JL, McCarthy BJ (2008) Descriptive epidemiology of primary spinal cord tumors. J. Neurooncol 87:173–179

Shah KV (2007) SV40 and human cancer: a review of recent data. Int J Cancer 120:215–223

Shete S, Hosking FJ, Robertson LB, Dobbins SE, Sanson M, Malmer B, Simon M, Marie Y, Boisselier B, Delattre JY, Hoang-Xuan K, El Hallani S, Idbaih A, Zelenika D, Andersson U, Henriksson R, Bergenheim AT, Feychting M, Lönn S, Ahlbom A, Schramm J, Linnebank M, Hemminki K, Kumar R, Hepworth SJ, Price A, Armstrong G, Liu Y, Gu X, Yu R, Lau C, Schoemaker M, Muir K, Swerdlow A, Lathrop M, Bondy M, Houlston RS (2009) Genome-wide association study identifies five susceptibility loci for glioma. Nat Genet 41:899–904

Terry MB, Howe G, Pogoda JM, Zhang FF, Ahlbom A, Choi W, Giles GG, Little J, Lubin F, Menegoz F, Ryan P, Schlehofer B, Preston-Martin S (2009) An international case-control study of adult diet and brain tumor risk: a histology-specific analysis by food group. Ann Epidemiol 19:161–171

Umansky F, Shoshan Y, Rosenthal G, Fraifeld S, Spektor S (2008) Radiation-induced meningioma. Neurosurg Focus 24:E7

Wöhrer A, Waldhör T, Heinzl H, Hackl M, Feichtinger J, Gruber-Mösenbacher U, Kiefer A, Maier H, Motz R, Reiner-Concin A, Richling B, Idriceanu C, Scarpatetti M, Sedivy R, Bankl HC, Stiglbauer W, Preusser M, Rössler K, Hainfellner JA (2009) The Austrian Brain Tumour Registry: a cooperative way to establish a population-based brain tumour registry. J Neurooncol 95:401–411

Wrensch M, Jenkins RB, Chang JS, Yeh RF, Xiao Y, Decker PA, Ballman KV, Berger M, Buckner JC, Chang S, Giannini C, Halder C, Kollmeyer TM, Kosel ML, LaChance DH, McCoy L, O'Neill BP, Patoka J, Pico AR, Prados M, Quesenberry C, Rice T, Rynearson AL, Smirnov I, Tihan T, Wiemels J, Yang P, Wiencke JK (2009) Variants in the CDKN2B and RTEL1 regions are associated with high-grade glioma susceptibility. Nat Genet 41:905–908

Wrensch M, Lee M, Miike R, Newman B, Barger G, Davis R, Wiencke J, Neuhaus J (1997) Familial and personal medical history of cancer and nervous system conditions among adults with glioma and controls. Am J Epidemiol 145:581–593

Chapter 2

Supratentorial Primitive Neuroectodermal Tumors

Mohit Singh and Juliette Hukin

Abstract Supratentorial primitive neuroectodermal tumor (sPNET) only represents 2.5–3% of childhood brain tumors. It has a worse prognosis than its posterior fossa counterpart and a different molecular signature has been demonstrated. The mainstay of therapy is gross total resection followed by adjuvant therapy that is age dependant, in older children this involves craniospinal radiation and chemotherapy, in the infant different approaches to minimize radiation have been attempted. Prognosis is variable between 5 and 30% 5 year survival, dependent on the child's age, the presence of dissemination at diagnosis and the treatment options available.

Keywords Neuroectodermal · Neuroepithelial stem cells · Cerebellum · Pediatric tumor · Leptomeninges · Pineoblastomas

Introduction

The term primitive neuroectodermal tumor or *PNET*, refers to tumors derived from neuroepithelial stem cells, cells that are arrested in different stages of diversification and differentiation (Louis et al. 2007). The central nervous system PNETs are classified based on their location relative to the tentorium. Most PNETs are infratentorial tumors arising in the cerebellum. They are referred to as medullobastomas and account for over 90% of all PNETs (Siffert and Allen, 1997). Supratentorial PNETs (sPNETs) are rare tumors and by definition, arise above the tentorium. The discussion below outlines some of the key points on this group of tumors, focusing on the pediatric population.

Incidence

Supratentorial PNETs account for 2.5–3% of all childhood brain tumors (Jakacki 1999). Although a primary pediatric tumor, it has been shown to occur in adults as well (Li et al. 2005). The majority of studies show a male predominance (Yang et al. 1999). sPNETs are more common in younger children, especially under 5 years of age (Dai et al. 2003).

Location

Most sPNETs arise from the cerebral hemispheres; the frontal, temporal or parietal lobes are the most common location. Supratentorial PNETs also commonly arise from the pineal region (Jakacki 1999). Less commonly deep regions in the brain are affected such as the basal ganglia, diencephalon and corpus collosum (Dirks et al. 1996). Deeper tumors are often found to have an intraventricular or peri-ventricular epicenter (Jakacki 1999). Many sPNETs are large and often involve vascular structures (Jakacki 1999).

Dissemination is often seen in sPNETs with the leptomeninges being involved at diagnosis or relapse. Extraneural metastases however, are uncommon (Dirks

J. Hukin (✉)
Neurology Division ACB, K3-145, British Columbia Children's Hospital, Vancouver, BC V6H3V4, Canada
e-mail: jhukin@cw.bc.ca

M.A. Hayat (ed.), *Tumors of the Central Nervous System, Volume 4*,
DOI 10.1007/978-94-007-1706-0_2,

et al. 1996), a recent review of the literature comments that out of 222 sPNETs patients reviewed, less than 0.5% had metastases outside the CNS (Johnston et al. 2008). This review also suggests that bone scans and bone marrow analysis to check for involvement of sites outside the CNS are not needed for patients with newly diagnosed sPNETs.

Signs and Symptoms

The clinical symptoms and progression of sPNETs tend to occur shortly before diagnosis and a differential diagnosis of all brain tumors must be included (Kuhn et al. 2007). Mostly, children present with general non-specific symptoms, including: headache, irritability, nausea, vomiting and balance difficulties (Abeloff 2008; Dirks et al. 1996). These symptoms are a sign of increased intracranial pressure (ICP). Factors that lead to increased ICP include: tumor volume, surrounding edema, the blockage of CSF within the ventricles and disruption of the flow of venous sinuses (Plum et al. 1980). Pineal tumors may compress the aqueduct of sylvius, causing hydrocephalus. Compression of the pretectal area produces Parinaud's syndrome, characterized by paralysis of upgaze, ptosis, and loss of pupillary light reflexes, along with retraction-convergence nystagmus (Abeloff 2008).

Supratentorial PNETs, can also produce different intracranial herniation syndromes. These include: cingulate gyrus herniation under the falx cereberi, diencephalic herniation, hippocampal gyrus herniation through the tentorial notch, which can compress the posterior cerebral artery and brain stem. Also, herniation of the cerebellar tonsils through the foramen magnum may be seen (Plum 1980).

Histology

The current World Health Organization (WHO) classification system relies on tumor cell of origin but also allows for grouping based on where these tumors may arise. Most childhood with brain tumors fall under tumors of neuroepithelial tissue. There are roughly nine broad types of tumors involving this tissue. According to the updated 2007 WHO classification system: astrocytic, oligodendroglial, oligoastrocytic, ependymal, pineal, neuronal-glial, choroid plexus, 'other' neuroepithelial tumors and embryonal tumors differentiate from neuroepithelial tissue (Louis et al. 2007). All PNETs fall under the embryonal tumor type.

PNETs are a heterogeneous group of embryonal tumors that may be poorly differentiated, showing properties along neuronal, astrocytic, ependymal, glial, muscular or melanotic lines (Girschick et al. 2001; Louis et al. 2007). They are a group of highly malignant, high-grade lesions. Although sPNETs are histologically indistinguishable from infratentorial medulloblastoma, they often respond poorly to medulloblastoma-specific therapy. The key to unlocking effective protocols of treatment for sPNET has not been histological analysis, but rather requires a deeper look at the cell types involved. Indeed, existing molecular genetic studies indicate that sPNETs have transcriptional and cytogenetic profiles that are different from those of medulloblastomas, thus pointing to a possible unique biological derivation for the sPNET.

Molecular Genetics

Studies focusing on the molecular genetics of sPNETs are very few, in contrast to PNETs as a group. It is important to appreciate the differences in the genetic make up of sPNETs as it may be key in helping us understand why therapy is not as effective and why prognosis is so poor for this group of tumors (Jakacki 1999; Li et al. 2005). Gains and losses in a variety of chromosomes, including, 6p, 16q and 17p, have been reported in medulloblastoma studies, the loss of chromosome arm 17p is reported to be the most frequent genetic abnormality (Burnett et al. 1997). The amplification of c-Myc, a transcriptional factor coded for by a proto-oncogene, and N-Myc, a transcriptional factor are thought to play a role in angiogenesis, and have also been implicated in PNET genesis (Pelengaris et al. 2002).

Since these well known genetic aberrations play a role in the tumor biology of medulloblastoma, it was hypothesized that the same could be implied for sPNETs. So far, the research has shown mixed results. A case study revealed that all chromosomes were

intact, showing no loss or gain of chromosomes and N-Myc and c-Myc were not amplified in the sPNET (Girschick et al. 2001). However, other studies have shown increased amplification of these very same factors (Li et al. 2005). It has also been shown that sPNETs show more losses than gains in chromosome number, with 4q loss seen in 50% of tumors studied (Li et al. 2005). Unlike their infratentorial counterparts, chromosome 17p was shown to be preserved in most of the sPNETs studied, suggesting unique events are involved in tumor formation (Burnett et al. 1997).

Abnormalities in cell signaling pathways have become one of the most recent targets to explain the behavior of sPNETs. The Ras 'superfamily' of signaling pathways has generated particular attention. This family of small GTPases is well known to control many different components of cell proliferation. The Rho protein family within the Ras superfamily have been of particular interest. These proteins are responsible for a variety of cellular processes, including, proliferation, motility, morphogenesis, vesicle movements and gene expression. Rho-GTPase activity has been found to be dysregulated in a variety of human cancers and may contribute to the formation of tumors (Durkin et al. 2007). Rho-GTPase is controlled by two types of larger regulatory proteins; the guanine nucleotide exchange factors (GEFs), which promote the exchange of GDP for GTP to generate the active state in signaling proteins, and the GTPase activating proteins (GAPs) which stimulate hydrolysis to bring about the inactive state (Durkin et al. 2007). The connection with the Rho GTPase and its possible contribution to formation of sPNETs is through a tumor suppressor gene named DLC-1, which stands for 'deleted in liver cancer'. In humans, the DLC-1 gene codes for a GAP regulatory protein, which is specific for Rho GTPase, called 'RhoGAP' which is essentially responsible for decreasing the activity of Rho GTPase. RhoGAP is being widely researched for its role in tumor suppression, regulation of cell proliferation as well as cytoskeletal organization (Durkin et al. 2007).

Loss of DLC-1 gene expression has been reported in many different types of human cancers, including breast, cervical, gastric and liver carcinomas among others (Durkin et al. 2007). Most recently a study was done to learn more about the role of DLC-1, which is located on chromosome 8p22, and its role in the development of PNETs (Pang et al. 2005). The results concluded that transcriptional silencing of DLC-1 through promoter hypermethylation is responsible for tumor formation in a subset of sPNETs. The study also showed that loss of DLC-1 through the mechanism of promoter hypermethylation was specific to sPNETs only.

Several other signaling pathways have been implicated in sPNET tumor genesis. The *Wingless (Wnt), Notch-Hes* and Sonic hedgehog-Gli (*Shh-Gli*) signaling pathways have all been implicated (Li et al. 2005). Out of these the *Shh-Gli* is the most deeply involved. The *Shh* protein and gene operate by stimulating an intracellular signal transduction pathway that contributes to the differentiation of many organs in the developing embryo, including, the notochord, floor plate and limbs (Arsic et al. 2004). The *Gli* protein is a critical part of this pathway as it is the primary mediator of transcriptional activation by *Shh.* Support for dysregulation of this pathways involvement comes from reports of increased expression of downstream targets of *Shh* signaling, such as N-MYC, and the loss of heterozygosity of the PTCH locus, a tumor suppressor gene involved in controlling *Shh* signaling (Zurawel et al. 2000). Although the clinical implication of these findings still needs to be investigated further, the involvement of signaling pathways in brain development lends support to the idea that sPNETs may be of congenital origin (Girschick et al. 2001).

The p53 tumor suppresser gene is located on chromosome 17p and is one of the most affected genes in cancer formation (Li et al. 2005). Li-Fraumeni syndrome (LFS) is a hereditary disorder that involves p53 and predisposes to a wide variety of early-onset tumors including astrocytic tumors, medulloblastomas and sPNETs. It has been reported that the mean onset of brain tumors in LFS is 16 years of age (Farrell et al. 2007).

Finally, sPNETs of the pineal region (Jakacki 1999) are also referred to as pineoblastomas. Pineal region tumors can be associated with a condition termed trilateral retinoblastoma. Usually, the term retinoblastoma refers to tumors arising from neurosensory cells of the retina (Paulino 1999). This is a disease that can occur with sporadic or heritable changes in the retinoblastoma gene, RB1, which is located on chromosome 13q. The association of an ectopic intracranial tumor with bilateral retinoblastoma is referred to as trilateral retinoblastoma. The histology of pineal and sPNETs occurring in the context of trilateral retinoblastoma is very similar to the histology of

intraocular retinoblastomas. It has been shown that during embryonic development, the pineal gland develops from neuroepithelial cells that have some features of photosensory differentiation, linked to the photoreceptors of the retina (Bajaj et al. 2007). The noted differences in histology of trilateral retinoblastoma associated PNETs of the pineal and suprasellar regions from other sPNETs implies that these tumors arise from slightly different cellular origins (Bajaj et al. 2007; Li et al. 2005).

Imaging

In infants with an open anterior fontanel transcranial ultrasound may identify an abnormal mass during the investigation of an enlarged head circumference and thus prompt further imaging. On CT imaging: sPNETs appear heterogeneous due to the variable presence of haemorrhage, necrosis, calcification, and cysts (Fig. 2.2a). Just over half of sPNETs demonstrate intratumoral calcification (Fig. 2.1a). As with other hypercellular tumors, the solid component of sPNETs typically appears as a hyperdense mass (Fig. 2.1a). With contrast the tumor usually enhances brightly heterogeneously. Despite the malignant nature of these lesions, there is often minimal or no edema (Fig. 2.1b).

MRI is the imaging modality of choice for distinguishing these lesions from other tumors and delineating the anatomical confines of the mass lesion. The typical appearance of a sPNET on MRI is that of a heterogeneous mass with relatively well-defined margins, and moderate to intense enhancement (Fig. 2.1c). On T1-weighted MRI, sPNETs are typically heterogeneously low signal but may be high signal depending on the presence of blood (Fig. 2.1a). On T2-weighted MRI, PNETs generally appear isointense to cerebral cortex but may also appear hyperintense (Fig. 2.1b). MRI plays a key role in detection of intracranial or spinal leptomeningeal dissemination. This is of particular importance, because 20–40% of sPNETs demonstrate evidence of such spread at presentation (Albright et al. 1995; Dirks et al. 1996).

Certain characteristics on MR imaging assist in differentiating PNETs from other tumors. Unlike other CNS neoplasms that can mimic PNETs, namely astrocytomas, ependymomas, choroid plexus carcinoma, and gangliogliomas, PNETs are usually isointense to

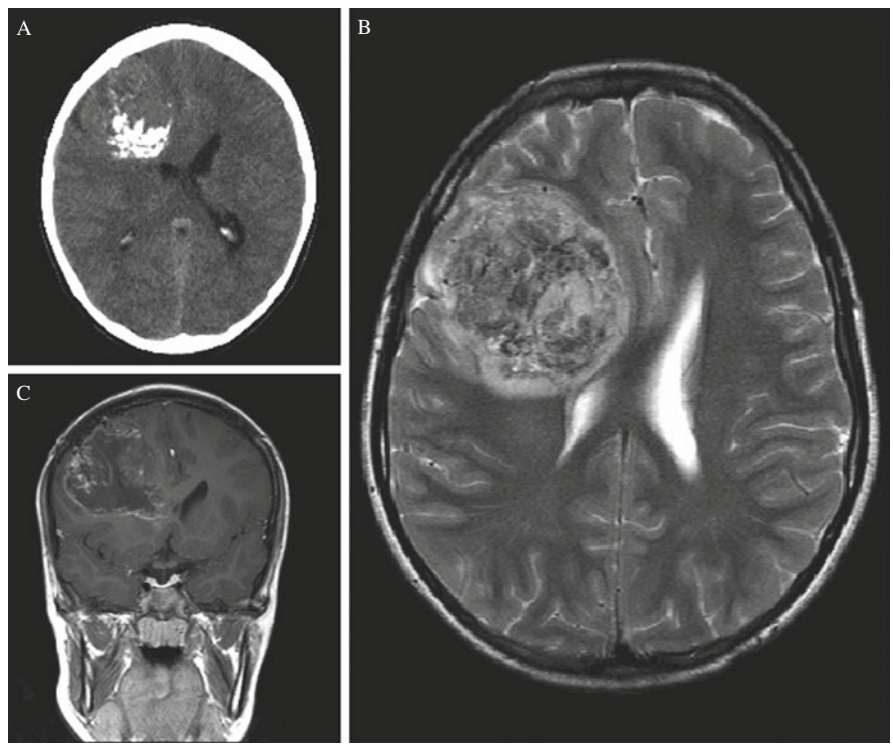

Fig. 2.1 (**a**) CT Brain: right frontal hyperdense mass with calcification, and compression of the frontal horn of the right lateral ventricle. (**b**) MRI Axial T2 weighted image: Heterogeneous with most areas being isointense or hyperintense. This well defined right frontal mass is causing distortion of the right lateral ventricle. Note the subfalcine herniation and little surrounding oedema. (**c**) MRI coronal T1 with contrast: heterogeneously low signal with peripheral contrast enhancement

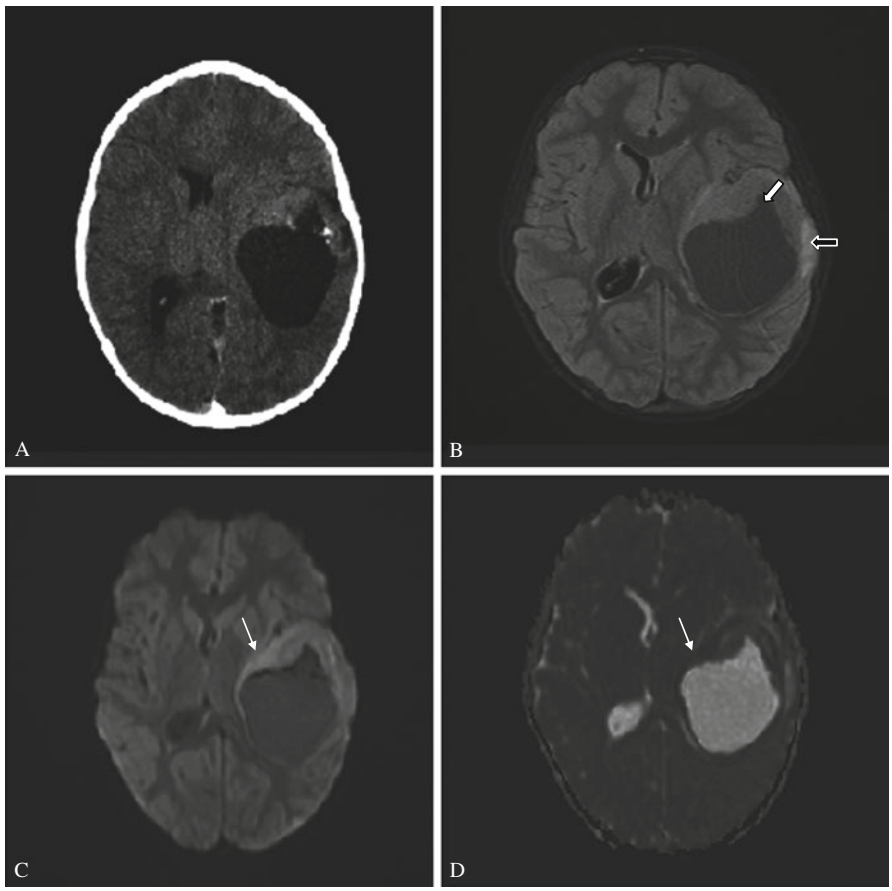

Fig. 2.2 (**a**) Axial CT Brain: temporal mass with large cystic component and surrounding high attenuation solid component with some calcification, with midline shift and compression of the left lateral ventricle and dilatation of the right. (**b**) FLAIR axial MRI: well defined solid component surrounding the cyst is isointense to cortex (⇧), with minimal perilesional edema (⬆). (**c**) Diffusion weighted axial MRI: increased signal in solid component around cyst. (**d**) Apparent diffusion coefficient map MRI: restricted diffusion in peripheral solid components of the tumor

cortex on FLAIR sequence MR scans (Fig. 2.2b). In addition, the solid components of sPNETs were found to have a high signal on diffusion-weighted MR imaging (Fig. 2.2c) (Klisch et al. 2000) with restricted diffusion on apparent diffusion coefficient map (Fig. 2.2d).

Prognosis

Prognostic factors of sPNETs have been under studied in comparison to medulloblastoma/PNETs. Since sPNETs are rare tumors, controversy surrounding their histological and pathological classification again factors in, making it difficult to understand fully the natural history of this disease. This is a major reason that the long-term survival in sPNET patients is so poor (Li et al. 2005). Survival is also influenced by different prognostic factors, both intrinsic and extrinsic to the tumor itself. Identifying these factors is crucial as it has an important role in treatment planning (Yang et al. 1999).

There are several other factors that influence outcome in sPNET patients. Age, for instance, is a prognostic factor known to influence the survival quite significantly. The 2 and 5 year survival rates were found to be 28 and 5.8% for those under age 3. They were much improved in comparison for those aged 3 and older at 72 and 29% (Li et al. 2005). It is important to think about the use of radiation therapy in treatment when considering age as a prognostic factor. While it is possible that younger age may equal more aggressive disease, the limited use of radiation in young children, which is a proven effective treatment, is likely a confounding factor (Johnston et al. 2008). Location may also play a role in prognosis, as pineal region tumors have shown to fare better than non-pineal and deep sPNETs (Dirks et al. 1996; Jakacki 1999). However this result is debated by a more recent study showing

a higher 4 year survival rate, 41–24%, for hemispheric versus pineal tumors respectively (Johnston et al. 2008). Evidence of dissemination is usually a reliable factor indicating a poor prognosis in patients (Mueller and Chang 2009).

Histological differentiation of the tumor has not been shown to be a reliable significant prognostic marker (Jakacki 1999). Also, although molecular genetics are the new frontier in developing a better understanding of sPNETs, little is known about how the implicated proteins and pathways affect prognosis. For example, studies analyzing the loss of chromosome 17p or abnormalities in p53 are poor prognostic factors in medulloblastoma, but the results cannot be extrapolated to sPNETs (Burnett et al. 1997). The treatment method used influences prognosis of sPNETs. Patients with sPNETs have a significantly worse prognosis than those with medulloblastoma, despite very similar therapies (Fangusaro et al. 2008). Surgical resection along with chemotherapy and radiation have been used in various combinations. A closer look at the different modalities of treatment for sPNETs and their effectiveness is explored in the next section.

Treatment

A multimodality approach including maximal safe surgical resection, chemotherapy and radiation is associated with the most favorable cure rate, however this may need to be modified depending on size, location and age of the patient.

Surgery

Surgical resection is the initial approach in patients presenting with sPNET (Mueller and Chang, 2009). Yang et al. (1999) examined treatment outcomes and prognostic factors in 28 cases of sPNETs. The degree of resection along with presence of tumor necrosis is statistically significant in determining risk of recurrence. More specifically, gross total resection and near total resection patients faired better than patients with subtotal, partial or biopsy type resections. The CCG–921 trial showed that children with residual tumor of 1.5 cm^2 or less had a survival of 40% after 4 years, those with tumor size greater than 1.5 cm^2, postoperative survival was only 13% after 4 years (Albright et al. 1995).

There is however some controversy surrounding the extent to which surgical excision of tumor dictates survival for patients. A retrospective clinical analysis of different regimens used to treat sPNETs in Canada for the past 10 years was recently completed (Johnston et al. 2008). The results showed no difference in outcome survival or event free survival in patients who had complete resection compared to those with incomplete resection. The authors concluded this was due to the effectiveness of adjuvant chemotherapy and radiation used post operatively. In addition a SIOP study of 68 patients with pineal or non pineal sPNETs did not demonstrate a statistically significant improvement in survival in those that had a gross total resection (Pizer et al. 2006). This observation held true regardless of tumor location and extent of metastases.

Radiation

Most evidence for the effectiveness of radiation comes from retrospective studies. Dosing, timing and target volume are still topics of debate. Radiation is typically used in children older than 3 years of age, and preferably older (Mueller and Chang, 2009). Age is carefully considered because it is important to avoid or limit radiation-induced damage to the developing brain, in particular its impact on neurocognitive development. Currently the dose of radiation recommended for children greater than 3 years old 36 Gy of craniospinal radiation plus a suggested total dose of 54–56 Gy to the focal tumor bed (Mueller and Chang, 2009; Pizer et al. 2006).

Some important knowledge regarding the role of radiation therapy in sPNET treatment comes from the German HIT 88/89 and HIT 91 trials (Timmermann et al. 2002). The purpose of these studies was to evaluate the role played by surgery, radiation and chemotherapy in treating children with sPNETs. In the HIT 88/89 trials patients were treated postoperatively with preirradiation chemotherapy (ifosfamide, etoposide, methotrexate, cisplastin, cytarabine). The chemotherapy was given starting 14 days after surgery.

External beam radiation then followed 4 weeks after chemotherapy in HIT 88/89. In the HIT 91 trial radiation was given 3 weeks following surgery, with maintenance chemotherapy (cisplastin, vincristine, lomustine) given 6 weeks after finishing radiation treatments. All patients were to be treated with fractionated recommended dosages of irradiation to the neuraxis, 35.2 Gy with additional boost provided to the supratentorial region involved, to 20 Gy.

The results of the HIT trials showed that immediate radiotherapy followed by maintenance chemotherapy was better than delaying radiation with preirradiation chemotherapy. There was an increased rate of early progression, 22% in the preirradiation group versus 4% in the immediate radiation with maintenance chemotherapy group. The study also showed the only significant prognostic factor for progression free survival was the dose and volume of radiation given. In fact, the progression free survival was noted to be 6.7% versus 49.3% for 15 of the 63 patients in these trials that had major violations in their radiotherapy (Timmermann et al. 2002). These major violations in radiotherapy were defined as craniospinal dose less than 35 Gy or local dose less than 54 Gy, or if no craniospinal irradiation was administered, or if no irradiation at all was performed.

The results of the HIT study were significant in reinforcing the importance of dose, volume and role of radiation in treating sPNETs. Similar results have been found in more recent studies as well. In the Canadian clinical analysis discussed above, the effects of adjuvant radiation and chemotherapy were studied in 48 pediatric patients (Johnston et al. 2008). This study found that when chemotherapy and radiation therapy were used concurrently, there was a significant improvement in survival rates. However, when multiple regression analysis was conducted, radiation therapy used according to recommended doses was found to be the only independent significant factor associated with improved survival ($p = 0.002$).

A recent look at the effectiveness of radiation therapy comes from Yale University, Mcbride et al. (2008) studied 15 children under 18 years old with non-pineal sPNETs. Initial treatment with surgery and chemotherapy was given to all patients. Radiation therapy was delivered as follows: upfront radiation (RT) in five patients, RT given at time of progression in five patients and five were given no RT. The results at follow up showed that all patients receiving the upfront RT were alive without any evidence of disease at a follow up averaging 4 years. However, only five of ten patients not receiving upfront RT were alive at follow up. There was a statistically significant difference in overall survival between the group of patients that received up-front RT and the group that did not ($P = 0.048$).

The retrospective SIOP/UKSSCG PNET-3 study looked at the effects of radiation therapy alone compared to pre radiation chemotherapy (alternating cycles of vincristine, etoposide, carboplatin and vincristine, etoposide and cyclophosphamide) for adjuvant treatment. Radiation was delivered in standard fractionated format, consisting of a craniospinal radiation dose of 35 Gy in 21 daily fractions. Followed by 20 Gy total dose to the primary tumor in 12 fractions (55 Gy total dose to the primary tumor) (Pizer et al. 2006). The results show no significant improvement for event free survival, 54% or outcome survival, 48% when comparing the pre chemotherapy plus radiation group to the radiation therapy alone group respectively. This study supports the value of radiation therapy as the mainstay of treatment in sPNET therapy.

The studies highlighted have shown there is a decrease in relapse rate with radiation use. It is important to consider however, that there is variation in tumor histology and molecular genetics of sPNET. With this in mind, there are cases that will respond well to chemotherapy without need for radiation. There is also the very important consideration of injury to developing brain cells of younger children with radiation. It is these factors that have lead to the increased development of chemotherapy and recent improvements in its effectiveness with increased intensity. The definite and important role of chemotherapy in treating sPNETs is discussed in the next section.

Chemotherapy

The most current review of the literature states that chemotherapy is effective in sPNETs as they are chemo-sensitive tumors. Chemotherapy is recommended as adjunctive therapy for newly diagnosed sPNETs. Intensive chemotherapy with autologous stem cell rescue is also beneficial in children of younger age to delay or avoid radiation therapy (Mueller and Chang, 2009).

As discussed in the previous section, various studies have tried to study the benefits of chemotherapy alone as well as in combination with radiation therapy. The combination of radiation and chemotherapy has shown to be effective in sPNETs in more recent studies (Fangusaro et al. 2008; Mueller and Chang, 2009). However, there were many disappointments in combination treatments before positive results were seen. A significant study highlighting the difficulty of finding a chemotherapy protocol to delay radiation treatments in infants and young children was conducted in Germany. The HIT-SKK87 and HIT-SKK 92 trial examined 29 pediatric patients studied under the age of 3. In the HIT-SKK87, children were divided into low risk (complete resection, no dissemination) or high risk (subtotal resection or metastases) (Timmermann et al. 2006). Low risk patients received maintenance chemotherapy until RT was administered after age 3, while high risk patients received induction chemotherapy post surgery followed by maintenance chemotherapy until age 3. For those in the HIT-SKK92, three cycles of methotrexate based chemotherapy was given after surgery.

The results of this study were not very encouraging. The progression-free survival (PFS) and overall survival (OS) rates after 3 years were 17 and 15%, for the SKK87 and SKK92 trials respectively. Twenty-four of twenty-nine children relapsed. There were a total of 15 patients in these trials that did not receive RT, of these, only one survived. These discouraging results led the authors to conclude that RT was vital to treatment of infants in sPNETs and that delay of RT be limited to a maximum of 6 months during initial therapy (Timmermann et al. 2006).

With continuing research however, there have been some positive and more effective findings in postponing radiation with chemotherapy in young patients. The Head Start I and II protocols explored delaying radiation by using intensive induction chemotherapy followed by consolidative chemotherapy and autologous hematopoietic cell rescue (AuHCR) in children newly diagnosed with sPNET. There were 43 patients studied in this study, with upper age limits of 6 years old for HS I trial and 10 years old for the HS II trial. Patients on HS I and patients with local disease on HS II received induction chemotherapy, five cycles every 3 weeks (vincristine, cisplastin, cyclophosphamide and etoposide) post surgery (Fanguraso et al. 2008).

Patients on HS II with evidence of metastatic disease were treated with high dose methotrexate and leucovorin rescue. If there was evidence of disease response (defined as tumor remission on MRI and clearance of malignant cells in CSF) patients received a single cycle of high dose consolidative chemotherapy (carboplatin, thiotepa and etoposide), which was followed by AuHCR. Post chemotherapy, the patients were then offered radiation if they were 6 years old at the time of diagnosis.

The results of the Head Start trials were encouraging. The estimated 5-year outcome survival and event free survival for the entire study for HSI was 39% and HSII was 49% respectively. Twenty-seven patients did not receive RT initially. At follow up times of 6.7 and 7.8 years respectively it was found that 12 out of 20 survivors in this category remained alive without any exposure to RT (Fanguraso et al. 2008). The Head Start study shows the possibility of successful deferral or even avoidance of radiation therapy in some patients with sPNET.

There are additional recent studies that support the role of chemotherapy in treating sPNETs. Using HDCT as first line chemotherapy post surgery and craniospinal radiation was investigated in an American study by Strother et al. (2001). Fifty-three patients with medulloblastoma and sPNET were enrolled, 19 with high-risk disease (presence of metastasis or >1.5 cm^2 residual tumor) and 34 with average risk disease (absence of metastatic disease and gross total resection of tumor or <1.5 cm^2 residual tumor), were examined. All patients were treated surgically to remove the maximal amount of tumor possible. Patients in the high-risk group were then treated with topotecan (topoisomerase I inhibitor) therapy for six weeks followed by standard craniospinal irradiation therapy. Low risk patients went straight to standard craniospinal irradiation post surgery. All patients were then started on four, 4 week cycles of high dose cyclophosphamide, cisplatin and vincristine, each followed by stem cell or bone marrow rescue. Forty-nine patients completed all four cycles. The median time to completion was 16.9 weeks and the median delivered dose intensities were 1014, 1023, 974, 991 $mg/m^2/wk$ for cycles 1 through 4. The results showed the 2-year progression free survival for the 34 average risk patients to be 93.6% (± 4.7%). Of the 19 high-risk patients, the 2-year progression free survival was found to be 73.7% (± 10.5%) (Sung et al. 2007). This study shows the role as well as the effectiveness of HDCT in pediatric patients post craniospinal radiation, however the results of longer followup from this study are awaited. These results

do need to be interpreted with some caution as it is unclear what proportion of the cohort was represented by sPNET, as medulloblastoma is known to have a better prognosis than sPNET.

Chemotherapy continues to be the area of focus for major studies on sPNET today. The above studies have determined there is a response to chemotherapy; the latest research is evaluating which combination and at what intensity can offer the best response. This is exemplified in the CCG protocols 99701, 99703 and Trilateral Retinoblastoma studies discussed below. In the CCG 99701 protocol now closed to accrual, the main purpose of the study was to determine a dose and duration of carboplatin to be used during radiation in children aged 3–21 years with embryonic brain tumors. Eligible patients were those with high risk (M1–M3 or >1.5 cc residual tumor remaining) PNET (supra/infra tentorial). Patients received carboplatin in a dose escalation format. This was given with daily craniospinal and local boost radiotherapy. Patients were then treated with vincristine and cyclophosphamide or vincristine, cyclophosphamide and cisplatin for maintenance chemotherapy. Although the EFS and OS for sPNETs are currently unavailable, carboplatin during radiation is being evaluated further in the randomization process of the current COG high risk protocol for CNS PNET tumors ACNS 0332.

In the CCG 99703 study, the main objectives were: to determine the dose limited toxicity of the drug thiotepa, as well as the viability of giving three cycles of high dose chemotherapy followed by peripheral blood stem cell rescue in infants with malignant brain tumors (6–35 months old). In this study, patients underwent six cycles of chemotherapy post surgery. The induction regimen of cisplatin, etoposide, cyclophosphamide, and vincristine followed by three cycles of consolidation with carboplatin, thiotepa and PBSC rescue. The results of this study are awaited with interest. The current COG study for infant PNET is the ACNS 0334 which is randomizing between the use of intravenous methotrexate or not during three cycles of induction followed by three cycles of consolidation therapy with stem cell rescue.

Trilateral retinoblastoma has historically had a very poor prognosis with only 5% long term survival in meta-analyses of the published literature of 94–104 patients (Paulino 1999; Kivelam 1999), those diagnosed on screening and smaller than 15 mm in size at diagnosis had a better prognosis. The median time to diagnosis of retinoblastoma was 6 months; the median time to diagnosis of intracranial sPNET was 21 months (range 0–84 months). The trilateral site is most commonly pineal. A recent study suggests the potential to cure these patients with a high intensity chemotherapy approach including stem cell harvest. Dunkel et al. (2010) report 5/13 patients surviving a median of 77 months (range 36–104 months) with this type of approach without radiation.

Conclusion

There has been tremendous expansion of knowledge in the area of sPNETs. The discovery that sPNETs are their own molecular entity, different from medulloblastomas, has lead to improvement in our understanding of their different biological behavior. With current studies also evaluating the molecular genetics of these tumors prospectively, there is promise to better understand what makes their prognosis so devastating in children. Advances in neurosurgical and radiological techniques have allowed improved resection with reduced morbidity. Delaying radiation in older children should be avoided. In recent years, the biggest advances have come in the form of optimizing chemotherapy regimens and doses to delay the use of radiation in young children and add to the benefits of radiation in older children to improve survival and overall function in the long-term. It will be important to evaluate functional outcome of these children as well as survival to adequately determine optimal therapy in future studies.

References

Abeloff M (2008) Cancers of the CNS. Abeloff's clinical oncology, 4th edn, Ch 70. Elsevier, Churchill Livingstone

Albright AL, Wisoff JH, Zeltzer P, Boyett J, Rorke LB, Stanley P, Geyer JR, Milstein JM (1995) Prognostic factors in children with supratentorial (nonpineal) primitive neuroectodermal tumors. A neurosurgical perspective from the Children's Cancer Group. Pediatr Neurosurg 22:1–7

Arsic D, Cameron V, Ellmers L, Quan QB, Keenan J, Beasley S (2004) Adriamycin disruption of the Shh-Gli pathway is associated with abnormalities of foregut development. J Pediatr Surg 39:1747–1753

Bajaj A, Bajaj SK, Bajaj N (2007) Bilateral retinoblastoma in early infancy: a case report. Kathmandu Univ Med J 5: 550–551

Burnett ME, White EC, Sih S, von Haken MS, Cogen PH (1997) Chromosome arm 17p deletion analysis reveals molecular genetic heterogeneity in supratentorial and infratentorial primitive neuroectodermal tumors of the central nervous system. Cancer Genet Cytogenet 97:25–31

Dai AI, Backstrom JW, Burger PC, Duffner PK (2003) Supratentorial primitive neuroectodermal tumors of infancy: clinical and radiologic findings. Pediatr Neurol 29:430–434

Dirks PB, Harris L, Hoffman HJ, Humphreys RP, Drake JM, Rutka JT (1996) Supratentorial primitive neuroectodermal tumors in children. J Neurooncol 29:75–84

Dunkel IJ, Jubran RF, Gururangan S, Chantada GL, Finlay JL, Goldman S, Khakoo Y, Obrein JM, Orjuela M, Rodriguez-Galindo C, Souweidane MM, Abramson DH (2010) Trilateral retinoblastoma: potentially curable with intensive chemotherapy. Pediatr Blood Cancer 54:384–387

Durkin ME, Yuan BZ, Zhou X, Zimonjic DB, Lowy DR, Thorgeirsson SS, Popescu NC (2007) DLC-1:a Rho GTPase-activating protein and tumour suppressor. J Cell Mol Med 11:1185–1207

Fangusaro J, Finlay J, Sposto R, Ji L, Saly M, Zacharoulis S, Asgharzadeh S, Abromowitch M, Olshefski R, Halpern S, Dubowy R, Comito M, Diez B, Kellie S, Hukin J, Rosenbulm M, Dunkel I, Miller D, Allen J, Gardner S (2008) Intensive chemotherapy followed by consolidative myeloablative chemotherapy with autologous hematopoietic cell rescue (AuHCR) in young children with newly diagnosed supratentorial primitive neuroectodermal tumors (sPNETs): report of the Head Start I and II experience. Pediatr Blood Cancer 50:312–318

Farrell CJ, Plotkin SR (2007) Genetic causes of brain tumors: neurofibromatosis, tuberous sclerosis, von Hippel-Lindau, and other syndromes. Neurol Clin 25:925–946

Girschick HJ, Klein R, Scheurlen WG, Kuhl J (2001) Cytogenetic and histopathologic studies of congenital supratentorial primitive neuroectodermal tumors: a case report. Pathol Oncol Res 7:67–71

Jakacki RI (1999) Pineal and nonpineal supratentorial primitive neuroectodermal tumors. Childs Nerv Syst 15:586–591

Johnston DL, Keene DL, Lafay-Cousin L, Steinbok P, Sung L, Carret AS, Crooks B, Strother D, Wilson B, Odame I, Eisenstat D, Mpofu C, Zelcer S, Huang A, Bouffet E (2008) Supratentorial primitive neuroectodermal tumors: a Canadian pediatric brain tumor consortium report. J Neurooncol 86:101–108

Kivelam T (1999) Trilateral retinoblastoma: a meta-analysis of hereditary retinoblastoma associated with primary ectopic intracranial retinoblastoma. J ClinOncol 17:1829–1837

Klisch J, Husstedt H, Hennings S, von Velthoven V, Pagenstecher A, Schumacher M (2000) Supratentorial primitive neuroectodermal tumours: diffusion-weighted MRI. Neuroradiology 42:393–398

Kuhn SA, Hanisch UK, Ebmeier K, Beetz C, Brodhun M, Reichart R, Ewald C, Deufel T, Kalff R (2007) A paediatric supratentorial primitive neuroectodermal tumour associated with malignant astrocytic transformation and a clonal origin of both components. Neurosurg Rev 30:143–149

Li MH, Bouffet E, Hawkins CE, Squire JA, Huang A (2005) Molecular genetics of supratentorial primitive neuroectodermal tumors and pineoblastoma. Neurosurg Focus 19:E3

Louis DN, Ohgaki H, Wiestler OD, Cavenee WK, Burger PC, Jouvet A, Scheithauer BW, Kleihues P (2007) The 2007 WHO classification of tumours of the central nervous system. Acta Neuropathol 114:97–109

McBride SM, Daganzo SM, Banerjee A, Gupta N, Lamborn KR, Prados MD, Berger MS, Wara WM, Haas-Kogan DA (2008) Radiation is an important component of multimodality therapy for pediatric non-pineal supratentorial primitive neuroectodermal tumors. Int J Radiat Oncol 72:1319–1323

Mueller S, Chang S (2009) Pediatric brain tumors: current treatment strategies and future therapeutic approaches. Neurotherapeutics 6:570–586

Pang J, Chang Q, Chung YF, Teo JG, Poon WS, Zhou LF, Kong X, Ng HK (2005) Epigenetic inactivation of DLC-1 in supratentorial primtive neuroectodermal tumor. Human Pathol 36:36–43

Paulino AC (1999) Trilateral retinoblastoma: is the location of the intracranial tumor important? Cancer 86:135–141

Pelengaris S, Khan M, Evan G (2002) c-MYC: more than just a matter of life and death. Nat Rev Cancer 2:764–776

Pizer BL, Weston CL, Robinson KJ, Ellison DW, Ironside J, Saran F, Lashford LS, Tait D, Lucraft H, Walker DA (2006) Analysis of patients with supratentorial primitive neuroectodermal tumours entered into the SIOP/UKCCSG PNET 3 study. Eur J Cancer 42:1120–1128

Plum F, Posner JB (1980) Structural causes of stupor and coma. The diagnosis of stupor and coma, 3rd edn, Ch 3: 93. F.A. Davis Company, Philadelphia

Siffert J, Allen JC (1997) Medulloblastoma. J Neuro-Oncol 24(68):181–209

Strother D, Ashley D, Kellie SJ, Patel A, Jones-Wallace D, Thompson S, Heideman R, Benaim E, Krance R, Bowman L, Gajjar A (2001) Feasibility of four consecutive high-dose chemotherapy cycles with stem-cell rescue for patients with newly diagnosed medulloblastoma or supratentorial primitive neuroectodermal tumor after craniospinal radiotherapy: results of a collaborative study. J Clin Oncol 19:2696–2704

Sung KW, Yoo KH, Cho EJ, Koo HH, Lim do H, Shin HJ, Ahn SD, Ra YS, Choi ES, Ghim TT (2007) High-dose chemotherapy and autologous stem cell rescue in children with newly diagnosed high-risk or relapsed medulloblastoma or supratentorial primitive neuroectodermal tumor. Pediatr Blood Cancer 48:408–415

Timmermann B, Kortmann RD, Kuhl J, Meisner C, Dieckmann K, Pietsch T, Bamberg M (2002) Role of radiotherapy in the treatment of supratentorial primitive neuroectodermal tumors in childhood: results of the prospective German brain tumor trials HIT 88/89 and 91. J Clin Oncol 20:842–849

Timmermann B, Kortmann RD, Kuhl J, Rutkowski S, Meisner C, Pietsch T, Deinlein F, Urban C, Warmuth-Metz M, Bamberg M (2006) Role of radiotherapy in supratentorial primitive neuroectodermal tumor in young children: results of the German HIT-SKK87 and HIT-SKK92 trials. J Clin Oncol 24:1554–1560

Yang HJ, Nam DH, Wang KC, Kim YM, Chi JG, Cho BK (1999) Supratentorial primitive neuroectodermal tumor in children: clinical features, treatment outcome and prognostic factors. Childs Nerv Syst 15:377–383

Zurawel RH, Allen C, Chiappa S, Cato W, Biegel J, Cogen P, de Sauvage F, Raffel C (2000) Analysis of PTCH/SMO/SHH pathway genes in medulloblastoma. Genes Chromosome Cancer 27:44–51

Chapter 3

Epileptic Seizures and Supratentorial Brain Tumors in Children

Roberto Gaggero, Alessandro Consales, Francesca Fazzini, Maria Luisa Garrè, and Pasquale Striano

Abstract Brain tumors represent about one third of the pediatric tumors. Epilepsy is overall associated with supratentorial brain tumors, that prevail in children under 3 years and over 10 years. Prevalence of seizures as first tumor symptom is 15–20%. In children under the 3 years of life, epilepsy is more frequent (until 70%), it can persists after the surgical intervention and in some cases an epileptic encephalopathy occurs. Epilepsy can began after surgery in other cases (10–40%), as a consequence of brain damage. Moreover, brain tumors are in a relevant percentage of cases (26–50%) the cause of a drug-resistant epilepsy, that can be successfully treated by surgery. The post surgical evolution is more favorable for patients with some particular tumor types (DNT, gangliogliomas). Pharmacological therapy of the epilepsy related with tumors is difficult, for an high frequency of side effects and of interactions with chemotherapy. The new AED are particularly promising not only for the favorable effect, but also for the lower incidence of side effects and of interactions.

Keywords Supratentorial tumor · Pediatric tumors · Astrocytoma · Medulloblastoma · Germ cell tumors · Seizures

R. Gaggero (✉)
Department of Neurosciences, Gaslini Children's Hospital, 16147 Genoa, Italy
e-mail: garob@iol.it

Introduction

Brain tumors represent a relevant clinical problem in children and the most frequent cause of death for malignancy under the 16 years of life (Wilne et al. 2007). The incidence of brain tumors in children ranges from 2.5 to 18/100,000 cases and makes up one third of all cases of pediatric tumors (Porter et al. 2010). The incidence is higher in the age from 4 to 9 years (Makino et al. 2010), with some differences related to the age. In fact, in children between 3 and 11 years infratentorial tumors are more frequent (57.5%), whereas in younger infants there is a predominance of supratentorial tumors.

The most frequent supratentorial tumor is astrocytoma (35–40%), followed by medulloblastoma (15–20%), anaplastic astrocytoma, glioblastoma (15%), ependymoma (10%), and craniopharyngioma (5%) (Rosemberg and Fujiwara 2005). Other tumor types include germ cell tumors (4.4%), gangliogliomas, meningiomas (2.5%), primitive neuroectodermal tumors (PNET) (1.9%), choroid plexus tumors (0.9%), and dysembryoplastic neuroepithelial tumor (DNT) (0.6%). Among infratentorial tumors, astrocytoma is the more frequent type (38%), followed by pilocytic astrocytomas, medulloblastomas, and ependymomas (Rosemberg and Fujiwara 2005).

As in adults, epilepsy may be the initial presenting features of a primary brain tumor in children (Liigant et al. 2001; Khan et al. 2006; Riva et al. 2006). However, it can also emerge during the course of therapy or as a late effect of tumor treatment (e.g., surgery, chemotherapy, radiotherapy) (Ullrich 2009), thus adding substantial morbidity to the patients (van

M.A. Hayat (ed.), *Tumors of the Central Nervous System, Volume 4*,
DOI 10.1007/978-94-007-1706-0_3,

Breemen et al. 2007). In addition, the medical management of epilepsy is often difficult in this age group, particularly due to the risk of side-effects deriving from use of AEDs as well as to their potential interactions with chemotherapy drugs (Khan and Onar 2006; van Breemen et al. 2007).

The mechanisms involved in the pathophysiology of tumor-related epilepsy are multiple, complex, varied, and-at least in part-not yet well defined. Several hypothesis have been proposed: the direct effects of the tumor, a focal cortical hyperexcitability, neurotransmitters abnormalities, and even the effect of metabolic products of the tumor itself (Ullrich 2009). Indeed, at level of peri-tumoral brain tissue, morphological changes and Ph variations, abnormalities in ion levels and amino acids, alterations of glutaminergic receptors, enzymatic modifications, and alterations of intercellular communication have been widely documented (Shaller et al. 2003). Moreover, several other mechanisms can influence the expression of epilepsy in brain tumors, including genetic changes, tumor malignancy, location, and age of onset (Kim et al. 2001; Khan et al. 2006; Riva et al. 2006).

Epilepsy as First Sign of the Tumor

The frequency of seizures in adults with brain tumors is generally high, ranging from 23 to 86% (Liigant et al. 2001; Riva et al. 2006), with highest percentages in low-grade tumors and lower in secondary tumors (Liigant et al. 2001) and in glioblastomas (Riva et al. 2006). Seizures occur as the first presentation symptom in about 85% of the cases (Riva et al. 2006). Association of epilepsy and brain tumors in children is lower: seizures occur in 15–20% of children with a cerebral tumor (Khan et al. 2006), most likely due to the fact that infratentorial tumors are more frequent in the pediatric age. Seizures represent a rare clinical onset of brain neoplasm, ranging from 10 to 15% in different series (Wilne et al. 2007).

A recent review on the clinical presentation of paediatric brain tumors (Wilne et al. 2007) reports that most frequent early symptoms of brain tumors are headache (33%), nausea and vomiting (32%), abnormalities of gait (27%). Seizures are reported only in 13% of cases and are more frequent (38%) as initial symptoms in tumors with supratentorial location. In a group of 98 children (Shady et al. 1994) with supratentorial brain tumors, mainly of glial type, 18 subjects (18.3%) were affected by seizures. In half of them seizures occurred at the onset and in 30% they were the unique symptom. Seizures were focal in 77% and EEG showed lateralized abnormalities in 88% of cases. In patients with seizures, tumors were cortical in 59%, whereas only 15% of cases with infratentorial lesions presented seizures. Epilepsy was associated with temporal and frontal localization of the lesion and with some particular type of tumors (in cases of gangliogliomas and oligoastrocytomas the prevalence of seizures was 88 and 86%, respectively). The cases with seizures as first sign of the tumor showed a favorable evolution.

Another paper (Gilles et al. 1992) investigated a large population of children and adolescents with brain tumors and showed that among 3291 cases only 14% presented seizures before the diagnosis. Prevalence was higher in patients with supratentorial lesions (22%) and in particular in subjects aged more than 14 years. In 50% of cases the period from the first seizure and the surgery was >1 year. In 89% of cases with seizures other symptoms were observed: consciousness disorder, mental impairment, gait and motor abnormalities. The main tumors characteristics were supratentorial and cortical localization, histology type (astrocytomas of different grade, ependymoma).

A particular and different condition is represented by brain tumors in very young children (under 3 years of life). They represent a particular clinical problem since their histological type and the immature stage of evolution of the nervous system (Michasky and Garrè 2004). The clinical presentation of the tumors in this period is peculiar; the prevalence of supratentorial localization (Rutledge et al. 1987; Chung et al. 1998; Mehrotra et al. 2009; Gaggero et al. 2009) can explain the high frequency of seizures as first symptom. The prevalent tumor types in this age are astrocytoma, primitive neuroectodermal tumor, papilloma or carcinoma of the choroid, teratoma, medulloblastoma, dermoid tumor, embryonal rhabdomyosarcoma (Gaggero et al. 2009).

In a group (Rutledge et al. 1987) of very early onset tumors (<1 year), 25–40% of the cases with a supratentorial location presented seizures at the onset and continue to suffer of epilepsy in 10–15% of cases. Mainly temporal mesial tumors were associated with seizures. In our experience (Gaggero et al. 2009), among 28

children evaluated, 20 (71.4%) suffered from epilepsy. Mean age at seizure onset was 18.7 months. In all cases, seizures recurrence was high, generally with a daily or weekly frequency. In fifteen (75%) children, epilepsy was an early manifestation or the presenting symptom of the tumor. In this group, seizures were focal with or without secondarily generalization in eight cases (53.3%) and generalized (spasms, tonic-clonic seizures, atypical absences) in the other seven individuals. Seizures remitted in 11 of these cases (73%) after surgical treatment, whereas in the other 4 epilepsy persisted and presented a long lasting severe course. Five (25%) subjects from this group suffered from occasional episodes of convulsive status epilepticus needing benzodiazepines rescue treatment. During the post-surgical evolution, other two (13%) children featured the clinical picture of an epileptic encephalopathy with stagnation in development, speech difficulties, and continuous spike-waves during sleep (CSWSS). Post-surgical follow-up ranged from 4 to 10 years. In this series, the outcome of epilepsy was generally good, with most children (76.4%) being seizure free or showing >90% improvement in seizure frequency after surgery. However, in about 20% of the cases, epilepsy persisted despite surgery and different antiepileptic drugs (AEDs) regimen. Best epilepsy outcome was observed in patients with low-grade tumors and without neurological deficits after surgery.

Epilepsy After Surgery or Other Tumor Treatments

In a significant number of patients (up to 45%) with brain tumors, epilepsy stars after the diagnosis and the treatment, often as consequence of the therapeutical procedures (Glantz et al. 2000). Part of them is represented by post-surgical seizures, that occur in the immediate period post-surgery (days or weeks). These cases are not frequent (12%) (Wang et al. 1994). In other cases, the seizures appear before the diagnosis and the treatment and they persist after surgery (Gaggero et al. 2009). In our experience (Gaggero et al. 2009), concerning epilepsy associated with brain tumors in infants (under 3 years), seizures began after surgery in 5 out of 20 cases (25%) and they became severe and drug resistant. Of these five children, four had focal seizures, with or without secondarily generalization. All these patients were affected by a serious neurological impairment (hemiplegia, mental disorders). Also one of these cases presented an epileptic encephalopathy with a continuous spike waves during slow sleep (CSWSS) EEG. So, in these cases the epilepsy is probably due to the brain damage.

A review of the neurological sequelae of brain tumors in children (Ullrich 2009) considers the effects of the different treatment: the lesions secondary to the surgery, the side effects of the chemotherapy, the consequences of the radiation. All these conditions can determine an epilepsy. Surgical resection remains the mainstay of therapy for most primary brain tumors, both for reduction of tumor burden and to provide histological diagnosis. For many tumors, surgical resection is the most important mode of therapy. The deficits and long-term effects resulting from neurosurgery are multifactorial and depend on the tumor location, the attempted degree of resection, the age of the patient, and the presurgical performance status. Direct neurological sequelae from surgical removal can include localized lesions, hydrocephalus and perioperative stroke, with consequent clinical symptoms (ataxia, hemiparesis, and persistent neurosensorial and neurocognitive deficits).

As regards chemotherapy, it should be kept in mind that some drug treatments may increase the risk of seizure occurrence. Thus, cyclosporine can be cause seizures and leucoencephalopathy (Gaggero et al. 2006) in 10% of the cases whereas cisplatin, vincristine and methotrexate are associated with seizures in 1% of the patients (Ullrich, 2009). Radiotherapy can determine a vasculopathy, especially in infants. In fact, in children under 3 years, these effects are more severe. The risk of developing severe brain damage after surgery and irradiation are peculiar in this subgroup of patients due to incomplete brain development (Michasky and Garrè 2004).

Neurosurgery and Drug-Resistant Epilepsy Secondary to Brain Tumors

Drug-resistant epilepsy can be secondary to brain tumors with a significant number of patients, including children. The surgical treatment of the drug-resistant epilepsy in pediatrics has become frequent in the last

decades. The results of this therapy are generally good. The tumors types vary in the different series. Prevalence of dysembryoplastic neuroepithelial tumors (DNT) ranges from 16 to 39% (Kim et al. 2001; Cossu et al. 2008; Zentner et al. 1997). Gangliogliomas frequency was 25–56% (Cossu et al. 2008; Zentner et al. 1997). Gangliocytomas: 8% (Cossu et al. 2008); oligodendrogliomas 26% (Kim et al. 2001); low grade astrocytomas 18% (Zentner et al. 1997; Cossu et al. 2008). The results of the surgery on the epilepsy were reported to be positive with high frequency of seizures free patients: from 67 to 74% (Van Oijen et al. 2006; Benifla et al. 2006; Cossu et al. 2008; Benifla et al. 2008).

The results are more favorable in the cases with brain tumors in comparison with the other etiological factors: the percentage of seizure free patients class was 71% (Zentner et al. 1997), 90% (Kral et al. 2001), 89% (Cossu et al. 2008). The favorable prognostic factors are an unique lesion, a temporal location, a complete lesionectomy, an older age at onset (Benifla et al. 2006; Van Oijen et al. 2006; Benifla et al. 2008; Cossu et al. 2008). Some specific tumors are in particular related with a more favorable outcome after surgery. Several series of dysembryoplastic neuroepithelial tumors (DNT) operated for a drug resistant epilepsy show a very high frequency of seizures free patients in childhood and adolescence: 83–100% (Nolan et al. 2004; Chang et al. 2010; Ozien et al. 2010). In some reports, after a more prolonged follow up, the percentage of remission trends to decrease (from 85 to 62% after 4 years) (Nolan et al. 2004). Also gangliogliomas are related with a favorable outcome in children: 90% seizure free (Ogiwara et al. 2010), 87.5% (Ozien et al. 2010).

In a high percentage of cases, tumors are associated with other cerebral lesions, that can represent a concomitant epileptogenic factor: mesial temporal sclerosis 13% (Benifla et al. 2006), cortical dysplasia 7% (Benifla et al. 2006) and 16% (Cossu et al. 2008), astrogliosis 12% (Benifla et al. 2006).

Antiepileptic Treatment

The use of chronic antiepileptic drugs (AED) for the treatment of the seizures is very frequent in patients with epilepsy secondary to brain tumors. The AED can be use after the first seizures before the tumor diagnosis or in the occasion of the surgical intervention or for the treatment of post-surgery epilepsy. In a recent paper (Sogawa et al. 2009), it has been reported that AED were used in 10% of 334 pediatric brain tumors patients. The most frequently used AED drugs were phenytoin and oxcarbazepine. Initial therapy was frequently changed because lack of efficacy and adverse effects. At last follow up the most common antiepileptic drugs were oxcarbazepine and levetiracetam. The patients started on newer-generation AED (levetiracetam, oxcarbazepine, lamotrigine) tended to remain on the same treatment more than did patients on older generation antiepileptic drugs: valproate, phenytoin and phenobarbital. Recently, several other reports confirm the prevalent efficacy and tolerability of the new AED, as levetiracetam, but the studies were performed mainly in adults and in small groups (Van Breemen et al. 2007).

A specific problem concerns the interference of the AED with the chemotherapeutic drugs. Several old AEDs (phenytoin, phenobarbital, carbamazepine) are metabolic inductors and they reduced the blood levels and the efficacy of the chemotherapy. So, enzyme inducing anticonvulsants drugs are generally not recommended because they can lead to insufficient serum levels of concomitant chemotherapeutic drugs (Vecht et al. 2003). However, because many AEDs and chemotherapeutics share common metabolic pathways via the hepatic cytochrome P450 (CYP) isoenzymes, there is potential for drug interactions. Likewise, chemotherapeutics can alter the pharmacokinetics of AEDs, resulting in decreased seizure control. Other agents, such as valproate, are enzyme-inhibiting AEDs that can impede the metabolism of other drugs, potentially increasing the serum concentration of chemotherapeutics (Vecht et al. 2003). A new generation of AEDs that are not metabolized by the CYP pathway is currently being developed. Among these, gabapentin and levetiracetam show the most promise in treating epileptic seizures in patients with brain tumors. Interactions between these newer AEDs and chemotherapeutic agents have not been reported. Thus far several drugs without enzyme induction effect are preferred (Vecht et al. 2003). The absence of interaction has been proved also in children with epilepsy and brain tumors (Ruggiero et al. 2010).

From a general point of view, the use of AED in patients with epilepsy secondary to brain tumors has

not been the object of specific studies. Their efficacy appears to be limited, their mechanisms of action are not specific for the epileptogenesis related with tumors. Some other actions of AED can be useful for the tumor treatment. For instance, it has been proposed an apoptosis effect on the tumoral cells by valproate, with a positive therapeutic result, but this observation remains controversial (Blaheta et al. 2005).

Another aspect concerning the use of AED in patients with epilepsy associated to brain tumors is represented by the anticonvulsant prophylaxis prescribed after surgery. For a long time it has been believed that preventing seizures with antiepileptic drugs (seizure prophylaxis) was effective and necessary, but the supporting evidence was little and mixed. The incidence of postoperative epilepsy following a subfrontal craniotomy did not exceed 12% when examined at various time periods during a 3-year postoperative course (Wang et al. 1994). Antiepileptic drugs were not warranted to reduce the incidence of postoperative seizures after the 1-month postoperative period and should not be used for long-term prophylactic therapy in children following a subfrontal craniotomy.

Ten years ago the Quality Standards Subcommittee of the American Academy of Neurology (Glantz et al. 2000) published the results of a meta-analysis of 12 studies, that have examined, either in randomized controlled trials or cohort studies, the ability of prophylactic anticonvulsants to prevent first seizures in patients with brain tumors. All these studies were dedicated to adult population. None have demonstrated efficacy. Only one of the 12 studies reported a significant difference in seizure frequency between the anticonvulsant prophylaxis and nonprophylaxis groups, and this difference favored the non-prophylaxis group. In contrast, deleterious interactions with cytotoxic drugs and corticosteroids are a major concern, and the incidence and severity of anticonvulsant side effects appear to be appreciably higher (20–40%) in brain tumor patients than in the general population of patients receiving anticonvulsants.

Despite the lack of definitive evidence, many physicians at that time continued to administer anticonvulsant medication prophylactically for preventing first seizures in patients with brain tumors, both adults and children (Stevens 2006).

Two years ago the conclusions of a study on antiepileptic drugs for preventing seizures in people with brain tumors (Tremont-Lukats et al. 2008), carried out according to Cochrane Criteria talked that here was no difference between the treatment interventions and the control groups in preventing a first seizure in participants with brain tumors. The evidence is neutral, neither for nor against seizure prophylaxis, in people with brain tumors. The decision to start an antiepileptic drug for seizure prophylaxis is ultimately guided by assessment of individual risk factors and careful discussion with patients. New AED as levetiracetam represent a new opportunity for the prevention of seizures.

In summary, AEDs usually show a modest efficacy; they can be useful for preventing seizure after surgery during the chemotherapy, whereas the long term action is less sure. They have to be employed in cases with partial tumor resection, cortical location, disseminated tumors and concomitant hemorrhages (Glantz et al. 2000; Tremont-Lukats et al. 2008; Ullrich 2009). Also the interruption of the therapy, after surgery and a favorable outcome, is possible (Khan et al. 2006). Sixty-two patients discontinued AEDs at a median time of 5.6 years from the first seizure. Median time since AED withdrawal was 2.3 years. Seizures recurred in 17 (27%) patients. Median seizure free period before AED withdrawal was 1.3 years. More than one tumor resection and whole-brain radiation treatment were associated with seizure recurrence. At seizure recurrence, control was re-established in 15 patients with AED reinstitution. Two patients with poor drug compliance continue to have seizures. In conclusions, AED withdrawal can be successfully achieved in majority of carefully selected patients.

Conclusion

The prevalence of brain tumors is elevated (about one third of pediatric tumors). Supratentorial tumors represent more than 50% of them and they are more frequent in children under 3 years and over 10 years. Epilepsy is overall associated with supratentorial brain tumors. Seizures can be the initial symptom of a brain tumor or they can occur during the evolution. In other cases, tumors of particular type can be the cause of a drug-resistant intractable epilepsy, that can be successfully treated by surgery. Seizures occur in 15–20% of children with brain tumors. Globally, seizures are

the first sign of a brain tumor with a low prevalence (only 10–15%). Seizures are focal in the majority of the cases. A particular problem is represented by the children under 3 years old. In this group, epilepsy is more frequent (up to 70%); it can persists after the surgical intervention and in some cases it evolves into an epileptic encephalopathy. Epilepsy can began after surgery in other cases (10–40%), as a consequence of brain damage. The prevalence is higher in children over 3 years old.

Drug-resistant epilepsy is secondary to a brain tumor in 26–50% of cases in the pediatrics. The results of the surgery is more favorable in children with brain tumors and epilepsy. The prevalence of seizure-free cases after surgery is 80–90%, compared with 60–70% of the cases with other etiology. The post surgical evolution is also more favorable for patients with some particular tumors (DNT, gangliogliomas). The pharmacological therapy of the epilepsy related with tumors is difficult with many side effects and interactions with chemotherapy. The new AED are particularly promising for the lower incidence of side effects and a good efficacy.

References

Benifla M, Otsubo H, Ochi A, Weiss SK, Donner EJ, Shroff M, Hawkins C, Drake JM, Elliot I, Smith ML, Snead OC, Rutka JT (2006) Temporal lobe surgery for intractable epilepsy in children: an analysis of outcomes in 136 children. Neurosurgery 59:1203–1213

Benifla M, Rutka JT, Otsubo H, Lamberti-Pasculli M, Elliot I, Sell E, Ramachandran Nair R, Ochi A, Weiss SK, Snead OC, Donner EJ (2008) Long-term seizure and social outcomes following temporal lobe surgery for intractable epilepsy during childhood. Epilepsy Res 82:133–138

Blaheta RA, Michaelis M, Driever PH, Cinatl J Jr (2005) Evolving anticancer drug valproic acid: insights into the mechanism and clinical studies. Med Res Rev 25: 383–397

Chang EF, Christie C, Sullivan JE, Garci PA, Berger MS, Barbaro NM (2010) Seizure outcomes after resection of dysembryoplastic neuroepithelial tumor in 50 patients Clinical article. J Neurosurg 5:123–130

Chung SK, Wang KC, Nam DH, Cho BK (1998) Brain tumor in the first year of life: a single institute study. J Korean Med Sci 13:65–70

Cossu M, Lo Russo G, Francione S, Mai R, Nobili L, Sartori I, Tassi L, Citterio A, Colombo N, Bramerio M, Galli C, Castana L, Cardinale F (2008) Epilepsy surgery in children: results and predictors of outcome on seizures. Epilepsia 49:65–72

Gaggero R, Consales A, Fazzini F, Mancardi MM, Baglietto MG, Nozza P, Rossi A, Pistorio A, Tumolo M, Cama A, Garrè ML, Striano P (2009) Epilepsy associated with supratentorial brain tumors under 3 years of life. Epilepsy Res 87:184–189

Gaggero R, Haupt R, Fondelli P, De Vescovi R, Marino A, Lanino E, Dallorso S, Faraci M (2006) Intractable epilepsy secondary to cyclosporine toxicity in children undergoing allogeneic hematopoietic bone marrow transplantation. J Child Neurol 21:861–866

Gilles FH, Sobel E, Leviton A, Hedley-Whyte ET, Tavare CJ, Sobel RA (1992) Epidemiology of seizures in children with brain tumors. The Childhood Brain Tumor Consortium. J Neuroonc 12:53–68

Glantz MJ, Cole BF, Forsyth PA, Recht LD, Wen PY, Chamberlain MC, Grossman SA, Cairncross JG (2000) Special Article Practice parameter: anticonvulsant prophylaxis in patients with newly diagnosed brain tumors. Neurology 54:1886–1893

Liigant A, Haldre S, Oun A, Linnamägi U, Saar A, Asserm T, Kaasik AE (2001) Seizures disorders in patients with brain tumors. Eur Neurol 45:46–51

Khan RB, Boop FA, Onar A, Sanford RA (2006) Seizures in children with low-grade tumors: outcome after tumor resection and risk factors for uncontrolled seizures. J Neurosurg 104 (Suppl 6) 377–382

Khan RB, Onar A (2006) Seizure recurrence and risk factors after antiepilepsy drug withdrawal in children with brain tumors. Epilepsia 47:375–379

Kim SK, Wang KC, Hwang YS, Kim KJ, Cho BK (2001) Intractable epilepsy associated with brain tumors in children: surgical modality and outcome. Child Nerv Syst 17: 445–452

Kral T, Kuczaty S, Blümck I, Urbach H, Clusmann H, Wiestler OD, Elger C, Schramm J (2001) Postsurgical outcome of children and adolescents with medically refractory frontal lobe epilepsies. Child Nerv Syst 17:595–601

Makino K, Nakamura H, Yano S, Kuratsu J; Kumamoto Brain Tumors Group (2010) Population-based epidemiological study of primary intracranial tumors in childhood. Child Nerv Syst 26:1029–1034

Mehrotra N, Shamji MF, Vassilyadi M, Ventureyra EC (2009) Intracranial tumors in first year of life: the CHEO experience. Child Nerv Syst 25:1563–1569

Michasky A, Garrè ML (2004) Infants tumors in brain and spine. In: Walker DA, Perilongo G, Punt JAG, Taylor R (ed) Tumors child. Arnold Publisher, London, pp 359–369

Nolan MA, Sakuta R, Chuang N, Otsubo H, Rutka JT, Snead OC, Hawkins CE, Weiss SK (2004) Dysembryoplastic neuroepithelial tumors in childhood: long-term outcome and prognostic features Neurology 62:2270–2276

Ogiwara H, Nordii DR, Di Patri AJ, Alden TD, Bowman C, Tomita T (2010) Pediatric epileptogenic gangliogliomas: seizure outcome and surgical results. J Neurosurg Pediatr 5:271–276

Ozien F, Gunduz A, Asan Z, Tandiveri T, Ozkara C, Yeni N, Yalcinkaya C, Ozyurt E, Uzan M (2010) Dysembryoplastic neuroepithelial tumors and gangliogliomas: clinical results of 52 patients. Acta Neurochir (Wien) 152:1661–1671

Porter KR, Mc Carthy BJ, Freels S, Kim Y, Davis FG (2010) Prevalence estimates for primary brain tumors in

the United States by age, gender, behavior, and histology. Neurooncology 2:520–527

Riva M, Salmaggi A, Marchioni E, Silvani A, Tomei G, Lorusso L, Merli R, Imbesi F, Russo A, for the Lombardia Neurooncology Group (2006) Tumor-associated epilepsy: clinical impact and the role of referring centres of a cohort of glioblastoma patients. A multicentre study from the Lombardia Neuro-oncology Group. J Neurol Sci 27: 345–351

Rosemberg S, Fujiwara D (2005) Epidemiology of pediatric tumors of the nervous system according to the WHO 2000 classification: a report of 1195 cases from a single institution. Child Nerv Syst 21:940–944

Ruggiero A, Rizzo D, Mastrangelo S, Battaglia D, Attinà G, Riccardi R (2010) Interactions between antiepileptic and chemotherapeutic drugs in children with brain tumors: is it time to change treatment? Pediatr Blood Cancer 54: 193–198

Rutledge SL, Snead OC, Morawetz R, Chandra-Sekar B (1987) Brain tumors presenting as seizure disorder in infants. J Child Neurol 2:214–219

Shady JA Black PM, Kupsky WJ, Tarbell NJ, Scott RM, Leong T, Holmes G (1994) Seizures in children with supratentorial astroglial neoplasms. Pediatr Neurosurg 21:23–30

Shaller B, Yaniv I, Michowitz S, Kornreich L, Schwartz M, Goldberg-Stern H, Cohen IJ (2003) Epilepsy associated with paediatric brain tumors: the neuro-oncologic perspective. Pediatr Neurol 29:232–235

Sogawa Y, Kan L, Levy AS, Maytal J, Shinnar S (2009) The use of antiepileptic drugs in pediatric brain tumor patients. Pediatr Neurol. 41:192–194

Stevens GH (2006) Antiepileptic therapy in patients with central nervous system malignancies. Curr Neurol Neurosci Rep 6:311–318

Tremont-Lukats IW, Ratilal BO, Armstrong T, Gilbert MR (2008) Antiepileptic drugs for preventing seizures in people with brain tumors. Cochrane Database Syst Rev 16(2):CD004424

Ullrich NJ (2009) Neurologic sequelae of brain tumors in children. J Child Neurol 24:1446–1454

Van Breemen MS, Wilms EB, Vecht CJ (2007) Epilepsy in patients with brain tumours: epidemiology, mechanisms, and management. Lancet Neurol 6:421–430

Van Oijen M, De Waal H, Van Rijen PC, Jennekens A, Van Huffelen AC, Van Nieuwenhuzen O; Dutch Collaborative Epilepsy Surgery Program (2006) Resective epilepsy surgery in childhood: the Dutch experience 1992-2002. Eur J Paediatr Neurol 10:114–123

Vecht CJ, Wagner GL, Wilms EB (2003) Treating seizures in patients with brain tumors: drug interactions between antiepileptic and chemotherapeutic agents. Semin Oncol 30(Suppl 19):49–52

Wang EC, Geyer JR, Berger MS (1994) Incidence of postoperative epilepsy in children following subfrontal craniotomy for tumor. Pediatr Neurosurg 21:165–172

Wilne SH, Collier J, Kennedy CR, Koller K, Grundy R, Walker D (2007) Presentation of childhood CNS tumours: a systematic review and meta-analysis. Lancet Oncol 8:685–695

Zentner J, Hufnagel A, Wolf HK, Ostertun B, Beherens F, Campos MG, Elger CE, Wiestler OD, Schramm J (1997) Surgical treatment of neoplasms associated with medically intractable epilepsy. Neurosurgery 41:378–383

Part II
Tumor to Tumor

Chapter 4

Breast Cancer Metastasis to the Central Nervous System

Marc R. Matrana and Nuhad K. Ibrahim

Abstract As breast cancer patients live longer, the development of central nervous system (CNS) metastases has become more prevalent. Clinically symptomatic breast cancer metastasis to the CNS is associated with significant morbidity and mortality. The blood-brain barrier (BBB) and the unique microenvironment and pathophysiology of the CNS create treatment challenges in this unique population. New therapeutic approaches are advancing the limits of the management of metastatic breast cancer to the CNS. Enhancements in surgical techniques and in targeted radiation are allowing better control of CNS metastases, while chemotherapy and targeted agents continue to play a major role in the treatment and research efforts. In addition to brain metastases, leptomeningeal carcinomatosis, spinal metastases and ocular metastases present particular challenges to clinicians and researchers. Future research efforts aimed at breast cancer patients with CNS metastases may focus on identifying patients at greater risk, enhancing treatment options, and identifying new diagnostic and predictive markers.

Keywords Breast cancer · CNS metastasis · Intrametastatic hemorrhage · Leptomeninges · WBRT · Intramedullary

Introduction

Rates of breast cancer have remained relatively stable since sharp increases in the 1980s related to the institution of widespread mammographic screening programs. Mortality has been steadily decreasing since the early 1990s. As patients live longer, the development of central nervous system (CNS) metastases has become more prevalent. Clinically symptomatic breast cancer metastasis to the CNS is associated with significant morbidity and mortality, and the CNS is often a site of disease progression even when other sites respond to treatment. The blood-brain barrier (BBB) and the unique microenvironment of the CNS constitute a biologically distinct milieu in which metastatic breast cancer exists. Although such cases are challenging to treat, new diagnostic advances and novel therapeutic approaches are advancing the limits of the management of metastatic breast cancer to the CNS. Enhancements in surgical techniques and in targeted radiation are allowing better control of CNS metastases, while chemotherapy and targeted agents continue to have negligible effect. The main goals of prolonging life, preserving neurological and cognitive functioning, and, most importantly, improving quality of life should continue to guide individualized treatment plans, taking into account patient and tumor variables.

N.K. Ibrahim (✉)
Department of Breast Medical Oncology, The University of Texas M.D. Anderson Cancer Center, Houston, TX 77030, USA
e-mail: nibrahim@mdanderson.org

M.A. Hayat (ed.), *Tumors of the Central Nervous System, Volume 4*,
DOI 10.1007/978-94-007-1706-0_4,

Epidemiology

Rates

The American Cancer Society estimated an incidence of nearly 1.4 million new cases of breast cancer worldwide in 2008. Female breast cancer incidence rates vary widely by geographic region, ranging up to 101.1 cases per 100,000 in the United States in 2002. In the United States, an estimated 192,370 women were diagnosed with invasive breast cancer in 2009. Over 1910 cases of male breast cancer were diagnosed the same year. Breast cancer is the second most common cancer associated with brain and other CNS metastases, after primary lung carcinoma (Barnholtz-Sloan et al. 2004). Although melanoma has a higher propensity for metastasis to the brain, the sheer volume of breast and lung cancer cases in the population makes CNS metastases from these cancers of a larger magnitude. Recent studies estimate that 8–10% of adult cancer patients will develop symptomatic brain metastases during their lives (Schouten et al. 2002), and 15–25% of these metastases will be from breast cancer. Moreover, breast cancer is the most common disease associated with leptomeningeal colonization.

Brain metastasis is rarely the presenting sign of breast cancer. The median latency between initial diagnosis and the development of clinically apparent brain metastasis is 2–3 years. The incidence of brain metastasis is also increasing, as survival for patients with breast cancer increases and detection improves with higher quality imaging technologies (Lin et al. 2004). In recent studies, the prevalence of clinically significant brain metastasis in breast cancer patients has ranged from 10 to 16%, although autopsy studies have found prevalence rates as high as 30–35% when accounting for those metastases not presenting clinically (Tsukada et al. 1983).

Risk Factors

A number of clinical risk factors for the development of CNS metastasis from breast cancer have been identified. Disease stage is an important risk factor. Less than 3% of patients presenting with early-stage breast cancer develop brain or other CNS metastases. Age is also an important risk factor. Patients younger than 40 years often have more aggressive disease and are more likely to develop CNS metastasis. The presence of pulmonary metastasis has also been shown to increase the risk of brain metastases from breast cancer. Race disparity in the development of brain metastasis in breast cancer has also been suggested. Barnholtz-Sloan et al. (2004) reported incidence proportions of brain metastases in patients from the Metropolitan Detroit Cancer Surveillance System. They found incidence percentages for brain metastasis of 4.6% for white patients with breast cancer compared with 7.4% for African American patients. The effects of confounders such as socioeconomic status, access to healthcare, and education on this observation are unknown.

The biological variability among individual tumors also creates differences in risk. Estrogen receptor-negative tumors metastasize to the brain at a higher rate than do estrogen receptor-positive tumors. Breast cancers that over express the oncogene Her2/neu have been associated with shorter time to progression and shorter overall survival. Amplification of this oncogene is also associated with a higher incidence of brain metastasis. This risk seems to be independent of treatment with trastuzumab, a large monoclonal antibody that does not cross the blood-brain barrier.

Patients with triple-negative breast cancers (which do not express estrogen or progesterone receptors or exhibit amplification of the Her2/neu oncogene) and often overlapping basal-like breast cancers also develop brain metastases at a high rate. In a retrospective study by Lin et al. (2008), 46% of patients with metastatic triple-negative disease developed clinically apparent brain metastasis before death.

Pathophysiology

In 1889, Paget theorized that breast cancer metastasis is ruled by both the “seed” (tumor cells) and the “soil” (the microenvironment). His theory still holds true today, as it did in his own time. It is understood however, that several steps are essential for metastases to form. First, tumor cells must invade the primary tumor border and enter the circulatory system; the cells need to survive in the circulation and successfully extravasate into the tissue of a distant site. Once relocated, tumor cells must rebound from quiescence

and form micrometastases. Progressive colonization to form a life-threatening metastasis must then ensue.

The epithelial-mesenchymal transformation theory (EMT) explains a set of events characterized by loss of cell adhesion, repression of E-cadherin expression, and increased cell mobility. EMT events are necessary for embryonic processes (such as mesoderm development and neural tube formation) but are also stimulated by several oncogenic signaling pathways. In theory, EMT processes may play an important role in the initiation of metastases.

The theory of the BBB is the most important construct for conceptualizing the underlying pathophysiology of brain metastases and for understanding the mechanisms of treatment resistance, which make managing breast cancer brain metastases or their recurrence so difficult. The BBB is formed from capillary endothelial cells that lack fenestrations and bind together with continuous tight junctions. The endothelial cells are further lined by pericytes, basement membrane, and astrocyte foot processes. This barrier has a high electrical resistance. Ions and small molecules have low permeability across the BBB, and it is virtually impossible for macromolecules and peptides to cross. Pinocytosis, which facilitates the transport of molecules through cells, is lacking in the BBB, further contributing to the exquisite selectivity observed in this microenvironment. While tumor cells often find a way around the discriminating system, the BBB is impervious to most drugs, making treatment challenging.

The BBB and the blood-cerebrospinal fluid (CSF) barrier protect the sensitive environment of the CNS. Metastatic lesions are similarly surrounded by endothelial cells to form a blood-tumor barrier, which accounts for the solitary discreet lesions usually represented by brain metastases. Brain metastases from breast cancer and other solid tumors are usually solid and well-circumscribed. In contrast to primary brain tumors, they tend not to infiltrate to surrounding brain tissue. Very little is known of this blood-tumor barrier, although a greater understanding may lead to the development of more efficacious therapies aimed at brain metastases.

Brain metastases from breast cancer and other solid tumors principally arise from hematogenous spread via arterial blood flow to the brain. Tumor cells most often lodge at the junction between gray and white matter, where blood vessels decrease in caliber, and in the distal vascular endpoint at the edges of arterial territories. Tumor cells are thought to adhere to the endothelial cells and escape into the brain tissue where they divide to form a metastatic focus.

CNS metastases can also originate from the venous circulation where individual cells may elude filtration by the pulmonary capillaries and eventually become trapped in the brain. Metastatic focuses in the lung may also break off and shower into the brain, forming nests of metastatic cells. It has further been postulated that cells from pelvic or abdominal metastases may even enter the posterior fossa or the leptomeninges via Batson's vertebral venous plexus, thereby bypassing the pulmonary circulation. Direct extension from bone and dural metastases and metastatic extension along cranial nerves can also explain the etiology of some breast cancer metastases into the brain.

Although metastatic brain lesions tend to be discrete and well-circumscribed, as opposed to infiltrating, they do tend to be numerous. A retrospective review by Evans et al. (2004) found that of breast cancer patients with brain metastases, 78% had multiple intracranial metastases, whereas 14% had solitary lesions. The remaining 8% had leptomeningeal disease.

Clinical Presentation

Breast cancer patients with brain metastases typically present with neurological sign or symptoms. Common presenting symptoms from brain metastases include headache, focal weakness, altered mental status or personality, seizures, and ataxia. According to Tsukada et al. (1983), the most common presenting symptoms in their series were gait disturbances (24%), seizures (23%), and headaches (16%). Less common presenting symptoms include cognitive disturbances (14%), nausea/vomiting (11%), and cranial nerve dysfunction (10%). Cerebellar symptoms and speech changes may be the initial presenting symptom in 2% of cases.

Classically, symptoms worsen gradually as tumors grow and edema worsens. Symptoms are typically progressive but can also occur acutely, especially in cases of intrametastatic hemorrhage. The types of symptoms that may develop are dependent on their neuroanatomic location(s). Lesions in the cerebellum and brain stem are less common than those in the cerebral hemispheres. Metastatic lesions in these areas can cause ataxia, cranial neuropathies, and upper motor

neuron dysfunction. Other signs of cerebellar lesions may include symptoms related to hydrocephalus, such as headache, memory problems, or behavioral changes.

There are no recommendations for formally screening neurologically asymptomatic breast cancer patients for brain metastases on a routine basis, although some physicians may occasionally order brain imaging as a part of extent-of-disease evaluation in certain subsets of patients with advanced, high-risk disease.

Diagnosis

Diagnosis of brain metastases is suggested by clinical presentation and confirmed by imaging. Magnetic resonance imaging (MRI) is widely accepted as the best diagnostic tool to detect brain metastases. T2-weigted images along with pre- and post-gadolinium-enhanced T1 sequences provide a more sensitive diagnostic tool than standard non-enhanced MRI or contrast-enhanced computed tomography (CT). Practitioners must weigh the relative benefits versus the risk of imaging. MRI is a fairly safe procedure, although gadolinium has recently been implicated in the development of nephrogenic systemic fibrosis, an often devastating condition that develops in patients with chronic kidney disease and end-stage renal disease exposed to gadolinium-based agents.

Other studies, such as lumbar puncture or positron emission tomography (PET), may be indicated in some specific situations, especially those in which symptoms such as headache, cranial neuropathy, or alterations in cognition suggest leptomeningeal carcinomatosis, when tumors have diffusely seeded the leptomeninges. Sensitivity rates in detecting leptomeningeal carcinomatosis have raised with advances in MRI technology, particularly improved T1-weighted images as well as the development of three-dimensional T1-weighted sequences and postcontrast fluid attenuated inversion recovery (FLAIR). Collie et al. (1999) noted a 100% sensitivity for detecting intracranial leptomeningeal carcinomatosis in 25 patients evaluated with gadolinium-enhanced MRI. However, the gold-standard diagnostic test for leptomeningeal metastases remains CSF cytology.

In some situations a tissue diagnosis to confirm brain metastasis may be warranted. Solitary brain lesions in breast cancer patients do not always represent breast cancer metastases and may actually be a primary parenchymal brain tumor, meningioma, CNS lymphoma, brain abscess, or a metastasis from a synchronous or metachronous malignancy. Excision of solitary lesions in patients who are fit for surgery provides both a diagnostic as well as therapeutic approach. Meningioma, in particular, should be ruled out in cases where the diagnosis is ambiguous, because of the unique higher incidence of meningioma seen in breast cancer patients.

Prognosis

Generally, the prognosis for breast cancer patients with brain metastasis is poor, but recent retrospective studies suggest that median survival is improving with newer treatments. Historically, survival for breast cancer patients with brain metastasis treated with whole brain radiotherapy (WBRT) was less than 6 months. A retrospective study of 112 breast cancer patients diagnosed with brain metastasis between 1997 and 2007 showed a significant improvement over the decade, with the median survival at 14.4 months in 2007 (Melisko et al. 2008). This is likely due to improved surgical and radiation treatments.

Since the introduction of trastuzumab for the treatment of HER2/neu-positive breast cancer, survival in patients with Her2/neu-positive breast cancer with brain metastasis has increased from an average of 3 months to a median of 23 months. Survival rates in patients with triple-negative disease and the presence of brain metastasis continue to be short, with survival ranging from 2.9 to 4.9 months in four recent studies. Other factors that improve prognosis include good performance status, stable or absent extra cranial metastasis, and a limited number of lesions within the CNS (Dawood et al. 2009; Nam et al. 2008).

Treatment Modalities

Surgery

Surgery provides rapid relief of symptoms and improves mass effect of large tumors. Surgery also improves local control of metastases and allows

for the collection of tissue for pathologic examination and diagnosis confirmation. As neuroanesthesia, neuroimaging, and neurosurgery have advanced, the safety of surgical resection of brain metastases has become a more effective approach in many patients. Technologies such as image guidance, preoperative and intraoperative functional mapping, and intraoperative ultrasounds and MRI have all led to improved outcomes.

In breast cancer patients with good performance status and a single brain lesion, resection is preferred when the lesion is located in area amicable to surgery. The risks and potential benefits of surgery must be considered in the ideal surgical candidate, as complications are common. Sawaya et al. (1998) reviewed the outcomes of 400 craniotomies in 327 patients with brain tumors (206 with glioma and 194 with metastasectomy). They found that even in good surgical candidates, 13% of patients suffered major complications including neurologic worsening and meningitis. Other risks include neurological complications (including stroke, seizure, or the development of focal neurological deficits), hemorrhage, tumor seeding, and infection. Other complications related to surgery, such as allergic reactions to anesthesia, worsening of pulmonary function, and long recovery times, must also be considered. Owing to high morbidity and mortality, surgery is generally not recommended for patients with a poor prognosis or those with rapidly progressive disease.

Whole-Brain Radiation Therapy

Whole-brain radiotherapy (WBRT) has traditionally been a mainstay of treatment for breast cancer patients with brain metastases, especially those not eligible for surgery due to tumor location, surgical risk factors, or the presence of multiple metastases. WBRT produces symptomatic relief of headache and seizures in 75–85% of patients. It also improves survival and quality of life in many cases (Soffietti et al. 2002). Although various dose-fractionation schedules have been compared in randomized studies, none has proven to be superior to another.

In patients with longer life expectancy (>6 months), a fraction size of less than 3 Gy is usually preferred. Lower doses reduce the incidence of late dementia, which is an uncommon but most undesirable side effect in long-term survivors (median latent period 4 months). The acute side effects of WBRT include alopecia, mild skin toxicity, mild-to-moderate fatigue, nausea and occasionally vomiting, and transient blockage of ears, whereas ataxia, urinary incontinence, and memory or cognitive disturbances are the known late side effects. Late radiation-induced dementia is rare, occurring in only 1.9–5.1% of patients.

The use of adjuvant (WBRT) following surgery is controversial. While several retrospective studies have failed to show a survival benefit in patients receiving adjuvant WBRT following surgery, a randomized clinical trial by Patchell et al. (1998) demonstrated that whole-brain radiation in addition to surgery improved local control and lengthened time to the development of new brain metastases, while decreasing the number of neurological deaths, but had no effect on overall survival. Radiation expected potential effect on the brain is even controversial. Some studies have shown that adjuvant radiation is associated with worsening neurocognitive function due to neurotoxicities; others suggest that whole-brain radiation improves neurocognitive function by controlling disease. Radiation therapy can cause neurocognitive decline, but the progression of brain metastases can also lead to serious deficits as well.

Stereotactic Radiosurgery

Stereotactic radiosurgery involves the delivery of precisely targeted and focal radiation to a single or multiple well-defined intracranial lesions. It can be used in the frontline or recurrent setting. The technique usually is performed with the use of a specifically adapted linear accelerator or a Gamma knife that can precisely target specific areas. Multiple well-collimated beams converge onto a small lesion to produce the treatment effect. The main advantage of radiosurgery is the significant dose fall-off at the target edge, allowing a clinically significant dose at the target while minimizing the dose to surrounding brain tissue and potentially limiting damage to normal brain parenchyma. Other advantages include a decreased risk of hemorrhage, infection, and tumor seeding and ultimately reduced costs, as there is no need for hospitalization. Radiosurgery can also often be performed on patients who have surgically inaccessible lesions or who are poor surgical candidates. Disadvantages of

radiosurgery include a relatively limited target diameter, usually no larger than 2.5–3 cm, slow tumor shrinkage and resolution of mass effect (usually over weeks to months), and the inability to obtain tissue for a pathologic diagnosis.

Radiosurgery can be used alone or in conjunction with other therapies. Adjuvant whole-brain radiation therapy is often given after stereotactic radiosurgery. In a Radiation Therapy Oncology Group (RTOG) trial, patients with 1–3 brain metastases were randomized to receive stereotactic radiosurgery with and without WBRT. The study found a survival benefit in the stereotactic radiosurgery group. Patients in the trial receiving stereotactic radiosurgery and WBRT had more stable or improved performance status than those in the WBRT-only group (Andrews et al. 2004).

Isolated radiosurgery has been compared with radiosurgery with adjuvant WBRT, and although median survival times were similar, comparisons of the development of new brain lesions and disease progression favored the combination of radiosurgery with adjuvant WBRT (Aoyama et al. 2006). The investigators of this study further argue that most breast cancer patients are even less appropriate candidates for isolated radiosurgery due to poorer prognosis and a greater likelihood of extra cranial metastases compared with brain metastases patients with other primary cancers.

Several studies have retrospectively compared the outcomes of patients with brain metastases who underwent radiosurgery versus traditional surgery, with various combinations of adjuvant WBRT. Although some mixed responses have been reported, overall the survival outcomes have been similar (Bindal et al. 1996). A prospective, randomized trial is under way, to minimize the problems of selection bias and confounders inherently found in retrospective reviews. Until more convincing data have been published, the risk-benefits ratio of individual patients taking into account co morbidities and tumor respectability among other factors should guide treatment.

Intracavitary and Interstitial Brain Irradiation

The United States Food and Drug Administration have approved the GliaSite Radiation Therapy System for the intracavitary treatment of brain tumors. A prospective phase II study of GliaSite brachytherapy (prescribed at a 60-Gy dose administered to a 10-mm depth) after resection of a single brain metastasis reported a local control rate, median patient survival time, and duration of functional independence similar to those found in patients receiving resection plus adjuvant WBRT (Rogers et al. 2006).

The use of the Photon Radiosurgery System (PRS), a miniature x-ray generator that can stereotactically irradiate intracranial tumors by using low-energy photons, has also been reported, but it has not been popularized. The procedure is usually performed at the time of biopsy, providing the advantage of combining diagnostic and treatment modalities during one procedure. The system obtained local control of cerebral metastases at rates that were comparable to those achieved through open resection and external stereotactic radiosurgery, but only two breast cancer patients were tested (Curry et al. 2005).

Salvage Cranial Irradiation

Even when cranial irradiation provides good control of brain metastases, metastatic lesions often recur and new lesions form. The question of whether it is appropriate to repeat cranial irradiation either with stereotactic radiosurgery or with WBRT in such patients has been controversial. Traditionally, reirradiation has been frowned upon as it is been thought to be associated with high rates of radiation necrosis, a dreaded adverse outcome that often leads to neurocognitive and other defects. More recently, several studies have evaluated repeated cranial irradiation in select high-performing patients with limited systemic disease.

Loeffler et al. (1990) treated 18 patients with 21 recurrent or persistent brain metastases with stereotactic radiosurgery. All but one patient had received prior radiotherapy. Inclusion criteria included a Karnofsky performance status score of at least 70% and no evidence of (or stable) systemic disease. They found that most of these patients showed neurologic improvement following treatment and had few complications. No cases of radiation necrosis occurred

To define a maximum dose of single-fraction stereotactic radiosurgery, the RTOG 90-05 trial analyzed

over 150 patients who had either recurrent primary brain tumors (36%) or recurrent brain metastases (64%). This study noted that the maximum tolerated doses of single-fraction radiosurgery were dependent on tumor size and defined a maximum dose base on the largest diameter of a lesion, as follows: 24 Gy for tumors ≤20 mm, 18 Gy for tumors 21–30 mm, and 15 Gy for tumors 31–40 mm. The authors further noted that CNS toxicity was more likely in patients with larger tumors (Shaw et al. 2000).

When patients develop multiple recurrent brain metastases after WBRT, salvage stereotactic radiation may not be possible. In these cases, some have argued that salvage WBRT may improve outcomes, whereas others have cautioned against the neurotoxicity related to this treatment strategy. A study by Wong et al. (1996) examined the cases of 86 patients who had repeated WBRT for recurrent CNS metastases. They found that 27% had resolution of neurologic symptoms, 43% had partial improvement of neurologic symptoms, and 29% had either no change or actually worsened after reirradiation. The median survival in this population following reirradiation was 4 months. The majority of these patients had no toxicity following reirradiation, although five patients developed radiation necrosis and one developed dementia

Radiation Sensitization

Numerous radiation sensitizers have been investigated in preclinical and clinical studies in attempts to increase the effectiveness of WBRT. Lonidamine, metronidazole, misonidazole, motexafin gadolinium, bromodeoxyuridine, and efaproxiral have all been studied in randomized controlled trials in patients with metastases from various types of cancer. All these agents failed to show benefit in local tumor control or overall survival, and all were associated with serious adverse events. Interestingly, a small subset of 42 breast cancer patients in the efaproxiral study showed a doubling of the median survival time with the addition of efaproxiral (Suh et al. 2006). This prompted a phase III randomized control study in breast cancer patients comparing WBRT with efaproxiral versus WBRT. The trial failed to demonstrate improvement in overall survival or any other endpoint (Suh et al. 2007).

Chemotherapy

Temozolomide

Temozolomide is an oral alkylating agent that crosses the blood-brain barrier. It is the standard drug used to treat grade IV astrocytoma (glioblastoma multiforme), and it is used to treat other primary brain tumors as well. Temozolomide achieves high concentrations in the CSF, exceeding 30% of plasma levels. Although often used in the treatment of brain metastases, temozolomide has limited activity as single agent in brain metastases of breast cancer, as shown in two different trials (Abrey et al. 2001; Christodoulou et al. 2001). In one of these trials, Abrey et al. treated 41 patients with brain metastases of solid tumors with temozolomide (5 days on, 23 days off), and none of the 10 patients with breast cancer responded. Christodoulou et al. evaluated 24 patients treated with temozolomide for brain metastases, four of whom had primary breast cancer. These authors did not distinguish outcomes by primary disease site. They found that 14 patients (58%) died or had clinical progression after a median of 45.5 days. DNA damage caused by such alkylating agents as temozolomide is repaired by O(6)-methyl-guanine-DNA-methyl-transferase (MGMT). MGMT is highly expressed in breast cancer tissue, which may account for the lack of efficacy of single-agent temozolomide in brain metastases in breast cancer patients. Theoretically, a dose-dense regimen of temozolomide may saturate available MGMT, thereby potentially increasing the effectiveness of the drug (Tosoni et al. 2008). Two Phase II clinical trials have evaluated dose-intensified temozolomide regimens in breast cancer patients with brain metastases, who had a history of WBRT (Friedman 2003; Trudeau et al. 2006). No responses were reported in either trial. Temozolomide with concomitant WBRT has also been tested in patients with brain metastases from various solid tumors. One study by Addeo et al. (2008) tested a dose-dense regimen of temozolomide given concurrently with WBRT and followed by a maintenance

dose. Twelve breast cancer patients and 15 lung cancer patients were enrolled in the study. The overall response rate to this treatment protocol was 48.1%. There was one complete response (CR) and six PRs among the breast cancer patients (Addeo et al. 2008). Treatment was well tolerated in most patients.

Temozolomide has been tested in combination with various other therapeutic agents, yielding mixed results. A study with temozolomide given in combination with capecitabine found an overall response rate of 18% in breast cancer patients with brain metastases previously treated with systemic chemotherapy. Half the patients had stable disease on this regimen, and the treatment was well tolerated (Rivera et al. 2006). In a study by Christodoulou et al. (2005), a combination of temozolomide and cisplatin noted a PR in 40% of breast cancer patients with brain metastases. When combined with irinotecan, temozolomide shows some preliminary evidence of efficacy, although trials are ongoing. In 17 patients with brain metastases and/or leptomeningeal disease with a history of prior treatments, Melisko et al. (2009) found that at 8 weeks, nine patients had stable disease. One patient had a partial response at 46 weeks, and a second patient maintained stable disease for 56 weeks on this regimen. Adverse events were mostly mild and included anemia, neutropenia, diarrhea, nausea, vomiting, and fatigue. Pegylated liposomal doxorubicin given concurrently with temozolamide has also been tested in a similar population. Temozolomide in the treatment of CNS metastases in breast cancer patients remains an area of active research. More data are needed to fully assess the benefits of this potentially promising agent.

Capecitabine

Capecitabine is an orally administered prodrug that is enzymatically converted to 5-fluorouracil in tumor cells, where it inhibits DNA synthesis. It has been shown to cross the blood-brain barrier in animal models and has been hypothesized to achieve sufficient concentrations in the brain to potentially reach clinical significance. Ekenel et al. (2007) analyzed seven breast cancer patients with brain metastases who were treated with capecitabine, five of whom had unsuccessfully undergone other treatments. Three patients had CR, three others had stable disease, and the final patient was not evaluated. The median overall survival was 13 months. Naskhletashvili et al. (2009) treated 10 breast cancer patients with brain metastases who had unsuccessfully undergone previous chemotherapy. Six of these patients had partial responses, three had stable disease, and one progressed. The median time to progression was 6 months.

Taxanes

Taxanes block mitosis by interfering with microtubules. They are most widely used in the treatment of breast cancer. They have limited ability to cross the blood-brain barrier. Patients have been shown to have CNS progression even while systemic disease is under control on taxanes, giving rise to the theory that the CNS acts as a sanctuary site where cancer cells are able to proliferate without being affected by the drug. Furthermore, in CNS substudy intergroup Phase III BIG 02-98 trial, researchers noted similar CNS relapse rates in taxane-treated breast cancer patients compared with controls (Pestalozzi et al. 2008). It has been suggested that taxane penetrance into the CNS may be improved after the blood-brain barrier is disrupted by radiotherapy, but no data have been reported to confirm this hypothesis. Little evidence is available to guide practitioners on the use of taxanes in breast cancer patients with CNS metastases, and much additional research is needed in this area.

Topotecan

Topotecan is a semi-synthetic camptothecin derivative that inhibits topoisomerase I, thereby inhibiting the repair of DNA super coiling and disrupting cell division. It has been shown to cross the blood-brain barrier, with continuous or prolonged infusions achieving higher concentrations in the CNS than standard shorter infusions. Oberhoff et al. (2001) evaluated the effects of topotecan in 16 patients with breast cancer metastases to the brain. Patients in this study received 1.5 mg/m^2 of daily topotecan for 5 days every 3 weeks. Of the 16 patients treated, 38% had a partial response and 31% had stable disease. Small studies of patients with metastases from various cancers (including breast cancer) have evaluated the simultaneous use of radiotherapy and topotecan. Response rates ranging from 33 to 72% have been reported, although fewer than

10 patients with breast cancer were treated in each study (Kocher et al. 2005; Hedde et al. 2007). Further studies with larger numbers of breast cancer patients are needed to adequately evaluate topotecan's initial efficacy.

Platinum

Platinum-based chemotherapy offers an alternative agent in metastatic patients who have been previously treated with other compounds. Cisplatin has the advantage of a low risk of bone marrow suppression, another important concern in patients who have received previous therapies. An autopsy study by Stewart et al. (1988) found that cisplatin crosses the blood-brain barrier in sufficient quantities to achieve therapeutic concentrations, especially when given in high doses.

A prospective study of 22 breast cancer patients with brain metastases found that a regiment of cisplatin plus etoposide achieved a response rate of 55%, with a median survival of 13 months (Cocconi et al. 1990). A similar study that analyzed the response to cisplatin plus etoposide in patients with brain metastases from various cancers, including 56 with breast cancer, found a 13% CR rate and 25% PR rate in those with breast cancer. The median survival time was 8 months (Franciosi et al. 1999).

Other Chemotherapeutic Agents and Combinations

Several other systemic chemotherapeutic agents have been used to treat CNS metastases in breast cancer patients. Cyclophosphamide, methotrexate, vincristine, doxorubicin, and 5-fluorouracil are among those agents that have shown efficacy in small studies or case series. Various combinations of systemic chemotherapy have been tested in breast cancer patients with CNS metastases with varying success. The combination of cyclophosphamide, methotrexate, and 5-fluorouracil has shown potential efficacy in a small study, which yielded a 76% response rate after two cycles. A similar study investigated the combination of cyclophosphamide, 5-flurouracil, and prednisone. A 52% response rate was noted using this regimen (Rosner et al. 1986).

Among the more promising novel agents under investigation is patupilone, a water-soluble, 16-membered macrocyclic polyketide that crosses the blood-brain barrier and is a potent inducer of tubulin dimerization. A study of 45 patients with brain metastases from breast cancer who has progressed after WBRT and were subsequently treated with patupilone found a response rate of 48% (Arslan et al. 2010).

Endocrine Therapy

Endocrine therapy is a mainstay of treatment for estrogen and/or progesterone receptor positive breast cancer; however, the role of hormonal manipulation in brain metastases from breast cancer is limited, and only a few case reports have addressed this issue in the literature. It has been determined that tamoxifen can achieve high levels in the brain. Salvati et al. (1993) reported three cases of prolonged stabilization of brain metastases from breast cancer that were treated with tamoxifen (5 years for two patients, and 6 years for the other). Much more research is needed in this area.

Targeted Agents

Trastuzumab

A probable risk factor for the development of CNS metastasis in breast cancer patients is the amplification of the oncogene HER2/neu. Trastuzumab is a humanized monoclonal antibody that binds to the HER2 receptor and inhibits tumor cell growth. It is used to treat breast cancer with HER2/neu amplification in the adjuvant and metastatic setting. Its introduction has changed the natural history of HER2/neu-positive disease.

Trastuzumab therapy is not without controversy. Some studies have reported higher rates of brain metastases in breast cancer patients treated with trastuzumab. The theory of the brain as a protected sanctuary site has been proposed, and the fact that brain metastases are seen at higher rates in breast cancer patients treated with trastuzumab likely results from the efficacy of the drug in the rest of the body. Improved overall survival in HER2/neu-positive patients treated

with trastuzumab allows more time for the development of brain metastases in a site that eludes the drug. Intrathecal formulation of trastuzumab is not available, and safety data are lacking. Studies are in progress of intrathecal administration and other CNS delivery methods to potentially overcome trastuzumab's inability to cross the blood-brain barrier and therefore assess its tolerability and efficacy.

Lapatinib

Lapatinib is an orally active tyrosine kinase inhibitor that binds HER1 and HER2 receptors, inhibiting downstream signaling. It can cross the blood-brain barrier and is thought to achieve clinically significant levels in the CNS. Lapatinib has the potential to be useful in cases of trastuzumab resistance. Promising results from animal models prompted wider-scale testing in humans. Lin et al. (2009) undertook a phase II study with single agent lapatinib in 242 patients with HER2-positive disease and confirmed CNS metastases and who had shown progression in their brain after WBRT. Responses were observed in 6% of patients, and 21% of patients experienced a $\geq$20% volumetric reduction in their brain lesions. A lapatinib plus capecitabine extension was undertaken in 50 study patients, and 20% experienced a CNS response, while 40% experienced a $\geq$20% volumetric reduction in their CNS lesions. Many patients had significant improvement in neurological symptoms.

Symptomatic and Supportive Treatment

While awaiting the effects of specific anti-tumor therapies, treatment aimed at controlling symptoms is vital. The control of intracranial pressure and edema, the prevention of seizures, and prophylaxis against venous thromboembolic disease are all important concerns.

Corticosteroids

Treatment with glucocorticoids to quickly alleviate increased intracranial pressure and brain edema associated with metastatic disease is usually initiated in symptomatic patients while awaiting the effects of treatments aimed at the cancer itself. Steroids are often used alone for symptom management and palliation or in combination with radiotherapy or other treatments. Because of its minimal mineralocorticoid effect and long half-life, dexamethasone is generally the preferred agent, although any other corticosteroid can potentially be effective. A starting daily dose of 4–8 mg/day divided into twice daily dosing is standard and typically results in marked neurological improvement within 24–72 h. More frequent dosing has been suggested in cases of rising intracranial pressure and/or impending herniation. Corticosteroids are associated with significant side effects, especially when used chronically. Most authors agree that, because of the potential toxicities, corticosteroids should not be used in asymptomatic or minimally symptomatic patients. Most also agree that steroids should be tapered or discontinued as quickly as possible. A dose reduction should be considered within 1 week of treatment initiation. In patients who have been on treatment for extended periods, abrupt discontinuation may initiate a rebound phenomenon, in which edema acutely worsens. The routine use of post-operative corticosteroids to reduce pain and edema is controversial, but it is clear that steroids should generally be minimized as much as possible unless brainstem, temporal, and cerebellar edema is prominent.

Anticonvulsants

Intracranial metastatic lesions may predispose patients to seizures, but given that brain metastases are more circumscribed in nature and less infiltrative than primary brain tumors, such risk is significantly lower. Although the question of whether to prophylactically use anticonvulsants in an attempt to prevent seizures has not been adequately addressed in the literature, most guidelines shy away from recommending seizure prophylaxis in this population. The morbidity and side effects of anticonvulsants is substantial, and the risks often outweigh potential benefits, especially in patients with a history of prior seizures. In those patients who are at higher risk for seizures or who have a history of prior seizure, the benefits and risks must be properly considered. In patients with recurrent seizures, standard treatment with anticonvulsants is warranted.

Routine use of prophylactic anticonvulsants after neurosurgery is debated, but generally, if anticonvulsants are given after surgery their use should be limited in the first few days to 1 week following the operative procedure.

Anticoagulation

Venous thromboembolic disease (VTE) is diagnosed in approximately 20% of patients with brain metastases. Unlike in patients with brain metastases from melanoma, choriocarcinoma, thyroid cancer, or renal cell carcinoma, CNS hemorrhage is not common in breast cancer patients with brain metastases. The use of bevacizumab, however, may increase this risk. The risks versus benefits of anticoagulation therapy should be weighed in breast cancer patients with brain metastases, but most patients can safely be given anticoagulants if necessary. Comorbid risk factors for VTE including, age, surgery, immobilization, and other features should be taken into account. Schiff and DeAngelis (1994) found that anticoagulation is more effective than Greenfield filters in most patients with brain metastases and venous thromboembolism. They further noted that recurrent VTE is diagnosed in as many as 40% of patients with brain metastases treated with inferior vena cava (IVC) filter alone. Venous thromboembolism is generally treated with low-molecular-weight heparin, which is favored in patients with brain metastases compared with warfarin. Routine VTE prophylaxis is not recommended in all patients with brain metastases, but in cases in which primary prophylaxis is desired (high-risk patients, personal or strong family history of clot formation, etc.), aspirin 325 mg daily is generally acceptable.

Leptomeningeal Disease

Leptomeningeal metastases are becoming more common in breast cancer patients as survival increases. Lobular carcinoma has a particular propensity to spread to the leptomeninges, and meningeal metastases may develop even in the environment of controlled systemic disease. Altundag et al. (2007) reviewed 420 cases of brain metastases originating from breast cancer. They found that 31.6% of patients with lobular carcinoma presented with isolated leptomeningeal disease. The presentation of leptomeningeal metastases varies but typically involves spinal symptoms such as leg weakness, mental status changes, and other neurologic signs. Multiple abnormalities involving different levels of the neuroaxis are highly suggestive of leptomeningeal disease. MRI remains the diagnostic imaging modality of choice when leptomeningeal disease is suspected, and cerebral spinal fluid cytology be the gold standard confirmatory test. For those patients with a poor prognosis, palliative radiation may be considered to lessen symptoms. In patients with relatively better prognosis, radiation (to relieve bulky disease or treat the obstruction of CSF flow) followed by intrathecal or intraventricular chemotherapy is preferred. Methotrexate and sustained-release cytarabine (DepoCyt) are the agents of choice, but other agents have been shown efficacy in small series or case reports. Two trials that compared DepoCyt and intrathecal methotrexate found similar response rates; however, DepoCyt seemed to have more toxicity but patients who received this treatment also had a significantly greater time to progression (Cole et al. 2003). A number of additional agents are currently available in clinical trials. These include novel immunotoxins and monoclonal antibodies, as well as commercially available therapies such as temozolomide and cytarabine.

Spinal Metastases

Intramedullary spinal cord metastases are rare but can have devastating clinical consequences. Spread of cancer to the spinal cord is thought to occur through hematogenous routes from arteries and vertebral venous plexuses, as well as via cerebral spinal fluid, and direct invasion from contiguous structures when tumors erode through the dura. Most patients with spinal cord metastases present with rapid progressive neurological deficits. Weakness, sensory loss, and urogenital dysfunction are the most common symptoms. MRI with gadolinium is the diagnostic test of choice when spinal cord metastases are suspected. Patients with intramedullary spinal cord metastases

have a median survival of 3–6 months from the time of diagnosis, and there is significant morbidity associated with this disease. Lee et al. (2007) reviewed six cases of intramedullary spinal cord metastases from primary breast cancer from their institution. These patients were treated with radiotherapy and had a median survival of 5.5 months. Treatment should be individualized, but options include surgery, radiotherapy, and chemotherapy. Steroids may be added to reduce edema. Steroids provide no survival benefit, but as in brain metastases, may reduce morbidity. Surgery aims at decompression of neural tissue and allows for pathological confirmation of diagnosis. Data are limited regarding the efficacy of surgery for intramedullary metastases, but it is generally considered in selected cases of a focal spinal mass in the face of limited systemic disease and relatively good prognosis. Evidence of the efficacy of chemotherapy for spinal metastases is similarly lacking but is generally considered palliative, rather than life prolonging. Radiotherapy remains the preferred treatment option for spinal cord metastases, providing various amounts of symptomatic relief for a large percentage of patients with this condition.

Ocular Metastases

Breast cancer has the highest rate of ocular metastasis of all cancers. The choroid is the most common site of involvement. Typically, patients present with visual symptoms, including loss of visual acuity, diplopia, the development of blind spots, and image distortions. Diagnosis is usually made via fundoscopic examination. Retinal detachment or hemorrhage is often noted. An MRI of the brain is indicated upon suspicion or diagnosis of ocular metastasis in order to rule out associated brain involvement, which occurs frequently. For those patients with worsening symptoms, palliative radiation therapy is indicated. Both eyes should be treated in bilateral disease. Maor et al. (1997) reported on 42 cases of metastatic breast cancer to the choroid treated by radiation therapy. Of the patients reviewed, 36% had bilateral ocular involvement and 64% had unilateral involvement. In 12 patients the choroid was the first site of metastasis. They noted a median survival after choroidal metastases of 10 months. These authors observed good visual responses in patients treated with radiation and recommended short courses of radiotherapy to the choroid for palliation.

Future Perspectives

Metastasis of breast cancer to the CNS continues to be a challenge for patients, practitioners, and researchers alike. Despite the available treatment approaches, it remains a problem of unmet needs. The prognosis gets poorer for patients who develop CNS metastasis irrespective of how well their systemic disease may be controlled. On the other hand, the seemingly increased incidence of such a pattern of spread makes it a problem of growing magnitude, as it directly compromises the survival of patients. Better control of established metastasis to the brain remains a challenge to be addressed. The benefits of total brain irradiation or stereotactic versus open resection with or without total brain radiation is well recognized; however, the overall outcome remains short of patients' objectives.

Newer approaches need to be developed. The CNS remains a sanctuary for breast cancer cells because the BBB prevents delivery of chemotherapy agents past this barrier. Development of effective antitumor agents that may enter the brain tissue may prove to be an effective research strategy. Another approach may be focused against the BBB itself to improve its permeability to chemotherapeutic agents. In tandem with such approaches, focus should also be on identifying patients who may be at higher risk of developing CNS metastasis. Enriching the patient population may enhance the research efforts in establishing both preventive and therapeutic approaches for such a problem. A nomogram had been developed for the identification of patients with metastatic systemic breast cancer who may be at high risk for metastasis to the brain (Fig. 4.1) (Graesslin et al, 2010). Its use may be a tool to identify patients at high risk and therefore enhance study designs by limiting the number of patients needed to test a therapeutic hypothesis. On the other hand, biologic markers or genetic profiles may also be indicators not only of high-risk patient population but also of targeted therapeutic potential.

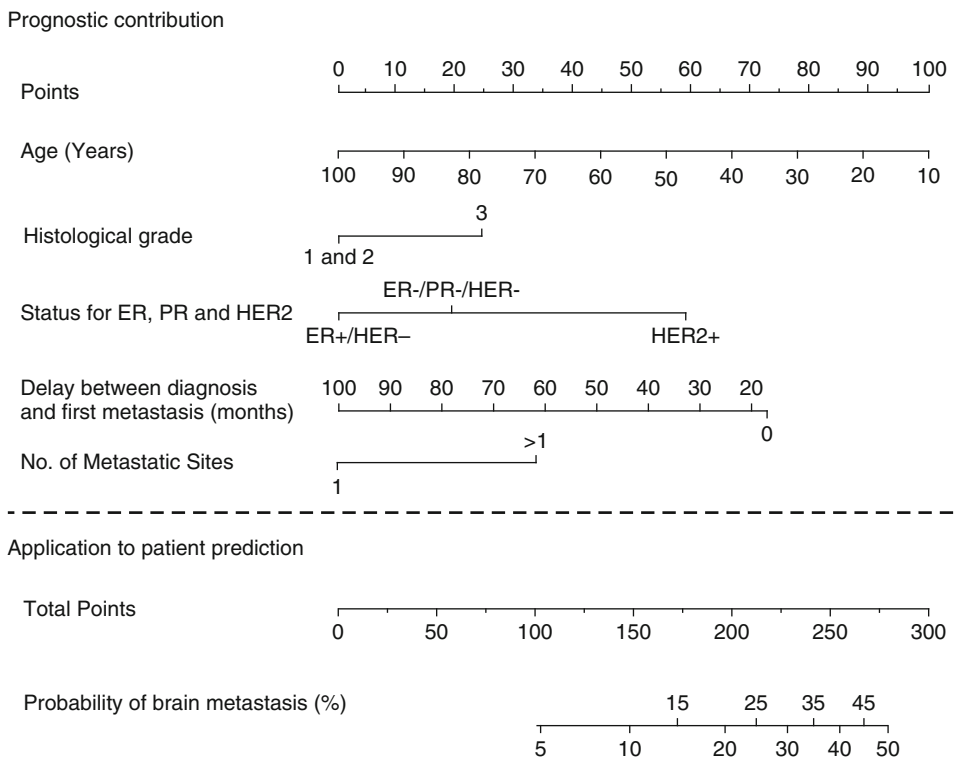

Fig. 4.1 Nomogram to estimate the probability of brain metastasis (BM) in metastatic disease other than brain breast cancer patients. Find the predictor points on the uppermost point scale that correspond to each patient variable and add them up. The total projected to the bottom scale indicates the probability of BM

References

Abrey LE, Olson JD, Raizer JJ, Mack M, Rodavitch A, Boutros DY, Malkin MG (2001) A phase II trial of temozolomide for patients with recurrent or progressive brain metastases. J Neurooncol 53(3):259–265

Addeo R, De Rosa C, Faiola V, Leo L, Cennamo G, Montella L, Guarrasi R, Vincenzi B, Caraglia M, Del Prete S (2008). Phase 2 trial of temozolomide using protracted low-dose and whole-brain radiotherapy for nonsmall cell lung cancer and breast-cancer patients with brain metastases. Cancer 113(9):2524–2531

Altundag K, Bondy ML, Mirza NQ, Kau SW, Broglio K, Hortobagyi GN, Rivera E (2007) Clinicopathologic characteristics and prognostic factors in 420 metastatic breast cancer patients with central nervous system metastasis. Cancer 110:2640–2647

Andrews DW, Scott CB, Sperduto DW, Flanders AE, Gaspar LE, Schell MC, Werner-Wasik M, Demas W, Ryu J, Bahary JP, Souhami L, Rotman M, Mehta MP, Curran WJ Jr. (2004, May 22) Whole brain radiation therapy with or without stereotactic radiosurgery boost for patients with the top three brain metastases: phase III results of the RTOG 9503 randomized trial. Lancet 363(9422):1665–1672

Aoyama H, Shirato H, Tago M, Nakagawa K, Toyoda T, Hatano K, Kenjyo M, Oya N, Hirota S, Shioura H, Kunieda E, Inomata T, Hayakawa K, Katoh N, Kobashi G (2006) Stereotactic radiosurgery plus whole-brain radiation therapy vs stereotactic radiosurgery alone for treatment of brain metastases: a randomized controlled trial. JAMA 7:295(21):2483–2491

Arslan C, Dizdar O, Altundag K (2010) Systemic treatment in breast-cancer patients with brain metastasis. Expert Opin Pharmacother 11(7):1089–1100

Barnholtz-Sloan JS, Sloan AE, Davis FG, Vigneau FD, Lai P, Sawaya RE (2004) Incidence proportions of brain metastases in patients diagnosed (1973 to 2001) in the Metropolitan Detroit Cancer Surveillance System. J Clin Oncol 22(14):2865–2872

Bindal AK, Bindal RK, Hess KR, Shiu A, Hassenbusch SJ, Shi WM, Sawaya R (1996) Surgery versus radiosurgery in the treatment of brain metastasis. J Neurosurg 84(5):748–754

Christodoulou C, Bafaloukos D, Kosmidis P, Samantas E, Bamias A, Papakostas P, Karabelis A, Bacoyiannis C, Skarlos DV (2001) Phase II study of temozolomide in heavily pretreated cancer patients with brain metastases. Ann Oncol 2(2):249–254

Christodoulou C, Bafaloukos D, Linardou H, Aravantinos G, Bamias A, Carina M, Klouvas G, Skarlos D (2005).

Temozolomide (TMZ) combined with cisplatin (CDDP) in patients with brain metastases from solid tumors: a Hellenic Cooperative Oncology Group (HeCOG) Phase II study. J Neurooncol 71(1):61–65

Cocconi G, Lottici R, Bisagni G, Bacchi M, Tonato M, Passalacqua R, Boni C, Belsanti V, Bassi P (1990) Combination therapy with platinum and etoposide of brain metastases from breast carcinoma. Cancer Invest 8(3–4):327–334

Cole BF, Glantz MJ, Jaeckle KA, Chamberlain MC, Mackowiak JI (2003) Quality-of-life-adjusted survival comparison of sustained-release cytosine arabinoside versus intrathecal methotrexate for treatment of solid tumor neoplastic meningitis. Cancer 97(12):3053–3060

Collie DA, Brush JP, Lammie GA (1999) Imaging features of leptomeningeal metastases. Clin Radiol 54(11):765–771

Curry WT Jr, Cosgrove GR, Hochberg FH, Loeffler J, Zervas NT (2005) Stereotactic interstitial radiosurgery for cerebral metastases. J Neurosurg 103(4):630–635

Dawood S, Broglio K, Esteva FJ, Yang W, Kau SW, Islam R, Albarracin C, Yu TK, Green M, Hortobagyi GN, Gonzalez-Angulo AM (2009) Survival among women with triple receptor-negative breast cancer and brain metastases. Ann Oncol 20(4):621–627

Ekenel M, Hormigo AM, Peak S, Deangelis LM, Abrey LE (2007) Capecitabine therapy of central nervous system metastases from breast cancer. J Neurooncol 85(2):223–227

Evans AJ, James JJ, Cornford EJ, Chan SY, Burrell HC, Pinder SE, Gutteridge E, Robertson JF, Hornbuckle J, Cheung KL (2004) Brain metastases from breast cancer: identification of a high-risk group. Clin Oncol (R Coll Radiol) 16(5):345–349

Franciosi V, Cocconi G, Michiara M, Di Costanzo F, Fosser V, Tonato M, Carlini P, Boni C, Di Sarra S (1999) Front-line chemotherapy with cisplatin and etoposide for patients with brain metastases from breast carcinoma, nonsmall cell lung carcinoma, or malignant melanoma: a prospective study. Cancer 85(7):1599–1605

Friedman HS (2003) Phase II trial of temozolomide for patients with progressive brain metastases. 2003 ASCO Annual Meeting (Central Nervous System Session, Poster Discussion)

Graesslin O, Abdulkarim BS, Coutant C, Huguet F, Gabos Z, Hsu L, Marpeau O, Uzan S, Pusztai L, Strom EA, Hortobagyi GN, Rouzier R, Ibrahim NK (2010) Nomogram to predict subsequent brain metastasis in patients with metastatic breast cancer. JCO 28:2032–2037

Hedde JP, Neuhaus T, Schüller H, Metzler U, Schmidt-Wolf IG, Kleinschmidt R, Losem C, Lange O, Grohe C, Stier S, Ko YD (2007) A phase I/II trial of topotecan and radiation therapy for brain metastases in patients with solid tumors. Int J Radiat Oncol Biol Phys 68(3):839–844

Kocher M, Eich HT, Semrau R, Güner SA, Müller RP (2005) Phase I/II trial of simultaneous whole-brain irradiation and dose-escalating topotecan for brain metastases. Strahlenther Onkol 181(1):20–25

Lee SS, Kim MK, Sym SJ, Kim SW, Kim WK, Kim SB, Ahn JH (2007) Intramedullary spinal cord metastases: a single-institution experience. J Neurooncol 84(1):85–89

Lin NU, Bellon JR, Winer EP (2008) CNS metastases in breast cancer. J Clin Oncol 22(17):3608–3617

Lin NU, Claus E, Sohl J, Razzak AR, Arnaout A, Winer EP (2008) Sites of distant recurrence and clinical outcomes in patients with metastatic triple-negative breast cancer: high incidence of central nervous system metastases. Cancer 113(10):2638–2645

Lin NU, Diéras V, Paul D, Lossignol D, Christodoulou C, Stemmler HJ, Roché H, Liu MC, Greil R, Ciruelos E, Loibl S, Gori S, Wardley A, Yardley D, Brufsky A, Blum JL, Rubin SD, Dharan B, Steplewski K, Zembryki D, Oliva C, Roychowdhury D, Paoletti P, Winer EP (2009) Multicenter phase II study of lapatinib in patients with brain metastases from HER2-positive breast cancer. Clin Cancer Res 15(4):1452–1459

Loeffler JS, Kooy HM, Wen PY Fine HA, Cheng CW, Mannarino EG, Tsai JS, Alexander E 3rd (1990) The treatment of recurrent brain metastases with stereotactic radiosurgery. J Clin Oncol 8(4):576–582

Maor M, Chan RC, Young SE (1977) Radiotherapy of choroidal metastases: breast cancer as primary site. Cancer 40(5):2081–2086

Melisko ME, Anderson M, Scott J et al. (2009) Phase II study of irinotecan and temozolomide in breast-cancer patients with brain metastases or leptomeningeal disease that has progressed after stereotactic radiosurgery or whole brain radiation. 2009 ASCO Breast Cancer Symposium, Abstract No. 237

Melisko ME, Moore DH, Sneed PK, De Franco J, Rugo HS (2008) Brain metastases in breast cancer: clinical and pathologic characteristics associated with improvements in survival. J Neurooncol 88(3):359–365

Nam BH, Kim SY, Han HS, Kwon Y, Lee KS, Kim TH, Ro J (2008) Breast cancer subtypes and survival in patients with brain metastases. Breast Cancer Res 10(1):R20

Naskhletashvili DR, Gorbounova VA, Bychkov MB, et al. (2009) Capecitabine monotherapy for patients with brain metastases from advanced breast cancer. 2009 ASCO Annual Meeting, Abstract No. 1102

Oberhoff C, Kieback DG, Wurstlein R, Deertz H, Sehouli J, van Soest C, Hilfrich J, Mesrogli M, von Minckwitz G, Staab HJ, Schindler AE (2001) Topotecan chemotherapy in patients with breast cancer and brain metastases: results of a pilot study. Onkologie 24(3):256–260

Patchell RA, Tibbs PA, Regine WF, Dempsey RJ, Mohiuddin M, Kryscio RJ, Markesbery WR, Foon KA, Young B (1998) Postoperative radiotherapy in the treatment of single metastases to the brain: a randomized trial. JAMA 280(17): 1485–1489

Pestalozzi BC, Francis P, Quinaux E, Dempsey RJ, Mohiuddin M, Kryscio RJ, Markesbery WR, Foon KA, Young B (2008) Is risk of central nervous system (CNS) relapse related to adjuvant taxane treatment in node-positive breast cancer? Results of the CNS substudy in the intergroup Phase III BIG 02-98 Trial. Ann Oncol 19(11):1837–1841

Rivera E, Meyers C, Groves M, Valero V, Francis D, Arun B, Broglio K, Yin G, Hortobagyi GN, Buchholz T (2006). Phase I study of capecitabine in combination with temozolomide in the treatment of patients with brain metastases from breast carcinoma. Cancer 107(6):1348–1354

Rogers LR, Rock JP, Sills AK, Vogelbaum MA, Suh JH, Ellis TL, Stieber VW, Asher AL, Fraser RW, Billingsley JS,

Lewis P, Schellingerhout D, Shaw EG (2006) Results of a phase II trial of the GliaSite radiation therapy system for the treatment of newly diagnosed, resected single brain metastases. J Neurosurg 105(3):375–384

Rosner D, Nemoto T, Lane WW (1986) Chemotherapy induces regression of brain metastases in breast carcinoma. Cancer 58(4):832–839

Salvati M, Cervoni L, Innocenzi G, Bardella L (1993) Prolonged stabilization of multiple and single brain metastases from breast cancer with tamoxifen. Report of three cases. Tumori79(5):359–362

Sawaya R, Hammoud M, Schoppa D, Hess KR, Wu SZ, Shi WM, Wildrick DM (1998) Neurosurgical outcomes in a modern series of 400 craniotomies for treatment of parenchymal tumors. Neurosurgery 42(5):1044–1055

Schiff D, DeAngelis LM (1994) Therapy of venous thromboembolism in patients with brain metastases. Cancer 73(2): 493–498

Schouten LJ, Rutten J, Huveneers HA, Twijnstra A (2002) Incidence of brain metastases in a cohort of patients with carcinoma of the breast, colon, kidney, and lung and melanoma. Cancer 94:2698–2705

Shaw E, Scott C, Souhami L, Dinapoli R, Kline R, Loeffler J, Farnan N (2000) Single dose radiosurgical treatment of recurrent previously irradiated primary brain tumors and brain metastases: final report of RTOG protocol 90-05. Int J Radiat Oncol Biol Phys 47(2):291–298

Soffietti R, Rudā R, Mutani RJ (2002) Management of brain metastases. Neurology 249(10):1357–1369

Stewart DJ, Mikhael NZ, Nair RC, Kacew S, Montpetit V, Nanji A, Maroun JA, Howard K (1988) Platinum concentrations in human autopsy tumor samples. Am J Clin Oncol 11(2): 152–158

Suh JH, Stea B, Nabid A, Kresl JJ, Fortin A, Mercier JP, Senzer N, Chang EL, Boyd AP, Cagnoni PJ, Shaw E (2006) Phase III study of efaproxiral as an adjunct to whole-brain radiation therapy for brain metastases. J Clin Oncol 24(1): 106–114

Suh J, Stea B, Tankel K, Marsiglia H, Belkacemi Y, Gomez H, et al. (2007). Phase 3 enrich (RT-016) comparative study of efaproxiral administered concurrent with whole brain radiation therapy (WBRT) in women with brain metastases from breast cancer. RT-35. Society for Neurooncology 12th Annual Meeting, Dallas, Texas

Tosoni A, Franceschi E, Ermani M, Bertorelle R, Bonaldi L, Blatt V, Brandes AA (2008) Temozolomide three weeks on and one week off as first line therapy for patients with recurrent or progressive low grade gliomas. J Neurooncol 89(2):179–185

Trudeau ME, Crump M, Charpentier D, Yelle L, Bordeleau L, Matthews S, Eisenhauer E (2006) Temozolomide in metastatic breast cancer (MBC): a phase II trial of the National Cancer Institute of Canada – Clinical Trials Group (NCIC-CTG). Ann Oncol 17(6): 952–956

Tsukada Y, Fouad A, Pickren JW, Lane WW (1983) Central nervous system metastasis from breast carcinoma. Autopsy study. Cancer 52(12):2349–2354

Wong WW, Schild SE, Sawyer TE, Shaw EG (1996) Analysis of outcome in patients reirradiated for brain metastases. Int J Radiat Oncol Biol Phys 34(3):585–590

Chapter 5

Melanoma to Brain Metastasis: Photoacoustic Microscopy

Xinmai Yang and Mark Cohen

Abstract Of skin malignancies, cutaneous melanoma carries the highest mortality due to its metastatic potential. This malignancy is known to metastasize to the brain, often leading to death. The ability to image the growth of melanoma brain metastases in vivo provides new insights into disease progression and response to therapies. We have recently used a reflection-mode photoacoustic microscopy (PAM) system to detect the growth of melanoma brain tumor in a small animal model. B16F10 murine melanoma tumor cells were stereotactically implanted in the brains of several Balb/C mice at the beginning of the study. Then, PAM was used to scan the region of implantation in the mouse brain, and growth of the melanoma was monitored until the disease became fatal. Results of the study demonstrated that PAM can be used to accurately detect and monitor melanoma brain metastasis growth noninvasively and transcranially in vivo.

Keywords Melanoma · Brain metastases · PAM · Metastatic brain tumor · Mouse brain · Orthotopic tumor model

Introduction

Malignant melanoma is one of the most lethal cancers and represents a significant public health problem in the United States. For patients with stage IV melanoma, the incidence of brain metastases has been reported to be as high as 10–40%, making melanoma the third most common metastatic brain tumor in the United States, following lung cancer and breast cancer (Xu et al., 2007). With effective treatments, survival time following central nervous system (CNS) metastases is between 2 and 5 months (Tarhini and Agarwala, 2004; Mori et al., 1998; Patchell et al., 1990; Yu et al., 2002). Without treatments, deterioration is enhanced leading to disease-related death. Recognition of the onset and progression of melanoma brain metastases in experimental models is necessary to identifying new research strategies that would be useful for the diagnosis and subsequent therapy of these fatal tumors in humans. Hence, in vivo monitoring of the formation and growth of melanoma brain metastases in live animals could have major applications to the design of improved therapies.

In this study, we utilize the photoacoustic microscopy (PAM) technique to detect the progress of melanoma brain tumors in mouse models in vivo (Staley et al., 2010). Photoacoustic (also called optoacoustic or thermoacoustic) imaging is based on the generation of photoacoustic waves by safely depositing short-pulsed optical energy into tissue (Wang, 2008a, b; Xu and Wang, 2006). Photoacoustic imaging overcomes the limitations of other existing optical imaging modalities and combines optical contrast with ultrasonic resolution. Photoacoustic imaging has demonstrated imaging depth up to 5 cm (Ku and Wang, 2005) with enhanced imaging resolution (from 2 to 500 μm) scalable to the imaging depth (Song and Wang, 2007; Wang, 2008a). Because photoacoustic imaging is based on optical absorption, it can be implemented quickly and inexpensively, with relatively simple instrumentation requirements and no

X. Yang (✉)
Department of Mechanical Engineering, The KU Bioengineering Research Center, University of Kansas, Lawrence, KS 66045, USA
e-mail: xmyang@ku.edu

M.A. Hayat (ed.), *Tumors of the Central Nervous System, Volume 4*,
DOI 10.1007/978-94-007-1706-0_5, © Springer Science+Business Media B.V. 2012

ionization. Formed photoacoustic images represent the distributions of optical absorption. Since melanin in melanoma has high optical absorption (e.g., about 1000 times of water at 700 nm wavelength), significant contrast between melanoma and background tissue can be achieved using photoacoustic imaging. Compared with other imaging modalities used to detect melanoma brain metastases noninvasively in vivo such as computed tomography (CT), magnetic resonance imaging (MRI), and positron emission tomography (PET) (Panigrahy and Bluml, 2009; Mishima et al., 1997), photoacoustic imaging is low cost, uses non-ionizing radiation and is based on sharp optical contrast. In contrast to high-resolution, purely optical imaging methods (Kienast et al., 2010), photoacoustic imaging can image much deeper and has no requirements for a cranial window.

Photoacoustic imaging has been applied to detect skin melanomas in small animal models (Oh et al., 2006; Zhang et al., 2006). Real-time detection of circulating melanoma cells using photoacoustic flow cytometry has also been proposed (Galanzha et al., 2008a, b; Zharov et al., 2006, 2007; Olszewski and Tarnok, 2008). In this chapter, we demonstrate the capability of photoacoustic imaging for noninvasive monitoring of the growth of melanoma brain tumors in a mouse model.

Methods and Materials

Our photoacoustic imaging system is identical to the one presented by (Song and Wang, 2007) for deep photoacoustic imaging. The system (Fig. 5.1) consists of an ultrasound transducer, a laser system, and receiving electronics. A Q-switched Nd:YAG laser (Surelite; Continuum, Santa Clara, CA) was used to pump a tunable OPO laser (Surelite OPO PLUS; Continuum, Santa Clara, CA) to obtain a 764 nm wavelength laser with a 10-Hz pulse repetition rate. The produced laser light forms a ring shape illumination after passing through two prisms and a conical lens and then is refocused inside the tissue sample by an optical condenser. At the tissue surface, the ring has a diameter of ~5 mm with a focal depth of ~3 mm for the current application. The subsequently generated ultrasonic waves are detected by a focused ultrasonic transducer (13-2506-R, Olympus-NDT, Waltham, MA), delivered to a pre-amplifier (5072PR, Olympus-NDT, Waltham, MA) with 30 dB gain, and finally collected by a personal computer through an A/D Scope Card (CS21G8-256MS, Gage, Lockport, IL) with a 500-MHz sampling rate. The conical and condenser lenses are driven by a three-dimension scanning translation stage to enable the transducer to mechanically

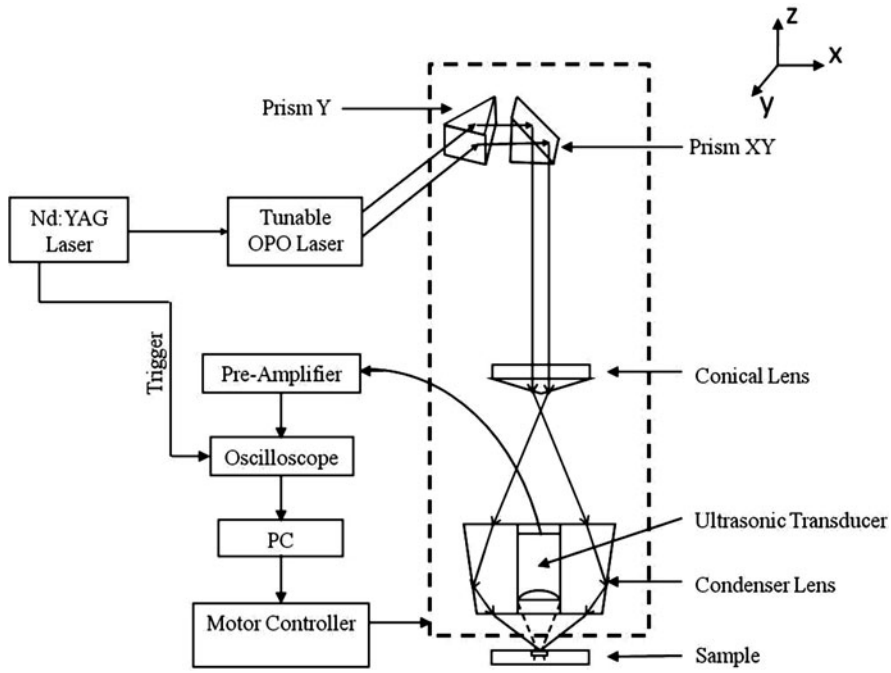

Fig. 5.1 Schematic of the PAM system

scan the targeted region. Two prisms are used to enable the optical beam-folding for a 2D mechanical scanning. In Fig. 5.1, prism Y indicates that the prism can move on the Y direction, while prism XY can move on both X and Y direction. The ultrasound transducer (15 mm focal length; 9.4 mm aperture size) has a central frequency of 25-MHz with 61% -6-dB fractional bandwidth and exhibits lateral resolution of 150 μm and axial resolution of 100 μm when used for photoacoustic imaging.

All in vivo imaging evaluations were done using an orthotopic murine melanoma model for metastatic melanoma to the brain on a stereotactic protocol approved by the University of Kansas Institutional Animal Care and Use Committee. B16F10 melanoma tumor cells grown in DMEM supplemented by 10% fetal bovine serum, 1% penicillin, and 1% streptomycin were harvested by trypsinization, washed in 1× phosphate-buffered saline, resuspended in 1× phosphate-buffered saline at a concentration of 2500 cells/μL, and kept on ice until injected intracranially. Balb/C mice were deeply anesthetized using a mixture of 87 mg/kg ketamine and 13 mg/kg xylazine through an intraperitoneal injection. The hairs on the top of the animals' heads were shaved to expose the skin, and animals were then appropriately positioned in a small animal stereotactic frame. Following liquid tear application to the eyes to prevent octular damage during anesthesia, povidone iodine was applied on the skin covering the skull around the anticipated midline incision site, and an alcohol pad was then used to wipe down the skin to remove excess povidone iodine and provide further sterilization. The calvarium was exposed via a midline incision of the scalp about ~5 mm in length, and a burr hole was drilled 1 mm anterior and 2 mm lateral (right) from the bregma by a Dremel 10.8 V 8000-03 with a rounded high speed cutter bit. A 10 μL blunt-tipped Hamilton syringe loaded with 2 μL was lowered into the hole. 3.3 mm from the cortical surface but retracted 0.3 mm to form a small pocket for the liquid to be injected, thereby introducing the cells into the right basal ganglia. The B16F10 cells were injected into the brain at a speed of 0.4 μL/min and a total volume of 2 μL (5000 cells injected per mouse). The syringe was left in place for about 1 minute following tumor cell injection to allow for pressure stabilization. After the intracranial injection, each animal was removed from the stereotactic frame, and the incision was closed with a surgical suture. Triple antibiotic ointment was added to the incision to help further prevent infection, and the animals were slowly warmed on a heating pad and monitored until they awakened.

Photoacoustic images of brain melanoma tumor implants were first acquired on the fifth day after the tumor cell injection. During the photoacoustic imaging, melanoma brain tumor-bearing mice were initially anesthetized with a mixture of 87 mg/kg ketamine and 13 mg/kg xylazine, and then the anesthesia was maintained with the inhalation of a mixture of pure oxygen and 1% isoflurane. The brain region where the melanoma cells were injected was then imaged. It took about 40 min scanning time get one photoacoustic image. The same process was repeated in the following days, and the growth of the brain melanoma tumor could be directly indicated from the photoacoustic images as the size of the tumor increased. The animals showed classic signs of morbidity approximately 2 weeks following the tumor injections.

Results and Discussions

Figure 5.2 highlights the depth profile referred to as a "B-scan" obtained by PAM non-invasively for a mouse brain. B-scans are line scans that contain the depth profile along the axis of interest – in this case either x or y. That is, using photoacoustics it is possible to form images that depict the acoustic response along the z-axis, allowing the visualization of a slice of data depth wise. Figure 5.2c represents the B-scan shown by the horizontal green line in Fig. 5.2b, running from left to right. Figure 5.2d is the B-scan shown by the blue vertical line, running from top to bottom, in Fig. 5.2b.

Maximum amplitude projection (MAP) of the photoacoustic images of the melanoma in mouse brain, which are formed by projecting the maximum photoacoustic amplitudes along z axis to its orthogonal plane, are presented in Fig. 5.3a–e. Photoacoustic signals from the scalp and skull were removed in the MAP images in order to clearly show the tumor inside the brain. Figure 5.3a–e were taken from an experimental animal on the day 5, day 8, day 10, day 13 and day 14 after the injection of tumor cells, respectively. On day 5 and day 8, the brain tumor signals are relatively

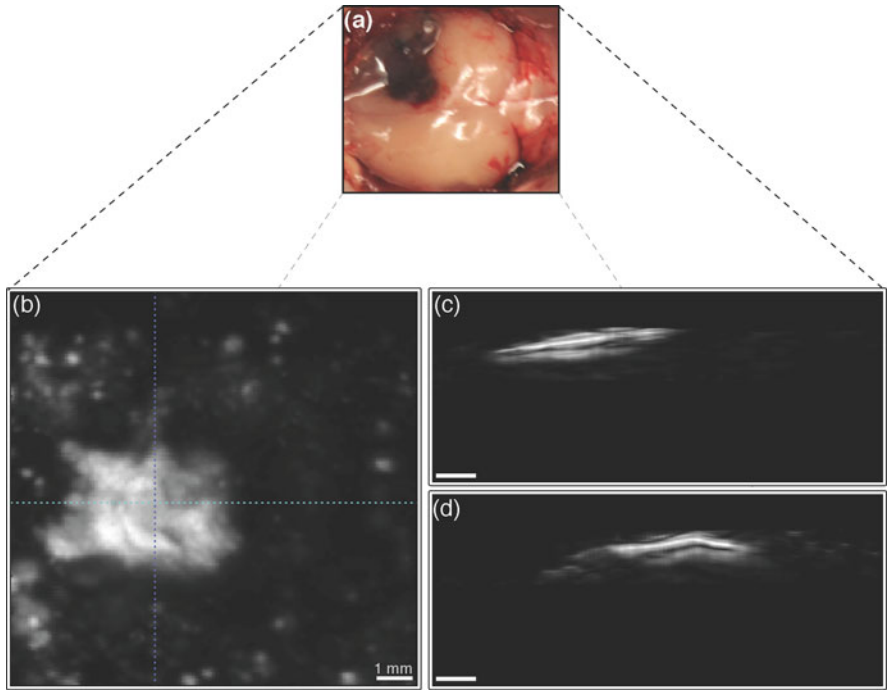

Fig. 5.2 Photograph and depth profile of tumor 11 days post-inoculation in mouse 2. (**a**) photograph taken after image acquisition and scalp and skill removal, showing the region of rumor growth in the cortex. (**b**) MAP image of the region in (**a**) obtained non-invasively. (**c**) Horizontal B-Scan along the *green line* in (**b**). (**d**) Vertical B-scan along the *blue line* in (**b**). Scale bar is the same in all images

weak because the tumor is still small. From the photoacoustic image, the signal to noise ratio (SNR) of the tumor region is 15 dB at day 5, the tumor size is around 1 mm in diameter and 0.3 mm in depth. On day 10, the photoacoustic signals from the melanoma brain tumor becomes dominate. The SNR of tumor region increases to 26 dB, and the size of the tumor increases to 2 mm in diameter and 0.7 mm in depth. The tumor continues to grow over the last two days before morbidity as the SNR of the tumor region increases to 30 dB, and the size is about 4 mm in diameter and over 1 mm in depth on day 14.

The corresponding B-mode (cross-sectional) photoacoustic images of the melanoma tumor from the same mouse are in Fig. 5.3f–j. These clearly show the depth of the melanoma tumor in the mouse brain on the five separate imaging days after injection. The brain melanoma was initially located about 2-3 mm deep underneath the skull. As the time elapses, the thickness of the melanoma brain increases. In the 14th day, the mouse died from the brain melanoma and the open skull photograph was taken and shown in Fig. 5.3k. The final size of the tumor is about 4 mm in diameter inside the brain. Both the size and depth information of the brain tumors are important in planning and verifying the treatment of primary brain tumors (e.g., glioma). This study showed PAM can monitor the brain tumor growth inside a small animal's brain noninvasively, and therefore, photoacoustic imaging is capable of being as an imaging tool to in vivo track the response of the brain tumor to therapies.

The ability of providing non-invasive brain tumor detection by PAM offers an important tool for small animal research. In addition, photoacoustic imaging has demonstrated the ability to image intracranial masses through a much thicker monkey brain (Yang and Wang, 2008). Based on success with monkey skulls and brains, this technique would likely be capable to perform human brain imaging, especially in the area of pediatric brain imaging where the skull is thinner and more easily penetrable by ultrasound waves. Although the current study only used one optical wavelength to detect brain tumors, photoacoustic imaging technique can be used to measure oxygenated hemoglobin (HbO_2) and de-oxygenated hemoglobin (Hb) separately when two or more optical wavelengths are used (Wang et al., 2006). The separated measurements of HbO_2 and Hb will shed more lights on the brain tumor imaging through the added detection of changes in brain function.

In conclusion, we have used a PAM system with a 25-MHz focused ultrasonic transducer and

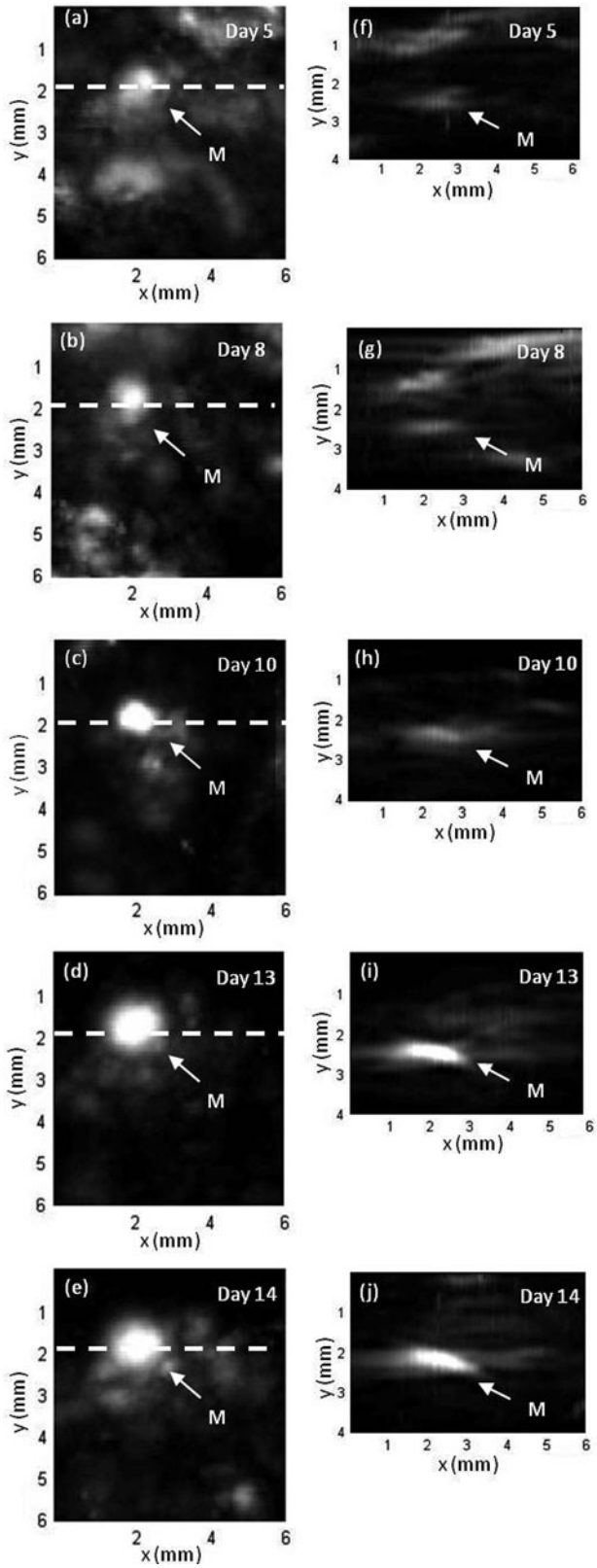

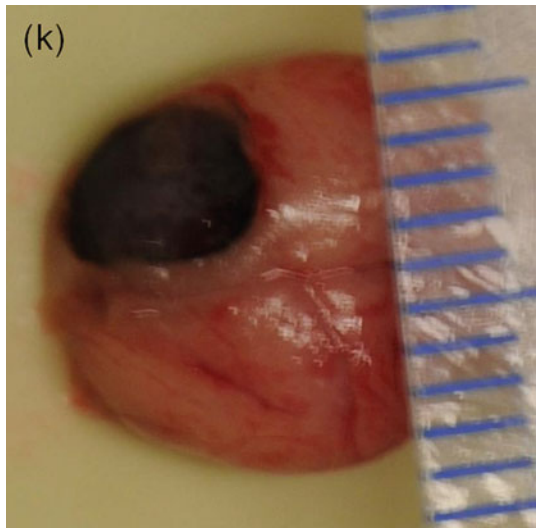

Fig. 5.3 Noninvasive MAP images of the brain melanoma in day 5 (**a**), day 8 (**b**), day 10 (**c**), day 13 (**d**), day 14 (**e**) after the injection of tumor cells, respectively. (**f**)–(**j**) The B-scan images corresponding to the *dashed line*s in (**a**)–(**e**), respectively. (**k**) Invasive anatomical photograph after the mouse death. All photoacoustic images are in the same intensity scale. M: melanoma brain tumor

demonstrated the capability of successfully detecting the growth of brain melanoma tumors in an orthotopic murine model of melanoma brain tumors. This technique has demonstrated successful evaluation of melanoma brain tumors and their response to therapy in a small animal model noninvasively and in real-time.

References

Galanzha EI, Shashkov EV, Kokoska MS, Myhill JA, Zharov VP (2008a) *In vivo* non-invasive detection of metastic melanoma in vasculature and sentinel lymph nodes by photoacoustic cytometry. Lasers Surg Med 263:81–81

Galanzha EI, Shashkov EV, Tuchin VV, Zharov VP (2008b) *In vivo* multispectral, multiparameter, photoacoustic lymph flow cytometry with natural cell focusing, label-free detection and multicolor nanoparticle probes. Cytom Part A 73A:884–894

Kienast Y, von Baumgarten L, Fuhrmann M, Klinkert WEF, Goldbrunner R, Herms J, Winkler F (2010) Real-time imaging reveals the single steps of brain metastasis formation. Nat Med 16:116–122

Ku G, Wang LHV (2005) Deeply penetrating photoacoustic tomography in biological tissues enhanced with an optical contrast agent. Opt Lett 30:507–509

Mishima Y, Imahori Y, Honda C, Hiratsuka J, Ueda S, Ido T (1997) *In vivo* diagnosis of human malignant melanoma with positron emission tomography using specific melanoma-seeking F-18-DOPA analogue. J Neuro-oncol 33:163–169

Mori Y, Kondziolka D, Flickinger JC, Kirkwood JM, Agarwala S, Lunsford LD (1998) Stereotactic radiosurgery for cerebral metastatic melanoma: factors affecting local disease control and survival. Int J Radiat Oncol Biol Phys 42: 581–589

Oh JT, Li ML, Zhang HF, Maslov K, Stoica G, Wang LHV (2006) Three-dimensional imaging of skin melanoma *in vivo* by dual-wavelength photoacoustic microscopy. J Biomed Opt 11:Article No. 034032

Olszewski WL, Tarnok A (2008) Photoacoustic listening of cells in lymphatics: research art or novel clinical noninvasive lymph test. Cytom Part A 73A:1111–1113

Panigrahy A, Bluml S (2009) Neuroimaging of pediatric brain tumors: from basic to advanced magnetic resonance imaging (MRI). J Child Neurol 24:1343–1365

Patchell RA, Tibbs PA, Walsh JW, Dempsey RJ, Maruyama Y, Kryscio RJ, Markesbery WR, Macdonald JS, Young B (1990) A randomized trial of surgery in the treatment of single metastases to the brain. N Engl J Med 322:494–500ial of surgery in the treatment of single metastases to the brain. *N. Engl. J. Med. 322*:494–500

Song KH, Wang LV (2007) Deep reflection-mode photoacoustic imaging of biological tissue. J Biomed Opt 12: Article No. 060503

Staley J, Grogan P, Samadi AK, Cui H, Cohen MS, Yang X (2010) Growth of melanoma brain tumors monitored by photoacoustic microscopy. J Biomed Opt 15: Article No. 040510

Tarhini AA, Agarwala SS (2004) Management of brain metastases, in patients with melanoma. Curr Opin Oncol 16: 161–166

Wang LV (2008a) Prospects of photoacoustic tomography. Med Phys 35:5758–5767

Wang LV (2008b) Tutorial on photoacoustic microscopy and computed tomography. IEEE J Select Topics Quantum Electron 14:171–179

Wang XD, Xie XY, Ku G, Wang LHV (2006) Noninvasive imaging of hemoglobin concentration and oxygenation in the rat brain using high-resolution photoacoustic tomography. J Biomed Opt 11: Article No. 024015

Xu MH, Wang LHV (2006) Photoacoustic imaging in biomedicine. Rev Sci Instrum 77: Article No. 041101

Xu N, Shu H, Marcus R, Crocker IR (2007) Radiation necrosis after stereotactic radiosurgery for metastatic brain disease. Int J Radiat Oncol Biol Phys 69:S163

Yang XM, Wang LV (2008) Monkey brain cortex imaging by photoacoustic tomography. J Biomed Opt 13: Article No. 044009

Yu C, Chen JCT, Apuzzo MLJ, O′Day S, Giannotta SL, Weber JS, Petrovich Z (2002) Metastatic melanoma to the brain: Prognostic factors after gamma knife radiosurgery. Int J Radiat Oncol Biol Phys 52:1277–1287

Zhang HF, Maslov K, Stoica G, Wang LHV (2006) Functional photoacoustic microscopy for high-resolution and noninvasive *in vivo* imaging. Nat Biotechnol 24:848–851

Zharov VP, Galanzha EI, Shashkov EV, Khlebtsov NG, Tuchin VV (2006) In vivo photoacoustic flow cytometry for monitoring of circulating single cancer cells and contrast agents. Opt Lett 31:3623–3625

Zharov VP, Galanzha EI, Shashkov EV, Kim JW, Khlebtsov NG, Tuchin VV (2007) Photoacoustic flow cytometry: principle and application for real-time detection of circulating single nanoparticles, pathogens, and contrast dyes *in vivo*. J Biomed Opt 12: Article No. 051503

Part III
Biomarkers and Diagnosis

Chapter 6

Extraaxial Brain Tumors: The Role of Genetic Polymorphisms

Luciana Oliveira de Almeida

Abstract Extraaxial tumors of the nervous system are extra-cerebral and often benign. Meningiomas, schwannomas and metastasis are the part of this group. The onset of a tumor occurs from the accumulation of genetic and epigenetic alterations in cells. To understand the molecular mechanism of tumor progression and metastasis formation is essential to identify the genes that accumulate these alterations. This study aimed at evaluating, through a case-control study, the influence of SNPs TP53 Pro47Ser and Arg72Pro, EGF + 61 and GSTP-1 Ile105Val on the development and prognosis of these tumors. Through the analysis of the polymorphisms Pro47Ser and Arg72Pro of the gene TP53, it was noticed that the polymorphic variant Ser47 is strongly associated with patients with extraaxial tumors and the presence of the variants Ser47 and Pro72 increase the risk of these tumors. Regarding the gene GSTP-1, it was concluded that the Val105 allele was more frequent among subjects with cancer and the presence of this allele in the population studied increased the risk of cancer in almost 6-fold. Finally, it was observed that the frequency of wild genotype G/G of the polymorphism EGF + 61 was higher among patients (particularly among those with low grade tumors) than among the control group and the presence of this allele may influence the risk of developing meningiomas, schwannomas and metastases in the subjects studied.

L.O. de Almeida (✉)
Oncogenetic Laboratory, Department of Medical Genetics, Rebeirao Preto Medical School, University of Sao Paulo, 14049-900 Ribeirao Preto, SP, Brazil
e-mail: lu_olive@yahoo.com

Keywords Extraaxial tumors · Meningiomas · Schwannomas · Val105 allele · Dermoid cysts · Epidermoid cysts

Introduction

Nervous system tumors constitute exclusive and heterogeneous populations of neoplasms including benign and malignant tumors. Although the incidence of these tumors is low compared to other cancers, tumors of the nervous system are among the most serious human malignancies, since they affect the organ responsible for coordinating and integrating all the vital activities in humans (Ohgaki and Kleihues 2005). Extraaxial tumors of the nervous system are extra-cerebral. They are often benign and their location can affect the treatment and prognosis. Meningiomas, schwannomas, metastases, dermoid and epidermoid cysts represent the vast majority of extraaxial tumors of the brain (Drevelegas 2005).

Meningiomas are the most common type of extraaxial tumors, originating in the meninges that cover the brain and spinal cord. They represent about 25% of all primary brain tumors, with an estimated annual incidence of six new cases per 100,000 subjects. However, the real incidence is probably higher since many benign meningiomas do not show the symptoms. In studies based on autopsies, 2.3% of subjects presented asymptomatic meningiomas which had not been diagnosed, suggesting that this type of tumor is more common than it is clinically detected (Lusis and Gutmann 2004).

According to the classification of nervous system tumors established by the World Health Organization

M.A. Hayat (ed.), *Tumors of the Central Nervous System, Volume 4*,
DOI 10.1007/978-94-007-1706-0_6,

(WHO), meningiomas present three grades of malignancy: benign meningiomas (Grade I), atypical meningiomas (Grade II) and anaplastic meningiomas (Grade III). About 90% of all meningiomas are benign, atypical meningiomas represent from 6 to 8% of cases and are defined histologically by an increase in the mitotic activity and a high risk of recurrence. Approximately 2–3% of meningiomas present malignant characteristics such as high mitotic activity and/or histological appearance similar to sarcomas, carcinomas or melanomas. They are associated with a poor prognosis and a survival lower than two years after the diagnosis (Wrobel et al. 2005).

Meningiomas show an increased incidence in relation to age, being more common in the sixth and seventh decade of life. Among adults, there is an incidence ratio of 3:2 between female and male, whereas in women, the annual incidence is estimated at 2.7 cases per 100,000 subjects, and among men, the incidence is 1–5 cases in 100,000. Anaplastic and atypical meningiomas are more common among men, which may be related to high rates of proliferation observed in meningiomas of male patients. In children and teenagers, meningiomas are equally rare in both genders with a tendency for developing more aggressive subtypes, usually associated with hereditary syndromes such as neurofibromatosis type 2, Gorlin syndrome and Cowden syndrome (Marosi et al. 2008).

Schwannomas (neurilemmomas or neurinomas) are benign tumors composed entirely of Schwann cells. They represent the second type of most common extraaxial tumor, constituting 5–10% of all intracranial tumors and approximately 29% of spinal tumors. Regarding its macroscopic appearance, schwannomas are typically well defined and often present a globular configuration. In small injuries, the nerve can be detected in the tumor, but in larger tumors the relationship between nerve and tumor becomes obscure. This type of tumor may develop at any age, but most frequently between 40 and 60 years there is a greater tendency for the occurrence in females in a ratio of 2:1 compared to men (Drevelegas 2005).

The presence of schwannoma is a very common feature in patients with neurofibromatosis type 2, a dominant hereditary disease with an incidence of one in 33–40 thousand subjects. It was recently discovered a new molecular and clinical syndrome distinct from NF2, observed in the onset of schwannomas, the Schwannomatosis. Patients with Schwannomatosis present multiple schwannomas. There are other rare genetic diseases in which multiple schwannomas may be present, as in Carney Complex. Based on this information, the schwannomas are classified into sporadic Schwannomas – occurring only once in a subject or schwannomas that occur multiple times in a single subject (Hanemann and Evans 2006). Genetic, chromosomal and molecular studies have provided some information on alterations related to the development of schwannomas. Schwannomas can be caused by the loss of function of the gene NF2 located in chromosome 22, responsible for encoding a protein whose product, named Merlin, is necessary for Schwann cells.

Metastases are the most feared features, more lethal and less effectively treated than a cancer can present, being also complex to be studied in detail. Studies which began in the mid-50s and are extended until the present day have shown that the process of metastatic formation depends on a sequence of uniform processes (Stafford et al. 2008). The first step required for the formation of metastasis is that cells of primary tumor detach from tumor stroma and migrate through the vascular system. These cells must survive to the transport and to blockages as the recognition of foreign cells presented by many tissues. In veins, these cells can cross the basement membrane and enter a totally unknown place. Occasionally, these cells may leave the veins, being protected from attacks of specific tissues (Rufini et al. 2007). Finally, the cells that complete all steps in the metastatic proliferation pathway colonize ectopic tissues. In recent years, this last step of the metastatic pathways, the colonization, has become the focus of several researches, since it offers the possibility to cultivate metastatic cells in a latent phase in a secondary site and then transform the place into a potential area for the development of therapeutic targets (Stafford et al. 2008).

Brain metastases are common complications in patients with systemic cancers. The tumor types most likely to expand to regions of the brain are lung, breast and melanoma. The survival of patients with brain metastases is less than one year (Chen 2007). Brain metastases are found most frequently in the supratentorial compartment, and can be calvarial, dural or leptomeningeal, and constitute the second form of the most common extraaxial cancer. Calvarial metastasis can develop in many patients with malignant tumors. Lung carcinomas, breast, liver and prostate are the most frequent primary neoplasias in which metastases

are derived. Metastases in the dural region are derived from breast, lung, prostate, melanoma and neuroblastoma tumors and less frequently from lymphomas and leukemias. Leptomeningial metastasis or meningeal carcinomatosis is usually the result of the progression of tumors of the nervous system, such as anaplastic astrocytoma, glioblastoma multiforme, ependymoma and medulloblastoma (Drevelegas 2005).

Single Nucleotide Polymorphisms

With the Human Genome Project completed, a large number of sequences located in "generic portions" of the genome is available. This fact may lead to the identification of all possible genetic variations in different human populations, as well as to associate its presence in individual phenotypes, including susceptibility to diseases and also to determine the functional impact of these variations. The most abundant source of variations in the human genome is SNPs – Single Nucleotide Polymorphisms (Suh and Vijg 2005). SNPs are substitutions of single base pairs occurring in the genomic DNA, generating different sequence alternatives (alleles) in normal subjects, and whose minimum allele frequency in the population may be 1% or greater. SNPs can be bi, tri or tetra-allelic polymorphisms, however in human populations, tri and tetra-allelic polymorphisms are rare or nonexistent.

Occurring approximately at each 500–1000 base pairs, SNPs are among the most common genetic variations. Initially, expectations were that SNPs were only a few thousand across the genome, but in the beginning of this century, the number of SNPs found increased about a thousand fold. Of the most known genes, 93% contain SNPs and 98% of these genes are at least 5 kb away from a SNP. Almost all genes are marked by one of these variable sequences (Sachidanandam et al. 2001). Because they are found throughout the genome, SNPs produce functional alleles or physiologically relevant, since in a coding region they may have an impact on the protein, in an intron they may influence the splicing mechanism and, in the promoter, they may modify the gene transcription.

Currently there is a great interest in large-scale study of SNPs which may be associated with genetic diseases, in order to be used in the pharmacogenomic research, studies on genetic populations and evolutionary biology, positional cloning and physical mapping (Smigielski et al. 2000). The association of SNPs with phenotypes of human diseases has great potential to direct clinical applications, through the discovery of novel and more specific genetic markers, for purposes of diagnosis and prognosis and possibly new therapeutic targets.

Methodology

Ninety subjects were studied and histopathological tests showed 48 meningiomas, 23 schwannomas and 19 metastasis. Sixty-eight were benign (grade I and II) and 22 malignant (grade III and IV). One hundred healthy subjects were included as control group. DNA extraction from tumor tissue and peripheral blood was performed using the phenol/chloroform technique. DNA was quantified and stored at –20°C until analysis. The primers were constructed from the genomic sequences obtained from the database SNP (dbSNP) NCBI (http://www.ncbi.nih.gov/SNP). With the target sequences, the primers were constructed with the *Gene Runner Software* (Version 3.05, Hasting Software, Inc.) to outflank the SNPs of interest and avoid the other polymorphic bases evidenced in the previous procedure. PCR was performed in a total volume of 25 μL with: 50 ng DNA, 1× buffer, 2 mM of $MgCl_2$, 0.4 μM of each primer, 50 μM of dNTPs, 0.5 U of Taq polymerase. The reaction consisted of 1 cycle at 95°C for 3 min and 35 cycles of 95°C (30 s), 54–60°C (30 s) and 72°C (30 s). The products obtained were submitted to the RFLP (*restriction fragment length polymorphisms*), incubated in the presence of enzymes Msp I, BstU I, Alu I, Pml I or BsmA I. The reactions were submitted to electrophoresis on polyacrylamide gel and stained with silver nitrate. For the statistical analysis Qui-square test, Fisher exact test, Kaplan–Meier and Log-rank test were used.

Epidermal Growth Factor (EGF) Polymorphism

The proliferative activity of cancer cells can be maintained through key mechanisms, including lack of autocrine control, which causes the cells to present

a decline in the need for exogenous growth factors. This independence is due to the ability of cancer cells to produce high levels of growth factors, and this ability depends on the activation of proto-oncogenes. Thus, the involvement of growth factors in the survival of cancer cells and in the induction of tumor proliferation through neoangiogenesis and the loss of apoptotic capacity contributes to the progression of various tumor types (Araujo et al. 2007).

The epidermal growth factor (EGF) is a member of the superfamily EGF of growth factors, which also includes TGFα, epiregulin, betacellulin and amphiregulin. EGF, like all growth factors, is related to the DNA synthesis, cell proliferation and mitogenic stimuli in epidermal tissues. EGF can induce the expression of cyclin D, a protein required for cell cycle progression, from phase G1 to S. EGF also acts as a survival factor to inhibit apoptosis and consequent promotion of tumor growth, and also along with TGFα, acts as angiogenic stimuli factor (Harari et al. 2007). As a mitogenic signal, EGF can activate DNA synthesis and cell proliferation. Thus, overexpression of EGF can increase levels of differentiation and proliferation, inhibit apoptosis and enhance the invasiveness capacity of cancer cells in several types of tumors, including nervous system tumors. It is suggested that both the expression of EGF and the cell division are regulated by the promoter of EGF. Thus, common genetic variations in the promoter region of EGF may contribute to differences in the expression of EGF and therefore to the susceptibility to diseases (Wang et al. 2008).

At present, only one polymorphism described in the EGF gene appears to be functional and it is associated with different types of tumors. Identified in 2002 by Shahbazi et al. (2002), this polymorphism is located in the region 5′UTR of the gene. It consists of a substitution of guanine (G) for adenine (A), which leads to an increase in the expression of EGF in mononuclear cells of the peripheral blood in culture. This SNP is located in 61 base pairs downstream of the EGF promoter and it was observed in 44% of the Caucasian population in Europe and in nearly 66% of patients with melanoma. Heterozygous subjects, carrying only one G allele had an increase of 2.7 fold in the susceptibility of developing melanoma compared with the homozygous population AA, in GG homozygous subjects, the increase observed was 4.9 fold (Shahbazi et al. 2002).

EGF protein is involved in nervous system development, including processes of growth, differentiation and maintenance of central nervous system. In brains of rodents, EGF production begins early in the embryonic development and after birth the expression of EGF is widely distributed throughout the brain, including brainstem, cerebral cortex, hippocampus, hypothalamus and thalamus. EGF protein is responsible for stimulating the proliferation of ectodermal and mesodermal cells besides regulating the development of neurons. Researches on the influence of EGF the human nervous system are very scarce, however, the EGF polymorphism 61G/A appears to be associated with an increase in the expression of EGF observed in biopsies of primary and secondary glioblastoma multiforme. This overexpression may be responsible for the development and progression of this type of cancer and may also be associated with increased aggressiveness of the disease (Puttonen et al. 2007).

In a case-control study, were observed significant differences in the genotypic frequencies between patients and controls ($p < 0.0001$). When compared to genotypic frequencies and gender of subjects, the G allele was more frequent in females than in males ($p = 0.021$). In relation to tumor subtypes and grade, the genotype A/A was present in metastasis ($p = 0.026$) but in low grade tumors ($p = 0.001$). People who carried G allele had 13 fold more chance to develop tumors than those who had A allele (Table 6.1). On the other hand, the survival did not affect this genotype (Fig. 6.1a).

Glutathione S-Transferase P1 (*GSTP1*) Polymorphism

The glutathione S-transferases (GSTs) constitute a superfamily of ubiquitin, multifunctional enzymes that play a fundamental role in cell detoxification of a large number of endogenous and exogenous chemicals with electrophilic functional groups. The process is performed through a combination of enzymes with a tripeptide glutathione. This reaction neutralizes the electrophilic sites of the toxins making their product more soluble in water. Additionally, these enzymes act to protect DNA against damage by mutagens (Ryberg et al. 1997).

In humans, five classes of GSTs enzymes were identified (GSTT-1, GSTM-1, GSTP-1, α and σ). Allelic

Table 6.1 EGF A61G polymorphism

		A/A (%)	G/A (%)	G/G (%)	*p*-value
Genotype and allele frequency	Case	2.3	23.3	74.4	<0.0001
	Control	23	45	32	
			G frequency	Case (0.86)	0,153
				Control (0.54)	
Gender of patients	Male	65.7	28.6	5.7	0.021
	Female	80	20	0	
Age of patients	Until 50	61.8	29.8	2.1	0.129
	Over 50	81.4	16.3	2.3	
Tumor subtype	Meningioma	75	20.8	4.2	0.026
	Schwannoma	78.3	21.7	0	
	Metastasis	68.4	31.6	0	
Tumor grade	High	54.2	29.1	16.7	0.001
	Low	75.8	21.2	3	
Cancer risk OR (95% CI)		1.0	0.18 (0.04–0.86)	24.07 (5.34–32.5)	
		p value	0.02	<0.0001	
			G frequency	13.14 (3.00–27.56)	<0.0001

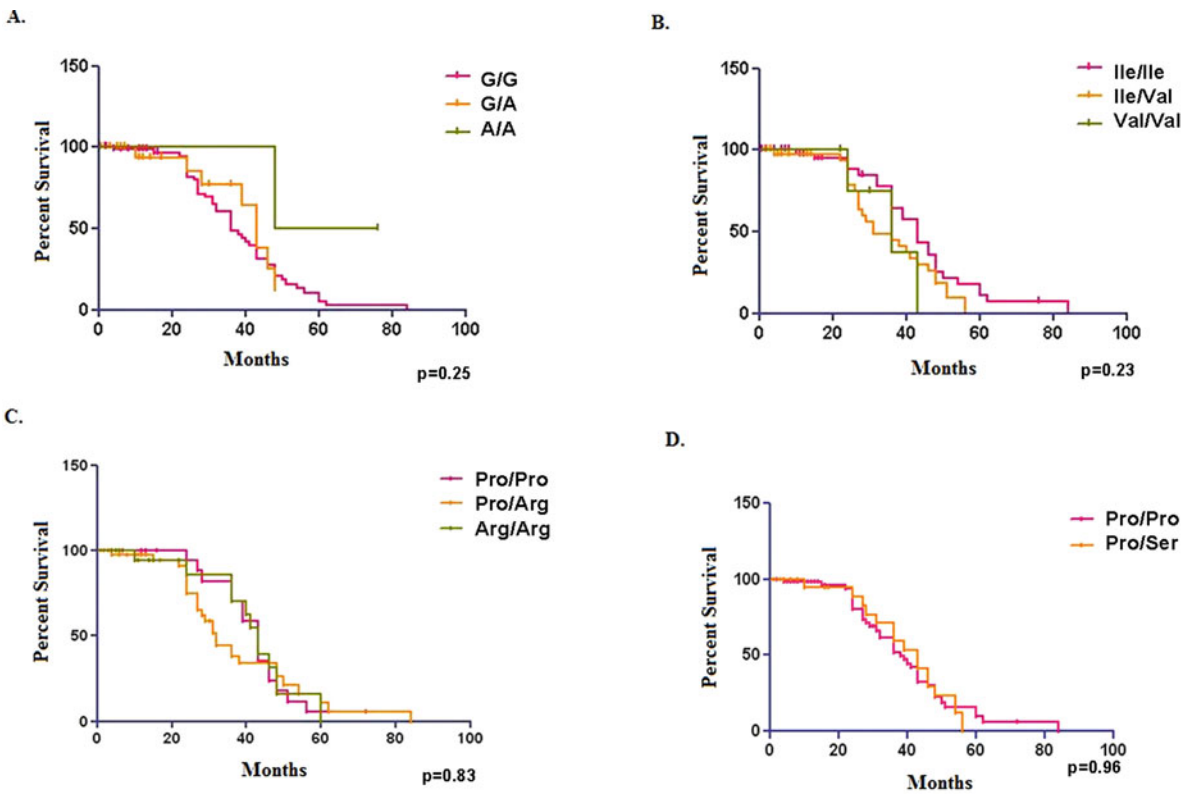

Fig. 6.1 Polymorphisms studied are not involved in the survival of patients with extraaxial brain tumors. (**a**) EGF A61G polymorphism, (**b**) GSTP-1 Ile105Val polymorphism, (**c**) TP53 Arg72Pro polymorphism and (**d**) TP53 Pro47Ser polymorphism

Table 6.2 GSTP-1 Ile105Val polymorphism

		Ile/Ile (%)	Ile/Val (%)	Val/Val (%)	*p*-value
Genotype and allele frequency	Case	53.3	41.1	5.6	<0.0001
	Control	87	13	0	
			Val frequency	Case (0.26) Control (0.07)	0,037
Gender of patients	Male	54.2	43	2.8	0.423
	Female	52.7	40	7.3	
Age of patients	Until 50	57.4	34	4.6	0.313
	Over 50	48.8	46.5	5.7	
Tumor subtype	Meningioma	50	41.7	8.3	0.042
	Schwannoma	52.2	43.5	4.3	
	Metastasis	63.1	36.9	0	
Tumor grade	High	54.2	37.5	8.3	0.637
	Low	53	42.4	4.6	
Cancer risk OR (95% CI)		1.0 *p*-value	0.19 (0.09–0.39) <0.0001	0.5 (0.02–0.93) 0.006	
			Val frequency	5.93 (2.93–11.98)	<0.0001

variants present in different genes can result in the absence or reduced efficiency of detoxification capacity, thereby increasing the susceptibility to cancer. The role of GSTs enzymes in detoxification mechanisms of carcinogenic components have led to the hypothesis that if the genotype of an individual encodes deficient levels of GSTs enzymes, or encodes a modified product that has lower affinity for its substrate, this may result in increased risk of cancer development. Polymorphisms in the genes GSTP-1, M-1 and T-1 are related to the loss or reduction of the enzymatic activity directed to important substrates, including those found in tobacco. Variations in expression and activity of GSTP-1 have been frequently associated with a large number of human tumors. GSTP-1 can metabolize and inactivate several anti-neoplastic drugs and also activate antineoplastic prodrugs. The gene product of GSTP-1 acts not only as an enzyme that metabolizes drugs, but also as a regulator of MAPKs, as a result of non-enzymatic activity (Moyer et al. 2008).

GSTP-1 has two not synonymous SNPs, resulting in genotypes Ile105Val and Ala114Val. These SNPs are associated with a variation in cancer risk and clinical response to therapy with anti-neoplastic agents. Val105 substitution results in a reduction in H site of the enzyme and, consequently, this variant can only bind to substrates less bulky than the variant Ile105 and thus, their specificity involves substrates different from those related to wild protein. Another difference among genotypes is the thermal stability. These characteristics may, in part, be responsible for the association observed among the variants and the process of carcinogenesis as well as the differences in response to antineoplastic drugs (Moyer et al. 2008).

In the present study, the Val allele ($p = 0.037$) and Val/Val genotype ($p < 0.0001$) were more frequently observed in patients than in controls. When they were grouped in the tumor subtypes, the Val allele was more frequent in the meningiomas and schwannomas ($p = 0.042$). It was not observed significant differences among genotypes and gender, age, tumor grade (Table 6.2) and survival of patients (Fig. 6.1b). In relation to the risk of cancer, subjects who showed Val allele had 6 fold more chance of developing extraaxial tumor.

TP53 Polymorphisms

TP53 gene represents one of the most studied tumor suppressor in Biology. Its product, the protein p53, is known as the "guardian of the genome", and represents a key regulator of cell growth. In response to stress signals such as genotoxic stress, hypoxia and oncogene activation, the protein p53 is stabilized after transcription. This stability can guide it through different pathways, depending on the origin of the cell or

cellular context, including cell cycle arrest, senescence or apoptosis. TP53 is the tumor suppressor gene most frequently mutated in human cancers, inactivated in 50% of tumors. In gliomas, TP53 presents mutations in 25% of cases. Somatic mutations occur mainly in astrocytomas and are less common in non-astrocytic brain tumors (Biros et al. 2002).

It is possible that the existence of natural variants of p53 may be related to the development of specific diseases, for example, by differences in the activity of these variant proteins in their pathways. Natural variants of p53 are studied in an attempt to understand their inter-individual differences in cancer risk and response to therapies. A critical region of p53 for signaling apoptosis, located between codons 64 and 92, encodes a gene region rich in proline, where there is a common polymorphism at codon 72, exon 4, in which a proline (CCC) or an arginine (CGC) originates three different genotypes: homozygous for arginine (Arg/Arg), homozygous for proline (Pro) and heterozygous (Arg/Pro). This SNP seems to affect the protein functions. The polymorphic allele arginine has an increased capacity to induce apoptosis when compared to the proline allele. This great apoptotic potential of the variant Arg appears to be related to its location in mitochondria (Hadhri-Guiga et al. 2007). It was observed that in homozygous the Arg allele has the capacity to induce apoptosis 15 fold larger than the Pro allele. Several results indicate that the Pro allele, with lower apoptotic efficiency is associated with an increased risk of tumor development.

Considering a risk factor for cancer and prognosis, there are controversies regarding this polymorphism. Some studies show that there is influence of polymorphism TP53 codon 72 on cancer risk whereas others indicate the opposite. A recent study suggested a possible association between this polymorphism and the susceptibility to high-grade adult and pediatric astrocytomas. Major research groups found an association between the variant Arg and increased risk for gastric cancer, breast, esophagus, skin, lung, and bladder. In contrast, other studies have demonstrated a relationship between the Pro allele (less apoptotic) and increased risk for other types of tumors such as thyroid, prostate, and nasopharynx (Hadhri-Guiga et al. 2007).

Analyzing extraaxial brain tumors, it was observed an increased number of patients carrier the Pro/Pro genotype ($p = 0.05$) and this genotype was more frequent in advanced age (more than 50 years old, $p = 0.011$). The presence of the Pro allele increases 3 fold the chance of tumor development (Table 6.3). However, the Pro allele is not involved in the survival of the subjects (Fig. 6.1c).

More recently, another polymorphism at codon 47 of the same exon 4 of TP53 showed also a significant decrease in the ability to induce apoptosis. The codon

Table 6.3 *TP53* Arg72Pro polymorphism

		Arg/Arg (%)	Arg/Pro(%)	Pro/Pro (%)	*p*-value
Genotype and allele frequency	Case	22.2	53.3	24.5	0.05
	Control	48	42	10	
			Pro frequency	Case (0.5)	0,385
				Control (0.31)	
Gender of patients	Male	20	51.4	28.6	0.535
	Female	23.6	54.5	21.9	
Age of patients	Until 50	29.8	44.7	25.5	0.011
	Over 50	14	62.8	23.2	
Tumor subtype	Meningioma	25	54.2	20.8	0.595
	Schwannoma	17.4	52.2	30.4	
	Metastasis	21	52.6	26.4	
Tumor grade	High	25	54.2	20.8	0.641
	Low	21.2	53	25.8	
Cancer risk		1.0	3.55 (1.82–6.94)	2.08 (0.85–5.08)	
OR (95% CI)		*p*-value	0.03	0.005	
			Pro frequency	3.23 (1.71–6.08)	0.003

Table 6.4 *TP53* Pro47Ser polymorphism

		Pro/Pro (%)	Pro/Ser(%)	*p*-value
Genotype and allele frequency	Case	73.3	26.7	0.001
	Control	99	1	
	Ser frequency		Case (0.26); Control (0.01)	<0.001
Gender of patients	Male	82.8	17.2	0.143
	Female	67.3	32.7	
Age of patients	Until 50	72.3	27.7	1.00
	Over 50	74.4	25.6	
Tumor subtype	Meningioma	79.2	20.8	0.264
	Schwannoma	60.8	39.2	
	Metastasis	73.7	26.3	
Tumor grade	High	72.7	27.3	0.748
	Low	75	25	
Cancer risk OR (95% CI)		1.0	1.28 (0.03–2.1)	
		p-value	0.01	

47 encodes proline (CCG) in p53 wild, but in a small number of subjects, it can encode serine (TCG). The polymorphic variant serine 47, which replaces the proline necessary in the recognition by kinases directed to proline, is a poor substrate for phosphorylation of p38 MAPK (Leite et al. 2006). Studies indicate that the variant Ser is a less effective substrate for phosphorylation of p38 MAPK, therefore, it presents 2–5 fold less capacity to induce apoptosis in vivo. In contrast, studies show no difference in its efficiency to bind to DNA, induce cell cycle arrest in G1 or its location in mitochondria compared to wild p53 (Li et al. 2005). In the present study, it was not found any Ser/Ser genotype carriers, although the Ser allele was frequently observed in patients ($p < 0.001$) and the presence of this allele increases in 1.28 fold the risk of extraaxial brain tumor development (Table 6.4).The survival of patients are not influenced by the Ser allele (Fig. 6.1d).

Discussion

Genes involved in tumorigenesis are considered potential molecular markers associated with susceptibility to cancer. The predisposition to important types of human cancers have been associated to genetic polymorphisms, which may present, along with other genetic changes, significant contributions to the origin and development of cancer and tumor behavior. Through a case-control study, this work aimed at investigating the relationship between single nucleotide polymorphisms *GSTP-1* Ile105V, *TP53* Pro47Ser *and* Arg72Pro and EGF+61 with and a susceptibility to extraaxial tumors of nervous system (meningiomas, schwannomas and metastases).

One of the most common polymorphisms of TP53 is located at codon 72 in exon 4, and refers to the substitution of an arginine (CGC) for a proline (CCC). It is proposed that the polymorphic variant at codon 72 introduces a potential susceptibility to the cancer development. The functional difference described in this polymorphism is that the genotype Arg/Arg induces apoptosis more efficiently than the genotype Pro/Pro. It was observed that the Pro72 allele appeared more frequently among subjects of the population who had cancer (frequency of 0.5) than among the control population (0.31). Statistical analyses suggested that the presence of Pro72 genotype can increase the risk of extraaxial tumors of the nervous system (OR = 3.23; IC = 1.71–6.08; $p = 0.003$), which may be explained by the reduced ability to induce apoptosis than the Pro allele has in comparison to the Arg allele. Biros et al. (2002) analyzed the Tp53 Arg72Pro polymorphism in meningiomas and astrocytomas, but no significant difference was observed regarding the distribution of genotype frequencies between case and control populations. Idbaih et al. (2007) studied the influence of SNP arg72Pro of TP53 on the risk of developing oligodendroglial tumors. They analyzed a group of 275 patients and found that the allele and genotype frequencies of codon 72 were similar between patients

and controls, suggesting an absence of relationship between this SNP and oligodendrogliomas.

There are few studies regarding the TP53 Pro47Ser polymorphism and susceptibility to cancer. Felley-Bosco et al. (1993) were the first group of researchers to demonstrate a significant decrease in the ability of allele Ser to induce apoptosis. Pinto et al. (2008) investigated the association between TP53 Pro47Ser polymorphism and the susceptibility to the development of gliomas, and found no association between them. Different results were obtained in this study, it was observed a significant difference in the frequency of allele Ser47 between case and control groups (0.26 and 0.01 respectively, $p < 0.001$) and also a slightly increase in the risk of developing extraaxial tumors of the nervous system between Ser47 allele carriers allele (OR = 1.28; IC = 0.03–2.10; $p = 0.01$). The process of apoptosis is essential for maintaining the balance between birth and cell death in tissues undergoing renovation, and the resistance to apoptosis is one of the most important characteristics of cancer cells, since it confers them a great power of survival and multiplication.

GSTP-1 is the family member of GSTs gene whose gene product is highly expressed in the brain. It presents a single-base polymorphism currently studied in cancer, the substitution A313G, which results in a change of amino acid Ile to Val at position 105. The substitution Ile105Val GSTP-1 is located near the substrate binding site, which can cause a reduction of enzymatic activity of GSTP-1. In this study, the genotype frequencies observed among patients were: 53.3% Ile/Ile, 41.1% Ile/Val and 5.6% Val/Val, however, significant differences were found when comparing these frequencies with those obtained in the control group: 87% Ile/Ile and 13% Ile/Val ($p < 0.0001$), and the occurrence of the polymorphic variant Val/Val was not observed among controls. Differences in allele frequencies were obseved, the frequency of Val105 was 0.26 among patients and 0.07 among controls ($p = 0.037$), suggesting that polymorphic allele Val105 may be involved in susceptibility to the development of meningiomas, schwannomas and metastasis.

There are few studies relating the GSTP-1 Ile105Val polymorphism to the risk of nervous system tumors and the results obtained are controversial. De Roos et al. (2003) analyzed 422 patients with glioma, 172 patients with meningiomas and 79 schwannomas and they observed that the presence of Val/Val genotype was associated with increased incidence of gliomas and schwannomas, and this risk increased according to the number of Val alleles (1.3-fold in Ile/Val and 2.1 fold in Val/Val). Schwartzbaum et al. (2007) analyzed 329 cases of glioblastomas and 546 meningiomas and found no association between the risk of nervous system tumors and the presence of polymorphism GSTP-1 Ile105Val. In this study, it was observed that the presence of Val105 allele is associated mainly with meningiomas ($p = 0.042$), but it showed no relation to schwannomas and metastases.

The most studied polymorphism of EGF consists of the substitution of a guanine (G) for adenine (A) in region 5′UTR of the gene. Studies indicate that this polymorphism is associated with the risk of developing some types of tumors such as melanoma, glioblastoma multiforme and gastric cancer. In glioblastoma multiforme and gastric cancer was also observed that the presence of G allele is a risk factor for carcinogenesis.

In this work it was evaluated the relationship between EGF polymorphism and the risk of developing extraaxial tumors of the nervous system. It were evaluated a total of 90 patients and 100 controls and the differences in genotype frequencies between the groups analyzed ($p < 0.0001$) were observed. Among patients, the frequencies were 74.4% for G/G, 23.3% for G/A and 2.3 for A/A, and among the control group the frequencies were 32% (G/G), 45% (G/A) and 23% (A/A), indicating that the presence of the G allele may be associated with the development of tumors. When evaluating the presence of the G allele and its association with cancer risk, it was found that G allele carriers had 13 times more chance of developing cancer ($p < 0.0001$) and, when it refers to the G/G genotype, these subjects had a chance even higher (OD = 24.07; IC= 5.34–32.50; $p < 0.0001$). A significant difference between the variants and tumor grade was also observed in which the G allele was found more frequently among patients with low grade tumors ($p = 0.001$) and the same allele was found in lower proportion in meningiomas ($p = 0.026$).

Among the nervous system tumors, EGF + 61 polymorphism is widely studied in glioblastomas, however, there are no studies relating this polymorphism to the extraaxial tumors. Vauleon et al. (2007) evaluated 209 patients with glioblastoma and 214 controls and found the presence of G/G in 21.1% of patients and 14% of controls. Costa et al. (2007) evaluated the association between EGF polymorphism + 61 and the risk

of gliomas, their results showed that the presence of the G allele confers a high risk of developing this type of tumor and the presence of G/G genotype increases in approximately 1.50 fold the risk of developing gliomas, glioblastomas and oligodendrogliomas.

In summary, genetic polymorphisms, as analyzed in this study, can influence the development and progression of extraaxial brain tumors and it might be used, in the future as tumor markers in a diversity of cancers.

Translated by Alessandra Almeida

References

Araujo A, Ribeiro R, Azevedo I, Coelho A, Soares M, Sousa B, Pinto D, Lopes C, Medeiros R, Scagliotti GV (2007) Genetic polymorphisms of the epidermal growth factor and related receptor in non-small cell lung cancer – a review of the literature. Oncologist 12:201–210

Biros E, Kalina I, Kohut A, Bogyiova E, Salagovic J, Sulla I (2002) Allelic and haplotype frequencies of the p53 polymorphisms in brain tumor patients. Physiol Res 51:59–64

Chen AM, Jahan TM, Jablons DM, Garcia J, Larson DA (2007) Risk of cerebral metastases and neurological death after pathological complete response to neoadjuvant therapy for locally advanced nonsmall-cell lung cancer: clinical implications for the subsequent management of the brain. Cancer 109:1668–1675

Costa BM, Ferreira P, Costa S, Canedo P, Oliveira P, Silva A, Pardal F, Suriano G, Machado JC, Lopes JM, Reis RM (2007) Association between functional EGF + 61 polymorphism and glioma risk. Clin Cancer Res 13:2621–2626

De Roos AJ, Rothman N, Inskip PD, Linet MS, Shapiro WR, Selker RG, Fine HA, Black PM, Pittman GS, Bell DA (2003) Genetic polymorphisms in GSTM1, -P1, -T1, and CYP2E1 and the risk of adult brain tumors. Cancer Epidemiol Biomarkers Prev 12:14–22

Drevelegas A (2005) Extra-axial brain tumors. Eur Radiol 15:453–467

Felley-Bosco E, Weston A, Cawley HM, Bennett WP, Harris CC (1993) Functional studies of a germ-line polymorphism at codon 47 within the p53 gene. Am J Hum Genet 53:752–759

Hadhri-Guiga B, Toumi N, Khabir A, Sellami-Boudawara T, Ghorbel A, Daoud J, Frikha M, Gargouri A, Mokdad-Gargouri R (2007) Proline homozygosity in codon 72 of TP53 is a factor of susceptibility to nasopharyngeal carcinoma in Tunisia. Cancer Genet Cytogenet 178:89–93

Hanemann CO, Evans DG (2006) News on the genetics, epidemiology, medical care and translational research of Schwannomas. J Neurol 253:1533–1541

Harari PM, Allen GW, Bonner JA (2007) Biology of interactions: antiepidermal growth factor receptor agents. J Clin Oncol 25:4057–4065

Idbaih A, Boisselier B, Marie Y, El Hallani S, Sanson M, Criniere E, Rodero M, Carpentier C, Paris S, Laigle-Donadey F, Ducray F, Hoang-Xuan K, Delattre JY (2007) TP53 codon 72 polymorphism, p53 expression, and 1p/19q status in oligodendroglial tumors. Cancer Genet Cytogenet 177:103–107

Leite JL, Manfrinatto JA, Mazzali M, Ward LS (2006) Polymorphisms at exon 4 of p53 and the susceptibility to herpesvirus types 6 and 1 infection in renal transplant recipients. Transpl Int 19:732–737

Li X, Dumont P, Della Pietra A, Shetler C, Murphy ME (2005) The codon 47 polymorphism in p53 is functionally significant. J Biol Chem 280:24245–24251

Lusis E, Gutmann DH (2004) Meningioma: an update. Curr Opin Neurol 17:687–692

Marosi C, Hassler M, Roessler K, Reni M, Sant M, Mazza E, Vecht C (2008) Meningioma. Crit Rev Oncol Hematol 67:153–171

Moyer AM, Salavaggione OE, Wu TY, Moon I, Eckloff BW, Hildebrandt MA, Schaid DJ, Wieben ED, Weinshilboum RM (2008) Glutathione s-transferase p1: gene sequence variation and functional genomic studies. Cancer Res 68:4791–4801

Ohgaki H, Kleihues P (2005) Epidemiology and etiology of gliomas. Acta Neuropathol 109:93–108

Pinto GR, Yoshioka FK, Clara CA, Santos MJ, Almeida JR, Burbano RR, Rey JA, Casartelli C (2008) WRN Cys1367Arg SNP is not associated with risk and prognosis of gliomas in Southeast Brazil. J Neurooncol 90:253–258

Puttonen S, Keltikangas-Jarvinen L, Elovainio M, Kivimaki M, Rontu R, Lehtimaki T (2007) Temperamental activity and epidermal growth factor A61G polymorphism in Finnish adults. Neuropsychobiology 56:208–212

Rufini V, Salvatori M, Fadda G, Pinnarelli L, Castaldi P, Maussier ML, Galli G (2007) Thyroid carcinomas with a variable insular component: prognostic significance of histopathologic patterns. Cancer 110:1209–1217

Ryberg D, Skaug V, Hewer A, Phillips DH, Harries LW, Wolf CR, Ogreid D, Ulvik A, Vu P, Haugen A (1997) Genotypes of glutathione transferase M1 and P1 and their significance for lung DNA adduct levels and cancer risk. Carcinogenesis 18:1285–1289

Sachidanandam R, Weissman D, Schmidt SC, Kakol JM, Stein LD, Marth G, Sherry S, Mullikin JC, Mortimore BJ, Willey DL, Hunt SE, Cole CG, Coggill PC, Rice CM, Ning Z, Rogers J, Bentley DR, Kwok PY, Mardis ER, Yeh RT, Schultz B, Cook L, Davenport R, Dante M, Fulton L, Hillier L, Waterston RH, Mcpherson JD, Gilman B, Schaffner S, Van Etten WJ, Reich D, Higgins J, Daly MJ, Blumenstiel B, Baldwin J, Stange-Thomann N, Zody MC, Linton L, Lander ES, Altshuler D (2001) A map of human genome sequence variation containing 1.42 million single nucleotide polymorphisms. Nature 409:928–933

Schwartzbaum JA, Ahlbom A, Lonn S, Warholm M, Rannug A, Auvinen A, Christensen HC, Henriksson R, Johansen C, Lindholm C, Malmer B, Salminen T, Schoemaker MJ, Swerdlow AJ, Feychting M (2007) An international case-control study of glutathione transferase and functionally related polymorphisms and risk of primary adult brain tumors. Cancer Epidemiol Biomarkers Prev 16:559–565

Shahbazi M, Pravica V, Nasreen N, Fakhoury H, Fryer AA, Strange RC, Hutchinson PE, Osborne JE, Lear JT, Smith AG, Hutchinson IV (2002) Association between functional polymorphism in EGF gene and malignant melanoma. Lancet 359:397–401

Smigielski EM, Sirotkin K, Ward M, Sherry ST (2000) dbSNP: a database of single nucleotide polymorphisms. Nucleic Acids Res 28:352–355

Stafford LJ, Vaidya KS, Welch DR (2008) Metastasis suppressors genes in cancer. Int J Biochem Cell Biol 40:874–891

Suh Y, Vijg J (2005) SNP discovery in associating genetic variation with human disease phenotypes. Mutat Res 573:41–53

Vauleon E, Auger N, Amiel AB, Donadey FL, Kaloshi G, Lejeune J, Delattre JY, Thillet J, Sanson M (2007) The 61 A/G EGF polymorphism is functional but is neither a prognostic marker nor a risk factor for glioblastoma. Cancer Genet Cytogenet 172:33–37

Wang Y, Tian T, Hu Z, Tang J, Wang S, Wang X, Qin J, Huo X, Gao J, Ke Q, Jin G, Ma H, Wang X, Shen H (2008) EGF promoter SNPs, plasma EGF levels and risk of breast cancer in Chinese women. Breast Cancer Res Treat 111:321–327

Wrobel G, Roerig P, Kokocinski F, Neben K, Hahn M, Reifenberger G, Lichter P (2005) Microarray-based gene expression profiling of benign, atypical and anaplastic meningiomas identifies novel genes associated with meningioma progression. Int J Cancer 114:249–256

Chapter 7

Central Nervous System Germ Cell Tumor

Takamitsu Fujimaki

Abstract Central nervous system germ cell tumors (CNSGCTs) are tumors of children and young adults. They affect mainly the pineal body, neurohypophysis ("suprasellar" area) and basal ganglia, but can arise in any other CNS location. Histologically, they are divided into germinoma and non-germinomatous germ cell tumors (NGGCTs), the latter including teratoma, embryonal carcinoma, choriocarcinoma, and yolk sac tumor. Teratomas are further subclassified into mature teratoma, immature teratoma, and teratoma with malignant transformation. Except for mature teratoma, all of these tumors are biologically malignant. Histologically, they resemble reproductive cells, fetal tissues, or related tissues such as placenta, and mixtures of these tumor subcategories are not rare. Initial symptoms include increased intracranial pressure due to obstructive hydrocephalus, abnormality of ocular movement and endocrine disorders. Some tumors of these subclasses produce humoral tumor markers, beta-human chorionic gonadotropin, alpha-fetoprotein or other markers, which can be used for differential diagnosis or clinical follow-up. Only mature teratoma can be cured with surgery alone, and the other tumors require adjuvant therapy for complete remission. Germinomas respond well to irradiation and can be cured, but platinum-based chemotherapy combined with reduced-dose irradiation has been recently used to minimize radiation-related toxicities or complications. As the other tumors cannot be cured by irradiation alone, more intensive platinum-based chemotherapy and radiation therapy including whole-neuroaxis irradiation are employed. Although better disease control and longer survival can now be achieved, the results of treatment are still not satisfactory. Therefore, development of new treatments, and improvements to existing ones, are needed for CNSGCTs.

Keywords CNSGCT · Germinoma · Teratoma · Embryonal carcinoma · Choriocarcinoma · Yolk sac tumor · Teratoma

Introduction

Central nervous system germ cell tumors (CNSGCTs) are malignant neoplasms affecting children and young adults. They show considerable histological variation and resemble germ cell tumors of the gonads or other extragonadal locations. In the Dictionary of Cancer Terms of the National Cancer Institute, the term "germ cell tumor" is used to define "a type of tumor that arises in the cells that give rise to sperm or eggs. Germ cell tumors can occur almost anywhere in the body, and can be either benign or malignant". In the CNS, these tumors arise chiefly in the pineal body, neurohypophysis ("suprasellar" area) and basal ganglia, but can affect any other area or structure.

Historically, tumors arising in the pineal region were referred to as "pinealoma" and were considered to arise from the pineal body. Tumors showing similar histology arising in other locations, especially near the pituitary gland, were called "ectopic pinealomas". Russel (1944) pointed out that these tumors resemble atypical teratoma of the testis and should be regarded as atypical teratomas. Friedman (1947) was

T. Fujimaki (✉)
Department of Neurosurgery, Saitama Medical University, Moroyama 350-0495, Japan
e-mail: tfujimak@saitama-med.ac.jp

M.A. Hayat (ed.), *Tumors of the Central Nervous System, Volume 4*,
DOI 10.1007/978-94-007-1706-0_7,

the first to call these tumors "germinoma" and considered that they arose from primordial germ cells. The terms "intracranial germ cell tumor" and "CNS germ cell tumor" have gradually been adopted since the 1970s in place of "pinealoma".

Epidemiology

The incidence of CNSGCTs is higher in Asian countries than in Europe or the United States, being 2.6% in the Japan Brain Tumor Registry, compared with 0.6% in the United States (The Committee of the Brain Tumor Registry of Japan 2009; Surawicz et al. 1999). In the pediatric population, its incidence among all intracranial neoplasms is 15% in Asian countries and 3% in Western countries.

CNSGCTs are most frequent in the second decade of life, followed in order by the first decade and the third decade. Boys are affected 2.5–3 times more frequently than girls. The pineal region is the most frequently affected site, followed by the neurohypophyseal (suprasellar) region and the basal ganglia, but these tumors can arise anywhere in the CNS including the spinal cord. Multiple locations, for example pineal and neurohypophyseal tumors, are not uncommon and tumor dissemination is also sometimes observed at the time of diagnosis. Most patients with pineal germ cell tumors are male, but both sexes are affected almost equally by neurohypophyseal (suprasellar) germ cell tumors (Matsutani et al. 1997).

Signs and Symptoms

Hydrocephalus due to compression of the aqueduct is the most common initial symptom of CNSGCTs, and approximately two thirds of affected patients present with it. Most patients with hydrocephalus show signs of increased intracranial pressure. Parinaud syndrome or upward gaze palsy is also frequent, and present in one third of the affected patients. Argyll Robertson pupils, characterized by bilateral myosis and lack of a light reflex with preservation of the accommodation reflex, is also observed (Fujimaki 2009). Visual field defect due to compression to the optic nerve has also been reported. Diabetes insipidus is often present before a diagnosis of neurohypophyseal GCT is made. Pan-hypopituitarism may also be present. Neurohypophyseal or hypothalamic GCT can cause symptoms mimicking anorexia nervosa (Berek et al. 1991). Pseudo-precocious puberty is a symptom caused by elevation of the level of hCG produced by GCTs (Fujimaki 2009). In GCT affecting the basal ganglia, hemiparesis or involuntary movements are initial symptoms, but the diagnosis may be delayed because neuroimaging features can be obscure in the initial stage (Sonoda et al. 2008) (see also Neuroimaging).

Histology and Classification

CNSGSTs have a wide variety of histological subclasses, including germinoma, embryonal carcinoma, choriocarcinoma, yolk sac tumor, and teratoma. Teratomas are further categorized into mature teratoma, immature teratoma, and teratoma with malignant transformation. Germinoma with syncytiotrophoblastic giant cells is a variant of germinoma (germinoma with STGC). Often CNSGCTs show a mixed histology comprising the aforementioned subcategories, and pure forms are relatively rare except for germinomas (Table 7.1). These tumors are considered to mimic elements of fetal and related tissues (Fujimaki 2009).

Germinomas show typical histological patterns, being similar to seminoma of the testis or dysgerminoma of the ovary. They are composed of two cell types: large polygonal or round cells with clear cytoplasm, round nuclei and clear nucleoli, and lymphocytes. The stroma may show a desmoplastic response. This histological appearance is known as the "two-cell

Table 7.1 Histological classification of central nervous system germ cell tumors

Germinoma
Germinoma with syncytiotrophoblastic giant cells (STGCs)
Embryonal carcinoma
Choriocarcinoma
Yolk sac tumor
Teratoma
Mature teratoma
Immature teratoma
Teratoma with malignant transformation

Table 7.2 Tumor markers used for immunohistochemistry

	Alpha-FP	hCG	Placental alkaline phosphatase	c-kit	CD30
Germinoma	−	−	+	+	−
Germinoma with STGC	−	+[a]	+	+	−
Embryonal carcinoma	−	−	+	+	+
Choriocarcinoma	−	+	±	−	−
Yolk sac tumor	+	−	±	−	−
Teratoma	+	−	−	−	−

[a]STGC cells.

pattern" (Sano et al. 1989). Germinoma with STGC contains large multinucleated cells with irregular cytoplasmic extensions resembling syncytiotrophoblasts. These cells are immunohistochemically positive for beta-hCG. Some investigators consider that these tumors show more aggressive clinical behavior than usual germinomas, but the true clinical significance of this germinoma variant is still not clear.

Embryonal carcinomas contain pleomorphic immature cells, forming sheet-like, papillary or tubular patterns. These cells sometimes resemble the large cells of germinoma. Choriocarcinomas are composed of cytotrophoblast-like and syncytiotrophoblast-like cells. Yolk sac tumors mimic endoderm of the yolk sac. They are composed of ovoid or flat cells with relatively small nuclei, forming a sinusoidal pattern and sometimes containing glomerulus-like structures known as "Schiller-Duval bodies".

Teratomas contain all three of the tridermic elements, i.e., cutaneous tissues or less frequently brain-like tissues as ectodermal elements, fatty tissue, cartilaginous tissue or muscle-like structures as mesodermic elements, and alimentary tract-like tissue or bronchus-like tissue as endodermic elements. Immature teratoma or teratoma with malignant transformation contains immature tissues or malignant elements, like those of sarcoma or adenocarcinoma (Rosenblum et al. 2007).

Tumor Markers

Some germ cell tumors produce tumor markers that can be helpful for differentiating the histological types. Typically, choriocarcinoma produces the beta subunit of human chorionic gonadotropin (beta-hCG), and yolk sac tumor produces alpha-fetoprotein. Germinoma with STGC also produces beta-hCG, although its level is usually <100 mIU/ml, whereas in choriocarcinoma it is >500 mIU/ml (Fujimaki 2009).

The serum levels of tumor markers are useful for differential diagnosis, monitoring the response to treatment, or detection of recurrence. Moreover, the level of beta-hCG in CSF is usually higher than that in serum, and is a sensitive marker for monitoring the clinical status of GCTs. Recently, it has been pointed out that very low but measurable levels of beta-hCG are also produced by usual germinoma (Katakami et al. 2003). Other than the aforementioned markers in body fluid, some proteins, such as placental alkaline phosphatase, c-kit or CD 30, are used for immunohistochemical differentiation of germ cell tumors (Table 7.2).

Neuroimaging

Differential diagnosis of pineal masses is limited. CNSGCT is the most probable diagnosis (Fig. 7.1), but rarer pineal parenchymal tumors such as pineocytoma or pineoblastoma need to be differentiated. For neurohypophyseal tumors, differential diagnosis includes craniopharyngioma, pituitary adenoma, pilocytic astrocytoma, or rarer lesions such as Langerhans cell histiocytosis. However, because the first three aforementioned tumors show a characteristic pattern, a possible diagnosis of "neurohypophyseal germ cell tumor" is not difficult. Basal ganglia germ cell tumors are invasive and sometimes difficult to diagnose initially because they are poorly enhanced with gadolinium (Sonoda et al. 2008). Ipsilateral hemispheric or peduncular atrophy has also been reported at locations for this tumor. Pineal tumors are usually accompanied by hydrocephalus. On CT scan, germinomas appear as relatively homogeneous masses with slightly high to high density, and sometimes with small cysts. The margins are somewhat obscure, and a calcified area may

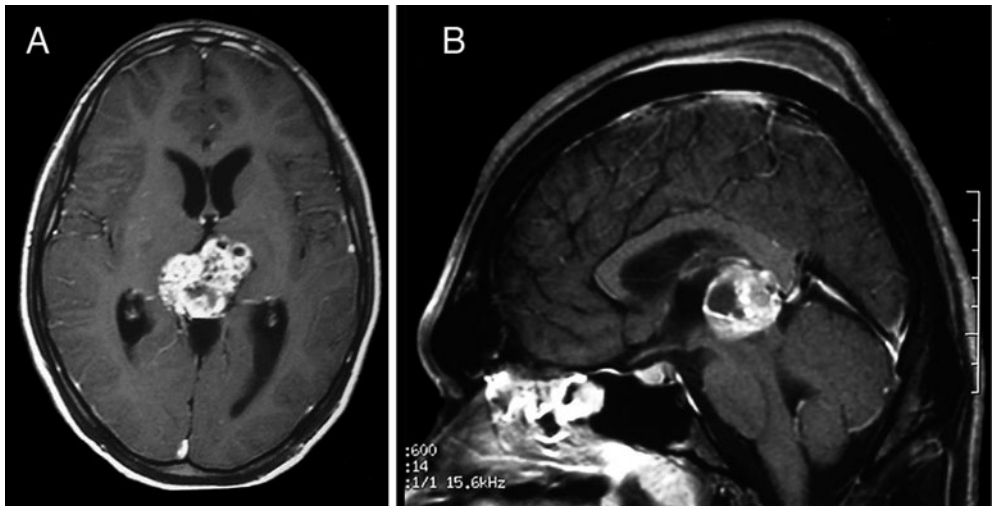

Fig. 7.1 (**a**) Gadolinium enhanced axial MR image of 14-year-old boy with pineal immature teratoma. (**b**) Gadolinium enhanced sagittal MR image of 18-year-old boy with pineal germinoma

be present, although this is not very large. On MRI images, germinomas show a clearer border with T1 low and T2 high signal intensity. Teratomas present as a heterogenous mass with a clear margin on both CT and MRI scans. They may contain fatty tissues, cysts or calcifications and show a characteristic pattern. Other subtypes, or mixed germ cell tumor, are difficult to diagnose on the basis of neuroimaging alone, but speculative diagnoses are possible with the aid of humoral tumor markers (Fujimaki et al. 1994; Fujimaki 2009). Differential diagnosis between pineal germ cell tumor and pineal parenchymal tumor is not easy, but if a tumor shows expansion to the cisternal space dorsal and caudal to the quadrigeminal plate, it may be a pineal parenchymal tumor.

Treatment

All CNSGCTs except for mature teratomas are malignant tumors requiring adjuvant radiation and/or chemotherapy. However, responsiveness to such adjuvant therapies varies among the histological subclasses, and the treatment strategy thus varies accordingly. To establish a diagnosis, surgery is the first step. Following advances in modern neurosurgery, biopsy or partial removal of a CNSGST can be done safely in most cases by an experienced neurosurgeon. Endoscopic biopsy at the time of third ventriculostomy to treat obstructive hydrocephalus provides another opportunity to acquire histological samples, but it has been reported that although samples obtained in this way are adequate for germinomas, they are not satisfactory for non-germinomatous GCTs (Luther et al. 2006). Instead of taking histological samples, provisional diagnosis can be made for tumors associated with a very high titer of beta-hCG (2000 mIU/ml or more, choriocarcinoma) or alpha-fetoprotein (2000 ng/ml or more, yolk sac tumor), and adjuvant therapy can be started (Kochi et al. 2003).

Hereafter the basic concepts for treatment strategies will be described for three groups: mature teratoma, germinoma, and non-germinomatous GCT.

Mature Teratoma

Mature teratomas are benign tumors that can be cured by surgery alone. However, except for true congenital teratomatous tumors of the newborn, pure mature teratomas are rare, and most are immature teratomas or teratomas with malignant transformation. Mixed histology with other germ cell tumors is also frequent. Treatments for these tumors are described later.

Germinoma

Germinomas respond well to radiation treatment, and long-term survival can be expected after radiation treatment alone. Pineal germinomas are often associated with increased intracranial pressure due to hydrocephalus, and affected patients can be well managed by ventriculo-peritoneal shunt followed by radiation therapy. Irradiation with a dose of 45–60 Gy, ranging from the involved field to the whole brain, can achieve long-term remission in many patients (Jennings et al. 1985). However, this radiation dose can cause late sequelae such as hypopituitarism, stenosis of major vessels including the intracranial carotid artery, or development of secondary tumors or cavernous malformations. Cognitive dysfunction as a long-term complication has also been reported.

In the 1980s, after the establishment of platinum-based chemotherapy for gonadal germ cell tumors, chemotherapy for intracranial germinomas was also introduced. Good responses were reported, but the recurrence rate was higher than that for radiation therapy (Yoshida et al. 1993; Kellie et al. 2004). Accordingly, a combination of irradiation and chemotherapy has since been employed for germinomas to reduce side effects (radiation) or enhance treatment efficacy (chemotherapy). The Japanese Pediatric Brain Tumor Study Group conducted a multi-institutional clinical study using this approach. After confirmation of the histological diagnosis, patients were given carboplatin-etoposide or cisplatin-etoposide combination chemotherapy followed by involved field irradiation with a dose of 24 Gy (Matsutani 2001). The 5-year overall and progression-free survival rates were 97.5 and 84.7%, respectively (Matsutani 2010). Silvani et al. (2005) treated germinoma patients with cisplatin-vinblastine and bleomycin followed by 30 Gy (germinoma) and 35 Gy (germinoma with STGC) of radiation to the tumor site, and reported a 48-month survival rate of 89.2%. Khatua et al. (2010) treated germinoma patients with carboplatin-etoposide chemotherapy followed by whole-ventricular irradiation to 21.6–25.5 Gy and a primary site boost to 30–30.6 Gy. The 3-year overall survival and event-free survival rates were 100 and 89.5%, respectively, with preserved cognitive function. Similar results were reported from a Korean group, but they stated that the recurrence rate was higher than for whole-neuroaxis irradiation. However, in that study, most of the chemo-radiation group received irradiation to the primary site, and not to the whole ventricle (Eom et al. 2008). Recurrence in the ventricular wall beyond the irradiation field has also been reported by the Japanese group (Matsutani 2010). It seems important to cover the whole ventricular system if chemotherapy followed by radiation is planned. For the basal ganglia, the planned irradiation field should certainly be wider.

For the management of hydrocephalus, endoscopic third ventriculostomy (ETV) has also been employed recently, and this allows endoscopic biopsy of pineal tumors to be done at the same time. If the tumor is a germinoma, endoscopic biopsy yields enough material for histological diagnosis (Luther et al. 2006).

There is some argument regarding the radiation field that should be used for germinomas. Because cerebrospinal fluid cytology is sometimes positive in germinoma patients, some have argued that they require whole-neuroaxis irradiation (Maity et al. 2004). However, many authors have stated that tumor control can be achieved by whole-ventricular-field irradiation alone (Shikama et al. 2005). This issue is still being debated among clinicians and investigators.

Non-germinomatous Germ Cell Tumor

These tumors include embryonal carcinoma, choriocarcinoma, yolk sac tumor, immature teratoma, teratoma with malignant transformation, and tumors showing a mixture of these histologic types. Unlike germinoma, the results of radiation therapy alone for these tumors have not been satisfactory, most patients dying within 2 years (Jennings et al. 1985). Spinal dissemination is also not rare. Therefore, various combinations of intensified radiation and chemotherapy have been tried for this type of tumor. The Japanese study group have tried ICE (ifosfamide-cisplatin-etoposide) chemotherapy and whole-neuroaxis irradiation followed by maintenance chemotherapy for embryonal carcinoma, choriocarcinoma, yolk sac tumor and their histologic mixtures (Matsutani 2001). The 5-year survival rate for this highly malignant group was 60%. The German Cooperative Trial of "protocol MAKEI89" for non-germinomatous germ cell tumors involved cisplatin-based chemotherapy and

craniospinal irradiation, and a 5-year event-free survival of 59% was reported (Calaminus et al. 2004). Using intensified cisplatin-based chemotherapy followed by neuroaxis and local boost irradiation, the Children's Oncology Group reported that 11 of 14 patients with non-germinomatous germ cell tumors were progression-free after a median follow-up period of 58 months (Kretschmar et al. 2007). Thus, although intensified chemo-radiotherapy seems to be effective for non-germinomatous germ cell tumors, the results are still less than ideal, since the disease control rate is still insufficient and the side effects and treatment- or disease-related sequelae are still problematic. An optimal treatment strategy for these patients has not yet been established.

In conclusion, the biology, responsiveness to treatment, and prognosis of CNSGCTs vary according to their histological class. Although recent advances in treatment have resulted in better disease control and survival of CNSGCT patients, overall survival is still less than satisfactory for some subcategories, aside from treatment side effects, recurrences and late sequelae. Methods for achieving earlier diagnosis, less invasive treatment and better management should be developed.

References

Berek K, Aichner F, Schmutzhard E, Kofler M, Langmayr F, Gerstenbrand F (1991) Intracranial germ cell tumor mimicking anorexia nervosa. Klin Wochenschr 69:440–442

Calaminus G, Bamberg M, Jurgens H, Kortmann RD., Sorensen N, Wiestler OD, Gobel U (2004) Impact of surgery, chemotherapy and irradiation on long term outcome of intracranial malignant non-germinomatous germ cell tumors: results of the German Cooperative Trial MAKEI 89. Klin Padiatr 216:141–149

Eom KY, Kim IH, Park CI, Kim HJ, Kim JH, Kim K, Kim SK, Wang KC, Cho BG, Jung HW, Heo DS, Kang HJ, Shin HY, Ahn HS (2008) Upfront chemotherapy and involved-field radiotherapy results in more relapses than extended radiotherapy for intracranial germinomas: modification in radiotherapy volume might be needed. Int J Radiat Oncol Biol Phys 71:667–671

Friedman NB (1947) Germinoma of the pineal; its identity with germinoma (seminoma) of the testis. Cancer Res 7:363–368

Fujimaki T (2009) Central nervous system germ cell tumors: classification, clinical features, and treatment with a historical overview. J Child Neurol 24:1439–1445

Fujimaki T, Matsutani M, Funada N, Kirino T, Takakura K, Nakamura O, Tamura A, Sano K (1994) CT and MRI features of intracranial germ cell tumors. J Neurooncol 19:217–226

Jennings MT, Gelman R, Hochberg F (1985) Intracranial germ-cell tumors: natural history and pathogenesis. J Neurosurg 63:155–167

Katakami H, Hashida S, Yamaguchi H, Yazawa S, Nakano S, Wakisaka S (2003) Central nervous system germ cell tumor, diagnosis and clinical course: development of ultrasensitive HCG-beta measurement and clinical application. Nippon Naibunpi Gakkai Zasshi 79(Suppl):58–60

Kellie SJ, Boyce H, Dunkel IJ, Diez B, Rosenblum M, Brualdi L, Finlay JL (2004) Intensive cisplatin and cyclophosphamide-based chemotherapy without radiotherapy for intracranial germinomas: failure of a primary chemotherapy approach. Pediatr Blood Cancer 43:126–133

Khatua S, Dhall G, O'Neil S, Jubran R, Villablance JG, Marachelian A, Nastia A, Lavey R, Olch AJ, Gonzalez I, Gilles F, Nelson M, Panigrahy A, McComb G, Krieger M, Fan J, Sposto R, Finlay J (2010) Treatment of primary CNS germinomatous germ cell tumors with chemotherapy prior to reduced dose whole ventricular and local boost irradiation. Pediatr Blood Cancer 55:42–46

Kochi M, Itoyama Y, Shiraishi S, Kitamura I, Marubayashi T, Ushio Y (2003) Successful treatment of intracranial nongerminomatous malignant germ cell tumors by administering neoadjuvant chemotherapy and radiotherapy before excision of residual tumors. J Neurosurg 99:106–114

Kretschmar C, Kleinberg L, Greenberg M, Burger P, Holmes E, Wharam M (2007) Pre-radiation chemotherapy with response-based radiation therapy in children with central nervous system germ cell tumors: a report from the Children's Oncology Group. Pediatr Blood Cancer 48:285–291

Luther N, Edgar MA, Dunkel IJ, Souweidane MM (2006) Correlation of endoscopic biopsy with tumor marker status in primary intracranial germ cell tumors. J Neurooncol 79:45–50

Maity A, Shu HK, Janss A, Belasco JB, Rorke L, Phillips PC, Sutton LN, Goldwein JW (2004) Craniospinal radiation in the treatment of biopsy-proven intracranial germinomas: twenty-five years' experience in a single center. Int J Radiat Oncol Biol Phys 58:1165–1170

Matsutani M (2001) Combined chemotherapy and radiation therapy for CNS germ cell tumors – the Japanese experience. J Neurooncol 54:311–316

Matsutani M (2010) Long-term follow-up of germinomas treated by ventricular irradiation with 24 Gy and concurrently administered carboplatin and etoposide chemotherapy. Neuro-oncology 12(6):ii28

Matsutani M, Sano K, Takakura K, Fujimaki T, Nakamura O, Funata N, Seto T (1997) Primary intracranial germ cell tumors: a clinical analysis of 153 histologically verified cases. J Neurosurg 86:446–455

Rosenblum M, Nakazato Y, Matsutani M (2007) CNS germ cell tumors. In: Luis D (ed) WHO classification of tumours of the central nervous system, 4th edn. International Agency for Research on Cancer, Lyon, 197–204

Russel DS (1944) The pinealoma: its relationship to teratoma. J Pathol Bacteriol 56:145–150

Sano K, Matsutani M, Seto T (1989) So-called intracranial germ cell tumours: personal experiences and a theory of their pathogenesis. Neurol Res 11:118–126

Shikama N, Ogawa K, Tanaka S, Toita T, Nakamura K, Uno T, Ohnishi H, Itami J, Tada T, Saeki N (2005) Lack of benefit of spinal irradiation in the primary treatment of intracranial germinoma: a multi-institutional, retrospective review of 180 patients. Cancer 104:126–134

Silvani A, Eoli M, Salmaggi A, Lamperti E, Fariselli L, Milanesi I, Broggi G, Solero CL, Giombini S, Boiardi A (2005) Combined chemotherapy and radiotherapy for intracranial germinomas in adult patients: a single-institution study. J Neurooncol 71:271–276

Sonoda Y, Kumabe T, Sugiyama S, Kanamori M, Yamashita Y, Saito S, Ariga H, Takai Y, Tominaga T (2008) Germ cell tumors in the basal ganglia: problems of early diagnosis and treatment. J Neurosurg Pediatr 2:118–124

Surawicz TS, McCarthy BJ, Kupelian V, Jukich PJ, Bruner JM, Davis FG (1999) Descriptive epidemiology of primary brain and CNS tumors: results from the Central Brain Tumor Registry of the United States, 1990–1994. Neuro-Oncology 1:14–25

The Committee of the Brain Tumor Registry of Japan (2009) Report of Brain Tumor Registry of Japan. Neurol Med Chir (Tokyo) 46(Suppl):5

Yoshida J, Sugita K, Kobayashi T, Takakura K, Shitara N, Matsutani M, Tanaka R, Nagai H, Yamada H, Yamashita J (1993) Prognosis of intracranial germ cell tumours: effectiveness of chemotherapy with cisplatin and etoposide (CDDP and VP-16). Acta Neurochir (Wien) 120: 111–117

Chapter 8

Microvascular Gene Changes in Malignant Brain Tumors

Matthew L. Dashnaw, Kevin A. Walter, and Eleanor B. Carson-Walter

Abstract Glioblastoma multiforme (GBM) is the most common primary brain tumor, and is associated with very poor survival. GBMs are known to elicit a strong angiogenic response from the host central nervous system (CNS) as they grow. As in other forms of cancer, this microvascular network delivers nutrients to the proliferating tumor and represents an attractive therapeutic target to impede tumorigenesis. In the CNS, however, the importance of the vascular network as a mediator of tumor morbidity and mortality is even more significant. Abnormal microvessels induced by the growing tumor lack a functional blood brain barrier, give rise to vasogenic edema and are prone to intracranial hemorrhage. Much work has been done to delineate the biochemical factors such as VEGF, PDGF, SF/HGF and others, responsible for inducing microvascular proliferation. Now, molecular studies using modern techniques for gene expression analysis have begun to determine the downstream changes induced in the microvascular endothelial cells themselves. Identification of the novel proteins specifically expressed by the tumor microvasculature promises to reveal additional targets that may one day be exploited for anti-angiogenic based therapies.

Keywords Glioblastoma multiforme · Brain tumor · Tumorigenesis · Intracranial hemorrhage · Microvasculature · Blood brain barrier

E.B. Carson-Walter (✉)
Department of Neurosurgery, University of Rochester, Rochester, NY 14642, USA
e-mail: Eleanor_carson-walter@urmc.rochester.edu

Introduction

GBMs account for approximately 60–70% of malignant gliomas. Despite optimal treatment, the median survival of affected patients is only 12–15 months. The GBM microvascular structure is markedly abnormal when compared to that of normal brain due to tumor specific angiogenic and vasculogenic processes. These microvascular changes directly contribute to the pathologic, imaging, and clinical characteristics of these tumors. Much work has been done to attempt to elucidate the mechanisms responsible for these microvascular changes. In particular, various pro-angiogenic factors have been identified and multiple clinical trials are currently underway that aim to block the signaling between these tumor factors and their endothelial cell targets. However, while these approaches are promising, there has been a paucity of data regarding the differences induced in the target endothelium itself. Now, endothelial specific studies of gene expression using techniques such as Serial Analysis of Gene Expression (SAGE) and gene microarrays have identified genes specifically expressed by glioma associated endothelial cells as compared to normal brain endothelial cells and raise the possibility that the proteins encoded by these genes represent novel therapeutic targets.

Microvasculature of Normal Brain – The Blood Brain Barrier

Within the CNS, the blood brain barrier (BBB) serves as an essential interface between the CNS and the peripheral circulatory system and functions as

M.A. Hayat (ed.), *Tumors of the Central Nervous System, Volume 4*,
DOI 10.1007/978-94-007-1706-0_8,

a dynamic regulator of ion balance, a facilitator of nutrient transport, and a barrier to potentially harmful molecules. A detailed discussion of BBB biology is beyond the scope of this chapter. In brief, the BBB exists primarily as a selective diffusion barrier at the level of the cerebral microvascular endothelium, characterized by the presence of tight cell–cell junctions and a lack of fenestrations. Attached at irregular intervals to the abluminal membrane of the endothelium are pericytes. Pericytes and endothelial cells are ensheathed by the basal lamina, a membrane 30–40-nm thick composed of collagen type IV, heparin sulfate proteoglycans, laminin, fibronectin, and other extracellular matrix proteins. The basal lamina is contiguous with the plasma membranes of astrocyte end-feet, which surround the cerebral capillaries.

Angiogenesis in Malignant Glioma

Formation of new blood vessels occurs by one of three methods: angiogenesis, vasculogenesis, or arteriogenesis. Angiogenesis is the formation of new blood vessels by rerouting or remodeling of existing ones, and is believed to be the primary method of vessel formation in malignant gliomas. The hypothesis that tumor growth is angiogenesis dependent was first proposed in 1971 (Folkman 1971). Sufficient exchange of nutrients and waste can be achieved by diffusion if tumor cells are situated within about 100 μm of blood vessels. Growth of tumors beyond this limit necessitates the recruitment of a new blood supply and consequently leads to the emergence of an angiogenic phenotype.

The fundamental stages of angiogenesis are well understood and can be summarized by the following steps. (1) Angiogenesis is initiated by breakdown of the existing blood vessels via degradation of the extracellular matrix (ECM). This allows for migration of endothelial cells and formation of new blood vessels by placement and alignment of endothelial cells via tubular morphogenesis and formation of a lumen (2). (3) Maturation of the vessel wall begins with the recruitment of pericytes and/or smooth muscle cells, which assemble along the endothelial cells outside the new vessel to stabilize it. (4) The process concludes with the formation of new basement membrane.

A histological examination of glioma tissues demonstrates that the tumor blood vessels are usually structurally and functionally different from vessels in the adjacent normal brain tissue. Malignant glioma vasculature is disorganized, tortuous, dilated, leaky, and hemorrhagic, often displaying dead-end structures. This abnormal new vasculature contributes to the peritumoral edema associated with malignant gliomas, as well as the contrast enhancement characteristic of malignant glioma on neuroimaging.

Initiation of Angiogenesis in Malignant Glioma

Angiogenesis in malignant gliomas is tightly regulated by the dynamic balance of pro- and anti-angiogenic factors. When the expression of pro-angiogenic molecules is balanced with that of anti-angiogenic molecules, angiogenesis does not take place. Most normal physiologic angiogenesis occurs only during embryonic development, wound healing or in naturally regenerating tissues such as the corpus luteum. During tumor angiogenesis, the tight regulation of the balance of expression of these molecules is disrupted and the resultant unregulated expression of pro-angiogenic molecules leads to uncontrolled and disorganized promotion of vessel proliferation.

Angiogenesis is believed to be triggered by low oxygen concentrations (hypoxia) resulting from deficits in the blood supply caused by the tumor's fast growth, or as a result of genetic alterations. In the setting of clinical hypoxia, glioma cells first accumulate around existing cerebral blood vessels and lift off the astrocytic foot processes, leading to the disruption of the normal contact between endothelial cells and the basement membrane. Affected endothelial cells express angiopoietin-2 (Ang-2) resulting in destabilization of the vessel wall and decreased pericyte coverage. Subsequently, these blood vessels become apoptotic and undergo involution. This vascular collapse leads to the death of neighboring tumor cells and the formation of a necrotic area. Exposure of brain tumor cells to hypoxia induces expression of hypoxia-inducible factor-1 (HIF-1α), a transcription factor that activates the transcription of VEGF and other proangiogenic factors in gliomas.

Mediators of Angiogenesis in Malignant Glioma

Much work has been done to identify the different growth factors and cytokines that are able to induce angiogenesis and trigger microvascular gene alterations in tumors. In addition, some of these proteins are upregulated in the tumor endothelium itself in addition to the surrounding tumor cells.

Vascular Endothelial Growth Factor (VEGF)

Over the past 20 years a large body of evidence has accumulated to support the role of the VEGF family of growth factors and their receptors as the most important mediators of tumor, including glioma, angiogenesis. The VEGF family includes six glycoproteins referred to as VEGF-A, VEGF-B, VEGF-C, VEGF-D, VEGF-E, and placental growth factor, which mediate their effects via several different receptors. VEGF-A (or $VEGF_{165}$) and its receptors are the best characterized signaling pathway in angiogenesis. In vivo, VEGF expression has been demonstrated to be temporally and spatially associated with key events in physiologic vasculogenesis and angiogenesis including endothelial cell proliferation, permeability, invasion, migration, survival and activation. It is generally agreed that VEGFR-2 (also known as KDR in humans) is the major receptor mediating the mitogenic, angiogenic and permeability-enhancing effects of VEGF-A.

The biological effects of VEGF are mediated through diverse signaling pathways. Through the Ras/mitogen-activated protein kinase (MAPK) signaling cascade, VEGF promotes endothelial proliferation, enhances vascular permeability and mediates endothelial migration. The phosphatidylinositol-3′ kinase (PI3K)/Akt is also of central importance in VEGF signaling. Activated VEGFR-2 mediates the phosphorylation of Akt, which potently inhibits endothelial cell apoptosis by interfering with downstream apoptotic signaling pathways. Akt also promotes endothelial cell migration and increases the expression of HIF-1α, contributing to a positive feedback loop of enhanced VEGF expression (Morales-Ruiz et al. 2000). Activation of endothelial nitric oxide synthase (eNOS) by Akt leads to the production of nitric oxide, which in turn promotes endothelial cell survival proliferation, migration and ECM remodeling. Among other effects, VEGF stimulates endothelial production of urokinase plasminogen activator (uPA), tissue-type plasminogen activator (tPA) and plasminogen activator inhibitor-1 (PAI-1). Plasminogen activators induce the conversion of plasminogen to plasmin, which breaks down ECM components, directly contributing to ECM remodeling.

Angiopoietins

Angiopoietin-1 (Ang-1) and Ang-2 are important endothelial growth factors implicated in glioma angiogenesis that signal via the Tie2 receptor tyrosine kinase (RTK) expressed on endothelial cells. Blood vessel stabilization, remodeling and maturation are mediated by Ang-1 activation of Tie-2. Ang-1 is also involved with enhanced endothelial cell survival, migration, and vessel sprouting by various mechanisms (Wong et al. 2009).

Ang-2 can act as an antagonist to Tie2 phosphorylation, which leads to destabilization of blood vessels and thus represents a checkpoint on Ang-1/Tie2-mediated angiogenesis. However, the biological effect of Ang-2 may depend on VEGF level. In the presence of endogenous VEGF, Ang-2 promotes vessel dilatation, remodeling of the basal lamina, proliferation and migration of endothelial cells, and stimulates sprouting of new blood vessels. In the absence of VEGF activity, Ang-2 becomes anti-angiogenic by promoting endothelial cell death and the regression of vessels.

Fibroblast Growth Factor (FGF)

Binding of FGF to its receptor causes transphosphorylation and activation of intrinsic tyrosine kinase, which results in signal transduction (Wong et al. 2009). Both acidic FGF (αFGF) and basic FGF (βFGF) are upregulated in GBM. These factors have an anti-apoptotic effect on endothelial cells and can induce proliferation and migration of the endothelium. Furthermore, FGF activation leads to remodeling of ECM and degradation of the basement membrane by inducing production of

plasminogen activator, collagenase and matrix metalloproteinases (MMPs) in endothelial cells.

Platelet-Derived Growth Factor β (PDGF-β)

PDGF-β and platelet-derived growth factor receptor β (PDGFRβ) have important roles in the development and differentiation of the vessel wall. PDGF-β is required for recruitment of pericytes and maturation of the microvasculature. The angiogenic effects of PDGF are mediated through PI3K/Akt, MAPK/ERK and STAT3 signaling (Sun et al. 2005). PDGF-β can also induce the expression of VEGF (Reinmuth et al. 2001).

Transforming Growth Factor-β (TGF-β)

In malignant gliomas, TGF-β and its receptors are highly expressed in areas of vascular hyperplasia and around necrotic regions. TGF-β induces endothelial production of PDGF-α and PDGF-β and promotes angiogenesis via the integrin signaling pathway (Dunn et al. 2000). TGF-β up regulates expression of αVβ3 integrin that, in turn, binds to MMP-2, which leads to degradation of the ECM and enhanced endothelial cell invasion (Platten et al. 2001).

Epidermal Growth Factor/Transforming Growth Factor-α

EGF and TGF-α are potent mitogenic factors for endothelial cells mediated by binding to the epidermal growth factor receptor (EGFR). EGFR and TGF-α are frequently expressed specifically on tumor endothelial cells (Maxwell et al. 1991). EGF also stimulates VEGF production in glioma cells. Furthermore, the constitutively active EGFR mutant, EGFRvIII, induces VEGF expression through Ras/MAPK and NF-kB signaling.

Scatter Factor/Hepatocyte Growth Factor (SF/HGF)

Expression of SF/HGF and its receptor c-MET is increased in both tumour and endothelial cells in GBM specimens. An autocrine or paracrine loop is believed to exist between glioma and endothelial cells, contributing to tumour progression and angiogenesis (Kunkel et al. 2001). Higher levels of SF/HGF correlate significantly with angiogenic activity in malignant glioma.

Interleukin-6 (IL-6) and Interleukin-8 (IL-8)

IL-6 and IL-8 are produced by gliomas and their expression correlates with the malignant behaviors in these tumors (Brat et al. 2005; Rolhion et al. 2001). IL-6 induces transcriptional activation of VEGF and regulates VEGF promoter activity (Loeffler et al. 2005).

IL-8 stimulates angiogenesis via the interaction with the C-X-C chemokine receptor 1 (CXCR1), CXCR2 and Duffy antigen receptor for cytokines (DARC) (Brat et al. 2005; Rolhion et al. 2001). IL-8 expression is upregulated during hypoxia in glioblastomas likely an independent inducer of endothelial cell tubular formation.

Tumour Necrosis Factor-α (TNF-α)

TNF-α is a potent inflammatory cytokine that is found in malignant gliomas. The TNF-α receptor (TNFR) is expressed by glioma and glioma endothelial cells (Chambaut-Guerin et al. 2000). TNF-α induces tumor angiogenesis indirectly via the activation of other angiogenic factors, including VEGF. In addition, TNF-α enhances VEGF, IL-8 and βFGF production by human microvascular endothelial cells and induces tubular morphogenesis in vitro.

Insulin-Like Growth Factor-1 (IGF-1)

Work by Hirano et al. (1999), suggests an association between microvascular proliferation and IGF-1 expression in glioma cells. This work showed that IGF-1 immunoreactivity is more intense in the tumor cells surrounding microvascular hyperplasia and in reactive astrocytes at the margins of tumor infiltration. In addition, glioma-associated endothelial cells are also immunopositive for IGF-1.

Neurotrophins

Signaling by neurotrophins and their receptors supports neuronal proliferation, differentiation and synapse formation. The neurotrophin family consists of four structurally related proteins: nerve growth factor (NGF), brain-derived neurotrophin factor (BDNF), neurotrophin-3 and neurotrophin-4. In addition to their neuronal effects, NGF and BDNF enhance endothelial cell survival and proliferation (Nico et al. 2008). NGF and BDNF bind primarily to the receptor kinases TrkA and TrkB, respectively, to mediate their effects.

Matrix Metalloproteinases (MMP)

The MMP family consists of four groups according to their substrates: collagenases, gelatinases, stromelysins and membrane associated MMP. MMPs are involved in the proteolytic degradation of ECM components and facilitate cell motility during invasion and angiogenesis. Gelatinases-A (MMP-2) and gelatinases-B (MMP-9) are highly expressed in astrocytomas and their levels correlate with histological grade. MMP-2 and MMP-9 proteolytically cleave and activate latent TGF-β, and promote angiogenesis (Yu and Stamenkovic 2000).

Gene Expression in Glioma Endothelial Cells

The endothelial cell response to tumor cell influence is clearly an important facet of GBM malignant progression. Targeting the tumor endothelial cells is likely to have several advantages over conventional cytotoxic approaches aimed at the tumor cells themselves. Endothelial cells are easily accessible via the bloodstream, obviating many of the pharmacokinetic difficulties associated with targeting the tumor cells. Second, each endothelial cell supports the growth of multiple surrounding tumor cells, so there is likely to be a significant bystander effect. Third, studies have shown that although the mutations that drive tumorigenesis are diverse, the vascular alterations associated with brain tumor progression are relatively conserved, suggesting that endothelial targeted therapy may be applicable to both primary and secondary, metastatic brain tumors (Liu et al. 2010). With these advantages in mind, there have been significant advances in the understanding of tumor associated endothelial cells. Genomic studies of glioma endothelial cell specific transcription have been completed using techniques including SAGE and laser capture based gene microarray analysis (Madden et al. 2004; Beaty et al. 2007; Pen et al. 2007). Endothelial cell gene expression patterns from glioma and nonneoplastic brain tissue have revealed distinct gene expression patterns and consistent up-regulation of certain glioma endothelial genes (Madden et al. 2004; Beaty et al. 2007; Pen et al. 2007). Of these genes, many encode cell surface proteins that hold particular promise for facilitating both therapeutic and diagnostic targeting.

Plasmalemmal Vesicle Associated Protein-1 (PLVAP)

Madden et al. (2004) identified PLVAP (also known as PV-1) as an upregulated endothelial gene transcript in malignant glioma using SAGE. PLVAP was one of 21 unique genes that were significantly induced in the microvasculature of high grade malignant glioma as compared to non-neoplastic brain vessels. PLVAP encodes a transmembrane protein that is associated with the caveolae of fenestrated microvascular endothelial cells and likely contributes to transendothelial transport. It is normally expressed in the lung, liver, kidney, and immature brain of rodents. However, intracerebral expression of PLVAP is silenced during normal differentiation of the blood–brain barrier, where transendothelial transport is inhibited. PV-1 expression, normally silenced in non-neoplastic human brain, is dramatically upregulated in highly vascularized, human malignant brain tumors in vivo and can be stimulated by VEGF in microvascular endothelial cells in vitro (Carson-Walter et al. 2005). Downregulation of PLVAP via PLVAP targeted siRNA, decreases endothelial tubule formation (Carson-Walter et al. 2005). Tumor-specific vascular induction of this protein is conserved in pre-clinical mouse models and it is hypothesized that this protein may play a functional role in BBB disruption, transendothelial trafficking and remodeling seen in malignant gliomas (Shue et al. 2008). A recent report demonstrated the ability of the anti-PLVAP antibody, MECA-32, to block leukocyte migration in vivo using a murine model of acute

peritonitis, suggesting that blocking PLVAP in brain tumor models via antibody mediated mechanisms may be blunt BBB leakiness as well (Keuschnigg et al. 2009).

Endosialin

Endosialin, also known as CD248 or tumor endothelial marker 1 (TEM1), was originally identified and characterized by St. Croix and colleagues in an analysis of genes specifically expressed by the tumor microvasculature of human colon carcinomas and murine tumor xenografts (St. Croix et al. 2000; Carson-Walter et al. 2001). Madden and coworkers further found that endosialin was specifically induced in the microvasculature of GBM (Madden et al. 2004). Since then multiple studies have confirmed its induction in malignant brain tumors (Brady et al. 2004; Simonavicius et al. 2008; Carson-Walter et al. 2009). Endosialin encodes a cell surface protein with significant structural homology to the thrombomodulin-like family of C-lectin domain proteins. However, the absence of endosialin from normal mature vessels differentiates it from thrombomodulin and its exact function remains unknown. When human GBM xenografts were implanted in endosialin KO mice, the resultant tumors had significantly increased numbers of vessels, suggesting that endosialin may play a role in the maturation or pruning of the proliferating microvasculature (Nanda et al. 2006; Carson-Walter et al. 2009). Interestingly, conflicting reports have suggested that endosialin is expressed by tumor pericytes, a subset of vascular leukocytes (CD45+ VE-cadherin+P1H12+CD34+CD31+TEM1+TEM7+ leukocytes), bone marrow derived mesenchymal stem cells and endothelial precursor cells, all of which may contribute to abnormal tumor vessels (Simonavicius et al. 2008; Bagley et al. 2009). All considered, targeting endosialin, perhaps via an antibody-toxin conjugate, may represent an attractive strategy for GBM therapy.

Chemokine (CXC Motif) Receptor 7 (CXCR7)

CXCR7 was another gene identified by SAGE analysis of GBM endothelium (Madden et al. 2004). Originally named RDC1, it was long classified as an orphan receptor. It is now known to serve as a receptor, along with CXCR4, for chemokine (CXC motif) ligand 12/stromal cell derived growth factor 1 (CXCL12/SDF-1) and CXCL11/interferon-inducible T cell alpha chemoattractant (I-TAC) (Burns et al. 2006). Upregulation of CXCR7 in both tumor and vasculature of aggressive primary and secondary brain tumors has since been confirmed by several groups (Liu et al. 2010; Hattermann et al. 2010). Though the function of CXCR7 in glioma progression and angiogenesis is unclear, it appears to physically cycle between the cell surface and the cytoplasm and may serve as a sink for the sequestration of CXCL12, mediate anti-apoptotic effects and potentially promote neural progenitor cell survival (Nauman et al. 2010; Hattermann et al. 2010; Bakondi et al. 2010). Structurally, CXCR7 is a G-protein coupled receptor, one of a family of proteins that has proven highly amenable to targeted drug development and, encouragingly, small molecular inhibitors of CXCR7 have already been reported (Burns et al. 2006).

Plexin Domain Containing 1 (PLXDC1)

PLXDC1 was identified in a separate SAGE-based genome-wide expression screen of glioblastoma endothelium (Beaty et al. 2007). Beaty and colleagues compared gene expression in glioma endothelial cells to normal brain endothelial cells and then further subtracted transcripts from blood cells and additional normal tissues. These analyses resulted in three gene transcripts, ANAPC10, CYP27B1 and PLXDC1, which were highly specific to GBM endothelial cells. Tumor vessel specific overexpression of the PLXDC1 protein was confirmed by immunohistochemistry. PLXDC1, also known as TEM7, likely encodes a type I transmembrane protein expressed on the endothelial cell surface, rendering it highly accessible to molecular targeting (Carson-Walter et al. 2001). While its exact function is unknown, it appears to interact and bind to components of the ECM, including the proteins cortactin and nidogen (Nanda et al. 2004; Lee et al. 2006). This interaction contributes directly to endothelial cell morphogenesis into microvessels. The identification PLXDC1 as well as potential ligands for the protein provides new opportunities for the design and delivery of therapeutic or imaging agents to GBMs.

Insulin-Like Growth Factor Binding Protein-7 (IGFBP7)

Pen et al. (2007) identified IGFBP7 in microarray study of laser-captured glioblastoma vessels as a selective marker of GBM vessels. IGFBP7 is a cell-adhesive glycoprotein with structural homology to insulin-like growth factor binding proteins but with lower binding affinity to IGF than other IGFBPs. The immunohistochemical analyses by Pen et al. (2007) suggest that IGFBP7 is produced by GBM endothelial cells and secreted into the ECM where it likely interacts with other components of the basal lamina and forms protein deposits that separate the vascular and parenchymal strands of the basement membrane. IGFBP7 could feasibly play a role in new vessel stabilization in GBM and targeting of IGFBP7 might promote tumor vessel regression. Interestingly, IGFBP7 has also been shown to stimulate endothelial production of the potent vasodilator PGI2 (Hata et al. 2000), which may contribute to the increased permeability of GBM vessels. In this case, therapeutic blockade of IGFBP7 function may be beneficial to the treatment of vasogenic edema and increased intracranial pressure.

Conclusion

There continues to be substantial excitement surrounding the promise of vascular-targeted therapies for the treatment of malignant brain tumors. In order to achieve improved clinical outcomes, however, it is critical to understand the biology of the tumor endothelial cells. Signaling pathways involving VEGF and other pro-angiogenic factors stimulate and maintain newly formed brain tumor blood vessels. But, while capable of supporting continued tumor growth, these immature vessels are structurally and functionally abnormal. Modern techniques for gene expression analysis provide the methods to identify new gene products that are associated with and/or contribute to the biology of this aberrant tumor endothelium and will provide unique targets for anti-angiogenic and anti-vascular therapies, as well as proteins that may prove to be useful diagnostic or imaging agents. Furthermore, insight into the genetic alterations induced in the tumor microvasculature will facilitate a better molecular understanding of the mechanisms of neoplastic progression, vasogenic edema and increased intracranial pressure characteristic of malignant brain tumors. Ultimately, these approaches will lead to a more complete comprehension of brain tumor angiogenesis and the development of rationally designed therapies for the treatment of CNS neoplasia.

References

Bagley RG, Weber W, Rouleau C, Yao M, Honma N, Kataoka S, Ishida I, Roberts BL, Teicher BA (2009) Human mesenchymal stem cells from bone marrow express tumor endothelial and stromal markers. Int J Oncol 34:619–627

Bakondi B, Shimada IS, Peterson BM, Spees JL (2010) Stromal-derived factor 1 alpha secreted by human CD133-derived multipotent stromal cells promotes neural progenitor cell survival through CXCR7. Stem Cells Dev Nov. 9 [Epub ahead of print]

Beaty RM, Edwards JB, Boon K, Siu IM, Conway JE, Riggins GJ (2007) PLXDC1 (TEM7) is identified in a genome-wide expression screen of glioblastoma endothelium. J Neurooncol 81:241–248

Brady J, Neal J, Sadakar N, Gasque P (2004) Human endosialin (tumor endothelial marker 1) is abundantly expressed in highly malignant and invasive brain tumors. J Neuropathol Exp Neurol 63:1274–1283

Brat DJ, Bellail AC, Van Meir EG (2005) The role of interleukin-8 and its receptors in gliomagenesis and tumoral angiogenesis. Neuro-oncology 7:122–133

Burns JM, Summers BC, Wang Y, Melikian A, Berahovich, R, Miao Z, Penfold ME, Sunshine MJ, Littman DR, Kuo CJ, Wei K, McMaster BE, Wright K, Howard MC, Schall TJ (2006) The novel chemokine receptor for SDF-1 and I-TAC involved in cell survival, cell adhesion and tumor development. J Exp Med 203:2201–2213

Carson-Walter EB, Hampton J, Shue E, Geynisman DM, Pillai PK, Sathanoori R, Madden SL, Hamilton RL, Walter KA (2005) Plasmalemmal vesicle associated protein-1 is a novel marker implicated in brain tumor angiogenesis. Clin Cancer Res 12:2649–2650

Carson-Walter EB, Watkins DN, Nanda A, Vogelstein B, Kinzler KW, St. Croix B (2001) Cell surface tumor endothelial markers are conserved in mice and humans. Cancer Res 61:6649–6655

Carson-Walter EB, Winans BN, Whiteman MC, Liu Y, Jarvela S, Haapasalo H, Tyler BM, Huso DL, Johnson MD, Walter KA (2009) Characterization of TEM1/endosialin in human and murine brain tumors. BMC Cancer 9:417

Chambaut-Guerin AM, Costa SL, Lefrancois T, Fages C, Gauthereau X, Tardy M (2000) Effects of retinoic acid and tumor necrosis factor alpha on GL-15 glioblastoma cells. Neuroreport 11:389–93

Dunn IF, Heese O, Black PM (2000) Growth factors in glioma angiogenesis: FGFs, PDGF, EGF, and TGFs. J Neurooncol 50:121–137

Folkman J (1971) Tumor angiogenesis: therapeutic implications. N Engl J Med 285:1182–1186.

Hata Y, Clermont A, Yamauchi T, Pierce EA, Suzuma I, Kagokawa H, Yoshikawa H, Robinson GS, Ishibashi T, Hashimoto T, Umeda F, Bursell SE, Aiello LP (2000) Retinal expression, regulation, and functional bioactivity of prostacyclin-stimulating factor. J Clin Invest 106:541–550

Hattermann K, Held-Feindt J, Lucius R, Muerkoster SS, Penfold ME, Schall TJ, Mentlein R (2010) The chemokine receptor CXCR7 is highly expressed in human glioma cells and mediates antiapoptotic effects. Cancer Res 70:3299–3308

Hirano H, Lopes MB, Laws ER Jr, Asakura T, Goto M, Carpenter JE, Karns LR, VandenBerg SR (1999) Insulin-like growth factor-1 content and pattern of expression correlates with histopathologic grade in diffusely infiltraing astrocytomas. Neuro Oncol 1:109–119

Keuschnigg J, Henttinen T, Auvinen K, Karikoski M, Salmi M, Jalkanen S (2009) The prototype endothelial marker PAL-E is a leukocyte trafficking molecule. Blood 114:478–484

Kunkel P, Muller S, Schirmacher P, Stavrou D, Fillbrandt R, Westphal M, Lamszus K (2001) Expression and localization of scatter factor/hepatocyte growth factor in human astrocytomas. Neuro-oncology 3:82–88

Lee HK, Seo IA, Park HK, Park HT (2006) Identification of the basement membrane protein nidogen as a candidate ligand for tumor endothelial marker 7 in vitro and in vivo. FEBS Lett 580:2253–2257

Liu Y, Carson-Walter EB, Cooper A, Winans BN, Johnson MD, Walter KA (2010) Vascular gene expression patterns are conserved in primary and metastatic brain tumors. J Neurooncol 99:13–24

Loeffler S, Fayard B, Weis J, Weissenberger J (2005) Interleukin-6 induces transcriptional activation of vascular endothelial growth factor (VEGF) in astrocytes in vivo and regulates VEGF promoter activity in glioblastoma cells via direct interaction between STAT3 and Sp1. Int J Cancer 115:202–213

Madden SL, Cook BP, Nacht M, Weber WD, Callahan MR, Jiang Y, Dufault MR, Zhang X, Zhang W, Walter-Yohrling J, Rouleau C, Akmaev VR, Wang CJ, Cao X, St. Martin TB, Roberts BL, Teicher BA, Klinger KW, Stan RV, Lucey B, Carson-Walter EB, Laterra J, Walter KA (2004) Vascular gene expression in nonneoplastic and malignant brain. Am J Pathol 165:601–608

Maxwell M, Naber SP, Wolfe HJ, Hadely-Whyte ET, Galanopoulos T, Neville-Golden J, Antoniades HN (1991) Expression of angiogenic growth factor genes in primary human astrocytomas may contribute to their growth and progression. Cancer Res 51:1345–1351

Morales-Ruiz M, Fulton D, Sowa G, Languino LR, Fujio Y, Walsh K, Sessa WC (2000) Vascular endothelial growth factor stimulated actin reorganization and migration of endothelial cells is regulated via the serine/threonine kinase Akt Circ Res 86:892–896

Nanda A, Buckhaults P, Seaman S, Agrawal N, Boutin P, Shankara S, Nacht M, Teicher B, Stampfl J, Singh S, Vogelstein B, Kinzler KW, St. Croix B (2004) Identification of a binding partner for the endothelial cell surface proteins tem7 and tem7r. Cancer Res 64:8507–8511

Nanda A, Karim B, Peng Z, Liu G, Qiu, W, Gan C, Vogelstein B, St. Croix B, Kinzler KW, Huso DL (2006) Tumor endothelial marker 1 (Tem1) functions in the growth and progression of abdominal tumors. Proc Natl Acad Sci USA 103: 3351–3356

Naumann U, Cameroni E, Pruenster M, Mahabaleshwar H, Raz E, Zerwes HG, Rot A, Thelen M (2010) CXCR7 functions as a scavenger for CXCL12 and CXCL11. PLoS One 5:e9175

Nico B, Mangieri D, Benagiano V, Crivellato E, Ribatti D (2008) Nerve growth factor as an angiogenic factor. Microvasc Res 75:135–141

Pen A, Moreno MJ, Martin J, Stanimirovic DB (2007) Molecular markers of extracellular matrix remodeling in glioblastoma vessels: microarray study of laser-captured glioblastoma vessels. Glia 55:559–572

Platten M, Wick W, Weller M (2001) Malignant glioma biology: role for TGF-beta in growth, motility, angiogenesis, and immune escape. Microsc Res Tech 52:401–410

Reinmuth N, Liu W, Jung YD, Ahmad SA, Shaheen RM, Fan F, Bucana CD, McMahon G, Gallick GE, Ellis LM (2001) Induction of VEGF in perivascular cells defines a potential paracrine mechanism for endothelial cell survival. FASEB J 15:1239–1241

Rolhion C, Penault-Llorca F, Kemeny JL, Lemaire JJ, Jullien C, Labit-Bouvier C, Finat-Duclos F, Verrelle P (2001) Interleukin-6 overexpression as a marker of malignancy in human gliomas. J Neurosurg 94:97–101

Shue EH, Carson-Walter EB, Liu Y, Winans BN, Ali ZS, Chen J, Walter KA (2008) Plasmalemmal vesicle associated protein-1 (PV-1) is a marker of blood-brain barrier disruption in rodent models. BMC Neurosci 9:29

Simonavicius N, Robertson D, Bax DA, Jones C, Huijbers IJ, Isacke CM (2008) Endosialin (CD248) is a marker of tumor-associated pericytes in high-grade glioma. Mod Pathol 21:308–315

St. Croix B, Rago C, Velculescu V, Traverso G, Romans KE, Montgomery E, Lal A, Riggins GJ, Lengauer C, Vogelstein B, Kinzler KW (2000) Genes expressed in human tumor endothelium. Science 289:1997–1202

Sun J, Wang DA, Jain RK, Carie A, Paquette S, Ennis E, Blaskovich MA, Baldini L, Coppola D, Hamilton AD, Sebti SM (2005) Inhibiting angiogenesis and tumorigenesis by a synthetic molecule that blocks binding of both VEGF and PDGF to their receptors. Oncogene 24:4701–4709

Wong ML, Prawira A, Kaye AH, Hovens CM (2009) Tumour angiogenesis: its mechanism and therapeutic implications in malignant gliomas. J Clin Neurosci 16:1119–1130

Yu Q and Stamenkovic I (2000) Cell surface-localized metrix metalloproteinase-9 proteolytically activates TGF-beta and promotes tumor invasion and angiogenesis. Genes Dev 14:163–176

Chapter 9

Role of MicroRNA in Glioma

Yongping You, Ning Liu, Chunsheng Kang, Peiyu Pu, and Zhen Fu

Abstract Gliomas are the most common type of malignant primary brain tumors. Despite the advances in surgery, radiation therapy, and chemotherapy, the prognosis of patients with gliomas has not improved significantly. MicroRNAs (miRNAs) are a class of 21–25 nucleotide long, non-coding RNAs that negatively regulate the expression of target genes by interacting with specific sites of mRNA. They control a wide array of biological processes, including cell differentiation, proliferation, and apoptosis. Recent studies show that miRNAs are aberrant expressed in gliomas and play a critical role in the development of gliomas, indicating a novel way to investigate the tumorigenesis, diagnosis and therapy of gliomas. Here we focus on recent findings of miRNA study in gliomas to emphasize the important and new highlights of miRNA involved in gliomas.

Keywords miRNA · Glioma · Brain tumors · Tumorigenesis · Gliomagenesis · Genome

Introduction

We are in the beginning of a new era in glioma research that started with the identification of a novel category of genes, the microRNAs (miRNAs). Regarding the history of these novel genes we can briefly mention that the important function of miRNAs was not known until the miRNA (let-7) was identified in a variety of organisms such as *C. elegans*, and most importantly in humans (Reinhart et al. 2000; Takamizawa et al. 2004). Since that time, miRNA-related research has become one of the most challenging fields in biomedical science and more than 1000 miRNAs have been identified and being added in miRNA databases. MiRNAs are short noncoding RNA located in noncoding regions or the introns of the genome, and regulate gene expression by interaction with complementary target sites in mRNAs. MiRNAs have been implicated in various biological processes including developmental timing, patterning and embryogenesis, differentiation and organogenesis, immune response, growth control and apoptosis. Each type of cell is likely to have a specific miRNA milieu to control gene expression. And each miRNA has the potential to regulate about 200 target genes according to recent computational predictions. Extensive studies have indicated that the alerted miRNA profile is identified in kinds of human disease. MiRNA expression signatures have been used to classify human disease and define miRNA markers that might predict a favorable prognosis.

MiRNA Process

MiRNAs are generated by a multistep process. The biogenesis of miRNAs involves a complex protein system, including members of the Argonaute family, Pol II-dependent transcription and the RNase IIIs Drosha and Dicer (Kim and Nam 2006). The primary miRNA transcripts (pri-miRNAs) are transcribed from the genome by RNA polymerase α, folding into a stem-loop structure which is essential for the maturation

Y. You (✉)
Department of Neurosurgery, The First Affiliated Hospital of Nanjing Medical University, Nanjing 210029, China
e-mail: Ypl9@njmu.edu.cn

M.A. Hayat (ed.), *Tumors of the Central Nervous System, Volume 4*,
DOI 10.1007/978-94-007-1706-0_9,

process. In animals, the pri-miRNAs are then cleaved by Drosha, in association with DGCR8/Pasha (Denli et al. 2004). The cleaving site is near the base of the stem-loop (Lee et al. 2003), generating the precursor miRNAs (pre-miRNAs). Then, pre-miRNAs are transported to cytoplasm by the RNA GTP-dependent transporter exportin 5.

In the cytoplasm, pre-miRNA is recognized by Dicer, and TAR RNA-binding protein (TRBP/TARBP2). Dicer cleaves pre-miRNA, generating a 21–25 nucleotide mature miRNA duplex. Generally, only one strand is selected as the biologically active mature miRNA and the other strand is degraded. The mature miRNA ultimately gets integrated into the RNA-induced silence complex(RISC), which is a trimeric complex composed Dicer, TRBP and a protein of the Argonaute superfamily (Ago2 in humans) (Gregory et al. 2005).

MiRNA-Mediated Gene Expression

In the canonical mode, miRNAs negatively regulate gene expression by base-pairing to target mRNAs with the miRNA 5′-proximal "seed" region (positions 2–8). Mature miRNAs allow RISC to recognize the mRNA 3′untranslated region (3′UTR) through the sequence complementarity with it in two ways, (1) perfect complementarity, followed by mRNA degradation; (2) imperfect complementarity, blockading mRNA translation. More recently, it has been demonstrated that miRNAs also can regulate target mRNAs by binding to coding sequence (CDS) region. Qin et al. (2010) showed that miR-24 can regulate human FAF1 (hFAF1) expression through binding to the CDS region of hFAF1 mRNA. All of them lead to the target gene repression at the post-transcriptional level. In addition, Tan et al. (2009) have reported that miR-10a targets a homologous DNA region in the promoter region of the hoxd4 gene and represses its expression, indicating that miRNA can inhibit gene expression in a novel transcriptional manner by binding the promoter region of the target. In the non-canonical mode, miRNAs can enhance gene expression through base-pairing to the mRNA 5′UTR. Tsai et al. (2009) found that miR-346 targets the 5′UTR of receptor-interacting protein 140 (RIP140) mRNA and up-regulates its protein expression.

Mirna Involvement in Glioma

An increasing body of literature has identified that a group of miRNAs are dysregulated in gliomas and involved in modulation of glioma development. The first study about miRNA expression profile of gliomas, reported by Ciafre work team (2005), found that some microRNAs were significantly altered in both glioblastoma tissues and glioblastoma cell lines using microarray, including up-regulated miR-21, miR-22, and down-regulated miR-181a and miR-181b, et al (Ciafre et al. 2005). In recent years, more and more researchers have been attracted to explore the biological significance of miRNAs in glioma progression. Here, we summarized the special expressed miRNAs identified from other independent expression profiling studies in gliomas (Table 9.1) (Godlewski et al. 2008; Guessous et al. 2010; Jiang et al. 2010; Kefas et al. 2010; Silber et al. 2008). Several altered miRNAs that have been characterized with regard to their biological function and mechanism in gliomagenesis are discussed in the following sections.

MiR-21

MiR-21, one of the most common up-regulated miRNAs, has been identified a key oncogenic miRNAs in gliomagenesis. Compared to normal brain tissue, miR-21 expression was seven to eleven folds in low grade astrocytomas, anaplastic astrocytomas and glioblastomas (Conti et al. 2009). Our and other studies confirmed overexpression of this miRNA in gliomas, indicating a critical role of miR-21 in glioma progression using miRNA oligonucleotide arrays, Northern blot and quantitative RT-PCR. In the first study exploring miR-21 function in gliomas, Chan et al. (2005) demonstrated that knockdown of miR-21 in cultured glioblastoma cell lines triggered the caspase activation and associated apoptotic cell death. Our recent data showed that reduction of miR-21 led to caspase 9 and 3 mediated mitochondrial apoptosis in glioma cell (Zhou et al. 2010b). Further study showed that miR-21 repressed p53-mediated apoptosis in response to chemotherapeutic agents such as doxorubicin and induced DNA damage, contributing to drug resistance in glioblastoma cells (Papagiannakopoulos et al. 2008). Knockdown of miR-21 enhanced the

Table 9.1 Special expressed miRNAs in glioma

Up-regulation				Down-regulation					
miRNA	Chrom.	miRNA	Chrom.	miRNA	Chrom.	miRNA	Chrom.	miRNA	Chrom.
miR-123	1	miR-210	11	miR-101	1	miR-29b	7	miR-299	14
miR-10b	2	miR-16	13	miR-137	1	miR-129	7	miR-323	14
miR-26a	3	miR-21	17	miR-181a	1	miR-124	8	miR-190	15
miR-425	3	miR-451	17	miR-181b	1	miR-7	9	miR-328	16
miR-9-2	5	miR-516-3p	19	miR-128-1	2	miR-31	10	miR-132	17
miR-25	7	miR-519d	19	miR-149	2	miR-511-1	11	miR-133a	18
miR-383	8	miR-125b-2	21	miR-153	2	miR-139	11	miR-187	18
miR-486	8	miR-155	21	miR-128-2	3	miR-483	13	miR-181c	19
miR-107	10	miR-185	22	miR-138	3	miR-17-92	14	miR-330	19
miR-125b-1	11	miR-221	X	miR-218	4	miR-154	14	miR-185	22
miR-130a	11	miR-222	X	miR-133b	6	miR-203		miR-326	11
miR-182	7			miR-34a	1				

chemo-sensitivity of human glioblastoma cells to taxol by inhibiting STAT3 expression and phosphorylation (Ren et al. 2010). In addition, miR-21 also promoted glioma cell migration and invasion by activating MMPs (Gabriely et al. 2008). These studies suggest that targeting miR-21 have a great therapeutic opportunity in glioblastomas.

Update, emerging studies have confirmed that miR-21 negatively regulates some specific targets which function as tumor suppressors, to modulate glioma pathogenesis. (1) PDCD4 (Programmed cell death 4): Chen et al. (2008) identified that reducing miR-21 increases PDCD4 and over-expression of miR-21 inhibits PDCD4-dependent apoptosis by targeting PDCD4 3′UTR in glioma cells. (2) PTEN: Zhou et al. (2010a) identified PTEN as a target of miR-21 in gliomas. Further, compared response of U251 (PTEN mutant) and LN229 (PTEN wild) cells to miR-21 antisense, similar growth and EGFR/Akt signal inhibitory in both of them by MTT assay, suggested that miR-21 could regulate EGFR/Akt pathway in a PTEN-independent manner, however, it would warrant further investigation. (3) LRRFIP1: Li et al. (2009b) revealed that miR-21 contributed to VM-26 resistance through depression LRRFIP1 (an inhibitor of NF-kappaB signaling), leading to the reduction of the cytotoxicity of chemotherapy drugs. (4) RECK and TIMP-3: miR-21 regulated MMP activities by targeting MMP inhibitors RECK and TIMP-3 to contributing glioma malignant phenotype (Gabriely et al. 2008). Other targets of miR-21 validated in other cancers included TPM1 (Zhu et al. 2007), FasL (Sayed et al. 2010) and MARCKS (Li et al. 2009a).

Regulation of miR-21 expression involves upstream factors that modulate miRNA biological process to affect levels of mature miRNAs, especially transcriptional regulatory. Computational analysis has identified several conserved enhancer elements were found in the consensus sequence upstream of the transcription start site of the pri-miR-21, including Foxo3a, STAT3, activator protein-1, CAAT/enhancer-binding protein-α and p53. Direct transcriptional regulation of miR-21 by Foxo3a, STAT3, activator protein-1 has been reported. In glioma cells, STAT3 negatively regulated miR-21 transcription in response to IFN-β treatment. However, the role of STAT3 activation is debatable because its overactivation has been reported to be oncogenic in glioma cell lines (Wang and Li 2010; Yuki et al. 2009). Loffler et al. (2007) showed that IL-6-dependent STAT3 activated the transcription of miR-21 in multiple myeloma cells. This discrepancy may arise from the difference in cytokine stimulus and cell type. Thus, the functional identification of regulatory genes which are responsible for controlling the spatial and temporal expression of specific miRNAs is in its early stages.

MiR-221/222

MiR-221/222, located in a cluster on chromosome Xp11.3, are overexpressed in glioblastomas (Zhang et al. 2009a). Our and other studies showed that single suppression of miR-221 or miR-222 induced lower glioma growth inhibition in vivo than co-suppression

of miR-221/222. As they share the same 'seed' sequence, short regions at their 5′ ends through which they bind their target sites in mRNA 3′UTRs, they have the same targets to regulate the same pathway synergeticly. According to bioinformatics analysis using 3 different target prediction programs (PicTar, TargetScan and miRanda) and Pathway Studio soft, about 70 common target genes of miR-221/222 were generated and 16 of them represented direct or indirect interaction with Akt (Zhang et al. 2010). Several genes have been evidenced, such as p27 (Zhang et al. 2009a), p57 (Medina et al. 2008), kit (He et al. 2005) and PTEN (Chun-Zhi et al. 2010). Recently, we have proved that miR-221/222 inhibited cell apoptosis by targeting proapoptotic gene PUMA in human glioma cells, indicating PUMA as a novel target of miR-221/222 that functions as apoptosis regulator (Zhang et al. 2009b). Additionally, overexpression of miR-221/222 cooperated to enhance malignant phenotype of U251 and C6 glioma cells by activating the Akt pathway. These findings suggest that the modulation of the mechanism responsible for miR-221/222 in glioma could be used as a therapeutic strategy to treat glioma.

MiR-181a and MiR-181b

MiR-181 family (miR-181a, miR-181b and miR-181c) was reported to be down-regulated by Ciafre et al. (2005). Our data showed that miR-181a and miR-181b were down-regulated in human glioma tissues and cells lines (U87, TJ950 and U251), and functioned as tumor suppressors to exert a great biological effect on glioma cells growth, invasion and apoptosis. Overexpressed miR-181a significantly sensitized glioma cells to radiation treatment concurrent with Bcl-2 down-regulation (Chen et al. 2010). However, little direct evidence exists to show the targets and mechanism of miR-181 involved in gliomagenesis.

MiR-7

As another tumor suppressor, miR-7, has been identified down-regulated in glioma tissues by Kefas et al. (2008). MiR-7 expression is decreased in glioblastomas through reduced processing of precursor miR-7 (Kefas et al. 2008). Further, miR-7 reduced viability and invasiveness of glioblastoma cells by directly targeting EGFR. In addition, miR-7 also suppressed the Akt pathway activation by repressing IRS-1 and IR S-2 proved to be another direct target of miR-7 independent of its EGFR inhibition.

MiR-26a

MiR-26a is another oncogenic miRNA in gliomas targeting critical cancer signaling pathways. Huse et al. identified miR-26a overexpression in a subset of high-grade gliomas (Huse et al. 2009). It has been shown that overexpression of miR-26a in glioma primarily was a consequence of amplification at the miR-26a-2 locus, a genomic event strongly associated with monoallelic PTEN loss. Further, miR-26a reduced PTEN levels and facilitates glioma formation in a well-characterized murine model system, and functionally substituted for loss of heterozygosity at the PTEN locus. Akt was also activated due to an upstream signal of PTEN.

MiR-128

MiR-128, was enriched in brain but down-regulated in glioma tissues and cell lines. Zhang et al. (2009c) demonstrated that miR-128 inhibited the proliferation of glioma cells through negatively regulating one of its targets, E2F3a. Moreover, knocking down of E2F3a had similar effect as overexpression of miR-128, and overexpression of E2F3a could partly rescue the proliferation inhibition caused by miR-128. In addition, Godlewski et al. (2008) showed that miR-128 caused a striking decrease in expression of the oncogene Bmi-1 by direct regulation of the Bmi-1 mRNA 3′UTR, with Akt phosphorylation, and up-regulation of p21levels.

MiR-124 and MiR-137

Silber et al. reported that the expression levels of microRNA-124 and microRNA-137 were significantly decreased in anaplastic astrocytomas and glioblastoma multiforme (Silber et al. 2008). Transfection of

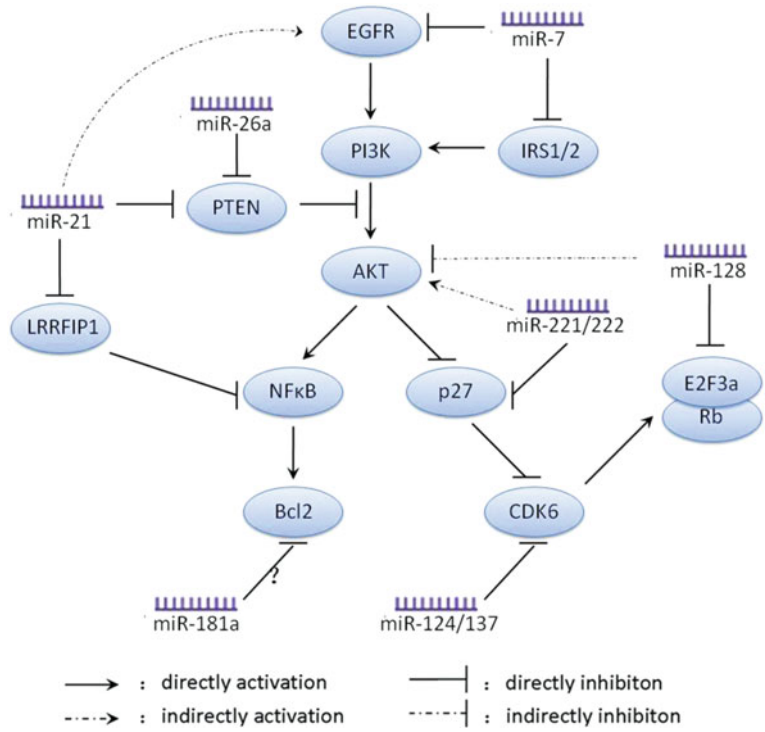

Fig. 9.1 The summary of miRNAs and EGFR/PTEN/AKT pathway involved in gliomas. Particular EGFR/PTEN/AKT signaling pathway affected by miRNAs is described in detail in the review

microRNA-124 or microRNA-137 induced G1 cell cycle arrest by inhibiting CDK6 expression in glioma cells.

Other miRNAs

Gal et al. demonstrated that transfection of glioblastoma cells by miR-451 can inhibited the cell growth (Gal et al. 2008). miR-10b is overexpressed in malignant glioma and associated with tumor invasive factors, uPAR and RhoC (Sasayama et al. 2009). MiR-10a is also found upregulated in glioblastomas (Ciafre et al. 2005; Silber et al. 2008). However, the function of these altered miRNAs remains unknown, and the expression levels of a few miRNAs in gliomas should be validated on larger, more representative cohorts of glioma patients.

Conclusion

In conclusion, since the discovery of miRNAs as a new class of gene regulators, lots of studies have emerged correlating altered expression levels and functions of particular miRNAs with the glioma. Interestingly and importantly, further analysis have identified that key signal components of the EGFR/PTEN/AKT pathway are the direct targets or downstream molecules of these specific miRNAs, indicating that these miRNAs participate in regulating EGFR/PTEN/AKT pathway, one of the most important signal pathways involved in gliomas (Fig. 9.1). However, molecular regulation of miRNAs in glioma, including miRNA upstream and downstream regulators and miRNA signal network, is comprehensive and still unclear, and a massive wealth of information is embedded and waiting to be discovered and extracted. Overall, we believe that these special miRNAs demonstrate a unique potential to result in a novel aspect of glioma progression and therapy, driving the field closer to the ultimate goal of improving patient survival rates and quality of life.

Acknowledgments This work was supported by China National Natural Scientific Fund (81072078 and 30872657), Jiangsu Province's Natural Science Foundation (BK2008475, 2010580), Program for Development of Innovative Research Team in the First Affiliated Hospital of NJMU, and Provincial Initiative Program for Excellency Disciplines, Jiangsu Province.

References

Chan JA, Krichevsky AM, Kosik KS (2005) MicroRNA-21 is an antiapoptotic factor in human glioblastoma cells. Cancer Res 65:6029–6033

Chen Y, Liu W, Chao T, Zhang Y, Yan X, Gong Y, Qiang B, Yuan J, Sun M, Peng X (2008) MicroRNA-21 down-regulates the expression of tumor suppressor PDCD4 in human glioblastoma cell T98G. Cancer Lett 272:197–205

Chen G, Zhu W, Shi D, Lv L, Zhang C, Liu P, Hu W (2010) MicroRNA-181a sensitizes human malignant glioma U87MG cells to radiation by targeting Bcl-2. Oncol Rep 23:997–1003

Chun-Zhi Z, Lei H, An-Ling Z, Yan-Chao F, Xiao Y, Guang-Xiu W, Zhi-Fan J, Pei-Yu P, Qing-Yu Z, Chun-Sheng K (2010) MicroRNA-221 and microRNA-222 regulate gastric carcinoma cell proliferation and radioresistance by targeting PTEN. BMC Cancer 10:367

Ciafre SA, Galardi S, Mangiola A, Ferracin M, Liu CG, Sabatino G, Negrini M, Maira G, Croce CM, Farace MG (2005) Extensive modulation of a set of microRNAs in primary glioblastoma. Biochem Biophys Res Commun 334: 1351–1358

Conti A, Aguennouz M, La Torre D, Tomasello C, Cardali S, Angileri FF, Maio F, Cama A, Germanò A, Vita G, Tomasello F (2009) miR-21 and 221 upregulation and miR-181b downregulation in human grade II-IV astrocytic tumors. J Neurooncol 93:325–332

Denli AM, Tops BB, Plasterk RH, Ketting RF, Hannon GJ (2004) Processing of primary microRNAs by the microprocessor complex. Nature 432:231–235

Gabriely G, Wurdinger T, Kesari S, Esau CC, Burchard J, Linsley PS, Krichevsky AM 2008. MicroRNA 21 promotes glioma invasion by targeting matrix metalloproteinase regulators. Mol Cell Biol 28:5369–5380

Gal H, Pandi G, Kanner AA, Ram Z, Lithwick-Yanai G, Amariglio N, Rechavi G, Givol D (2008) MIR-451 and Imatinib mesylate inhibit tumor growth of Glioblastoma stem cells. Biochem Biophys Res Commun 376:86–90

Godlewski J, Nowicki MO, Bronisz A, Williams S, Otsuki A, Nuovo G, Raychaudhury A, Newton HB, Chiocca EA, Lawler S (2008) Targeting of the Bmi-1 oncogene/stem cell renewal factor by microRNA-128 inhibits glioma proliferation and self-renewal. Cancer Res 68:9125–9130

Gregory RI, Chendrimada TP, Cooch N, Shiekhattar R 2005. Human RISC couples microRNA biogenesis and posttranscriptional gene silencing. Cell 123:631–640

Guessous F, Zhang Y, Kofman A, Catania A, Li Y, Schiff D, Purow B, Abounader R (2010) microRNA-34a is tumor suppressive in brain tumors and glioma stem cells. Cell Cycle 9:1031–1036

He H, Jazdzewski K, Li W, Liyanarachchi S, Nagy R, Volinia S, Calin GA, Liu CG, Franssila K, Suster S, Kloos RT, Croce CM, de la Chapelle A (2005) The role of microRNA genes in papillary thyroid carcinoma. Proc Natl Acad Sci USA 102:19075–19080

Huse JT, Brennan C, Hambardzumyan D, Wee B, Pena J, Rouhanifard SH, Sohn-Lee C, le Sage C, Agami R, Tuschl T, Holland EC (2009) The PTEN-regulating microRNA miR-26a is amplified in high-grade glioma and facilitates gliomagenesis in vivo. Genes Dev 23:1327–1337

Jiang L, Mao P, Song L, Wu J, Huang J, Lin C, Yuan J, Qu L, Cheng SY, Li J (2010) miR-182 as a prognostic marker for glioma progression and patient survival. Am J Pathol 177:29–38

Kefas B, Comeau L, Erdle N, Montgomery E, Amos S, Purow B (2010) Pyruvate kinase M2 is a target of the tumor-suppressive microRNA-326 and regulates the survival of glioma cells. Neuro Oncol 11:1102–1112

Kefas B, Godlewski J, Comeau L, Li Y, Abounader R, Hawkinson M, Lee J, Fine H, Chiocca EA, Lawler S, Purow B (2008) microRNA-7 inhibits the epidermal growth factor receptor and the Akt pathway and is down-regulated in glioblastoma. Cancer Res 68:3566–3572

Kim VN, Nam JW (2006) Genomics of microRNA. Trends Genet 22:165–173

Lee Y, Ahn C, Han J, Choi H, Kim J, Yim J, Lee J, Provost P, Rådmark O, Kim S, Kim VN (2003) The nuclear RNase III Drosha initiates microRNA processing. Nature 425:415–419

Li T, Li D, Sha J, Sun P, Huang Y (2009a) MicroRNA-21 directly targets MARCKS and promotes apoptosis resistance and invasion in prostate cancer cells. Biochem Biophys Res Commun 383:280–285

Li Y, Li W, Yang Y, Lu Y, He C, Hu G, Liu H, Chen J, He J, Yu H (2009b) MicroRNA-21 targets LRRFIP1 and contributes to VM-26 resistance in glioblastoma multiforme. Brain Res 1286:13–18

Loffler D, Brocke-Heidrich K, Pfeifer G, Stocsits C, Hackermüller J, Kretzschmar AK, Burger R, Gramatzki M, Blumert C, Bauer K, Cvijic H, Ullmann AK, Stadler PF, Horn F (2007) Interleukin-6 dependent survival of multiple myeloma cells involves the Stat3-mediated induction of microRNA-21 through a highly conserved enhancer. Blood 110:1330–1333

Medina R, Zaidi SK, Liu CG, Stein JL, van Wijnen AJ, Croce CM, Stein GS (2008) MicroRNAs 221 and 222 bypass quiescence and compromise cell survival. Cancer Res 68: 2773–2780

Papagiannakopoulos T, Shapiro A, Kosik KS (2008) MicroRNA-21 targets a network of key tumor-suppressive pathways in glioblastoma cells. Cancer Res 68:8164–8172

Qin W, Shi Y, Zhao B, Yao C, Jin L, Ma J, Jin Y (2010) miR-24 regulates apoptosis by targeting the open reading frame (ORF) region of FAF1 in cancer cells. PLoS One 5:e9429

Reinhart BJ, Slack FJ, Basson M, Pasquinelli AE, Bettinger JC, Rougvie AE, Horvitz HR, Ruvkun G (2000) The 21-nucleotide let-7 RNA regulates developmental timing in *Caenorhabditis elegans*. Nature 403:901–906

Ren Y, Zhou X, Mei M, Yuan XB, Han L, Wang GX, Jia ZF, Xu P, Pu PY, Kang CS (2010) MicroRNA-21 inhibitor sensitizes human glioblastoma cells U251 (PTEN-mutant) and LN229 (PTEN-wild type) to taxol. BMC Cancer 10:27

Sasayama T, Nishihara M, Kondoh T, Hosoda K, Kohmura E (2009) MicroRNA-10b is overexpressed in malignant glioma and associated with tumor invasive factors, uPAR and RhoC. Int J Cancer 125:1407–1413

Sayed D, He M, Hong C, Gao S, Rane S, Yang Z, Abdellatif M (2010) MicroRNA-21 is a downstream effector of AKT that

mediates its antiapoptotic effects via suppression of Fas ligand. J Biol Chem 285:20281–20290

Silber J, Lim DA, Petritsch C, Persson AI, Maunakea AK, Yu M, Vandenberg SR, Ginzinger DG, James CD, Costello JF, Bergers G, Weiss WA, Alvarez-Buylla A, Hodgson JG (2008) miR-124 and miR-137 inhibit proliferation of glioblastoma multiforme cells and induce differentiation of brain tumor stem cells. BMC Med 6:14

Takamizawa J, Konishi H, Yanagisawa K, Tomida S, Osada H, Endoh H, Harano T, Yatabe Y, Nagino M, Nimura Y, Mitsudomi T, Takahashi T (2004) Reduced expression of the let-7 microRNAs in human lung cancers in association with shortened postoperative survival. Cancer Res 64:3753–3756

Tan Y, Zhang B, Wu T, Skogerbø G, Zhu X, Guo X, He S, Chen R (2009) Transcriptional inhibition of Hoxd4 expression by miRNA-10a in human breast cancer cells. BMC Mol Biol 10:12

Tsai NP, Lin YL, Wei LN (2009) MicroRNA mir-346 targets the 5′-untranslated region of receptor-interacting protein 140 (RIP140) mRNA and up-regulates its protein expression. Biochem J 424:411–418

Wang K, Li PF (2010) Foxo3a regulates apoptosis by negatively targeting miR-21. J Biol Chem 285:16958–16966

Yuki K, Natsume A, Yokoyama H, Kondo Y, Ohno M, Kato T, Chansakul P, Ito M, Kim SU, Wakabayashi T (2009) Induction of oligodendrogenesis in glioblastoma-initiating cells by IFN-mediated activation of STAT3 signaling. Cancer Lett 284:71–79

Zhang J, Han L, Ge Y, Zhou X, Zhang A, Zhang C, Zhong Y, You Y, Pu P, Kang C (2010) miR-221/222 promote malignant progression of glioma through activation of the Akt pathway. Int J Oncol 36:913–920

Zhang CZ, Kang CS, Pu PY, Wang GX, Jia ZF, Zhang AL, Han L, Xu P (2009a) Inhibitory effect of knocking down microRNA-221 and microRNA-222 on glioma cell growth in vitro and in vivo. Zhonghua Zhong Liu Za Zhi 31:721–726

Zhang C, Kang C, You Y, Pu P, Yang W, Zhao P, Wang G, Zhang A, Jia Z, Han L, Jiang H (2009b) Co-suppression of miR-221/222 cluster suppresses human glioma cell growth by targeting p27kip1 in vitro and in vivo. Int J Oncol 34:1653–1660

Zhang Y, Ren Y, Moore L, Mei M, You Y, Xu P, Wang B, Wang G, Jia Z, Pu P, Zhang W, Kang C (2009c) MicroRNA-128 inhibits glioma cells proliferation by targeting transcription factor E2F3a. J Mol Med 87:43–51

Zhou X, Ren Y, Moore L, Mei M, You Y, Xu P, Wang B, Wang G, Jia Z, Pu P, Zhang W, Kang C (2010a) Downregulation of miR-21 inhibits EGFR pathway and suppresses the growth of human glioblastoma cells independent of PTEN status. Lab Invest 90:144–155

Zhou X, Zhang J, Jia Q, Ren Y, Wang Y, Shi L, Liu N, Wang G, Pu P, You Y, Kang C (2010b) Reduction of miR-21 induces glioma cell apoptosis via activating caspase 9 and 3. Oncol Rep 24:195–201

Zhu S, Si ML, Wu H, Mo YY (2007) MicroRNA-21 targets the tumor suppressor gene tropomyosin 1 (TPM1). J Biol Chem 282:14328–14336

Chapter 10

Glioblastoma Multiforme: Cryopreservation of Brain Tumor-Initiating Cells (Method)

Tan Boon Toh, Yuk Kien Chong, Beng Ti Ang, and Carol Tang

Abstract Tumor-initiating cells isolated from glioblastoma multiforme (GBM) have been shown to possess the ability to self-renew and contribute to tumor recurrence following chemo- and radiation therapies. In many instances, clinical material is limited, compounded by a lack of methods to preserve such cells at convenient time points. Although GBM-initiating cells grown in spheroid manner have been shown to maintain their integrity through serial transplantation in immune-compromised mice, practically, it is not always possible to have access to suitably-aged animals to continuously maintain these cells. We therefore explored vitrification as a cryopreservation technique for GBM-initiating cells. An efficacious cryopreservation technique would have to rely on unique assays to measure the behavior of *bona fide* tumor-initiating cells in the heterogeneous neurospheres. We show evidence that essential traits such as stemness, multipotentiality profiles and karyotypic hallmarks were maintained with vitrification. Transcriptome analysis showed that vitrified and non-vitrified samples in either of stem-like or differentiated states clustered together, providing evidence that vitrification did not alter the transcriptome profile of frozen cells. Importantly, our vitrified cells reformed serially transplantable glioma xenografts that recapitulated the human disease morphology. Our work demonstrates that vitrification of tumor neurospheres preserves the biological phenotype and genetic profiles of these cells, supporting its use as a cryopreservation method.

C. Tang (✉)
Department of Research, National Neuroscience Institute, Singapore 308433, Singapore
e-mail: carol_tang@nni.com.sg

Keywords Glioblastoma multiforme · Neurospheres · Glioma xenografts · Cryopreservation · Cancer stem cells · Vitrification

Introduction

There is compelling evidence demonstrating that the bulk of tumor cells is generated by a subpopulation of self-renewing, multipotent, and tumor-initiating cells, commonly termed cancer stem cells (CSCs) (Reya et al. 2001). The first evidence of CSCs came from a study on acute myeloid leukaemia (Bonnet and Dick 1997). Subsequently, various groups have demonstrated the existence of CSCs through transplantation studies using prospectively isolated tumor cells in a variety of solid tumors including breast, colon and brain (Al-Hajj et al. 2003; O'Brien et al. 2007; Ricci-Vitiani et al. 2007; Singh et al. 2003). Glioblastoma multiforme (GBM) is the most prevalent primary tumor of the adult central nervous system, with a median survival of approximately 12 months after diagnosis. In brain tumors, stem-like cells termed brain tumor stem cells (BTSCs) have been identified. BTSCs are largely undifferentiated, multipotent, and possess the ability to reform tumor xenografts with characteristics of the original parental tumor. Furthermore, BTSCs can be maintained and propagated as tumor neurosphere cultures in defined serum-free condition, a paradigm that is adopted from the traditional neurosphere culture (Reynolds and Weiss 1992, 1996). In addition, Lee and colleagues have shown that tumor stem-like cells grown in serum-free condition closely mimic the genotype, gene expression profile and biology of their parental tumors (Lee et al. 2006).

M.A. Hayat (ed.), *Tumors of the Central Nervous System, Volume 4*,
DOI 10.1007/978-94-007-1706-0_10,

Thus, the establishment of a tumor neurosphere repository with preservation of essential features of tumor heterogeneity would provide an invaluable resource to investigate the disease. Such a method would also allow us to return to the same experimental cell line passages in order to reduce variability in experimental replication.

Vitrification: Biology

Vitrification is a process of glass-like solidification in which an aqueous solution is prevented from crystallization by rapid cooling (Rall et al. 1987). Vitrification has been commonly used for the cryopreservation of embryos at different developmental stages from various species such as murine, rabbit, sheep and bovine (Ali and Shelton 1993; Kasai et al. 1990, 1992; Saha et al. 1996). Furthermore, human and mouse multi-cell embryos have been successfully cryopreserved using this strategy (Mukaida et al. 1998). This highlights the feasibility of cryopreserving cell aggregates. In addition, it has been demonstrated that vitrified embryonic stem cells retained their pluripotency and viability upon thawing (Reubinoff et al. 2001). Taken together, vitrification could provide an effective means of storage of brain tumor-initiating cells cultured as spherical structures.

In many studies involving the prospective isolation of tumor-initiating cells, only small amounts of clinical material are available, and this limitation is compounded by lack of appropriate methods to preserve such cells at convenient time points. In brain tumors for instance, it has been demonstrated that in vivo serial passaging of tumor neurospheres can provide a means to reliably maintain such primary cell lines (Galli et al. 2004); however in practice, it is not always possible to have access to suitably-aged immune-compromised mice. Cryopreservation of spherical structures with 10% dimethyl sulfoxide (DMSO) using conventional slow freezing methods has been reported to yield low cell viability (Chong et al. 2009; Tan et al. 2007). On the other hand, utilizing a high content of fetal bovine serum (FBS) as cryoprotectant increases cell viability but induces cellular differentiation, resulting in the loss of stem-like traits (Chong et al. 2009; Ha et al. 2005). The preservation of stemness quality is important as previous work has shown that tumorigenicity is abrogated when BTSCs are induced to differentiate (Piccirillo et al. 2006). To define vitrification as an effective tool, we investigated several properties with unique assays to probe the cellular heterogeneity of tumor cells. We show evidence that specific BTSC properties are maintained by vitrification.

Vitrification and Thawing of Human Glioblastoma-Derived Neurospheres (Methodology)

Materials and Solutions Preparation

Borosilicate glass capillaries (0.78 mm in diameter)
Cryotubes (4.5 ml) with holes punched in the upper section through the lid and middle section across the vial to allow liquid nitrogen movement
Liquid Nitrogen
DMEM-HEPES (Holding medium): 20% FBS, 1 M HEPES in DMEM medium (filtered solution through a pre-wet 0.22 μm pore-size filter).
1 M sucrose solution: 1 M sucrose, 20% FBS in DMEM-HEPES medium (filtered solution through a pre-wet 0.22 μm pore-size filter).
10% Vitrification Solution (VS1): 10% DMSO, 10% ethylene glycol in DMEM–HEPES medium.
20% Vitrification solution (VS2): 20% DMSO, 20% ethylene glycol, 30% of the 1 M sucrose solution in DMEM–HEPES medium.
0.2 M sucrose solution (SS1): 20% of the 1 M sucrose solution in DMEM–HEPES medium.
0.1 M sucrose solution (SS2): 10% of the 1 M sucrose solution in DMEM–HEPES medium.

Vitrification Procedure

The following procedure is applicable for vitrifying tumor neurospheres (50–100 μm) from one T75 culture flask. See Fig. 10.1 for illustrations.

1. Collect the tumor neurospheres from the T75 culture flask and transfer to a 15-ml disposable centrifuge tube (Fig. 10.1a).
2. Centrifuge for 5 min at 150*g*, at room temperature.

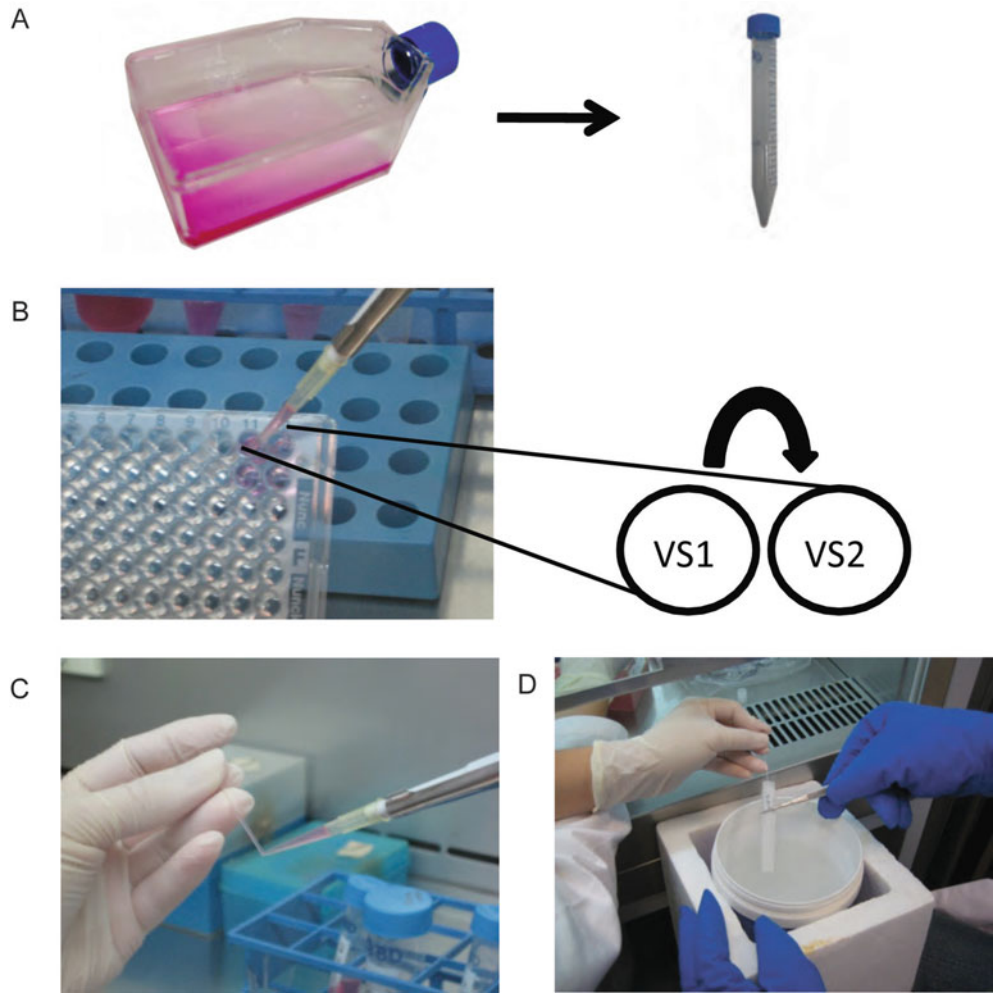

Fig. 10.1 Outline of vitrification procedure. (**a**) Tumor neurospheres are collected in pellet form by centrifugation. (**b**) Tumor neurospheres in DMEM-HEPES are transferred into VS1 solution for 1 min and subsequently into VS2 solution for an additional 25 s. (**c**) Suspension of tumor neurospheres in vitrification solution is drawn into a fine borosilicate capillary using a micropipettor fitted with a 200 μl pipette tip. (**d**) Capillary filled with suspension of tumor neurospheres is immediately plunged into a cryovial containing liquid nitrogen

3. Aspirate and discard the supernatant. Gently tap the base of the tube to disperse the pellet of tumor neurospheres.
4. Resuspend the tumor neurospheres in 200–300 μl of DMEM–HEPES medium.
5. Transfer 100 μl of well-suspended spheres in DMEM–HEPES into a well containing 100 μl of 10% vitrification solution (VS1). Incubate the suspension for 1 min at room temperature (Fig. 10.1b).
6. Transfer the total contents in the well to the next well containing 100 μl of 20% vitrification solution (VS2). Incubate the suspension for 25 s at room temperature (Fig. 10.1b).
7. Immediately contact one end of the borosilicate capillary with the suspended solution at a 30° angle to the plane of the flask. The solution should be drawn up by capillary action. Fill up the entire straw using a micropipettor fitted with a 200 μl pipette tip containing the solution (Fig. 10.1c).
8. Plunge the capillary into the cryotube containing liquid nitrogen (Fig. 10.1d).

Comments: It takes an experienced operator 2 min to freeze a capillary. Taking up to 3 min per capillary is still acceptable. The viability of the cells

may be affected with prolonged duration to freeze the capillary. Freezing is the critical step in the storage process.

Thawing Procedure

(1) Collect the cryotube containing the capillaries in a receptacle with liquid nitrogen. Remove the capillary using a forcep from the storage cryotube.
(2) Immediately, submerge one end of the capillary containing the vitrified liquid column (containing the tumor neurospheres) into the well containing 100 μl of 0.2 M sucrose solution (SS1).
(3) As soon as the liquid column melts (almost immediate), reverse capillary action will draw out the liquid into the well containing SS1. Residual liquid trapped in the capillary can be retrieved by inserting a micropipettor fitted with a 200 μl pipette tip to draw out remaining liquid.
(4) After 1 min, transfer the total contents in the well to the next well containing 100 μl of 0.1 M sucrose solution (SS2).
(5) After 5 min, transfer the total contents in the well to the next well containing 100 μl of DMEM–HEPES media.
(6) After 5 min, transfer the total contents in the well into a 15 ml centrifuge tube containing 5 ml of DMEM–HEPES. Repeat steps 1–5 if more capillaries are to be thawed.
(7) Collect the tumor neurospheres by centrifugation for 5 min at 200*g*, at room temperature.
(8) Discard supernatant and gently tap the tube to disperse the pellet of tumor neurospheres.
(9) Wash the cells with 5 ml of serum-free DMEM-F12 medium and repeat step 7 to collect the tumor neurospheres.
(10) Resuspend the tumor neurospheres in serum-free DMEM-F12 medium supplemented with growth factors (20 ng/ml each of EGF, bFGF and hLIF, 1× B27 growth supplement and 5 μg/ml heparin) and transfer into culture flask.
(11) Place the culture in a humidified 37°C, 5% CO_2 incubator. Inspect for viable tumor neurospheres after 24 h.

Vitrification Maintains the Biological Profiles of Brain Tumor Neurospheres

An important criterion for efficacious vitrification is the preservation of cellular properties upon thawing after long-term cryopreservation. We analysed essential properties such as viability, expression of stem cell markers, multipotentiality, karyotypic hallmarks, transcriptome profiles and the ability to recapitulate glioma pathophysiology in immune-compromised mice. Our data show that vitrification best maintained the morphology and initial frozen tumor neurosphere size (50–100 μm) with little or no cell death (Fig. 10.2a(i)). In addition, no visible differentiation was observed at the initial phase of culture establishment. However, although tumor neurospheres cryopreserved in 90% FBS yielded the best viability, clear signs of differentiation were observed upon 5–10 days post-thawing (Fig. 10.2a(ii), arrowhead).

We carried out quantitative real-time RT-PCR and immunofluorescence studies to assess the preservation of stemness and multipotentiality of cryopreserved tumor neurospheres. Our results show that gene expression of stemness state markers such as Nestin, SRY-box containing gene-2 (Sox-2), Complementarity Determinant 133 (CD133), Musashi-1 (Msi-1), Bmi-1, Nanog and Octamer-4 (Oct-4) were widely preserved after vitrification. Immunofluorescent staining of stemness and multipotentiality profiles of vitrified and non-vitrified samples demonstrated preservation of stem-like markers such as Nestin, Msi-1 and Oct-4. Induction of differentiation of vitrified cells and their non-vitrified counterparts displayed similar ability to form neurons, astrocytes and oligodendrocytes (Fig. 10.2b), supporting that vitrification preserves the multipotentiality property of the cells. Interestingly, differentiated tumor neurospheres displayed high percentages of Nestin and Msi-1 markers, indicating the retention of self-renewal potential in otherwise normally terminally differentiated cells. In addition, some of the differentiated tumor stem cells displayed co-staining for GFAP (glial fibrillary acidic protein, astrocytes) and TuJ1 (neuronal class III β-tubulin, neurons; Fig. 10.2b(ii)). These observations may reflect an aberrant regulatory pathway that characterizes the abnormalities in tumor-initiating cells (Hemmati et al. 2003; Yuan et al. 2004).

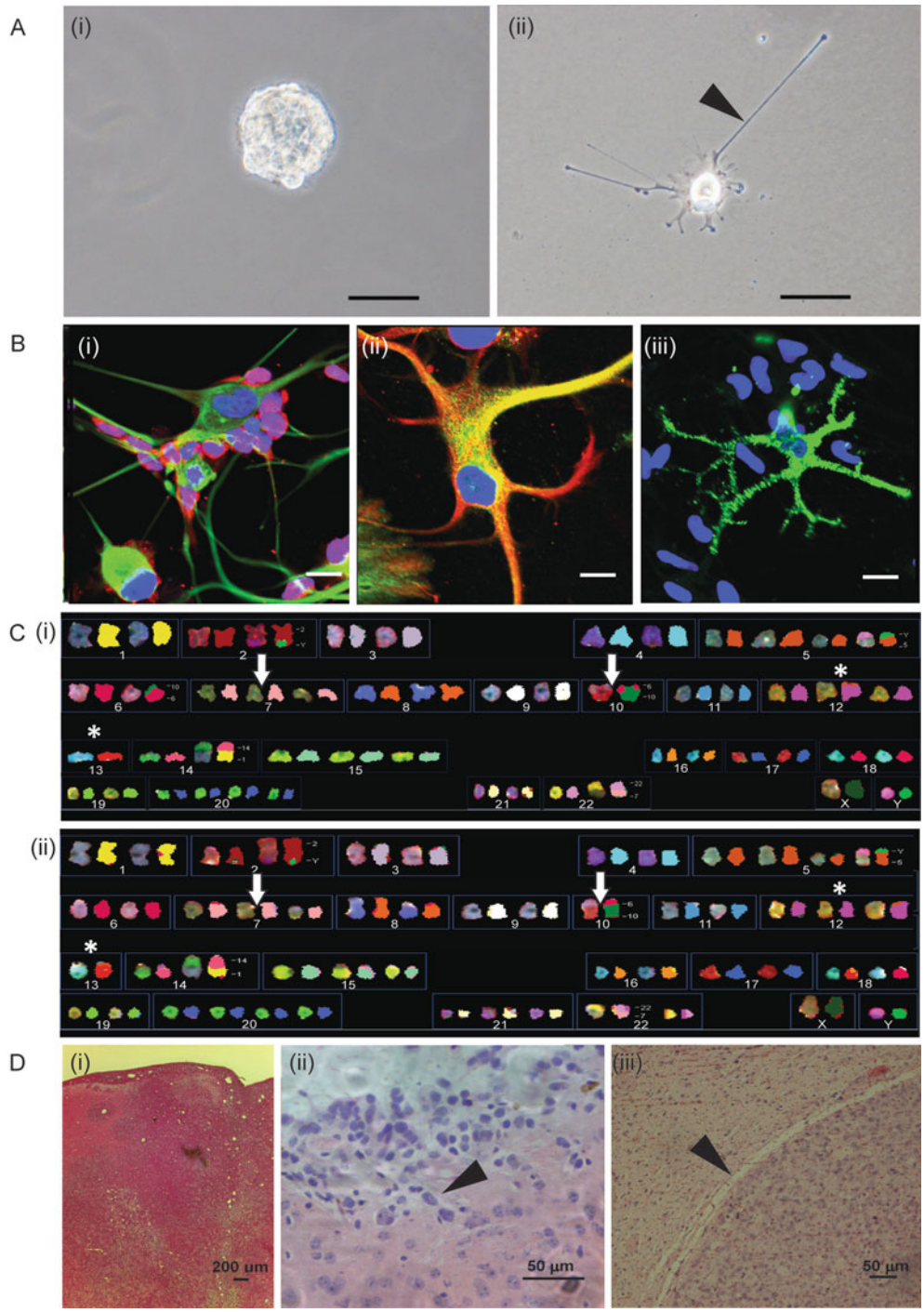

Fig. 10.2 Vitrification maintains the biological profiles of brain tumor neurospheres. (**a**) Morphology of viable tumor neurospheres 5–10 days of initial thawing after (i) vitrification and (ii) 90% FBS (note signs of differentiation, *arrowhead*). Scale bar: 100 µm. (**b**) Immunofluorescent staining of multipotentiality markers in vitrified cells showing the ability to form (i) neurons (TuJ1, *green* and Msi-1, *red*), (ii) astrocytes (GFAP, *red* and TuJ1, *green*) and (iii) oligodendrocytes (O4, *green*) upon differentiation with serum. Scale bar: 20 µm. (**c**) Spectral karyotyping of (i) non-vitrified and (ii) vitrified cells demonstrate the preservation of karyotypic hallmarks (polysomy of chromosome 7 and loss of chromosome 10, *arrows*) of glioblastoma multiforme. (**d**) Vitrified tumor neurospheres form tumor xenografts that recapitulate the extensive infiltration nature of glioma pathophysiology as seen in patients (i and ii, *arrowhead*) whereas commercially procured glioma cell lines generate tumors with well-defined margins (iii, *arrowhead*). (**c**) and (**d**) (i, ii) were reproduced (Chong et al. 2009) with permission from John Wiley and Sons

To ascertain that vitrification preserves the karyotypic integrity and hallmarks of GBM, we karyotyped all vitrified and non-vitrified tumor neurospheres. Our spectral karyotypic data show that all tumor neurospheres were of tumor origin and that they preserved karyotypic hallmarks of GBM, specifically polysomy of chromosome 7 (containing epidermal growth factor receptor, EGFR) and loss of chromosome 10 (containing phosphatase and tensin homolog, PTEN; Fig. 10.2c(i) and (ii), arrows). Interestingly, we also observed aneusomy of chromosomes 12 and 13 across all tumor neurosphere samples (Fig. 10.2c(i) and (ii), asterisks).

A major difficulty in the understanding of GBM classification is the inability to predict different patient outcomes on the basis of histopathological features. Gene expression-based molecular classification of GBM into four distinct subtypes, each with unique genomic aberrations has been demonstrated, highlighting the need to develop different therapeutic approaches that target these different subtypes (Verhaak et al. 2010). In addition, intrinsic gene expression profiling of glioma subtypes has shown that different genetic changes drive gene expression profiles and that molecular classification may prove to be a better predictor of patient outcome than histology (Gravendeel et al. 2009). Hence, the gene expression of tumor-initiating cells is an important property to analyse. We show by unsupervised gene expression clustering that vitrified tumor neurospheres clustered closely with its respective non-vitrified counterpart, indicating that vitrification preserves the genetic profiles of tumor neurospheres. Unexpectedly, one of the tumor neurosphere lines which showed changes in karyotype due to prolonged in vitro serial passaging continued to cluster with its non-vitrified form. This highlights that the quality of tumor sphere lines must rely on a combination of assays aimed at measuring tumor stem cell frequency, and that vitrification provides a reliable means to preserve biological properties of low passage cells.

A key feature in identifying bona fide brain tumor-initiating cells is the ability to create serially transplantable xenografts that recapitulate glioma pathophysiology. We orthotopically implanted our vitrified tumor neurospheres that were grown in defined serum-free medium into non-obese diabetic/ severe combined immunodeficiency (NOD-SCID) mice and examined the histology of the gliomas formed. We observed intracranial tumors with extensive cerebral infiltration (Fig. 10.2d(i) and (ii), arrowhead), a pathognomonic feature of human GBMs that is distinct from the spatially constrained, well-delineated tumors (Fig. 10.2d(iii), arrowhead) generated by commercially procured serum-grown cells. Our results demonstrate that vitrification preserves the biological phenotype and genetic profiles of the cells.

Discussion

Traditionally, clinical tissue specimens are maintained either as frozen samples stored in liquid nitrogen or embedded in paraffin wax blocks. These conventional ways of storage do not allow for isolation and subsequent cultivation of live cells. Here, we propose the use of a modified vitrification method for human brain tumor neurospheres that enrich for tumor-initiating cells. Vitrification is a process involving the use of high cryoprotectant concentration in combination with high cooling rates. As such, ice crystal formation that causes cell injury during cooling and warming are minimised. We have carefully investigated the genetic profiles and the preservation of stem cell-like characteristics of vitrified neurospheres. Our method may also be applicable to other tumor types where neoplastic stem-like cells can be grown in spheroid manner e.g. mammospheres and prostaspheres from breast and prostate cancers respectively (Chen et al. 2007; Lang et al. 2001; Lawson et al. 2007; Woodward et al. 2007). We envisage that a combination of vitrification and in vivo serial passaging in immune-compromised mice will provide a convenient means of preserving the tumor-initiating population and facilitate subsequent experimental designs.

Acknowledgements This work was supported by grants from the Biomedical Research Council of Singapore (to CT) and Singapore Institute for Clinical Sciences, Agency for Science, Technology and Research (to BTA).

References

Al-Hajj M, Wicha MS, Benito-Hernandez A, Morrison SJ, Clarke MF (2003) Prospective identification of tumorigenic breast cancer cells. Proc Natl Acad Sci USA 100:3983–3988

Ali J, Shelton J (1993) Successful vitrification of day-6 sheep embryos. J Reprod Fertil 99:65–70

Bonnet D, Dick JE (1997) Human acute myeloid leukemia is organized as a hierarchy that originates from a primitive hematopoietic cell. Nat Med 3:730–737

Chen MS, Woodward WA, Behbod F, Peddibhotla S, Alfaro MP, Buchholz TA, Rosen JM (2007) Wnt/beta-catenin mediates radiation resistance of Sca1+ progenitors in an immortalized mammary gland cell line. J Cell Sci 120:468–477

Chong YK, Toh TB, Zaiden N, Poonepalli A, Leong SH, Ong CE, Yu Y, Tan PB, See SJ, Ng WH, Ng I, Hande MP, Kon OL, Ang BT, Tang C (2009) Cryopreservation of neurospheres derived from human glioblastoma multiforme. Stem Cells 27:29–39

Galli R, Binda E, Orfanelli U, Cipelletti B, Gritti A, De Vitis S, Fiocco R, Foroni C, Dimeco F, Vescovi A (2004) Isolation and characterization of tumorigenic, stem-like neural precursors from human glioblastoma. Cancer Res 64:7011–21

Gravendeel LA, Kouwenhoven MC, Gevaert O, de Rooi JJ, Stubbs AP, Duijm JE, Daemen A, Bleeker FE, Bralten LB, Kloosterhof NK, De Moor B, Eilers PH, van der Spek PJ, Kros JM, Sillevis Smitt PA, van den Bent MJ, French PJ (2009) Intrinsic gene expression profiles of gliomas are a better predictor of survival than histology. Cancer Res 69:9065–9072

Ha SY, Jee BC, Suh CS, Kim HS, Oh SK, Kim SH, Moon SY (2005) Cryopreservation of human embryonic stem cells without the use of a programmable freezer. Hum Reprod 20:1779–1785

Hemmati HD, Nakano I, Lazareff JA, Masterman-Smith M, Geschwind DH, Bronner-Fraser M, Kornblum HI (2003) Cancerous stem cells can arise from pediatric brain tumors. Proc Natl Acad Sci USA 100:15178–15183

Kasai M, Hamaguchi Y, Zhu S, Miyake T, Sakurai T, Machida T (1992) High survival of rabbit morulae after vitrification in an ethylene glycol-based solution by a simple method. Biol Reprod 46:1042–1046

Kasai M, Komi J, Takakamo A, Tsudera H, Sakurai T, Machida T (1990) A simple method for mouse embryo cryopreservation in a low toxicity vitrification solution, without appreciable loss of viability. J Reprod Fertil 89:91–97

Lang SH, Sharrard RM, Stark M, Villette JM, Maitland NJ (2001) Prostate epithelial cell lines form spheroids with evidence of glandular differentiation in three-dimensional Matrigel cultures. Br J Cancer 85:590–599

Lawson DA, Xin L, Lukacs RU, Cheng D, Witte ON (2007) Isolation and functional characterization of murine prostate stem cells. Proc Natl Acad Sci USA 104:181–186

Lee J, Kotliarova S, Kotliarov Y, Li A, Su Q, Donin NM, Pastorino S, Purow BW, Christopher N, Zhang W, Park JK, Fine HA (2006) Tumor stem cells derived from glioblastomas cultured in bFGF and EGF more closely mirror the phenotype and genotype of primary tumors than do serum-cultured cell lines. Cancer Cell 9:391–403

Mukaida T, Wada S, Takahashi K, Pedro PB, An TZ, Kasai M (1998) Vitrification of human embryos based on the assessment of suitable conditions for 8-cell mouse embryos. Hum Reprod 13:2874–2879

O'Brien CA, Pollett A, Gallinger S, Dick JE (2007) A human colon cancer cell capable of initiating tumour growth in immunodeficient mice. Nature 445:106–110

Piccirillo SG, Reynolds BA, Zanetti N, Lamorte G, Binda E, Broggi G, Brem H, Olivi A, Dimeco F, Vescovi AL (2006) Bone morphogenetic proteins inhibit the tumorigenic potential of human brain tumour-initiating cells. Nature 444: 761–765

Rall WF, Wood MJ, Kirby C, Whittingham DG (1987) Development of mouse embryos cryopreserved by vitrification. J Reprod Fertil 80:499–504

Reubinoff BE, Pera MF, Vajta G, Trounson AO (2001) Effective cryopreservation of human embryonic stem cells by the open pulled straw vitrification method. Hum Reprod 16: 2187–2194

Reya T, Morrison SJ, Clarke MF, Weissman IL (2001) Stem cells, cancer, and cancer stem cells. Nature 414:105–111

Reynolds BA, Weiss S (1992) Generation of neurons and astrocytes from isolated cells of the adult mammalian central nervous system. Science 255:1707–1710

Reynolds BA, Weiss S (1996) Clonal and population analyses demonstrate that an EGF-responsive mammalian embryonic CNS precursor is a stem cell. Dev Biol 175:1–13

Ricci-Vitiani L, Lombardi DG, Pilozzi E, Biffoni M, Todaro M, Peschle C, De Maria R (2007) Identification and expansion of human colon-cancer-initiating cells. Nature 445: 111–115

Saha S, Otoi T, Takagi M, Boediono A, Sumantri C, Suzuki T (1996) Normal calves obtained after direct transfer of vitrified bovine embryos using ethylene glycol, trehalose, and polyvinylpyrrolidone. Cryobiology 33:291–299

Singh SK, Clarke ID, Terasaki M, Bonn VE, Hawkins C, Squire J, Dirks PB (2003) Identification of a cancer stem cell in human brain tumors. Cancer Res 63:5821–5828

Tan FC, Lee KH, Gouk SS, Magalhaes R, Poonepalli A, Hande MP, Dawe GS, Kuleshova LL (2007) Optimization of cryopreservation of stem cells cultured as neurospheres: comparison between vitrification, slow-cooling and rapid cooling freezing protocols. Cryo Lett 28:445–460

Verhaak R, Hoadley K, Purdom E, Wang V, Qi Y, Wilkerson M, Miller C, Ding L, Golub T, Mesirov J, Alexe G, Lawrence M, O'Kelly M, Tamayo P, Weir B, Gabriel S, Winckler W, Gupta S, Jakkula L, Feiler H, Hodgson J, James C, Sarkaria J, Brennan C, Kahn A, Spellman P, Wilson R, Speed T, Gray J, Meyerson M, Getz G, Perou C, Hayes D (2010) Integrated genomic analysis identifies clinically relevant subtypes of glioblastoma characterized by abnormalities in PDGFRA, IDH1, EGFR, and NF1. Cancer Cell 17: 98–110

Woodward WA, Chen MS, Behbod F, Alfaro MP, Buchholz TA, Rosen JM (2007) WNT/beta-catenin mediates radiation resistance of mouse mammary progenitor cells. Proc Natl Acad Sci USA 104:618–623

Yuan X, Curtin J, Xiong Y, Liu G, Waschsmann-Hogiu S, Farkas DL, Black KL, Yu JS (2004) Isolation of cancer stem cells from adult glioblastoma multiforme. Oncogene 23:9392–9400

Chapter 11

Relationship Between Molecular Oncology and Radiotherapy in Malignant Gliomas (An Overview)

Filippo Alongi, Arturo Chiti, Pierina Navarria, and Marta Scorsetti

Abstract Radiotherapy is currently in the midst of new developments both in technology and radiobiology. Recent papers have greatly enriched the current knowledge of radiation oncology, especially radiobiology and molecular oncology, and this has changed the oncology practice in radiation therapy in just a few years. The long-term objective of the translational research program in radiation oncology, also for central nervous system tumors such as glioblastoma multiforme (GBM), is to improve the therapeutic window, minimizing the damage to normal tissue and increasing the efficacy of radiation in eradicating cancer. The correct determination of the single patient profile as well as single tumor behaviour, with multidisciplinary approach is one of the next challenges in radiation oncology. This conceptual revolution will derive from the stronger correlations between new radiobiological data and experimental results in molecular oncology that are increasingly becoming available and ready to be translated into clinical practice. Some of the most interesting issues regarding relationships between molecular oncology and radiotherapy are: the availability of new, more effective drugs to prescribe in conjunction with radiation, the possibility to reduce intrinsic radioresistance or, on the contrary, to enhance radiosensitivity with innovative molecular targeted agents, the increasing potential application of cancer stem cells with radiotherapy, the impact of new molecular tracers for functional imaging of brain in radiotherapy treatment planning and in response evaluation. These issues are analysed and discussed in the present overview in regard to the recent literature on the topic.

Keywords Glioblastoma multiforme · Molecular oncology · Stem cells · Grade IV astrocytoma · Temozolomide · Cytotoxic agents

Introduction

Recent investigations have gradually enriched the current knowledge of cancer behaviour before, during and after radiotherapy treatments, especially in the field of radiobiology and molecular oncology. This confirms the growing interest of radiation researchers in conducting preclinical studies at their centres and translating the results as soon as possible to clinical radiotherapy practice.

GBM is the most common and malignant type of tumour in the central nervous system, classified as grade IV astrocytoma by the World Health Organisation (WHO). Radiotherapy after surgery, or exclusively in selected cases considered unsuitable for surgery, is the treatment of choice combined with new generation chemotherapy.

Despite initial treatment with surgical resection, radiotherapy, and chemotherapy, GBM virtually recurs in all cases. Both the tumour feature and its therapeutic multidisciplinary approach often result in profound impact on quality of life. This frustrating issue forced scientists to improve translational research efforts in molecular oncology and also in radiation therapy in a series of investigational preclinical and clinical studies.

F. Alongi (✉)
IRCCS Humanitas, Via Manzoni 56, 20089, Rozzano, Italy
e-mail: Filippo.alongi@humanitas.it

M.A. Hayat (ed.), *Tumors of the Central Nervous System, Volume 4*,
DOI 10.1007/978-94-007-1706-0_11,

The most interesting data to emerge from recent preclinical and clinical research into relationships between molecular oncology and radiotherapy in GBM, are: the advent of novel, more effective drugs to be used in conjunction with radiotherapy, molecular targeted agents as modulation factors of intrinsic radioresistance/radiosensitivity, the potential applicability of cancer stem cells in radiotherapy, the role of the new molecular tracer in functional brain imaging. In particular, newer imaging methods which explore the biological and molecular characteristics of brain tumour tissue by positron emission tomography (PET) represents a promising approach to integrate into treatment planning for high precision radiotherapy and post-treatment evaluation, even when radiation is combined with new targeted molecules.

In brief, brain tumors, especially those with high-grade histological behaviour, can represent one of the most challenging malignancies because of their anatomical location, aggressiveness, and high radial infiltrative capacity. Thus, more consolidated clinical results will probably require improvements in molecular oncology regarding combined approaches, particularly of radiation with innovative agents.

Chemotherapy, Targeted Agents and Radiation Therapy

More than three decades ago, the role of some basic mechanisms was established through which radiotherapy and chemotherapy might interact to improve their combined efficacy (Steel et al. 1979). In diffusely infiltrating high-grade gliomas, the real role of combined radiation and chemotherapy has remained historically controversial. Based on recent studies and developments, various types of further potential interactions between radiotherapy and drugs could become the object of preclinical and clinical investigations.

In GBM patients, Temozolomide, an alkylating agent with simple oral administration and a favorable toxicity profile, has been largely used in conjunction with and after radiotherapy. In fact, the addition of Temozolomide concomitant with radiotherapy, and for the 6 months following the radiotherapeutic course, proved superior to radiotherapy alone (Stupp et al. 2005). With this new combined approach, the expected median survival is established around 15 months, with a 2-year survival rate of 26.5%.

Prior to the Temozolomide era, many cytotoxic agents, most often nitrosoureas and other alkylating agents, have been added to surgery and radiotherapy since the 1970s. However, after publication by Stupp et al. of encouraging efficacy results from a phase II trial in patients with GBM (Stupp et al. 2005), most of clinical trials were addressed prevalently to different temozolomide administration schedules, in addition to radiotherapy.

Recently, research has increased our knowledge into the molecular pathways fundamental for gliomatosis and aggressiveness of malignant gliomas. Newer agents have been developed against these targets, including receptor tyrosine kinases, intracellular signalling molecules, epigenetic abnormalities, and tumor vasculature and cancer microenvironment. Some of these new targeted agents, could have a potential impact on improving clinical results in GBM, especially if prescribed synergistically with radiotherapy.

Several signalling pathways are frequently overexpressed in glioblastoma: some of them are vascular endothelial growth factor (VEGF), platelet-derived growth factor (PDGF), fibroblast growth factor, and epidermal growth factor.

Based on an improved knowledge of tumour vasculature biology, many new agents are being developed in preclinical models. Angiogenesis inhibitors are able to interrupt the process of angiogenesis to prevent new tumor blood-vessel formation. Vascular disrupting drug agents aim to cause direct damage to the existing tumor endothelium. Lead agents in both categories have now advanced into clinical trials. At the same time, it has been established that radiotherapy may achieve vasculature damage on endothelium in solid tumours (Garcia-Barros et al. 2003). Indeed, the application of such new combined approaches, by means of vascular target agents with radiation, could offer new more effective treatment opportunities.

In recent years, antiangiogenesis agents have been evaluated mainly in the treatment of GBM. Because VEGF plays has a fundamental role in the process of angiogenesis, therapeutic approaches targeting VEGF and VEGFR signalling are rational. The use of such

molecules in brain tumor treatment has been developed. Currently, there are several clinical studies dedicated to this approach, including the better definition of molecules that bind specifically to VEGF ligands and those that directly target VEGF receptors.

Bevacizumab, an anti-VEGF monoclonal antibody, was the first antiangiogenic therapy approved for use in cancer by the Food and Drug Administration for the treatment of recurrent GBM in 2009, the first new drug for Malignant Gliomas in over a decade. Several prospective trials are ongoing into Bevacizumab in recurrent GBM patients. To date, in patients with recurrent/refractory GBM, Bevacizumab, alone or in combination with other drugs and/or radiation, has produced good response rates and an encouraging improvement in median survival (7–9 months). However the role of Bevacizumab in the combined modality first-line treatment of patients with GBM has not been definitively assessed.

The feasibility and safety of concurrent administration of Bevacizumab and radiotherapy has already been demonstrated (Gruber et al. 2009). Because continued efforts are needed to confirm and increase these good early results, ongoing phase 3 studies are evaluating the combination of Bevacizumab with Temozolomide and radiotherapy.

To better explore new molecular oncology pathways to improve radiation in GBM patients, other targeted molecules, already applied in other cancers, are currently under investigation in clinical studies. Sorafenib, is an oral vascular endothelial growth factor receptor tyrosine kinase inhibitor recently prescribed with a good rate of response in renal cell carcinoma. It was hypothesized that, when Sorafenib is added to standard radiotherapy and Temozolomide in the first-line treatment, it could optimize the opportunity to improve therapy of patients with GBM. However the addition of this new target tailored molecule did not clearly appear to improve treatment efficacy when compared with the standard therapy approaches of malignant gliomas (Hainsworth et al. 2010).

From these and other data, our emerging knowledge of the molecular pathophysiology of malignant gliomas will improve therapeutic target selection in the future. Rigorous pre-clinical evaluation will be essential to better define the correct strategy regarding combinations of drugs that are most likely to be more effective and sufficiently tolerable with radiotherapy.

Modulation Factors of Radioresistance and Radiosensitivity

Malignant gliomas are typically defined as radioresistant tumours. This behaviour was clinically confirmed with the high rates of recurrence after radiotherapy.

To modulate radio-resistance of GBM, and enhance the possible radio-sensitivity of some cancer cell subpopulations in the tumour mass, several strategies in preclinical and clinical research have been initially evaluated.

From a purely radiobiological point of view, particular types of fractionation and dosage has been explored in GBM patients. Survival advantage has been demonstrated with post operative radiation therapy to doses of 50–60 Gy and, to date, standard radiotherapy of GBM is a total dose of 60 Gy in 30–33 fractions. Whether there is any benefit in administering doses >60 Gy using conventional treatment has not been demonstrated and increasing doses up to 90 Gy has not proven to alter the course of this disease significantly (Fitzek et al. 1999). Dose intensification with new radiation techniques using three-dimensional conformal radiotherapy or Intensity Modulated Radiation Therapy (IMRT), or boosting with Stereotactic Radiotherapy has still not demonstrated to improve results.

Several studies have used hyperfractionation or accelerated fractionation to escalate dose, hypothesizing a possible radiation sensitivity of GBM to low dose per fraction, without real significant improvements (Payne et al. 1982; Deutsch et al. 1989). Only one single experience achieving better survival results, using multiple daily fractionation combining radiotherapy with misonidazole in malignant astrocytoma patients, has been reported (Shin et al. 1985).

New fractionation schemes have been recently applied and validated in subsets of GBM patients treated with radiotherapy. A group of 100 patients with GBM over 60 years of age were randomized to receive standard radiotherapy of 60 Gy in 30 fractions or a shorter course of 40 Gy in 15 fractions. Overall survival between the two arms was not different, assessing that the short course of RT seems to be a reasonable treatment option for older patients with GBM (Roa et al. 2004).

Particle beam therapy is a fascinating new challenge in physical and biological application of radiotherapy. Despite theoretical gain with respect to better radiation dose conformity and/or radiobiologic advantage especially in radio-resistant tumors, particle beam therapy has been investigated in most trials, but this innovative approach has failed to demonstrate improved survival in high grade brain tumors compared to standard high energy X-ray radiation therapy. A Recent meta-analysis suggested that neutron beam therapy did not improve the survival of high-grade glioma patients, while there is no definitive conclusion regarding carbon therapy (Maucort-Boulch et al. 2010).

A way to enhance intrinsic radiosensitivity of high-grade gliomas could be represented by the combination with radio sensitizer molecules. To be able to significantly enhance cure rates by modulating the response of malignant gliomas to radiation is a fascinating possibility. The increased use of new drugs, able to literally "enhance" the effect of radiation, will eventually become a reality in the near future for patients with GBM.

As already reported, the standard of care for GBM patients remains the multidisciplinary approach with extensive surgery followed by radiotherapy with concomitant and adjuvant Temozolomide. Other combinations including molecular factors combined with radiotherapy, newer chemotherapeutic agents, radio sensitizers, and other agents are the most interesting target of ongoing studies. The good response rate of radiation with Temozolamide in malignant glioma could be due to the radio sensitizing activity of the alkylating agent and it would appear to establish that radio sensitization can improve clinical results.

Hypermethylation of methylguanine methyltransferase (MGMT) gene has been extensively shown as correlated with better results in GBM. The protein derived from MGMT gene has in fact a crucial role in repairing of alkylated DNA and it is either absent or greatly impaired in some types of GBM tumors. One study has shown that MGMT methylation status seems to have a predictive role in estimating sensitivity to alkylating molecules such as Temozolamide (Hegi et al. 2005). However, the predictive usefulness of MGMT status has not been rigorously analysed with regard to sensitivity to other treatments, such as radiation. To address this issue, MGMT methylation status was analyzed in a cohort of 225 patients with GBM treated with radiotherapy (Rivera et al. 2010). In patients who received radiotherapy alone following resection, methylation of the MGMT promoter was correlated with an improved response to radiotherapy. Unmethylated tumors were twice as likely to progress during radiation treatment. From this data it was suggested that MGMT promoter methylation appears to be a predictive biomarker of radiation response.

Some promising radio sensitizer agents have been explored in other anatomical districts such as head and neck tumours, in which radiotherapy is more effective when associated with chemotherapy. Prior to the Temozolamide era, misonidazole, a hypoxic cell radio sensitizer or bromodeoxyuridine, a halogenated pyrimidine that incorporates into DNA to radio sensitize cells, failed to obtain additional survival in GBM patients compared to patients treated with radiation and carmustine or radiation and vincristine, lomustine, and procarbazine.

However, recent preclinical and clinical data has provided a rationale to further investigate the combination of new targeted molecules with radiation, especially to modulate the known radio-resistance of high grade gliomas.

A reduction of EGFR signalling inducted in Glioma cells in vitro resulted in a modulation of response to radiation with greater radio sensitivity expression (O'Rourke et al. 1998). Inversely, a mutant expression, constitutively active EGFR was found to produce radioresistance primarily through activation of the PI3K pathway (Li et al. 2004).

Imatinib, an inhibitor of alpha- and beta-platelet-derived growth factor receptors (PDGFR) and other tyrosine kinases, is a well established treatment in gastrointestinal stromal cancer and chronic myeloid leukemia. In other malignant tumours, such as malignant gliomas protein kinases are usually involved in mutations or can alter their up-down regulation.

It was evaluated in an in vitro study whether radiation could sensitize astrocytoma cell lines to the effects of imatinib. For this purpose, T98G and MOG-G-UVW astrocytoma cells were treated with imatinib alone or in combination with gamma radiation (Ranza et al. 2009). The authors achieved that Imatinib conferred greater radio sensitivity on the astrocytoma cells in vitro giving a significant drop in colony formation compared with radiation alone. However the combination of Imatinib and radiation may result in unexpected toxicities that are not observed with treatment alone.

Based on improved knowledge of the tumour vasculature features, new molecular agents are being developed that exhibit these effects in preclinical models. Some experiences suggesting that caspase-2 was acting upstream of mitochondria after irradiation in several tumors, such as GBM. The rationale of this potential radio sensitizer is that inhibitor of apoptosis proteins, which are expressed at high levels in a series of tumors, block apoptosis at the core of the apoptotic machinery by inhibiting caspases. So therapeutic modulation of inhibitor of apoptosis proteins could target a key control point in resistance and can represent a promising strategy to enhance radio sensitivity in human cancers.

To enhance radio sensitivity of malignant glioma further interesting molecular pathways involving apoptosis and repair mechanisms after radiation are in the initial phase of preclinical exploration. In irradiated cells irreversible radiation damage is definitively expressed by the DNA chain double strand break. The hepatocyte growth factor/Met signalling pathway is up-regulated in several tumors, with downstream mediators playing a role in DNA double strand break repair. The effect of the anti-hepatocyte growth factor monoclonal antibody, AMG102, on the response to ionizing radiation in a model of glioblastoma multiforme in vitro and in vivo was partially investigated. Initial results seem to be promising, assessing for modulation of Met signalling with AMG102 the role of a new radiation sensitizer (Buchanan et al. 2010).

Signal transducer and activator of transcription pathways serve to block the apoptosis process, keeping cells alive in very toxic environments such as chemotherapy or ionizing radiation. Recent promising experimental data indicate that Phosphatidyl-inositol 3-kinase/protein kinase B (Akt) is a signal transducer modulating apoptosis with a potential role for radio sensitizing human malignant glioma (Chautard et al. 2010). This type of mechanism modulating apoptosis, to decrease the high tumor radio resistance, is a fascinating issue still under preclinical investigation.

The COX-2 protein is frequently overexpressed in human malignant gliomas, thus targeting the COX-2 pathway might improve glioma therapy. COX-2 expression is low in most normal tissues and can be up-regulated under various pathological conditions and also by irradiation. In a preclinical study, the effects of the selective COX-2 inhibitor meloxicam alone and in combination with irradiation on human glioma cells in vitro were recently investigated. The conclusion was that selective COX-2 inhibitor exerted COX-2 independent growth inhibition and radiosensitization of human glioma cells, leading the way toward a new fashionable type of targeted drug therapy to combine with radiation in malignant glioma patients (Bijnsdorp et al. 2007).

However, more established elements regarding clinical application modality of these new agents are expected in the near future.

Cancer Stem Cells and Radiotherapy

The selective inactivation of tumor cells in a solid mass is the most important finding related to the eradication of tumors by means of radiation without severely damaging healthy surrounding tissue. Radiotherapy has been the most effective nonsurgical treatment, but recent experimental research reports that tumors can be expected to recur after ionizing radiation treatment even if only one cancer stem cell survives (Meyn et al. 2009). Cancer stem cells are a specific subpopulation of cancer cells with high tumorigenic potential. It should be investigated in terms of clinical application, how cancer stem cells can be selectively destroyed, and whether they may respond differently to more selective radiotherapy and a more selective combined radio-pharmacological modality.

Glioblastoma is the most common brain tumor in adults. The mechanisms leading to glioblastoma are not well known but preclinical studies support that inactivation of tumor suppressor genes in neural stem cells is needed and sufficient to induce glial cancers. According to the cancer stem cell hypothesis, all cancer stem cells must be destroyed in order to definitively cure cancer. In particular, in the human brain, the subventricular zone represented by the 3–5 mm thick lateral periventricular region of the lateral ventricles, and the subgranular layer, a subregion of the hippocampal formation, have been shown to harbor normal brain stem cells (Singh et al. 2003). It was suggested that the neural stem cell niches in the brain that may harbor cancer stem cells, can provide innovative targets for therapy approach; researchers have hypothesized that higher radiation doses to these neural stem cell niches improve patient survival by eradicating potential cancer stem cells. In a retrospective radiation dose-distributional analysis of 55 adult

patients with Grade 3 or Grade 4 glial cancer treated with radiotherapy and temozolamide at UCLA, it was showed that patients whose bilateral subventricular zone received greater than 43 Gy had a significant improvement in progression-free survival when compared to patients who received a minor dose (Evers et al. 2010). This study permitted authors to hypothesize that the prescription of a defined dose to the periventricular region, targeting the stem cell niches, may be a way to improve treatment responses in patients with high-grade gliomas.

To investigate the possibility that cancer stem cells may represent the source of the radio-resistant subpopulation, the effect of ionizing radiation on human glioma models was investigated using both patient surgical specimens and human glioma xenografts maintained in immunocompromised mice. A resistance to radiation was shown to be due to increased activation of the DNA damage checkpoint (Rich et al. 2007). It was also discovered that these subpopulations of tumor stem cells can stimulate tumor angiogenesis through increased expression of vascular endothelial growth factor. The exploitation of this pathway will probably provide therapeutic targets to sensitize cancer stem cells to cytotoxic therapies in combination with radiation, to improve cancer patient treatment and not exclusively for brain tumours.

Molecular and Biological Imaging for Radiotherapy

Molecular oncology in functional imaging has become fundamental for tumor staging, for biologic definition, and for delineation of target volumes in radiation oncology.

Biological heterogeneity of neoplastic cells is an important factor in the variable radiosensitivity within a tumor mass. Selective dose escalation with modern types of radiotherapy to the more radioresistant parts of the lesion is considered feasible after the use of dose painting based on increased availability of molecular imaging technologies such as PET (Positron Emission Tomography), SPECT (Single Photon Emission Tomography) and MR imaging/spectroscopy.

High metabolism, high proliferation, and increased hypoxia now represent the targets for higher doses of radiation. New biological molecules, fundamental in the tumor profile, are being studied to reveal these and other features in detail. Hypoxia, for example, is known to be involved in the radioresistance of cancer. Hypoxia can be measured using 18F-FDG, 18F-labeled nitroimidazoles, and 64Cu-ATSM, and has been demonstrated as a prognostic factor in many clinical studies. When using 18F-FMISO PET, it was shown that malignant gliomas seem to have a different level of oxygenation (Valk et al. 1992). However, the real influence of hypoxia in the combined treatment of high-grade gliomas is unclear and still under evaluation.

"Theragnostic imaging" in radiotherapy is a new term to describe the introduction of molecular images to define and more selectively treat each voxel of tumor volume with dose painting based on biological and functional characterization (Bentzen 2008).This type of approach is currently being routinely applied in several radiotherapy centres, prevalently for some solid cancers, such as tumors of the head and neck district, or in the thorax.

In the brain, PET can also give molecular information that can influence Radiation therapy practice. FDG PET has been largely used in several types of neoplasm but is still problematic for brain cancers due to high background signal which comes from the central nervous system tissue. A study reported the real impact of FDG PET for GTV delineation in malignant gliomas in 18 patients. Although FDG uptake was regionally related to anaplastic areas, it was shown to be of limited value in target volume (Gross et al. 1998).

Many new PET radiopharmaceuticals do not have this functional limit and are currently at various stages of clinical development. Amino acids are the predominant molecules used for the imaging of central nervous system tumours. Cancer cell uptake of radiolabelled amino acids is established as increased compared to normal tissues. In normal brain cells, amino acid uptake is lower, due to their nearly exclusive glucose metabolism. Currently available PET tracers are 11C-labelled methionine (MET) and 18F-labelled fluoroethyl-L-tyrosine (FET).

MET PET can provide useful information in initial diagnosis and differentiating tumor recurrence from radiation necrosis. Sensitivity, specificity, and accuracy of MET PET has been reported as around 80–85%. The use of MET PET was estimated to impact the treatment program in 50% of the brain cases. It has been reported that, with the integration of MET PET, the intended management was changed in half of the cases (Yamane

et al. 2010). The main message was that the accuracy of MET PET for tumour detection and tumour tissue extension seems to be significantly higher in comparison to MR, CT or FDG-PET. However, ongoing randomized multicenter studies with MET PET will allow to assess the benefit for patients resulting from the molecular imaging approach.

In early detection, radiation treatment response in glioma patients is uncertain: contrast enhancement in magnetic resonance imaging can mimic tumor resistance or progression because influenced chemoradiation treatment. In several settings, PET using the amino acid tracer 18F-fluoroethyltyrosine (FET) seems to be a promising method for treatment volume definition, response evaluation and monitoring in patients with glioblastomas at an early stage (Piroth et al. 2010).

In PET imaging, another issue of increasing interest for radiotherapy and molecular oncology is the possibility to accurately define tumor biology, also in Gliomas. The thymidine analogue 18F-fluorothymidine (FLT) levels seems to be strictly correlated with cell proliferation measured by Ki-67 (Ullrich et al. 2008).

The feasibility of 18F-Galacto-RGD PET for imaging of avb3 expression on new vasculature was recently reported in patients with squamous cell carcinoma of head and neck (Beer et al. 2007). The avb3 integrin is a cell receptor involved in tumour-induced angiogenesis and metastasis. A targeted molecule that interacts blocking this receptor is currently under investigation also for malignant gliomas. This type of molecular imaging could be used in combined treatment when radiation is prescribed with drugs targeted to this newer neo-vasculature induction mechanism.

Biological mapping of the brain parenchyma is possible also through evaluation of oxygen modifications in the local tissue with improved MR technologies. The definition of functionally eloquent parts of brain with MR allow surgeons to perform more accurate surgical resection or radiation oncologists to define better target volume to irradiate while avoiding injury to critical areas. Functional MR modalities can provide unique metabolic, pathological and physiological data not available in anatomic MR. Molecular based MR techniques can also potentially improve the treatment response of brain tumors. Choline (Cho) to *N*-acetylaspartate (NAA) and Cho to creatine (Cr) ratios are examples of values that can be used to grade malignancy of gliomas. The possibility to increase definition of the molecular aspect of brain tumour behaviour can consequently influence volumes and doses in radiotherapy planning.

Conclusion

The long-term objective of the translational research program in radiation and molecular oncology is to improve the therapeutic window, minimizing the damage to normal tissue and increasing the efficacy of radiation in eradicating cancer.

One of the issues of major interest is the research into innovative drugs that could replace standard chemotherapy or that could enhance its potential efficacy, when used concomitantly with radiation.

Radiosensitizer agents combined with radiation in GBM patients, as well as in other cancer patients, could be a promising way toward reducing radioresistance and improving radiation treatment response.

To assess definitively whether cancer stem cells can represent the source of the resistant subpopulation of tumors, future investigations should improve knowledge and their potential application in radiotherapy and molecular oncology, also for brain cancers.

New tracers have proven to be potentially useful for imaging malignant gliomas. Molecular imaging application in the central nervous system can overcome the current limit of neuroimaging in brain and newer molecules are currently under evaluation. The availability of new tracers will improve radiation therapy and better define the entire treatment volume, or evaluate subvolumes of disease with different malignant behaviour to irradiate selectively with different doses during the same course of radiotherapy.

In summary, molecular oncology and radiotherapy are currently in strict relationship and several developments in both are awaited over the next few years.

References

Beer AJ, Grosu AL, Carlsen J, et al. (2007) Feasibility of (18F)Galacto-RGD PET for imaging of avb3 expression on neovasculature in patients with squamous cell carcinoma of head and neck. Clin Cancer Res 13:6610–6616

Bentzen SM (2008) Dose painting and theragnostic imaging: towards the prescription, planning and delivery of biologically targeted dose distributions in external beam radiation oncology. Cancer Treat Res 139:41–62

Bijnsdorp IV, van den Berg J, Kuipers GK, Wedekind LE, Slotman BJ, van Rijn J, Lafleur MV, Sminia P (2007) Radiosensitizing potential of the selective cyclooxygenase-2 (COX-2) inhibitor meloxicam on human glioma cells. Neuro-oncology 85:25–31

Buchanan IM, Scott T, Tandle AT, Burgan WE, Burgess TL, Tofilon PJ, Camphausen K (2010, July 12) Radiosensitization of glioma cells by modulation of Met signaling with the hepatocyte growth factor neutralizing antibody, AMG102. J Cell Mol Med [Epub ahead of print]

Chautard E, Loubeau G, Tchirkov A, Chassagne J, Vermot-Desroches C, Morel L, Verrelle P (2010) Akt signaling pathway: a target for radiosensitizing human malignant glioma. Neuro-oncology 12(5):434–443

Deutsch M, Green SB, Strike TA, et al. (1989) Results of a randomized trial comparing BCNU plus radiotherapy, streptozotocin plus radiotherapy, BCNU plus hyperfractionated radiotherapy, and BCNU following misonidazole plus radiotherapy in the postoperative treatment of malignant glioma. Int J Radiat Oncol Biol Phys 16(6):1389–1396

Evers P, Lee PP, DeMarco J, Agazaryan N, Sayre JW, Selch M, Pajonk F (2010) Irradiation of the potential cancer stem cell niches in the adult brain improves progression-free survival of patients with malignant glioma. BMC Cancer 10:384

Fitzek MM, Thornton AF, Rabinov JD, et al. (1999) Accelerated fractionated proton/photon irradiation to 90 cobalt gray equivalent for glioblastoma multiforme: results of a phase II prospective trial. J Neurosurg 91:251–260

Garcia-Barros M, Paris F, Cordon-Cardo C, Lyden D, Rafii S, Haimovitz-Friedman A, Fuks Z, Kolesnick R (2003) Tumor response to radiotherapy regulated by endothelial cell apoptosis. Science 300(5622):1155–1159

Gross MW, Weber WA, Feldmann HJ, et al. (1998) The value of F-18-fluorodeoxyglucose PET for the 3-D radiation treatment planning of malignant gliomas. Int J Radiat Oncol Biol Phys 41:989–995

Gruber ML, Raza S, Gruber D, Narayana A (2009) Bevacizumab in combination with radiotherapy plus concomitant and adjuvant temozolomide for newly diagnosed glioblastoma: update progression-free survival, overall survival, and toxicity [abstract]. J Clin Oncol :91 s. Abstract 2017

Hainsworth JD, Ervin T, Friedman E, Priego V, Murphy PB, Clark BL, Lamar RE (2010) Concurrent radiotherapy and temozolomide followed by temozolomide and sorafenib in the first-line treatment of patients with glioblastoma multiforme. Cancer 116(15):3663–3669

Hegi ME, Diserens AC, Gorlia T, et al. (2005) MGMT gene silencing and benefit from temozolomide in glioblastoma. N Engl J Med 352:997

Li B, Yuan M, Kim IA, Chang CM, Bernhard EJ, Shu HK (2004) Mutant epidermal growth factor receptor displays increased signaling through the phosphatidylinositol-3 kinase/AKT pathway and promotes radioresistance in cells of astrocytic origin. Oncogene 23:4594–4602

Maucort-Boulch D, Baron MH, Pommier P, Weber DC, Mizoe JE, Rochat J, Boissel JP, Balosso J, Tsujii H, Amsallem E (2010) Rationale for carbon ion therapy in based on a review and a meta-analysis of neutron beam trials. Cancer Radiother 14(1):34–41

Meyn RE, Milas L, Ang K (2009) The role of apoptosis in radiation oncology. Int J Radiat Biol 85:107–115

O'Rourke DM, Kao GD, Singh N, et al. (1998) Conversion of a radioresistant phenotype to a more sensitive one by disabling erbB receptor signaling in human cancer cells. Proc Natl Acad Sci USA 95:10842–10847

Payne DG, Simpson WJ, Keen C, et al. (1982) Malignant astrocytoma: hyperfractionated and standard radiotherapy with chemotherapy in a randomized prospective clinical trial. Cancer 50(11):2301–2306

Piroth MD, Pinkawa M, Holy R, Klotz J, Nussen S, Stoffels G, Coenen HH, Kaiser HJ, Langen KJ, Eble MJ (2011) Prognostic value of early [18F] fluoroethyltyrosine positron emission tomography after radiochemotherapy in glioblastoma multiforme. Int J Radiat Oncol Biol Phys 80(1):176–184

Ranza E, Bertolotti A, Facoetti A, Mariotti L, Pasi F, Ottolenghi A, Nano R (2009) Influence of imatinib mesylate on radiosensitivity of astrocytoma cells. Anticancer Res 29(11):4575–4578

Rich JN (2007) Cancer stem cells in radiation resistance. Cancer Res 67(19):8980–8984

Rivera AL, Pelloski CE, Gilbert MR, Colman H, De La Cruz C, Sulman EP, Bekele BN, Aldape KD (2010) MGMT promoter methylation is predictive of response to radiotherapy and prognostic in the absence of adjuvant alkylating chemotherapy for glioblastoma. Neuro-oncology 12(2): 116–121

Roa W, Brasher PM, Bauman G, Anthes M, Bruera E, Chan A, Fisher B, Fulton D, Gulavita S, Hao C, Husain S, Murtha A, Petruk K, Stewart D, Tai P, Urtasun R, Cairncross JG, Forsyth P (2004) Abbreviated course of radiation therapy in older patients with glioblastoma multiforme: a prospective randomized clinical trial. J Clin Oncol 22(9):1583–1588

Shin KH, Urtasun RC, Fulton D, et al. (1985) Multiple daily fractionated radiation therapy and misonidazole in the management of malignant astrocytoma. A preliminary report. Cancer 56(4):758–760

Siemann DW, Horsman MR (2004) Targeting the tumor vasculature: a strategy to improve radiation therapy. Expert Rev Anticancer Ther 4(2):321–327

Singh SK, Clarke ID, Terasaki M, Bonn VE, Hawkins C, Squire J, Dirks PB (2003) Identification of a cancer stem cell in human brain tumors. Cancer Res 63:5821–5828

Steel GG, Peckham MJ (1979) Exploitable mechanisms in combined radiotherapy–chemotherapy: the concept of additivity. Int J Radiat Oncol Biol Phys 5:85–91

Stupp R, Mason WP, van den Bent MJ, et al. (2005) Radiotherapy plus concomitant and adjuvant temozolomide for glioblastoma. N Engl J Med 352:987–996

Ullrich R, Backes H, Li H, Kracht L, Miletic H, Kesper K, Neumaier B, Heiss WD, Wienhard K, Jacobs AH (2008) Glioma proliferation as assessed by 3′-fluoro-3′-deoxy-L-thymidine positron emission tomography in patients with newly diagnosed high-grade glioma. Clin Cancer Res 14(7):2049–2055

Valk PE, Mathis CA, Prados MD, et al. (1992) Hypoxia in human gliomas: demonstration by PET with fluorine-18-fluoromisonidazole. J Nucl Med 33:2133–2137

Yamane T, Sakamoto S, Senda M (2010) Clinical impact of (11)C-methionine PET on expected management of patients with brain neoplasm. Eur J Nucl Med Mol Imaging 37(4):685–690

Chapter 12

High-Grade Brain Tumours: Evaluation of New Brain Lesions by Amino Acid PET

Robert Pichler, Sabine Spiegl-Kreinecker, and Gabriele Wurm

Abstract Amino acid PET provides very sensitive means to detect brain tumours, especially gliomas, and might therefore influence decision-making including selection for active treatment. Malignant cells show increased amino acid transport and are therefore a possible target for isotope labelled amino acid imaging, whereas FDG PET does not provide optimal diagnostic value in brain tumours due to high back-ground activity in brain. Most promising ^{18}F-FET seems to require the prerequisites for brain tumour imaging. FET PET is a ^{18}F-labeled amino acid (tyrosine) that can be produced in large amounts for clinical purposes. FET PET may be used for evaluation of newly diagnosed brain lesions including optimal guidance of biopsies, treatment monitoring of high grade glioma and improved treatment planning of radiotherapy. Sensitivity of FET PET for high grade glioma can be estimated at 90% or even higher, but cerebral gliomatosis may appear FET negative. On the other hand FET PET is not useful to exclude any brain glioma as many low grade gliomas do not show marked uptake of this tracer. Low grade gliomas without marked FET uptake have far better prognosis in respect to malignant transformation and death than have FET avid lesions. Evaluation of newly observed brain lesions by FET PET will most probably be included in the standard diagnostic approach.

Keywords Gliomas · FET PET · Amino acid transport · Brain lesions · Choline · Hemiplegia

Introduction

Amino acid PET provides very sensitive means to detect brain tumours, especially gliomas, and might therefore influence decision-making including selection for active treatment. On the other hand, progress in brain tumour treatment has been painfully slow and prognosis for glioblastomas remains amongst the worse of all cancer types (Herholz 2010). Hopefully the future will bridge this gap between diagnostic and therapeutic possibilities.

According to the broad access of MRI in the setting of neurological patients intracerebral lesions being consistent with primary brain tumour or at least of unknown significance are rather frequently observed. Thus, MRI has evolved as the most important diagnostic tool for initial assessment of pathologies of the central nervous system. Morphological imaging techniques are usually able to demonstrate precisely the presence of a brain lesion, in terms of its size and its relation with surrounding brain structures (Del Sole et al. 2004), however, this technique lacks specificity in the non-invasive assessment of histopathology. Metabolic imaging of brain tumours with radiolabeled amino acids has been shown to be a valuable method to improve the diagnostic accuracy in combination with anatomic radiological methods (Pauleit et al. 2004; Jager et al. 2001), especially after diagnosis to accurately delineate the extension of tumour for initial staging or during follow-up after therapy.

R. Pichler (✉)
Transportation Research Institute, The University of Michigan, Ann Arbor, MI 481 09-2150, USA
e-mail: Robert.pichler@gespag.at

M.A. Hayat (ed.), *Tumors of the Central Nervous System, Volume 4*,
DOI 10.1007/978-94-007-1706-0_12,

Isotope Labelled Amino Acids in Nuclear Medicine and Neurooncology

Amino acids enter cells mainly via specific transport systems. Malignant cells show increased amino acid transport and are therefore a possible target for isotope labelled amino acid imaging. Although PET with FDG is proven to be useful for diagnosis and therapeutic management in a variety of tumours, in tissues with high background, such as brain, difficulties in image interpretation occur (Haberkorn 2004). Additionally, many brain tumours including even glioblastoma do no capture FDG sufficiently (Pötzi et al. 2007; Pichler et al. 2010a).

Historically ^{123}I labelled tyrosine has been used for brain tumour imaging since 20 years (Langen et al. 1990; Biersack et al. 1989) as a marked accumulation of tracer was reported in human brain tumors. Langen and coworkers demonstrated tracer uptake in about 80% of investigated gliomas. So ^{123}IMT was considered a suitable SPECT tracer of amino acid uptake. Some advantage of SPECT gamma camera systems is the broad availability – on the other hand the poor spatial resolution of SPECT compared to PET represents a major disadvantage. With growing numbers of PET and PET/CT cameras especially in and nearby neurosurgical centres the use of ^{123}I and ^{99m}Tc labelled compounds – as MIBI – or ^{201}Tl will loose relevance further on.

Comparably long ^{11}C labelled methionine for PET imaging is available, the method has also been compared on a patient basis to ^{123}IMT (Langen et al. 1997). The diagnostic impact of ^{11}C-MET on brain tumour imaging and the technical superiority of a PET resolution system have been published since the 1980s, so the main pro of this compound is a large body of evidence of usefulness in clinical practice. The short half-life of ^{11}C of 20 min which enforces the presence of an on-site cyclotron is rather unpractical. Additionally the specificity of the compound for tumour imaging might not be optimal compared to others as accumulation in inflammatory tissue may occur.

The development of ^{18}F labelled amino acid compounds has helped to overcome these restrictions. ^{18}F-DOPA is available since about 1985 mostly for evaluation of Parkinson's disease (Calne et al. 1985) and was also shown to detect brain tumours (Heiss et al. 1996). Some regional centres as Graz in Austria still rely on this compound for brain tumour imaging. But it has to be concerned that the marked physiological striatal uptake is undesirable for glioma imaging. Also rather strong and persistent uptake can be observed in inflammatory processes and hyperaemia e.g. after stroke – see Fig. 12.1. Last but not least

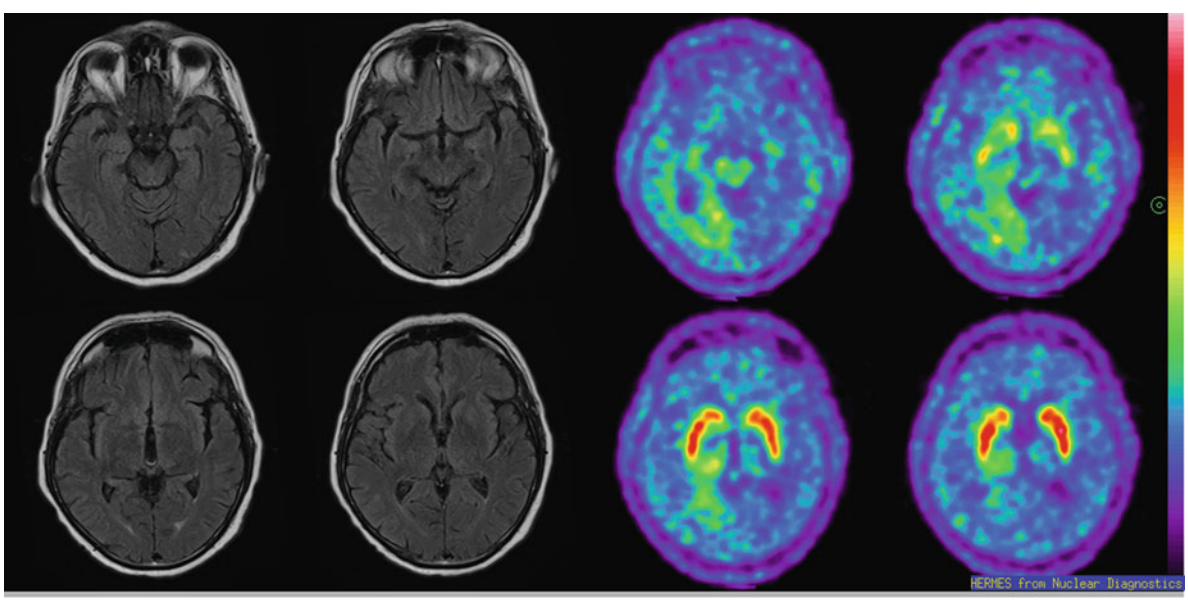

Fig. 12.1 The 71 year old male patient suffered from acute stroke involving the right posterior cerebral artery. We present the MRI and DOPA PET images (subacute) from September 2010, the tracer is accumulated markedly in hyperaemic area surrounding yet unviable brain tissue of the right temporo-occipital lobe. There was no brain tumour

technical reasons limiting the production of larger radiotracer quantities impeded that this compound became first choice in amino acid glioma imaging.

Most promising ^{18}F-FET seems to require the prerequisites for brain tumour imaging. FET PET is a ^{18}F-labeled amino acid (tyrosine) that can be produced in large amounts for clinical purposes (Langen et al. 2006). This amino acid is not incorporated into proteins, the uptake by tumor cells is mediated by amino acid transporters (Heiss et al. 1999). Weber et al. (2000) published a series of patients with intracerebral tumorous lesions comparing ^{11}C-MET and ^{18}F-FET in 2000. For all lesions there was a close correlation between MET and FET uptake. It is likely that the clinical experience with ^{11}C-MET in brain tumour imaging can be partly extrapolated to FET. Further on the discussion is focused upon the data already available for FET in glioma imaging. In Central Europe this tracer has become commercially available since 2005, in the meanwhile FET can be obtained in most European countries.

A valid alternative to this compound seems to be ^{18}F-FLT. This ^{18}F labelled thyronine compound has effect fully been used for glioma diagnosis. A significant correlation between kinetic modelling and the percentage of Ki-67-positive cells has been observed (Backes et al. 2009). This finding might qualify this tracer especially for the use in clinical trials, at least in high grade gliomas. Nevertheless, comparative evaluation concluded that ^{18}F-FLT should not be considered for evaluation of recurrent low grade gliomas (Tripathi et al. 2009), as only one third of low grade gliomas presented any relevant tracer uptake. Therefore caution is recommended in respect to this radiopharmakon when evaluating brain lesions of unproven histology.

It has to be mentioned, that ^{11}C or ^{18}F labelled choline, a small molecule that represents a substrate for phospholipids metabolism in the cell membrane, has also been introduced for brain glioma imaging.

The Role of FET PET in Glioma Imaging

FET PET may be used for evaluation of newly diagnosed brain lesions including optimal guidance of biopsies, treatment monitoring of high grade glioma and improved treatment planning of radiotherapy.

Tumour or Not To Be Tumour

Nonspecific incidental brain lesions are being detected more frequently because of an increasing number of screening MRI scans of the brain (Floeth et al. 2008). Combined use of MRI and FET PET in patients with cerebral gliomas significantly improves the identification of cellular glioma tissue (Pauleit et al. 2005).

Our group evaluated 88 patients with leading clinical symptoms of seizures, headache and neurological deficits as hemiplegia, generally of new onset. MRI presented a new diagnosed lesion possibly compatible with brain tumour. Overall 51/60 operated persons had positive FET PET imaging and 86% of neoplastic brain lesions were FET positive, including three cases with brain metastasis and one intracerebral lymphoma. Among the low grade brain tumours (WHO I–II) 13/19 were FET positive, this indicates a sensitivity of 68%. The diagnostic approach for non-operated persons was based upon longitudinal observation by clinical observation or re-MRI examination. Ours study presented high sensitivity of FET PET for high grade glioma (sensitivity was 93% for all malignant entities) – for example see Fig. 12.2 – but cerebral gliomatosis may appear FET negative. On the other hand FET PET is not useful to exclude any brain glioma as many low grade gliomas do not show marked uptake of this tracer. But there seems to be a place in the primary diagnostic approach of lesions with unknown significance, because FET-PET is able to avoid unnecessary invasive diagnosis in lesions without uptake and to advocate a wait and see strategy (Pichler et al. 2010a).

What is the prognostic impact of a FET negative lesion? Floeth et al. (2008), showed that low grade gliomas without marked FET uptake had far better prognosis in respect to malignant transformation and death than had FET avid lesions. Combining the metabolic data with MRI criteria additionally helped to estimate individual prognosis.

The intensity of uptake may help to differentiate tumour grading, but there exists substantial overlap so the impact for individual patient management is very limited. It was intended to overcome this problem by measurement of FET tumour kinetics (Pöpperl et al. 2007), but these promising results did not lead to broad acceptance in other centres.

Of course parallel use of radiological imaging by MRI – ideally including spectroscopy (Stadlbauer et al.

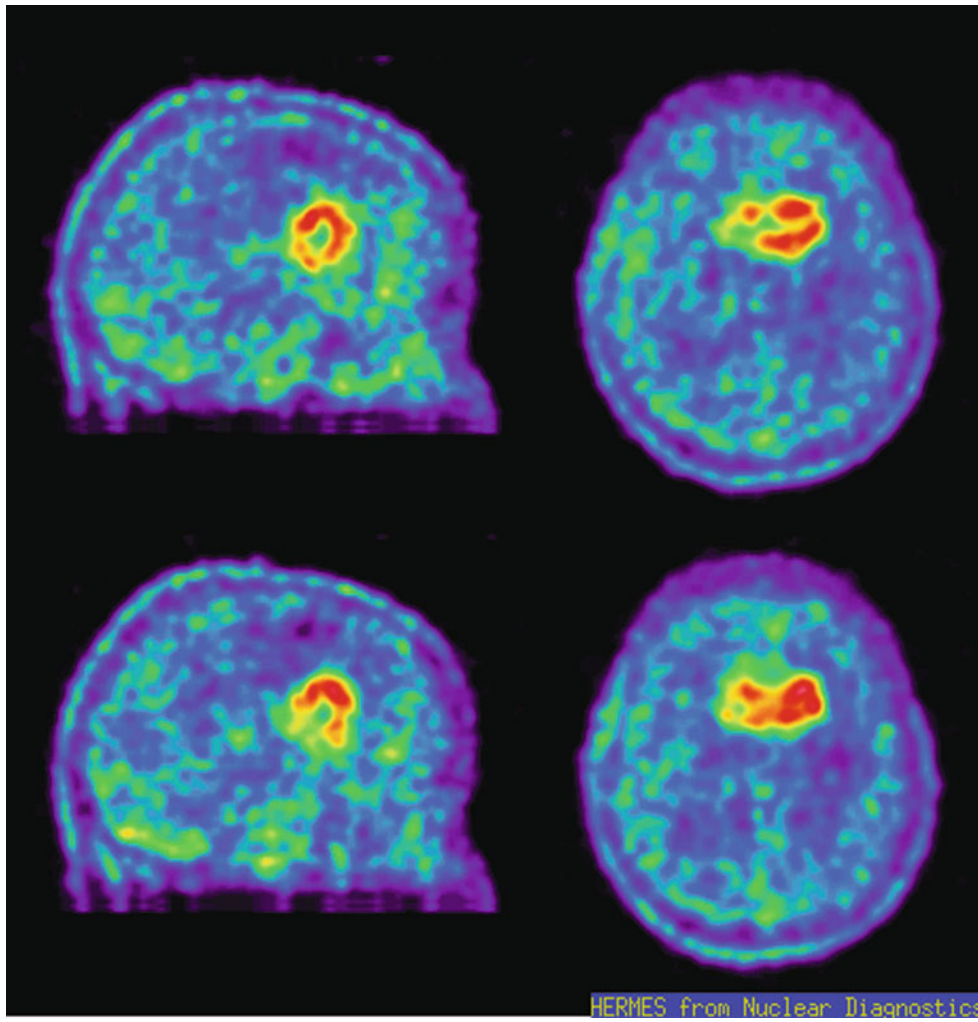

Fig. 12.2 A huge tumour in the corpus callosum was observed in this 61 year old female patient, FET PET presented marked uptake in the lesion with a central defect indicating necrosis (sagittal and transversal images). Biopsy revealed a glioblastoma

2008) – is necessary. It has to be stressed that fusion imaging with MRI should be done in all patients and that bimodal image interpretation should represent an essential part of medical report analysis.

Target selection for diagnostic biopsies is a major point of imaging. Combined use of MRI and FET PET in patients with cerebral gliomas significantly improves the identification of cellular glioma tissue and allows definite histological tumour diagnosis (Pauleit et al. 2005).

Anyhow, some pitfalls of false FET-positive benign lesions have been described, as brain abscess (Floeth et al. 2006), stroke (Pichler et al. 2010a) and radiation-induced astrogliosis (Pichler et al. 2010b). It has to be mentioned that also by MR imaging benign lesions mimicking supratentorial tumours can be observed (Wurm et al. 2003).

Monitoring Therapy Response

Besides surgery, radiotherapy, chemotherapy and combined radiochemotherapy that are the essential therapeutic options for high-grade glioma experimental therapy as convection-enhanced delivery of cytotoxic or radiation-emitting substances may be available. Glioblastoma still has very poor prognosis,

but a broader range of therapeutic alternatives as anti-angiogenetic factors go in line with a demand for early and precise monitoring of therapeutic success and/or detection of recurrence.

The extent of magnetic resonance imaging contrast enhancement has been used as an early post radiotherapy indicator of therapeutic response, but this approach is limited by the difficulty of distinguishing tumour and unspecific treatment effects (Piroth et al. 2011). This dilemma might be solved by the combined imaging with FET, as Rachinger et al. (2005), could show a sensitivity of 100% and a specificity of 93% for tumour recurrence using FET, whereas the specificity of MRI was only 50%. A shorter time gap for FET-PET examination after e.g. radiotherapy compared to MRI might be considered advantageous. Quantification of FET uptake in tumour lesions seems mandatory in longitudinal observation to objectify tumour progress or treatment response.

Prognostic data might be obtained early by FET imaging (Piroth et al. 2011), especially in combination with information about immune-histochemical tumour characteristics as Ki67. Another example of utmost prognostic importance is the O6-methylguanine DNA methyltransferase protein expression in tumor cells (Spiegl-Kreinecker et al. 2010) which influences response to chemotherapy.

FET PET Guided Radiotherapy

Using FET PET-CT planning, the size and geometrical location of gross and biological tumour volumes differs in the majority of patients compared to conventional methods (Weber et al. 2008). Vees et al. (2009), also showed that gross tumour volumes defined on PET-based techniques are usually smaller (but add tumour extension in one third of patients) compared to MRI guided volumes. Hopefully the information provided by metabolic images will help to optimize the therapeutic success of radiotherapy which still has to be proven.

Further Developments

Somatostatin-Receptor Imaging

It is evident that not all brain tumours are gliomas, some entities – preferably in knowledge of tumour histology – can be considered as candidates for other PET imaging modalities than amino acid PET. Most promising are the ^{68}Ga labelled compounds DOTATOC and DOTANOC for somatostatin receptor imaging. PNET and medulloblastoma as well as meningiomas (see Fig. 12.3) present a high density of somatostatin receptors and are therefore candidates for imaging with those compounds. Some usefulness for PET/CT radiotherapy planning has already been published (Nyuyki et al. 2010).

Imaging of Angiogenesis

Angiogenesis is a critical process in many pathological processes including cancer. Vascular endothelial

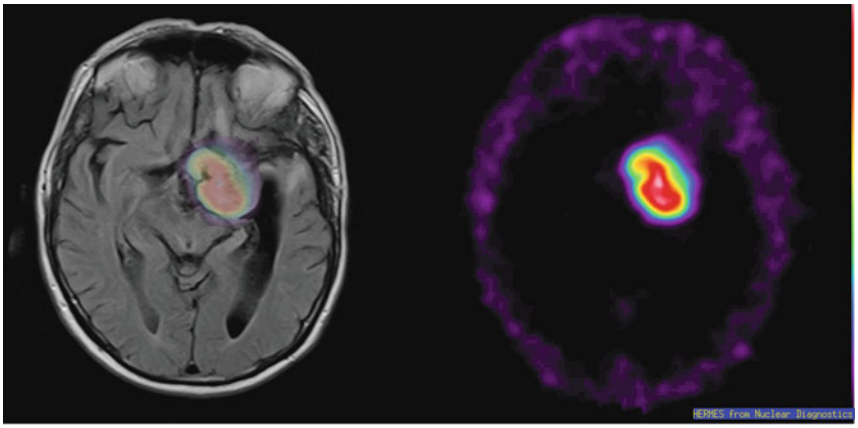

Fig. 12.3 E ^{68}Ga-DOTANOC PET (and fusion images with MRI) from August 2010 present a high tracer uptake in this meningioma originating from the left sphenoid bone and infiltrating the temporal lobe. Due to high somatostatin-receptor density possible specific therapeutic approaches for the 75 year old male patient were discussed

growth factor receptor signalling pathway plays a pivotal role in regulating angiogenesis. Quantitative PET imaging of VEGF receptor expression is possible via a ^{64}Cu labelled PET radiopharmacon (Chen et al. 2009), other markers of angiogenesis can be labelled by radioiodine. Such imaging methods could be helpful for monitoring antiangiogenic treatment.

Conclusion

MRI still represents the principal and essential imaging method in brain tumours, especially for anatomy and morphological tumour information. But metabolic nuclear medicine imaging con provide useful additional information about viability, treatment response and tumour extension in brain tumours especially in high grade gliomas. It can be estimated that amino acid PET by FET will become the most popular nuclear medicine imaging option for brain tumour. Evaluation of newly observed brain lesions by FET PET will most probably be included in the standard diagnostic approach.

References

Biersack HJ, Coenen HH, Stöcklin G, Reichmann K, Bockisch A, Oehr P, Kashab M, Rollmann O (1989) Imaging of brain tumors with L-3-[^{123}I]iodo-alpha-methyl tyrosine and SPECT. J Nucl Med 30:110–112

Backes H, Ullrich R, Neumaier B, Kracht L, Wienhard K, Jacobs AH (2009) Noninvasive quantification of ^{18}F-FLT human brain PET for the assessment of tumour proliferation in patients with high-grade glioma. Eur J Nucl Med Mol Imaging 36:1960–1967

Calne DB, Langston JW, Martin WR, Stoessl AJ, Ruth TJ, Adam MJ, Pate BD, Schulzer M (1985) Positron emission tomography after MPTP: observations relating to the cause of Parkinson′s disease. Nature 317:246–248

Chen K, Cai W, Li ZB, Wang H, Chen X (2009) Quantitative PET imaging of VEGF receptor expression. Mol Imaging Biol 11:15–22

Del Sole A, Moncayo R, Tafuni G, Lucignano G (2004) Position of nuclear medicine techniques in the diagnostic work-up of brain tumors. Q J Nucl Med Mol Imaging 48:76–81

Floeth FW, Pauleit D, Sabel M, Reifenberger G, Stoffels G, Stummer W, Rommel F, Hamacher K, Langen KJ (2006) ^{18}F-FET PET differentiation of ring-enhancing brain lesions. J Nucl Med 47:776–782

Floeth FW, Sabel M, Stoffels G, Pauleit D, Hamacher K, Steiger HJ, Langen KJ (2008) Prognostic value of ^{18}F-fluoroethyl-L-tyrosine PET and MRI in small nonspecific incidental brain lesions. J Nucl Med 49:730–737

Haberkorn U (2004) Future clinical applications of PET: amino acid and nucleoside imaging. In: Ell PJ, Gambhir SS (eds) Nuclear medicine in clinical diagnosis and treatment. Churchill Livingston, London, pp 329–343

Heiss P, Mayer S, Herz M, Wester HJ, Schwaiger M, Senekowitsch-Schmidtke R (1999) Investigation of transport mechanism and uptake kinetics of O-(2-[^{18}F]fluoroethyl)-L-tyrosine in vitro and in vivo. J Nucl Med 40:1367–1373

Heiss WD, Wienhard R, Wagner H, Lanfermann A, Thiel A, Herholz K, Pietrzyk U (1996) F-Dopa as an amino acid tracer to detect brain tumors. J Nucl Med 37:1180–1182

Herholz K (2010) Amino acid PET and clinical management of glioma patients. Eur J Nucl Med Mol Imaging 37:683–684

Jager PL, Vaalburg W, Pruim J, de Vries EG, Langen KJ (2001) Radiolabeled amino acids: basic aspects and clinical applications in oncology. J Nucl Med 42:432–445

Langen KJ, Coenen HH, Roosen N, Kling P, Muzik O, Herzog H, Kuwert T, Stöcklin G, Feinendegen LE (1990) SPECT studies of brain tumors with L-3-[^{123}I] iodo-alpha-methyl tyrosine: comparison with PET, ^{124}IMT and first clinical results. J Nucl Med 31:281–286

Langen KJ, Hamacher K, Weckesser M, Floeth F, Stoffels G, Bauer D, Coenen HH, Pauleit D (2006) O-(2-[^{18}F]fluoroethyl)-L-tyrosine: uptake mechanisms and clinical applications. Nucl Med Biol 33:287–294

Langen KJ, Ziemons K, Kiwit JCW., Herzog H, Kuwert T, Bock WJ, Stöcklin G, Feinendegen LE, Müller-Gärtner HW 1997. 3-[^{123}I]iodo-α-methyltyrosine and [methyl-^{11}C]-L-methionine uptake in cerebral gliomas: a comparative study using SPECT and PET. J Nucl Med 38:517–522

Nyuyki F, Plotkin M, Graf R, Michel R, Steffen I, Denecke T, Geworski L, Fahdt D, Brenner W, Wurm R (2010) Potential impact of ^{68}Ga-DOTATOC PET/CT on stereotactic radiotherapy planning of meningiomas. Eur J Nucl Med Mol Imaging 37:310–318

Pauleit D, Floeth F, Hamacher K, Riemenschneider MJ, Reifenberger G, Müller HW, Zilles K, Coenen HH, Langen KJ (2005) O-(2-[^{18}F]fluoroethyl)-L-tyrosine PET combined with MRI improves the diagnostic assessment of cerebral gliomas. Brain 128:678–687

Pauleit D, Floeth F, Tellmann L, Hamacher K, Hautzel H, Müller HW, Coenen HH, Langen KJ (2004) Comparison of *O*-(2-^{18}F-fluoroethyl)-L-tyrosine PET and 3-^{123}I-iodo-α-methyl-L-tyrosine SPECT in brain tumors. J Nucl Med 45:374–381

Pichler R, Dunzinger A, Wurm G, Pichler J, Weis S, Nußbaumer K, Topakian R, Aigner RM (2010a) Is there a place for FET PET in the initial evaluation of brain lesions with unknown significance? Eur J Nucl Med Mol Imaging 37:1521–1528

Pichler R, Wurm G, Nußbaumer K, Kalev O, Silyé R, Weis S (2010b) Sarcoidois and radiation-induced astrogliosis causes pitfalls in neuro-oncologic positron emission tomography imaging by *O*-(2-[^{18}F]fluoroethyl)-L-tyrosine. J Clin Oncol 28:e753–755

Piroth MD, Pinkawa M, Holy R, Klotz J, Nussen S, Stoffels G, Coenen HH, Kaiser HJ, Langen KJ, Eble MJ (2011)

Prognostic value of early [^{18}F]fluoroethyltyrosine positron emission tomography after radiochemotherapy in glioblastoma. Int J Radiat Oncol Biol Phys 80:176–184

Pöpperl G, Kreth FW, Mehrkens JH, Herms J, Seelos K, Koch W, Gildehaus FJ, Kretzschmar HA, Tonn JC, Tatsch K (2007) FET PET for the evaluation of untreated gliomas: correlation of FET uptake and uptake kinetics with tumour grading. Eur J Nucl Med Mol Imaging 34:1933–1942

Pötzi C, Becherer A, Marosi C, Karanikas G, Szabo M, Dudczak R, Kletter K, Asenbaum S 2007. [^{11}C] methionine and [^{18}F] fluorodeoxyglucose PET in the follow-up of glioblastoma multiforme. J Neurooncol 84:305–314

Rachinger W, Goetz C, Pöpperl G, Gildehaus FJ, Kreth FW, Holtmannspötter M, Herms J, Koch W, Tatsch K, Tonn JC (2005) Positron emission tomography with O-(2-[^{18}F]fluoroethyl)-L-tyrosine versus magnetic resonance imaging in the diagnosis of recurrent gliomas. Neurosurgery 57:505–511

Spiegl-Kreinecker S, Pirker C, Filipits M, Lötsch D, Buchroithner J, Pichler J,, Silye R, Weis S, Micksche M, Fischer J, Berger W (2010) O6-Methylguanine DNA methyltransferase protein expression in tumor cells predicts outcome of temozolomide therapy in glioblastoma patients. Neuro-oncology 12:28–36

Stadlbauer A, Prante O, Nimsky C, Salomonowitz E, Buchfelder M, Kuwert T, Linke R, Ganslandt OM (2008) Metabolic imaging of cerebral gliomas: spatial correlation of changes in O-(2-^{18}F-fluoroethyl)-L-tyrosine PET and proton magnetic resonance spectroscopic imaging. J Nucl Med 49:721–729

Tripathi M, Sharma R, D′Souza M, Jaimini A, Panwar P, Varshney R, Datta A, Kumar N, Garg G, Singh D, Grover RK, Mishra AK, Mondal A (2009) Comparative evaluation of F-18 FDOPA, F-18 FDG, and F-18 FLT-PET/CT for metabolic imaging of low grade gliomas. Clin Nucl Med 34:878–883

Vees H, Senthamizhchelvan S, Miralbell R, Weber DC, Ratib O, Zaidi H (2009) Assessment of various strategies for ^{18}F-FET PET-guided delineation of target volumes in high-grade glioma patients. Eur J Nucl Med Mol Imaging 36: 182–193

Weber DC, Zilli T, Buchegger F, Casanova N, Haller G, Rouzaud M, Nouet P, Dipasquale G, Ratib O, Zaidi H, Vees H, Miralbell R (2008) [^{18}F]Fluoroethyltyrosine-positron emission tomography-guided radiotherapy for high-grade glioma. Radiat Oncol 3:44

Weber WA, Wester HJ, Grosu AL, Herz M, Dzewas B, Feldmann HJ, Molls M, Stöcklin G, Schwaiger M (2000) O-(2-[^{18}F]fluoroethyl)-L-tyrosine and L-[methyl-^{11}C]methionine uptake in brain tumours: initial results of a comparative study. Eur J Nucl Med 27:542–549

Wurm G, Parsaei B, Silye R, Fellner FA (2003) Distinct supratentorial lesions mimicking cerebral gliomas. Acta Neurochir (Wien) 146:19–26

Chapter 13

Cyclic AMP Phosphodiesterase-4 in Brain Tumor Biology: Immunochemical Analysis

B. Mark Woerner and Joshua B. Rubin

Abstract Cyclic AMP plays a significant role in the biology of brain tumors and represents an important therapeutic target. Intracellular levels of cAMP are regulated through its synthesis via adenylyl cyclases and its degradation by phosphodiesterases (PDEs). There are eleven families of PDEs (1 through 11) as well as multiple sub-families from which numerous isoforms are generated by alternate mRNA splicing. We, and others have found that specific PDE isoforms exhibit tumor promoting qualities and that PDE inhibitors possess potent anti-tumor activity. In order to investigate the molecular basis for PDE actions in brain tumor biology, we rigorously examined the patterns of PDE isoform expression. In the following chapter we focus on the PDE4 sub-family of cAMP specific hydrolases and discuss several challenges that arise when examining their patterns of expression by western blotting, immuno-histochemistry and immuno-fluorescence.

Keywords Cyclic AMP · PDE inhibitors · Adenylyl cyclases · PDE4 · Neoplasms · Rolipram

Introduction

Central to advancing the care for patients with malignant neoplasms are efforts to delineate how cancer cells differ from their normal counterparts, and the identification of biological targets whose activity, when normalized, corrects the cancer phenotype and re-establishes normal growth control. In this regard we and others have described the tumor promoting actions of cyclic adenosine monophosphate (cAMP) phosphodiesterases and the antitumor effects of phosphodiesterase inhibitors. In the following chapter we will focus on the unique biology of the cAMP phosphodiesterase-4 (PDE4) family of cAMP hydrolases as it pertains to brain tumors and the experimental challenges that arise when studying patterns of PDE4 expression.

Furman and Shulman (1977) first recognized the relationship between abnormally low levels of cAMP and brain tumor growth. They found that both the activity of the cAMP synthetase, adenylate cyclase, and cAMP levels were inversely correlated with the degree of malignancy of brain tumors. The importance of PDE4 to tumor biology was first suggested by the antitumor activity of the PDE4 inhibitor Rolipram when tested in vitro against breast and lung carcinoma cell lines (Drees et al. 1993; Merz et al. 1998). More recently, McEwan et al. demonstrated Rolipram activity against colon carcinoma cells (McEwan et al. 2007), and we found that decreased cAMP levels stimulate brain tumor growth in vivo and that drugs that can elevate cAMP, including Rolipram, exhibit significant antitumor effects (Goldhoff et al. 2008; Yang et al. 2007). These studies strongly suggest that the PDE4 family of enzymes and PDE4 inhibitors be vigorously evaluated as vital targets to oncology.

Phosphodiesterases hydrolyze intracellular cAMP and cGMP to their respective 5' monophosphate forms, and thereby function as negative regulators of multiple cyclic nucleotide-dependent processes. The

J.B. Rubin (✉)
Division of Pediatric Hematology/Oncology, Department of Pediatrics, Washington University School of Medicine, St. Louis, MO 63110, USA
e-mail: Rubin_J@kids.wustl.edu

M.A. Hayat (ed.), *Tumors of the Central Nervous System, Volume 4*,
DOI 10.1007/978-94-007-1706-0_13,

PDE superfamily contains 11 subfamilies that are distinguished by sequence homology, substrate affinity, enzyme kinetics, and modulation by specific regulators (Conti and Jin 1999). The PDE4 subfamily is highly specific for cAMP and abundant in the brain (Cherry and Davis 1999). PDE4 was found to be the predominant isoform expressed in approximately two-thirds of 60 human tumor cell lines (Marko et al. 2000), and expression correlated with malignancy in mouse keratinocyte derived carcinoma lines (Marko et al. 1998). PDE4 expression was also evaluated in six human glioblastoma multiforme (GBM) cell lines where it was found to be present, but at lower levels than PDE1, a combined cAMP/cGMP hydrolase (Marko et al. 2000). We found that several histological subtypes of brain tumors expressed high levels of PDE4 and that PDE4 inhibition, in combination with standard radiation and chemotherapy, promoted a unique tumor regression in an intracranial xenograft model of GBM (Goldhoff et al. 2008).

The PDE4 family of phosphodiesterases can be further subdivided into four subfamilies derived from separate genes (A–D). From these four genes at least 35 different functional isoforms are generated (Lugnier 2006). Through distinct combinations of localization motifs, regulatory sites and protein–protein interacting domains, the multiplicity of PDE4 isoforms performs a wide array of tissue and subcellular compartment specific functions (Lynch et al. 2006). For instance, only PDE4D5 regulates PKA-dependent heterotrimeric G protein switching by β_2 – adrenergic receptors (Lynch et al. 2005). Similarly, PDE4D3 and PDE4C2, but not PDE4A4 or PDE4B1, are required for basal AKAP450-tethered protein kinase type II activity (McCahill et al. 2005).

The range of function and form within the PDE4 family constitutes an experimental challenge for those

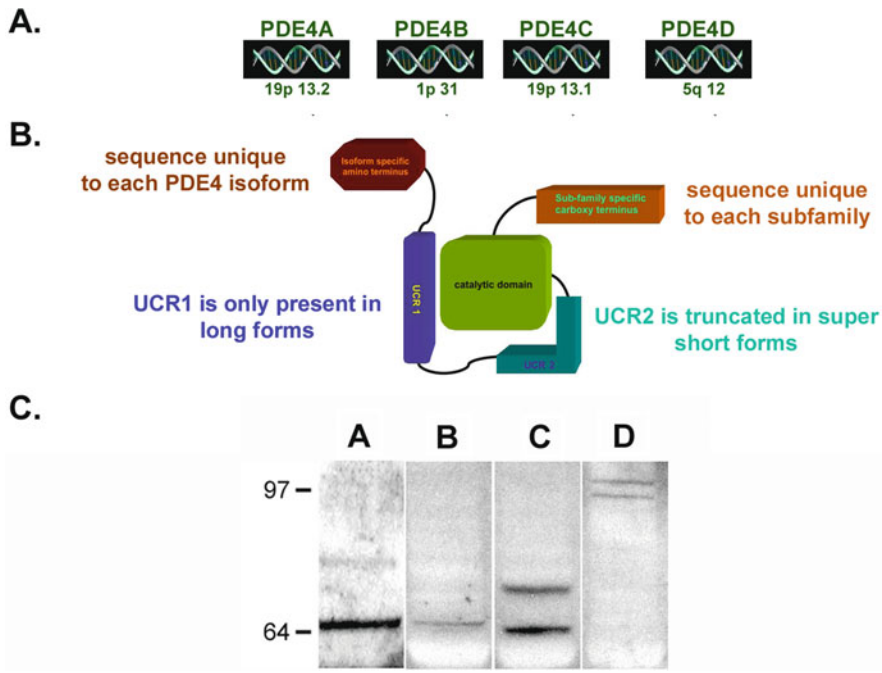

Fig. 13.1 PDE4 exists as multiple isoforms. (**a**) Chromosomal location of the four PDE4 genes (A–D). (**b**) Domain organization of PDE4 isoforms consisting of unique isoform specific amino terminus, upstream conserved regions (UCR) 1 and 2, catalytic domain and subfamily (A–D) specific carboxy terminus. Long forms contain all five domains. Short and supershort forms do not contain UCR1. Supershort forms contain a truncated UCR2. (**c**) Western blots of U87 glioblastoma cells probed with the human specific antibody for PDE4A (Houslay) and with PDE4 subfamily specific antibodies from FabGennix lanes B through D. U87 cells express PDE4A isoforms of 66 and 80 kDa likely corresponding to PDE4A1 and PDE4Ax. The PDE4B antibody also reveals a band at 66 kDa indicating that U87 cells also express PDE4B4. Two isoforms of PDE4C are evident in U87 cells at 64 and 73 kDa. These correspond PDE4C2 and PDE4C3, respectively. Finally, the PDE4D antibody reveals a high molecular weight doublet corresponding to PDE4D3 at 95 kDa and PDE4D5 at 105 kDa

interested in evaluating changes in expression or localization as a basis for a difference in PDE4 activity. It is likely that functionally significant variations in PDE4 activity result from modulation in the expression or localization of a limited number of isoforms. Thus, antibody reagents that cannot distinguish between isoforms may, in some circumstances, be less useful than those that can. In this regard some consideration for the domain organization of the PDE family is warranted. The fundamental domain organization of PDE4 includes unique, isoform specific amino-terminal regions, two regulatory domains referred to as upstream conserved regions (UCR1 and UCR2), a highly conserved catalytic unit, and a subfamily or gene specific carboxy terminal domain (Fig. 13.1). The multiplicity of PDE4 isoforms arises from splice variants that are derived from the four PDE4 genes (A–D). This results in three groups of PDE4 molecules: the long isoforms which include complete UCR1 and UCR2, the short isoforms which contain only UCR2, and the super-short isoforms which contain a truncated UCR2. Thus, while the potential exists to utilize isoform specific reagents directed against the unique amino termini, most commercially available antibodies are directed against the carboxy-terminus and recognize all the members of one PDE4 subfamily without further distinction. Finally, while the carboxy-termini of PDE4B, PDE4C, and PDE4D are conserved between humans and rodents, the carboxy termini of human and rodent PDE4A diverge considerably.

Materials and Methods

Phosphodiesterase function is dependent upon which PDE4 isoforms are expressed, what their subcellular localization is, and what other proteins they are in complex with. Each of these elements of PDE4 function can be assessed with immunochemical methods. It is imperative that only the appropriate antibody reagents be utilized. Commercially available antibodies include those directed against a synthetic peptide common to most of the PDE4 subtypes and belonging to the PDE4A and D subfamilies. Alternatively, there are antibodies directed against the carboxy-terminus that can distinguish between members of different subfamilies. Furthermore, there are some isoform specific antibodies as well as antibodies against phosphorylated PDE4, such as the phospho-PDE4A-selective antibody. Finally, while many commercial antibody specifications indicate cross-reaction between human and animal PDE4, the sequence divergence between murine and human PDE4A can make this less likely, and caution should be used when identification of the immunizing peptide is treated as proprietary information. In the following sections we provide detailed protocols for investigating PDE4 protein expression.

Western Blotting

Materials

1. Cell lysates were obtained from U87 cells, an established human brain tumor cell lines (ATTC)
2. Phosphate buffered saline (PBS), pH 7.35
3. RIPA buffer: 150 mM NaCl, 10 mM Tris (pH 7.2), 0.1% SDS, 1.0% Triton X-100, 1% deoxycholate and 5 mM EDTA
4. Protease inhibitor cocktail: (1 mM phenylmethylsulfonyl fluoride, 10 mM benzamidine, aprotinin 5 μg/ml, leupeptin 5 μg/ml)
5. Protein Assay Bio-Rad DC Bradford system
6. NuPAGE LDS Sample Buffer (4X) Invitrogen (NP0007)
7. NuPAGE DTT Sample Reducing Agent Invitrogen (NP0004)
8. Molecular weight marker SeeBlue Plus2 Invitrogen (LC5925)
9. NuPAGE 10% Bis-Tris Gel Invitrogen (NP0301)
10. NuPAGE MOPS SDS Running Buffer Invitrogen (NP0001)
11. Gel running apparatus
12. Nitrocellulose Membrane Amersham
13. Transfer apparatus
14. NuPAGE Transfer Buffer Invitrogen (NP0006)
15. Tris buffered saline with 0.01% Tween-20 in TBST (pH 7.6)
16. Bovine serum albumin (BSA)
17. Antibodies used and their concentrations were as follows:
    a. hPDE4A-PDE-46 noncommercial polyclonal antibody made against human PDE4A (GST 788-886) used at a dilution of 1:400 (kind gift from M.D. Houslay)

b. PDE4B- FabGennix (PD4-201AP) made against undisclosed synthetic peptides corresponding to N- & C-terminal region common to all PDE4B subtypes, used at a concentration of 1 μg/ml
c. PDE4C-FabGennix (PD4-301AP) made against an undisclosed synthetic peptide common to all PDE4C subtypes, used at a concentration of 1 μg/ml
d. PDE4D-FabGennix (PD4-401AP) made against an undisclosed synthetic peptide common to all PDE4D subtypes, used at a concentration of 1 μg/ml

18. Goat anti-Rabbit-HRP Biorad (170-6515) used at a dilution of 1:25,000
19. Chemiluminescent Detection SuperSignal West Pico Pierce (34080)

Methods

Western blotting is a method for quantifying protein expression in cell or tissue lysates. Under the denaturing conditions described below, electrophoresis of proteins through an acrylamide gel will result in their separation based on size. Immunolabeling of separated protein bands provides a reliable method for identification of individual proteins such as specific isoforms of PDE4. The coupling of antibody labeling to photon-emitting reactions or fluorescent tags supports the quantitation of relative protein abundance. Thus, Western blotting can identify which PDE4 isoforms are expressed and provide information regarding relative levels of expression between different cell lines or tissues as well as information regarding up- or down-regulation of specific isoforms under different growth conditions or in response to different stimuli (Fig. 13.1).

(1) Human astrocytoma cells (U87) are grown in serum supplemented media on 10 cm plates. When the cells are confluent, the plates are removed from the incubator and placed onto ice and rinsed two times with ice cold PBS.
(2) Remove the PBS and add 0.5 ml RIPA lysis buffer supplemented with protease inhibitor cocktail to each 10 cm plate.
(3) Scrape cells with a cell scraper into the RIPA buffer and transfer to microfuge tube.
(4) Incubate on ice for 10 min. Vortex every few minutes to dissolve cell membranes. Alternatively, cells and tissue can be solubilized in a sonicator.
(5) Centrifuge samples at 10,000 rpm for 5 min in a microfuge to pellet insoluble material.
(6) Remove supernatant and discard the pellet.
(7) Determine protein concentration of the supernatant with an assay kit according to manufacturer's instructions. We typically utilize the Bradford Assay (Bio-Rad).
(8) Take a volume of supernatant that corresponds to 25 μg of protein, add 4X concentrate of sample buffer and 10% by volume of DTT and heat to 70° C in boil proof Eppendorf tube for 10 min.
(9) Load cooled mixture onto a 10% Bis-Tris gel. Load 5 μl of molecular weight markers into a separate lane.
(10) Run gels at 100 V for 115 min or until a 17 kDa marker has run off the gel.
(11) Prepare the gel and nitrocellulose membranes for transfer by equilibrating in transfer buffer for 10 min.
(12) Gels and nitrocellulose paper are then mounted into a transfer apparatus.
(13) Transfer of proteins occurs at 150 V for 120 min.
(14) Membranes (now blots) are removed from transfer apparatus. Non-specific antibody labeling is reduced by soaking the membrane for 1 h at room temperature (R.T.) in 4% BSA in TBST.
(15) Primary antibodies are added to blots for overnight incubation at R.T. in 5 ml plastic sealable baggies and placed onto a nutator.
(16) The next day, blots are rinsed in TBST 3 times for 10 min/wash.
(17) Secondary antibody conjugated to HRP is added to blots at a concentration of 1:25,000 for 90 min at R.T. on the nutator.
(18) Blots are rinsed in TBST 3 times for 10 min/wash and then developed in chemiluminescent reaction system according to manufacturers instructions; we prefer the West Pico Substrate from Pierce.
(19) Blots are finally wrapped in Saran wrap, placed into a light tight cassette and developed with X-ray film in the dark room. Start with a 2 min exposure and change time as appropriate to develop bands on film.
(20) Use molecular weight marker lane to gauge molecular weights of the bands.
(21) To quantify protein expression, scan blots and quantify bands using Image J software from the

NIH, a free imaging software that can be downloaded at http://rsbweb.nih.gov/ij/download.html

Immunohistochemistry

Materials

1. Tissue sections were obtained from archival tissue blocks sectioned to 5 μm and placed onto positively coated (+) slides. Slides were dried in an oven for 1 h at 35°C.
2. Antigen Retrieval Solution Citrate buffer (pH 6.0) DAKO (S1699).
3. PAP Pen hydrophobic marker Vector (H-4000).
4. Tris buffered saline with 0.01% Tween-20 in TBST (pH 7.6).
5. Hydrogen peroxide 30 wt% solution in water Sigma-Aldrich (216763)
6. Avidin/Biotin Blocking Kit Vector (SP-2001)
7. Antibody diluent: 1% Milk in TBS (pH 7.6) heated to and held at 60ºC for 1 hour. After cooling, add 2% BSA, 0.1% Triton X-100, and 0.01% sodium azide
8. Normal swine serum Jackson ImmunoResearch (014-000-121)
9. Antibodies used and their concentrations were as follows:
   a. hPDE4A-PDE-46 (GST 788-886) used at a dilution of 1:400
   b. Swine anti-Rabbit Biotin Conjugate DAKO (E0431) used at a dilution of 1:450
10. Streptavidin-HRP DAKO (P0397) used at a dilution of 1:450
11. Diaminobenzidine Chromogen DAKO (K4366)
12. Hematoxylin Counterstain Gill 2 Richard-Allan Scientific (72504)
13. Permount Fisher Scientific (SP15)
14. Xylenes and alcohols found in a typical histology staining system

Methods

Immunohistochemistry is a method for detecting and localizing proteins of interest in tissue sections. Investigators can determine which cell types express a particular protein through colocalization of that protein and a second protein whose expression is limited to a specific cell type. As an example (Fig. 13.2), we found that hPDE4A was localized to cells that had been found to express glial fibrillary acidic protein (GFAP) in serial sections (data not shown). In this fashion we were able to conclude that astrocytoma cells express PDE4A.

(1) Deparaffinize slides and bring to H_2O (2 washes in xylene 5 min/wash, 2 washes in 100% EtOH 5 min/wash, 1 wash in 90% EtOH for 5 min and then place into 100% dH_2O. All washes are done at R.T.
(2) Antigen Retrieve in 0.01 M sodium citrate (pH 6.0) at 95°C for 10 min, cool down on desktop for 10 min.
(3) Rinse slides briefly in dH_2O, circle tissue with PAP Pen.
(4) Block endogenous peroxide with H_2O_2 (3% in TBST for 15 min at R.T.).
(5) Wash briefly in TBST.
(6) Block with avidin/biotin for 15 min at R.T., each reagent following manufacturers instructions.
(7) Wash briefly in TBST after each block.
(8) Block with 10% normal swine serum in diluent for 1 h at R.T.
(9) Drain blocking solution and incubate in primary antibody overnight at R.T.
(10) The next day, wash three times in TBST for 10 min/wash at R.T.
(11) Incubate in Secondary Swine α Rabbit-Biotin conjugate for 90 min at a dilution of 1:450 at R.T.
(12) Wash 3 times in TBST for 5 min/wash at R.T.
(13) Incubate in streptavidin–HRP for 60 min at a dilution of 1:450 at R.T.
(14) Wash three times in TBST for 5 min/wash at R.T.
(15) Develop in DAB following manufacturers instructions for 5 min or until there is sufficient staining.
(16) Counterstain with hematoxylin.
(17) Dehydrate through a series of alcohols and xylenes.
(18) Mount with Permount, allow to dry overnight and photograph.

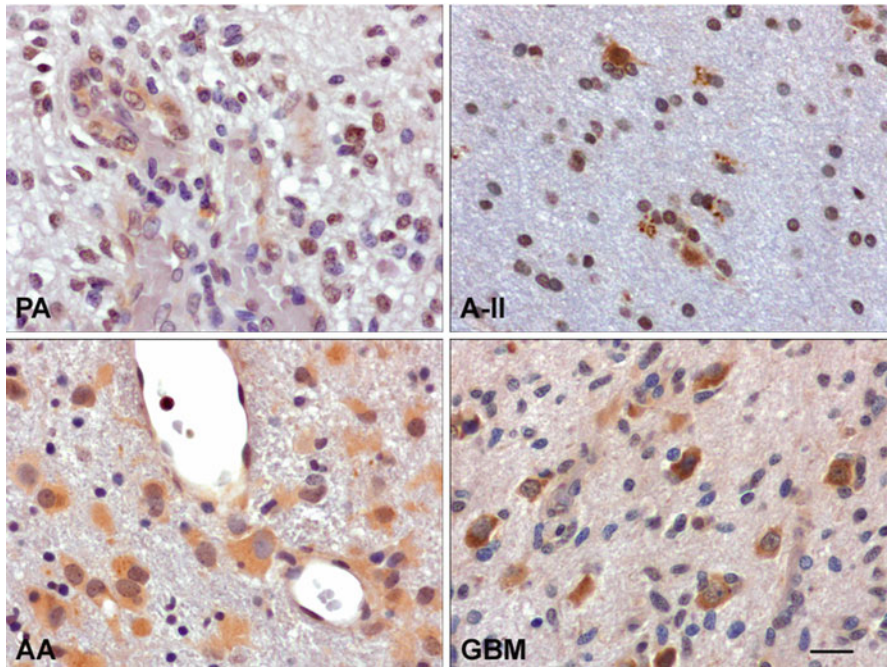

Fig. 13.2 Astrocytomas of all grades express PDE4. Immunohistochemical staining of human tumor specimens. PA – Grade I Pilocytic Astrocytoma; A-II – Grade II Astrocytoma; AA – Grade III Anaplastic Astrocytoma; GBM – Grade IV Glioblastoma stained using a human specific PDE4A antibody. In all cases positive staining for PDE4A appears *brown*. Scale bar is 20 μm

Immunocytochemistry

Materials

1. DAOY cells, an established human medulloblastoma cell line (ATCC) engineered to express murine PDE4A1.
2. Fixative, Prefer, an aqueous glyoxal fixative obtained from Anatech Ltd.
3. Tris buffered saline with 0.01% Tween-20 in TBST (pH 7.6)
4. Antibody Diluent: pH 7.6 Tris Buffered Saline (TBS) with 2% IgG free BSA Jackson ImmunoResearch (001-000-161), 0.1% Triton X-100 and 0.01% sodium azide
5. Normal Donkey serum Jackson ImmunoResearch (017-000-121)
6. Antibodies used and their concentrations were as follows:
   a. PDE4A-Abcam (ab 14607) C-terminal region specific antibody raised against an undisclosed peptide, used at a concentration of 4 μg/ml
   b. 58 K Golgi Protein- Abcam (ab27043) made against full length purified native rat protein and used at a concentration of 1 μg/ml
   c. Donkey anti-Rabbit AlexaFluor 555 Molecular Probes (A-31572) used at a dilution of 1:2000
   d. Donkey anti-Mouse AlexaFluor 488 Molecular Probes (A-21202) used at a dilution of 1:2000
7. DAPI 4', 6-diamidino-2-phenyl-indole dihydrochloride Molecular Probes (D-1306) 14.3 mM stock at a dilution of 1:10,000
8. Immu-Mount mounting media Thermo Scientific (9990402)

Methods

Immunocytochemistry is a method for detecting and localizing proteins of interest in cells grown in culture. Through the use of multiple antibodies and fluorophore detection techniques, more than one protein can be detected simultaneously. Thus, co-localization of a protein of interest with a marker of a subcellular organelle can identify that organelle as a domain in which the protein functions. As an example, the subcellular localization of virally encoded murine PDE4A1 to the Golgi membranes of Daoy cells was achieved by double labeling cells with an antibody directed against murine PDE4 and a second antibody

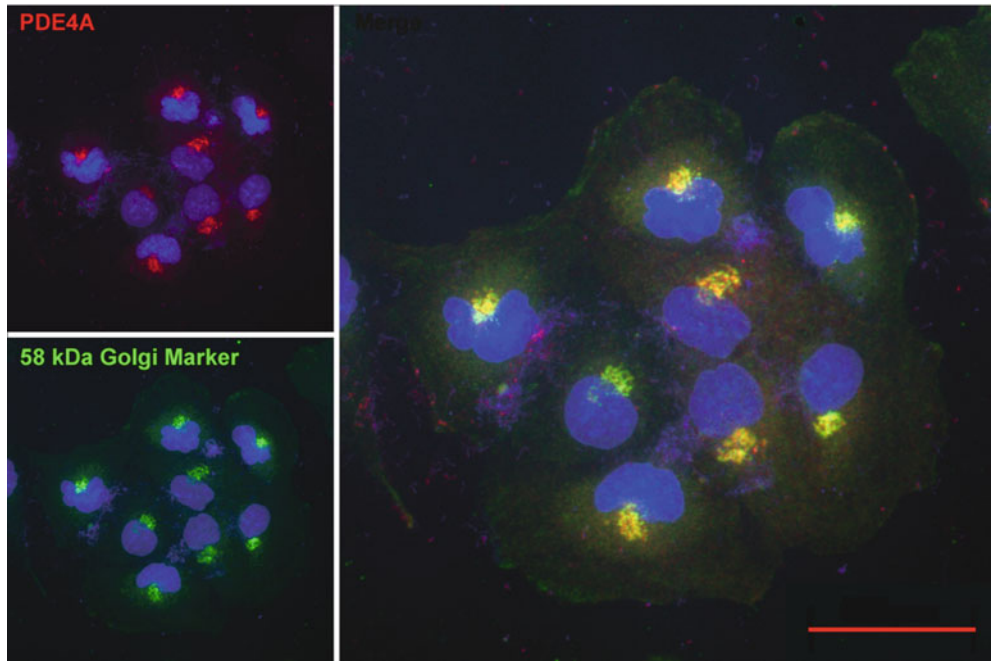

Fig. 13.3 PDE4A1 is localized to the Golgi. Daoy medulloblastoma cells were infected with lentivirus encoding murine PDE4A1. Immunofluorescent co-localization of murine PDE4A (*red*) and a 58 kDa Golgi Marker (*green*) reveals that the two proteins are co-localized as evidenced by *yellow* appearance when the color channels are combined. Nuclei are stained with DAPI. Scale bar is 20 μm

directed against the 58KD Golgi Marker. The use of green and red fluorophores allows for the detection of protein colocalization through the merging of the green and red images and the generation of a yellow signal in the regions of co-localization (Fig. 13.3).

(1) Human DAOY medulloblastoma cells expressing murine PDE4A1 are grown on coverslips.
(2) Rinse with ice cold TBS twice briefly.
(3) Fix with ice-cold fixative for 15 min on ice.
(4) Wash 2 times with TBST for 1 min/wash at R.T.
(5) Permeabilize cells with 0.5% Triton X-100 for 10 min at R.T.
(6) Wash three times in TBST for 10 min/wash at R.T.
(7) Block with 5% normal donkey serum in diluent for 60 min at R.T.
(8) Remove blocking solution without rinsing.
(9) Incubate in both primaries overnight at 4°C.
(10) The next day, wash three times in TBST for 10 min/wash.
(11) Incubate in both secondary Alexafluors for 90 min at R.T.
(12) Remove antibody solution and incubate with DAPI for 10 min at R.T.
(13) Wash three times TBST for 10 min/wash at R.T.
(14) Mount with Immu-Mount.

Results and Discussion

A strong relationship exists between malignant brain tumor growth and low levels of cAMP (Furman and Shulman 1977; Racagni et al. 1983). In general, low levels of cAMP may be attained through either inhibition of adenylate cyclase as occurs downstream of Gi-coupled G protein coupled receptors (Sunahara and Taussig 2002), or through increased action of phosphodiesterases (Lugnier 2006). We have generated data to support both mechanisms for maintaining low levels of cAMP (Goldhoff et al. 2008; Warrington et al. 2007; Yang et al. 2007) and present data here that indicate PDE4 is highly expressed in both astrocytomas and medulloblastomas (Figs. 13.1, 13.2, and 13.3).

It is not realistic to speak of cAMP levels as if a single level applies to the entire cell. Indeed, fluorescent probes for cAMP levels have made it clear that cAMP levels change within microdomains suggesting that it is microdomains of cAMP that regulate cellular function (Ponsioen et al. 2004). In this regard the described functions of the PDE4 family are particularly relevant. The extended family of PDE4 isoforms allows not only for tissue specific expression of PDE4 activity but subcellular localization of different isoforms, which support the spatial resolution of cAMP signaling. As an example, we have found that PDE4A1 stimulates brain tumor growth (Goldhoff et al. 2008; Yang et al. 2007). This particular isoform of PDE4 is localized to the Golgi (Fig. 13.3). Thus, the cAMP-sensitive mediators of PDE4A1 effects must also be localized to this domain.

Utilizing the methods described above it is possible to detect individual PDE4 isoforms in tissue and cells and to localize PDE4 to particular cells and to subcellular compartments (Figs. 13.2 and 13.3). These studies provide the foundation for generating hypotheses about specific PDE4 isoforms and function. Coupled with techniques to generate mutant PDE4 isoforms in which localization, catalytic and protein–protein interacting domains are disrupted, these kinds of studies allow investigators to dissect out the dependence of specific PDE4 functions on particular PDE4 domains (Huston et al. 2006; Scotland and Houslay 1995; Shakur et al. 1993).

Among the most attractive aspects of PDE4 inquiry is the number of clinically available PDE4 inhibitors. Currently there is an active program for the evaluation of PDE inhibition in the treatment of chronic obstructive pulmonary disease (Spina 2008). There are nearly twenty clinically available, some with known isoform specificity. This has the advantage of efficacy for specific indications without excessive toxicity or off target effects. Ample preclinical investigation, demonstrating a potential application would stand the chance of rapid translation.

Rolipram, a pan-PDE4 inhibitor, was developed as an anti-depressant (Wachtel and Schneider 1986) and has also been evaluated as an anti-inflammatory in multiple sclerosis (Dyke and Montana 2002). It is relatively well tolerated with nausea and emesis the limiting toxicities. Rolipram penetrates into the central nervous system and does not induce its own metabolism. Based on the activity of cAMP analogues as antitumor cell agents, Rolipram has been evaluated for antitumor cell activity in a limited number of in vitro studies. Antitumor activity has been described for chronic B-cell leukemia cells (Siegmund et al. 2001), acute lymphocytic leukemia (Ogawa et al. 2002) as well as for an astrocytoma cell line (Chen et al. 2002). Further, we have evaluated Rolipram in an extensive in vivo study in which we compared the antitumor effect of Rolipram alone to Rolipram in combination with conformal radiotherapy and temozolomide in an intracranial xenograft model of glioblastoma multiforme. Rolipram, in combination with radiation and temozolomide was observed to promote significant tumor regression (Goldhoff et al. 2008). These data again emphasize the importance of cAMP to brain tumor growth and the importance of PDE4 to cAMP regulation in brain tumors.

The scope of investigations into identifying individual PDE4 isoforms, their physiological roles, their subcellular localization, associated interacting proteins and the impact of specific inhibitors on numerous biological functions and in diseases will be a richly promising and rewarding line of work for some time to come.

References

Chen TC, Wadsten P, Su S, Rawlinson N, Hofman FM, Hill CK, Schonthal AH (2002) The type IV phosphodiesterase inhibitor rolipram induces expression of the cell cycle inhibitors p21(Cip1) and p27(Kip1), resulting in growth inhibition, increased differentiation, and subsequent apoptosis of malignant A-172 glioma cells. Cancer Biol Ther 1:268–276

Cherry JA, Davis RL (1999) Cyclic AMP phosphodiesterases are localized in regions of the mouse brain associated with reinforcement, movement, and affect. J Comp Neurol 407:287–301

Conti M, Jin SL (1999) The molecular biology of cyclic nucleotide phosphodiesterases. Prog Nucl Acid Res Mol Biol 63:1–38

Drees M, Zimmermann R, Eisenbrand G (1993) 3′,5′-Cyclic nucleotide phosphodiesterase in tumor cells as potential target for tumor growth inhibition. Cancer Res 53: 3058–3061

Dyke HJ, Montana JG (2002) Update on the therapeutic potential of PDE4 inhibitors. Expert Opin Investig Drugs 11:1–13

Furman MA, Shulman K (1977) Cyclic AMP and adenyl cyclase in brain tumors. J Neurosurg 46:477–483

Goldhoff P, Warrington NM, Limbrick DD Jr, Hope A, Woerner BM, Jackson E, Perry A, Piwnica-Worms D,

Rubin JB (2008) Targeted inhibition of cyclic AMP phosphodiesterase-4 promotes brain tumor regression. Clin Cancer Res 14:7717–7125

Huston E, Gall I, Houslay TM, Houslay MD (2006) Helix-1 of the cAMP-specific phosphodiesterase PDE4A1 regulates its phospholipase-D-dependent redistribution in response to release of Ca2+. J Cell Sci 119:3799–3810

Lugnier C (2006) Cyclic nucleotide phosphodiesterase (PDE) superfamily: a new target for the development of specific therapeutic agents. Pharmacol Ther 109:366–398

Lynch MJ, Baillie GS, Mohamed A, Li X, Maisonneuve C, Klussmann E, van Heeke G, Houslay MD (2005) RNA silencing identifies PDE4D5 as the functionally relevant cAMP phosphodiesterase interacting with beta arrestin to control the protein kinase A/AKAP79-mediated switching of the beta2-adrenergic receptor to activation of ERK in HEK293B2 cells. J Biol Chem 280:33178–33189

Lynch MJ, Hill EV, Houslay MD (2006). Intracellular targeting of phosphodiesterase-4 underpins compartmentalized cAMP signaling. Curr Top Dev Biol 75:225–59

Marko D, Pahlke G, Merz KH, Eisenbrand G (2000) Cyclic 3′,5′-nucleotide phosphodiesterases: potential targets for anticancer therapy. Chem Res Toxicol 13:944–948

Marko D, Romanakis K, Zankl H, Furstenberger G, Steinbauer B, Eisenbrand G (1998) Induction of apoptosis by an inhibitor of cAMP-specific PDE in malignant murine carcinoma cells overexpressing PDE activity in comparison to their nonmalignant counterparts. Cell Biochem Biophys 28:75–101

McCahill A, McSorley T, Huston E, Hill EV, Lynch MJ, Gall I, Keryer G, Lygren B, Tasken K, van Heeke G, Houslay MD (2005) In resting COS1 cells a dominant negative approach shows that specific, anchored PDE4 cAMP phosphodiesterase isoforms gate the activation, by basal cyclic AMP production, of AKAP-tethered protein kinase A type II located in the centrosomal region. Cell Signal 17:1158–1173

McEwan DG, Brunton VG, Baillie GS, Leslie NR, Houslay MD, Frame MC (2007) Chemoresistant KM12C colon cancer cells are addicted to low cyclic AMP levels in a phosphodiesterase 4-regulated compartment via effects on phosphoinositide 3-kinase. Cancer Res 67:5248–5257

Merz KH, Marko D, Regiert T, Reiss G, Frank W, Eisenbrand G (1998) Synthesis of 7-benzylamino-6-chloro-2-piperazino-4-pyrrolidinopteridine and novel derivatives free of positional isomers. Potent inhibitors of cAMP-specific phosphodiesterase and of malignant tumor cell growth. J Med Chem 41:4733–4743

Ogawa R, Streiff MB, Bugayenko A, Kato GJ (2002) Inhibition of PDE4 phosphodiesterase activity induces growth suppression, apoptosis, glucocorticoid sensitivity, p53, and p21(WAF1/CIP1) proteins in human acute lymphoblastic leukemia cells. Blood 99:3390–3397

Ponsioen B, Zhao J, Riedl J, Zwartkruis F, van der Krogt G, Zaccolo M, Moolenaar WH, Bos JL, Jalink K (2004) Detecting cAMP-induced Epac activation by fluorescence resonance energy transfer: Epac as a novel cAMP indicator. EMBO Rep 5:1176–1180

Racagni G, Pezzotta S, Giordana MT, Iuliano E, Mocchetti I, Spanu G, Sangiovanni G, Paoletti P (1983) Cyclic nucleotides in experimental and human brain tumors. J Neurooncol 1:61–67

Scotland G, Houslay MD (1995) Chimeric constructs show that the unique N-terminal domain of the cyclic AMP phosphodiesterase RD1 (RNPDE4A1A; rPDE-IVA1) can confer membrane association upon the normally cytosolic protein chloramphenicol acetyltransferase. Biochem J 308 (Pt 2):673–681

Shakur Y, Pryde JG, Houslay MD (1993) Engineered deletion of the unique N-terminal domain of the cyclic AMP-specific phosphodiesterase RD1 prevents plasma membrane association and the attainment of enhanced thermostability without altering its sensitivity to inhibition by rolipram. Biochem J 292 (Pt 3):677–686

Siegmund B, Welsch J, Loher F, Meinhardt G, Emmerich B, Endres S, Eigler A (2001) Phosphodiesterase type 4 inhibitor suppresses expression of anti-apoptotic members of the Bcl-2 family in B-CLL cells and induces caspase-dependent apoptosis. Leukemia 15:1564–1571

Spina D (2008) PDE4 inhibitors: current status. Br J Pharmacol 155:308–315

Sunahara RK, Taussig R (2002) Isoforms of mammalian adenylyl cyclase: multiplicities of signaling. Mol Interv 2:168–184

Wachtel H, Schneider HH (1986) Rolipram, a novel antidepressant drug, reverses the hypothermia and hypokinesia of monoamine-depleted mice by an action beyond postsynaptic monoamine receptors. Neuropharmacology 25:1119–1126

Warrington NM, Woerner BM, Daginakatte GC, Dasgupta B, Perry A, Gutmann DH, Rubin JB (2007) Spatiotemporal differences in CXCL12 expression and cyclic AMP underlie the unique pattern of optic glioma growth in neurofibromatosis type 1. Cancer Res 67:8588–8595

Yang L, Jackson E, Woerner BM, Perry A, Piwnica-Worms D, Rubin JB (2007) Blocking CXCR4-mediated cyclic amp suppression inhibits brain tumor growth *in vivo*. Cancer Res 67:651–658

Part IV
Imaging

Chapter 14

Molecular Imaging of Brain Tumours Using Single Domain Antibodies

Abedelnasser Abulrob, Umar Iqbal, Boguslaw Tomanek, and Danica Stanimirovic

Abstract Glioblastoma multiforme (GBM) is the most malignant type of brain neoplasm with an average patient survival of 15 months under the current treatment regime. The failure of therapeutic approaches including surgical resections is due to multiple factors, including molecular diversity of GBMs, invading micro-metastases, presence of tumor stem cells, molecular drug resistance, as well as difficulties of delivering therapeutics across the vascular brain-tumor barrier. Non-invasive imaging of molecular make-up of GBM could facilitate the identification of critical disease features and tailoring of treatments to individual disease variants, respectively. Development of such molecular imaging agents requires integration of tumor biomarker discovery with the development of biomarker-targeting molecular imaging agents, and their validation in pre-clinical disease models. This chapter will describe processes and techniques involved in the pre-clinical development of molecular imaging agents for brain tumors, with the particular emphasis on workflows leading from biomarker selection to developing single-domain antibody-targeted imaging probes to visualize and evaluate biomarker expression by in vivo imaging using various imaging modalities.

Keywords Magnetoencephalography · Molecular imaging agents · Brain neoplasm · Single-domain antibody · BOLD technique · Biomarker expression

A. Abulrob (✉)
Institute for Biological Sciences, National Research Council of Canada, Ottawa, ON, Canada
e-mail: Abedelnasser.abulrob@nrc-cnrc.gc.ca

Introduction

Molecular Imaging

The Society for Nuclear Medicine broadly defines *molecular imaging* as the visualization, characterization, and measurement of biological processes at the molecular and cellular levels in humans and other living systems. *Molecular imaging agents* are probes used to visualize, characterize, and measure biological processes in living systems. Both endogenous molecules and exogenous probes can be molecular imaging agents.

The broader definitions of molecular imaging separate anatomy from function and equate molecular imaging with functional studies that use contrast media and radiopharmaceuticals whose biodistribution does not have a strong mass dependency, and include measurements of blood flow, blood volume, perfusion, glomerular filtration, phagocytosis, hepatocyte clearance and bone adsorption. A recent publication by Thakur and Lentle (2006) narrowed the definition of molecular imaging by eliminating several of these approaches such as MRI using the blood oxygen level dependent (BOLD) technique, MR diffusion tensor sequences, and magnetoencephalography among others. A further refinement of the scope of molecular imaging addresses specific and saturable binding of a probe to a target protein. This implies low capacity targets such as enzymes and receptors. In the post genomic era, approaches involving proteomics, genomics, antisense mRNA, reporter genes, protein–protein interactions, and others expanded the inventory of potential targets for molecular imaging probe development from less than a hundred to thousands,

M.A. Hayat (ed.), *Tumors of the Central Nervous System, Volume 4*,
DOI 10.1007/978-94-007-1706-0_14,

particularly in the field of oncology. In this chapter, molecular imaging will be interpreted as in vivo imaging of the expression, abundance or activity of a specific biomarker (protein) using contrast agents specifically targeted/designed to bind/recognize this biomarker.

Molecular imaging instrumentation comprises tools that enable visualization and quantification in space and over time of signals from molecular imaging agents. The techniques used include radiotracer imaging/nuclear medicine, magnetic resonance (MR) imaging, MR spectroscopy, optical imaging, ultrasound, and others. The combination of multiple imaging modalities often offers synergistic advantages over any modality alone, such as improved sensitivity, better spatial resolution, and access to combined molecular, anatomical and functional information. Many hybrid systems that combine two or more imaging modalities, such as PET-CT or PET-MRI, are often used in molecular imaging.

In the last decade, the strong impetus for the development of molecular imaging diagnostics came from the quest for personalized medicine – therapy tailored to patient populations exhibiting specific molecular characteristics. This was made possible through genome-scale biomarker discovery efforts, as well as advancements in enabling technologies for contrast agent design and synthesis. This chapter will review recent progress in developing targeted probes for molecular imaging of brain tumors that combine biomarker selection with molecular imaging agent design and validation using a spectrum of enabling technologies ranging from antibody engineering to nanotechnology.

Brain Tumor Biomarkers

A *biomarker* is defined as a physical sign or laboratory measurement (in body fluids or by non-invasive imaging) that occurs in association with a pathological process and that has putative diagnostic and/or prognostic utility. A biomarker that is expected to predict the effect of a therapeutic intervention and is intended to serve as a substitute for a clinical endpoint is called a *surrogate end point*. For brain tumors clinically useful biomarkers should be able to provide information on: (a) early presence or spread of the disease; (b) differential diagnosis based on molecular characteristics, (c) prognosis based on progressive or invasive nature of the disease, (d) choice of treatment protocols (e.g., drug resistance), (e) tumor response to selected treatment, and (f) early disease recurrence.

Over last decade, efforts to discover useful GBM biomarkers have been focused on identification of 'typical' or common gene mutations as well as on the application of gene microarrays to identify differentiating molecular signatures of GBMs derived by biopsy or surgery. Several growth factors and their cognate receptors were found to be up-regulated or mutated in gliomas including platelet-derived growth factor (PDGF)-A, -B/PDGFR-α, -β, and epidermal growth factor (EGF)/EGFR (Wong et al. 1987). The EGFR gene is amplified in 40% of GBMs and these tumors often acquire additional genomic rearrangement of EGFR gene resulting in the expression of truncated receptor that shows constitutive tyrosine kinase activity, aberrant receptor signaling and processing (Nagane et al. 2001). The most common rearrangement of the EGFR gene (occurs in 50–60% of those that have the amplified EGFR) is an in-frame deletion of 801 bp, which make up exons 2–7 in the mRNA (known as EGFRvIII) that confers a dramatically enhanced tumorigenicity to GBM cells (Nishikawa et al. 1994). EGF- or PDGF-receptor activation results in stimulation of downstream signals including the PI3 kinase/AKT pathway, RAF/MAPK/ERK pathway and PLC-γ/PKC pathway. Activation of AKT causes a loss of function of the tumor suppressor gene PTEN (phosphatase and tensin homologue on chromosome 10), which is frequently found in GBMs. Other commonly seen gene mutations in human GBMs are deletion of INK4A-ARF (occurs in 60% GBMs) and alteration of p53 and MDM2 protein, all involved in the regulation of cell cycle. Primary and secondary GBMs are clinically and genetically different. Whereas de novo GBMs are characterized by EGFR amplification/overexpression, deletion of PTEN and INK4A-ARF, and over-expression of MDM2 protein, secondary GBMs occur in younger patients and involve serial accumulation of genetic alterations often associated with PDGFR amplification/overexpression and p53 hyper-activation.

The vasculature of GBM is heterogeneous, disorganized and tortuous with irregular diameter (Jain et al. 2007) and abnormalities in cellular (endothelial cells and pericytes) and acellular constituents. Endothelial cell hyperplasia is accompanied with increased vessel wall thickness, wide interendothelial junctions and 'openings' such as endothelial fenestrae, vesicles and transcellular holes, abnormal pericyte coverage and discontinuous basement membrane that often projects into the tumor parenchyma. The tumor vascular network exhibits erratic branching patterns and lacks hierarchy; tumor vessels are often described as immature. Structural abnormalities are associated with the aberrant function including a heterogeneous blood-brain barrier (BBB) disruption and vasogenic brain edema leading to increased interstitial fluid pressure.

Abnormal vascular gene expression is a key signature of tumor vessels. For example, VEGF/VEGFR-2 signaling is responsible for the increase in tumor vessel permeability (Machein et al. 1999), while down-regulation of anti-thrombotic molecules, such as antithrombin III, and overexpression of thrombomodulin cause intratumoral haemorrhage and intravascular thrombosis (Isaka et al. 1994). While GBM vessels lose the expression of several junctional molecules including VE-cadherin, claudin-1, -3, -5, and occludin, they show increased expression of the ATP binding cassette transporters, including P-glycoprotein and ABCG2, therefore, limiting the delivery of drugs into the brain. VEGF/VEGFR-2 complexes, integrins $\alpha v\beta 3$, $\alpha 5\beta 1$, endoglin (CD105), thrombospondin-1 receptor (CD36), Thy-1, prostate-specific membrane antigen (PSMA) and tumor endothelial markers (TEMs) (St Croix et al. 2000) have all been documented at higher levels in tumor compared to normal vessels. Genomic profiling technologies have contributed to the identification of novel markers in tumor endothelium that could be exploited for diagnostic or therapeutic purposes (St Croix et al. 2000). In a recent study (Pen et al, 2007), 69 differentially expressed genes were identified in the laser-capture microdissected vessels from human glioblastomas; one of these biomarkers, IGFBP7, was shown to be robustly and selectively upregulated in glioblastoma vessels, secreted by tumor endothelium and deposited in the tumor vessel basal lamina.

Brain tumor vascular biomarkers are particularly suitable for developing molecular imaging approaches. The rate of angiogenesis in brain tumors is prognostic and can differentiate between lower grades astrocytomas and glioblastomas. Furthermore, a majority of vascular antigens that are 'phenotypic' of tumor vessels could be accessed systemically, without need to cross the blood-tumor barrier (BTB). Tumor vessels (over)express a variety of drug efflux transporters important for choosing chemotherapeutics to circumvent drug resistance. Specific vascular imaging biomarkers can also aid differential diagnosis between radiation necrosis and tumor recurrence. Finally, tumor vessels can be targeted therapeutically to either inhibit angiogenesis or 'stabilize' vessels to enable better delivery of chemotherapeutics; responses to these therapies could be evaluated using vessel-targeted molecular imaging. In addition, *molecular* vascular changes assessed by molecular imaging techniques could be combined and correlated with *functional* vascular responses using blood oxygen level dependent (BOLD) technique, perfusion imaging, or neurovascular coupling by fMRI.

Despite notable progress in brain tumor biomarker discovery using gene and protein screening techniques, challenges remain in translating these biomarkers/biomarker signatures into tools useful in clinical decision-making. Critical features of the brain tumor biomarker exploitable for molecular imaging include *selectivity* to diseased tissue, enabling good contrast-to-noise ratio, *specificity* to the disease, enabling accurate diagnosis of the disease, *abundant expression* so that it can be reliably detected even with less sensitive techniques, such as MRI, and *accessibility* to systemically injected molecular imaging contrast agents. For example, for intratumoral biomarkers that have good predictive value (e.g., mutated/deleted EGFR), the imaging agent has to cross the brain–tumor barrier to access the biomarker; although dysfunctional, the brain-tumor barrier is restrictive for some small molecules and chemotherapeutics due to upregulation of efflux pumps, as well as for biologics due to preservation of relatively tight junctional complexes. Furthermore, high interstitial pressure within the tumor due to edema restricts free diffusion of therapeutic/imaging agents within the tumor. In contrast, some brain tumor vascular biomarkers are accessible from the systemic compartment and could be targeted by both small molecules and biologics; however, most of these biomarkers lack selectivity and their prognostic/predictive link to disease remains obscure.

Application of Domain Antibodies in Molecular Imaging

After selecting appropriate and informative biomarker conforming to criteria outlined in the previous section, its detection by non-invasive imaging necessitates the development of 'targeting' molecules that bind to the biomarker with sufficient specificity and affinity. These targeting molecules should be functionalized with the contrast appropriate for a specific imaging modality, e.g., fluorescent label for optical imaging, radiochemical for PET/SPECT, paramagnetic molecule for MRI, or a combination of these for multimodal imaging.

Biomarker targeting molecules have typically been small molecule radiopharmaceuticals or small organic probes developed as agonist/antagonist of specific brain receptors, neurotransmitters or misfolded proteins. During the last decade, biologics, including peptides and antibodies, have expanded the field of molecular imaging agent design for various indications including cancer and atherosclerosis. With the help of sophisticated bioconjugation and radiolabeling techniques, numerous peptide-based agents have been developed and evaluated for delivery of PET radionuclides to the specific molecular targets in preclinical and clinical studies. As compared to macromolecules, such as proteins or antibodies, low-molecular-weight peptides are advantageous for in vivo molecular imaging applications due to favorable pharmacokinetics. A relatively new class of cell penetrating peptides (CPPs) has opened the possibility of targeting contrast agents to intracellular and intranuclear targets, by introduction of membrane-transducing peptides in the design of new contrast agents. Whereas antibodies have higher specificity and affinity than peptides, the implementation of antibodies in molecular imaging has been limited by their extended circulation persistence, which is responsible for increased background activity. More recently, recombinant antibody fragments have been produced that retain high affinity for target antigens, and display a combination of rapid, high-level tumor targeting with concomitant clearance from normal tissues and the circulation in animal models. They also provide a useful building block for intermediate-sized recombinant fragments that can be tailored for improved targeting, clearance properties and avidity.

Single domain antibodies (sdAbs) are variable domains (VHH) of heavy chain antibodies, naturally occurring in camelid species (Hamers-Casterman et al. 1993). These antibody fragments have MW of 13 kDa, the 10th of the size of IgG (150 kDa), generally display high solubility and stability and can be readily produced in yeast, plant, and mammalian cells. Recombinant sdAbs have several advantages over conventional antibodies and the single chain variable fragments (scFv) derived from the V-domains of conventional antibodies, including high thermal stability, high refolding capacity, and good tissue penetration in vivo (Iqbal et al. 2010b; Dumoulin et al. 2002; Doyle et al. 2008). They often recognize targets inaccessible to conventional antibodies, such as sites in G protein-coupled receptors, protein cavities and active sites of enzymes (Lauwereys et al. 1998; Dumoulin et al. 2002). sdAb are typically isolated from non-immune camelid libraries by process of bio-panning against specific antigen, when they often have lower (nM–μM) affinities, or by clonal expansion of B-cells in the lymphoid organs of the immunized animals, when their affinities range from pM to nM. sdAbs can be readily cloned into various formats by fusion to other proteins or peptides, thereby tailoring their utility for certain diagnostic and/or therapeutic applications. Tandem cloning of two identical sdAbs connected by a linker peptide yields a bivalent reagent with higher avidity for the antigen (Roovers et al. 2007). Tandem cloning to an sdAb with a distinct specificity, e.g., for serum albumin, can help target the reagent to a particular compartment and/or help to increase the in vivo half life of the reagent (Roovers et al. 2007). A bivalent hcAb can be reconstituted by genetic fusion to the Fc-domain of any conventional antibody, e.g., mouse or human IgG1. sdAbs exhibit fast pharmacokinetic profiles (Iqbal et al. 2010b), desirable in molecular imaging applications where fast clearance from the circulation in combination with appropriate specificity and affinity can result in high signal/background ratios within reasonable time after contrast agent injection.

In examples described in this chapter, sdAbs isolated against two glioblastoma biomarkers, one intratumoral and one vascular, were evaluated in preclinical in vivo molecular imaging applications. The studies involved the design and recombinant production of sdAbs and various fusion molecules to tailor their affinity and pharmacokinetics, their bioconjugation with the optical contrast agent and their subsequent evaluation in the orthotopic glioblastoma model in mice using time-domain optical imaging. One of these

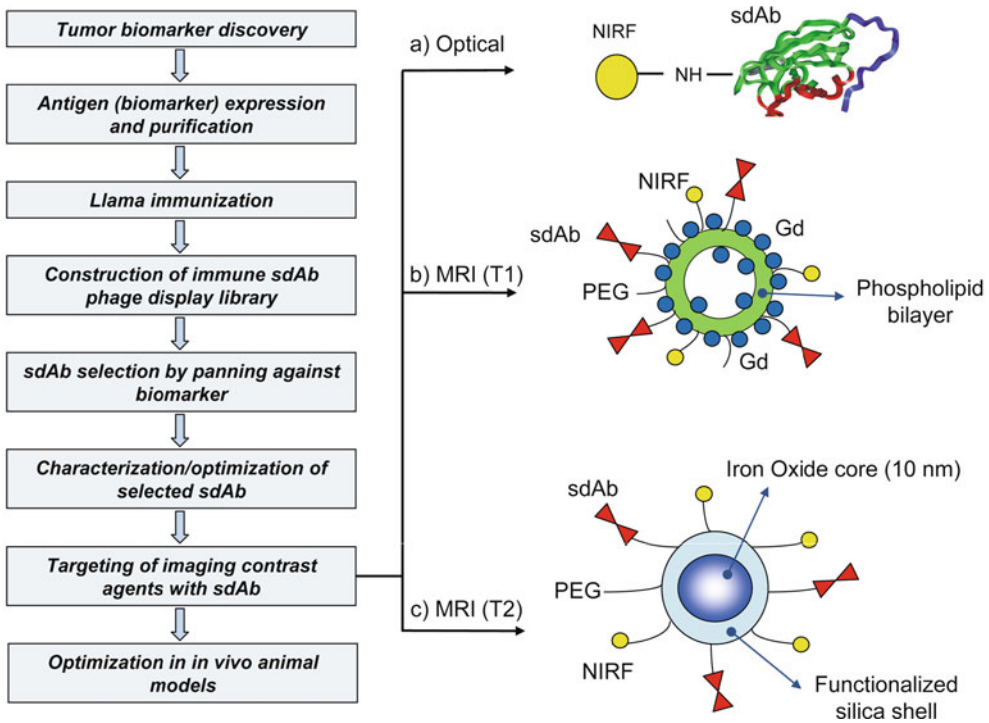

Fig. 14.1 Schematic of the approach used to develop single-domain antibody-targeted molecular imaging agents for brain tumors and conceptual drawings of described targeted imaging probes for optical and MR imaging modalities

antibodies was further evaluated as targeting agent for various nanoparticle formulations designed to exhibit contrast properties in MRI. The schematic of the development, optimization and bioconjugation workflow to develop sdAbs – targeted molecular imaging probes for various imaging modalities and their conceptual drawings are shown in Fig. 14.1.

Molecular Imaging Using Single Domain Antibodies Against EGFR

As discussed in "Brain Tumor Biomarkers" section, over-expression of EGFR and the presence of EGFRvIII has been considered one of molecular hallmarks of glioblastoma tumors. Because this biomarker is found in >50% of GBMs, has low expression in normal brain, is prognostic (i.e., correlates with tumor invasiveness), and is cell-surface expressed, it is considered an attractive target for molecular imaging purposes. However, the blood-tumor barrier limits the access to this parenchymal target. The study by Iqbal et al. (2010a), describes the development and characterization of the camelid sdAb, EG2, that recognizes both EGFR and EGFRvIII, as well as two additional recombinant formats of this sdAab, pentameric EG2 (V2C-EG2) and fusion with the human Fc-domain (EG2-hFc). All three antibody formats were bioconjugated with the near-infrared optical contrast, Cy5.5, and evaluated in the orthotopic GBM model (over-expressing both EGFR and EGFRvIII) in nude mice using time-domain in vivo optical imaging. The molecular size, apparent affinity and plasma half-lives of tested constructs are shown in Table 14.1. It is important to note that, although V2C-EG2 has higher molecular weight than EG2-hFc, its circulation half-life is shorter due to lack of Fc region and the susceptibility of the sdAb pentamerizing scaffold to proteolytic degradation in the circulation. Among the three constructs, EG2-hFc demonstrated the highest accumulation and retention in orthotopic GBM over a 72-h prospective imaging protocol (Fig. 14.2a), compared to early and transient tumor signal enhancement 1h after injection observed with V2C-EG2 and EG2. Whereas the short circulation half-lives of EG2 and

Table 14.1 Characteristics of three single-domain antibody constructs evaluated for in vivo imaging of orthotopic glioblastoma tumors

Construct	MW (kDa)	Apparent affinity	Plasma half-life
EG2 (monomeric)	15	55 nM (EGFR)–97 nM (EGFRvIII)	5 min
V2C-EG2 (pentameric)	128	10–40× greater than EG2	70 min
Fc-EG2 (dimeric)	80	50–600× greater than EG2	12 h

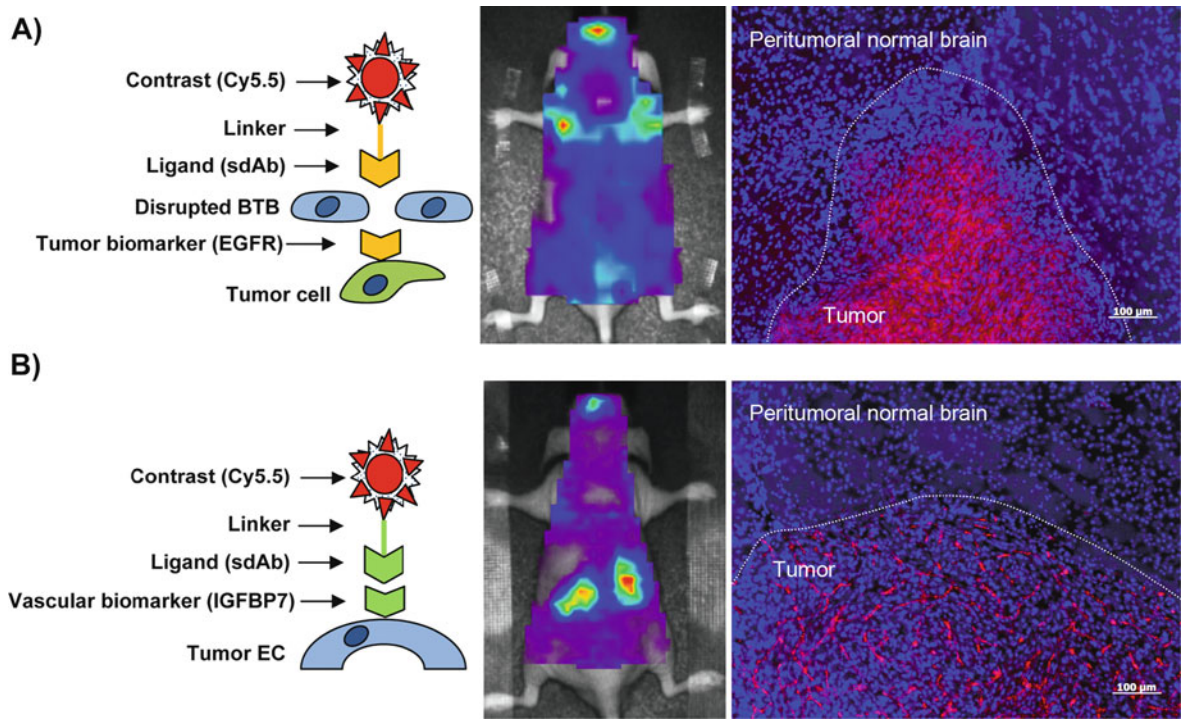

Fig. 14.2 Molecular imaging of vascular and tumor-cell biomarkers in orthotopic glioblastoma model in nude mice using single-domain antibody ligands coupled to the near-infrared fluorescent probe, Cy5.5. (**a**) Conceptual schematic (*left*) of a molecular imaging probe developed against tumor cell-specific biomarker, EGFR. Representative whole body image (*middle panel*) of a mouse bearing orthotopic glioblastoma tumor 72 h after intravenous injection of the probe (Cy5.5-Fc-EG2sdAb; Table 14.1). Fluorescence microcopy analysis of excised tumor (*right panel*) shows Cy5.5-Fc-EG2sdAb-originating fluorescence (*red*) localized to tumor parenchyma (blue-cell nuclei), suggesting that brain-tumor barrier in this model is disrupted sufficiently to allow passage of a biologic-based molecular imaging agent. (**b**) Conceptual schematic (*left*) of a molecular imaging probe developed against the tumor vessel-specific biomarker, IGFBP7. Representative whole body image (*middle panel*) of a mouse bearing orthotopic glioblastoma tumor 4 h after intravenous injection of the probe (Cy5.5-IGFBP7sdAb). Fluorescence microcopy analysis of excised tumor (*right panel*) shows Cy5.5-IGFBP7sdAb-originating fluorescence (*red*) localized selectively to brain tumor vessels (blue-cell nuclei)

V2C-EG2 enabled fast post-injection detection of the tumor-accumulated contrast, the combined effects of moderate molecular size, increased apparent affinity due to bivalent display, and longer circulation half-life of EG2-hFc produced a superior tumor targeting and retention as well as good signal-to-noise ratio as early as 24 h after injection. Similarly, high tumor targeting by EG2-hFc (at 24–44 h) compared to EG2 and V2C-EG2 has also been observed in PET/microCT imaging of xenograft (subcutaneous) pancreatic tumor (Bell et al. 2010). These experiments also indicated that the blood-tumor barrier in the orthotopic GBM model used in the study is non-restrictive for penetration of molecules as large as 80 kDa, which is not the case in clinical GBMs, where the blood–tumor barrier is largely intact, and requires an invasive osmotic disruption for delivery of even small molecular weight therapeutics. Therefore, although studies described here show successful single-domain antibody tailoring to the imaging application, the interpretation of the

data was largely driven by the characteristics of the model and could not be directly translated to the clinical realm. Given the more restrictive BTB, high interstitial tumor pressure (Jain 1994) and high tumor volume compared to experimental GBM, smaller antibody formats may actually be beneficial due to facilitated tumor penetration and better intratumoral diffusion.

Molecular Imaging Using Single Domain Antibody Against Vascular Target IGFBP7

Recently, Pen et al. (2007) described insulin-like growth factor binding protein-7 (IGFBP7) as a highly specific vascular biomarker of GBM. IGFBP7 is a 31 kDa secreted protein overexpressed in various tumor blood vessels with little or no expression in normal blood vessels (Akaogi et al. 1996; St Croix et al. 2000). In GBM vessels, IGFBP7 is induced in tumor endothelial cells by TGFβ-1 released by glioblastoma cells, and is deposited in the vascular basal lamina (Pen et al. 2007; Pen et al. 2008). Subsequent studies indicated that IGFBP7 is involved in late phase of angiogenesis in GBM tumors (Pen et al. 2008). Interestingly, IGFBP7 deposition was found in virtually all GBM vessels in both tissue sections of surgically removed human tumors, as well as in host vessels in orthotopic human GBM tumors implanted into nude mice (Pen et al. 2007; Iqbal et al. 2010a). Most importantly, IGFBP7 expression was not detectable in vessels in non-tumor brain tissue. Furthermore, vascular IGFBP7 expression/deposition was a good differentiator between GBM and lower grade gliomas (unpublished observation from the same laboratory). Since IGFBP7 has been implicated in GBM angiogenesis, it could provide a measure of the intensity of angiogenesis in the tumor, or the response of the tumor to anti-angiogenic treatments.

From IGFBP7-immunized llama sdAb library (generated using protocols shown in Fig. 14.1), an IGFBP7 sdAb with a moderate 40-nM affinity was selected and its binding to GBM vessels in human and orthotopic GBM confirmed by immunochemistry. The antibody was then bioconjugated with the near-infrared probe, Cy5.5, and evaluated in vivo by optical imaging in orthotopic GBM model in nude mice. IGFBP7 sdAb injected i.v. produced a fast (as early as 10 min) and persistent (up to 4 h) tumor signal with high contrast to noise ratio (Fig. 14.2b), which was not detectable in animals injected with either a 100-fold excess of unlabeled IGFBP7 sdAb, or with control isotypic sdAb (Iqbal et al. 2010a). The subsequent evaluation of excised tumors by in situ fluorescence imaging (Fig. 14.2b, right), revealed exclusive localization (binding) of injected IGFBP7 sdAb to virtually all glioblastoma vessels with no presence in peritumoral vessels or vessels of the contralateral hemisphere. These studies indicated that the affinity of IGFBP7 sdAb was sufficient to allow an efficient 'capture' by antigen-expressing glioblastoma vessels despite its fast pharmacokinetics (circulation half-life of 7 min). The antibody also displayed high selectivity to pathological vessels and specificity to its antigen, and achieved a rapid and robust contrast enhancement in experimental orthotopic GBM in whole-body imaging, emphasizing the importance of biomarker characteristics (listed in Section 1.2) for achieving successful molecular imaging detection.

This has been underscored further by previous attempts to develop methods for molecular imaging of tumor vessels. ^{64}Cu-labeled vascular endothelial growth factor 121 ($VEGF_{121}$), a ligand for the endothelial target, VEGFR-2, up-regulated in angiogenic vessels, has been developed for noninvasive imaging of VEGFR expression in small animals (Cai et al. 2006). Similar to anti-IGFBP7 sdAb, $VEGF_{121}$ has a low nanomolar affinity for VEGFR and fast clearance from the body due to its small size (25 kDa). In pre-clinical studies, it became evident that VEGFR expression was heterogenous in a mouse subcutaneous tumor model of GBM, as well as that targeting ligand had to compete with endogenous tumor-expressed VEGF for binding to VEGFR (Cai et al. 2006). Another well-studied biomarker of GBM tumor vessels, $\alpha_v\beta_3$ integrin, has been targeted by a variety of RGD containing peptide ligands for non-invasive imaging of tumors. In a recent study where [^{18}F]Galacto-RGD peptide was used for noninvasive PET assessment of $\alpha_v\beta_3$ integrin expression in patients with GBM (Schnell et al. 2009), the GBMs had very heterogeneous tracer uptake that correlated well with immunohistochemically determined $\alpha_v\beta_3$ expression. However, in contrast to both VEGFR and IGFBP7, the $\alpha_v\beta_3$ integrin expression is associated with both sprouting vessels and with tumor cells (Schnell et al. 2009), making it difficult to differentiate the origin of molecular imaging signal.

Single Domain Antibody-Targeted Small Unilamellar Vesicles

Whereas various formats of sdAbs can be optimized for optical and PET molecular imaging by bioconjugation to appropriate tracers, MR molecular imaging remains challenging due to limited sensitivity of its probes (Gupta and Weissleder 1996). As the major determinant of the contrast in 3H-MR images are the relaxation times, T1 and T2, of the tissue protons, paramagnetic substances are necessary for contrast enhancement. Paramagnetic complexes of metal ions, such as Gd(III) or Mn(II) have been successfully used as MRI contrast agents since the late 1980s. However, the main obstacle to their use in molecular imaging is high sensitivity required when biological targets are present in low concentrations. The challenge of high relaxivity has been tackled using the vast armory of nanotechnology tools, including dendrimers, nanotubes, micelles, nanovesicles and metal-based nanoparticles (Cormode et al. 2010). The use of liposomes capable of carrying high payloads of Gd has been suggested as a viable strategy (Glogard et al. 2002). Furthermore, to achieve targeting to specific molecular recognition sites, a variety of targeting peptides or antibodies attached to liposome-based imaging reporters have been developed to date (Zhang et al. 2009; Strijkers et al. 2010). However, these formulations often had pharmacokinetic properties unsuitable for imaging applications due to polydispersity and bulky size (~100–400 nm). Recently, we reported that a long- and short-chain phospholipid mixture (e.g., dimyristoyl phosphatidylcholine, DMPC, and dihexanoyl phosphatidylcholine, DHPC, respectively), doped with a long-chain charged lipid (dimyristoyl phosphatidylglycerol, DMPG) spontaneously forms *small unilamellar vesicles* (sULV) with a low-polydispersity (Nieh et al. 2003, 2004, 2005). The size (diameter) of these sULVs ranges from 10 to 40 nm, and can be obtained in a controlled manner without multistage filtration (Nieh et al. 2003, 2004; Yue et al. 2005). In subsequent studies, sULVs were used as nanoscaffolds to achieve a high load of Gd(III) by incorporating PEGylated phospholipid, distearoyl phosphoethanolamine-*N*-[amino (polyethylene glycol) 2000] (DSPE-PEG2000-Amino) and Gd DTPA-bis-oleate (Gd-DTPA-BOA). Furthermore, these Gd-sULV were bioconjugated with the anti-IGFBP7 sdAbs to target the payload to GBM vessels, as well as the near infrared dye, Cy5.5, to achieve multi-modality applications (Fig. 14.1, conceptual drawing).

Gd load was estimated at 30,000 Gd per ULV nanoparticle; the T1 relaxivity in water at 9.4T was 2220 + 280 and 23800 + 5270/mM/sec for the 20 and 40 mol% Gd-DTPA-BOA in ULV contrast formulation, respectively. In vivo pharmacokinetic analysis of *Gd*-sULV's indicated a plasma half life of 1.67 h and an apparent volume of distribution (Vss) of 1.004 ml. Therefore, the PK parameters of the Gd-sULV indicate a full clearance of nanoparticles within 8 h (~5 half-lives).

In vivo optical imaging experiments in orthotopic GBM model, showed peak tumor signal at 2–4 h with IGFBP7 sdAb-targeted Gd-ULVs, whereas non-targeted Gd-sULVs-Cy5.5 demonstrated a negligible passive accumulation. In both groups, the highest optical signal originated from the liver, followed by the kidneys and spleen. Brain sections analyzed by fluorescent microscopy at the peak tumor signal (4 h) showed the exclusive presence of the injected anti-IGFBP7 sdAb- Gd-sULV-Cy5.5 in GBM vessels. This was further confirmed in T1 weighted MRI images obtained at 9.4T, where intracranial tumors became more enhanced 2 h after the injection of IGFBP7 sdAb-Gd-sULV, but not the nontargeted Gd-sULV. These studies established that nanoscale lipid vesicles optimized to sizes between 10 and 40 nm exhibit good pharmacokinetic profiles for imaging applications. These vesicles can carry high load of paramagnetic contrast, and exhibit high target avidity when functionalized with multiple targeting sdAbs, sufficient to improve MRI detection sensitivity for molecular imaging applications.

Single-Domain Antibody-Targeted Iron Oxide Nanoparticles

Progress in mMRI has been further propelled by advances in nanosynthesis leading to reproducible production of nanoparticles with controlled physical and chemical properties including size, shape, core and shell type, as well as surface modifications (Di Marco et al. 2007). Superparamagnetic iron oxide nanoparticles (SPIO) have been often utilized as MR imaging

probes able to efficiently shorten T2 and particularly T2* of water protons. While the NPs' core reduces T2, the coating (shell) is added to prevent aggregation and sedimentation of the particles in aqueous solution, provide chemical stability, allow functionalization and reduce potential toxicity. Therefore, the iron oxide core has been coated with gold and silica (Tromsdorf et al. 2009), creating core/shell NP. Furthermore Fe_3O_4 and Fe_3O_4/Au NPs have been synthesized with a polymeric shell, such as poly(ethylene glycol) or dextran to enable binding of targeting moieties. Recently, targeted contrast agents comprising superparamagnetic nanoparticles bioconjugated with biological objects, such as antibodies (Suwa et al. 1998) or liposomes (Hamzah et al. 2009) have been reported; these contrast agents found recent applications in diagnosis of cancer and inflammation (Reimer and Tombach 1998).

Targeting of iron-oxide nanoparticles with sdAbs raised against the vascular GBM target, IGFBP7, has been recently described (Iqbal et al. 2010a). Iron-oxide NPs were synthesized, PEGylated and functionalized with Cy5.5 and IGFBP7 sdAb as described (Iqbal et al. 2010a; see conceptual drawing in Fig. 14.1), yielding stable and water soluble NPs with a hydrodynamic diameter of 33 nm, polydispersity of 0.17, and a circulation half-life of approximately 24 h. Bioconjugation of sdAb to the iron oxide NPs increased the average hydrodynamic diameter to 42 nm with a polydispersity of 0.375. Proof-of-concept studies using optical imaging as surrogate, demonstrated a progressive increase in GBM tumor vs. contralateral brain signal ratio, peaking at 72 h after anti-IFGBP7sdAb-PEGylated NPs-Cy5.5 injection, and no specific accumulation of non-targeted NPs in the tumor. Sections from GBM tumour-bearing mice receiving anti-IGFBP7sdAb-PEGylated NPs-Cy5.5 demonstrated co-localization of Cy5.5 fluorescence with tumor vessels, compared with virtual absence of Cy5.5 fluorescence in the contralateral healthy brain or in tumour sections from animals injected with non-targeted PEGylated NPs-Cy5.5. Preliminary MRI data using a commercially available iron oxide NP coated with dextran and targeted with the anti-IGFBP7 sdAb displayed stable and measurable MRI contrast of the brain tumour for up to 24 h, whereas the nontargeted NP had no measurable contrast at 24 h and had cleared completely from the brain tumor. T_2 relaxation times were significantly lower ($p < 0.005$) for the anti-IGFBP7 single domain antibody-targeted iron oxide nanoparticle in the tumor than in the healthy brain 10 min, 2 and 24 hour after contrast injection when compared to non-targeted contrast agent. Although further optimization of this targeted nanoparticle is necessary to adjust circulation half-life and evaluate general and organ toxicity, the example provides an initial demonstration of successful targeting of T2 contrast nanoparticles with single-domain antibodies raised against a vascular glioblastoma biomarker.

In both examples of targeted ULVs and iron oxide nanoparticle described in sections above, a successful transition between optical and MRI modalities has been achieved using developed multimodal imaging agents. Multimodality imaging using small-molecule-based probes is challenging due to the limited number of attachment points for alternative modalities and potential interference with its receptor binding affinity. In contrast, use of large surface nanoparticles in molecular imaging affords attachment of hundreds or even thousands, of imaging labels or a combination of labels for different imaging modalities leading to signal amplification, as well as multiple, potentially different, targeting ligands providing for enhanced binding affinity and specificity. Single domain antibodies against molecular GBM targets were shown in our studies to be versatile targeting ligands that can be used to functionalize various contrast-bearing nanoparticles.

Challenges and Perspectives

Although conceptually feasible, many obstacles remain in developing molecular imaging agents for brain tumors. The first and the most critical element is the selection of the biomarker that could be exploited for the development of molecular imaging agent. Whereas parenchymal tumor biomarkers, cell surface or intracellular, could potentially be accessed by small molecule (radio)ligands provided that they escape multiple and usually overexpressed efflux transporters at both blood-tumor barrier and tumor cells themselves, these targets would not be readily accessible for targeting biologics or biologics-functionalized imaging nanoparticles due to the restrictive nature of brain-tumor barrier. In contrast, tumor vascular targets/biomarkers are better suited to biologics-based molecular imaging probes, provided that they are selective, specific and sufficiently abundant. Although

many different targeting molecules could be used to recognize such biomarkers, the body of work summarized here demonstrates that domain antibodies have some distinct advantages for this application due to their small size and stability as well as relative ease with which they can be engineered to optimize affinity, avidity, and circulation life-times to specific application.

Even when a solid proof of concept for imaging application has been obtained in animal studies, translation into clinical applications remains a challenge. The principal reasons are lack of animal models that well recapitulate characteristics of human glioblastomas as well as 'transition' from preclinical imaging modalities (usually optical and microPET/SPECT) to accessible and widely used clinical imaging modalities (MRI and PET-CT). The advantage of approaches presented in this chapter is the ability to introduce multimodality early on in the targeted contrast agent development to accomplish target validation and agent optimization in animal models using optical imaging, while enabling translation to clinically more relevant MRI and PET modalities.

Since currently most molecular imaging agents are injectable small molecules, the 'transition' of the field to targeting biologics will remain a challenge for the near future. Biologics may be inherently costly for such applications, although in the paradigm of personalized medicine they in the end may reduce overall cost of treatment. Furthermore, regulatory issues associated with approval of injectable contrast agents, essentially treating them as a 'drug', remain sufficiently restrictive to allow their fast penetration into clinical practice.

Notwithstanding these challenges, the future promise of molecular imaging providing a clinician or neurosurgeon with information critical for successful management of deadly brain tumors, including identification of micro-metastases and stem cells, presence/enrichment in specific proteins or enzymes, molecular aberrations (e.g., gene methylation) that can be therapeutically targeted, as well as observing 'drug in action' on particular target, remains exciting. The advancement in enabling technologies necessary to develop clinically useful molecular imaging probes has already reached a critical mass, and preclinical proof of concept for few such agents has been obtained; the ultimate challenge in the near future will remain translating these promising approaches into clinical realm.

References

Akaogi K, Okabe Y, Sato J, Nagashima Y, Yasumitsu H, Sugahara K, Miyazaki K (1996) Specific accumulation of tumor-derived adhesion factor in tumor blood vessels and in capillary tube-like structures of cultured vascular endothelial cells. Proc Natl Acad Sci USA 93:8384–8389

Bell A, Wang ZJ, Arbabi-Ghahroudi M, Chang TA, Durocher Y, Trojahn U, Baardsnes J, Jaramillo ML, Li S, Baral TN, O'Connor-McCourt M, Mackenzie R, Zhang J (2010) Differential tumor-targeting abilities of three single-domain antibody formats. Cancer Lett 289:81–90

Cai W, Chen K, Mohamedali KA, Cao Q, Gambhir SS, Rosenblum MG, Chen X (2006) PET of vascular endothelial growth factor receptor expression. J Nucl Med 47:2048–2056

Cormode DP, Jarzyna PA, Mulder WJ, Fayad ZA (2010) Modified natural nanoparticles as contrast agents for medical imaging. Adv Drug Deliv Rev 62:329–338

Di Marco M, Sadun C, Port M, Guilbert I, Couvreur P, Dubernet C (2007) Physicochemical characterization of ultrasmall superparamagnetic iron oxide particles (USPIO) for biomedical application as MRI contrast agents. Int J Nanomed 2:609–622

Doyle PJ, Arbabi-Ghahroudi M, Gaudette N, Furzer G, Savard ME, Gleddie S, McLean MD, Mackenzie CR, Hall JC (2008) Cloning, expression, and characterization of a single-domain antibody fragment with affinity for 15-acetyl-deoxynivalenol. Mol Immunol 45:3703–3713

Dumoulin M, Conrath K, Van Meirhaeghe A, Meersman F, Heremans K, Frenken LG, Muyldermans S, Wyns L, Matagne A (2002) Single-domain antibody fragments with high conformational stability. Protein Sci 11:500–515

Glogard C, Stensrud G, Hovland R, Fossheim SL, Klaveness J (2002) Liposomes as carriers of amphiphilic gadolinium chelates: the effect of membrane composition on incorporation efficacy and in vitro relaxivity. Int J Pharm 233:131–140

Gupta H, Weissleder R (1996) Targeted contrast agents in MR imaging. Magn Reson Imaging Clin N Am 4:171–184

Hamers-Casterman C, Atarhouch T, Muyldermans S, Robinson G, Hamers C, Songa EB, Bendahman N, Hamers R (1993) Naturally occurring antibodies devoid of light chains. Nature 363:446–448

Hamzah J, Altin JG, Herringson T, Parish CR, Hammerling GJ, O'Donoghue H, Ganss R (2009) Targeted liposomal delivery of TLR9 ligands activates spontaneous antitumor immunity in an autochthonous cancer model. J Immunol 183:1091–1098

Iqbal U, Albaghdadi H, Luo Y, Arbabi M, Desvaux C, Veres T, Stanimirovic D, Abulrob A (2010a) Molecular imaging of glioblastoma multiforme using anti-insulin-like growth factor-binding protein-7 single domain antibodies. Br J Cancer 103:1606–1616

Iqbal U, Trojahn U, Albaghdadi H, Zhang J, O'Connor-McCourt M, Stanimirovic D, Tomanek B, Sutherland G, Abulrob A (2010b) Kinetic analysis of novel mono- and multivalent VHH-fragments and their application for molecular imaging of brain tumors. Br J Pharm 160:1016–1028

Isaka T, Yoshimine T, Maruno M, Kuroda R, Ishii H, Hayakawa T (1994) Altered expression of antithrombotic molecules in human glioma vessels. Acta Neuropathol 87:81–85

Jain RK (1994) Barriers to drug delivery in solid tumors. Sci Am 271:58–65

Jain RK, di Tomaso E, Duda DG, Loeffler JS, Sorensen AG, Batchelor TT (2007) Angiogenesis in brain tumours. Nat Rev Neurosci 8:610–622

Lauwereys M, Arbabi Ghahroudi M, Desmyter A, Kinne J, Hölzer W, De Genst E, Wyns L, Muyldermans S (1998) Potent enzyme inhibitors derived from dromedary heavy-chain antibodies. EMBO J 17:3512–3520

Machein MR, Kullmer J, Fiebich BL, Plate KH, Warnke PC (1999) Vascular endothelial growth factor expression, vascular volume, and, capillary permeability in human brain tumors. Neurosurgery 44:732–740

Nagane M, Lin H, Cavenee WK, Huang HJ (2001) Aberrant receptor signaling in human malignant gliomas: mechanisms and therapeutic implications. Cancer Lett 162 Suppl: S17–S21

Nieh MP, Harroun TA, Raghunathan VA, Glinka CJ, Katsaras J (2003) Concentration independent spontaneously forming biomimetic vesicles. Phys Rev Lett 91:158105

Nieh MP, Harroun TA, Raghunathan VA, Glinka CJ, Katsaras J (2004) Spontaneously formed monodisperse biomimetic unilamellar vesicles: effect of charge, dilution and time. Biophys J 86:2615–2629

Nieh MP, Raghunathan VA, Kline SR, Harroun TA, Huang CY, Pence J, Katsaras J (2005) Spontaneously formed unilamellar vesicles with path dependent size distribution. Langmuir 21:6656–6661

Nishikawa R, Ji XD, Harmon RC, Lazar CS, Gill GN, Cavenee WK, Huang HJ (1994) A mutant epidermal growth factor receptor common in human glioma confers enhanced tumorigenicity. Proc Natl Acad Sci USA 91:7727–7731

Pen A, Moreno MJ, Durocher Y, Deb-Rinker P, Stanimirovic DB (2008) Glioblastoma-secreted factors induce IGFPB7 and angiogenesis by modulating Smad-2-dependent TGF-β signalling. Oncogene 27:6834–6844

Pen A, Moreno MJ, Martin J, Stanimirovic DB (2007) Molecular markers of extracellular matrix remodelling in glioblastoma vessels: microarray study of laser-captured glioblastoma vessels. Glia 15:559–572

Reimer P, Tombach B (1998) Hepatic MRI with SPIO: detection and characterization of focal liver lesions. Eur Radiol 8:1198–1204

Roovers RC, van Dongen GA, van Bergen en Henegouwen PM (2007) Nanobodies in therapeutic applications. Curr Opin Mol Ther 9:327–335

Schnell O, Krebs B, Carlsen J, Miederer I, Goetz C, Goldbrunner RH, Wester HJ, Haubner R, Popperl G, Holtmannspotter M, Kretzschmar HA, Kessler H, Tonn JC, Schwaigner M, Beer AJ (2009) Imaging of integrin alpha(v)beta(3) expression in patients with malignant glioma by 18F Galacto-RGD positron emission tomography. Neuro-oncology 6: 861–870

St Croix B, Rago C, Velculescu V, Traverso G, Romans KE, Montgomery E, Lal A, Riggins GJ, Lengauer C, Vogelstein B, Kinzler KW (2000) Genes expressed in human tumor endothelium. Science 289:1197–1202

Strijkers GJ, Kluza E, Van Tilborg GA, van der Schaft DW, Griffioen AW, Mulder WJ, Nicolay K (2010) Paramagnetic and fluorescent liposomes for target-specific imaging and therapy of tumor angiogenesis. Angiogenesis 13:161–173

Suwa T, Ozawa S, Ueda M, Ando N, Kitajima M (1998) Magnetic resonance imaging of esophageal squamous cell carcinoma using magnetite particles coated with anti-epidermal growth factor receptor antibody. Int J Cancer 75:626–634

Thakur M, Lentle BC (2006) Report of a summit on molecular imaging. Am J Roentgenol 186:297–299

Tromsdorf UI, Bruns OT, Salmen SC, Beisiege U, Weller H (2009) A highly effective, nontoxic T1 MR contrast agent based on ultrasmall PEGylated iron oxide nanoparticles. Nano Lett 9:4434–4440

Wong AJ, Bigner SH, Bigner DD, Kinzler KW, Hamilton SR, Vogelstein B (1987) Increased expression of the epidermal growth factor receptor gene in malignant gliomas is invariably associated with gene amplification. Proc Natl Acad Sci USA 84:6899–6903

Yue B, Huang CY, Nieh MP, Glinka CJ, Katasaras J (2005) Highly stable phospholipid unilamellar vesicles from spontaneous vesiculation: a DLS and SANS study. J Phys Chem 109:609–616

Zhang D, Feng XY, Henning TD, Wen L, Lu WY, Pan H, Wu X, Zou LG (2009) MR imaging of tumor angiogenesis using sterically stabilized Gd-DTPA liposomes targeted to CD105. Eur J Radiol 70:180–189

Chapter 15

Quantitative Analysis of Pyramidal Tracts in Brain Tumor Patients Using Diffusion Tensor Imaging

Rubén Cárdenes, Emma Muñoz-Moreno, Rosario Sarabia-Herrero, Daniel Argibay-Quiñones, and Marcos Martín-Fernández

Abstract Diffusion Tensor Imaging (DTI) is an image modality that provides information about the nerve fiber tracts in the brain white matter. In this chapter, we describe the use of DTI to quantify the damage in fiber tracts due to brain tumors. A quantification method for this modality is useful to understand the neurological effects of the tumor in a given patient, such as motor and/or sensitive disorders, as well as to help in surgical planning for the resection of the tumor. The quantification of the state of fiber tracts and its comparison with the values obtained before resection and with healthy tracts, is also of paramount importance for the follow-up of the patient after tumor resection. As an example, we show the quantification of the pyramidal tract using two measures: integrity and connectivity. The fiber tract is automatically identified in any subject by means of a specific fiber tracking algorithm, so robust comparison between control subjects and patients can be performed, as well as comparison between the two hemispheres of a same subject. Diffusion tensor based measures are defined to quantify the state of fiber bundles, taking into account both the intrinsic properties of the fibers and the similarity to healthy control fibers. A 2D mapping of the tracts is also provided to perform comparisons among a given population, and to visually analyze the tract damages. Experiments show the results obtained in a set of 10 tumor patients, and 10 control subjects.

Keywords Brain tumor · DTI · Pyramidal tract · Brain white matter · Multiple sclerosis · Fiber tracts

Introduction

Quantification of Diffusion Tensor Imaging (DTI) data sets has become a demanding practice in clinical environments for the evaluation of neurological diseases (Smith et al. 2006), due to its capability to identify and measure the fiber structure of the brain white matter, which is not possible to obtain using conventional magnetic resonance imaging (MRI). Some works have increased the interest in using this imaging modality, providing evidence that changes in the structure of the brain white matter in specific areas could be directly related to some diseases such as multiple sclerosis (Audoin et al. 2007; Pagani et al. 2005; Roosendal et al. 2009), epilepsy (Diehl et al. 2008; McDonald et al. 2008), or schizophrenia (Kubicki et al. 2005).

If a robust and automatic method to measure the state of the fiber tracts is available, it could be possible to measure how affected is a specific fiber bundle of the brain due to the presence of a tumor, and also to know its evolution and the level of success of a resection procedure in follow up studies. Moreover, such a quantification method could also give a better understanding of the state of important fiber tracts for a better surgical planning. Furthermore, due to the information provided by this modality, these techniques will also give a measure related to the connection between two or more areas of the brain. Additionally, comparing the differences between both hemispheres, and differences against healthy patients, these techniques could

R. Cárdenes (✉)
Laboratory of Image Processing, University of Valladolid, Valladolid, Spain
e-mail: ruben@lpi.tel.uva.es

M.A. Hayat (ed.), *Tumors of the Central Nervous System, Volume 4*,
DOI 10.1007/978-94-007-1706-0_15,

give more objective measures of the amount of injury produced by brain tumors. Despite the efforts already made to correctly quantify DTI data, there is still low agreement on what is the best methodology to compare different DTI data sets. Although quantification methods along fiber tracts have become important and have been shown to be reproducible (Partridge et al. 2005), the measures proposed up to date to quantify DTI data are limited to isolated standard tensor properties such as the anisotropy and the diffusivity. However, in (Cárdenes et al. 2010a) a more global study that takes into account several properties involved in the fiber tracts, is used to better characterize bundles of interest.

Background

Diffusion Tensor Imaging

Conventional neuroimaging modalities allow identifying different kinds of tissues in the brain, such as gray and white matter, but the complex fiber structure that makes up the white matter cannot be visualized. Diffusion Imaging techniques provide information about such fiber structures based on the measure of the molecular diffusion in the tissues, that is mainly in the direction of the neuron axons that form the nerve fiber tracts (Basser et al. 1994). Thus, if this direction can be identified, the nerve fiber trajectories can be estimated by means of a technique known as tractography or fiber tracking (Mori and van Zijl 2002). In this way, 3D representations of the fiber bundles can be visualized, and the connectivity within the brain can be studied. Besides, measures along the fiber bundles can also be done, in order to analyze, for instance, if they have been damaged due to a given pathology.

To measure the diffusion in the brain a MRI acquisition protocol is defined. The DTI is computed from a set of Diffusion Weighted MRIs (DW-MRI). Each of these images is acquired by exciting the tissue with a specific pulse sequence named *Stejskal-Tanner* sequence (Stejskal and Tanner 1965), that applies a pulse gradient in a given direction. In this way, an image representing the molecular diffusion in such direction is obtained, where darker areas correspond to regions where diffusion is higher and brighter areas involve lower diffusion. In order to obtain information about the diffusion in all the 3D space, a set of gradients must be applied, so the diffusion in a set of directions is measured. At each point of the image, these measures are combined into a Diffusion Tensor (DT), that is a mathematical entity describing the diffusion in every direction. DT is a symmetrical second order positive definite tensor, and can be represented by a 3×3 symmetric matrix. From the eigen-analysis of this matrix, the shape, magnitude and principal directions of the diffusion can be analyzed. Thus, DT can be viewed as an ellipsoid whose axis directions are defined by the eigenvectors, and the axis length is described by the corresponding eigenvalues.

In DTI, the anisotropy of the diffusion processes in the brain tissues can be quantified, for instance by means of a quantity called *fractional anisotropy* (*FA*) that is related to the relative amount of diffusion in a predominant direction, and which allows distinguishing between gray and white matter. The myelin coat and cell membranes of the axons constrain the diffusion, and force it to be parallel to the axon direction. Thus, in the white matter, which is composed by nerve fibers, the diffusion is clearly anisotropic, while in the gray matter, there is no preferred direction for diffusion, that is, diffusion is isotropic. Therefore, if a DT is represented as an ellipsoid, as aforementioned, when it is mostly isotropic, that is, in absence of fibers, the DT would become a sphere, since diffusion is equal in any direction of the space. On the other hand, in the white matter, where there are fiber tracts, DTs are represented by cigarette-shape ellipsoids. Other information that can be extracted from the diffusion tensor, is the *mean diffusivity* (*MD*) that is related to the overall amount of diffusion, (independently on the direction). Changes in *MD* or *FA* have been associated to some pathologies, such as epilepsy, multiple sclerosis or brain ischemia (Sundgren et al. 2004). The shape of the diffusion also provides information about the fiber structures. In (Westin et al. 2002) a set of geometrical coefficients are defined, that distinguish between linear, planar or spherical diffusion: linear is related to fiber tracts, planar occurs when two or more fiber tracts are crossing in the same voxel of the image, and spherical diffusion appears in the gray matter.

Regarding the diffusion direction, if the axons are aligned to form a fiber bundle, it can be assumed that the main eigenvector of the tensor describes the fiber tract orientation at each voxel. If we follow the path indicated by these vectors along the image, the

fiber trajectories can be identified, and images as the one shown in Fig. 15.2 can be obtained. The relation between these fiber tracts and the anatomical nerve structures previously described has been shown in (Mori et al. 2005). To identify anatomically the fiber tracts computed from DTI, manual selection of the fibers is usually performed. However, to avoid this tedious task, automatic segmentation algorithms, as the one described here, have been proposed. Thus, the damage in a given tract can be easily measured and related to the neurological problems observed in a particular patient.

Quantification Methods based on Diffusion Tensor Imaging

The most common way to perform quantification of DTI data, has been the use of scalar magnitudes related to the diffusion tensor. In particular, the *FA* and the *MD* have been used, see for instance (Pierpaoli and Basser 1996). However, due to the advance in computer fiber tracking techniques, a more recent trend has been to search for differences in relevant anatomical fiber tracts (Correia et al. 2008), measuring the length, the weighted length, the number of fibers in a tract, etc. Then, a more sophisticated approach is to quantify the connectivity between brain regions (Hagmann et al. 2003; O'Donnell et al. 2002; Skudlarski et al. 2008) usually regarded as the amount of fibers joining these regions. The main problem of fiber tract based measure techniques is that the same tract has to be identified in every data set under study to make robust comparisons. Therefore, some atlas-based approaches have been proposed (Hagler et al. 2009; Hua et al. 2008; Lawes et al. 2008; Pagani et al. 2005) to overcome this problem.

On the other hand, there also exist some specific studies of brain tumors using DTI. For instance the works in (Inoue et al. 2005; Kinoshita et al. 2008; Price et al. 2003) explore tumor characteristics using *FA* and *MD*, but they do not analyze how the tumor affects specific fiber structures. There exist however other works that use tractography to study brain tumors, quantifying along fiber tracts instead of using standard voxel based measures. That is the case of the work proposed by (Yu et al. 2005) who studied the pyramidal tract, corpus callosum and optic radiation for surgical planning and post operative evaluation. In that work, they propose to classify the tracts affected by tumors in three different groups: those whose fibers have been displaced by the tumor (simple displacement), those with disrupted fibers due to the tumor (single disrupted) and those whose fibers were displaced and also disrupted (displacement with disruption). As we will see later, the anatomical tracts are usually generated from some regions of interest or seeds. The location of these regions are studied in the work proposed by (Schonberg et al. 2006) in the pyramidal tract and the superior longitudinal fasciculus of tumor patients, using functional information from functional Magnetic Resonance Imaging (fMRI) in order to obtain fibers with the same functional relationship. In this chapter, a proposal to perform DTI quantification in the pyramidal tract is described more thoroughly. This methodology consists in the automatic identification of the fiber tract of interest from the DTI and the definition of specific magnitudes to measure the integrity of the fibers, their deviation from an average population and finally their connectivity. To show an example of the performance of this proposal, the proposed method is applied in a dataset of 10 patients harboring brain tumor, whose pyramidal tract is analyzed and compared with healthy subjects.

Materials and Methods

Materials and Participants

For this study, 10 tumor patients have been selected. Selection criteria included adult patients diagnosed of harboring a brain tumor affecting the pyramidal tract of only one hemisphere, either cortically or subcortically, for which they were subsequently operated upon. We will refer to these 10 patients as P1 to P10. The pathological diagnosis of the patients' tumors corresponded to two anaplastic astrocytomas located cortico-subcortically in the motor area in the two cases, in P4 (left), and in P7 (right); four astrocytomas: parieto-occipital left in P1, in the motor area subcortically right in P2, parietal right in P5 and temporal right in P8; one left parietal meningioma, in P3; one multiform glioblastoma located in the left internal capsule

and cerebral peduncle in P10, and two cerebral breast metastasis located cortico-subcortically in the left posterior frontal lobe in P6, and parieto-occipital left in P9. All these patients underwent a preoperative tractography to identify the distortion of the pyramidal tract induced by the tumor. Additionally, two groups of 30 and 10 control subjects have participated in this work. The first group of 30 subjects, aged from 24 to 62 years old, with mean age of 32.4, was used to build a DTI model, and the second one of 10 subjects, aged from 23 to 56 years old, with mean age of 32.9, was selected to perform comparison studies with the patients. All the controls that participated in this study were right handed healthy volunteers, without any known neurological disorder nor image artifacts encountered after scanning.

Automatic Fiber Tract Extraction

The quantification method analyzes the fiber tracts affected by the tumor. Therefore, the first step is the extraction of the fiber tract of interest. To do that, an automatic algorithm is proposed, that first computes the fibers in all the brain and then selects the ones that belong to a given anatomical tract. The computation of the fiber tracts is made by means of a fourth order *Runge-Kutta* algorithm to interpolate the vector field composed by the major eigenvector of the diffusion tensor at each voxel. Each of the image voxels belonging to the white matter (that is, those whose *FA* is higher than a given threshold) are considered as a seed for fiber trajectory estimation. Once all the fiber tracts have been computed, the bundle of interest must be selected. To do that, each anatomical tract is defined based on a set of regions through which it must pass or not. These regions are identified on a model of a DTI brain taking into account the Mori's atlas in (Mori et al. 2005).

To build the model, the set of 30 healthy subjects described previously has been considered. One of the volumes has been selected as reference, and all the others have been aligned with it. The transformation that is applied to each of the DTI volumes to become aligned to the reference is computed by means of a registration algorithm based on DTI, as described in (Muñoz-Moreno and Martin-Fernandez 2009). To obtain the optimum alignment of the images, the registration takes into account the physical interpretation of the DT, and searches for matching in shape, direction and amount of diffusion. Once all the volumes are aligned, the value at each voxel is averaged, so an average healthy brain DTI is obtained. Afterwards, the regions of interest required to identify the fiber tracts are selected in the model. In this case, the fibers belonging to the pyramidal tract are selected as the ones passing through the posterior limb of the internal capsule, so this region is selected in the image as the seed region. To identify the anatomical tract of interest in a patient, the image from the patient (data image) is registered against the model image previously described, so a geometrical transformation is obtained. The application of this transformation to the model will align it to the data image. Therefore, the regions that correspond to each of the anatomical fiber tracts in the model are transformed and aligned to the analogous region in the image under analysis. Then, tractography is computed on the data image, and the anatomical fiber bundles are identified as the fibers crossing the regions that now are identified over the data image. Since the fiber tracking is performed over the image under analysis, this method is robust in the presence of tumors that can displace fibers with respect to their normal (healthy) trajectories. One of the advantages of the automatic identification of the fiber bundles, besides avoiding the tedious task of manual segmentation, is that the tracts identified in the different images are comparable and measures can be performed along the fibers and their variability between different datasets can be analyzed. Below, a proposal to carry out this quantification is described.

Quantification

Here, some measure indices are described for the quantification of fiber tracts, that therefore can be used to know to what extent these fibers are affected by the presence of a brain tumor. First, an integrity measure of fiber bundles is defined, and then a mapping of the fibers to a 2D plane is described to define more robust measures among subjects. Finally a tract connectivity measure, which includes several fiber tract features is defined to perform more global and robust

comparisons. For further details, see (Cárdenes et al 2010a).

Tract Integrity Measure

The integrity of fiber tracts is defined here using two intrinsic features of the tensors: the *FA* and the radial diffusivity. The first quantity is an anisotropy measure, limited between zero and one, which increases with the directionality of the tensors involved in the fiber tract. A high *FA* value means that the diffusion is produced in a predominant direction, meaning that a high number of axons are aligned in that direction. Consequently, low *FA* values can be associated to a low number of aligned axons involved. On the other hand, diffusivity is a measure of the magnitude of the diffusion produced at each voxel. *MD* is the average diffusivity produced in a voxel, i.e. in all directions and is often used in the literature (Pagani et al. 2005; Audoin et al. 2007; McDonald et al. 2008). Diffusivity can be divided into more descriptive values which are, diffusion in the direction parallel to the fibers, called axial diffusivity $D_{ax} = \lambda_1$, and in the direction perpendicular to the fibers: perpendicular or radial diffusivity $D_{\text{rad}} = 1/2\ (\lambda_2 + \lambda_3)$, where λ_1, λ_2 and λ_3 are the tensor eigenvalues ordered in descending order. Therefore a high value of D_{ax} is related to a high diffusion along the fiber, and a high value of D_{rad} is related to a high diffusion in the perpendicular direction to the fiber. The relation between these quantities is already included in the *FA*, so only one of them is used in the integrity measure. For this reason only D_{rad} is used, whose high values are associated to loss of myelin as stated by (Song et al. 2003). It can be stated that *FA* and D_{rad} are good descriptors to characterize the inherent properties of the fibers, and can be used to define an integrity measure for a given tract. Taking these properties in mind, a fiber tract presents more integrity when its amount of anisotropy is high, and the diffusion along the perpendicular direction of the fibers is low. Thus, the integrity measure can be defined as the total amount of *FA* computed at the points involved along the fiber paths, divided by the total amount of radial diffusivity, or equivalently the relation between the average *FA* and the average D_{rad}:

$$I = \frac{\overline{FA}}{\overline{D_{\text{rad}}}}$$

2D Tract Mapping

The integrity measure can be defined as a longitudinal measure in the sense that it is computed along a given fiber trajectory and does not use the transverse direction or information between neighboring fibers. Hence, a 2D tract mapping can be used to add information about the direction transversal to the fiber and to visualize and obtain additional measures from the fiber profiles in a two dimensional way. The mapping consists in projecting the fiber tracts into a plane, starting from the seeds. The *FA* values along the fibers are stored in a 2D matrix where the rows represent the longitudinal dimension and the columns represent the transverse dimension. The implementation of this mapping is easy in the pyramidal tract, because the fibers can be ordered from anterior to posterior direction, and the longitudinal dimension is ordered from inferior to superior. Then, the 2D mapping is done by representing the fibers points in a 2D image, as if the fibers were individually transformed into straight lines, and placed one beside the other in an anterior to posterior ordering. Notice that all fibers points are represented in the map, and only transverse spatial relations of such points are altered to fit into a 2D image. The 2D maps obtained by means of this procedure are illustrated in Fig. 15.1 for a patient with a tumor that affects the left hemisphere. From top to bottom on each map it is represented the superior to inferior direction, and from left to right the anterior to posterior direction of the fibers. In this figure it is also shown the filtered maps obtained using Gaussian filtering to homogenize areas of different integrity in the maps. The representation of the *FA* using this procedure simplifies the analysis of the tracts and provides useful visual information of the global state of the pyramidal tracts. It is possible for instance, to observe zones with a particular low *FA*, and to analyze the shape and size of affected zones. For this reason, the information provided by these maps is extremely useful to make quantitative analysis of the pyramidal tracts.

In order to quantify the state of a fiber tract robustly using these maps, a new measure is defined comparing the map of an individual subject with an average map constructed from healthy volunteers. To better illustrate this idea, in Fig. 15.1 it is also shown the error maps in the two hemispheres, representing the differences of this subject with respect to an average one.

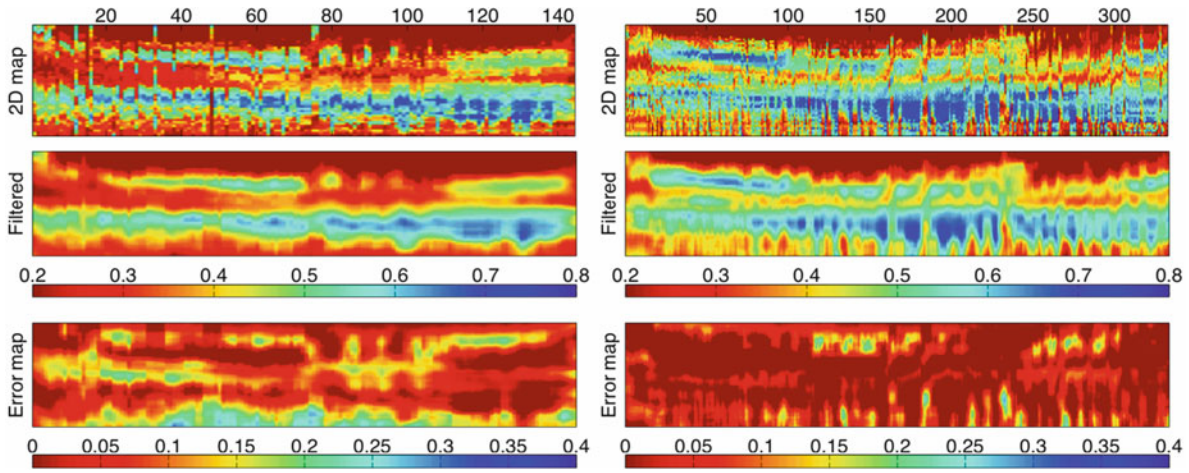

Fig. 15.1 2D FA maps, filtered maps, and error maps, for a patient (P6) with a tumor in the left hemisphere. *Left*: maps corresponding to the left hemisphere. *Right*: maps corresponding to the right hemisphere

To construct the average maps (one for each hemisphere), that we will denote as model maps, a group of 10 healthy subjects are used. Therefore for each of the 10 healthy subjects the 2D *FA* map is obtained, and then filtered and resized to a common image size, to finally average them all. Based on these model maps it is possible to measure the deviation of a given subject map from the map of an average population, by computing the average difference of the subject maps points that are below the *FA* value in the model map, as follows:

$$E_{\mathrm{m}} = \frac{\sum_{i=1}^{L} (M_i - X_i)\, u\,(M_i - X_i)}{\sum_{i=1}^{L} u\,(M_i - X_i)}$$

where M_i are the values of the model map, X_i the values of the subject map, $u(x)$ is the Heaviside step function, and L is the total number of pixels in the map. Notice that using $u(M_i - X_i)$ only the points with *FA* values lower than the model are considered because higher FA values indicate a normal behavior of the fiber, which is not relevant in pathological cases. We will refer to this measure as the *deviation from the model* or E_{m}.

Figure 15.2 shows the pyramidal tracts of the same patient as in Fig. 15.1, with a tumor in the left hemisphere. The tracts are colored using the *FA* values between 0.2 and 0.7 (top row) and using the diffusivity between 0.065 and 0.125 (bottom row). This figure shows clearly the reduction of *FA* in the right pyramidal tract, especially in the posterior area, which is more affected by the tumor, and the increase in the diffusivity in that area.

Tract Connectivity Measure

Due to the intrinsic nature of fibers, which are neuronal connections, a natural way of measuring these structures is accounting for their connectivity. A connectivity measure should give us a way to measure the degree of connection between two or more regions of the brain. The connectivity can be defined based on three contributions: one corresponding to the global intrinsic properties of the fiber tract, a second one derived from the deviation with respect to the healthy model, and a third one based on the number of fibers of the bundle:

$$C = I + \alpha_1(1 - \beta E_{\mathrm{m}}) + \alpha_2 N$$

where I is the *integrity* measure, E_{m} is the *deviation from the model*, and the parameters α_1 and α_2 and β are weight factors used to sum comparable magnitudes. In the experiments performed in this work the values used are 5, 0.01 and 10 respectively. The reason to choose a low value for α_2 with respect to α_1 is because N has a high variability, near 20% in the control group, and therefore its contribution has to be limited with respect to the others in order to avoid a high bias. The connectivity measure defined here increases with the anisotropy *FA* and the number of

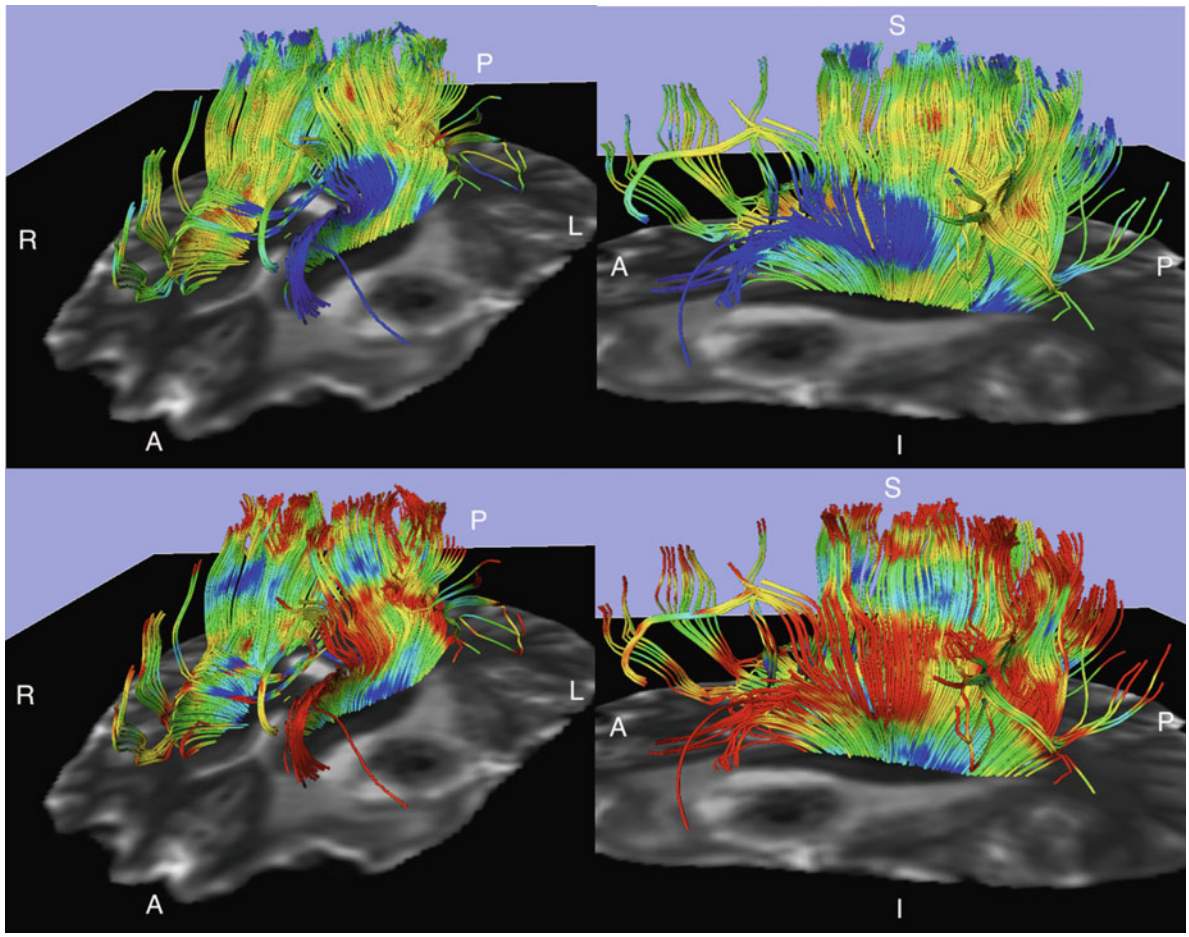

Fig. 15.2 Tractography images, showing the pyramidal tract of a patient (P6) harboring a tumor in the left hemisphere. *Left column*: *top left* view, *right column*: *left view*. *Top row*: fibers colored according to FA values. *Bottom row*: fibers colored according to MD values

fibers N, and decreases with the radial diffusivity D_{rad} and the deviation from the model E_{m}.

Experiments

The experiments reported here have been carried out on the data sets of 10 patients (numbered from P1 to P10) selected as described before, previous to the intervention, as well as on 10 control subjects. The measures reported here are the integrity I, and the connectivity C, but other measures such as the deviation from the model E_{m}, as well as the classic measures such as average FA, average radial diffusivity D_{rad}, and number of fibers N have been also computed to obtain the first two. These measures, together with all the processing made on the tensor datasets, have been carried out using *SATURN* software (Cárdenes et al. 2010b).

In Fig. 15.3 (top row) the integrity and connectivity measures are shown for the control and the patient groups, distinguishing between the two hemispheres. It is clear from these figures how the control group differentiate from the patient group, where asymmetry between left and right hemisphere values are clearly noticeable, showing how the pyramidal tracts are affected by the tumor, compared to the controls and also compared to the contralateral hemisphere. This is especially clear for patients P7, P8, P9 and P10 in the I measure, and P4, P6, P7, P8, P9 and P10 in the C measure. It is also noticeable that the control group presented very similar values between

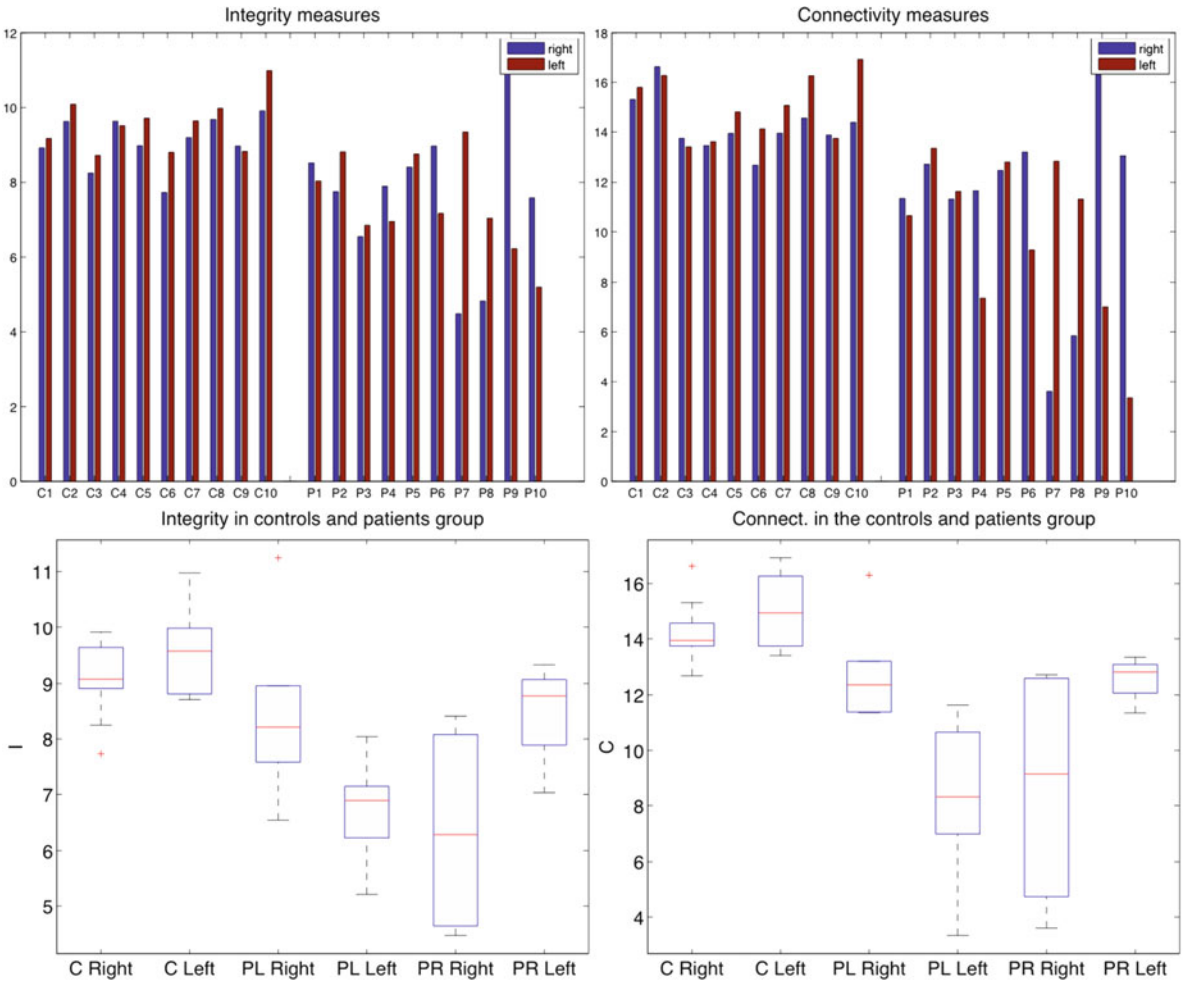

Fig. 15.3 *Top row*: integrity and connectivity measures for the control (C1 to C10) and patient (P1 to P10) groups, in blue the values for the right hemisphere and in red for the left hemisphere. *Bottom row*: mean and std of the integrity and connectivity measures in the control group (C), the patient group with tumor in the right (PR), and patients with tumor in the left (PL), divided by hemispheres

both hemispheres in all the measures, and also similar values among different subjects. In this study, only patients P1, P2, P3 and P5, did not have significant differences between both hemispheres, due to the small pyramidal tract zone affected by the tumor. However, their integrity and connectivity values were below the mean values obtained in the control group. In Fig. 15.3 (bottom row) it is also shown the mean and standard deviation (std) obtained for the two groups. This time the patient group is divided into two groups: PL which are patients with the left hemisphere affected (P1, P3, P4, P6, P9 and P10) and PR, patients with the right hemisphere affected (P2, P5, P7 and P8). It is clear from this figure that *I* and *C* measures present higher average values and lower std values in the control group than in the pathological groups (PL left and PR right).

Discussions and Conclusions

The quantification methodology based on DTI can effectively characterize the pyramidal tracts in tumor patients, allowing to compare them against healthy tracts, such as those obtained in control subjects and against contralateral fiber bundles of the same patient. The quantification method shows to be effective when

it is based on key features extracted from the fiber tracts, such as the anisotropy and diffusivity of the regions involved in the fiber tract and the number of fibers of the tract. Moreover, it turns out to be even more useful if a population based measure is included, such as the difference between the patient's tract and a model extracted from the tracts of a set of control healthy subjects. It has been shown that the combination of intrinsic properties of the fibers such as *FA* and D_{rad}, in the integrity measure, provides values that discriminate better between pathologic and healthy fiber tracts than using single *FA* or single *MD*.

The experiments carried out here show that this methodology is valid to quantify correctly the pyramidal tracts of tumor patients, in the sense that these measures distinguish clearly healthy pyramidal tracts from affected ones. Two main comparison experiments have been carried out in this work. First, a comparison between hemispheres of the same patient shows clear differences between the healthy and the affected side of the same patient as shown in Fig. 15.3. Second, comparison with controls is shown to be useful to detect affected tracts, which are related to reduced connectivity values, as shown also in Fig. 15.3. Such information has proven useful for clinicians not only to plan surgery but also for counseling patients in the preoperative period, and the method can also be employed successfully to evaluate the evolution of patients.

The 2D mapping technique used in this methodology, has been useful to normalize the tract to a standard space in which measures can be done easily. Therefore, comparison between individual subjects and data coming from control population becomes easier using these maps. The measure derived from them, called deviation from the model E_{m}, provides useful information about the state of the tract, and can perform more robust fiber tract quantification than other classic methods. This 2D mapping of the pyramidal tract has also clear advantages for visual inspection of tracts, obtaining a new insight of the state of the fiber tract, providing information about the global state of the fibers, and local abnormalities such as holes or bands located at particularly important anatomical regions. The integrity measure, the deviation from the model measure and the number of fibers of the bundle, are finally combined to define a connectivity measure which gives an aggregate measure about the degree of connection of the pyramidal tract. This quantity is a connectivity measure because its values are increased as they approach to the ideal pyramidal tract provided by the model, when the number of fibers increase, and when the axons in the fibers are strongly aligned in the fibers directions. The measures reported here also correlate well with the clinical state of the patients considered in this work. Taking advantage of the simplicity of the procedure, and its ability to account for most of the information obtained from the DTI data, this methodology can be used to study other fiber bundles that could be affected by tumors, such as the corpus callosum, the superior longitudinal fasciculus or the inferior longitudinal fasciculus, for instance, and it can be also used to quantify or detected fiber tracts that are affected by other neurological disorders such as multiple sclerosis, epilepsy, etc.

References

Audoin B, Guye M, Reuter F, Duong M-VA, Confort-Gouny S, Malikova I, Soulier E, Viout P, Chérif AA, Cozzone PJ, Pelletier J, Ranjeva J-P (2007) Structure of WM bundles constituting the working memory system in early multiple sclerosis: a quantitative DTI tractography study. NeuroImage 36:1324–1330

Basser P, Mattiello J, Le Bihan D (1994) MR diffusion tensor spectroscopy and imaging. Biophys J 66:259–267

Cárdenes R, Muñoz-Moreno E, Sarabia-Herrero R, Rodríguez-Velasco M, Fuertes-Alja JJ, Martin-Fernandez M (2010a) Analysis of the pyramidal tract in tumor patients using diffusion tensor imaging, NeuroImage 50:27–39

Cárdenes R, Muñoz-Moreno E, Tristan-Vega A, Martin-Fernandez M (2010b) Saturn: a software application of tensor utilities for research in neuroimage, Comput Meth Prog Biol 97:264–279

Correia S, Lee SY, Voorn T, Tate DF, Paul RH, Zhang S, Salloway SP, Malloy PF, Laidlaw DH (2008) Quantitative tractography metrics of white matter integrity in diffusion-tensor MRI. NeuroImage 42:568–581

Diehl B, Bush RM, Duncan JS, Piao Z, Tkach J, Lüders HO (2008) Abnormalities in diffusion tensor imaging of the uncinate fasciculus related to reduced memory in temporal lobe epilepsy. Epilepsia 49:1409–1418

Hagler DJ, Ahmadi ME, Kuperman J, Holland D, McDonald CR, Halgren E, Dale AM (2009) Automated white-matter tractography using a probabilistic diffusion tensor atlas: application to temporal lobe epilepsy. Hum Brain Mapp 30:1535–1547

Hagmann P, Thiran, J-P, Jonasson L, Vandergheynst P, Clarke S, Meuli R (2003) DTI mapping of human brain connectivity: statistical fibre tracking and virtual dissection. NeuroImage 19:545–554

Hua K, Zhang J, Wakana S, Jiang H, Li X, Reich DS, Calabresi PA, Pekar JJ, van Zijl PCM, Mori S (2008) Tract

probability maps in stereotaxic spaces: analysis of white matter anatomy and tract-specific quantification. NeuroImage 39:336–347

Inoue T, Ogasawara K, Beppu T, Ogawa A, Kabasawa H (2005) Diffusion tensor imaging for preoperative evaluation of tumor grade in gliomas. Clin Neuro Neurosurg 107: 174–180

Kinoshita M, Hashimoto N, Goto T, Kagawa N, Kishima H, Izumoto S, Tanaka H, Fujita N, Yoshimine T (2008) Fractional anisotropy and tumor cell density of the tumor core show positive correlation in diffusion tensor magnetic resonance imaging of malignant brain tumors. NeuroImage 43:29–35

Kubicki M, Park H, Westin CF, Nestor PG, Mulkern RV, Maier SE, Niznikiewicz M, Connor EE, Levitt JJ, Frumin M, Kikinis R, Jolesz FA, McCarley RW, Shenton ME 2005. DTI and MTR abnormalities in schizophrenia: Analysis of white matter integrity. NeuroImage 26:1109–1118

Lawes INC, Barrick TR, Murugam V, Spierings N, Evans DR, Song M, Clark CA (2008) Atlas-based segmentation of white matter tracts of the human brain using diffusion tensor tractography and comparison with classical dissection. NeuroImage, 39:62–79

McDonald CR, Ahmadi ME, Hagler DJ, Tecoma ES, Iragui VJ, Gharapetian L, Dale AM, Halgren E (2008) Diffusion tensor imaging correlates of memory and language impairments in temporal lobe epilepsy. Neurology 71:1869–1876

Mori S, van Zijl PCM (2002) Fiber tracking: principles and strategies – a technical review. NMR Biomed 15: 468–480

Mori S, Wakana, S, Nagae-Poetscher LM, van Zijl PCM (2005) MRI atlas of human white matter. Elsevier, Amsterdam, The Netherlands

Muñoz-Moreno E, Martin-Fernandez M (2009) Characterization of the similarity between diffusion tensors for image registration. Comput Biol Med 39:251–265

O'Donnell L, Haker S, Westin CF (2002) New approaches to estimation of white matter connectivity in diffusion tensor MRI: elliptic PDEs and geodesics in a tensor-warped space. Proceedings of MICCAI 459–466, Tokyo, Japan

Pagani E, Filippi M, Rocca MA, Horsfield MA (2005) A method for obtaining tract-specific diffusion tensor MRI measurements in the presence of disease: applications to patients with clinically isolated syndromes suggestive of multiple sclerosis. NeuroImage 26:258–265

Partridge S, Mukherjee P, Berman J, Henry RG, Miller SP, Lu Y, Glenn OA, Ferreiro DM, Barkovich AJ, Vigneron DB (2005) Tractography-based quantification of diffusion tensor imaging parameters in white matter tracts of preterm newborns. J Magn Reson Imaging 22:467–474

Pierpaoli C, Basser PJ (1996) Toward a quantitative assessment of diffusion anisotropy. Magn Reson Med 36:893–906

Price SJ, Burnet NG, Donovan T, Green HAL, Peña A, Antoun NM, Pickard JD, Carpenter TA, Gillard JH, (2003) Diffusion tensor imaging of brain tumors at 3T: a potential tool for assessing white matter tract invasion? Clin Radiol 58: 455–462

Roosendal SD, Geurts JJG., Vrenken H, Hulst HE, Cover KS, Castelkins JA, Pouwels PJW, Barkhof F (2009) Regional DTI differences in multiple sclerosis patients. NeuroImage 44:1397–1403

Schonberg T, Pianka P, Hendler T, Pasternak O, Assaf Y (2006) Characterization of displaced white matter by brain tumors using combined DTI and fMRI. NeuroImage 30:1100–1111

Skudlarski P, Jagannathan K, Calhoun VD, Hampson M, Skudlarska BA, Pearlson G (2008) Measuring brain connectivity: diffusion tensor imaging validates resting state temporal correlations. NeuroImage 43:554–561

Smith S M, Jenkinson M, Johansen-Berg H, Rueckert D, Nichols TE, Mackay CE, Watkins KE, Cicarelli O, Cader MZ, Matthews PM, Behrens TEJ (2006) Tract-based spatial statistics: Voxelwise analysis of multi-subject diffusion data. NeuroImage 31:1487–1505

Stejskal EO, Tanner JE (1965) Use of spin-echoes in a pulse magnetic field gradient to study anisotropic diffusion and flow. J Chem Phys 43:3597–3603

Song SK, Sun SW, Ju WK, Lin SJ, Cross AH, Neufeld AH (2003) Diffusion tensor imaging detects and differentiates axon and myelin degeneration in mouse optic nerve after retinal ischemia. NeuroImage 20:1714–1722

Sundgren PC, Dong Q, Gómez-Hassan D Mukherji SK, Maly P, Welsh R (2004) Diffusion tensor imaging of the brain: review of clinical applications. Neuroradiology 46:339–350

Westin, C-F, Maier SE, Mamata H, Nabavi A, Jolesz FA, Kikinis R (2002) Processing and visualization of diffusion tensor MRI. Med Image Anal 6:93–108

Yu CS, Li KC, Xuan Y, Ji XM, Qin W (2005) Diffusion tensor tractography in patients with cerebral tumors: a helpful technique for neurosurgical planning and postoperative assessment. Eur J Radiol 56:197–204

Chapter 16

Differentiation Between Gliomatosis Cerebri and Low-Grade Glioma: Proton Magnetic Resonance Spectroscopy

Virginie Callot, Damien Galanaud, and Patrick J. Cozzone

Abstract The distinction between gliomatosis cerebri (GC) and low-grade glioma (LGG), based on histological and MR criteria, is a matter of debate. In this chapter, the diagnostic and prognostic value of proton MR Spectroscopy in the characterization of infiltrating gliomas is illustrated.

Keywords Gliomatosis cerebri · Neuroepithelial neoplasms · Glial tumor · Astrocytic tumor · Oligodendroglial · Low-grade glioma

Introduction

Gliomatosis cerebri (GC) is a rare tumor – less than 300 cases have been reported in the literature (Taillibert et al. 2006) – considered as a malignant lesion of poor prognosis.

In the 1993 World Health Organization (WHO) classification, GC has been classified as a type of neuroepithelial neoplasms of unknown origin (Kleihues et al. 1993) and it has been defined as a diffuse glial tumor infiltrating the brain extensively, involving more than two lobes, frequently bilaterally and often extending to infratentorial structures, with typical absence of features such as vascular proliferation and necrosis. GC has been classified as a type of astrocytic tumor in the 2007 WHO classification (Louis et al. 2007); however an oligodendroglial or mixed cell type proliferation is commonly found at the biopsy. It should be noted that no clear histological feature can differentiate a GC from a more common WHO grade II or III glioma.

The diagnosis of GC is usually made on the basis of both histology and neuroimaging. However, biopsy specimens are often difficult to evaluate because of heterogeneous tumor process, which makes difficult the precise quantification of tumoral and normal elements and thus the assessment of the degree of aggressiveness of the tumor.

Magnetic resonance imaging (MRI), which is the radiologic method of choice, is also often nonspecific. Infiltration of two lobes or more, absence of contrast enhancement and necrosis are indeed common in infiltrative gliomas and the differential diagnosis between the two subtypes of tumors rely on more subtle findings, reported by Peretti-Viton et al. (2002), such as a predominant involvement of the white matter or the absence of significant "focal" mass effect. To overcome this problem, it has recently been suggested that the use of proton MR spectroscopy (MRS) may aid in the differential diagnosis of gliomatosis cerebri and low-grade glioma (Galanaud et al. 2003).

Methodology

^{1}H-MR Spectroscopy

MRS allows in vivo non invasive explorations of the molecular constituents (metabolites) involved in the physiopathology of the tumors. Clinical proton MRS methods include single-voxel spectroscopy (SVS) and multi-voxel 2D and 3D chemical shift imaging (2D and 3D CSI). SVS produces a single spectrum from a

P.J. Cozzone (✉)
Centre de Résonance Magnétique Biologique et Médicale (CRMBM), UMR 6612, CNRS, Université de la Méditerranée, Faculté de Médecine, 27 boulevard Jean Moulin, 13385 Marseille cedex 05, France
e-mail: Patrick.cozzone@univmed.fr

M.A. Hayat (ed.), *Tumors of the Central Nervous System, Volume 4*,
DOI 10.1007/978-94-007-1706-0_16,

single voxel, whereas CSI can be displayed as spectral maps, colored metabolic images, and individual spectra. MRS explorations are performed at short or long echo times, which provide the ability to control the T_2 contrast of spectral peaks (short T_2 metabolite signals decay faster and the corresponding peaks are therefore not seen on long echo time spectra). Due to technical limitations, such as field strength and examination time, only a few compounds can however routinely be detected in a clinical context. The principal metabolites of particular importance are:

- *N*-acetyl aspartate (NAA), detected at 2.02 and 2.6 ppm, which is an amino acid present almost exclusively in neurons. Its decrease corresponds to neuronal injury,
- choline-containing compounds (Cho), detected at 3.2 ppm, which are mostly involved in cell membrane metabolism. They increase whenever there is cellular proliferation, inflammation or demyelination,
- creatine/phosphocreatine (Cr), detected at 3.02 and 3.9 ppm, which is involved in energy storage. It is a marker of overall cellular density and has often been used as an internal standard for semi-quantitative evaluation of metabolic changes of other brain metabolites,
- glutamate/glutamine (Glx), detected at 2.05 and 2.5 ppm, which is involved in excitatory and inhibitory neurotransmission,
- myo-inositol (mI), detected at 3.56 ppm, which is a sugar only present in glia, that is reduced when there is a specific suffering of these cells and increased in cases of glial activation or proliferation,
- lactate (Lac), detected at 1.35 ppm, which is produced under conditions of anaerobic glycolysis. It indicates hypoxic conditions as well as hypermetabolic glucose consumption and in some cases macrophagic invasion, and finally
- lipids (Lip) and macromolecules, detected between 0.9 and 1.3 ppm, which usually correlate to the extent of tissue necrosis.

Patient Population

Nine patients with GC (mean age 52 ± 16 years) and nine patients with LGG (mean age 54 ± 17 years) were enrolled within a period of 20 months after being referred to the Neurosurgery Department of the Timone Hospital in Marseille. All patients were examined by conventional MR imaging shortly before being included in the study.

Patients were considered to have GC (nine patients) when they met the following criteria (Peretti-Viton et al. 2002):

(1) the glial neoplasm infiltrated at least 2 lobes and was documented by brain biopsy,
(2) the patient had no history of focal glioma,
(3) there was a lack of significant focal mass effect,
(4) the lesion involved mostly white matter and/or the basal ganglia, and,
(5) there was a lack of significant contrast enhancement (<1 cm^2) on imaging studies at the time of diagnosis.

When patients did not fulfill the last four criteria, a diagnosis of infiltrating glioma was made. The mean time between the first symptoms (seizures (seven patients), psychomotor slowing (five patients), intracranial hypertension (five patients), dysarthria (two patients), hemiparesis (one patient) and ataxia (one patient)) and the diagnosis was 1.5 ± 1.5 months. Survival times ranged from 1 to 22 months. Treatment consisted of nitrosourea-based chemotherapy (nine patients) and radiotherapy (three patients). Among the eight patients with adequate follow-up, two patients sustained neurological improvement under therapy. None exhibited a neuroimaging-verified decrease in tumor volume.

The nine patients with LGG were documented by stereotactic brain biopsy. The tumors were classified as oligodendroglioma (six patients), oligoastrocytoma (two patients) and astrocytoma (one patient). Treatment consisted of nitrosourea-based chemotherapy and radiotherapy. All but one of the patients were alive without progression of their disease after 24 months of follow-up.

Eighteen healthy volunteers (mean age 24 ± 6 years) were additionally included to determine the regional metabolite levels in different areas of the normal brain.

All volunteers and patients gave informed consent to participate to the study, which was approved by the Ethics Committee of our institution. The first MR

examination of the protocol was performed before any treatment.

MR Protocol

All exams were performed on a 1.5-tesla system (Magnetom Vision, Siemens, Erlangen, Germany). The MRI protocol included at least one FLAIR acquisition and one T_1-weighted acquisition before and after administration of a gadolinium-based contrast agent (DOTAREM, Guerbet, Paris, France). The MRS protocol included both SVS and CSI.

The SVS was performed using the manufacturer STEAM sequence (TR/TE 1500/20 ms, voxel size 20 × 20 × 20 mm). Single-voxel acquisitions were performed in the bulk of the gliomatosis infiltration in seven of nine patients with GC and in contrast-enhancing areas in the other two patients. In patients with low grade glioma, the voxel was positioned in an area of tumor infiltration which appeared homogeneous and non cystic on the FLAIR sequence.

The CSI acquisitions were performed in the axial plane using a home-designed sequence (Galanaud et al. 2001), with the following parameters: TR 1500 ms, slice thickness 15 mm, FOV 230 mm spectroscopic volume of interest 20 × 20 × 15 mm^3. The slice was positioned in areas of maximum extension of tumor and/or in contrast-enhancing areas. If these areas were different, CSI was performed at both locations. An echo time of 135 ms was used in all patients and volunteers. Acquisition at short echo time (TE 22 ms) was performed in 7 of 9 patients with GC, 4 of 9 patients with LGG and 9 of the 18 volunteers.

Data Analysis

The MRS data are analyzed using a dedicated software (Le Fur et al. 2010), developed on IDL (Interactive Data Language, Research System Inc., Boulder, CO, USA) and adapted from the magnetic resonance user interface software package (MRUI, http://sermn02.uab.cat/mrui/). Automated packages, now available on most of clinical systems, can also be used, as well as the LCModel software (http://s-provencher.com/pages/lcmodel.shtml). Resonances were assigned according to those described in ^{1}H-MR Spectroscopy section. Signals from NAA, Cho, Cr and Lac were recorded from both long and short echo time spectra, whereas Ins and Glx signals were recorded on the short echo time spectra.

Absolute quantification is not yet routinely performed because it requires a determination of the relaxation times of all metabolites, which is too time-consuming to be clinically acceptable for the patient, and water signal cannot be used as a reliable reference since the amount of water is variable among the tumors due to the presence of edema and differences in cellular morphology. In this study, the brain metabolites were measured using relative quantitation and data were displayed as ratios of the signal area of a given metabolite over the sum (S) of signal areas of all metabolites detected on the same spectrum. The regions of interest for analysis the CSI spectra were: (1) a homogeneous-appearing, non contrast-enhancing part of the gliomatosis or low grade glioma infiltration and (2) a normal-appearing whiter matter area of the same tissue structure, usually located in the parieto-occipital region. Acquisitions that could not be reliably analyzed because of insufficient quality of the spectra were discarded in 2 LGG. For the volunteers, only normal-appearing white matter in the right and left parieto-occipital regions were analyzed.

Statistical Analysis

Statistical analysis was performed using Statview software (Abacus Inc., Berkeley, CA, USA) for classic univariate analysis. Comparisons between patients with GC or LGG and healthy volunteers for each metabolite ratio were performed by applying a Kruskal–Wallis analysis followed by a discriminating Scheffé test with Bonferroni correction. The metabolic ratios individually discriminating among groups by univariate statistical analysis were selected to perform a principal component analysis (PCA) with the objective to separate GC, LGG and control populations. The multivariate analysis by PCA was performed using Excel software (Microsoft, Redmond, WA, USA) with Statbox (Grimmersoft, Paris, France). All values are reported as means ± standard deviations. *P*-values less than 0.05 were considered significant. When the three groups were compared (Bonferroni correction), *p*-values lower than 0.0167 were considered significant.

Results

Typical spectra recorded at short and long echo time from patients with GC, LGG and an healthy volunteer (NV) are displayed in Fig. 16.1. The tumor process in the two patients harboring glial neoplasm was characterized by markedly elevated Ins (Fig. 16.1b and e) and reduced NAA levels (Fig. 16.1b, c, e, and f). The Cho level was additionally more elevated and the NAA more reduced in LGG (Fig. 16.1, middle) than GC (top) and NV (bottom).

The metabolic ratios obtained in the different experimental conditions (SVS, CSI) and the statistical differences observed between groups ($n = 9$ GC, $n = 9$ LGG and $n = 18$ NV) are summarized in Table 16.1.

Overall, at short echo time, LGGs were characterized by lower NAA/S and higher Cho/S ratios than GCs and higher Cho/S and Ins/S ratios and lower

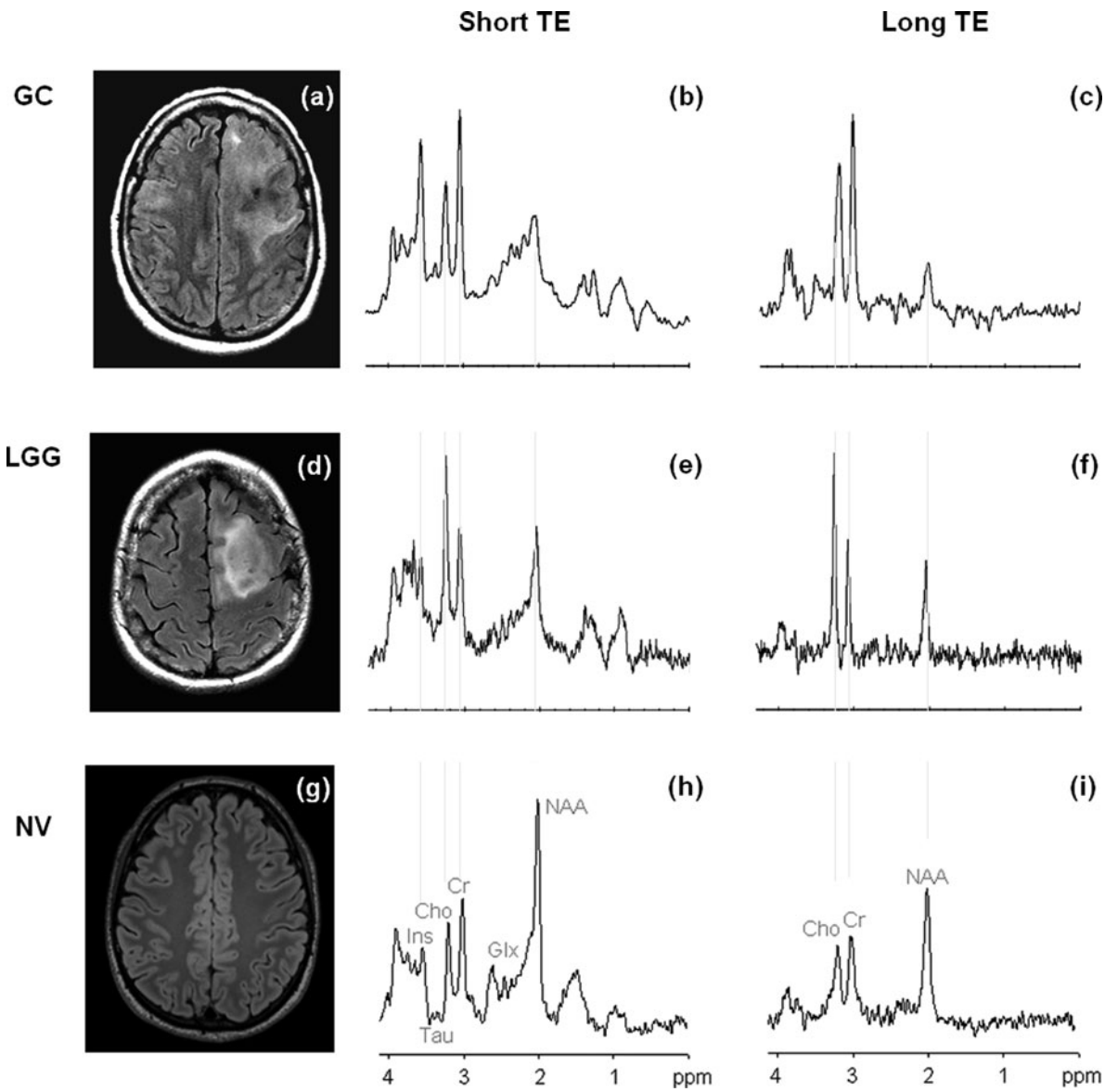

Fig. 16.1 Short (**b**, **e**, **h**) and long (**c**, **f**, **i**) echo time spectra collected in patients with GC (*top*), LGG (*middle*) and a normal volunteer NV (*bottom*)

Table 16.1 Metabolic ratios in regions of GCs, LGGs and normal-appearing white matter of normal volunteers (NV). Values are expressed as means ± standard deviation. A *p*-value lower than 0.0167 corresponds to statistically significant differences

MRS method	GC	LGG	NV	Statistical difference
SVS (TE 20 ms)	*N*=7	*N*=5	*N*=18	
NAA/S	0.178±0.052	0.169±0.063	0.278±0.056	GC vs. NV, LGG vs. NV
Cr/S	0.176±0.044	0.130±0.035	0.152±0.021	GC vs. LGG
Cho/S	0.114±0.039	0.208±0.053	0.126±0.022	GC vs. LGG, LGG vs. NV
Ins/S	0.217±0.060	0.184±0.095	0.109±0.017	GC vs. NV, LGG vs. NV
Glx/S	0.329±0.090	0.328±0.108	0.314±0.057	
CSI (TE 22 ms)	*N*=7	*N*=4	*N*=9	
NAA/S	0.290±0.105	0.173±0.091	0.364±0.072	LGG vs. NV
Cr/S	0.217±0.058	0.222±0.057	0.167±0.043	
Cho/S	0.125±0.065	0.258±0.062	0.111±0.024	GC vs. LGG, LGG vs. NV
Ins/S	0.176±0.048	0.130±0.046	0.068±0.022	GC vs. NV, LGG vs. NV
Glx/S	0.154±0.106	0.222±0.070	0.273±0.0101	
CSI (TE 135 ms)	*N*=9	*N*=9	*N*=16	
NAA/S	0.365±0.075	0.256±0.073	0.535±0.036	GC vs. LGG, GC vs. NV, LGG vs. NV
Cr/S	0.346±0.083	0.234±0.081	0.244±0.022	GC vs. LGG, GC vs. NV
Cho/S	0.289±0.036	0.474±0.078	0.221±0.036	GC vs. LGG, GC vs. NV, LGG vs. NV

NAA/S ratios than healthy brain. GCs were characterized by higher Cr/S and lower Cho/S ratios than LGGs, and lower NAA/S and higher Ins/S ratios than healthy brain tissue. From both short and long echo time CSI acquisitions, it was verified that the Cr levels in normal white matter in patients with GC, patients with LGG and healthy volunteers, were similar (data not shown), making thus the contralateral level of Cr a suitable internal reference.

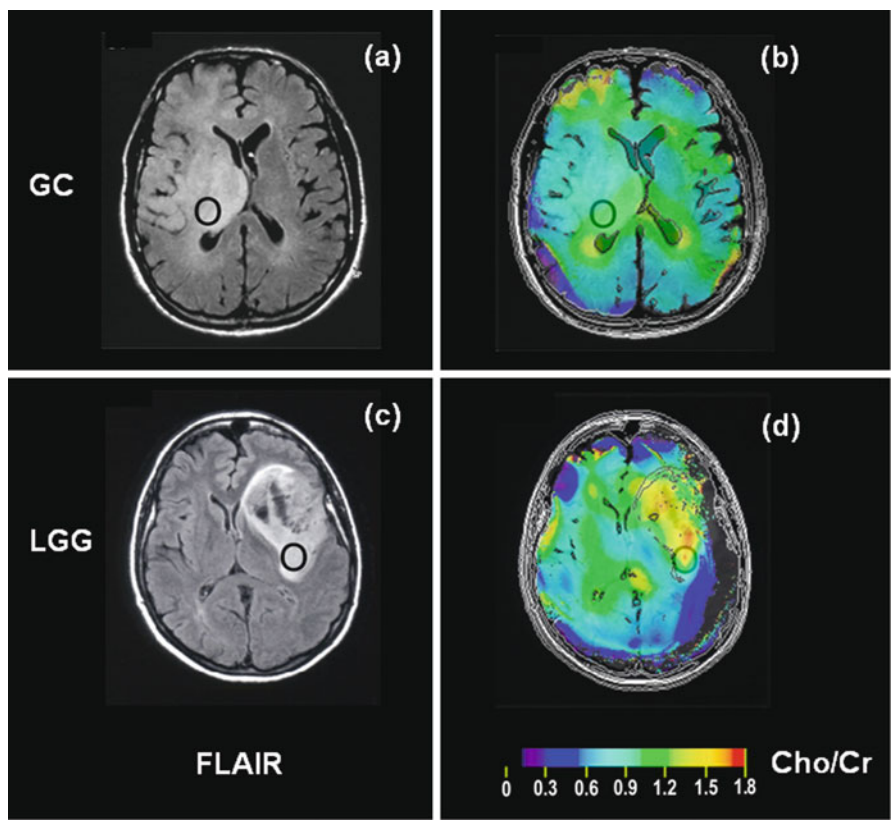

Fig. 16.2 FLAIR images (**a**, **c**) and Cho/Cr maps (**b**, **d**), obtained in a patient with GC (*top*) and a patient with LGG (*bottom*). By visual inspection of the metabolic color maps, the two tumor processes can clearly been distinguished

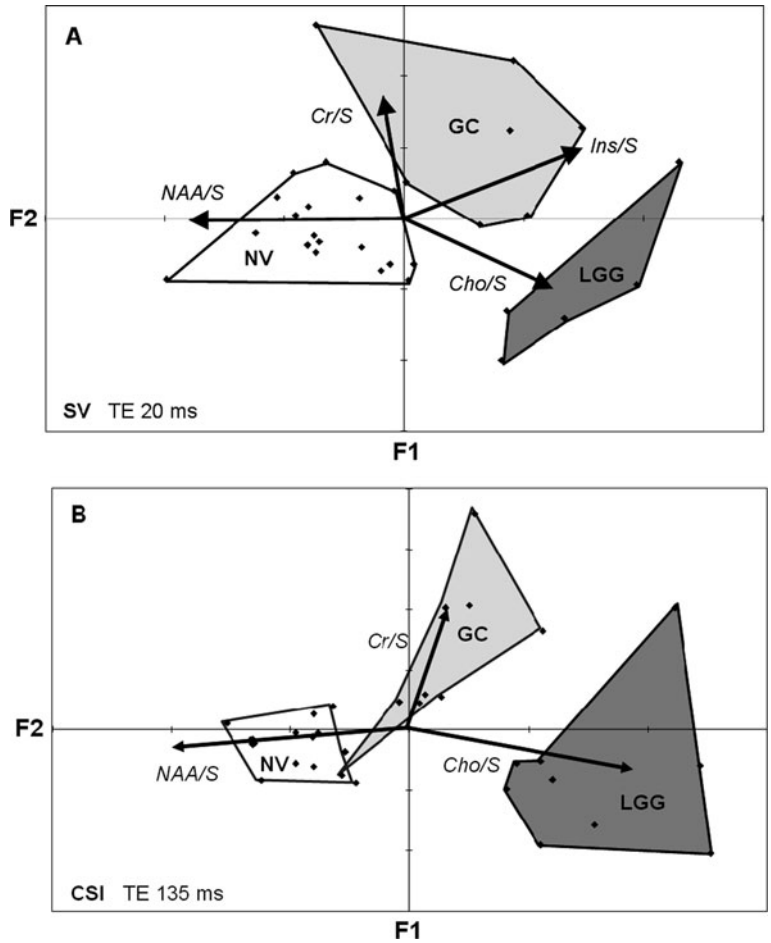

Fig. 16.3 Principal component analysis of the results performed at short (**a**) and long (**b**) echo times. The two axis (F1 and F2) explain 77% (**a**) and 99% (**b**) of the total variance

At long echo time, LGGs were characterized by reduced levels of Cr and NAA and a more elevated concentration of Cho than GCs. Lactate was detected in three patients. GCs were characterized by an elevated level of Cr, a reduced level of NAA, an absence of lactate and a less elevated level of Cho than LGGs. Cho/Cr maps recorded from patients with GC and LGG are illustrated on Fig. 16.2. These two patients, who were not differentiated according to the WHO criteria, displayed different Cho/Cr metabolic maps. The level of Cho is only slightly elevated in the patient with GC and the level of Cr is markedly elevated, which leads to a reduction of Cho/Cr in the lesion compared to normal white matter. On the contrary, because the Cho concentration is elevated and the Cr level is normal or reduced in the patient with LGG, an elevated Cho/Cr ratio is observed in the tumor compared to normal brain parenchyma. By using the metabolic ratio, which undergoes opposite variations in GC and LGG, the metabolic differences between GC and LGG are enhanced, enabling thus their separation by visual inspection of the metabolic maps. This capacity of distinguishing the two tumor processes was further emphasized by performing PCA and adding the NAA information (Fig. 16.3b).

The PCA performed with the spectroscopic parameters derived from short echo time acquisitions (Cho, Cr, NAA and Ins) clearly separated all individuals from each of the three groups (NV, GC, and LGG), as shown on Fig. 16.3a.

Discussion

Treatment of glial tumors has markedly improved in the last 10 years. Availability of new chemotherapeutic agents such as temozolomide and avastin has lead to an increased survival of a significant subgroup of patients. However, some patients still have a dismal prognosis

and fail to respond to usual treatments. Some histological markers, such as the oligodendroglial cell type or methylation of the MGMT precursor have been shown to be of prognostic value and/or predict the response to treatment. They are however insufficient to reliably determine the evolution of the patient at an individual level, and two subjects with a similar histology can have very different outcomes.

Gliomatosis cerebri is a still poorly understood glial neoplasm. Its histology is similar to the more common types of low-grade gliomas but its prognosis is poor, comparable to a high-grade glioma. It more successfully responds to chemotherapy regimens aimed at grade III–IV tumors (temozolomide) rather than those more classically used in grade II lesions (PCV regimen) (Levin et al. 2004). It can be seen as the most infiltrative subtype of glioma and the radiologic criteria used to define this tumor emphasize the combination of extensive infiltration (two lobes or more) and low tumor cell density (lack of focal mass effect).

MR spectroscopy shows marked differences between low-grade gliomas and gliomatosis cerebri. The former has the classical spectrum of a glioma, with an elevation in choline, reflecting the proliferation of glial cells, associated to a marked reduction of NAA, mirroring the replacement of neurons by these tumor cells. Myo-inositol may sometimes be slightly elevated depending on the dedifferentiation of the tumor. On the contrary, gliomatosis cerebri has a unique profile among intracranial tumors. Choline is only marginally elevated reflecting the low tumor cell density. On the contrary, there is a simultaneous increase in Creatine and myo-inositol. Other authors have also reported similar results (Gutowski et al. 1999). Elevated Creatine and myo-inositol has previously been reported in pathologies such as Steinert's myotonic dystonia and been related to an increased glial metabolism (Chang et al. 1998). It appears unlikely that these metabolites originated from the neoplastic cells, since their density is low and their metabolism is usually abnormal, resulting in a reduction in the resonance of Creatine (Negendank et al. 1996; Ziegler et al. 2001). The most likely explanation is an increased metabolism and/or an increased density of the normal glia, which is present within the tumor. Since the stereotactic biopsies used to make the pathological diagnosis cannot evaluate this parameter, this is a clear added value of MRS for the diagnosis of this disease, as compared to both conventional MRI and histopathology.

Acknowledgments The authors are indebted to the neurosurgeons (Prof. Grisoli and Roche, Dr. Mettelus and Fuentès), neurooncologists (Prof. Chinot, Dr Barrié-Attarian) and anatomopathologist (Prof. Figarella-Branger) of the Hôpital de la Timone and Hôpital Sainte-Marguerite. This work receives the support of CNRS (Centre National de la Recherche Scientifique, UMR 6612), ANR (Agence Nationale de la Recherche), ARC (Association pour la Recherche contre le Cancer).

References

Chang L, Ernst T, Osborn D, Seltzer W, Leonido-Yee M, Poland RE (1998) Proton spectroscopy in myotonic dystrophy: correlations with CTG repeats. Arch Neurol 55:305–311

Galanaud D, Chinot O, Nicoli F, Confort-Gouny S, Le Fur Y, Barrie-Attarian M, Ranjeva JP, Fuentes S, Viout P, Figarella-Branger D, Cozzone PJ (2003) Use of proton magnetic resonance spectroscopy of the brain to differentiate gliomatosis cerebri from low-grade glioma. J Neurosurg 98:269–276

Galanaud D, Le Fur Y, Nicoli F, Denis B, Confort-Gouny S, Ranjeva JP, Viout P, Pelletier J, Cozzone PJ (2001) Regional metabolite levels of the normal posterior fossa studied by proton chemical shift imaging. MAGMA 13:127–133

Gutowski NJ, Gomez-Anson B, Torpey N, Revesz T, Miller D, Rudge P (1999) Oligodendroglial gliomatosis cerebri: (1)H-MRS suggests elevated glycine/inositol levels. Neuroradiology 41:650–653

Kleihues P, Burger PC, Scheithauer BW (1993) The new WHO classification of brain tumours. Brain Pathol 3:255–268

Le Fur Y, Nicoli F, Guye M, Confort-Gouny S, Cozzone PJ, Kober F (2010) Grid-free interactive and automated data processing for MR chemical shift imaging data. MAGMA 23:23–30

Levin N, Gomori JM, Siegal T (2004) Chemotherapy as initial treatment in gliomatosis cerebri: results with temozolomide. Neurology 63:354–356

Louis DN, Ohgaki H, Wiestler OD, Cavenee WK, Burger PC, Jouvet A, Scheithauer BW, Kleihues P (2007) The 2007 WHO classification of tumours of the central nervous system. Acta Neuropathol 114:97–109

Negendank WG, Sauter R, Brown TR, Evelhoch JL, Falini A, Gotsis ED, Heerschap A, Kamada K, Lee BC, Mengeot MM, Moser E, Padavic-Shaller KA, Sanders JA, Spraggins TA, Stillman AE, Terwey B, Vogl TJ, Wicklow K, Zimmerman RA (1996) Proton magnetic resonance spectroscopy in patients with glial tumors: a multicenter study. J Neurosurg 84:449–458

Peretti-Viton P, Brunel H, Chinot O, Daniel C, Barrie M, Bouvier C, Figarella-Branger D, Fuentes S, Dufour H, Grisoli F (2002) Histological and MR correlations in Gliomatosis cerebri. J Neurooncol 59:249–259

Taillibert S, Chodkiewicz C, Laigle-Donadey F, Napolitano M, Cartalat-Carel S, Sanson M (2006) Gliomatosis cerebri: a review of 296 cases from the ANOCEF database and the literature. J Neurooncol 76:201–205

Ziegler A, von Kienlin M, Decorps M, Remy C (2001) High glycolytic activity in rat glioma demonstrated in vivo by correlation peak 1H magnetic resonance imaging. Cancer Res 61:5595–5600

Chapter 17

Peripheral Nerve Sheath Tumors: Diagnosis Using Quantitative FDG-PET

Elizabeth Shurell and Fritz C. Eilber

Abstract Malignant peripheral nerve sheath tumors (MPNST) compose a fraction of all soft tissue sarcomas, but are life-threatening and present difficult diagnostic and therapeutic challenges. Benign peripheral nerve sheath tumors, including schwannomas or neurofibromas, can often be managed conservatively unless symptomatic. MPNSTs require aggressive multimodality treatment (surgery, radiation therapy, ± chemotherapy). MPNSTs can arise from pre-existing neurofibromas in patients with neurofibromatosis type 1 (NF1) or can develop sporadically in the general population. Peripheral nerve sheath tumors are often pathologically heterogeneous or in difficult anatomic locations often making needle biopsy unreliable or unfeasible. Current standard imaging of these tumors rely on computed tomography (CT) or magnetic resonance imaging (MRI), both of which characterize size and local invasiveness, but do not provide reliable insight into the presence of malignant transformation. Clinical manifestations of malignant transformation classically rely on reported symptoms of new neurological deficits, rapid increase in size, change in palpated density from soft to hard, and unremitting pain. Investigations into the glycolytic phenotype of peripheral nerve sheath tumors with [18F] 2-Fluoro-2-deoxy-D-glucose positron emission tomography (FDG-PET) have been performed to identify potential areas of malignant degeneration. Lower tumor FDG uptake has proven to correlate with benign peripheral nerve sheath tumors, which can be distinguished from the high FDG uptake of its malignant counterpart, MPNST. Clinicians may employ this imaging modality to help identify MPNSTs, guide biopsies, direct therapies, measure response to treatment, and survey for tumor recurrence.

Keywords MPNST · Soft tissue sarcomas · Schwannomas · Neurofibromas · NF1 · Nerve sheath

Introduction

Malignant peripheral nerve sheath tumors (MPNST) compose a small fraction of all soft tissue sarcomas, but are life-threatening and present difficult diagnostic and therapeutic challenges. Benign peripheral nerve sheath tumors, including schwannomas or neurofibromas, can often be managed conservatively unless symptomatic. MPNST require aggressive multimodality treatment (surgery, radiation therapy, ± chemotherapy). MPNSTs can arise from pre-existing neurofibromas in patient with neurofibromatosis type 1 (NF1) or can develop sporadically in the general population. Peripheral nerve sheath tumors are often pathologically heterogeneous making needle biopsy frequently unreliable.

Radiographic differentiation of a MPNST from a benign peripheral nerve sheath tumor is often challenging (Benz et al. 2010a). MRI and CT have commonly been used with size and rapidity of growth being important factors to identify potential areas of malignant transformation. Clinically, physicians look to identify symptoms of new neurological deficits, rapid increase in size, change in palpated density

F.C. Eilber (✉)
Division of Surgical Oncology, UCLA, Los Angeles, CA 90095-1782, USA
e-mail: fceilber@mednet.ucla.edu

M.A. Hayat (ed.), *Tumors of the Central Nervous System, Volume 4*,
DOI 10.1007/978-94-007-1706-0_17,

from soft to hard, and unremitting pain (Ferner and Gutmann 2002). Despite this methodic clinical evaluation and serial cross sectional imaging, the reliability with which we can confidently diagnose a MPNST is poor. Recent studies investigating the glycolytic phenotypes of soft tissue sarcomas have highlighted the potential role of PET imaging with FDG to identify areas of malignant degeneration. Using FDG PET, we can now more accurately identify MPNSTs.

Glycolytic Phenotyping

Fluoro-2-deoxy-D-glucose (FDG) is an analog of glucose, a common substrate of metabolism in the human body. Using radiolabeled FDG, areas of high glucose metabolism, such as the brain, liver, and myocardium can be easily identified using PET imaging. Tumor cells and certain infectious processes also have increased FDG uptake. When introduced into the extracellular environment, FDG is transported intracellularly and phosphorylated by hexokinase to FDG 6-phosphate (Kostakoglu et al. 2003). This phosphorylation causes structural changes in FDG that prevent further metabolism or extracellular transport, thereby allowing build-up and detection by PET scanning. This process is called "metabolic trapping" and is the basis for FDG-PET imaging of tumors (Chang et al. 2006; Kostakoglu et al. 2003).

Quantitative Evaluation of Metabolic Activity

FDG uptake in tumors is directly proportional to the metabolic activity of viable tumor cells, which have an increased demand for glucose (Kostakoglu et al. 2003). Quantitative data can be obtained from FDG PET images using the standardized uptake value (SUV) that provides a comparative means to evaluate multiple areas of FDG uptake. Standardized uptake values can be measured by identifying the area of greatest FDG accumulation in the suspected lesion. The mean SUV is then calculated by dividing the activity of the tracer (Ci/mL) in the region of interest divided by the injected dose of tracer (Ci) by patient weight (g) (Chang et al. 2006; Kostakoglu et al. 2003). Body weight and radioactive decay, among other issues, must also be taken into account as they impact SUV interpretations (Kostakoglu et al. 2003). SUV_{max}, obtained by measuring the maximum rather than mean activity in the region of interest, has been shown to allow for the best comparison between studies because of high reproducibility and low inter-observer variability (Benz et al. 2008b).

Imaging of Benign Peripheral Nerve Sheath Tumors

Schwannomas

Schwannomas are benign tumors originating from the nerve sheath that are slow-growing, well-encapsulated, usually solitary, and have little to no potential for malignant transformation. Schwannomas are a distinctive lesion in Neurofibromatosis Type 2 (NF-2), but can also be associated with other genetic syndromes such as Carney complex and schwannomatosis (Ferner 2010; Landry et al. 2009; Lu-Emerson and Plotkin 2009). The imaging of schwannomas is most accurately performed with MRI, although these lesions can also be seen using ultrasound or CT. On MRI, schwannomas usually appear as well-defined rounded or oval lesions distributed along the course of a peripheral nerve and are of low to intermediate signal intensity on T1-weighed images and high signal intensity on proton density, T2-weighted images (MacCollin et al. 2005). Attempts at characterizing schwannomas with FDG-PET have been largely unsuccessful; schwannomas show highly variable SUV_{max} measurements, which do not correspond to increased tumor size, apoptotic rate, Ki-67 proliferation index, or expression of markers of glucose utilization (glucose-transport protein 1 and hexokinase II) (Beaulieu et al. 2004; Benz et al. 2010a; Benz et al. 2010b; Steinhart et al. 2003). Studies using FDG-PET imaging of schwannomas report SUV_{max} ranges from 1.9 to 7.2, and 2.3 to 8.3, and one case report measured a standardized uptake value of 12 in a thoracic paravertebral schwannoma (Beaulieu et al. 2004; Benz et al. 2010a; Benz et al. 2010b; Shah et al. 2000). Interestingly, schwannomas exhibit a significantly higher SUV_{max} than

neurofibromas (mean: 4.2 ± 1.9 versus 2.3 ± 0.7 g/mL respectively) (Benz et al. 2010b). The cause for this variability remains unknown and further research is needed to delineate the root of this differential glucose utilization in schwannomas. Given this wide variance in measured SUV_{max}, differentiating schwannomas from MPNSTs using metabolic glucose uptake is less reliable (Benz et al. 2010b).

Neurofibromas

Neurofibromas are composed of axons, Schwann cells, perineural cells, mast cells, fibroblasts, and collagen fibrils (Korf 1999). These tumors can be localized to cutaneous, subcutaneous, spinal nerve root, or plexiform lesions (Ferner 2010). Both plexiform and subcutaneous neurofibromas appear to have the potential for malignant degeneration, although MPNSTs most commonly arise from the plexiform variety of neurofibroma and require frequent monitoring with imaging (Ferner 2010).

Occasionally neurofibromas may grow rapidly within a short period of time, causing significant morbidity and increasing the suspicion for malignant degeneration, and other lesions may undergo a period of quiescence or may even spontaneously regress. Patients with neurofibromas commonly undergo MRI imaging to evaluate change in growth prior to enrollment in a clinical trial or as a means to clinically monitor rapid growth. Classic imaging with MRI reveals a target appearance on MRI with a hypointense central portion on both T1- and T2-weighted images, in contrast to schwannomas which area relatively homogenous in appearance (MacCollin et al. 2005). Metabolic imaging of these benign lesions could provide a noninvasive means of predicting which lesions will require therapy and which can be monitored conservatively.

Using FDG-PET imaging, Fisher et al. (2008) found that a SUV_{max} greater than 2 in benign lesions accurately predicted which tumors would undergo significant growth over a 1 year period of time. In that study, lesions with an SUV_{max} greater than 2 underwent a 27% increase in volume over 1 year compared to a 4% growth in volume for lesions with an SUV_{max} less than two (Fisher et al. 2008). Fisher and colleagues predict that FDG-PET imaging may facilitate more timely intervention before benign peripheral nerve sheath tumor growth causes significant impairment. Furthermore, FDG-PET imaging may provide valuable information to assess benign peripheral nerve sheath tumor response to therapeutic intervention, as tumor growth may arrest spontaneously (Fisher et al. 2008).

Imaging of Malignant Peripheral Nerve Sheath Tumors

MPNSTs share many characteristics with other malignant soft tissue sarcomas, including rapid growth and high metastatic potential. As MPNSTs are a particularly aggressive histologic subtype of soft tissue sarcoma, early diagnosis is imperative. A noninvasive means of identifying suspicious lesions has many clinical benefits, especially as MPNSTs are often heterogeneous lesions that are frequently not amenable to biopsy. MPNST is one of the leading causes of mortality in NF-1 patients, and metastasize in 39% of cases, most commonly to lung (Ducatman et al. 1986; Rasmussen et al. 2001). Sporadic cases of plexiform neurofibromas (not associated with NF-1) have a 3 to 5% risk of malignant transformation, and patients with NF-1 have a reported 10–20% risk of MPNST development, and therefore all require frequent monitoring (Ducatman et al. 1986; Evans et al. 2002; Tucker et al. 2005). Historically, the standard in imaging of MPNSTs has been MRI, which provides insight into local extent of disease, growth, and heterogeneity of the tumor without providing distinct information regarding the malignant nature of the tumor (Li et al. 2008). However, with the expanding knowledge of FDG-PET imaging and the glycolytic phenotyping of soft tissue tumor, imaging of the malignant transformation has become more accurate.

Differentiating Benign Peripheral Nerve Sheath Tumors from MPNSTs Using Quantitative FDG-PET Imaging

CT was the primary imaging modality to monitor tumor growth and size. MPNSTs are generally larger in size than benign peripheral nerve sheath tumors, but there is considerable overlap in size and CT cannot

consistently and correctly distinguish MPNSTs from benign peripheral nerve sheath tumors (Benz et al. 2010). MRI, with its fine detail and ability to delineate infiltrative margins and tumor heterogeneity, has given clinicians a window into tumor progression. However, multiple studies have underscored the limitations of MRI as a modality to detect malignant transformation (Mautner et al. 2003).

Recently, forty peripheral nerve sheath tumors were evaluated for malignancy using FDG-PET imaging, with measured SUV_{max} comparisons providing a basis for judgment. Benz et al. (2010a) found that the mean SUV_{max} for MPNSTs was significantly higher than that for benign PNSTs (mean: 12.0 ± 7.1 versus 3.4 ± 1.8 g/mL; $P < 0.001$). Both MPNST lesions arising in patients with NF-1 and cases of sporadic MPNSTs had similar SUV_{max} measurements (Benz et al. 2010a). Using receiver operating characteristic curves to define optimum cutoff values for differentiation of malignancy, a SUV_{max} of 6.1 g/mL was identified as an optimum threshold for separating malignant from benign tumors (Benz et al. 2010a). This resulted in a sensitivity of 94% and specificity of 91% for detecting MPNSTs. Although there was some variability in SUV_{max} within each subgroup, the positive and negative predictive values for malignancy by FDG-PET were 89% and 95% respectively, and the diagnostic accuracy was 93% ($P < 0.001$) (Benz et al. 2010a). There is still considerable debate about the ideal SUV_{max} threshold with ranges from 1.8 to 6.1 g/mL, though recent data supports values higher than 3 (Benz et al. 2010a; Brenner et al. 2006; Cardona et al. 2003; Ferner et al. 2008; Warbey et al. 2009).

Further Clinical Application of FDG-PET Imaging in MPNSTS

Prognosis

FDG-PET can potentially be useful in predicting prognosis. Eary et al. (2002) previously revealed that SUV is an independent and significant predictor of survival in 209 patients with different types of sarcoma. Brenner et al. (2006) observed marked variability in NF-1-related MPNST metastatic potential and survival. Using FDG-PET imaging, Brenner and colleagues discovered that tumor SUV of greater than 3 g/mL reliably identified patients at high risk for metastases with a limited life expectancy and an SUV of less than 3 g/mL indicated low-risk patients in whom a more favorable outcome was likely. In this study, SUV predicted long-term survival with an accuracy of 94%, compared with 69% predictive value for tumor grade (Brenner et al. 2006).

Biopsy Guidance

Currently, the diagnosis of MPNST is made pathologically from an excised specimen. MPNSTs are often heterogeneous, with areas of necrosis, fibrosis, and benign tissue adjacent to the tumor. Biopsy of these lesions can give erroneous results that either under or overestimate the clinical impact of the peripheral nerve sheath tumor. FDG-PET paired with CT images can give accurate stereotactic information about areas with increased likelihood of harboring MPNST. By coupling lesions with high SUV_{max} with CT-obtained anatomical coordinates, an appropriate target tissue for biopsy can be identified.

Response to Treatment

Change in tumor size does not necessarily correlate with clinical response to therapy in soft tissue sarcomas (Miki et al. 2010). MPNSTs are heterogeneous tumors, and CT and MRI cannot reliably distinguish tumor necrosis or shrinkage as part of the tumor growth pattern or as a result of therapy (Benz et al. 2008a). FDG-PET imaging can give clinicians a window into the metabolic response of a MPNST to radiotherapy and/or chemotherapy. There have been multiple reports of FDG-PET accurately characterizing response to treatment in high grade soft tissue sarcomas and many other malignancies (Benz et al. 2008a; Benz et al. 2009; Chander et al. 2004; Evilevitch et al. 2008). Benz et al. (2008a) evaluated 20 patients with high-grade sarcomas who underwent chemotherapy or chemotherapy plus external beam radiation and determined that changes in FDG-PET accurately predicted response to treatment. In that study, the SUV_{max} decreased from a baseline value of 11.22± 8.23 to

4.58 ± 3.34 post treatment (Benz et al. 2008a). Percent change of SUV_{max} was significantly more pronounced in histopathologic responders (defined as <5% viable tumor cells on pathologic analysis) than in nonresponders (Benz et al. 2008a). Later studies deduced that a threshold of 35% reduction in FDG uptake/SUV_{max} could accurately predict histopathologic response with sensitivity of 100% and specificity of 67% (Benz et al. 2009). Therefore, FDG-PET can provide clinicians with valuable information that assesses tumor treatment response and may guide cessation or continuation of therapy.

Surveillance

Local recurrence and metastases are common in MPNSTs and therefore diligent follow-up is required after therapy (Ducatman et al. 1986). If recurrent tumors are identified early then surgery can be attempted. It is therefore imperative to frequently monitor these patients for recurrent MPNST with serial imaging. CT and MRI are often useful for volumetric and growth analysis, however in areas previously treated with radiotherapy, these imaging modalities are insufficient at differentiating tumor recurrence from post-irradiation fibrosis. Metabolic sampling with FDG-PET may provide an accurate noninvasive means of monitoring for tumor recurrence. Further studies are needed to support the use of FDG-PET imaging for assessment of MPNST recurrence.

Future Directions

The correlation of glucose utilization with malignant transformation in peripheral nerve sheath tumors has been well-documented, however more research is needed to highlight influential pathways allowing for FDG-PET detection. Correlation between expression of glucose transporters and SUV_{max} values in lung and pancreatic cancers have been confirmed, however this area of research has not yet extended to MPNSTs. Evaluation of the causal determinants of FDG metabolic trapping would be useful in the evaluation of MPNSTs and could allow for more finite discrimination of sarcoma subtypes.

Conclusion

Differentiating MPNSTs from benign peripheral nerve sheath tumor is challenging and relies on a combination of clinical, radiographic, and pathologic data. FDG-PET is a functional imaging technique that permits the visualization and quantification of glucose metabolism in peripheral nerve sheath tumors and is proving to be an important non-invasive imaging modality for tumor detection, malignant characterization, staging, treatment monitoring and surveillance.

References

Beaulieu S, Rubin B, Djang D, Conrad E, Turcotte E, Eary JF (2004) Positron emission tomography of schwannomas: emphasizing its potential in preoperative planning. Am J Roentgenol 182(4):971–974

Benz MR, Allen-Auerbach MS, Eilber FC, Chen HJ, Dry S, Phelps ME, Czernin J, Weber WA (2008a) Combined assessment of metabolic and volumetric changes for assessment of tumor response in patients with soft-tissue sarcomas. J Nucl Med 49(10):1579–1584

Benz MR, Czernin J, Allen-Auerbach MS, Tap WD, Dry SM, Elashoff D, Chow K, Evilevitch V, Eckardt JJ, Phelps ME, Weber WA, Eilber FC (2009) FDG-PET/CT imaging predicts histopathologic treatment responses after the initial cycle of neoadjuvant chemotherapy in high-grade soft-tissue sarcomas. Clin Cancer Res 15(8):2856–2863

Benz MR, Czernin J, Dry SM, Tap WD, Allen-Auerbach MS, Elashoff D, Phelps ME, Weber WA, Eilber FC (2010a) Quantitative F18-fluorodeoxyglucose positron emission tomography accurately characterizes peripheral nerve sheath tumors as malignant or benign. Cancer 116(2): 451–458

Benz MR, Dry SM, Eilber FC, Allen-Auerbach MS, Tap WD, Elashoff D, Phelps ME, Czernin J (2010b) Correlation between glycolytic phenotype and tumor grade in soft-tissue sarcomas by 18F-FDG PET. J Nucl Med 51(8):1174–1181

Benz MR, Evilevitch V, Allen-Auerbach MS, Eilber FC, Phelps ME, Czernin J, Weber WA (2008b) Treatment monitoring by 18F-FDG PET/CT in patients with sarcomas: interobserver variability of quantitative parameters in treatment-induced changes in histopathologically responding and nonresponding tumors. J Nucl Med 49(7):1038–1046

Brenner W, Friedrich RE, Gawad KA, Hagel C, von Deimling A, de Wit M, Buchert R, Clausen M, Mautner VF (2006) Prognostic relevance of FDG PET in patients with neurofibromatosis type-1 and malignant peripheral nerve sheath tumours. Eur J Nucl Med Mol Imaging 33(4):428–432

Cardona S, Schwarzbach M, Hinz U, Dimitrakopoulou-Strauss A, Attigah N, Mechtersheimer section sign G, Lehnert T (2003) Evaluation of F18-deoxyglucose positron emission tomography (FDG-PET) to assess the nature of neurogenic tumours. Eur J Surg Oncol 29(6):536–541

Chander S, Westphal SM, Zak IT, Bloom DA, Zingas AP, Joyrich RN, Littrup PJ, Taub JW, Getzen TM (2004) Retroperitoneal malignant peripheral nerve sheath tumor: evaluation with serial FDG-PET. Clin Nucl Med 29(7):415–418

Chang JM, Lee HJ, Goo JM, Lee HY, Lee JJ, Chung JK, Im JG (2006) False positive and false negative FDG-PET scans in various thoracic diseases. Korean J Radiol 7(1):57–69

Ducatman BS, Scheithauer BW, Piepgras DG, Reiman HM, Ilstrup DM (1986) Malignant peripheral nerve sheath tumors. A clinicopathologic study of 120 cases. Cancer 57(10): 2006–2021

Eary JF, O'Sullivan F, Powitan Y, Chandhury KR, Vernon C, Bruckner JD, Conrad EU (2002) Sarcoma tumor FDG uptake measured by PET and patient outcome: a retrospective analysis. Eur J Nucl Med Mol Imaging 29(9): 1149–1154

Evans DG, Baser ME, McGaughran J, Sharif S, Howard E, Moran A (2002) Malignant peripheral nerve sheath tumours in neurofibromatosis 1. J Med Genet 39(5):311–314

Evilevitch V, Weber WA, Tap WD, Allen-Auerbach M, Chow K, Nelson SD, Eilber FR, Eckardt JJ, Elashoff RM, Phelps ME, Czernin J, Eilber FC (2008) Reduction of glucose metabolic activity is more accurate than change in size at predicting histopathologic response to neoadjuvant therapy in high-grade soft-tissue sarcomas. Clin Cancer Res 14(3): 715–720

Ferner RE (2010) The neurofibromatoses. Pract Neurol 10(2):82–93

Ferner RE, Golding JF, Smith M, Calonje E, Jan W, Sanjayanathan V, O'Doherty M (2008) [18F]2-fluoro-2-deoxy-D-glucose positron emission tomography (FDG PET) as a diagnostic tool for neurofibromatosis 1 (NF1) associated malignant peripheral nerve sheath tumours (MPNSTs): a long-term clinical study. Ann Oncol 19(2):390–394

Ferner RE, Gutmann DH (2002) International consensus statement on malignant peripheral nerve sheath tumors in neurofibromatosis 1. Cancer Res 62(5):1573–1577

Fisher MJ, Basu S, Dombi E, Yu JQ, Widemann BC, Pollock AN, Cnaan A, Zhuang H, Phillips PC, Alavi A (2008) The role of [18F]-fluorodeoxyglucose positron emission tomography in predicting plexiform neurofibroma progression. J Neurooncol 87(2):165–171

Korf BR (1999) Plexiform neurofibromas. Am J Med Genet 89(1):31–37

Kostakoglu L, Agress H Jr, Goldsmith SJ (2003) Clinical role of FDG PET in evaluation of cancer patients. Radiographics 23(2):315–340

Landry CS, Waguespack SG, Perrier ND (2009) Surgical management of nonmultiple endocrine neoplasia endocrinopathies: state-of-the-art review. Surg Clin North Am 89(5):1069–1089

Li CS, Huang GS, Wu HD, Chen WT, Shih LS, Lii JM, Duh SJ, Chen RC, Tu HY, Chan WP (2008) Differentiation of soft tissue benign and malignant peripheral nerve sheath tumors with magnetic resonance imaging. Clin Imaging 32(2): 121–127

Lu-Emerson C, Plotkin SR (2009) The neurofibromatoses. Part 2: NF2 and schwannomatosis. Rev Neurol Dis 6(3):E81–86

MacCollin M, Chiocca EA, Evans DG, Friedman JM, Horvitz R, Jaramillo D, Lev M, Mautner VF, Niimura M, Plotkin SR, Sang CN, Stemmer-Rachamimov A, Roach ES (2005) Diagnostic criteria for schwannomatosis. Neurology 64(11):1838–1845

Mautner VF, Friedrich RE, von Deimling A, Hagel C, Korf B, Knöfel MT, Wenzel R, Fünsterer C (2003) Malignant peripheral nerve sheath tumours in neurofibromatosis type 1: MRI supports the diagnosis of malignant plexiform neurofibroma. Neuroradiology 45(9):618–625

Miki Y, Ngan S, Clark JC, Akiyama T, Choong PF (2010) The significance of size change of soft tissue sarcoma during preoperative radiotherapy. Eur J Surg Oncol 36(7):678–683

Rasmussen SA, Yang Q, Friedman JM (2001) Mortality in neurofibromatosis 1: an analysis using U.S. death certificates. Am J Hum Genet 68(5):1110–1118

Shah N, Sibtain A, Saunders MI, Townsend E, Wong WL (2000) High FDG uptake in a schwannoma: a PET study. J Comput Assist Tomogr 24(1):55–56

Steinhart H, Triebswetter F, Wolf S, Gress H, Bohlender J, Iro H (2003) Growth of sporadic vestibular schwannomas correlates with Ki-67 proliferation index. Laryngorhinootologie 82(5):318–321

Tucker T, Wolkenstein P, Revuz J, Zeller J, Friedman JM (2005) Association between benign and malignant peripheral nerve sheath tumors in NF1. Neurology 65(2):205–211

Warbey VS, Ferner RE, Dunn JT, Calonje E, O'Doherty MJ (2009) [18F]FDG PET/CT in the diagnosis of malignant peripheral nerve sheath tumours in neurofibromatosis type-1. Eur J Nucl Med Mol Imaging 36(5):751–757

Chapter 18

Tumor Resection Control Using Intraoperative Magnetic Resonance Imaging

Venelin M. Gerganov, Mario Giordano, Rudolf Fahlbusch, Madjid Samii, and Amir Samii

Abstract Intraoperative imaging is one of the major advancement in brain tumor surgery in the last years. The golden standard is intraoperative high-field magnetic resonance imaging. Different types of intraoperative scanner are currently utilized. A schematic classification can be based on the strength of the magnetic field: low field and high field scanner. Low field transportable intraoperative MRI (iMRI) systems can be used without structural operating room modifications. On the other hand, the field of view is restricted and there is no possibility to obtain spectroscopy and/or diffusion tensor imaging (DTI). High field systems are more expensive and require a dedicated operating theatre. On the other hand, they provide an optimal quality of the images with better identification of tumor remnants. The utility of this tool has been studied and verified in two main categories of tumors: gliomas and pituitary adenomas. In glioma surgery the iMRI is useful to estimate the extent of tumor removal, to evaluate the safety of further resection and to update the navigation dataset. Its application in pituitary adenoma surgery can improve the cure rate by indentifying small tumor remnants. The correct use of iMRI requires a standardized workflow. The main phases are: preparation with preoperative imaging, integration of the data with the navigation system, first imaging control after resection, update of the navigation to perform further tumor removal and final MRI control.

Keywords Gliomas · Pituitary adenomas · iMRI · Subcortical structures · Intracranial tumors · Tumor resection

Introduction

The optimal management of patients with brain gliomas remains controversial and challenging. Over the past decades, however, a growing amount of evidence suggests that the extent of resection correlates with patients' survival, especially in case of low grade gliomas (Keles et al. 2001; McGirt et al. 2008). Radical tumor removal has been shown to be associated with longer life expectancy for both low- and high grade gliomas (Claus et al. 2005; Sanai et al. 2008). The main limiting factors of complete removal are the location of the tumor in close proximity to highly eloquent cortical and subcortical structures and its poor demarcation from surrounding brain tissue were. The implementation of new technologies in the last decades strongly influenced the practice of neurosurgery, allowing performing safer and more radical surgeries. Various intraoperative imaging techniques, such as ultrasonography, computerized tomography and magnetic resonance imaging (MRI), have been introduced to provide an objective assessment of surgeons' activity (Hadani et al. 2001; Lunsford et al. 1984; Trobaugh et al. 1994). In particular, they enhance the surgeon's ability to detect residual tumor and its relationship to critical neurological structures.

Image-guided frameless navigation, using anatomical and functional datasets, allows the surgeon to perform targeted approaches to intracranial tumors thus

V.M. Gerganov (✉)
International Neuroscience Institute, Hannover, Germany
e-mail: vgerganov@gmail.com

M.A. Hayat (ed.), *Tumors of the Central Nervous System, Volume 4*,
DOI 10.1007/978-94-007-1706-0_18, © Springer Science+Business Media B.V. 2012

minimizing the operative morbidity (Barnett 1999; Kikinis et al. 1996). The navigation systems initially have been based on preoperatively acquired images, which was a major limitation: during the surgery, brain shift caused by loss of cerebrospinal fluid, head position, and tumor debulking can lead to significant decrease of system accuracy (Nabavi et al. 2001; Nimsky et al. 2000; Roberts et al. 1998). Intraoperative image acquisition allows for update of navigation data and reliable localization of residual tumor. MRI is the most advance intraoperative imaging modality that provides high quality anatomic and functional data required for safely planning and performing the surgery. The use intraoperative magnetic resonance imaging (iopMRI) was first introduced by the groups of Black (Black et al. 1997) and Fahlbusch (Steinmeier et al. 1998) in the 1990s.

Intraoperative Magnetic Resonance Imaging Setup

Several iopMRI concepts have been developed and are still used, regarding the operating room setup, type of scanner, strength of the magnetic field, and logistical organization.

Low Field iopMRI

The first low field system, used by Black et al. (1997), included two fixed vertically oriented magnets (0.5 T), the so-called "Double Doughnut". The head of the patient was positioned between the magnet and surgery was performed "in situ". This allowed performing image acquisition at any time without movement of the surgical table. On the other hand, this system caused space limitations for the surgeon and required MRI compatible instruments. Fahlbusch et al. (2001) and Steinmeier et al. (1998) developed the concept of an open magnet, initially with field strength of 0.2 T. The patient was positioned on a rotating table with the head at the limit of the 5-Gauss line, allowing the use of standard surgical instruments during the surgery. The table was moved in order to position the head into the centre of the magnet. In one study, this group assessed the reliability of this tool during pituitary adenoma surgery comparing the surgeon estimation of tumor removal with the image findings (7). The newly acquired information allowed performing additional removal in 27% of all cases, even if the surgeon assumed a complete resection before the control. On the other hand, in 30% there were difficulties in the interpretation of the images caused by artifacts, mainly due to metal debris from the diamond drill or blood in the resection cavity. Hadani et al. (2001) reported on their experience with the PoleStar N10 for the treatment of 20 patients with gliomas and pituitary adenomas. The system is composed by a compact ultra-low field system including a 0.12 T magnet with two vertically oriented poles with a 25 cm gap mounted on a transportable gantry that could be positioned under the surgical table when not in use for scanning allowing the employ of standard surgical instruments.

The second generation of this system, the PoleStar N20, is still used during surgeries of both pituitary adenomas (Gerlach et al. 2008) and gliomas (Schulder et al. 2006). It includes a 0.15 T magnet with a larger field of view, better images quality, and shorter of acquisition time. Gerlach et al. (2008) assessed that in the treatment of pituitary adenomas this system was reliable to demonstrate an adequate decompression of the optic system. On the other hand the visualization of small remnants in the sellar and parasellar space seemed to be more difficult due to the artifacts created by the skull base. The impact of this device utilization for resection control in glioma surgery has been demonstrated to be similar to that of its predecessor N10 (Schulder et al. 2006).

One advantage of these low field transportable iopMRI systems is the possibility to use them without structural operating room modifications. On the other hand the field of view, which they provide, is restricted; this can be a limiting factor in the removal of large lesions and can reduce the accuracy of the navigation system due to the increased spatial distortion at the periphery (Kanner et al. 2002). Another important limit of this system is the absence of imaging sequences for spectroscopy and diffusion tensor imaging (DTI) helpful for the update of functional data.

High Field iopMRI

The early results obtained using low field iopMRI for resection of intracranial lesions led in recent years to further elaboration of this technology. The introduction of high field magnets has been an important advancement. The use of 1.5 T magnets led to a remarkable improvement of image quality with an improved signal-to-noise ratio. The image quality is comparable to preoperative diagnostic imaging in terms of tumor extension, extent of resection, and anatomical changes during the surgery (Truwit and Hall 2006). Another important advantage of high field scanners is the possibility to provide, besides the standard anatomical sequences, other imaging modalities, such as diffusion tensor imaging and spectroscopy. These techniques play a major role in the surgery of gliomas allowing the reconstruction of fiber tracts and the identification of metabolites in peritumoral area perioperatively.

Nimsky et al. (2004) in a study on 47 patients operated for high- and low-grade glioma using a 1.5 T scanner found that 41.2% of the complete resected tumors were attributable to further tumor removal after MRI control. The use of 1.5 T iopMRI was validated also for pituitary adenomas: the rate of complete removal can be increased, after the identification of tumor remnants, from 58 to 82% (Nimsky et al. 2006). Moreover, in comparison with the low field systems, it allows a better identification of tumor extension in the sellar space and cavernous sinus.

Only few recent reports have been published about 3 T magnets for intraoperative use (Jankovski et al. 2008; Pamir et al. 2010; Truwit and Hall 2006). An interesting approach to reduce the costs for these expensive facilities is their use as shared resources: the scanner can be installed in a shielded room adjacent and interconnected to the operating theatre. This allows employing the system for outpatient diagnostic sessions when it is not required for intraoperative control. The introduction of 3 T scanners obviously further increases the spatial resolution of the imaging. It offers further a significant improvement in detection of metabolites during spectroscopy (Pamir et al. 2010). On the other hand, the increased magnetic field strength can also led to a stronger susceptibility to artifacts. Further clinical studies are needed to demonstrate if the use of 3 T magnets can give benefits comparable to the ones achieved with the change from 0.5 to 1.5 T.

Indication for iopMRI

The use of iopMRI can be theoretically extended to the surgery of any intracranial and spinal lesions. The utility of this tool, however, has been studied and verified in two main categories of tumors: gliomas and pituitary adenomas.

Glioma Surgery

The currently most widely accepted goal of glioma surgery is to perform a radical removal without new postoperative neurological deficits. iopMRI plays a major role to achieve the best surgical result minimizing the risk of postoperative morbidity. The first objective is of course the evaluation of the extent of surgical resection: due to the infiltrative nature and variable appearance of gliomas, it might be difficult to differentiate the lesion from normal brain tissue. The second objective, achieved with the introduction of high-field magnets, is to evaluate the safety of further surgical removal by updating the fiber tracking and spectroscopic data. Finally, the imaging performed during the operation is used to update the frameless navigation system in order to compensate the effect of brain shift.

Pituitary Adenoma Surgery

Successful removal of hormonally active pituitary adenomas is evaluated with postoperative endocrinological studies. In contrast, there is no marker to assess the grade of resection of non-secreting adenomas (Nimsky et al. 2006). Postoperative MRI controls, performed before the second postoperative month are difficult to interpret due to postoperative artifacts and therefore are unreliable (Dina et al. 1993). One of the principal indications fore the use of iopMRI is surgery of pituitary tumors (Fahlbusch et al. 2001). It has been

shown to improve the cure rate by recognizing the presence and the location of tumor remnants, thus allowing further resection (Nimsky et al. 2006). In this regard, the high-field setup is an important advancement: even small remnants – of 3–4 mm size (Nimsky et al. 2006) – can be detected in the intra- and parasellar areas, which was impossible with the low-field scanners (Gerlach et al. 2008).

Other Indications

Besides surgery of gliomas and pituitary tumors, the iopMRI has been applied in a wide spectrum of procedures. The removal of other space occupying lesions such as craniopharyngiomas, Rathke cleft cysts and meningiomas have benefited from its application (Nimsky et al. 2005). It allows further reliable evaluation of the extent of resection in epilepsy surgery during the operative procedure. Its role in correcting an initially incomplete resection, particularly in lesional cases, has been demonstrated (Buchfelder et al. 2000, 2002). Surgery of vascular lesions, including arteriovenous malformations, cavernomas and aneurysms clipping, has also been successfully performed under iopMRI control (Levy et al. 2009; Sutherland et al. 2002). Drainage of brain abscesses, puncture and aspiration of cystic intracranial lesions, and management of hydrocephalus have been carried out with iopMRI control to obtain immediate feedback control (Kollias and Bernays 2001). The iopMRI has been also used to evaluate the adequacy of resection in patients undergoing transoral resection of C-2 lesions causing craniocervical junction compression (Kaibara and Bernays 2001).

Workflow

In order to understand the practical application of a modern iopMRI, it is important to clarify all the steps of the image acquisition procedure. We will describe the procedures, as used in one of the currently most sophisticated setups, which integrates all surgical and diagnostic tools.

Operating Area Setup

The operating room is radiofrequency shielded and equipped with a high-field open-bore 1.5-T MR imager. The scanner has an integrated rotating table that permits a variable position angle between the magnet and the patient with the head placed always at the level of the 5-Gauss. This distance permits the use of normal surgical instruments without risk to be influenced by the magnetic field. The MRI unit is integrated with a neuronavigation system. The surgical microscope is fixed on the ceiling outside the 5-Gauss line. The MRI-compatible respirator and anesthesia monitoring system are placed outside the 200-Gauss line. A computer control-room is separated by glass wall from the radiofrequency-shielded operating theatre. This room is used to setup the scanner sequences, visualize the intraoperative images and plan the surgery with the frameless navigation system.

Preoperative Steps

After anaesthesia induction, the patient is positioned; the head is fixed in a special designed headrest-coil unit with five pins. Three pins are placed laterally (two on one side and one on the opposite) and 2 – inferiorly. Care is taken to position the head according to the specific surgical strategy, although the particular design and less adjustability of the headrest, compared with to the classical 3-point head fixation devices, can cause difficulties. The second half of the headrest coil is then placed above the head: it contains the fiducial markers for automatic registration of the frameless navigation systems. In case of a transsphenoidal surgery is to be preformed without navigational guidance, the head fixation is not required: a flexible coil adapted around the head is sufficient.

The preoperative imaging includes a three-dimensional data set with the following sequences: T1-weighted magnetization prepared rapid acquisition gradient echo (MPRAGE) slice thickness 1 mm, field of view 320 mm^2, echo time (TE) 3.5 ms, repetition time (TR) 2150 ms; T2-weighted thickness 1 mm, field of view 320 mm^2, TE: 505 ms, TR: 3200 ms;

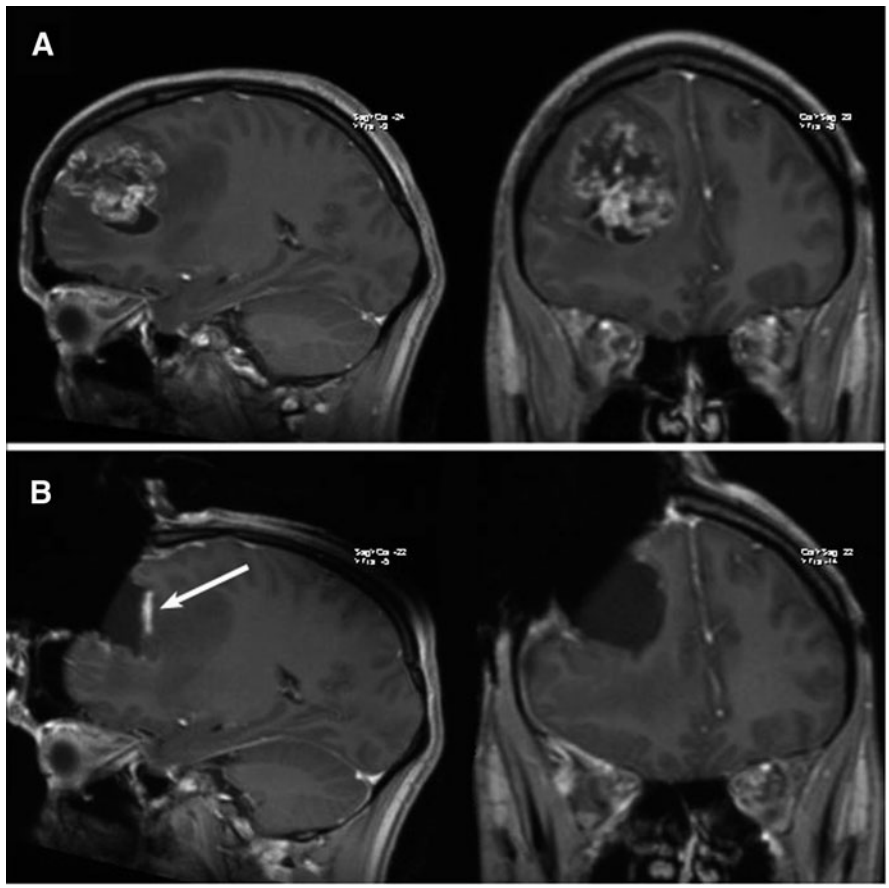

Fig. 18.1 (**a**) Preoperative sagittal and coronal T1-weighted MRI with contrast enhancement of a patient harbouring a right frontal glioblastoma. (**b**) First intraoperative MRI control showing the total removal of the lesion. In this case the surgery was finished without further imaging. The sagittal image shows a linear hyperintensity on the dorsal side of the resection cavity due to a small blood collection (*white arrow*)

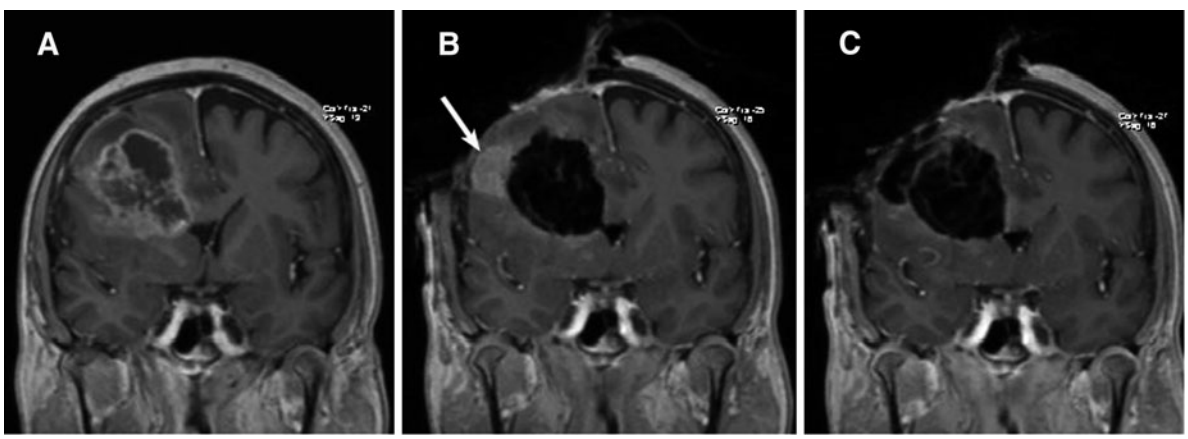

Fig. 18.2 (**a**) Preoperative coronal T1-weighted MRI with contrast enhancement of a patient harbouring a right frontoparietal glioblastoma. (**b**) First intraoperative control showing a contrast-enhancing tumor remnant adjacent to the resection cavity (*white arrow*). In this case further resection was achieved. (**c**) Final intraoperative imaging showing the total resection of the lesion

DTI slice thickness 3 mm, field of view 320 mm^2, TE: 107 ms, TR: 3000 ms. For contrast enhancing lesions, intravenous gadopentate dimeglumine (0.2 mL/kg) is administered before scanning. Fluid-attenuated inversion recovery (FLAIR) and/or echo planar imaging dark fluid sequences can be obtained whenever deemed necessary.

The imaging data are then transferred to the navigation workstation and integrated with the functional data (fMRI) obtained one day before the surgery. The planning is performed, considering the specific for the lesion and the operation, information. It includes tumor segmentation, functional area depiction (motor and/or speech areas), fiber tracking (pyramidal tract, visual tract, arcuate fasciculus, and/or fornix).

The preoperative plan is then transferred to the navigation system and automatic registration is done before removing the upper part of the headrest-coil.

For transsphenoidal surgery navigation is rarely used and preoperative imaging is performed using T1-weighted spin echo coronal and sagittal spin echo sequences (slice thickness: 3 mm; FOV: 230 mm; TR: 500 ms; TE: 9.5 ms) and T2-weighted turbo-spin echo sequences (slice thickness: 3 mm; FOV: 230 mm; TR: 4570 ms; TE: 120 ms). An MRI compatible nasal speculum is used during surgery.

Intraoperative Imaging and Evaluation of Tumor Resection

The surgeon decides when to perform the first MRI control, based on intraoperative findings and progress of the surgery. Image acquisition is carried out to: verify of an expected complete resection, verify an expected partial resection with residual tumor in high-eloquent brain area or involving important fiber tracts, or to update the dataset for the frameless navigation system.

Prior to image acquisition, the resection area is filled with water or absorbable haemostatic gelatin sponge. The oxidize cellulose as haemostatic agent is avoided to prevent image artifacts. The upper part of the headrest-coil is positioned in a sterile fashion and the patient is covered with sterile draping before rotating the table in the scanning position.

The same MRI sequences as preoperatively are performed and the surgical team evaluates the images. If a complete resection is confirmed, the surgery can be finished without further MRI controls. In case a remnant is seen, the images are transferred to the navigation workstation and the region of interest is segmented. After reconstruction of the white matter fibers and fusion with the functional data, the surgical team decides if it is safe to perform further tumor resection or the risk of injury to eloquent structures is too high (surgical goal achieved). If the resection is continued, further MRI controls are performed until the goal has been reached (Figs. 18.1 and 18.2). Similar imaging protocol is used in transsphenoidal surgeries.

Conclusion

MRI is the most advanced and reliable tool for intraoperative control of tumor resection currently available. Besides increasing the safety of surgery, it allows for more radical resections, which – as shown by recent studies – have a definitive survival benefit for the patients.

References

Barnett GH (1999) The role of image-guided technology in the surgical planning and resection of gliomas. J Neurooncol 42:247–258

Black PM, Moriarty T, Alexander E 3rd, Stieg P, Woodard EJ, Gleason PL, Martin CH, Kikinis R, Schwartz RB, Jolesz FA (1997) Development and implementation of intraoperative magnetic resonance imaging and its neurosurgical applications. Neurosurgery 41:831–842; discussion 842–835

Buchfelder M, Fahlbusch R, Ganslandt O, Stefan H, Nimsky C (2002) Use of intraoperative magnetic resonance imaging in tailored temporal lobe surgeries for epilepsy. Epilepsia 43:864–873

Buchfelder M, Ganslandt O, Fahlbusch R, Nimsky C (2000) Intraoperative magnetic resonance imaging in epilepsy surgery. J Magn Reson Imaging 12:547–555

Claus EB, Horlacher A, Hsu L, Schwartz RB, Dello-Iacono D, Talos F, Jolesz FA, Black PM (2005) Survival rates in patients with low-grade glioma after intraoperative magnetic resonance image guidance. Cancer 103:1227–1233

Dina TS, Feaster SH, Laws ER, Jr, Davis DO (1993) MR of the pituitary gland postsurgery: serial MR studies following transsphenoidal resection. AJNR Am J Neuroradiol 14:763–769

Fahlbusch R, Ganslandt O, Buchfelder M, Schott W, Nimsky C (2001) Intraoperative magnetic resonance imaging during transsphenoidal surgery. J Neurosurg 95:381–390

Gerlach R, du Mesnil de Rochemont R, Gasser T, Marquardt G, Reusch J, Imoehl L, Seifert V (2008) Feasibility of Polestar N20, an ultra-low-field intraoperative magnetic resonance imaging system in resection control of pituitary macroadenomas: lessons learned from the first 40 cases. Neurosurgery 63:272–284; discussion 284–275

Hadani M, Spiegelman R, Feldman Z, Berkenstadt H, Ram Z (2001) Novel, compact, intraoperative magnetic resonance imaging-guided system for conventional neurosurgical operating rooms. Neurosurgery 48:799–807; discussion 807–799

Jankovski A, Francotte F, Vaz G, Fomekong E, Duprez T, Van Boven M, Docquier MA, Hermoye L, Cosnard G, Raftopoulos C (2008) Intraoperative magnetic resonance imaging at 3-T using a dual independent operating room-magnetic resonance imaging suite: development, feasibility, safety, preliminary experience. Neurosurgery 63:412–424; discussion 424–416

Kaibara T, Hurlbert RJ, Sutherland GR (2001) Transoral resection of axial lesions augmented by intraoperative magnetic resonance imaging. Report of three cases. J Neurosurg 95:239–242

Kanner AA, Vogelbaum MA, Mayberg MR, Weisenberger JP, Barnett GH (2002) Intracranial navigation by using low-field intraoperative magnetic resonance imaging: preliminary experience. J Neurosurg 97: 1115–1124

Keles GE, Lamborn KR, Berger MS (2001) Low-grade hemispheric gliomas in adults: a critical review of extent of resection as a factor influencing outcome. J Neurosurg 95:735–745

Kikinis R, Gleason PL, Moriarty TM, Moore MR, Alexander E 3rd, Stieg PE, Matsumae M, Lorensen WE, Cline HE, Black PM, Jolesz FA (1996) Computer-assisted interactive three-dimensional planning for neurosurgical procedures. Neurosurgery 38:640–649; discussion 649–651

Kollias SS, Bernays RL (2001) Interactive magnetic resonance imaging-guided management of intracranial cystic lesions by using an open magnetic resonance imaging system. J Neurosurg 95:15–23

Levy R, Cox RG, Hader WJ, Myles T, Sutherland GR, Hamilton MG (2009) Application of intraoperative high-field magnetic resonance imaging in pediatric neurosurgery. J Neurosurg Pediatr 4:467–474

Lunsford LD, Parrish R, Albright L (1984) Intraoperative imaging with a therapeutic computed tomographic scanner. Neurosurgery 15:559–561

McGirt MJ, Chaichana KL, Attenello FJ, Weingart JD, Than K, Burger PC, Olivi A, Brem H, Quinones-Hinojosa A (2008) Extent of surgical resection is independently associated with survival in patients with hemispheric infiltrating low-grade gliomas. Neurosurgery 63:700–707; author reply 707–708

Nabavi A, Black PM, Gering DT, Westin CF, Mehta V, Pergolizzi RS Jr, Ferrant M, Warfield SK, Hata N, Schwartz RB, Wells WM, 3rd, Kikinis R, Jolesz FA (2001) Serial intraoperative magnetic resonance imaging of brain shift. Neurosurgery 48:787–797; discussion 797–788

Nimsky C, Fujita A, Ganslandt O, Von Keller B, Fahlbusch R (2004) Volumetric assessment of glioma removal by intraoperative high-field magnetic resonance imaging. Neurosurgery 55:358–370; discussion 370–351

Nimsky C, Ganslandt O, Cerny S, Hastreiter P, Greiner G, Fahlbusch R (2000) Quantification of, visualization of, compensation for brain shift using intraoperative magnetic resonance imaging. Neurosurgery 47:1070–1079; discussion 1079–1080

Nimsky C, Ganslandt O, Fahlbusch R (2005) 1.5 T: intraoperative imaging beyond standard anatomic imaging. Neurosurg Clin N Am 16:185–200, vii

Nimsky C, von Keller B, Ganslandt O, Fahlbusch R (2006) Intraoperative high-field magnetic resonance imaging in transsphenoidal surgery of hormonally inactive pituitary macroadenomas. Neurosurgery 59:105–114; discussion 105–114

Pamir MN, Ozduman K, Dincer A, Yildiz E, Peker S, Ozek M M (2010) First intraoperative, shared-resource, ultrahigh-field 3-Tesla magnetic resonance imaging system and its application in low-grade glioma resection. J Neurosurg 112:57–69

Roberts DW, Hartov A, Kennedy FE, Miga MI, Paulsen KD (1998) Intraoperative brain shift and deformation: a quantitative analysis of cortical displacement in 28 cases. Neurosurgery 43:749–758; discussion 758–760

Sanai N, Berger MS (2008) Glioma extent of resection and its impact on patient outcome. Neurosurgery 62:753–764; discussion 264–756

Schulder M, Salas S, Brimacombe M, Fine P, Catrambone J, Maniker AH, Carmel PW (2006) Cranial surgery with an expanded compact intraoperative magnetic resonance imager. Technical note. J Neurosurg 104:611–617

Steinmeier R, Fahlbusch R, Ganslandt O, Nimsky C, Buchfelder M, Kaus M, Heigl T, Lenz G, Kuth R, Huk W (1998) Intraoperative magnetic resonance imaging with the magnetom open scanner: concepts, neurosurgical indications, and procedures: a preliminary report. Neurosurgery 43:739–747; discussion 747–738

Sutherland GR, Kaibara T, Wallace C, Tomanek B, Richter M (2002) Intraoperative assessment of aneurysm clipping using magnetic resonance angiography and diffusion-weighted imaging: technical case report. Neurosurgery 50:893–897; discussion 897–898

Trobaugh JW, Richard WD, Smith KR, Bucholz RD (1994) Frameless stereotactic ultrasonography: method and applications. Comput Med Imaging Graph 18:235–246

Truwit CL, Hall WA (2006) Intraoperative magnetic resonance imaging-guided neurosurgery at 3-T. Neurosurgery 58:ONS-338–345; discussion ONS-345–336

Chapter 19

Brain Tumors: Clinical Applications of Functional Magnetic Resonance Imaging and Diffusion Tensor Imaging

Raimund Kleiser, Janpeter Nickel, Rüdiger J. Seitz, Johannes Trenkler, and Gabriele Wurm

Abstract One of the most exciting methodologies in the clinical neurosciences evolving toward the end of the twentieth century was functional magnetic resonance imaging (fMRI). Whereas MRI is used to produce structural images of subjects' brain the functional component allows an in vivo measurement of brain activity. fMRI has provided new insights into human cognitive functions. Till now it was mainly used for basic scientific questions and has provided foundations for at least five large-scale neurocognitive networks identified in the human brain, namely for spatial attention, language, memory-emotion, executive function, and face and object recognition. In addition, white matter tractography based on diffusion tensor imaging (DTI) has become a well-accepted noninvasive tool for exploring the white matter architecture of the human brain in vivo. These two MR techniques are complementary in describing functional and anatomical components of grey and white matters. Furthermore, fMRI is useful to define the seed regions for DTI, because large interindividual anatomical variations make it difficult to define tracking seed areas based reliably on macroanatomical landmarks. An accurate definition of seed regions for the reconstruction of a specific neuronal pathway becomes even more challenging in patients suffering from space occupying brain lesions due to the displacement of the tissue and the distortion of anatomical landmarks around the lesion. Therefore, fMRI and DTI play a growing role in clinical neuroimaging with increasing applications in neurosurgical planning using neuronavigation. By means of neuronavigational devices both modalities can intuitively be used during surgical procedures. The goal of tumor surgery is to optimize the extent of resection, while minimizing the risk of a permanent neurological deficit. Because the tumor may infiltrate eloquent areas and because of major intersubject anatomical and functional variability, cortical functional organization, subcortical connectivity and brain plasticity can be studied at an individual scale. Presurgical functional neuroimaging and tractography can show the relationships between eloquent regions and the tumor, and consequently the cortical and subcortical structures essential for brain functions can be identified and preserved. In addition, post-operative control and longitudinal neuroimaging studies are important to study adaptive changes in network behaviour and to monitor the effects of brain plasticity.

Keywords fMRI · Diffusion tensor imaging · Neuronavigation · Brain functions · Tumor growth · Brain tissue

Introduction

Patients with brain tumors present a complex clinical situation. This is due to the fact that brain tumors induce structural changes of the brain which are local owing to tumor growth and more widespread related to mass effects. However, the human brain readily adapts functionally to pathological changes of the nervous system. In fact, it was shown by functional imaging

R. Kleiser (✉)
Institute of Radiology, Landes-Nervenklinik Wagner-Jauregg, 4020 Linz, Austria
e-mail: raimund.kleiser@gespag.at

M.A. Hayat (ed.), *Tumors of the Central Nervous System, Volume 4*,
DOI 10.1007/978-94-007-1706-0_19,

that motor representations may occur in abnormal locations due to plastic reorganization of the brain tissue adjacent to the brain tumor (Krings et al. 2002; Seitz et al. 1995; Wunderlich et al. 1998). These plastic changes do not occur only in cerebral mass lesions but are found also in vascular brain diseases such as stroke and are thought to be related to changes of excitability of the cerebral cortex (Butefisch et al. 2006).

This plastic capacity of the human brain is most pronounced in congenital space occupying lesions and may result in a remapping of function into the non-affected contralesional hemisphere (Nickel et al. 2007). Consequently, it typically takes weeks to many months until a brain tumor becomes clinically apparent by neurological deficits. More frequently, brain tumors are discovered by computed tomography (CT) or MRI when a patient presents because of a first epileptic seizure. In this situation the burning question is how the patient can be treated optimally. This clinical challenge then is to identify the location of the tumor, establish its pathological entity (histological diagnosis), and to plan the optimal therapeutic strategy.

Typically, neurosurgical resection of the tumor is the backbone of treatment. However, any neurosurgical procedure has to take in account the targeted benefit of the tumor resection against the potential risk of neurological deficits resulting from surgical brain damage. Thus, neurosurgery is complex and delicate. It is probably the type of surgery most feared by patients, because the brain is our body's most personally relevant organ. That is the reason that technical and methodological innovations are increasing the safety of neurosurgical procedures such as functional imaging and neuronavigation-guided surgery; and that is why they are very important.

In the first paragraph we describe the technology of neuronavigation because the integration of different imaging techniques such as fMRI, DTI, single photon emission tomography (SPECT), and positron emission tomography (PET) provide an optimized work flow and application for neurosurgery based on the neuronavigation system. The term neuronavigation is used to describe a set of computer-assisted technologies used by neurosurgeons to guide or to "navigate" within the three-dimensional confines of the skull or the vertebral structures during neurosurgical operations. The term neuronavigation, thus, is synonymous with image-guided surgery, computer-assisted or computer-aided surgery, or interactive image-guided neurosurgery. After a methodological description of fMRI, DTI, and PET we focus on the combination of these complimentary and essential modalities.

Results of the benefits of neuronavigation especially by integration of fMRI and DTI will be highlighted and exemplarily described in single case studies. Furthermore, in two longitudinal neuroimaging studies we demonstrate the characteristics of the network activity pre- and post-surgery and how to monitor the effects of brain plasticity. Finally, the integration of fMRI and DTI for clinical application is discussed in comparison to the "gold standard" of cortical stimulation mapping.

Methodology

Navigational Guided Neurosurgery

Neuronavigation was developed within the last 15 years in order to improve the safety of brain surgery and to improve functional outcome of the patients' suffering from different kinds of intracranial lesions. Neuronavigation is recognized as the next evolutionary step of stereotactic surgery, a set of techniques that date back to the early 1900s and that gained popularity during the 1940s. In its infancy, the purpose of stereotactic and neuronavigationally guided technologies was to create a mathematical model describing a coordinate system for the space within the closed structure of the skull. The history of neuronavigation, thus, is quite short, but full of highly promising achievements. The advent of neuronavigation, however, would have been impossible without the development of modern imaging technology, electronics, and space technology.

The examinations done by highly sophisticated neuroimaging technologies are related to the actual patient's brain during surgery. Computer-graphic modelling and accelerated manipulation of data through complex mathematical algorithms with recent computer technologies facilitate the real-time quantitative spatial depiction of images of a patient's brain creating an individual "fiducial coordinate system". This fiducial spatial system uses fiduciary or natural landmarks as a reference to describe with high accuracy the position of specific structures within a defined space. The entire neuronavigation surgery process can easily be compared to location and directional tracking systems

used for cars and ships; it is, in effect, a kind of a global positioning system for the neurosurgeon. The image-guided camera performs much like a satellite that detects signals from vehicles or instruments that are equipped with special tracking devices.

Steps Involved in a Neuronavigation Procedure

There are four broad steps in neuronavigation procedures as summarized below.

Step 1 – A diagnostic image of the patient's anatomy is loaded into the neuronavigation computer work station. Usually, a CT and/or MRI scan of the patient is taken the day before or the day of surgery. Similar to navigating in a city on the basis of landmarks, a surgeon uses landmarks in the image scan. The surface of the head, however, often needs artificial markers because the head is relatively featureless, except for facial features. Therefore, mostly artificial landmarks on the patient's head are used to serve as markers. As alternative, natural landmarks of the head (tip of the nose, bridge of the nose, the inner angel of the eye, etc.) can be used as natural fiducials and superimposed on the 3D images (Vlieger et al. 2004).

Step 2 – The scan is then used to create a 3D model of the patient's brain anatomy. Thus, the patient's unique anatomy can be viewed on the computer monitor of the neuronavigation workstation. Then, entry point, target points, risk zones, targeted resection borders, and vessels are built and displayed in a 3D-manner. Eventually, surgical trajectories and the targeted boarder of the resection area are defined on the computed image, and can be anticipated even during the planning period.

Step 3 – These data are transferred to the computer in the operating room. After anaesthesia is administered and before start of surgery, the surgeon maps the patient's anatomy to the 3D model of the scanned information, using an image-guided probe at the patient's anatomy; this process is known as registration process (also called reference process). As the registration process begins, the neurosurgeon touches the centre of the fiducials that have been placed on the patient's head or touches natural landmarks with an image-guided instrument (image-guided pointer or probe). Then the neurosurgeon touches that point on the screen with the instrument. Point by point, on the patient's head in the operation room and then on the monitor, the neurosurgeon builds a correlation between the head and the screen image. By matching the scan with the real anatomy of the individual patient during surgery, the neurosurgeon can accurately "see" the location of the instrument tip in the brain; registration thus means matching a patient's physical anatomy with the 3D computer scan information.

Step 4 – As the surgeon moves an instrument in the body, its position is precisely calculated. The neurosurgeon now can track instrumentation as it proceeds into the operative field as well as view its relative position and trajectory to the operative field allowing the visualization of exact placement and direction of the moving instrument or the microscope. During surgery, the tip of surgical instruments or of focus of the surgical microscope will be displayed dynamically as cross-hairs in all three orthogonal anatomical views on the monitor. This also enables the neurosurgeon to visualize the proximity of the instruments to critical anatomic structures, such as eloquent brain regions, cerebral arteries, venous structures, and cranial nerves. Ultimately, neuronavigation helps the surgeon to accurately detect where he or she is working in the patient's body at every moment during surgery.

Multimodal Image Guidance During the Surgical Procedure

Moreover, one can use the neuronavigation device as a common platform to merge complementary information modalities. Correlation of anatomic and structural details with functional information from different imaging modalities (fMRI, DTI, SPECT, PET, etc) contributes to the surgical script in a variety of diagnoses in neurosurgery. Multimodal neuronavigation with multimodal information injected into the overlay (head-up) display of a neurosurgical microscope thus extends the use of neuronavigation. Most neuronavigation systems today use the principle of multimodal and multi-informational neuronavigation by means of a modern data fusion environment.

Incorporation of functional data provided by fMRI with neuronavigation helps to avoid destruction of

the eloquent areas of the brain during surgery. Some studies today report on the relative merits and problems of the navigational systems and also highlight the role of functional brain mapping and intraoperative MRI, when integrated with neuronavigation, in surgical decision-making aiming at radical tumor resection with minimal morbidity.

Benefit of Neuronavigation During Neurosurgical Procedures

Image-guided surgery systems provide advanced procedure planning, and they enable surgeons to more accurately identify ideal surgical entry points and targets. The physician can "practice and check" the surgery, can try alternative approaches, and assess possible difficulties, before the real surgery takes place. Neuronavigation enables the surgeon to reduce the size of incision necessary to perform an operation. Trauma may be minimized due to smaller sized and better centred skin incisions and craniotomies and due to approaching the target lesion with less dissection of intact brain parenchymal tissue. By enabling the surgeon to navigate through the delicate landscape of the brain more accurately, the surgeon can remove a brain tumor, possibly without impacting healthy tissue (Auer et al. 2007; Gumprecht et al. 2002). The precise neuronavigation technology enables the surgeon to directly focus on the problem, which may mean the patient spends less time on the operating table. The duration of the procedure can be decreased, and the surgeon's feeling of safety can be improved. Despite more radical removal of lesions, the overall invasiveness of the operation can be decreased.

When trauma to the body is minimized, the patient may spend less time in recovery and may experience fewer complications. These benefits often lead to shorter hospital stays. This technology may mean better long-term results and decrease the need for repeat surgeries. In certain cases, tumor biopsies can be performed with a neuronavigation surgery system with great accuracy and with minimal trauma to the patient.

Thus, neuronavigation gives us a detailed "road map" of the brain or spine, which means that only a limited incision is necessary to get exactly where the surgeon needs to focus. This reduces pain and recovery time for patients, and it reduces the risk of damage to the tissue or the surrounding areas. The ability to relate the position of a real surgical instrument in the surgeon's hand or the microscope's focal point to the location of the imaged pathology, updated in real time in an integrated operating room, highlights the modern version of this set of technologies at its finest. In its current form, neuronavigation has adapted to modern neuroimaging technologies, to real-time imaging capabilities, to new technologies to transfer the information in the operating room for 3-D localization, and to new and better algorithms to handle data via more sophisticated computer technologies.

Applications of Neuronavigation

Neuronavigation technology can be used in a variety of patients, including tumor removal, aneurysm repair, cyst removal or spine repair using pins or screws. In *tumor surgery*, increased extent of tumor resection is associated with prolonged survival (Jenkinson et al. 2007; Vlieger et al. 2004). Neuronavigation gives surgeons image-guided precision for delicate procedures. Navigation combined with intra-operative imaging allow the surgeon to "see" whether he or she has successfully removed the entire tumor and avoid damage to surrounding healthy tissue (Wu et al. 2004; Zhang et al. 2008).

The management of *medically refractory epilepsy* poses both a valuable therapeutic opportunity and a formidable technical challenge to epilepsy surgeons. Despite its success, the neurosurgical treatment of epilepsy remains a clinical decision-making and technical challenge for which there is still room for improvement. Recent advances in the capabilities and dispersion of intraoperative neuronavigation and neuromonitoring underscore how the modern epilepsy surgeon is becoming increasingly armed with adjunctive technologies that hold promise to improve surgical outcomes (Pirotte et al. 2005). For many patients, surgery for intractable epilepsy provides not only freedom or substantial relief from seizures, but also functional improvement and increased quality of life. In particular, image-based neuronavigation and electrophysiological neuromonitoring represent versatile and informative modalities that can assist a surgeon in performing safe and effective resections. In patients with medically refractory epilepsy, neuronavigation technologies evolve with demonstrated and potential

utility. Precise intraoperative localization of the underlying structural and functional processes is crucial in this regard (Wurm et al. 2000, 2003). In *cavernoma surgery*, an operation with the guidance of neuronavigation is safe and can decrease the occurrence of disability following the procedure (Wurm and Fellner 2004; Zhao et al. 2007).

Our Patients Series

We use the neuronavigation device as a common platform to merge complementary information modalities. Correlations of anatomic and structural details with functional information contribute to the surgical script in various neurosurgical procedures. In most cases, at least two different information modalities contribute to planning and surgical guidance in every patient. Immediately following the operative procedure, the surgeon answers a set of questions regarding the reasons for the application of neuronavigation, and the efficiency and safety of navigation. Detailed analysis of the location of the operative procedure, histopathological findings and outcome is performed.

We found that the main benefits of neuronavigation in neurosurgery are precision of targeting even in small and deep-seated targets, safe manipulation in critical brain areas, accurate placement of electrodes, and correlation of electro-clinical information modalities with underlying structures. Furthermore, neuronavigation provides individual tailoring of craniotomy and corticotomy. It is, however, less reliable for verification of resection boundaries in the case of gliomas. Neuronavigational localization and its combination with image fusion and functional investigations greatly improves discussion within the interdisciplinary team. Thus, the neuronavigation concept proves its value in neurosurgery by linking anatomic, pathologic and functional data of the individual patient. Enhanced by the integration of multimodal information, neuronavigation significantly improves the available treatment options (Wurm et al. 2000, 2003).

Functional Magnetic Resonance Imaging

fMRI is a type of specialized MRI scan. fMRI rests on the supposition that there is a relationship between brain function and cerebral blood dynamics. When a neural event occurs in a region of the brain, there is a subsequent increase in local blood flow that changes the ratio of oxyhemoglobin to deoxyhemoglobin in the local microvasculature of the activated region. This change leads to an increase in fMRI signal that has been called the blood oxygenated level-dependent (BOLD) response. Thus, fMRI is an indirect measure of neural activity. There is a possible mismatch between the location of the BOLD signal and the actual site of neural activity that can be reduced to a maximum error of 3–6 mm with dedicated MR imaging and postprocessing techniques. The BOLD signal reflects the total amount of deoxyhemoglobin ($dHBO_2$), and is thus a complex function of cerebral blood flow (CBF), the cerebral rate of oxygen metabolism ($CMRO_2$), cerebral blood volume (CBV), and the magnetic field strength. Furthermore, the interpretation of changes in the BOLD signal can be complicated by variations in these physiological quantities due to factors such as age, disease, or the presence of vasoactive agents.

BOLD is the most widely used fMR imaging method, but others such as perfusion fMRI based upon arterial spin labeling (ASL) methods offers another useful complement to BOLD fMRI. In contrast to BOLD, it can provide quantitative measures of both baseline and functional changes in CBF that can aid in the interpretation of the BOLD signal change. Changes in CBF are thought to be more directly linked to neuronal activity than BOLD, so that perfusion fMRI also has the potential to offer more accurate measures of the spatial location and magnitude of neural function. The CBV fMRI is expected to show only microvascular activation regions, which are localized in the brain parenchyma. However, different types of ASL sequences are still under development and have some restrictions especially in regard to number of the acquired image volume and spatial resolution compared to BOLD fMRI. Nevertheless, CBV fMRI can be combined with other fMRI methods to study different aspects of the hemodynamic responses during functional activation and/or physiological challenges. The spatial and temporal characteristics of these multi-modal fMRI responses can provide us with a tool for quantitative evaluation of brain physiology, from which one can study how the brain regulates its blood supply and maintains homeostasis during normal state and in pathology.

Task Design and Image Analysis Methods

The choice of the cerebral activation paradigm is perhaps one of the most difficult issues, because not enough is known regarding how exactly brain functions are organized. The choice of a paradigm depends on the objective of a study and it deserves careful consideration. What stimuli are presented depends firstly on what functions one wants to measure, and secondly on how closely comparison stimuli can be matched. For an fMRI experiment one has to devise a task which contains at least two different conditions in order to create a meaningful activation paradigm. During an investigation based on the block design, the patient performs a task of usually 20–30 s, in which specific brain functions are invoked and alternated with periods of a control task. Calculated and compared to a rest condition with nearly no specific brain activation, the whole brain activation related to the performed task is shown. To identify a particular function, the control task should invoke all the functions that are involved in the experimental stimuli, except for the function of interest.

Although regions involved in both tasks remain undetected, cognitive processes involved in processing stimuli are generally complex, and can differ considerably between subjects. Accordingly, there are various cognitive functions that require more than one type of control stimulus due to complicated interactions between brain systems. One way of dealing with this is to devise multiple tasks, each of which contains the function of interest plus several functions that need to be filtered out. This is referred to as "conjunction design", and is used for instance in language studies, e.g., in order to isolate "language comprehension".

Temporal resolution of fMRI is generally low, as the BOLD response lags behind the neural response by several seconds and lasts for a single event up to 10–20 s. Methods to increase temporal resolution have received considerable attention in recent years, and it is referred to as the "event-related", "fast event-related" or "single-event" design. This term is, however, generally used to indicate the type of data analysis that is applied, in that the hemodynamic BOLD response is an important factor in building the factors for image analysis.

A task may involve presentation of a series of experimental stimuli with an interval of 2 or 3 s, alternating with series of comparison stimuli. The data can be analyzed with a boxcar function with on and off periods, but alternatively each stimulus can be modelled as a task-related brief event. This impulse function can be transformed to a series of BOLD response curves. Extractions of the BOLD response from the data require a special scheme of varying stimulus onset times and/or inter stimulus intervals, and can be achieved without any comparison stimuli.

Characteristics of the brain processes that are invoked by a stimulus determine whether a block design or an event-related design should be used. For instance, perception of simple visual stimuli involves predictable rapid and brief instances of neuronal activity, and can be modelled adequately. Memory tasks, however, cannot be modelled very well in time, making it difficult to construct an adequate impulse function. In this case a block design may be better suited. Even more complicated is the situation with patients, when, for example, strategies to perform a task are changed. Small differences in the instruction or comprehension can induce major differences in activated brain regions. Therefore, it is necessary that all confounds (e.g., functions one is not interested in) are controlled.

Many of the currently available fMRI data analysis programs make use of multiple regression algorithms based on the General Linear Model. This type of analysis essentially determines whether the fMRI signal time series in each voxel correlates with the task, showing the events that take place when the task is performed, as well as factors that contribute to noise in the dataset. Once an fMRI protocol, which includes data acquisition method (pulse sequence), task design (paradigm) and image analysis (preprocessing and statistical algorithms) has been composed at which all of them can affect the quality measures, it can be tested in an fMRI experiment. Interpretation of results of fMRI experiments is rarely straightforward, and it is important to test the results on the basis of validity, sensitivity, and reliability. Performance is a valuable measure in fMRI because it can indicate not only whether a function is invoked, but also the demand imposed by the task on the underlying brain system. In addition, the quantification of different performance parameters can be used for a parametric statistic analysis and can contribute to a more specific view.

Most MR imaging units today have software for real-time automatic analysis and display results during

imaging. The corresponding performance is not a trivial issue and in neuropsychology, performance is generally the readout variable, and is used to characterize a persons' cognitive abilities. In fMRI, task performance can give rise to problems in image interpretation. Poor performance may be associated with abnormal task solving strategies. For example, the strategy determines how much the working memory system is taxed, and this affects the levels of brain activity as measured with fMRI. In addition, the level of difficulty may also be adjusted for each individual subject, based on a practice session before scanning. An alternative solution is to adjust the statistical analysis to performance by separating scans acquired during correct responses from scans acquired during incorrect responses.

Abnormal fMR imaging activation can, of course, be truly false-positive resulting from movement artefacts or low statistical threshold, but it can also represent variations in normal anatomy and physiology or reflect brain plasticity. On the other hand, failure to detect activity can be caused by several factors; some of them are difficult or impossible to control. Furthermore, a tumor can distort the brain or cause blood flow abnormalities that may alter or diminish the BOLD signal. Absence does not necessarily imply absence of relevant neural activity. Even activity inside the tumor can be detected and may be functionally relevant.

Diffusion Tensor Imaging

DTI is a promising MRI method for studying noninvasively the anatomical organization of major white matter fibre systems. White matter bundles carry functional information between brain regions. The diffusion of water molecules is hindered across the axes of these bundles such that measurements of water diffusion can reveal information regarding the location of large white matter pathways (for a review see Mori and van Zijl 2002).

A key obstacle for accurate reconstruction of neuronal fibres is the selection of a suitable tracking algorithm. In certain areas of the white matter, such as the corona radiata or the occipital white matter where an abundant crossing and/or merging of different fibre systems takes place, the main diffusion intravoxel direction does not necessarily correspond to the main fibre direction. This is due to the tensor's voxel averaged quantity and the limited resolution of available DTI acquisitions (Jones 2003). Consequently, simple tracking algorithms, which incorporate only the main diffusion direction for determining the propagation pathway (or track) are not adequate in such anatomically complex areas, and the reconstructed trajectories are often compromised by the wrong directional information (Lazar and Alexander 2003; Tournier et al. 2002). Recently, sophisticated tracking algorithms have been developed to overcome these limitations, particularly to ameliorate tracking results in crossing and branching situations (Parker et al. 2002). This problem can be addressed by using a tracking algorithm called "advanced Fast Marching" (aFM), which has been specifically developed in order to improve reconstruction of white matter trajectories in anatomically complex areas. The quality of the aFM algorithm was evaluated and compared with other tracking algorithm by reconstructing different neuronal fibre systems and networks in the human brain (Staempfli et al. 2007).

Combination of fMRI and DTI

Accurate preoperative localization and visualization of the displaced or infiltrated fibre tracts in relation to intracranial tumors is crucial for treatment planning and potentially for the post-operative prognosis. One of the first publications by Witwer et al. (2002) demonstrated displaced fibre tracks on directionally color-coded maps. Goebell et al. (2006) showed different fractional anisotropy (FA) values in the centre as compared to the periphery of gliomas as well as in the adjacent normal appearing white matter. They also found differences in FA ratios between low-grade and high-grade tumors.

New developments aim at presurgical, intraoperative, and follow-up post-surgical applications of DTI to provide relevant information related to the tumor affected tissue. fMRI-driven fibre tracking methods are the most recent clinical application in this direction (Schonberg et al. 2006; Kleiser et al. 2010). Guye et al. (2003) applied the basic fast marching tracking algorithm in order to perform fMRI driven fibre tracking. Thereby, probabilistic connectivity maps of healthy

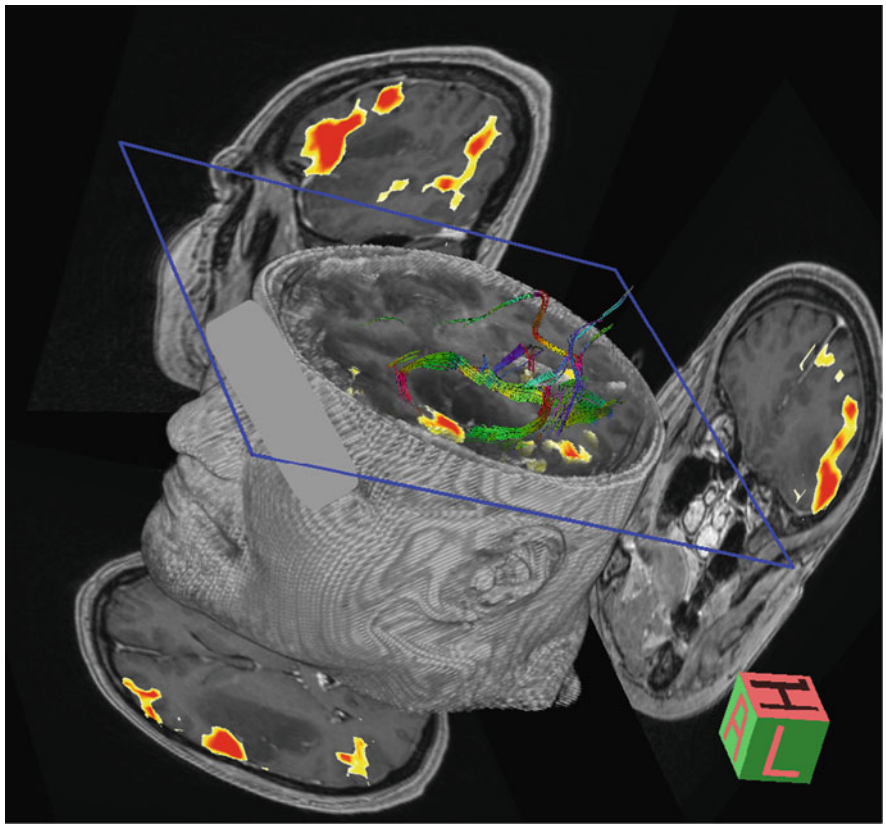

Fig. 19.1 fMRI-driven fiber tracking method. Functional imaging in a patient with a tumor in the left insula and opercula: BOLD-activation during language task: visible are Broca and Wernicke area and additional – compensatory – activation in the frontopolar, posterior temporal and parietal lobe. DTI seeding in Broca and Wernicke: fiber connections between primary language areas are displaced bending around the tumor mass

subjects were computed and compared with a map of a patient suffering from a tumor.

A main issue in the field of DTI-based fibre tractography is the definition of a tracking seed region that would be appropriate for the reconstruction of white matter tracts relevant to a specific functional system or network. If seed areas are slightly misplaced by only a few voxels, the reconstructed trajectories may represent tracks from different white matter fibre systems. Intersubject anatomical variations make it difficult to define tracking seed areas based merely on reliable anatomical landmarks, even in brains of healthy subjects. This problem becomes more difficult in the presence of a space occupying intracranial pathological processes, as e.g., tumor, where the definition of functionally relevant tracking seed regions based on anatomical landmarks becomes more challenging due to displacement or infiltration of the surrounding tissue and a potential reorganization of involved functional systems. To overcome this obstacle, a combined approach of DTI and fMRI can be performed where seed areas for the DTI tracking algorithm are defined based on fMRI activation patterns specific to individual patient. Taken together fMRI-driven fiber tracking method is an accurate, reliable and safe technique of detection of cortical areas and white matter pathways for the function (Fig. 19.1).

Positron Emission Tomography

In clinical applications, a very small amount of labelled compound called radiopharmaceutical or radiotracer is administered into the patient usually by intravenous injection. After an appropriate uptake period, the concentration of tracer in tissue and its localization is measured by the PET scanner. During its decay process, the radionuclide emits a positron which, after travelling a short distance (3–5 mm), encounters an electron from the surrounding environment. The two particles combine and "annihilate" each other resulting in the emission in opposite directions of two gamma rays of 511 keV each, which are detected

by coincidence. Amino acid PET data using O-(2-[18F]fluoroethyl)-L-tyrosine (FET) as a tracer have recently been established as diagnostic marker for gliomas. Contrary to structural MRI with contrast-agent, the i.v.-injection of FET does not result in a passive accumulation in the tumorous lesions facilitated by a defect of the blood–brain–barrier. Rather, FET enhancements result from an active transport of FET into tumor cells through an intact cell membrane. The increased uptake is mediated by a selective overexpression of specialized transport-proteins in the cell membrane of the glioma cells. Therefore, increased FET-uptake indicates vital tumor tissue.

Coregistration of fMRI and Amino Acid PET

Amino acid PET is established to identify glioma tissue. In presurgical evaluation this helps to plan a maximal resection of gliomas. Especially in patients with brain tumors in so called eloquent cortex areas, i.e., cortex areas inheriting primary functions such as sensorimotor or language representations, fMRI as well as amino acid PET have been proposed as tools for planning surgery (Nariai et al. 1997). The goal is to achieve a maximal excision of tumor tissue combined with a minimal disruption of the patient's sensorimotor and language abilities, i.e., to tailor the tumor resection line with respect to brain function and thereby optimize the functional outcome for the patient. A multimodal coregistration of fMRI and PET can, therefore, be used to localize sensorimotor and language function in relation to tumor amino acid uptake at a glance.

In a group analysis, the sensitivity of the lesion-to-brain ratio of FET uptake for the detection of tumor tissue using a threshold for the FET ratio (uptake in tumor compared to healthy tissue, so called tumor-to-brain ratio, TBR) of 1.6 was 92% and the specificity 81%. Another criterion for using this specific threshold is the fact that in histologically proven peritumoral tissue the mean ratio of FET uptake was 1.2 ± 0.4 versus 2.6 ± 0.9 for the samples taken from tumor tissue ($p < 0.001$) (Pauleit et al. 2005). The resulting intermediate value of 1.6 for the TBR is, therefore, one standard deviation from both ratios.

The combined use of MRI and FET-PET in patients with cerebral gliomas significantly improves the identification of cellular glioma tissue and thus, has been proposed favorable over the exclusive use of MRI in planning for cerebral glioma resection (Rachinger et al. 2005).

In a series of 11 patients with left hemispheric gliomas (WHO II–IV) the spatial relation between fMRI and FET-PET was investigated prior to surgery. fMRI was done using a sentence completion task, amino acid uptake in tissue was measured with FET-PET, then fMRI and PET-images were coregistrated in Talairach stereotaxic space (Nickel et al. 2007) (Fig. 19.2).

In this series, FET-uptake and fMRI-activations were spatially distinct. Using a threshold of 1.60 for the FET-tumor-to-brain ratio the mean distance between FET-uptake-volume and fMRI-activation in language related areas was 14 ± 8 (2–29) mm. This suggests that, in general, uptake of FET in vital tumor tissue and functional activation of surrounding brain tissue as measured with fMRI are spatially distinct. The combined use of fMRI and FET-PET, therefore, appears to be one promising approach for presurgical evaluation of structure-to-function relations in patients with gliomas, as it may help to estimate a safety margin for resection and the functional potential of the peritumoral tissue.

Clinical Examples

Integration of fMRI and DTI in Neurosurgery Planning with their Impact

In the years 2008–2010 ~250 fMRI examinations in our hospital were used to confine eloquent brain areas. The functional data were used for the operative procedure due to their close neighbourhood to the lesion demonstrating good profit in clinical practice. The choice of the MR parameters between different institutes is more or less standardized. For the following described measurements we used a 1.5 T Siemens Symphony Tim scanner with the standard 12-channel head matrix coil. For fMRI a gradient-echo T2*-weighted echo-planar MR sequence was used (TR/TE = 3000/50 ms, FOV = 192 × 192 mm, matrix = 64 × 64, voxel size 3 × 3 × 3 mm), for DTI a single shot echo-planar imaging sequence (TR/TE = 3600/110 ms, FOV = 220 × 220 mm, matrix = 128 × 128, voxel size 1.7 × 1.7 × 6 mm, averages = 4, 12

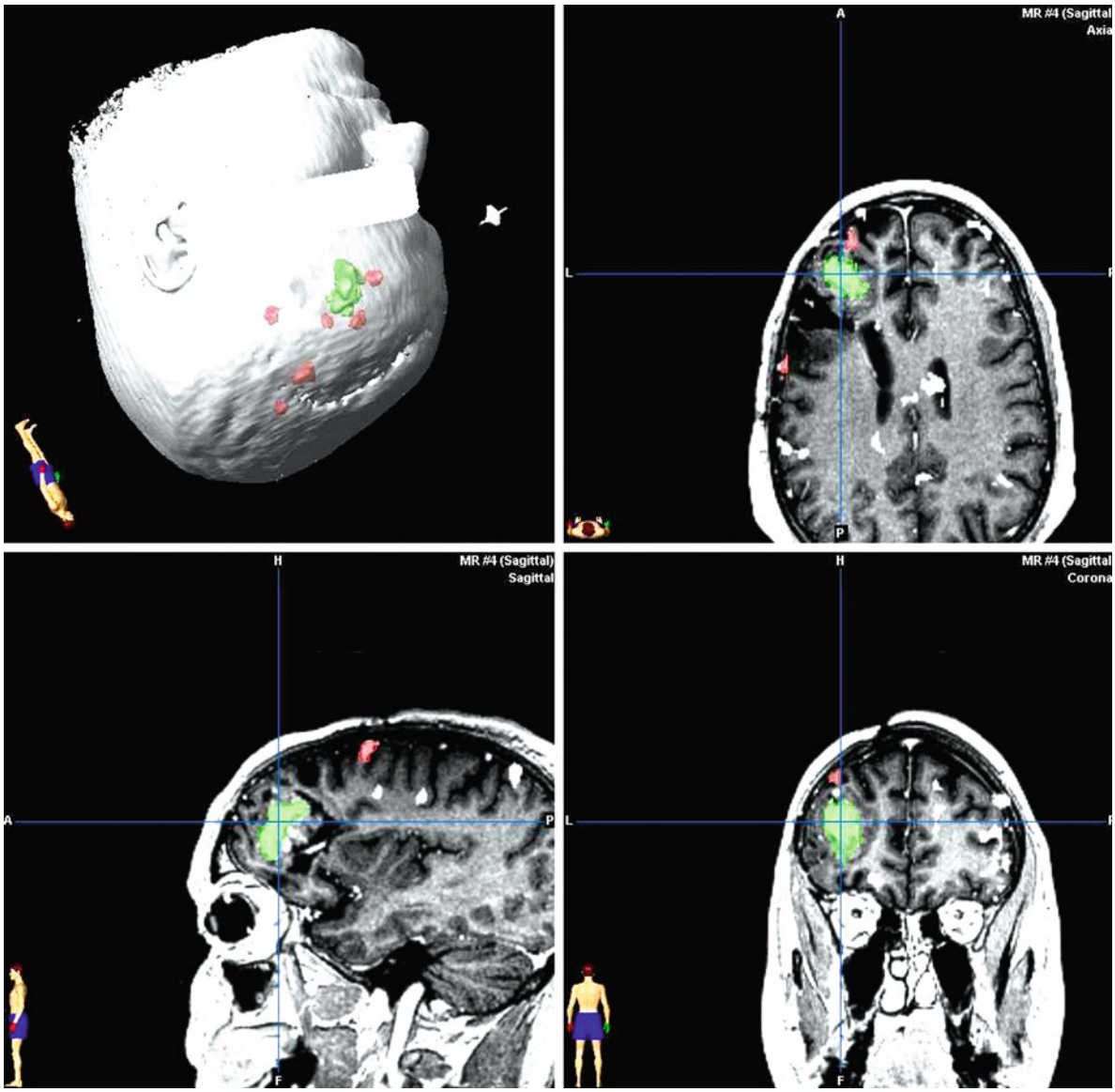

Fig. 19.2 Screenshot from the neuronavigation software BrainLab® showing a co-registration of language-fMRI (*red spots*) and FET-PET (*green spot*) on to the structural 3D-T1 MRI of the patient

non-colinear directions, *b*-values 0, 1000 s/mm^2), for anatomical data a 3D T1-MPRage, and in addition an axial 2D T1- and T2-weighted sequence.

In the current prospective study we evaluated our experience with the integration of fMRI and DTI with a more standardised evaluation. Up to now 15 tumor patients were examined. The stimulus paradigms for fMRI were adapted and optimized to the tumor location and the individual characteristics of the subject. The paradigms included cognitive, semantic, sensorimotor and visual tasks. A typical fMRI paradigm lasted ∼5 min. Usually up to ten different paradigms were necessary to scan the adjacent functional areas around the tumor.

We designed a questionnaire containing following parameters: (1) approach, (2) trajectory, (3) resection border. Neurosurgeons were requested to decide on approach, trajectory, and resection borders *without* and afterwards *with* the additional information provided by fMRI and DTI.

We collected the data of 15 patients with fMRI and 3 of those additionally with DTI. This was taken into account only if fibre pathways between special functional areas were under suspect to be interrupted by the tumor, as between Broca's and Wernicke's area or for the optic pathway. We found BOLD activation near the tumor in 86% of all patients confirming the excellent stimulus adaptation for the individual subjects. Furthermore, the expected functional areas were displaced by the tumor in ~40% of the patients. The direction was unpredictable and therefore the uncertainty relevant for the neurosurgeon. This is reflected in the change of the neurosurgical approach in 33% of the patients, the trajectory in 27%, and the resection border in 54% when fMRI data were available. In this pilot study we succeeded in demonstrating feasibility and benefit of incorporating fMRI and DTI data in our multimodal neuronavigation concept.

It influenced surgical strategies: altering overall strategy – biopsy versus resection, avoiding destruction of brain areas with permanent loss of function, and altering the kind and duration of postoperative therapy. In the following we detail three cases who exemplarily demonstrate the influence of fMRI and DTI information on the decision of trajectory, approach and resection border and the expected consequences:

Patient 1

A 68 year old male patient sustained a first epileptic seizure, beginning in the right upper extremity with secondary generalisation. When admitted to the hospital the patient had no neurologic deficit and no further seizures. CT- and MR-imaging was performed, and cavernous hemangioma was diagnosed in the left central parietal region with typical surrounding hemosiderin ring and intrinsic bleeding in various stages. Furthermore, a MRI-SWI-investigation was performed whether surrounding bleeding showed distinct borders in the left central region.

Originally, a direct transsulcal approach was planned to remove the cavernous angioma and the surrounding bleeding. However, considering the eloquent region in addition a preoperative functional MRI and DTI was planned. After integrating these advanced MR-imaging it could be shown that the originally planned trajectory was directly going through the eloquent region. Thus, it was decided to go more dorsally through another cerebral sulcus, which meant that another trajectory with a longer approach to the cerebral lesion was used. The surgical performance was done neuronavigationally guided in March, 2010. Postoperatively, the patient remained neurologically intact and up to now did not show any seizures again. He has normal life quality and is apt to perform all procedures of normal daily life. In case of damage to the left central region one would have expected that the patient was at high risk to sustain permanent right hemiparesis (Fig. 19.3a).

Patient 2

A 37 year old female patient got the incidental diagnosis of a huge left frontal glioma, which extended to the left frontoparietal opercula. At that time the patient was completely free of neurological or psychiatric symptoms. She had been seizure-free. According to the borders of the diagnosed tumor it was suspected that only very few tumor reductions would be possible in this young patient, which expecting that prognosis of the tumor would be very poor.

However, fMRI and DTI was done in order to augment the neuronavigational guided operation with these examinations in addition to implemented PET images to the neuronavigation workstation. After implementation of all images it could be shown that the eloquent regions had been displaced far laterally, and that the most enhancing tumor parts which were considered to be the most malignant part of the tumor would be able to be completely resected. This was discussed with the patient who is a psychologist and was able to have a good knowledge of her disease and on her prognosis. It was decided together to remove as much tumor as possible. The microsurgical neuronavigational guided procedure was performed in May, 2008. The tumor turned out to be a glioblastoma multiforme WHO°IV, and postoperative radiotherapy and chemotherapy were performed.

Up to now the patient is fully symptom-free, free of seizures and is fully able to work in her former profession. The regularly performed MR- and PET-images do not show any contrast enhancing lesion and show the patient free of tumor progression. If the surgical operation would have touched regions of eloquence, for example, regions responsible for verbal speech, the patient of course would not be able to work in her profession again (Fig. 19.3b).

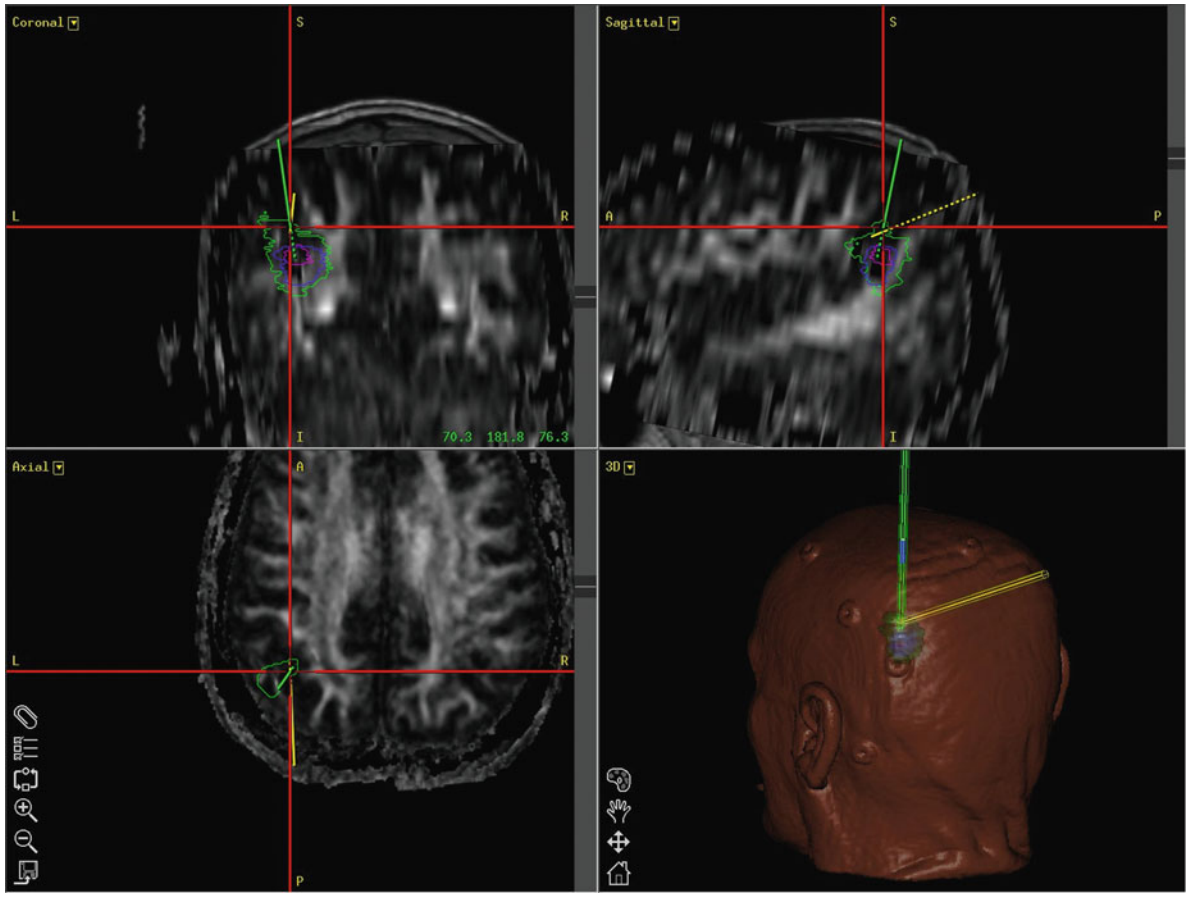

Fig. 19.3a Improvement of approach, trajectory, or resection using the example of three patients; please compare patient paragraphs for details. *Patient 1*: approach with fMRI yellow line, without fMRI green line

Patient 3

A 45 year old female patient, who was working as a teacher sustained epileptic seizures and was admitted for cerebral MR-imaging. In these examinations a left frontolateral low-grade glioma was diagnosed and the patient was admitted to our hospital. The tumor was located in the left frontal operculum, which means in the Broca region in the right-handed patient. With this diagnosis it was originally suspected that only tumor biopsy would be possible, knowing that this performance could only provide diagnosis but no help for prognosis and progression-free survival. Therefore, the patient was sent for fMRI with adjusted speech tasks. In this examination the left frontal operculum was totally engaged by the tumor, whereas all speech regions had been displaced to the surrounding areas. The maximum resection was discussed with the patient. The patient herself wanted to have the most radical resection, which was considered to be possible and the microsurgical neuronavigational-guided surgery including fMRI was performed in December, 2005.

After the operation the patient was totally symptom-free and seizure-free. She showed only very small residual tumor of the oligodendroglioma WHO°II, and this residual tumor has not shown any progress for 5½ years. Without the knowledge of the fMRI-examination only a biopsy would have been done or the patient would have been at risk to have permanent neurological deficit (Fig. 19.3c).

In addition to benefiting the individual patients' potentially altering prognosis and quality of life, the cost of nursing care could be reduced, implying a significant economic impact.

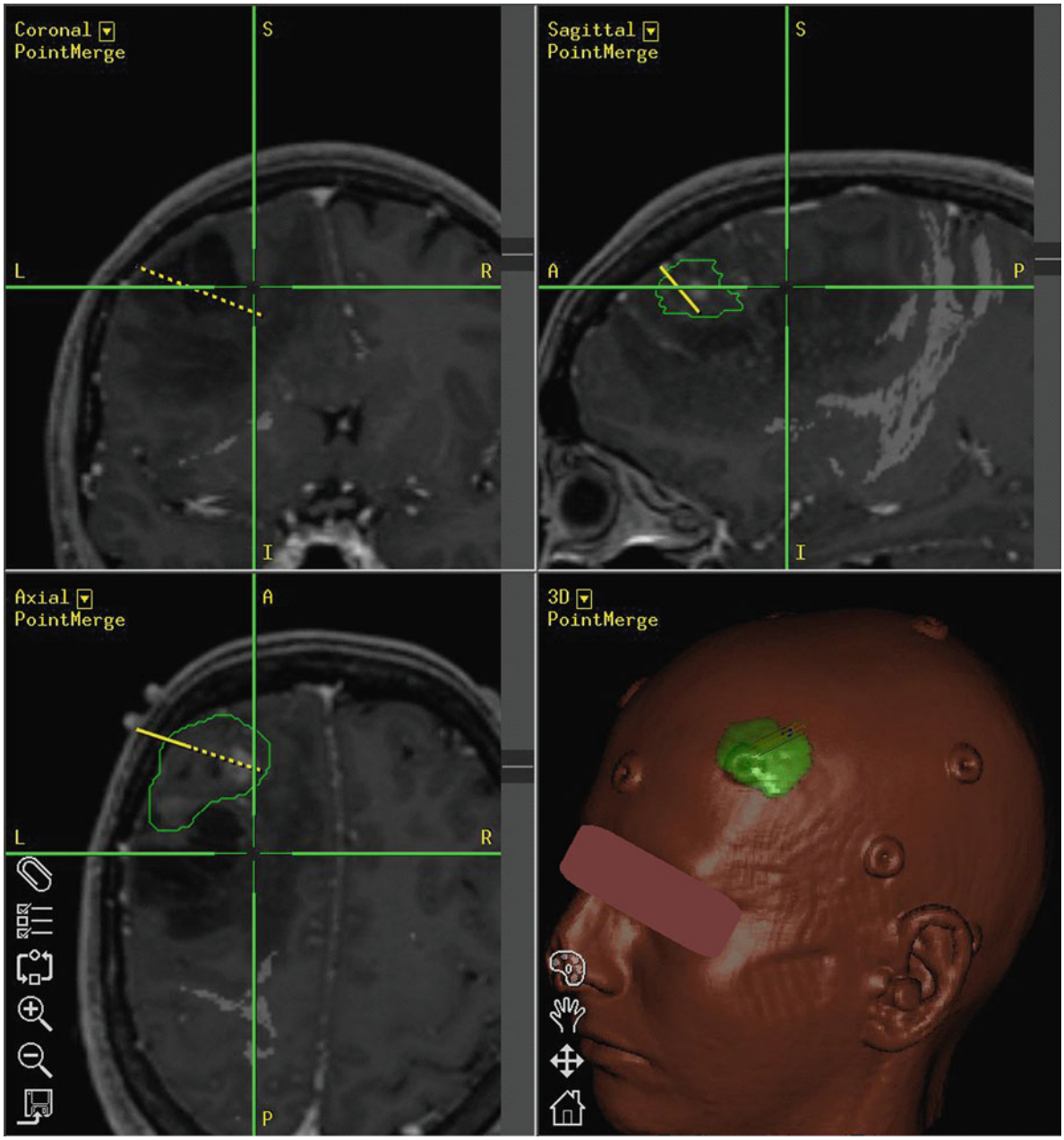

Fig. 19.3b *Patient 2*: PET activation (*green*) inside the tumor area indicating the most malignant part of the tumor. DTI (*white*) shows fibres around the tumor

Patients with Longitudinal Language-fMRI in Gliomas

The following case samples demonstrate the feasibility and the potential of serial language fMRI investigations in patients with gliomas. Two different cortical strategies of functional compensation, namely intrahemispheric adjustment and transhemispheric shift are revealed (Fig. 19.4).

For both patients a systematic clinical neurological examination as well as detailed neuropsychological testing were performed alongside the fMRI scans. The neuropsychological assessment comprised language memory (Rivermead Behavioural Memory Test), verbal fluency (word generation task from the AAT),

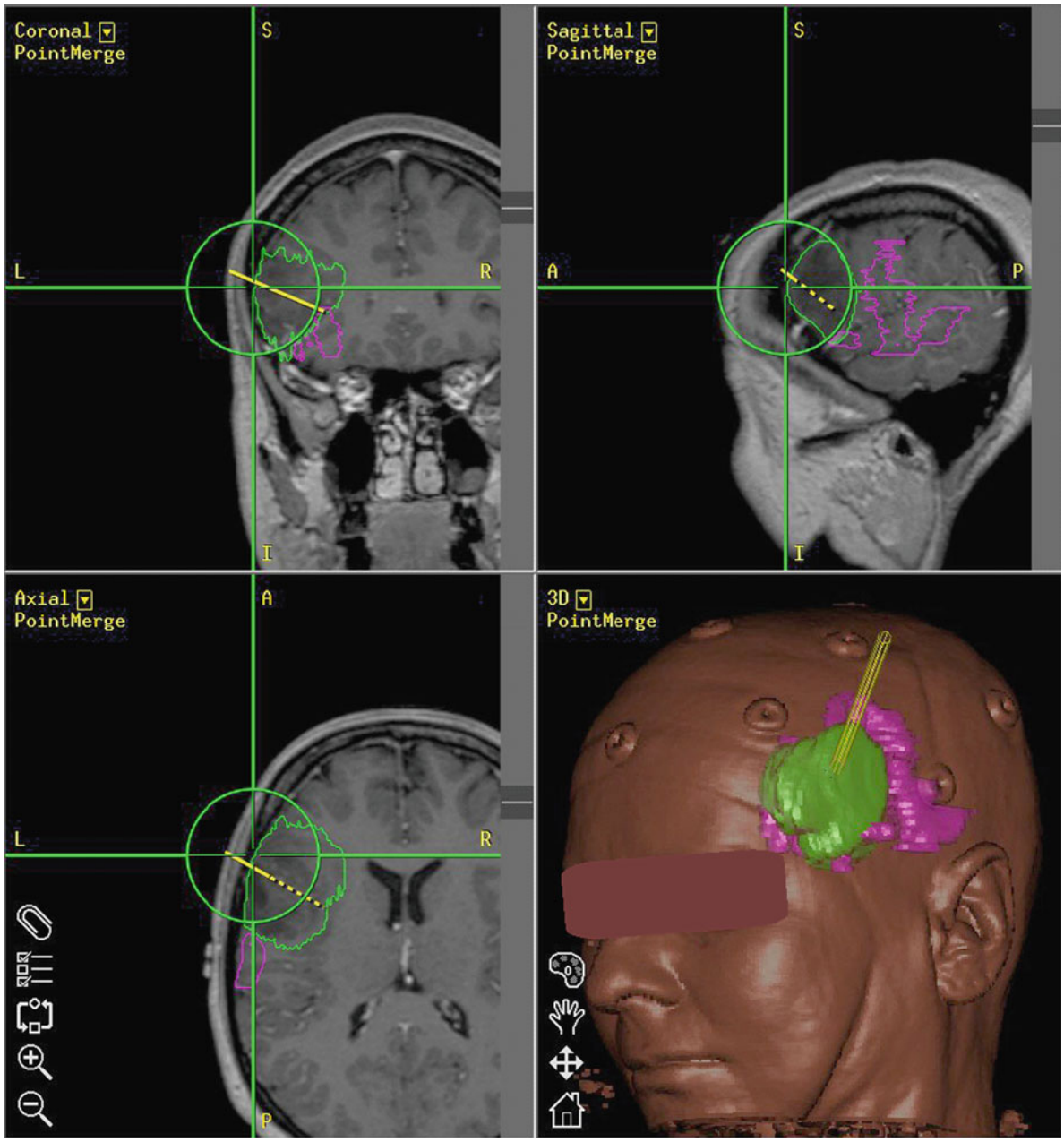

Fig. 19.3c *Patient 3*: fMRI activation (*pink*) of eloquent areas near to critical resection border of the tumor (*green*)

frontal lobe tasks (Digit-Span and Block-Span), and tests for reading, writing and handedness (Edinburgh Handedness Scale).

fMRI was realised using covert speech in a sentence completion task with inflectional processing of verbs. This paradigm has got a high capacity to demonstrate the cerebral language network (Jorgens et al. 2007; Kleiser et al. 2005; Sach et al. 2004).

Patient 1

The patient is male, age 36 years at first admission and suffered from a low-grade glioma arising from the left insular cortex confirmed to be a diffuse astrocytoma of WHO°II. The clinical neurological examination did not reveal a focal deficit, the results of the neuropsychological assessment confirmed below average scores

for language memory and verbal fluency while frontal lobe tasks showed average or even above average scores.

Initial fMRI for language demonstrated a typical left hemispheric pattern of activity in this right-handed patient. Activation for expressive function of language were displaced from the typical location in the inferior frontal gyrus ("Broca's area") due to local tumor-growth immediately neighbouring the glioma in the border between T1-tumor area and the surrounding healthy-appearing tissue. Given the picture of a large low-grade glioma in eloquent cortex with rather moderate clinical impairment (well controlled epilepsy, only slight to moderate cognitive deficits) the patient was taken in a regime of regular, close meshed clinical and MRI follow-up investigations (Fig. 19.4).

At age 38 years, structural MRI and FET-PET of the same patient pointed to a progression of the glioma. Apart from an increased verbal fluency the neuropsychological tests showed stable results and language fMRI confirmed a left hemispheric language activation pattern with multiple spots of activation surrounding the tumor mass that had grown further into the left frontal and temporal lobe. The tumor mass was reduced surgically using fMRI-guided intraoperative cortical stimulation mapping for language testing, and neuropathological analysis of the resected specimen confirmed a progression towards an anaplastic astrocytoma (WHO III).

Postoperative MRI confirmed a good reduction of tumor mass. Fortunately, the results of the neuropsychological tests remained stable and also fMRI confirmed the appearance of widespread left-hemispheric language activation. An irradiation therapy was performed after the surgery and another follow-up fMRI was done ~9 months after the surgery. The clinical neurological status remained stable and even neuropsychological tests showed a slight improvement for verbal fluency and frontal-lobe tasks (digit span forward). fMRI in consistence with the previous results, demonstrated the foreknown left hemispheric activation pattern.

At the time of the last follow-up, a little more than 1 year after surgery (patient age 40 years), the neuropsychological results were even more stabilized towards average and above average values. Language fMRI again demonstrated the widespread left fronto-temporal activations and the clinical-neurological status also remained stable. In this patient, longitudinal language fMRI was in agreement with the clinical and neuropsychological status and aided in performing a functionally safe surgery. Thereby the partial resection of the glioma did not do harm to the spots of fMRI activation in the surrounding eloquent cortex and the partially displaced left-hemispheric language function in this patient with a large left-hemispheric tumor mass was preserved. Over time, this patient had a stable pattern of multiple left fronto-temporal activations in language fMRI. This represents a functionally qualified intrahemispheric adaption due to cortical plasticity of the language network within the affected dominant hemisphere.

Patient 2

The patient was examined for the first time when he was aged 29 years and suffered from a high-grade glioma growing in the left frontal lobe confirmed to be an anaplastic oligodendroglioma of WHO III. The clinical neurological examination did not reveal a focal deficit, the results of the neuropsychological assessment confirmed right handedness and a below average score for verbal fluency (percent-rank 30%), while the other tests showed average or even above average scores.

Initial fMRI for language demonstrated a left hemispheric activity at the borderline of tumor and tissue with normal T1-signal intensity in MRI in the inferior frontal gyrus of the left hemisphere ("Broca's Area"), but additionally showed a similar activation in the inferior frontal gyrus of the right hemisphere ("Broca analogue"). No further activation was seen in the left frontal lobe due to the large tumor mass (Fig. 19.4). Given the picture of a large high-grade glioma in eloquent cortex with a moderate clinical impairment (well controlled epilepsy, moderate cognitive deficits) the patient was chosen for combined surgical resection and consecutive irradiation therapy.

Partial resection of the tumor (using fMRI-guided intraoperative cortical stimulation mapping for language testing) resulted in a significant reduction of the mass effect, and language fMRI confirmed the bilateral Broca-activation in the sentence completion task. The clinical status nine months after the surgery was unchanged and the neuropsychological tests showed a trend towards lower percent-ranks, but did not demonstrate a substantial worsening.

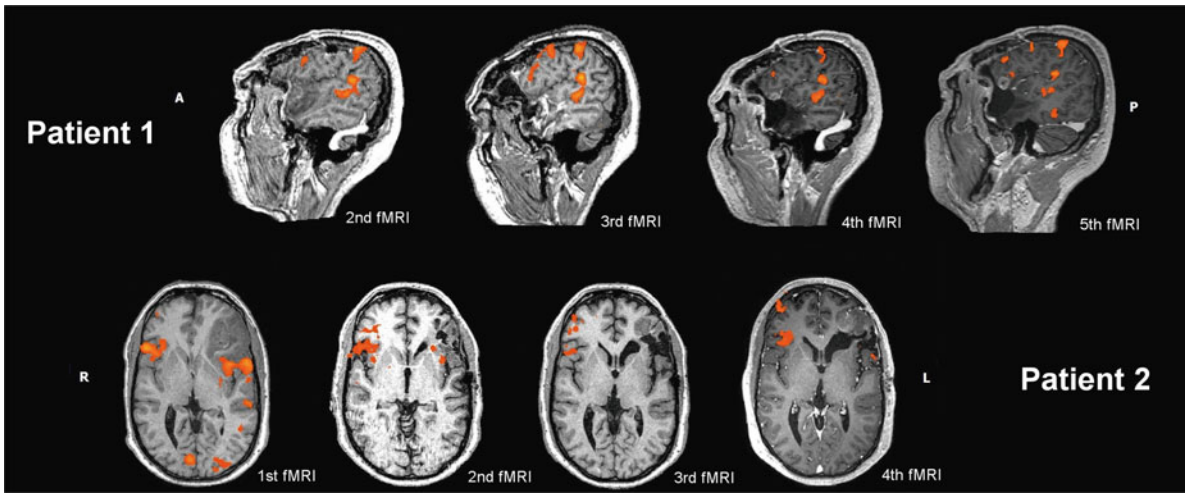

Fig. 19.4 Representative similar sections from the longitudinal language fMRI-sessions of patient 1 (four subsequent measurements, sagittal sections of the left hemisphere, *top row*) and patient 2 (4 subsequent scans, transversal sections, *bottom row*) using the same paradigm and contrast, please compare to the section *Patients with Longitudinal Language-fMRI in Gliomas* for details

In the mean time the status remained stable and another follow-up was performed when the patient had become 31 years old and a new enhancement of contrast agent in MRI had appeared during the regular MRI scans. Due to suspicion of a relapse of the high-grade glioma another resection was planned. Functional MRI for language again showed a bilateral pattern of activation, now with the activation of the right hemisphere preponderating the one in the originally "dominant" left hemisphere. The scores of the neuropsychological tests resembled those of the initial assessment. Reresection was performed (again using fMRI-guided intraoperative cortical stimulation mapping for language testing) and was limited in extent by the persistent left-hemispheric language-representation.

On the last follow-up, performed when the patient was 32 years old (∼13 months from the second surgery), the tumor mass had regained in T1-volume, although the volume of contrast-agent was lower than before. Language fMRI now showed a pattern with a clear right hemispheric preponderance, whereas the scores of the neuropsychological tests showed an improvement for verbal fluency and in the visually guided frontal lobe tasks as well as a decrease for the verbally mediated frontal lobe functions and verbal memory.

In this patient, longitudinal language fMRI again was in agreement with the clinical and neuropsychological status and aided in performing a functionally safe surgery two times. Thereby the partial resection of the glioma protected the fMRI activation near the original "Broca Area". Over time, this patient developed a pattern of bilateral language representation in fMRI that was dominated by the right hemispheric activations in the end. This represents an at least partial functionally qualified interhemispheric adaption due to cortical plasticity of the language network with a shift of functions towards the primary nondominant hemisphere.

Discussion

MRI has considerably improved the potential to plan and perform neurosurgery of cerebral space occupying lesions. In particular, neuronavigation allows surgeons to pinpoint to specific areas of the brain or the spine during the planning period as well as during the operation itself. Moreover, the neuronavigation equipment is able to generate a detailed, three-dimensional image of the area of interest. Similar to a driver of a car who uses the global positioning system to find the way on the road, the neurosurgeon relies on these images to confirm the position of his or her instruments in the patient's brain. As the instrument moves, the neuronavigation software calculates position and

transfers the information to the computer, which in turn shows the direction of the moving surgical instrument. The purpose of this system is to guide the surgeon's instrument to a selected target. Then, the neuronavigation system will give specific directions as how to proceed. Therefore, neuronavigation enables neurosurgeons to track instruments in relation to a patient's anatomy and to track the anatomy itself during a surgical procedure. Currently, neuronavigation is an indispensable part of the neurosurgical reality with a significant impact in each neurosurgical procedure. Neuronavigation systems are now used routinely in medical centres throughout the world. Today's neuronavigation systems are versatile and safe, and there are no adverse effects, complications or surgical mortality due to the neuronavigation devices. Image-guided surgery systems can increase accuracy levels in identifying and removing lesions of the CNS. Neuronavigation systems, however, are not robotic in design; the neurosurgeon still holds and guides the surgical instruments. It might be possible that robotics will be integrated with image-guided surgery systems in the future but today's systems are still directly dependent upon the neurosurgeon performing the procedure.

There is a debate on the issue whether intraoperative cortical stimulation mapping (CSM) and presurgical fMRI constitute complementary or contradictory information regarding the localization of brain function on cortical level. Questions to be asked in this context usually are: are both methods directly comparable at all? What is the degree of concordance of both methods? Can one method be substituted by the other one?

First of all, one has to note that there are substantial methodological differences between both approaches that hinder a direct comparison. In the context of presurgical functional mapping, motor function is often reduced to a short repetitive movement ("tapping") that is based on a simple and automated function in which the cortical representation is restricted to well-defined areas. This pattern is quite uniform and most commonly includes the primary sensory-motor cortex (M1/S1), the supplementary motor area (SMA) and the cerebellum. On the other hand, language-stimulation is being treated very differently among research groups. This is also due to the fact that it has many aspects: speaking (overt and soundless/covert), listening, writing, reading, grammar, prosody, naming, verbal fluency, verbal memory, and native and foreign languages. Accordingly, language is arranged in multiple cortical representations interacting in a widespread and dynamic cortical network. A wide variety of fMRI-paradigms for language exists but is not directly comparable. The calculated fMRI-activation maps vary not only according to the paradigm, but also alternative statistical methods including the individual thresholding (p-, q- or z-values) procedures that have influence on the resulting activation maps.

There are several elements of uncertainty within fMRI studies of patients. Amongst others there is the individual degree of compliance by the patient during the data-acquisition and also the amount of movement of the patients during the data-acquisition. During post-processing, the quality of the alignment between functional and structural data and machine-dependent factors of the scanner can influence the results. Generally, there is a variety of tools and statistical models available for computing the activation maps. Although there are no universal standards for quantification and visualization of the data, results can be assumed to be comparable (but not identical) across laboratories. CSM, on the other hand, is performed by application of a local stimulation current directly to the cortex during (awake) surgery. The physiological effect is the induction of a local (synchronous) hyperpolarisation or depolarization that may cause induction or inhibition of brain function. There are numerous methodological variables of CSM, such as the distance of the pins of the bipolar electrode, the frequency and magnitude of the stimulation current, its shape and duration and also the duration of the repetitive or continuous stimulation ("train").

Table 19.1 shows a general view on the stimulation parameters used for CSM from publications of worldwide neurosurgical centres. A wide range of the values used in the different stimulation parameters can be depicted: the amplitude of the stimulation current varies from 2 to 20 mA, the duration of the single stimulation pulse varies from 0.2 to 4.0 ms, the stimulation frequency is 40, 50 or 60 Hz, and there are various wave forms used with a total duration of the stimulation from 1 to 6 s. This shows that, although many neurosurgeons claim CSM to be the "gold standard" of functional mapping, this procedure is not standardized and, therefore, comparisons between different sites performing CSM as well as intermodal comparisons to fMRI are not straight forward.

Table 19.1 Variability of CSM – parameters among studies and centers

Author and year	Clinic located in	L/M	Amplitude (mA)	Single pulse duration (ms)	Frequency of pulses (Hz)	Pulse wave form and total duration of stimulation
Bello et al. (2006, 2008)	Milan/I	L	2 + 0.5 (3.5–5.5)	1.0	60	Train of biphasic square-wave pulses for up to 4 s, amplitude below threshold producing after discharges
Bello et al. (2006), Duffau (2001)	Paris/F	M	+ 2 <18 <4 awake	1.0	60	Biphasic square-wave pulses (1 ms single phase duration) for 1 s, maximum amplitude awake 4 mA
Eisner et al. (2001)	Munich/GER	M/L	5–35 5–20	0.2	50	Train of square-wave pulses for 3–6 s
Fandino et al. (1999)	Zurich/CH	M	2 + 0.5/1 <10	1–4	50–60	"brief" trains of bipolar square-wave pulses
FitzGerald et al. (1997)	Charlestown/USA	M/L	+ 1 3–7	0.5	50	Biphasic pulses (0.5 ms single phase duration !), threshold motor < language
Ojemann et al. (1996)	St. Louis/USA	M/L	0–10 3–5	?	?	Language: amplitude 05–1 mA below threshold producing after discharges
Picht et al. (2006)	Berlin/GER	L	0–20 M 14	?	60 (40)	3 (2–4) sec
Pouratian et al. (2004)	Los Angeles/USA	M/L	+ 2 <16	200	50	5 s train of square pulses, amplitude 2 mA below threshold producing after discharges – motor: single train – language: 5 s intervals
Quinones-Hinojosa et al. (2003)	San Francisco/USA	L	2–6	1.0	60	Biphasic square-waves pulses (1 ms single phase duration)
Roessler et al. (2005)	Vienna/AUS	M	+ 2 < 25	2–4	50	Train of square-waves pulses
Roux et al. (2000, 2003)	Toulouse/F	M L	+ 2	1.0	60	Train of biphasic square-wave pulses, max. 4 s, amplitude below producing after discharges
Rutten et al. (2002)	Utrecht/NL	L	+ 2 M 12 (8–15)	0.3	40	5 s of monophasic square impulses, amplitude below producing after discharges
Seeck et al. (2006)	Genève/CH	L	1–11	0.3	50	Train 2–5 s, amplitude below producing after discharges
Skirboll et al. (1996)	Seattle/USA	L	2–8	–	–	"few" seconds, amplitude below producing after discharges
Skirboll et al. (1996)	Seattle/USA	M	2–16	1.0	60	Train of biphasic, square wave impulses (1 ms single phase duration)
Suess et al. (2006)	Berlin/GER	M	15 ± 8	0.3	400	5 impulses
Yetkin et al. (1997)	Wisconsin/USA	M + L	10	?	?	?

L/M = parameters used for language and/or motor cortical stimulation mapping = values not given in the paper.

Notably, CSM shows a direct cortical effect (induction or disturbance) only if the area of stimulation is essential for the specific brain function, and the investigator has to make sure to monitor all possible effects of the stimulation. CSM also suffers from various elements of uncertainty: the magnitude of the local cortical resistance is not defined and it is not clear whether its magnitude varies spatially, and also the spatial distortion of the signal is not defined. It is at least plausible to argue for the existence of possible remote effects transmitted by associate fibres. In an intraoperative setting it is hardly possible to make sure that all possible effects are being detected. Furthermore, the application of a local cortical current inherits the possibility to cause epileptogenic (after-) discharges and even may induce seizures. Table 19.2 summarizes the divergent methodological difference variables and pitfalls of CSM and fMRI in direct comparison.

In the past, several studies have compared individual findings of fMRI and CSM in patients. It is noted that the use of the terms "specificity" and "sensitivity" seems to be inconsistent in these publications. This is due to the fact that this difference is caused by the (arbitrary) choice of the viewing direction when comparing fMRI with CSM or CSM with fMRI, respectively.

One of the first publications on this issue was done by FitzGerald et al. (1997). They compared the results of five different language fMRI-tasks with the results of CSM in a series of 11 patients with lesions in the dominant hemisphere. Counting the findings that showed a spatial overlap between both methods (the "Touch"-criteria), they calculated a sensitivity of 33–92% and a specificity of 40–88%. Using weaker spatial criteria (both methods within 2 cm) sensitivity increased to 67–100%, while the specificity went down to 0–50% in the individual patients. Overall, the authors reported a wide interpersonal variability with a range of the individual sensitivity from 0 to 100%, the spatial comparison was realized by digitizing intraoperative photographs and overlaying them onto the functional MR language map (FitzGerald et al. 1997).

Roux et al. (2003) reported a comparison between fMRI and CSM in 14 right-handed patients with left hemispheric tumors using naming or verb generation and calculated a sensitivity of 22–36% and a specificity of 97–98%. When using the combined task (naming and verb generation) the values were 59 and 97%, respectively. In this study fMRI was used as the predictor for the calculation in the statistical model (Roux et al. 2003). Rutten et al. (2002) investigated language fMRI and CSM in 13 patients with temporal lobe epilepsy. Their sensitivity was said to be 92% with a specificity of 61%. The authors also calculated a positive predictive value of 51% (range 14–100%) and a negative predictive value of 100% in 10 of the 11 patients (Rutten et al. 2002).

Although sample sizes in these studies were rather small and clinical features as well as the technical setting for fMRI and CSM varied substantially between

Table 19.2 Methodological confrontation of CSM and fMRI

fMRI	*CSM*
Principle	
fMRI shows a *relative hyperperfusion* in brain areas *generally involved* (essentially and supplementarily, no focus on the internal hierarchy) relative to a *control condition*	CSM shows a direct cortical effect (induction or disturbance) only if the area of stimulation is essential for a certain function
Variables	
– Alternatives in analysis/statistical method – Thresholding (p-, q- or z-values) – Clipping	– Distance of the pins of the bipolar electrode – Frequency and amplitude of the stimulation – Shape and duration of the stimulation current – Duration of repetitive or continuous stimulation ("train")
Elements of uncertainty	
– Compliance of the patients during the data-acquisition – Movements of the patients during the data-acquisition – Quality of the alignment between functional and structural data – Machine-dependent factors (MRI scanner) – No universal standard for quantification and visualization of the data	– Cortical resistance not defined – Spatial distortion of the signal not defined – Possible remote effects may occur (associate fibers?) – Are all possible effects detectable? – Possibility of epileptogenic (after-) discharges/induced seizures

centres, these comparative studies suggested that fMRI overall seems to have a good negative predictive value and specificity (true negatives) on the one hand and a rather weak positive predictive value and sensitivity (true positives) on the other hand. The fact that specificity and negative predictive value suggest a good concordance between both methods seems to justify the use of fMRI to pre-screen functionally "silent" cortical regions. This is a proper goal of preinvasive diagnostic procedure because it helps to identify the regions that are accessible for surgery in terms of the cortical transsection needed to make a lesion accessible.

The rather poor sensitivity and positive predictive value for fMRI/CSM may be due to the aforementioned fundamental differences in characterizing a brain function by both methods (essential sites in CSM, nonhierarchical involvement in fMRI), the large interindividual variability of both methods, the diversity of the elements of uncertainty and variables of both methods and also due to the fact that often very different paradigms are used for fMRI and CSM investigations in the same patient.

Consequently, it seems that in terms of pre- and intra-surgical functional mapping, fMRI and CSM are complementary methods and should be used in a synergistic way. One cannot replace one method by the other. Both methods will surely be optimized in the future. A desirable standardization will, thereby, also enable better prospective comparative studies in patients to further evaluate the interaction of both techniques. In particular, fMRI provides essential information in combination with DTI and PET.

Beside the fact that fMRI and DTI techniques are complementary in describing functional and anatomical components of grey and white matter, fMRI is useful to define the seed regions for DTI. The additional information provided by fMRI is important considering the large intersubject anatomical variations of the human brain, particularly in the presence of a space occupying pathological process affecting the spatial position of anatomical landmarks. Thus, fMRI-guided DTI fiber tracking allows the identification of tracking start regions reliably based on functional anatomy rather than solely on anatomical landmarks (Kleiser et al. 2010). This is shown in healthy volunteers as well as in tumor patients. Furthermore, DTI benefits from the combination with fMRI in order to reconstruct fibers related to specific functional areas. In cases of intracranial tumors, the fMRI approach compliments and enhances the accuracy of DTI information for preoperative planning. This is realized by defining the relevant functionally related structures as accurate start regions for fiber tracking with advanced tracking techniques. This is crucial in complex areas such as the (motor)cortex region where many different neuronal systems are tightly packed, especially in the presence of tumors. If start regions are slightly shifted in this area, the combined fMRI/DTI approach can prevent the obstacle of estimating completely different fiber systems which might belong to the target system. The complementary information obtained from fMRI and DTI provides a quantitative estimate related to both the structural integrity of the white matter and the functional status of the interconnected relevant cortical areas that may be displaced or infiltrated by the tumor. This information can be used to enhance pre-surgical planning and intrasurgical decision making, but also to predict post-operative functional outcome and thus improve patient counselling.

In conclusion, a careful design of fMRI paradigms will benefit interpretation of brain imaging results. Many of the important design issues can be dealt with before any fMRI scans are acquired. This is based on prior knowledge regarding the neuronal mechanisms underlying the function of interest and mathematical properties of the input functions. All stages of an fMR imaging experiment are tightly interwoven and slight changes in MR hardware, task design, task performance, or data analysis can significantly change the resulting brain activation maps. Unfortunately, yet no standardization and user-independent fMR imaging protocols that can be easily and reliably used for surgical purposes, or even for simpler tasks, are available. This makes it more difficult, because in general the interpretation of fMR imaging maps requires the common expertise of neurologists, radiologist, psychologists, neurosurgeons, and physicists. Therefore, in the future a standardization of fMRI setup for clinical routine multicenter studies is desirable. In addition, if task performance is not monitored, the investigator is left with uncertainty regarding the cause of poor results and/or unexpected activation pattern.

Additional information is needed from other modalities to increase reliability and to decide which information from which modality in different individual neurosurgical cases is trustful. fMR imaging maps should be used as an adjunct to existing clinical

techniques and be compared with CSM and, in particular, with patients outcome for continuous optimization of fMR imaging protocols. Additional techniques such as iMR will compensate for brain shift and contribute to a better outcome (Liu et al. 2003). The fMRI imaging maps can be implemented in neuronavigational systems for intraoperative use, and confounding factors require a continuous feedback from surgical practice so that fMR imaging protocols can be validated and optimized.

The foremost advantage of MR imaging is that any sensorimotor or cognitive function of interest can, in principle, be studied once appropriate experimental conditions are divides. It is, therefore, not limited to the regions of the brain that have been damaged or to the function that is disturbed. Healthy subjects can also be studied and data can be used for modelling of brain processes. Furthermore, one of the challenges in the next years will be to differentiate between brain areas which are indispensable or not. Pre-surgery fMRI enables studying the individual cortical functional organization before any resection and to map the subcortical structures throughout the resection. It enables to understand the pathophysiology of cerebral eloquent areas, allowing a study of the anatomo-functional connectivity, and to tailor the resection according to individual cortico-subcortical functional boundaries. In addition, post-operative control and longitudinal neuroimaging studies are important to study adaptation of the residual network and to monitor the effects of brain plasticity related to rehabilitation.

References

Auer T, Schwarcz A, Janszky J, Horvath Z, Kosztolanyi P, Doczi T (2007) Application of functional MR-images acquired at low field in planning of neurosurgical operation close to an eloquent brain area. Ideggyogy Sz 60:35–40

Bello L, Acerbi F, Giussani C, Baratta P, Taccone P, Songa V, Fava M, Stocchetti N, Papagno C, Gaini SM (2006) Intraoperative language localization in multilingual patients with gliomas. Neurosurgery 59:115–125

Bello L, Gambini A, Castellano A, Carrabba G, Acerbi F, Fava E, Giussani C, Cadioli M, Blasi V, Casarotti A, Papagno C, Gupta AK, Gaini S, Scotti G, Falini A (2008) Motor and language DTI fiber tracking combined with intraoperative subcortical mapping for surgical removal of gliomas. Neuroimage 39:369–382

Butefisch CM, Kleiser R, Seitz RJ (2006) Post-lesional cerebral reorganisation: evidence from functional neuroimaging and transcranial magnetic stimulation. J Physiol Paris 99: 437–454

Duffau H (2001) Acute functional reorganisation of the human motor cortex during resection of central lesions: a study using intraoperative brain mapping. J Neurol Neurosurg Psychiatry 70:506–513

Eisner W, Steude U, Burtscher J, Bise K (2001) Surgery of lesions in the motor strip combining a stereotactically-guided mini-craniotomy with electrophysiological mapping of the motor cortex. Minim Invasive Neurosurg 44:230–233

Fandino J, Kollias SS, Wieser HG, Valavanis A, Yonekawa Y (1999) Intraoperative validation of functional magnetic resonance imaging and cortical reorganization patterns in patients with brain tumors involving the primary motor cortex. J Neurosurg 91:238–250

FitzGerald DB, Cosgrove GR, Ronner S, Jiang H, Buchbinder BR, Belliveau JW, Rosen BR, Benson RR (1997) Location of language in the cortex: a comparison between functional MR imaging and electrocortical stimulation. AJNR Am J Neuroradiol 18:1529–1539

Goebell E, Paustenbach S, Vaeterlein O, Ding XQ, Heese O, Fiehler J, Kucinski T, Hagel C, Westphal M, Zeumer H (2006) Low-grade and anaplastic gliomas: differences in architecture evaluated with diffusion-tensor MR imaging. Radiology 239:217–222

Gumprecht H, Ebel GK, Auer DP, Lumenta CB (2002) Neuronavigation and functional MRI for surgery in patients with lesion in eloquent brain areas. Minim Invasive Neurosurg 45:151–153

Guye M, Parker GJ, Symms M, Boulby P, Wheeler-Kingshott CA, Salek-Haddadi A, Barker GJ, Duncan JS (2003) Combined functional MRI and tractography to demonstrate the connectivity of the human primary motor cortex in vivo. Neuroimage 19:1349–1360

Jenkinson MD, du Plessis DG, Walker C, Smith TS (2007) Advanced MRI in the management of adult gliomas. Br J Neurosurg 21:550–561

Jones DK (2003) Determining and visualizing uncertainty in estimates of fiber orientation from diffusion tensor MRI. Magn Reson Med 49:7–12

Jorgens S, Kleiser R, Indefrey P, Seitz RJ (2007) Handedness and functional MRI-activation patterns in sentence processing. Neuroreport 18:1339–1343

Kleiser R, Staempfli P, Valavanis A, Boesiger P, Kollias S (2010) Impact of fMRI-guided advanced DTI fiber tracking techniques on their clinical applications in patients with brain tumors. Neuroradiology 52:37–46

Kleiser R, Wittsack HJ, Butefisch CM, Jorgens S, Seitz RJ (2005) Functional activation within the PI-DWI mismatch region in recovery from ischemic stroke: preliminary observations. Neuroimage 24:515–523

Krings T, Topper R, Willmes K, Reinges MH, Gilsbach JM, Thron A (2002) Activation in primary and secondary motor areas in patients with CNS neoplasms and weakness. Neurology 58:381–390

Lazar M, Alexander AL (2003) An error analysis of white matter tractography methods: synthetic diffusion tensor field simulations. Neuroimage 20:1140–1153

Liu H, Hall WA, Truwit CL (2003) The roles of functional MRI in MR-guided neurosurgery in a combined 1.5 Tesla MR-operating room. Acta Neurochir Suppl 85:127–135

Mori S, van Zijl PC (2002) Fiber tracking: principles and strategies – a technical review. NMR Biomed 15:468–480

Nariai T, Senda M, Ishii K, Maehara T, Wakabayashi S, Toyama H, Ishiwata K, Hirakawa K (1997) Three-dimensional imaging of cortical structure, function and glioma for tumor resection. J Nucl Med 38:1563–1568

Nickel J, Sabel M, Floeth F, Stoffels G, Langen KJ, Seitz RJ (2007) Multimodal Evaluation of Brain Tumours – FET-PET, fMRI and Cortical Stimulation Mapping for Tailoring Therapy. J Neurol 254 (Suppl. 3):III/9

Ojemann JG, Miller JW, Silbergeld DL (1996) Preserved function in brain invaded by tumor. Neurosurgery 39:253–258

Parker GJ, Wheeler-Kingshott CA, Barker GJ (2002) Estimating distributed anatomical connectivity using fast marching methods and diffusion tensor imaging. IEEE Trans Med Imaging 21:505–512

Pauleit D, Floeth F, Hamacher K, Riemenschneider MJ, Reifenberger G, Muller HW, Zilles K, Coenen HH, Langen KJ (2005) O-(2-[18F]fluoroethyl)-L-tyrosine PET combined with MRI improves the diagnostic assessment of cerebral gliomas. Brain 128:678–687

Picht T, Kombos T, Gramm HJ, Brock M, Suess O (2006) Multimodal protocol for awake craniotomy in language cortex tumour surgery. Acta Neurochir (Wien) 148:127–137

Pirotte B, Neugroschl C, Metens T, Wikler D, Denolin V, Voordecker P, Joffroy A, Massager N, Brotchi J, Levivier M, Baleriaux D (2005) Comparison of functional MR imaging guidance to electrical cortical mapping for targeting selective motor cortex areas in neuropathic pain: a study based on intraoperative stereotactic navigation. AJNR Am J Neuroradiol 26:2256–2266

Pouratian N, Cannestra AF, Bookheimer SY, Martin NA, Toga AW (2004) Variability of intraoperative electrocortical stimulation mapping parameters across and within individuals. J Neurosurg 101:458–466

Quinones-Hinojosa A, Ojemann SG, Sanai N, Dillon WP, Berger MS (2003) Preoperative correlation of intraoperative cortical mapping with magnetic resonance imaging landmarks to predict localization of the Broca area. J Neurosurg 99:311–318

Rachinger W, Goetz C, Popperl G, Gildehaus FJ, Kreth FW, Holtmannspotter M, Herms J, Koch W, Tatsch K, Tonn JC (2005) Positron emission tomography with O-(2-[18F]fluoroethyl)-L-tyrosine versus magnetic resonance imaging in the diagnosis of recurrent gliomas. Neurosurgery 57:505–511

Roessler K, Donat M, Lanzenberger R, Novak K, Geissler A, Gartus A, Tahamtan AR, Milakara D, Czech T, Barth M, Knosp E, Beisteiner R (2005) Evaluation of preoperative high magnetic field motor functional MRI (3 Tesla) in glioma patients by navigated electrocortical stimulation and postoperative outcome. J Neurol Neurosurg Psychiatry 76:1152–1157

Roux FE, Boulanouar K, Ibarrola D, Tremoulet M, Chollet F, Berry I (2000) Functional MRI and intraoperative brain mapping to evaluate brain plasticity in patients with brain tumours and hemiparesis. J Neurol Neurosurg Psychiatry 69:453–463

Roux FE, Boulanouar K, Lotterie JA, Mejdoubi M, LeSage JP, Berry I (2003) Language functional magnetic resonance imaging in preoperative assessment of language areas: correlation with direct cortical stimulation. Neurosurgery 52:1335–1345

Rutten GJ, Ramsey NF, van Rijen PC, Noordmans HJ, van Veelen CW (2002) Development of a functional magnetic resonance imaging protocol for intraoperative localization of critical temporoparietal language areas. Ann Neurol 51: 350–360

Sach M, Seitz RJ, Indefrey P (2004) Unified inflectional processing of regular and irregular verbs: a PET study. Neuroreport 15:533–537

Schonberg T, Pianka P, Hendler T, Pasternak O, Assaf Y (2006) Characterization of displaced white matter by brain tumors using combined DTI and fMRI. Neuroimage 30: 1100–1111

Seeck M, Pegna AJ, Ortigue S, Spinelli L, Dessibourg CA, Delavelle J, Blanke O, Michel CM, Landis T, Villemure JG (2006) Speech arrest with stimulation may not reliably predict language deficit after epilepsy surgery. Neurology 66:592–594

Seitz RJ, Huang Y, Knorr U, Tellmann L, Herzog H, Freund HJ (1995) Large-scale plasticity of the human motor cortex. Neuroreport 6:742–744

Skirboll SS, Ojemann GA, Berger MS, Lettich E, Winn HR (1996) Functional cortex and subcortical white matter located within gliomas. Neurosurgery 38:678–684

Staempfli P, Rienmueller A, Reischauer C, Valavanis A, Boesiger P, Kollias S (2007) Reconstruction of the human visual system based on DTI fiber tracking. J Magn Reson Imaging 26:886–893

Suess O, Suess S, Brock M, Kombos T (2006) Intraoperative electrocortical stimulation of Brodman area 4: a 10-year analysis of 255 cases. Head Face Med 2:20

Tournier JD, Calamante F, King MD, Gadian DG, Connelly A (2002) Limitations and requirements of diffusion tensor fiber tracking: an assessment using simulations. Magn Reson Med 47:701–708

Vlieger EJ, Majoie CB, Leenstra S, den Heeten GJ (2004) Functional magnetic resonance imaging for neurosurgical planning in neurooncology. Eur Radiol 14:1143–1153

Witwer BP, Moftakhar R, Hasan KM, Deshmukh P, Haughton V, Field A, Arfanakis K, Noyes J, Moritz CH, Meyerand ME, Rowley HA, Alexander AL, Badie B (2002) Diffusion-tensor imaging of white matter tracts in patients with cerebral neoplasm. J Neurosurg 97:568–575

Wu JS, Zhou LF, Gao GJ, Mao Y, Du GH (2004) Integrating functional magnetic resonance imaging in neuronavigation surgery of brain tumors involving motor cortex. Zhonghua Yi Xue Za Zhi 84:632–636

Wunderlich G, Knorr U, Herzog H, Kiwit JC, Freund HJ, Seitz RJ (1998) Precentral glioma location determines the displacement of cortical hand representation. Neurosurgery 42:18–26

Wurm G, Fellner FA (2004) Implementation of T2*-weighted MR for multimodal image guidance in cerebral cavernomas. Neuroimage 22:841–846

Wurm G, Ringler H, Knogler F, Schnizer M (2003) Evaluation of neuronavigation in lesional and non-lesional epilepsy surgery. Comput Aided Surg 8:204–214

Wurm G, Wies W, Schnizer M, Trenkler J, Holl K (2000) Advanced surgical approach for selective amygdalohippocampectomy through neuronavigation. Neurosurgery 46:1377–1382

Yetkin FZ, Mueller WM, Morris GL, McAuliffe TL, Ulmer JL, Cox RW, Daniels DL, Haughton VM (1997) Functional MR activation correlated with intraoperative cortical mapping. AJNR Am J Neuroradiol 18:1311–1315

Zhang Y, Wang S, Zhuo Y, Yang MQ, Zhao YL, Zhang D, Wang R, Xu L, Wang B, Chen L, Zhao JZ (2008) Functional magnetic resonance imaging-integrated neuronavigation and protection of brain function. Zhonghua Yi Xue Za Zhi 88:2–6

Zhao J, Wang Y, Kang S, Wang S, Wang J, Wang R, Zhao Y (2007) The benefit of neuronavigation for the treatment of patients with intracerebral cavernous malformations. Neurosurg Rev 30:313–318

Chapter 20

Trigeminal Neuralgia: Diagnosis Using 3-D Magnetic Resonance Multi-Fusion Imaging

Toru Satoh, Keisuke Onoda, and Isao Date

Abstract Most instances of idiopathic trigeminal neuralgia (TN) are caused by neurovascular contact (NVC) between the offending vessels and the affected trigeminal nerve. Pre-treatment analysis of the MR imaging findings on the severity of the NVC may predict the outcomes of microvascular decompression (MVD) surgery or radiosurgical treatment. In order to visualize the spatial relationships of the NVC, we have developed a method for three-dimensional (3-D) magnetic resonance (MR) multi-fusion imaging, reconstructed with a perspective volume-rendering algorithm, by compositing co-registered data sets of 3-D MR cisternograms, 3-D MR angiograms (non-contrasted and contrast-enhanced), and 3-D computed tomographic (CT) angiograms in a single 3-D image. Technical aspects of the fusion imaging were documented with some comments regarding the MR sequences to characterize the NVC. Severity analysis of the NVC revealed that the NVC in the affected trigeminal nerve was observed more frequently and much more severely than that at the contra-lateral and normal nerves in controls. Pre-operative MVD surgical simulation and inner-view observation from inside the nerve were depicted for the virtual reality. Moreover, comparative fusion images were reconstructed by superimposing the post-MVD images over pre-MVD simulation, which may confirm the success of the nerve decompression by surgical treatment. Consequently, the 3-D MR multi-fusion imaging may be useful for adjunctive diagnosis, planning of the best treatment strategy, and post-treatment follow-up in patients with TN.

Keywords Trigeminal neuralgia · Neurovascular compression syndrome · Cranial nerves · Meckel cave · MVD · NVC

Introduction

Idiopathic trigeminal neuralgia (TN) is a neurovascular compression syndrome caused by hyperactive dysfunction of the cranial nerves (Jannetta 1977) and is characterized by paroxysmal, lancinating facial pains, or a variety of sensory experiences. TN is the most common neuralgia with an annual incidence of 27 cases per 100,000 persons every year (Bennetto et al. 2007). The incidence is higher in females and increases with age. Most instances are caused by the neurovascular contact (NVC) between the offending vessels and the affected trigeminal nerve along the course from the orifice of the Meckel cave to the rootlet at the brainstem. Diagnosis of the TN is primarily established based on the clinical features of the facial pains, which initially responds to carbamazepine. In addition, the existence of a suspected NVC depicted by neuroradiological studies can be a valuable adjunctive in confirming a diagnosis, and may be important in the decision-making process when determining the best treatment strategy for patients with TN.

Recent advances in magnetic resonance (MR) imaging technology have provided us with fine volumetric data regarding the anatomic elements composing the NVC, including the trigeminal nerve and artery or vein, with surrounding brain parenchyma, dura

T. Satoh (✉)
Department of Neurological Surgery, Ryofukai Satoh Neurosurgical Hospital, 5-23-23 Matsunaga, Fukuyama, Hiroshima 729-0104, Japan
e-mail: ucsfbtrc@urban.ne.jp

M.A. Hayat (ed.), *Tumors of the Central Nervous System, Volume 4*,
DOI 10.1007/978-94-007-1706-0_20,

mater, and cranial base bones. The offending vessels causing the NVC can be seen on the source images in a two-dimensional (2-D) planar fashion. However, a physician can discern the spatial relationships of the nerve–vessel complex more easily in three-dimensional (3-D) displays. By using the most up-to-date image-reconstruction techniques with post-processing computer medical visualization software, the precise architecture of a complicated NVC can be virtually depicted in 3-D.

We have developed a 3-D MR multi-fusion imaging technique by compositing co-registered data sets of a 3-D MR cisternogram, a 3-D MR angiogram (non-contrasted and contrast-enhanced), and a 3-D computed tomographic (CT) angiogram in a single 3-D image (Satoh et al. 2007a, b; 2009). With these images, the characteristics of the NVC, especially regarding the severity of compression, can be morphologically classified and evaluated not only from outside as a virtual surgical simulation but also from inside the nerve or vessels as a virtual inner-view observation. Moreover, comparative fusion imaging for pre- and post-microvascular decompression (MVD) surgical simulation can confirm the success of the nerve decompression by the MVD surgery during post-operative follow-up period. The usefulness of 3-D MR multi-fusion imaging for diagnosis, treatment planning, and post-treatment follow-up in patients with TN is discussed herein.

Technical Aspects on the 3-D MR Multi-Fusion Imaging

Imaging Procedure

MR cisternography: Imaging was performed with MR imaging scanners (Signa Excite EchoSpeed 1.5 T; GE Healthcare, Milwaukee, Wis). The heavily T2-weighted MR cisternography was performed with a standard quadrature head coil, using a 3D fast spin-echo (FSE) sequence with the following parameters: TR/ TE, 4000/ 160 ms; NEX, 1; echo-train length, 128; bandwidth, 41.67–15.63 kHz; matrix, 256 × 256; section thickness, 0.6 mm; section interval, 0.6 mm; FOV, 16 cm; voxel size, 0.6 × 0.6 × 0.6 mm; and total imaging time, 768–803 sec. A total of 96 continuous axial source images were acquired. Alternatively, so-called steady-state "T2 high-resolution" MR cisternography was conducted by a fast imaging employing steady-state acquisition-phase cycling (FIESTA) sequence with the following parameters: TR/ TE, 6.4/2.6 ms; NEX, 1; section thickness, 0.6 mm; FOV, 16 cm; voxel size, 0.6 × 0.6 × 0.6 mm; total imaging time, 301 s; source images 96.

MR angiography: With the same scanning baseline, MR angiography (non-contrasted) was carried out by using a 3D time-of-flight spoiled gradient-recalled (TOF SPGR) sequence: TR/TE, 25–35/4.0–2.6 ms; NEX, 2; flip angle, 20°; matrix, 192 × 128; section thickness, 1.2 mm; section interval, 0.6 mm; FOV, 16 cm; without magnetization transfer contrast; zero-fill interpolation processing, 2 times; 120 sections in total (two slabs); overlap of eight sections; voxel size, 0.8 × 1.3 × 0.6 mm; and total imaging time, 468–529 s. A total of 104 continuous axial source images were obtained. In addition, contrast-enhanced MR angiography was repeatedly performed and was started 3 min after 0.1 mmol/kg intravenous administration of meglumine gadopentate (Magnevist; Schering Japan Co., Tokyo, Japan) via the antecubital vein.

CT angiography: Independently, CT angiography was performed by using a multi-detector CT scanner (Activion-16; Toshiba Medical Systems, Tokyo, Japan). The protocol used was as follows: 100 mL of Iomeron (iodine concentration 350 mg/mL; Eizai Pharmaceutical, Tokyo, Japan) injected at a rate of 3 mL/s into the antecubital vein with a power injector (Dynamic CT injector MCT320P; Medrad, Pittsburgh, PA), table speed of 10 mm/s, 0.5-mm collimation, 120-kV peak, 200 mA, 20-cm field of view, a 512 × 512 matrix; and total imaging time, 8 s. A total of 201 sections were obtained with a section thickness of 0.5 mm. Data from the source axial images were reconstructed every 0.5 mm with a 16-cm field of view on the console, producing voxel size of 0.3 × 0.3 × 0.5 mm.

Image Processing

Technical aspects of reconstruction of the 3-D MR multi-fusion imaging have been described previously (Satoh et al. 2007a, b; 2009). Briefly, all volumetric data sets from the MR cisternography, and the MR and CT angiographies were transferred to a workstation (Ziostation; Ziosoft, Tokyo, Japan). 3-D

MR cisternograms were reconstructed by means of a perspective volume-rendering algorism, where the information regarding the entire area with lower signal intensity than cerebrospinal fluid (CSF) was selected from the whole volume-rendering data set without targeting or trimming of the region of interest. The perspective 3-D MR and 3-D CT angiograms were independently reconstructed by rendering the data sets with higher MR signal intensity and CT attenuation values, respectively, than the background.

The 3-D multi-fusion images were then reconstructed by compositing four co-registered independent data sets, including the heavily T2-weighted 3-D FSE MR cisternogram, or the steady-state "T2 high-resolution" FIESTA MR cisternogram, the TOF SPGR 3-D MR angiogram (non-contrasted and contrast-enhanced), and the steady-state contrast-enhanced subtraction 3-D CT angiogram, in a single 3-D image. The overall time required to reconstruct a picture of multi-fusion imaging was within 90 s per image after the completion of data acquisition.

Comments on MR Sequences

Several MR imaging sequences have been employed to depict the structures composing the NVC, including MR cisternography with FSE sequences or "T2 high-resolution" and MR angiography with or without gadolinium contrast enhancement.

T2-weighted 3-D FSE MR cisternography: Traditional heavily T2-weighted MR cisternography, obtained by using a simple 3-D FSE sequence, with fine adjustment of TR/TE (TR, 4000 ms; TE, 160 ms in the present study), can depict the vascular structures as complete flow voids with a profoundly low signal intensity (black blood), the cranial nerves and brain parenchyma, with moderately low signal intensity, and the CSF, with profoundly high signal intensity (Satoh et al. 2007a, b; 2009). These features may be useful in discriminating the boundary of the offending artery and the vein from the trigeminal nerve within the cerebellopontine angle (CPA) cistern and nerve rootlet at the brainstem.

Steady-state "T2 high-resolution" MR cisternography: In contrast, recent so-called steady-state "T2 high-resolution" MR cisternography, obtained by steady-state sequences such as FIESTA (Chávez et al. 2005), constructive interference in steady-state (CISS) (Naraghi et al. 2004; Leal et al. 2010), and balanced fast field echo (BFFE) (Miller et al. 2008), can depict the intra-cisternal structures including cranial nerves, vascular structures, and brain parenchyma with dark hypo-intense signals (black blood). These structures are in contrasted to the surrounding CSF with bright hyper-intense signals. Several inherent pitfalls may exist when dealing with these "T2 high-resolution" imaging sequences (Satoh et al. 2007a). First, the signal intensities of intra-cisternal anatomical elements are uniform and similar, making it difficult to distinguish the boundary of adjacent nerves and vessels from each other at the site of the NVC. Second, because the images are composites of the gradient echo and spin echo sequences, a relatively hyper-intense area related to susceptibility artifacts can unexpectedly appear within the large vessels. Third, the CSF flow-related artifacts may cause heterogeneous signal intensity distribution within the CPA cistern. This heterogeneity may result in concomitance of the ghost shadows in the intra-cisternal space on the reconstructed images, making it difficult to depict the NVC. The above susceptibility and flow-related artifacts may be enhanced with a higher magnetic field strength imager such as 3-T (Miller et al. 2008) in comparison to those with 1.5-T. Therefore, in the assessment of the NVC, prediction of the offending vessels can be possible, but it is difficult to define the precise severity of the NVC by the steady-state "T2 high-resolution" MR cisternogram alone.

MR angiography: MR angiography obtained by the TOF SPGR sequence is a T1-weighted gradient echo image. By using non-contrasted MR angiography, the cranial nerves and brain parenchyma are depicted with relatively low signal intensity and the CSF with low signal intensity; these are contrasted to the vascular structures with profoundly high signal intensity (bright blood). The arteries and large veins within the CPA cistern are clearly visualized in contrast to the adjacent brainstem and cerebellum. The steady-state contrast-enhanced MR angiography, obtained by the 3-D TOF SPGR sequence with an intravenous administration of contrast medium, can enhance the depiction of vessels with a relatively slow flow velocity due to the T1-shortening effect of intravascular paramagnetic agents. The arterial branches such as the rostral and caudal tributaries of the superior cerebellar artery and venous components such as the superior petrosal veins and their tributaries draining into the petrosal

sinuses are represented more clearly than those with non-contrasted MRA.

Vascular structures represented by the TOF SPGR sequence with or without contrast-enhancement, however, do not indicate the pure luminal morphology, as shown by digital angiography and subtraction CT angiography (Satoh et al. 2004, 2007a). The MR angiogram represents the intravascular flow information caused by an inflow effect related mainly to the peak flow velocity within the vessel lumen, with or without the T1- shortening effect. Due to flow-related artifact, a tortuous and hair-pin curved artery may infrequently show signal loss at the beginning of the branching sites. Moreover, when the offending artery travels tortuously around the NVC, the artery may often be depicted running in an aberrant course just at the site of contact due to complex blood flow-related artifact (Fig. 20.1).

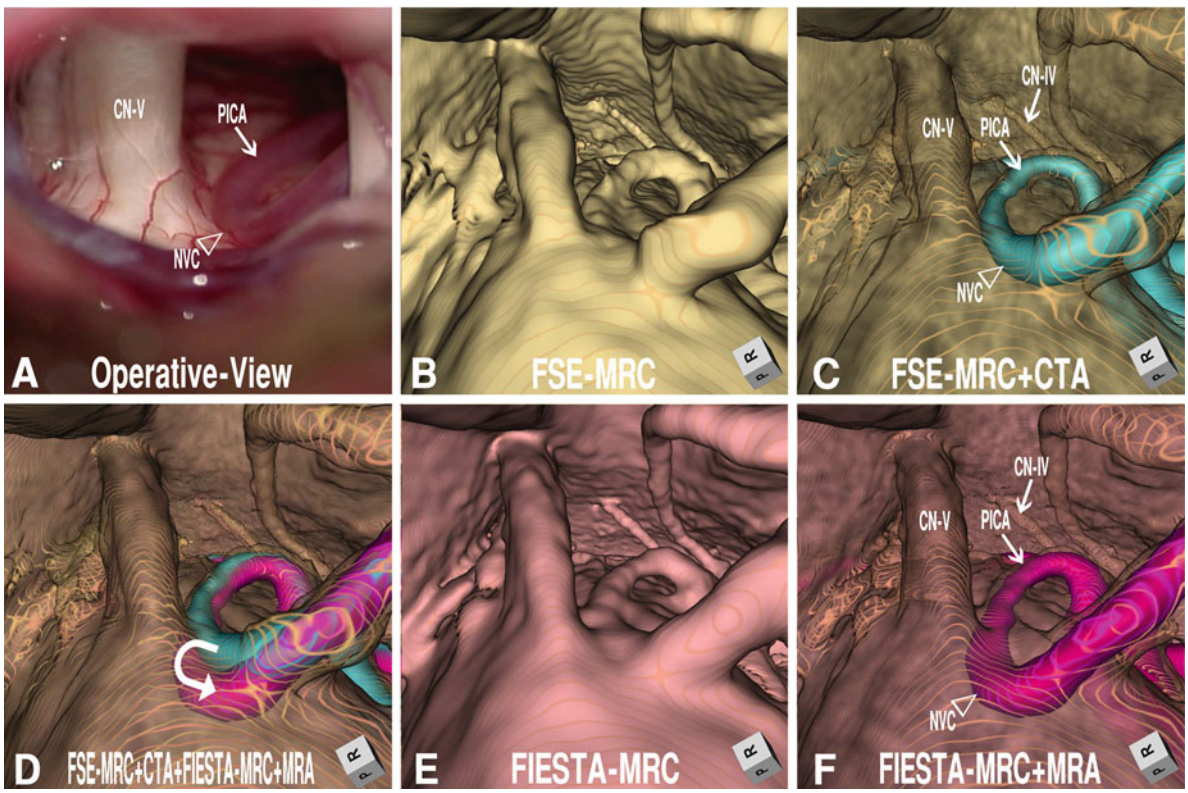

Fig. 20.1 Comparative depiction of the NVC (*right* TN). (**a**) Operative view. The right trigeminal nerve (CN-V) is compressed by the offending posterior inferior cerebellar artery (PICA). The severity of the NVC (*empty-arrowhead*) is classified as moderate at MVD surgery. (**b**) 3-D FSE MR cisternogram (rendered in *brown*) (FSE-MRC), reconstructed by using FSE sequence. (**c**) 3-D MR fusion image compositing of 3-D FSE MR cisternogram (in *brown*) and 3-D CT angiogram (in *bluish-green*) (FSE-MRC+CTA). The offending right PICA runs tortuously and hair-pin curved just at the site of NVC (*empty-arrowhead*), resulting in moderate degree of compression. The anatomical relationship of the NVC and its severity depiction is quite consistent with regard to the actual operative field (**a**). (**d**) Comparative depiction of fusion image of 3-D FIESTA MR cisternogram (in *wine-red*, **f**) and 3-D MR angiogram (in *magenta*, **f**) superimposed over the 3-D FSE MR cisternogram (in *brown*, **c**) and 3-D CT angiogram (in *bluish-green*, **c**) (FSE-MRC +CTA+ FIESTA-MRC+MRA). Difference in the running course of the offending PICA at the NVC (*curved arrow*) between the 3-D MR angiogram with 3-D FIESTA MR cisternogram and the 3-D CT angiogram with 3-D FSE MR cisternogram is clearly depicted. (**e**) 3-D FIESTA MR cisternogram (in *wine-red*), reconstructed by using FIESTA sequence. (**f**) 3-D MR fusion image, compositing of FIESTA MR cisternogram (in *wine-red*) and 3-D MR angiogram (*in magenta*) (FIESTA-MRC+MRA). The offending PICA runs in an aberrant course due to complex blood flow-related artifact with TOF SPGR MR angiogram. The spatial relationship of the NVC depicted by a fusion image in composition of FIESTA MR cisternogram and TOF SPGR MR angiogram looks similar to the operative view (**a**), but is subtly different in the detail. CN-IV, trochlear nerve; CN-V, trigeminal nerve; FIESTA, fast imaging employing steady-state acquisition-phase cycling; FSE, fast spin-echo, MVD, microvascular decompression; NVC, neurovascular contact; PICA, posterior inferior cerebellar artery; TOF SPGR, time-of-flight spoiled gradient-recalled

As mentioned above, with a fusion image reconstructed by compositing the steady-state "T2 high-resolution" MR cisternogram and the MR angiogram, prediction of the offending vessels may be possible, but the arterial components depicted by the MR angiogram may not represent the real degree of compression; this point may require careful consideration in evaluating the severity of the NVC (Fig. 20.1d–f). Instead, a fusion image with a composition of FSE MR cisternogram and CT angiogram can depict the extent of morphological changes between the offending vessels and the affected trigeminal nerve, so that the anatomical relationship of the NVC may be visualized clearly; severity of the NVC can be precisely assessed with this combination (Fig. 20.1b–d).

3-D Image Reconstruction

With the recent progress in computer medical visualization software, 3-D images of MR cisternography, MR angiography, and CT angiography can be reconstructed in a short time. The perspective view makes objects far away seen small, and those close by seen large. These perspective projection images provide 3-D visualization of the anatomical relationships as a virtual endoscopic picture, which is similar to the microscopic view in the neurosurgical operative fields. Though the 3-D reconstructed images do not embody more information than the source 2-D planar data set used to render them, the 3-D images provide spatial relationships of the trigeminal nerve and offending vessels making up the NVC through the clear 3-D visualization of each element with anatomical continuity.

3-D MR Multi-fusion Imaging

The 3-D multi-fusion images are reconstructed by compositing the black blood heavily T2-weighted 3-D FSE MR cisternogram, the bright blood TOF SPGR 3-D MR angiogram (non-contrasted and contrast-enhanced), and the steady-state contrast-enhanced subtraction 3-D CT angiogram in a single 3-D image. We have used it for the pre-operative depiction and severity analysis of NVC in patients with TN. Moreover, the boundary volume-rendering technique is used to depict the boundary of the contours of the intra- and juxta-cisternal objects as a series of clear rings or zebra stripes, so that the underlying structures can be visualized directly through the spaces between rings (Satoh et al. 2004; 2007a, b; 2009). By referring to the overlapped non-contrasted 3-D MR angiogram, contrast-enhanced 3-D MR angiogram and 3-D CT angiogram, the vascular components depicted on the 3-D MR cisternogram (rendered as a series of rings) can be discriminated from the complicated intra-cisternal structures, including the trigeminal nerve and its rootlet at the brainstem. With 3-D MR multi-fusion imaging, the severity of the NVC can be assessed primarily based on the 3-D MR cisternogram, with reference to the vascular components represented on the 3-D MR and CT angiograms.

Serial display of those images may allow for tracing the arteries back to a trunk of the basilar artery or veins to a large vein draining into the superior petrosal vein and sinus, and also trigeminal nerve from the nerve rootlet at the brainstem along to the Meckel cave. We can decide which elements are arteries, veins, and nerves depicted on the 3-D MR cisternogram, and then assess the details of the NVC. The static images and their animated display for surgical simulation can provide virtual reality for surgical access during MVD surgery; those are quite consistent with regard to the actual operative trajectory and fields. Additionally, the 3-D MR multi-fusion imaging may provide us with information regarding both the vascular morphology (FSE 3-D MR cisternogram and 3-D CT angiogram) and the intravascular flow condition (TOF SPGR 3-D MR angiogram) in a single composited 3-D image. Each complements the characteristics and limitations of the other, and may enhance the advantages of each.

Severity Analysis of MR Imaging Findings of the Neurovascular Contact

Incidence and Significance

The pathogenesis of the TN is proposed to be a NVC; however, physicians are often confronted with a diagnostic dilemma in patients with TN due to the lack of a reference standard to detect the NVC. With recent

advances in MR imaging and image-reconstruction techniques, the existence of the NVC is often discovered, or at least suspected, on the affected trigeminal nerve, with an incidence ranging from 57 to 88% (Anderson et al. 2006; Satoh et al. 2009; Miller et al. 2009; Leal et al. 2010). However, the NVC is not infrequently observed on the asymptomatic nerve contra-lateral to the affected side, as well as on the normal trigeminal nerve in a control subject without TN, with an incidence ranging from 17 to 71% (Anderson et al. 2006; Satoh et al. 2009; Miller et al. 2009; Leal et al. 2010). Variations in incidence may not reflect the insensitivity of detecting the NVC, but instead may result from various reference criteria to evaluate the MR imaging findings of the NVC. Furthermore, it remains unclear whether the MR evidence regarding the NVC indicates that the NVC is symptomatic and linked to the cause of TN or asymptomatic and observed incidentally.

Effects on the Clinical Outcomes

As for the intra-operative findings of the NVC (Sindou et al. 2007), outcomes after MVD for TN may be related to the characteristics of the NVC found during surgery. MVD can be similarly effective at proximal and distal locations of the NVC, but the more severe the degree of compression exerted on the nerve root, the better the outcomes in terms of long-term relief after MVD. Moreover, in the treatment with Gamma Knife radiosurgery (Sheehan et al. 2010), pain relief correlates with a higher dose to the point of the NVC. In addition to demyelination of the trigeminal nerve, vessel wall changes as a result of a higher radiation dose may relate to the degree of relief following radiation therapy. The MR evidence regarding the NVC may affect the strategy for the radiosurgical treatment of TN with improvements in radiosurgical targeting, dose planning, and resulting clinical outcomes.

The severity of the NVC may be related to the degree of nerve compression produced by the offending vessels, so that severe NVC may result in morphological changes, including deformation, displacement, distortion, indentation, and atrophy of the trigeminal nerve. The above NVC features can be discerned by the pre-operative MR imaging. Therefore, determination of the severity of the NVC on the MR imaging findings could affect selection of a candidate for the best treatment strategy with respect to good clinical outcomes.

Our Results Regarding the Severity Analysis

By using the 3-D MR fusion imaging, we analyzed the MR imaging findings of the NVC in the affected ($n = 66$), contra-lateral ($n = 66$), and normal ($n = 78$) trigeminal nerves (Satoh et al. 2009). The NVC was observed more frequently in the affected trigeminal nerves (85%, $p < 0.01$, χ^2 test) than in the contra-lateral (35%) and normal (31%) trigeminal nerves. Because an innocent juxtaposition of the trigeminal nerve and vessels occurs with some frequency, the presence of the NVC itself did not appear to be the cause of TN. Therefore, the severity of the NVC was classified as follows: severe, NVC with a vessel contacting the trigeminal nerve covering >20% of the nerve circumference; moderate, with <20% contact; simple, with slight touch; and none. The severity of the NVC in the affected trigeminal nerve showed more severe compression (moderate 30% and severe 38%) than that at the contra-lateral (6 and 0%, respectively) and normal (8 and 0%, respectively) trigeminal nerves ($p < 0.01$, Mann–Whitney U test).

The above results indicate that a trend toward greater compression severity of the NVC is more frequently found at the affected trigeminal nerve than at the contra-lateral and normal trigeminal nerves. Consequently, when moderate-to-severe NVC is observed at the affected trigeminal nerve in patients with TN, the NVC may be a cause of TN. Although a simple NVC may not be sufficient to explain the cause of TN, any degree of NVC in the affected trigeminal nerve may be a cause. In addition, the NVC in patients who underwent MVD surgery for TN was more severe (moderate to severe, 83%) than that in patients with medical treatment (46%, $p < 0.01$, Mann–Whitney U test).

MR imaging findings of the NVC may be an important factor, but it is neither necessary nor sufficient to cause TN (Satoh et al. 2009; Miller et al. 2009). It has been reported that a few patients with TN may not exhibit any evidence of the offending vessels,

but simple morphological changes on the trigeminal nerve, including a curved and deformed running course of the nerve axis (Ishikawa et al. 2002). In these cases, TN may be caused not by a NVC, but an adhesive thickening of the arachnoid membranes or arachnoiditis. Consequently, prediction of the NVC severity using the 3-D MR multi-fusion imaging may provide useful information in selecting patients who are most likely to benefit from MVD surgery or from other approaches such as radiosurgical treatments or percutaneous destructive techniques.

Clinical Application of the 3-D MR Multi-fusion Imaging

Virtual Reality for the Pre-surgical Simulation

With a 3-D MR multi-fusion imaging, the presence of offending vessels and the sites of the NVC can be assessed pre-operatively for surgical simulation, and visualized in a 3-D display from various viewpoints within the CPA cistern. Because retraction of the cerebellar surface and dissection of the arachnoid membranes are usually performed during MVD surgery, the pre-operative visualization of the NVC may not be identical to the intra-operative fields. The displacement of the anatomical elements following surgical manipulation always compromises a comparison of the pre- and intra-operative studies.

In our studies, the shapes and relationships of nerve-vessel structures were compared between the surgical simulation images and the actual intra-operative views (Satoh et al. 2007a, b; 2009). As a result, pre-operative simulation images with 3-D MR multi-fusion imaging through the surgical access (microscopic view) were quite consistent with the intra-operative trajectory and findings. The pre-operative surgical simulation provided not only a realistic depiction, but also further understanding of the spatial anatomical relationships of the NVC beyond the operative view. Moreover, a blinded surgical trajectory can be discerned through endoscopic viewpoints projected from various directions within the CPA cistern (neuroendoscopic view). Consequently, 3-D MR multi-fusion imaging allows the surgeon to look around the trigeminal nerve, to examine its ventral surface, and to trace its vascular anatomy, which may be obscured from view during actual MVD surgery.

Virtual Inner-View for the Severity Analysis

The severity of the NVC has been evaluated based on the source axial or multi-planar reconstruction images; however, the exact site of the NVC may remain unclear due to the difficulties in finding an imaging plane perfectly perpendicular to the course of the nerve in 2D fashion. With the inner-view of the 3-D MR multi-fusion imaging, the 3-D anatomical relationship of the NVC is projected along the nerve axis from the nerve rootlet at the brainstem toward the orifice of the Meckel cave. According to the extent of the nerve circumference in contact with the vessel, the severity of the NVC could be assessed and graded objectively, as described previously (Satoh et al. 2009). Because the 3-D relationships of the NVC can be assessed from inside the affected trigeminal nerve, without interruption caused by the offending vessels compressing the nerve from outside, the inner-view can be a reference standard for assessment of the severity of the NVC.

Comparison Between the Pre- and Post-Surgical Images

For neurosurgeons, 3-D visualization and prediction of the severity of the NVC with 3-D MR multi-fusion imaging in patients with TN can provide not only valuable pre-operative assessment to execute MVD surgery, but also post-operative educational comprehension based on review of the operative videotapes. During the MVD surgery, decompression of the NVC is usually carried out by a transposition of the offending vessels away from the nerve, an interposition of the prosthetic materials between the vessels and the brainstem, or, if necessary, a coagulation and excision of the certain offending veins (Ichikawa et al. 2011).

In the past, after the completion of MVD surgery, however, there has been nothing to confirm the

success of the above surgical intervention. However, by reconstructing the 3-D MR fusion imaging post-operatively, spatial and anatomical relationships between the decompressed trigeminal nerve and the former offending vessels after MVD surgery can easily be depicted and assessed in 3-D. In comparison with the pre-operative fusion images, post-operative images confirm the disappearance of compression at the NVC (Fig. 20.2). The former offending artery transposed away from the nerve or moved over the interposed prosthetic material can easily be depicted in 3-D.

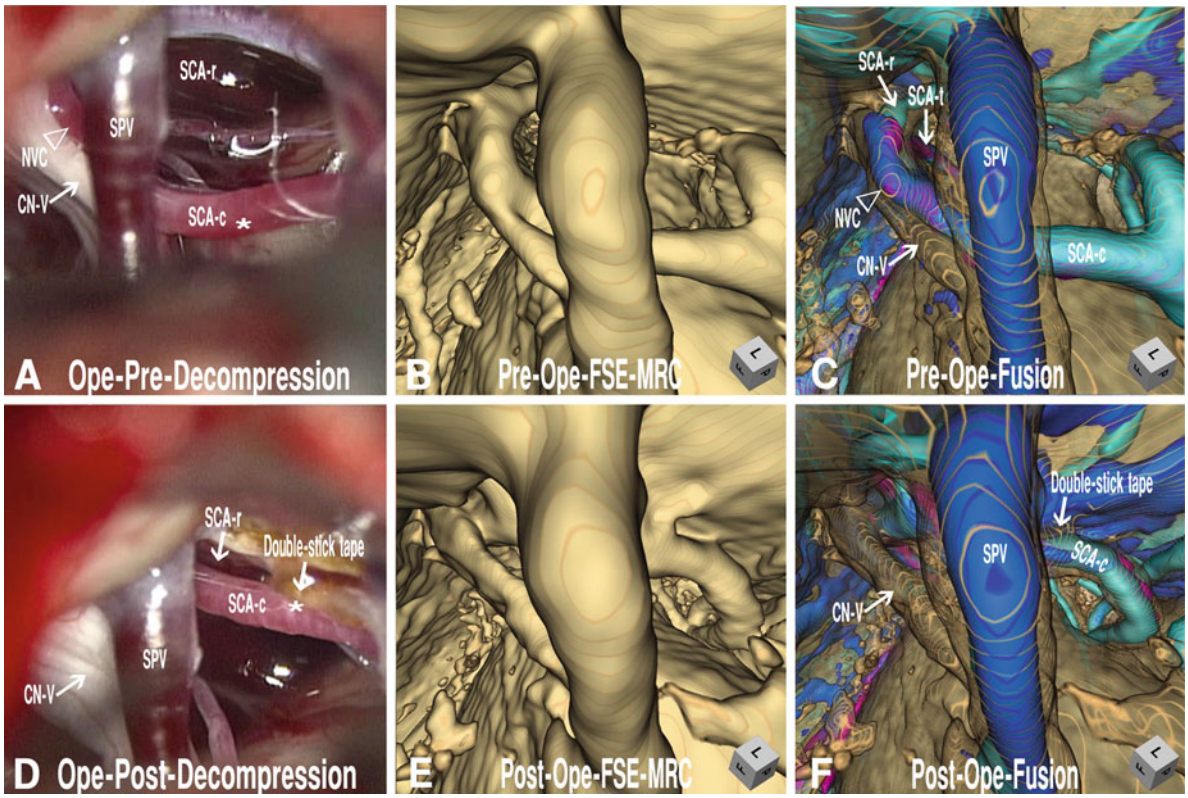

Fig. 20.2 Comparative depiction of the pre- and post-MVD surgical simulation (*right* TN). (**a**) Operative view before decompression of the NVC (Ope-Pre-Decompression). The right trigeminal nerve is severely compressed by the offending right SCA. The NVC (*empty-arrowhead*) is shown at the mid-1/3 in the cisternal course of the trigeminal nerve from the superomedial direction by the trunk of the SCA (SCA-t) bifurcating into the rostral (SCA-r) and caudal (SCA-c*) tributaries. (**b**) Pre-operative 3-D FSE MR cisternogram (rendered in *brown*) (Pre-Ope-FSE MRC). (**c**) Pre-operative 3-D MR multi-fusion image for MVD simulation (Pre-Ope-Fusion), reconstructed by compositing of 3-D FSE MR cisternogram (in *brown*), 3-D MR angiogram (non-contrasted in magenta, contrast-enhanced in indigo), and 3-D CT angiogram (in *bluish-green*). The anatomical relationship of the NVC (*empty-arrowhead*) is consistent with the operative field (**a**). (**d**) Operative view after decompression of the NVC (Ope-Post-Decompression). The offending caudal tributary of the right SCA (SCA-c*) is transposed to the tentorium by using double-stick tape, resulting in decompression of the NVC. (**e**) Post-operative 3-D FSE MR cisternogram (in *brown*) (Post-Ope-FSE-MRC). (**f**) Post-operative 3-D MR multi-fusion image for MVD simulation (Post-Ope-Fusion); a composition of 3-D FSE MR cisternogram (in *brown*), 3-D MR angiogram (non-contrasted in *magenta*, contrast-enhanced in *indigo*), and 3-D CT angiogram (*bluish-green*). In comparison with the pre-operative images (**b**, **c**), post-operative images (**e**, **f**) depict the anatomical relationship of the NVC, and confirms the complete decompression of the NVC. The affected nerve with deformation and bended nerve axis before MVD restores the normal columnar shape and straight running course after MVD. CN-V, trigeminal nerve; FSE, fast spin-echo, MVD, microvascular decompression; NVC, neurovascular contact; NVC, neurovascular contact; SCA-c, caudal tributary of the superior cerebellar artery; SCA-r, rostral tributary of the superior cerebellar artery; SCA-t, trunk of the superior cerebellar artery; SPV, superior petrosal vein; PICA, posterior inferior cerebellar artery

When the decompression of the affected nerves has been successfully completed by MVD surgery, the nerves may be restored to their normal and original shapes (Fig. 20.2). Due to the reversibility inherent in the nerve itself, pre-operative findings of the certain morphological changes may be recovered post-operatively. After MVD surgery, affected nerves with deformation, distortion, and indentation may be recovered to elliptic and columnar in shape. In addition, the deformed nerve axis and displaced running course of the affected nerve can be returned to its normal shape within the CPA cistern. Reversibility of nerve morphology may be observed intra-operatively before completion of MVD surgery, but precise restoration of the nerve shape can be depicted and assessed with a post-operative fusion imaging. As a result, with comparison between the pre- and post-MVD fusion images, it is possible to understand and confirm the dissolution of the NVC by MVD surgery.

Comparative Fusion Imaging for Pre- and Post-Surgical Simulation

Moreover, we can reconstruct comparative images by superimposing the post-operative 3-D MR cisternograms, 3-D MR angiograms (non-contrasted and contrast-enhanced), and 3-D CT angiograms over the pre-operative simulation images. With the comparative fusion images for pre- and post-MVD simulation, alteration in the anatomical elements making of the NVC may be depicted and compared directly and widely beyond the limits of the operative fields. In the case of the trigeminal nerve compressed and penetrated by a large tributary vein emptying in to the superior petrosal vein and sinus, pre-operative assessment of the venous draining pathway may provide useful information as to whether that vein can be sacrificed and excised (Fig. 20.3). After cutting off the offending vein during MVD surgery, an alternative venous pathway draining into the superior petrosal sinus via the other superior petrosal veins, instead of the sacrificed vein, can be depicted and confirmed. As a result, with comparative fusion imaging for pre- and post-MVD simulation, it may be possible to assess the success, insufficiency, or failure of the surgical treatment during the post-operative follow-up period.

Comparative 3-D MR Multi-fusion Imaging for Recurrence

Finally, in cases that the patient's symptoms of TN might recur again, repeated study of the 3-D MR multi-fusion imaging may provide useful information for the treatment strategy. The cause of recurrence (Amador and Pollock 2008) can be discerned, as can whether re-compression of the nerve occurred due to slipping out of the interposed materials or re-positioning of the displaced vessels. Alternatively, granuloma formation around the inserted materials, the existence of another offending vessel originating afterwards, deformity of the nerve axis due to adhesion and arachnoiditis might cause recurrence of TN. With the fusion imaging, the cause to the recurrence of TN after MVD surgery can be predicted in some cases. The above results may contribute to the selection of patients who are most likely to benefit from re-execution of MVD surgery. The comparative 3-D MR multi-fusion imaging may provide valuable information regarding the decision-making process for the best treatment strategy in either cases of primary and recurrent TN.

In conclusion, diagnosis of the TN is primarily established based on the clinical features of facial pains, so that MR imaging findings of NVC alone do not necessarily establish it as a cause of TN. However, MR evidence of the existence of a suspected NVC can be a valuable adjunctive to confirm the diagnosis. Prediction of the severity of the NVC with 3-D MR fusion imaging may provide useful information in selecting patients who are most likely to benefit from MVD surgery or from other approaches such as radiosurgical treatment or percutaneous destructive techniques. Moreover, comparative fusion images reconstructed by superimposition of the post-MVD images over pre-MVD simulation can confirm the success of the nerve decompression by the MVD surgery. Consequently, 3-D MR multi-fusion imaging could become a powerful tool to discern the real NVC, and may be useful for the diagnosis, planning of best treatment strategy, and follow-up in patients with TN. More work is required to validate the imaging techniques with improvements in the computer medical visualization software, to qualify the source volumetric data sets, and then to clarify the significance of the MR imaging findings of the NVC regarding the pathogenesis of TN.

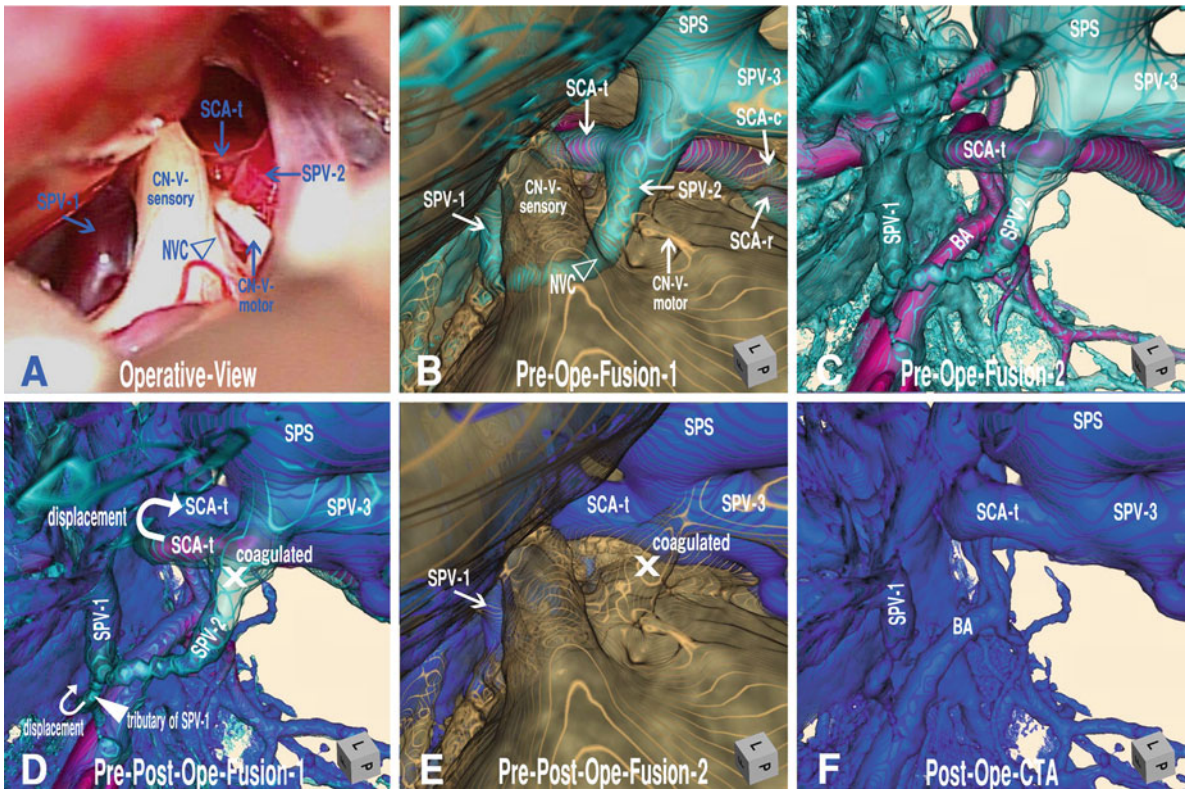

Fig. 20.3 Comparative fusion imaging for pre- and post-MVD simulation (*left* TN). (**a**) Operative view of the NVC before surgical intervention (Operative-View). The left trigeminal nerve is compressed and penetrated by the offending superior petrosal vein (SPV-2) at the proximal 1/3 in the cisternal course of the nerve. Decompression of the NVC (*empty-arrowhead*) is accomplished by a coagulation and excision of the SPV-2. (**b**) Pre-operative 3-D MR multi-fusion image for MVD simulation (Pre-Ope-Fusion-1), reconstructed by compositing of 3-D FSE MR cisternogram (rendered in *brown*), 3-D MR angiogram (non-contrasted, in *magenta*), and 3-D CT angiogram (in *bluish-green*). The anatomical relationship of the NVC is quite consistent with the actual operative field (**a**). (**c**) Pre-operative fusion image for vascular simulation (Pre-Ope-Fusion-2), by compositing of 3-D MR angiogram (non-contrasted, in *magenta*) and 3-D CT angiogram (in *bluish-green*). Pre-operative arterial and venous draining pathway is assessed widely beyond the limits of the operative fields (**a**). (**d**) Pre- and post-operative comparative fusion image for vascular simulation (Pre-Post-Ope-Fusion-1), by compositing of the pre-operative 3-D MR angiogram (non-contrasted, in *magenta*), pre-operative 3-D CT angiogram (in *bluish-green*), and superimposed post-operative 3-D CT angiogram (in *indigo*). After coagulated and cutting off the offending vein (SPV-2, **X**) during MVD surgery, an alternative venous pathway draining into the superior petrosal sinus via the other superior petrosal veins (SPV-1, SPV-3), instead of the sacrificed vein (SPV-2), is depicted clearly. *Curved arrows* indicate the movement of trunk of the SCA (SCA-t) and a tributary of the superior petrosal vein (*arrowhead*) draining into the SPV-1, respectively, by the surgical intervention. (**e**) Comparative pre- and post-operative fusion image (Pre-Pos-Ope-Fusion-2); post-operative 3-D CT angiogram (in *indigo*) superimposed over the pre-operative 3-D FSE MR cisternogram (in *brown*). The effect of the surgical intervention is indicated (**X**) in relation to the post-operative remaining vascular structures. (**f**) Post-operative 3-D CT angiogram (in *indigo*) (Post-Ope-CTA), showing the post-operative vascular anatomy for comparison to the pre-operative image (**b**–**d**). BA, basilar artery; CN-V-motor, motor bundle of the trigeminal nerve; CN-V-sensory, sensory bundle of the trigeminal nerve; FSE, fast spin-echo, MVD, microvascular decompression; NVC, neurovascular contact; NVC, neurovascular contact; SCA-c, caudal tributary of the superior cerebellar artery; SCA-r, rostral tributary of the superior cerebellar artery; SCA-t, trunk of the superior cerebellar artery; SPV, superior petrosal vein

References

Amador N, Pollock BE (2008) Repeat posterior fossa exploration for patients with persistent or recurrent idiopathic trigeminal neuralgia. J Neurosurg 108: 916–920

Anderson VC, Berryhill PC, Sandquist MA, Ciaverella DP, Nesbit GM, Burchiel KJ (2006) High-resolution three-dimensional magnetic resonance angiography and three-dimensional spoiled gradient-recalled imaging in the evaluation of neurovascular compression in patients with trigeminal neuralgia: a double-blinded pilot study. Neurosurgery 58:666–673

Bennetto L, Patel NK, Fuller G (2007) Trigeminal neuralgia and its management. BMJ 334:201–205

Chávez GR, Antonio AF, De Salles AAF, Solberg TD, Pedroso A, Espinoza D, Villablanca P (2005) Three-dimensional fast imaging employing steady-state acquisition magnetic resonance imaging for stereotactic radiosurgery of trigeminal neuralgia. Neurosurgery 56:E628

Ichikawa T, Agari T, Kurozumi K, Maruo T, Satoh T, Date I (2011) 'Double-stick tape' technique for transposition of an offending vessel in microvascular decompression: technical case report. Neurosurgery 68:onsE377–382

Ishikawa M, Nishi S, Aoki T (2002) Operative findings in cases of trigeminal neuralgia without vascular compression: Proposal of a different mechanism. J Clin Neurosci 9:200–204

Jannetta PJ (1977) Observations on the etiology of trigeminal neuralgia, hemifacial spasm, acoustic nerve dysfunction and glossopharyngeal neuralgia: definitive microsurgical treatment and results in 117 patients. Neurochirurgia 20: 145–154

Leal PRL, Hermier M, Froment JC, Souza MA, Cristino-Filho G, Sindou M (2010) Preoperative demonstration of the neurovascular compression characteristics with special emphasis on the degree of compression, using high-resolution magnetic resonance imaging: a prospective study, with comparison to surgical findings, in 100 consecutive patients who underwent microvascular decompression for trigeminal neuralgia. Acta Neurochir 152: 817–825

Miller J, Acar F, Halilton, B, Burchiel K (2008) Preoperative visualization of neurovascular anatomy in trigeminal neuralgia. J Neurosurg 108:477–482

Miller J, Acar F, Halilton, B, Burchiel K (2009) Radiographic evaluation of trigeminal neurovascular compression in patients with and without trigeminal neuralgia. J Neurosurg 110:627–632

Naraghi R, Hastreiter P, Tomandl B, Bonk A, Huk W, Fahlbusch R (2004) Three-dimensional visualization of neurovascular relationships in the posterior fossa: technique and clinical application. J Neurosurg 100:1025–1035

Satoh T, Ekino C, Ohsako C (2004) Transluminal color-coded three-dimensional magnetic resonance angiography for visualization of signal intensity distribution pattern within an unruptured cerebral aneurysm: preliminarily assessment with anterior communicating artery aneurysms. Neuroradiology 46:628–634

Satoh T, Onoda K, Date I (2007a) Preoperative simulation for microvascular decompression in patients with idiopathic trigeminal neuralgia: visualization with three-dimensional magnetic resonance cisternogram and angiogram fusion imaging. Neurosurgery 60:104–114

Satoh T, Onoda K, Date I (2007b) Fusion imaging of three-dimensional magnetic resonance cisternograms and angiograms for the assessment of microvascular decompression in patients with hemifacial spasms. J Neurosurg 106:82–89

Satoh T, Omi M, Nebeshima M, Onoda K, Date I (2009) Severity analysis of neurovascular contact in patients with trigeminal neuralgia: assessment with the inner view of the 3D MR cisternogram and angiogram fusion imaging. AJNR Am J Neuroradiol 30:603–609

Sheehan JP, Ray DK, Monteith S, Yen CP, Lesnick J, Kersh R, Schlesinger D (2010) Gamma Knife radiosurgery for trigeminal neuralgia: the impact of magnetic resonance imaging-detected vascular impingement of the affected nerve. J Neurosurg 113:53–58

Sindou M, Leston J, Decullier E, Chapuis F (2007) Microvascular decompression for primary trigeminal neuralgia: long-term effectiveness and prognostic factors in a series of 362 consecutive patients with clear-cut neurovascular conflicts who underwent pure decompression. J Neurosurg 107:114–1163

Chapter 21

Epilepsy-Associated Brain Tumors: Diagnosis Using Magnetic Resonance Imaging

Horst Urbach

Abstract In 20–30% of patients with long-term drug-resistant epilepsy neuroepithelial tumours are found. Glioneuronal tumours are much more frequent than glial tumours. Gangliogliomas and dysembryoplastic neuroepithelial tumours (DNTs) are well characterized, both clinically and on MRI. Both tumour types are located in the cortex or in the cortex and subcortical white matter, gangliogliomas most commonly in the mesial temporal lobe (around the collateral sulcus). Both tumour types have typical imaging features, and from both, location and imaging features, they can be usually distinguished from glial tumors. This distinction is important since more than 70% of patients with drug resistant epilepsy caused by gangliogliomas and DNTs get seizure free following extended lesionectomy.

Keywords Epilepsy · Gangliogliomas · Mesial temporal lobe · Glioneuronal tumours · Glial tumors · DNTs

Introduction

In 20–30% of patients with long-term drug-resistant epilepsy intra-axial brain tumours are found (Luyken et al. 2003; Urbach et al. 2004). Tumor identification and characterization benefits from high-resolution MRI which is capable to display different tumor components within the diseased cortex and subcortical white matter. Clinically, two different groups exist in this cohort. The first contains typical epilepsy-associated tumours such as gangliogliomas, dysembryoplastic neuroepithelial tumours (DNTs), angiocentric gliomas, pleomorphic astrocytomas (pXAs), and supratentorial pilocytic astrozytomas, WHO grade I, with an usually benign behaviour. The second group consists of diffuse astrocytomas, WHO grade II, oligodendrogliomas, WHO grade II, with a 5-year-survival rate of 50–65%, and a few anaplastic cases, classified as WHO grade III, with a median survival time of 2–3 years. Histopathologically, glioneuronal and glial tumours can be distinguished. Among the glioneuronal tumours, gangliogliomas and DNTs are well characterized on MRI. Another tumor with a characteristic MR imaging pattern designed as angiocentric glioma has recently been added to the WHO classification of brain tumors (Louis et al. 2007). Due to the uncertain histogenesis it is grouped in the category "other neuroepithelial tumors". Within the spectrum of glial tumours a so-called isomorphic astrocytoma is likely associated with a clinically more benign behaviour (Blümcke et al. 2004; Schramm et al. 2004).

Glioneuronal Tumors

Gangliogliomas

Gangliogliomas are usually benign intraaxial neoplasms that were first described by Perkins in 1926. They are composed of dysplastic neurons and neoplastic glial cells. Both cell populations may show

H. Urbach (✉)
Radiologische Klinik, Neuroradiologie, Universitatsklinikum Bonn, 53105 Bonn, Germany
e-mail: Horst.urbach@ukb.uni-bonn.de

M.A. Hayat (ed.), *Tumors of the Central Nervous System, Volume 4*,
DOI 10.1007/978-94-007-1706-0_21,

heterogeneity, with the morphological spectrum ranging from a predominantly neuronal phenotype to a predominant glial population. Some gangliogliomas may also exhibit clear cell morphology which makes the differential diagnosis of oligodendrogliomas or DNT difficult. However, the immunohistochemical profile of gangliogliomas (e.g., expression of the stem cell epitope CD34) usually allows a specific diagnosis (Blümcke et al. 1999; Blümcke and Wiestler 2002).

The vast majority of gangliogliomas correspond to WHO grade I, in larger series around 10% of the tumours were classified as WHO grade II and 5% as WHO grade III tumours, respectively (Blümcke and Wiestler 2002; Luyken et al. 2004; Majores et al. 2008). Overall recurrence rate is around 7%, but distinctly higher for grade II (33%) and grade III (60%) tumors. If there is tumor recurrence, a significant portion of patients suffers from glioblastomas (around 45%) (Majores et al. 2008).

The above mentioned three-tiered classification of gangliogliomas has been abandoned in the 2007 WHO classification, which now only distinguishes benign WHO grade I and anaplastic WHO grade III gangliogliomas (Louis et al. 2007). From a clinical point of view, extratemporal location, male gender, age at surgery <40 years, a history without epilepsy, incomplete tumor resection, and histopathological presence of a gemistocytic cell component have been identified as poor prognostic outcome parameters (Majores et al. 2008; Rumana et al. 1999).

On MRI, gangliogliomas are consistently located in the cortex or in the cortex and subcortical white matter and have a spatial preponderance for the parahippocampal and lateral temporo-occipital gyri (Fig. 21.1). The classical imaging feature is the combination of intracortical cyst(s), a circumscribed area of cortical (and subcortical) signal increase on FLAIR and T2-weighted images and a contrast enhancing nodule (Fig. 21.1). Calcifications are present in 1/3 of cases (Zentner et al. 1994). If contrast enhancement is absent (≈50% of cases), gangliogliomas may be difficult to distinguish from cortical dysplasias. Especially, in these cases intracortical cysts are highly diagnostic. Gangliogliomas typically have no perifocal oedema. If oedema is present, malignant degeneration (from the glial component) to a WHO grade II or III ganglioglioma or anaplastic glial tumours including PXA with anaplastic features should be suspected.

DNTs

Dysembryoplastic neuroepithelial tumours are always WHO grade I intraaxial neoplasms that were first described by Daumas-Duport in 1988 (Daumas-Duport et al. 1988). Their histopathological hallmark is the so-called glioneuronal element, which contains oligodendrocyte-like cells attached to bundles of axons and neurons floating in a myxoid interstitial fluid (Daumas-Duport et al. 2000). If only the glioneuronal element is present, it is referred to as simple variant. Complex DNT variants additionally may contain glial nodules resembling astrocytomas, oligodendrogliomas or oligoastrocytomas, foci of cortical dysplasia, calcification and hemorrhages. Tumor growth or recurrence is extremely rare, it may occur in the complex variant group also characterized by an earlier seizure onset, and more extratemporal locations (Campos et al. 2009).

Even 20 years after their initial description, around 15% of DNTs are misclassified as low-grade astrocytomas or oligodendrogliomas (Fig. 21.2). It is rather the oligodendrocyte-like cells of the glioneuronal element than adjacent glial nodules as part of the complex DNT variant that cause these misclassifications (Campos et al. 2009).

On MRI, DNTs appear as usually multilobulated cysts, rarely only one large cyst is present. The cysts represent the glioneuronal element and are located in the cortex or in the cortex and subcortical white matter, sometimes single smaller cysts are located in the vicinity of the tumor, from which they are clearly separated. The multilobulated cysts are either oriented in a ball-like fashion or perpendicular to the cortical surface, they are characteristically hypointense on T1-weighted and strongly hyperintense on T2-weighted images. On FLAIR images, they have a mixed signal intensity, most of the "lobuli within the cyst" are hypointense. On DWI, DNTs are hypointense. Parts of the glioneuronal element may show contrast enhancement, which may vary on follow-up examinations in that way, that sharply marginated contrast-enhancing nodules occur while others have disappeared (Campos et al. 2009). Calcifications are found in 10% of DNTs, mostly within the deeper located tumor portions, usually in the vicinity of the contrast enhancing regions and – if rarely present – always in the vicinity of hemorrhage (Campos et al. 2009).

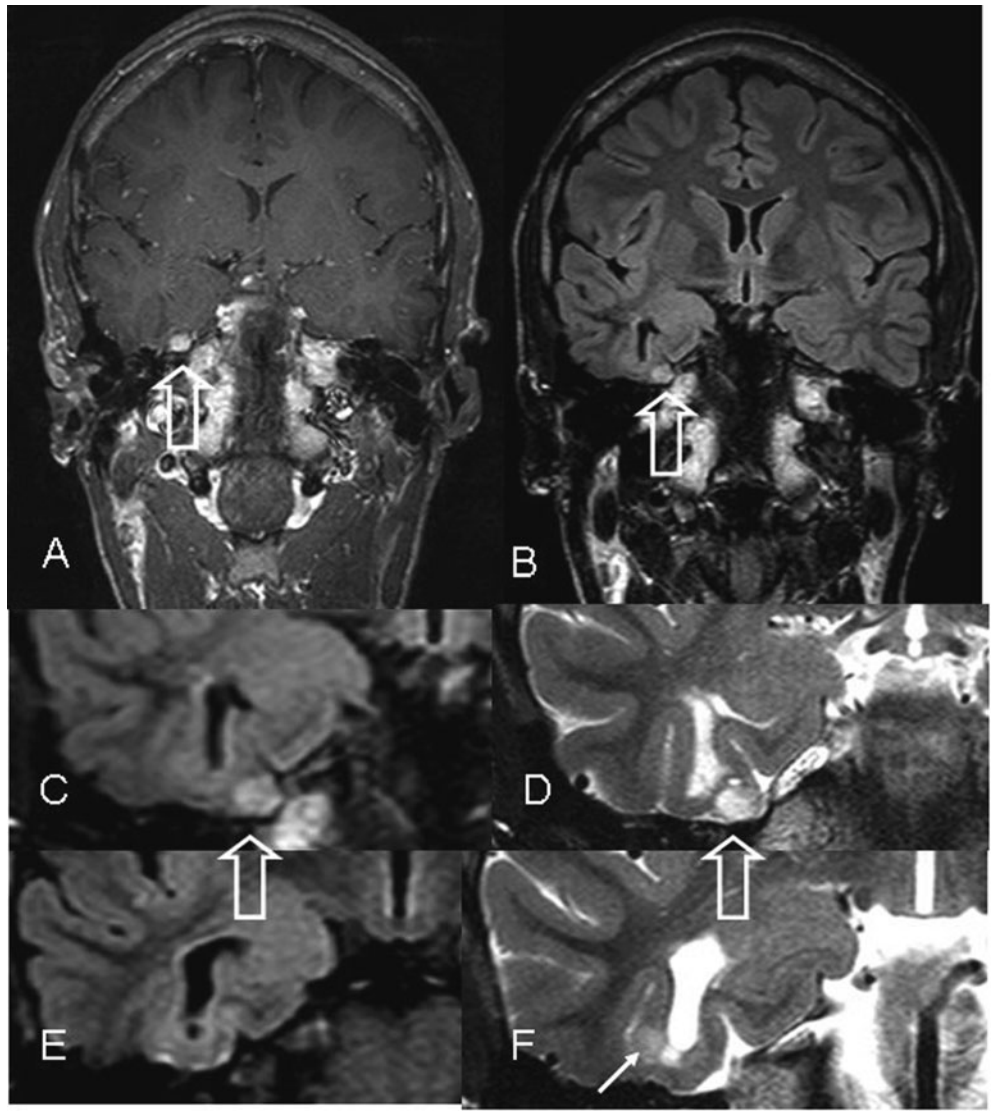

Fig. 21.1 Ganglioglioma WHO grade I of the right lateral occipito-temporal gyrus. Note the different cortical tumor components: (**a**) contrast-enhancing nodule (**a**: *hollow arrow*) rather extends the cortical surface (**b–d**: *hollow arrow*). The non-enhancing tumor component is somewhat inhomogenous which is better visible on the high-resolution T2-weighted fast spin echo images (**f**: *arrow*) than on the FLAIR image (**e**)

Angiocentric Gliomas

This new WHO entity was initially described by two different groups from Paris, France and Houston, U.S.A. in together 18 patients almost always suffering from epileptic seizures since childhood (Lellouch-Tubiana et al. 2005; Wang et al. 2005). Histologically, the variably infiltrative tumours have features of both astrocytoma and ependymoma, the most striking neuropathological features are an angiocentic polarity with gliofibrillary acidic protein (GFAP) positive fusiform and bipolar astrocytic cells arranged around blood vessels. Due to the uncertain histogenesis, angiocentric glioma was grouped with astroblastoma and chordoid glioma of the third ventricle in the category of 'Other neuroepithelial tumours', previously designated

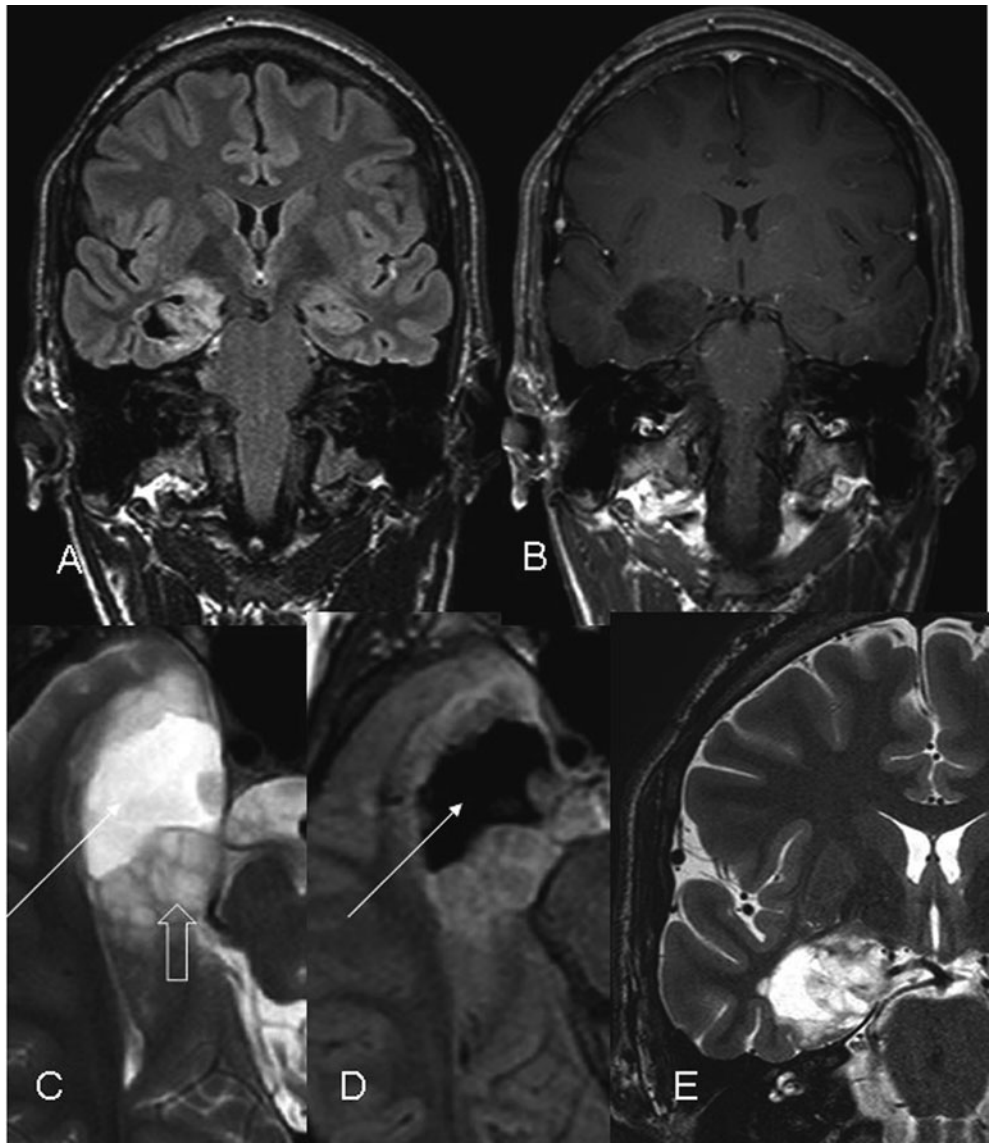

Fig. 21.2 Dysembryoplastic neuroepithelial tumor (DNT) of the right uncus involving the amygdala, hippocampal head and parahippocampal gyrus. A central CSF-filled cavity resulted from incomplete tumor resection 14 years before (**c**, **d**: *arrows*), after which the tumor was classified as oligodendroglioma WHO grade II. Note the multiple cysts representing the glioneuronal element as MRI hallmark of a DNT (**c**: *hollow arrow*). Smaller cysts sometimes clearly separated from the tumor are even more characteristic (**a**, **c**, **e**: *thick arrow*)

'Tumours of uncertain origin'. Due to its benign clinical behaviour and the possibility of curative surgery, the angiocentric glioma is assigned to WHO grade I (Louis et al. 2007).

On MRI, these tumours are located in the cortex and subcortical white matter with a stalk like extension to the lateral ventricle. On T1-weighted SE sequences, the involved cortical gyri are isointense with an intrinsic rim like hyperintensity. On T2-weighted and FLAIR sequences the tumours are hyperintense. There are no calcifications or contrast enhancement (Fig. 21.3).

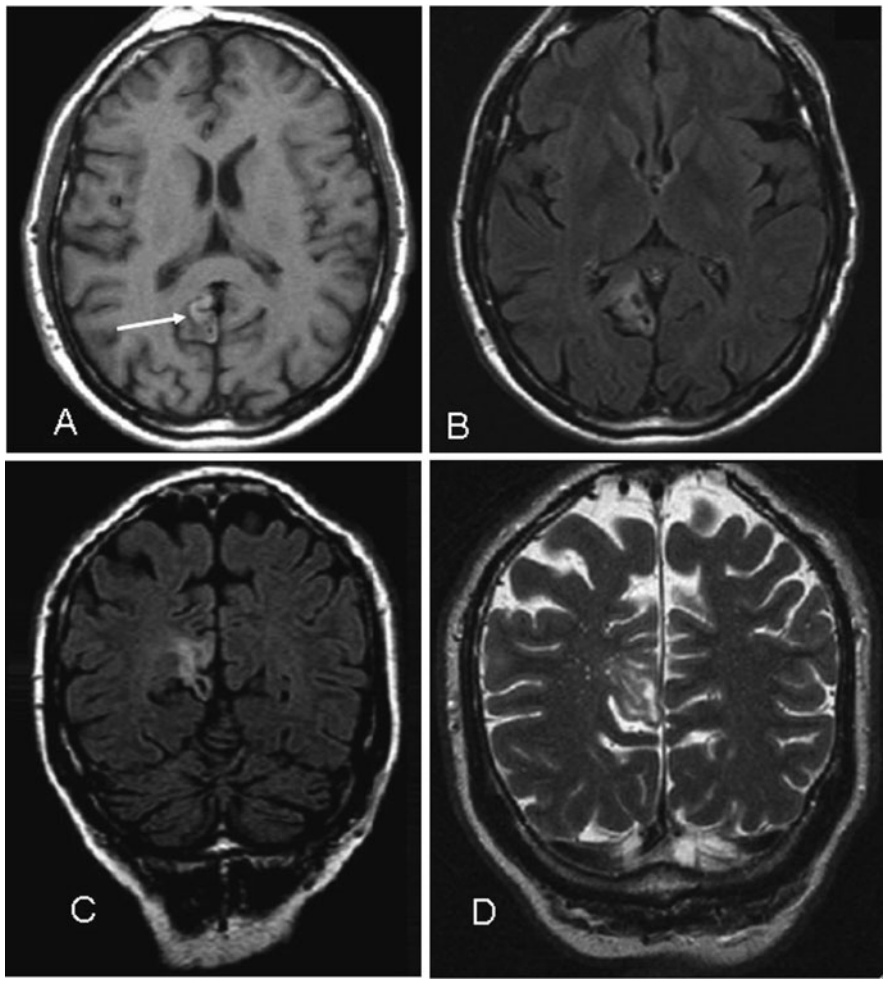

Fig. 21.3 Angiocentric glioma of the right occipital lobe. A cortical hyperintensity on unenhanced T1-weighted images is characteristic for this tumor (**a**: *arrow*). Note also the missing space-occupying effect of this tumor (**a**–**d**)

Glial Tumors

Pilocytic Astrocytomas

Pilocytic astrocytomas are generally circumscribed, slowly growing, often cystic astrocytomas, histologically characterized by a biphasic pattern with varying proportion of compacted bipolar cells with Rosenthal fibres and loose textured multipolar cells with microcysts and granular bodies. They correspond to WHO grade I tumors although rarely anaplastic pilocytic astrocytomas are found. Recently, a histopathological variant designed as pilomyxoid astrocytoma occurring at a younger age and characterized by a significant worse prognosis has been added to the WHO classification of brain tumors (Louis et al. 2007; Linscott et al. 2008)

On MRI, pilocytic astrocytomas are well-circumscribed mass lesions with a cystic portion and a contrast-enhancing mural nodule. It may be impossible to distinguish this tumor from a gangli-oglioma, calcifications, e.g. which are present in 1/3 of gangliogliomas, would favour the diagnosis ganglioglioma and larger tumors the diagnosis pilocytic astrocytoma, respectively. In rare cases, a pilocytic astrocytoma spreads through the subarachnoid space, although histologically it may be still a WHO grade I tumor. If there is subarachnoid spread and intratumoral hemorrhage, a pilomyxoid variant should be suspected (Linscott et al. 2008).

Diffuse Astrocytomas

Diffusely infiltrating astrocytomas apply to a group of astrocytic tumours that are usually divided into the following clinico-pathologic entities: Diffuse astrocytoma (WHO grade II), anaplastic astrocytoma (WHO grade III), glioblastoma multiforme (WHO grade IV, and variants. Recently, a rare variant with a clinically more benign behaviour has been described in young patients suffering from long standing drug resistant seizures (Blümcke et al. 2004; Schramm et al. 2004). This isomorphic astrocytoma is histologically characterized by a low cellularity, lack of mitotic activity, and highly differentiated astroglial elements infiltrating into adjacent brain parenchyma.

On MRI, astrocytomas typically grow diffusively within the white matter, which is hyperintense and swollen on FLAIR and T2-weighted images and hypointense and swollen on T1-weighted images, respectively. Focal areas of contrast enhancement indicate malignant degeneration to a WHO grade III (or even grade IV) tumor. However, even non-enhancing mass lesions can be anaplastic, here the degree of inhomogeneity (on T1-weighted images) may indicate anaplastic dedifferentiation. On the other side of the spectrum, the recently described isomorphic astrocytoma has a very homogenous appearance on T1-weighted, FLAIR, and T2-weighted images; the relatively low signal intensity on T1-weighted images might be explained by the low cellularity of the tumor. Some of the astrocytomas associated with temporal lobe epilepsy predominantly grow within the limbic system, the reason for this growing pattern is not entirely clear.

Oligodendrogliomas and Oligoastrocytomas

Oligodendrogliomas are diffusively infiltrating tumours composed of cells with rounded homogenous nuclei and, on paraffin sections, a swollen, clear cytoplasm (honeycomb appearance). Histologically and clinically, WHO grade II and grade III tumours are distinguished. If tumours contain a conspicuous mixture of two neoplastic cell types morphologically resembling the tumour cells in oligodendroglioma and diffuse astrocytoma, they are designed oligoastrocytomas. Oligoastrocytomas are more frequent than pure oligodendrogliomas.

On MRI, (pure) oligodendrogliomas are inhomogenous tumours who tend to infiltrate the cortex and adjacent leptomeninges. Characteristic for this tumor are nodular or clumped calcifications which are found in 70–90% of cases on CT. Contrast enhancement is variable and usually irregular.

Recent advances in molecular genetics show among others a combined loss of chromosomes 1p and 19q as a powerful predictor of chemotherapeutic response and survival in oligodendrogliomas. On MRI, however, oligodendrogliomas with a combined loss show rather indistinct borders and diffuse enhancement on T1-weighted images, while oligodendrogliomas without a combined 1p/19q loss have rather sharp borders and a ring-like enhancement (Nutt et al. 2005).

PXAs

Pleomorphic xanthoastrocytomas are astrocytic tumours with superficial location in the cerebral hemispheres and involvement of the meninges. They correspond histologically to WHO grade II, for lesions with significant mitotic activity (5 or more mitoses per 10 high power fields) the term PXA with anaplastic features may be used. It has been postulated that PXAs originate from subpial astrocytes. However, the demonstration of synaptophysin and neurofilament protein in some PXAs can be taken as evidence for neuronal differentiation and suggests a more complex histogenesis.

On MRI, PXAs have typical imaging features with a meningo-cerebral contrast enhancement on T1-weighted and white matter edema on T2-weighted and FLAIR images. Calcifications are possible and as a glial tumor, a PXA usually has a space-occupying effect. However, it may be impossible to distinguish a PXA from a ganglioglioma in some cases, which in part can be explained by composite PXA-GG lesions (Furuta et al. 1992; Yeh et al. 2003)

Differential Diagnosis and Summary

Several lesions (focal cortical dysplasias, limbic encephalitis, herpes and other viral encephalitis, abscess, multiple sclerosis, vascular malformations

including cavernoma, epidermoid, meningioangiomatosis, others) may sometimes mimic tumors and cause drug-resistant epilepsy, especially in a temporo-mesial location. The most common tumor-like lesion is the cavernoma, which by means of MRI can be classified into four types (Zabramski et al. 1994). Type II cavernomas with signal characteristics indicating loculated areas of hemorrhage and thrombosis of varying age and large areas of hemosiderin-stained brain best visible on T2-weighted gradient echo or susceptibility-weighted (SWI) images are more likely to cause seizures than type III or type IV cavernomas which may develop de novo and are often asymptomatic. Another common lesion with a characteristic MRI appearance is the epidermoid. The epidermoid is nearly isointense to CSF in all except Diffusion-weighted (DWI) MRI sequences, on which it is distinctly hyperintense, If DWI is not routinely performed, one has to look carefully for focal widening of the subarachnoid space.

In series from large epilepsy surgery centres, the majority of patients with long term epilepsy associated tumours have gangliogliomas (Luyken et al. 2003; Ruban et al. 2009). The second common tumor is the DNT, which has an even more specific MR imaging appearance caused by the glioneuronal element as histopathological hallmark of this tumor (Campos et al. 2009). A new WHO entity designed as angiocentric glioma is characterized by an intrinsic cortical hyperintensity on T1-weighted images (Lellouch-Tubiana et al. 2005; Wang et al. 2005). Even if it not always possible to distinguish these tumours on MRI, in a case of a characteristic MRI pattern, a different histopathological diagnosis should be mistrust. At least, a cortical or cortical/subcortical located glioneuronal tumour must be distinguished from an infiltratively growing glial tumour, so that in doubtful cases extended immunohistochemical investigations (e.g., CD34 immunohistochemistry) are mandatory.

References

Blümcke I, Giencke K, Wardelmann E, Beyenburg S, Kral T, Sarioglu N, Pietsch T, Wolf HK, Schramm J, Elger CE, Wiestler OD (1999) The CD34 epitope is expressed in neoplastic and malformative lesions associated with chronic, focal epilepsies. Acta Neuropathol 97:481–490

Blümcke I, Luyken C, Urbach H, Wiestler OD, Schramm J (2004) A new clinico-histopathological subtype of low-grade astrocytoma associated with long-term epilepsy and benign prognosis. Acta Neuropathol 107: 381–388

Blümcke I, Wiestler OD (2002) Gangliogliomas: an intriguing tumor entity associated with focal epilepsies. J Neuropathol Exp Neurol 61:575–584

Campos AR, Clusmann H, von Lehe M, Niehusmann P, Becker AJ, Schramm J, Urbach H (2009) Simple and complex dysembryoplastic neuroepithelial tumors (DNT): clinical profile, MRI and histopathology. Neuroradiology 51: 433–443

Daumas-Duport C, Pietsch T, Lantos PL (2000) Dysembryoplastic neuroepithelial tumour. In: Kleihues P, Cavenee K (eds) Pathology and genetic of tumours of the nervous system. IARC Press, Lyon, pp 103–106

Daumas-Duport C, Scheithauer BW, Chodkiewicz JP, Laws ER Jr, Vedrenne C (1988) Dysembryoplastic neuroepithelial tumor: a surgically curable tumor of young patients with intractable partial seizures. Report of thirty-nine cases. Neurosurgery 23:545–556

Furuta A, Takahashi H, Ikuta F, Onda K, Takeda N, Tanaka R (1992) Temporal lobe tumor demonstrating ganglioglioma and pleomorphic xanthoastrocytoma components. Case report. J Neurosurg 77:143–147

Lellouch-Tubiana A, Boddaert N, Bourgeois M, Fohlen M, Jouvet A, Delalande O, Seidenwurm D, Brunelle F, Sainte-Rose C (2005) Angiocentric neuroepithelial tumor (ANET): a new epilepsy-related clinicopathological entity with distinctive MRI. Brain Pathol 15:281–286

Linscott LL, Osborn AG, Blaser S, Castillo M, Hewlett RH, Wieselthaler N, Chin SS, Krakenes J, Hedlund GL, Sutton CL (2008) Pilomyxoid astrocytoma: expanding the imaging spectrum. AJNR Am J. Neuroradiol 29:1861

Louis DN, Ohgaki H, Wiestler OD, Cavenee WK, Burger PC, Jouvet A, Scheithauer BW, Kleihues P (2007) The 2007 WHO classification of tumours of the central nervous system. Acta Neuropathol 114:97–109

Luyken C, Blümcke I, Fimmers R, Urbach H, Wiestler OD, Schramm J (2003) The spectrum of long-term epilepsy associated tumors: long-term seizure and tumor outcome and neurosurgical aspects. Epilepsia 44:822–830

Luyken C, Blümcke I, Fimmers R, Urbach H, Wiestler OD, Schramm J (2004) Supratentorial gangliogliomas. Histopathological grading and tumor recurrence in 184 patients with a median follow-up of eight years. Cancer 101:146–155

Majores M, von Lehe M, Fassunke J, Schramm J, Becker AJ, Simon M (2008) Tumor recurrence and malignant progression of gangliogliomas. Cancer 113:3355–3363

Nutt CL (2005) Molecular genetics of oligodendrogliomas: a model for improved clinical management in the field of neurooncology. Neurosurg Focus 19: E2:1–9

Perkins OC (1926) Gangliogliomas. Arch Pathol Lab Med 2: 11–17

Ruban D, Byrne RW, Kanner A, Smith M, Cochran EJ, Roh D, Whisler WW (2009) Chronic epilepsy associated with temporal tumors: long-term surgical outcome. Neurosurg Focus 2:E6.

Rumana CS, Valadka AB, Contant CF (1999) Prognostic factors in supratentorial ganglioglioma. Acta Neurochir (Wien) 141:63–69

Schramm J, Luyken C, Urbach H, Fimmers R, Blümcke I (2004) Evidence for a clinically distinct new subtype of grade II astrocytomas in patients with long-term epilepsy. Neurosurgery 55:340–358

Urbach H, Hattingen J, von Oertzen J, Luyken C, Clusmann H, Kral T, Kurthen M, Schramm J, Blümcke I, Schild HH (2004) MRI in the presurgical evaluation of patients with drug-resistant epilepsy. AJNR Am J Neuroradiol 25: 919–926

Wang M, Tihan T, Rojiani AM, Bodhireddy SR, Prayson RA, Iacuone JJ, Alles AJ, Donahue DJ, Hessler RB, Kim JH, Haas M, Rosenblum MK, Burger PC (2005) Monomorphous angiocentric glioma: a distinctive epileptogenic neoplasm with features of infiltrating astrocytoma and ependymoma. J Neuropathol Exp Neurol 64:875–881

Yeh DJ, Hessler RB, Stevens EA, Lee MR (2003) Composite pleomorphic xanthoastrocytoma-ganglioglioma presenting as a suprasellar mass: case report. Neurosurgery 52:1465–1469

Zabramski JM, Wascher TM, Spetzler RF, Johnson B, Golfinos J, Drayer BP, Brown B, Rigamonti D, Brown G (1994) The natural history of familial cavernous malformations: results of an ongoing study. J Neurosurg 80:422–432

Zentner J, Wolf HK, Ostertun B, Hufnagel A, Campos MG, Solymosi L, Schramm J (1994) Gangliogliomas: clinical, radiological and histopathological findings in 51 patients. J Neurol Neurosurg Psychiatry 57:1497–1502

Chapter 22

Growth of Malignant Gliomas In Vivo: High-Resolution Diffusion Tensor Magnetic Resonance Imaging

Jinyuan Zhou

Abstract Diffusion tensor imaging (DTI) can provide information noninvasively about tissue microstructure and microdynamics at the near-cellular level. In this Chapter, we review the use of high-resolution DTI to visualize the growth patterns of brain tumor xenografts in vivo in animals. The possible eventual clinical applications of the results to humans are also discussed.

Keywords Gliomas · Brain parenchyma · Necrosis · Angiogenesis · DT-MRI · Tissue microstructure

Introduction

Gliomas are highly heterogeneous and infiltrative. Early histological studies have revealed that malignant gliomas in humans usually consist of cores of solid tumors (often mixed with necrosis) and regions of edematous or normal brain tissue infiltrated by tumor cells. Solid tumor masses are generally defined by the volume exhibiting gadolinium (Gd) contrast enhancement. These masses may destroy the brain parenchyma, and are often accompanied by endothelial proliferation and the formation of new microvessels. The histologic criteria for the diagnosis of high-grade gliomas include necrosis and angiogenesis. In contrast, individual infiltrating tumor cells do not destroy brain parenchyma, and are usually not associated with angiogenesis or Gd enhancement. They migrate preferentially along blood vessels and white matter fiber tract pathways, and can spread quite a distance from the solid tumor mass, even outside regions of T_2 hyperintensity. It is widely recognized that residual tumor cells that remain after resection and local radiation are the source of tumor recurrence (Albert et al. 1994).

Diffusion tensor magnetic resonance imaging (DT-MRI) can provide information noninvasively about tissue microstructure and microdynamics at a scale comparable to cell dimensions (Basser et al. 1994). A great number of recent studies in humans (Gauvain et al. 2001; Sinha et al. 2002) and in animals (Zhang et al. 2007; Kim et al. 2008) have suggested that diffusion tensor imaging (DTI) may be sensitive to the microscopic structures of gliomas. Although there are contradictory results, most investigators believe that DT-MRI may be useful for detecting gliomas, evaluating the extent of tumor invasion, distinguishing between solid tumor cores and peritumoral edema, and differentiating tumors from radiation necrosis and other abnormalities. The purpose of this chapter is to review the use of high-resolution DTI to visualize the growth patterns of malignant gliomas in vivo in animals, and the possible eventual clinical applications of the results to humans.

Diffusion Tensor Imaging

The study of water diffusion remains one of the most important topics in NMR spectroscopy and imaging. Diffusion-weighted MRI (DWI) was introduced for clinical studies in 1986 by Le Bihan et al. (1986). Later, two landmark articles were published in 1990 by Moseley et al. (1990a, b), who reported that DWI

J. Zhou (✉)
Johns Hopkins School of Medicine, Department of Radiology, 600 N. Wolfe Street, Park 336, Baltimore, MD 21287, USA
e-mail: jzhou@mri.jhu.edu

M.A. Hayat (ed.), *Tumors of the Central Nervous System, Volume 4*,
DOI 10.1007/978-94-007-1706-0_22,

offers an accurate approach for the early detection of cerebral ischemia, and that diffusion was anisotropic in tissues. Currently, DWI has become a routine, almost indispensable MRI modality for the clinical examination of diseases, including stroke and tumors. It is known that water diffusion is anisotropic in several biological tissues, such as brain white matter and muscles, and that this anisotropy must be characterized by a tensor (Basser et al. 1994). DTI measures these diffusion constants and fits them into a simplified tensor model, from which several types of information, such as the extent (average apparent diffusion coefficient, ADC_{av} or ADC, for simplicity) and fractional anisotropy (FA) of diffusion and its predominant orientation, can be calculated. DTI can detect and visualize the three-dimensional (3D) structures and the architecture of well-ordered tissues at the microscopic level. In axonal tracts, where neuronal fibers are coherently arranged in the same direction, the measured diffusion anisotropy is high, and the diffusion orientation is along the direction of fiber trajectories. Because of this capability, DTI has been used to map white matter tracts in the living brain (Mori et al. 1999).

DTI data processing is somewhat complicated, but many types of software (Jiang et al. 2006) can be used for this purpose. Briefly, the diffusion tensors ($\overline{\overline{D}}$) are usually calculated using a log-linear fitting method. Three pairs of eigenvalues (λ_1, λ_2, and λ_3) and eigenvectors ($\boldsymbol{V}_1$, $\boldsymbol{V}_2$, and $\boldsymbol{V}_3$) are calculated for each pixel. The eigenvector associated with the largest eigenvalue is referred to as the primary eigenvector ($\boldsymbol{V}_1$). Then, isotropic ADC and FA are calculated according to the equations (Basser and Pierpaoli 1996):

$$\mathrm{ADC} = \mathrm{Trace}(\overline{\overline{D}})/3 = (\lambda_1 + \lambda_2 + \lambda_3)/3 = \bar{\lambda} \tag{22.1}$$

$$\mathrm{FA} = \sqrt{3/2[(\lambda_1 - \bar{\lambda})^2 + (\lambda_2 - \bar{\lambda})^2 + (\lambda_3 - \bar{\lambda})^2}/\sqrt{\lambda_1^2 + \lambda_2^2 + \lambda_3^2} \tag{22.2}$$

The orientation of water diffusion can be visualized through directionally encoded color (DEC) maps (Pajevic and Pierpaoli 1999), which are generated by combining the images of the primary eigenvector ($\boldsymbol{V}_1$) and FA into RGB images. In the DEC images, red is assigned to the medial-lateral orientation, green to the anterior–posterior orientation, and blue to the superior-inferior orientation (perpendicular to the figure). The ratios among the green, red, and blue components of each pixel are defined by the ratios of the x, y, and z components of the primary eigenvector, and the intensity is proportional to the FA. The orientation information may also be visualized by vector images, in which the measured $\boldsymbol{V}_1$ at each pixel is visualized by a small line segment overlaid on DEC images, with a length proportional to its FA value. Finally, isotropic DW images are obtained through the average of DW images with different diffusion gradient directions.

Similar to conventional MRI, what DTI detects in a voxel is an average of the entire voxel. Larger voxel size generally results in larger partial volume effects and may yield ambiguous DTI results. In contrast, higher resolution DTI would have a decreasing signal-to-noise ratio (SNR) due to the smaller voxel volume. This low SNR would lead to apparently increased FA values (Farrell et al. 2007), an error that is even more significant for low FA tissue, such as gray matter and tumor rims, which will be described in this chapter. To increase SNR in humans, high (3 T) or ultra-high (7 T) field MRI and parallel imaging (32-channel phased-array receiver), in combination with zoomed MRI and an increased number of acquisitions, may be utilized. Currently, most human DTI studies with 3 T use a voxel size of 8–10 mm^3, with an acquisition time of 3–5 min. On the other hand, animal DTI studies are generally performed at a much higher spatial resolution (an in-plane resolution of 0.1–0.3 mm and a slice thickness of 1–1.5 mm) at field strengths of 4.7 T or higher. The scan time is usually as long as 1–2 h, because parallel imaging is generally not available.

Growth of Experimental Brain Tumors In Vivo

It is known that after implantation, tumor cells will accumulate around vessels, proliferate rapidly, and pack closely in the initial stage, which is then followed

by vascular apoptosis and involution and tumor necrosis (Zagzag et al. 2000). In addition, angiogenesis will occur as a later event in tumor progression. The dynamics of malignant tumor growth have been investigated in vitro and in vivo by many different researchers (Deisboeck et al. 2001; Bru et al. 2003).

Using high-resolution DTI at submillimeter resolution, it was recently demonstrated (Zhang et al. 2007; Kim et al. 2008) that high FA values and, thus, highly organized microstructures exist in various experimental brain tumor models. Of these observations, Zhang et al. (2007) used two established rat tumor models (9L, F98) and patient-derived human glioblastoma xenografts in rats with a spatial resolution of $0.33 \times 0.33 \times 1.5\ mm^3$. Kim et al. (2008) used two rat brain tumor models, 9L and F98, at an imaging resolution of $0.23 \times 0.23 \times 1\ mm^3$. Lope-Piedrafita et al. (2008) and Asanuma et al. (2008) used the established C6 glioma model in rats with an imaging resolution of $0.16 \times 0.16 \times 1\ mm^3$ and $0.2 \times 0.2 \times 1\ mm^3$, respectively. The quantitative analysis of tumor properties revealed by the sub-mm DTI technique clearly showed that the rims of the tumors have significantly higher FA values than the central regions. However, the differences in ADC between the centers and rims are small, and most are not significant. Furthermore, it has been shown that the tumor rims have significantly higher FA values than the contralateral striatum.

Figure 22.1 shows an example of the high resolution DT-MRI results of 9L tumors and human glioblastoma xenografts in rats (Zhang et al. 2007). In the T_2-weighted images and ADC maps, regions with tumors are relatively homogeneous and have higher signal intensities than the striatum on the contralateral side. However, the FA maps show high contrast and interesting patterns within the tumors, which consist of small, dark centers with low diffusion anisotropy and rims with a high degree of diffusion anisotropy. In the DEC and vector images, it is particularly interesting that water diffusion directionality in the rims of the tumors forms a circular pattern for 9L tumors and a radial pattern for human glioblastoma xenografts. Moreover, it was observed that these well-organized DTI patterns appear at an early stage post-implantation and seemingly enlarge with tumor growth (Zhang et al. 2007). Over time, some of the tumors develop several small confluent tumor foci, with each having a center and a structured rim.

The fact that there is a high degree of diffusion anisotropy within the tumor rims implies that water diffusion is coherently, not randomly, distributed in certain tumor regions. This clearly demonstrates the formation of highly ordered cellular structures during tumor growth. To examine the existence of distinctive cellular organizational patterns within tumors, H&E staining was performed. It was shown under high magnification that the orientation of individual tumor cells and the adjacent interstitial spaces form a circular pattern for 9L and F98 tumors or a radial pattern for human glioblastoma xenografts in the rims of the tumors (Zhang et al. 2007). Thus, the diffusion patterns of water molecules observed by DTI may reflect the patterns of the interstitial water motion and cellular organization within these tumors.

High-resolution DT-MRI reveals unique microstructures inside brain tumor xenografts, which consist of disordered central zones with low diffusion anisotropy and highly organized peripheral structures (rims) with high diffusion anisotropy, and which have circular or radial orientations. It is possible that these rims of increased FA within the tumors are an imaging marker predictive of highly proliferating, viable tumor areas versus those that mainly reflect dying and dead tumor cells, cell debris, and edema. Currently, it is not clear how these organized microstructures appear with the growth of the tumors and why the FA values in the tumor rims could be larger than those in the gray matter of the brain. However, the existence of the well-organized microstructures within the tumors, unique for different tumor cell lines, may support the hypothesis of self-organization in biological systems, as suggested previously by Deisboeck et al. (2001). Based on that hypothesis, it was shown in vitro that wild-type U87 tumor cells invade in a spherically symmetric manner, while mutant U87-ΔEGFR tumor cells with enhanced malignancy produce a branching pattern in the invasive region (Deisboeck et al. 2001).

Growth of Human Brain Tumors

Using DTI, brain tumor cores, peritumoral edema, and adjacent brain tissues, including white matter tracts and the cerebral cortex, have been examined intensively in recent years (Gauvain et al. 2001; Sinha et al. 2002). To elucidate the effects of infiltrating

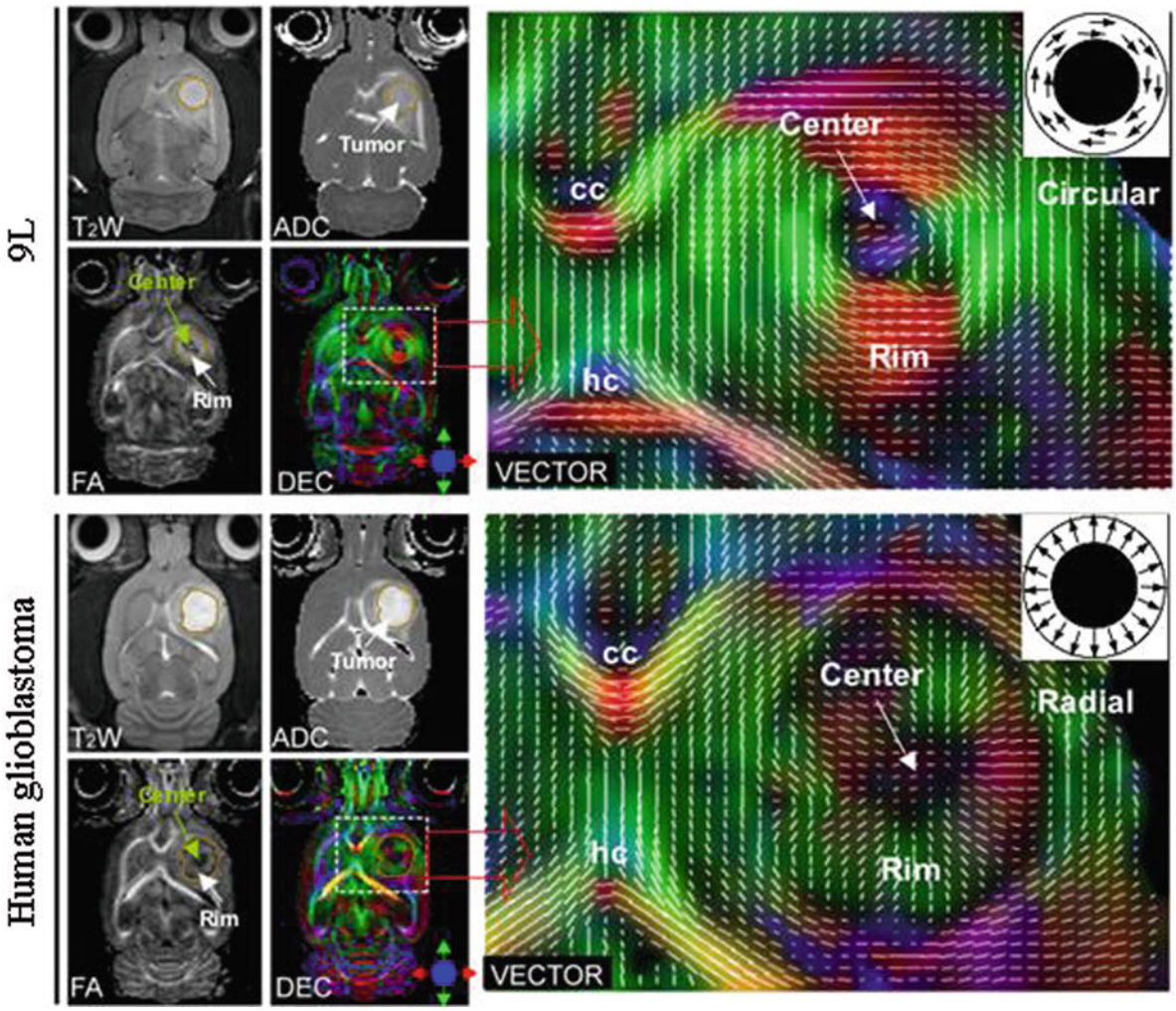

Fig. 22.1 In vivo MR images of 9L gliosarcoma and human glioblastoma xenografts in rats. Post-implantation days were 11 (9L) and 26 (human glioblastoma). The tumor regions are hyperintense on T_2W and ADC. T_2W hyperintense regions were manually defined and overlaid on other images. In FA maps, the tumors consisted of central zones with low diffusion anisotropy and peripheral structures (rim) with high diffusion anisotropy. DTI revealed unique microstructures (circular orientation for 9L, radial orientation for human glioblastoma) inside tumors, as seen clearly in DEC and vector images. Reprinted from Zhang et al. (2007) with permission from Wiley-Liss, Inc

brain tumors on the fiber tracts, the abnormalities in the brain have been categorized by displaced, edematous, infiltrated, and disrupted diffusion patterns (Field et al. 2004). In brain areas infiltrated by isolated tumor cells, tissue microstructures are still dominated by white matter tracts, but their FA values are substantially decreased. It was reported (Gauvain et al. 2001) that fiber tract FA was "negatively" correlated with cell density. Malignant gliomas in humans include areas of necrosis, micro- or macro-hemorrhage, and cystic components, in which FA is expected to disappear totally, and no specific diffusion patterns would be observed for white matter tracts.

However, some recent DTI observations in humans at 3 T have demonstrated that high FA values exist within certain regions of human gliomas. For example, it was reported by Beppu et al. (2003, 2005) and Kinoshita et al. (2008) that the FA values in the Gd-enhancing region are "positively" correlated with the tumor cell density, vascularity, and MIB-1 index (a predictor of proliferation activity). In the Gd-enhancing solid tumor cores, tumor cells proliferate

rapidly and may pack closely in a coherent way, and the brain parenchyma is completely destroyed (Kelly et al. 1987). Therefore, tumor cell organization would predominantly affect FA values. To understand these seemingly contradictory results, it was suggested by Beppu et al. (2005) that the FA value is determined by a balance between factors that decrease it (fiber destruction or displacement) and factors that increase it (tumor cell arrangement and vascularity). It seems likely that well-organized microstructures within human gliomas may exist, but are not readily characterized due to mixture with the fiber tracts of the brain.

In particular, it was reported by Kashimura et al. (2007), at 3 T, that the FA values of Gd-enhancing lesions were $\sim 0.28 \pm 0.04$ for recurrent tumors and 0.17 ± 0.03 for radiation necrosis. This case study, although no distinctive diffusion directionality was found, suggests that high-resolution DTI at high-field strengths may add value to standard MRI for differentiating necrosis from tumor recurrence. The use of DTI to differentiate between radiation necrosis and tumor regrowth has been an ongoing topic of interest. It is possible that the observation of the unique diffusion patterns in human brain tumors is mainly hampered by spatial resolution limitations, but may become clearer as spatial resolution for DTI improves to the submillimeter level in all directions in the future.

Conclusion

The highly organized diffusion patterns inside brain tumors have not fully been characterized in either animals or humans, as yet. These findings at the near-cellular level differ substantially from the current thinking that tumors are totally disordered. Therefore, this unique use of high-resolution DTI may provide certain significant methodological innovations in tumor diagnosis and therapy:

(i) The distinctive diffusion patterns inside solid tumors may be characteristic for identifying the tumor cores. The findings would offer a pattern-based MRI approach that can help to better define actively growing, viable tumor regions with high proliferation activity, potentially allowing more targeted treatments. (ii) The unique diffusion patterns in solid tumors can be used to distinguish between injured brain tissue and recurrent tumors noninvasively. If the hypothesis can be confirmed, high-resolution DTI would offer an important option for the noninvasive assessment of radiation necrosis. (iii) Although somewhat speculative, different tumor cell lines may have specific microstructures, and the circular versus radial pattern difference may be associated with the proliferative and invasive potential of solid tumors. (iv) The primary diffusion orientation of water molecules inside tumors may be related to the direction and distribution of oxygen, nutrients, and drugs. The findings may influence the design criteria for drugs and potentially allow better decisions concerning tumor chemotherapy.

Acknowledgments This work was supported in part by grants from NIH (RR015241) and the Dana Foundation.

References

Albert FK, Forsting M, Sartor K, Adams H-P, Kunze S (1994) Early postoperative magnetic resonance imaging after resection of malignant glioma: objective evaluation of residual tumor and its influence on regrowth and prognosis. Neurosurgery 34:45–60

Asanuma T, Doblas S, Tesiram YA, Saunders D, Cranford R, Pearson J, Abbott A, Smith N, Towner RA (2008) Diffusion tensor imaging and fiber tractography of C6 rat glioma. J Magn Reson Imag 28:566–573

Basser PJ, Mattiello J, LeBihan D (1994) MR diffusion tensor spectroscopy and imaging. Biophys J 66:259–267

Basser PJ, Pierpaoli C (1996) Microstructural and physiological features of tissues elucidated by quantitative-diffusion-tensor MRI J Magn Reson Series B 111:209–219

Beppu T, Inoue T, Shibata T, Kurose A, Arai H, Ogasawara K, Ogawa A, Nakamura S, Kabasawa H (2003) Measurement of fractional anisotropy using diffusion tensor MRI in supratentorial astrocytic tumors. J Neuro-oncol 63:109–116

Beppu T, Inoue T, Shibata Y, Yamada N, Kurose A, Ogasawara K, Ogawa A, Kabasawa H (2005) Fractional anisotropy value by diffusion tensor magnetic resonance imaging as a predictor of cell density and proliferation activity of glioblastomas. Surg Neurol 63:56–61

Bru A, Albertos S, Subiza JL, Garcia-Asenjo JL, Bru I (2003) The universal dynamics of tumor growth. Biophys J 85:2948–2961

Deisboeck TS, Berens ME, Kansal AR, Torquato S, Stemmer-Rachamimov AO, Chiocca EA (2001) Pattern of self-organization in tumour systems: complex growth dynamics in a novel brain tumour spheroid model. Cell Prolif 34: 115–134

Farrell JAD, Landman BA, Jones CK, Smith SA, Prince JL, van Zijl PCM, Mori S (2007) Effects of signal-to-noise ratio on the accuracy and reproducibility, of diffusion tensor imaging-derived fractional anisotropy, mean diffusivity, and principal

eigenvector measurements at 1.5T. J Magn Reson Imaging 26:756–767

Field AS, Alexander AL, Wu YC, Hasan KM, Witwer B, Badie B (2004) Diffusion tensor eigenvector directional color imaging patterns in the evaluation of cerebral white matter tracts altered by tumor. J Magn Reson Imaging 20:555–562

Gauvain KM, McKinstry RC, Mukherjee P, Perry A, Neil JJ, Kaufman BA, Hayashi RJ (2001) Evaluating pediatric brain tumor cellularity with diffusion-tensor imaging. Am J Roentgenol 177:449–454

Jiang H, van Zijl PC, Kim J, Pearlson GD, Mori S (2006) DtiStudio: resource program for diffusion tensor computation and fiber bundle tracking. Comput Methods Programs Biomed 81:106–116

Kashimura H, Inoue T, Beppu T, Ogasawara K, Ogawa A (2007) Diffusion tensor imaging for differentiation of recurrent brain tumor and radiation necrosis after radiotherapy – three case reports. Clin Neurol Neuros 109:106–110

Kelly PJ, Daumas-Duport C, Kispert DB, Kall BA, Scheithauer BW, Illig JJ (1987) Imaging-based stereotaxic serial biopsies in untreated intracranial glial neoplasms. J Neurosurg 66:865–874

Kim S, Pickup S, Hsu O, Poptani H (2008) Diffusion tensor MRI in rat models of invasion and well-demarcated brain tumors. NMR Biomed 21:208–216

Kinoshita M, Hashimoto N, Goto T, Kagawa N, Kishima H, Izumoto S, Tanaka H, Fujita N, Yoshimine T (2008) Fractional anisotropy and tumor cell density of the tumor core show positive correlation in diffusion tensor magnetic resonance imaging of malignant brain tumors. NeuroImage 43:29–35

Le Bihan D, Breton E, Lallemand D, Grenier P, Cabanis E, Laval-Jeantet M (1986) MR imaging of intravoxal incoherent motions: application to diffusion and perfusion in neurologic disorders. Radiology 161:401–407

Lope-Piedrafita S, Garcia-Martin ML, Galons J-P, Gillies RJ, Trouard TP (2008) Longitudinal diffusion tensor imaging in a rat brain glioma model. NMR Biomed 21:799–808

Mori S, Crain BJ, Ckacko VP, van Zijl PC (1999) Three dimensional tracking of axonal projections in the brain by magnetic resonance imaging. Ann Neurol 45:265–269

Moseley ME, Cohen, Y., Kucharczyk J, Mintorovitch J, Asgari HS, Wendland MF, Tsuruda J, Norman D (1990a) Diffusion-weighted MR imaging of anisotropic water diffusion in cat central nervous system. Radiology 176:439–445

Moseley ME, Kucharczyk J, Mintorovitch J, Cohen Y, Kurhanewicz J, Derugin N, Asgari H, Norman D (1990b) Diffusion-weighted MR imaging of acute stroke – correlation with T2-weighted and magnetic susceptibility-enhanced MR imaging in cats. Am J Neuroradiol 11:423–429

Pajevic S, Pierpaoli C (1999) Color schemes to represent the orientation of anisotropic tissues from diffusion tensor data: application to white matter fiber tract mapping in the human brain. Magn Reson Med 42:526–540

Sinha S, Bastin ME, Whittle IR, Wardlaw JM (2002) Diffusion tensor MR imaging of high-grade cerebral gliomas. Am J Neuroradiol 23:520–527

Zagzag D, Amirnovin R, Greco MA, Yee H, Holash J, Wiegand SJ, Zabski S, Yancopoulos GD, Grumet M (2000) Vascular apoptosis and involution in gliomas precede neovascularization: a novel concept for glioma growth and angiogenesis. Lab Invest 80:837–849

Zhang J, van Zijl PCM, Laterra J, Salhotra A, Lal B, Mori S, Zhou J (2007) Unique patterns of diffusion directionality in rat brain tumors revealed by high-resolution diffusion tensor MRI. Magn Reson Med 58:454–462

Part V
Therapy

Chapter 23

Resection of Brain Lesions: Use of Preoperative Functional Magnetic Resonance Imaging and Diffusion Tensor Tractography

Erik Magnus Berntsen and Asta Kristine Håberg

Abstract Blood-oxygenation-level-dependent functional magnetic resonance imaging (BOLD fMRI) and diffusion tensor imaging (DTI) are specialized MRI-techniques used to map eloquent cortices and neural tracts in gray and white matter of the brain, respectively. By having the patient performing given tasks while inside the MRI-scanner (e.g. finger tapping), it is possible to map the cortical areas active during task performance (e.g. primary motor cortex) and visualize them as color maps overlain anatomical MRI-images. The most commonly areas mapped before neurosurgery in patients with brain lesions are primary motor and language areas. By acquiring DTI-images and further process them using a technique called tractography, it is possible to map important neural tracts and visualize them as fiber bundles (e.g. the corticospinal tract). The results from these examinations may be helpful during planning and resection of brain lesions, by providing information on functional eloquent cortices and important white matter tracts in close proximity to the lesion, as the goal of surgery is to maximize resection without inflicting neurological damage. This functional information may also be incorporated into neuronavigation systems and utilized during surgery, thus named functional neuronavigation. The following chapter will give an introduction to the basis of BOLD fMRI and DTI, as well as their methodological considerations and how to perform these investigations in practice, followed by how they have been utilized for preoperative mapping and functional neuronavigation so far. Finally, some suggestions to future directions are given.

Keywords Brain lesions · fMRI · Diffusion tensor imaging (DTI) · Motor and language regions · Diffusion tensor tractography (DTT)

Introduction

Magnetic resonance imaging (MRI) is a key stone in imaging of all brain lesions with a high degree of anatomical detail offering valuable information with regard to both diagnostics and treatment. In the last two decades additional MRI-techniques such as blood-oxygenation-level-dependent functional MRI (BOLD fMRI) and diffusion tensor imaging (DTI) have emerged. BOLD fMRI is used for mapping of eloquent cortices (e.g., motor and language regions) by using color-coded statistical maps overlaid on anatomical images of the brain. DTI can be used for mapping of white matter and through an analysis called diffusion tensor tractography (DTT) such images can visualize the white matter neural tracts as three-dimensional fiber bundles. Together with conventional anatomical imaging, functional imaging with BOLD fMRI and DTT can be helpful during planning and resection of brain lesions, as the goal of neurosurgery is to maximize resection without inflicting neurological deficits. This functional information from the MRI images may also be incorporated into neuronavigation systems and utilized during surgery, thus named functional neuronavigation. Preoperative mapping and functional neuronavigation during neurosurgery are

E.M. Berntsen (✉)
Department of Radiology, St. Olavs Hospital, University Hospital of Trondheim, N-7006, Trondheim, Norway; MI Lab and Department of Circulation and Medical Imaging, Norwegian University of Science and Technology, Trondheim, Norway
e-mail: erik.berntsen@stolav.no; erik.berntsen@gmail.com

M.A. Hayat (ed.), *Tumors of the Central Nervous System, Volume 4*,
DOI 10.1007/978-94-007-1706-0_23,

currently the best-established clinical application of BOLD fMRI and DTT. There are however important pitfalls to be aware of when using these technique which we will discuss in the following chapter. Finally we will also give some thoughts on future directions for BOLD fMRI and DTT for use in preoperative planning.

Magnetic Resonance Imaging

Magnetic resonance imaging (MRI) is an imaging technique able to depict inner organs of the human body based on the physical properties of unpaired atomic nuclei in the organ. As the two major components of the human body, water and fat, are abundant with hydrogen atoms (^{1}H), this is the nuclei most commonly used for medical imaging. By placing the hydrogen atoms in a large static magnetic field and manipulate them with electromagnetic fields, it is possible to derive information about tissue properties at specific spatial localizations and thereby produce images of the organ examined. Different tissue properties may be derived and used for image production. For a quantitative introduction to the theoretical basis of MRI other more detailed textbooks are recommended, e.g., *MRI – The Basics* (Hashemi et al. 2003) or *Magnetic Resonance Imaging: Physical Principles and Sequence Design* (Haacke et al. 1999).

The first MRI-image of in vivo human anatomy was acquired in 1977 by Peter Mansfield and Andrew A. Maudsley and was a cross section through Maudley's finger revealing *considerable anatomical detail, particularly of the soft tissue regions* taking 23 min to produce. In clinical practice today MRI is primarily used to identify tissue pathology using a combination of different MRI sequences (e.g., T_1 and T_2 weighting). MRI sequences depicting tissue function and metabolism are, however, rapidly evolving and increasingly used in the clinic, such as BOLD fMRI, DTI and magnetic resonance spectroscopy.

Functional Magnetic Resonance Imaging

Blood-oxygenation-level-dependent functional MRI (BOLD fMRI), hereafter referred to as fMRI, is a specialized MRI-technique using a T_2^*-weighted gradient echo sequence. The basis for this technique was first reported in 1990 by Ogawa and colleagues. They discovered that this sequence was sensitive to changes in the concentration of de-oxygenated hemoglobin (deoxy-Hb) in blood. Furthermore, they reported signal changes around the vessels in the rat brain at different levels of blood oxygenation, and based on this suggested that this sequence could be used to study regional brain activity, similar to positron emission tomography (PET) (Ogawa et al. 1990). These discoveries were the basis of functional neuroimaging with fMRI and the following numerous papers using fMRI to study human brain function that has come the last two decades.

The Basis of the BOLD Signal

The physical basis of the BOLD signal lay in the physical properties of deoxy-Hb, as it is paramagnetic and thus influences the MRI signal. Changes in the level of deoxy-Hb compared to oxygenated-Hb (oxy-Hb) will therefore give a variation in the measured MRI signal, known as the BOLD signal (Ogawa et al. 1990). The neurophysiological underpinnings of the BOLD signal are related to secondary changes in local cerebral blood flow, volume, and level of oxygenation, which in turn is related to metabolism following neuronal activity, the so-called neurovascular coupling. The complex mechanism of this neurovascular coupling is not fully understood and several models are proposed, but none of these fully explain all aspects of the biophysics giving rise to the BOLD signal (Buxton et al. 2004). The most intuitive and simplified explanation is that local neuronal activity requires an increased local metabolism with an increased need for glucose and oxygen. Increased neuronal activation initiates a feed forward reaction leading to changes in the local blood supply. A local increase in blood flow and concomitant increase in blood volume, supplying the extra glucose and oxy-Hb needed is thus ensured. The amount of oxy-Hb delivered is, however, greater than the amount of oxygen extracted, giving a paradoxical local increase in oxy-Hb and thus a local decrease in the concentration of deoxy-Hb. Even though the neurovascular coupling is not understood in detail, it has been shown that fMRI activations do reflect increase in neural activity and mostly the input and intra-cortical

processing in a given cortical area (Logothetis and Pfeuffer 2004). Furthermore, it has been shown that fMRI has good concordance with other brain mapping techniques such as intraoperative motor evoked potentials and intraoperative electrocortical mapping (Lehericy et al. 2000; Bizzi et al. 2008)

Methodological Considerations Regarding the BOLD Signal

The T_2^*-weight echo planar imaging sequence (EPI) used for fMRI is very sensitive to inhomogeneities in the magnetic field and prone to artifacts, giving rise to signal loss as well as spatial and intensity distortions. Signal loss is in particular a problem in regions where there is crossing between tissues (e.g., brain tissue close to air filled sinuses) and metal shavings from prior operations. There exist strategies for avoiding or overcoming these problems. One approach is to use alternative MRI-sequences not based on T_2^*-weighting, but rather spin echo BOLD fMRI or arterial spin labeling. There are also methods for mapping of B_0-field variations which are used to unwarp distortions after acquisition. For echo planar imaging, scans with opposite phase encoding polarities can be applied to eliminate spatial distortions and recover signal dropout. The extent of these B_0 inhomogeneities varies with the strength of the static magnetic field, which also affects the BOLD signal. It has been shown that an increased proportion of the BOLD signal arises from the brain tissue (and thus the active neurons) rather than draining veins at higher field strengths. Furthermore, the contrast-to-noise ratio also increases with higher field strength, giving a stronger BOLD signal.

A Tool for Research or the Clinic?

Functional MRI has grown to be one of the most important tools in neuroscience having the undisputable advantage of non-invasively mapping brain functions at high spatial and fair temporal resolution. There has also been a great interest in using fMRI in clinical research to study diseases of the brain such as Parkinson's and Alzheimer's disease, schizophrenia and bipolar disorder, amongst others. In clinical practice fMRI was first used for preoperative mapping prior to surgery of epileptic foci, neoplastic brain tumors and arteriovenous malformations as a supplement to the intracarotid amytal test (Wada test) and invasive mapping (Jack et al. 1994; Morris et al. 1994; Latchaw et al. 1995). Other areas of clinical use have been explored, such as imaging of auditory cortex prior to cochlear implantation. Preoperative mapping is currently the best-established clinical application of fMRI (Matthews et al. 2006).

Adapting fMRI to clinical practice raises several concerns. When used as a research tool, fMRI studies are most often performed at a group level, having no direct consequence for the individual participant. When used for clinical purposes, however, the investigation is done on an individual basis, possibly having major consequences for each patient. Thus, when using fMRI for preoperative mapping it is of utmost importance to avoid false negatives, i.e., no fMRI-activation in brain areas active during task performance, as they could lead to resection of eloquent cortices. Similarly, false positive, i.e., fMRI-activation in brain areas not active during task performance, could lead to limited resection of the brain lesion. These issues necessitate that fMRI has as high sensitivity and specificity as the gold standard mapping technique direct cortical stimulation (DCS). The sensitivity and specificity of fMRI varies among brain regions. Most studies find better sensitivity and specificity for fMRI of motor areas than for language areas when compared to DCS, probably due to the larger ontogenetic and phylogenetic stability of the primary motor area, at both macroscopic and microscopic levels (Jack et al. 1994; Roux et al. 1999; Giussani et al. 2010). Moreover, language areas show larger individual variability with regard to lateralization and are more complex due to their involvement in more complex cognitive functions. These issues make many clinicians reluctant to use fMRI alone for mapping of language areas. Instead preoperative fMRI is combined with intraoperative DCS to lower the risk of postoperative language deficits (Giussani et al. 2010). Nevertheless, as language fMRI holds great potential for future development and application its use in the clinic is growing.

fMRI in Practice and Methodological Considerations

An fMRI investigation consists of several steps, starting with a subject lying inside the MRI scanner performing a particular task at given times, while MR images are acquired. After scanning, these images need to be pre-processed before statistical analysis is performed in order to produce color-coded statistical parametric activation maps. Thereafter, these activation maps need to be interpreted. Obviously the process from image acquisition to interpreted functional maps consists of several steps each vulnerable to different sources of error. Thus, expertise in fMRI acquisition, analysis and functional neuroanatomy is required to perform these investigations accurately. Several books on these topics have been written and are recommended for further reading (Jezzard et al. 2001; Friston et al. 2007).

Tasks

The cortical area to be mapped determines which task(s) the patient performs. Preoperative mapping using different motor and language tasks are the most frequent. For motor tasks the subjects are instructed to do for instance finger-tapping when a finger or other symbol is presented. For language tasks the subjects are instructed to do for instance word generation covertly without moving the tongue or mouth when a letter is presented. Covert word generation is necessary in order to avoid both movement artifacts and artifacts due to changes in the amount of air in the mouth in relation to vocalization. It is important that the subjects undergoing an fMRI investigation are able to perform the given task, i.e., that he/she performs the task when indicated by the instructions (at the right time) in order for correct analysis of the collected MRI data. This may be controlled fairly well by observing the subject if a motor task is performed, or by using some sort of response device to monitor task performance within each block of activity. However, controlling a covertly executed language task is difficult. One possibility is to ask the patients afterwards how it went and to perform the task again outside the scanner to get an impression of performance. Such post-scanning evaluations will, however, be subjective and effects such as fatigue could impact results, hence results may be confounded. Another possibility is to have the subjects push a response button each time they solve a particular task (i.e., produce a new word). This will, however, make the task much harder to perform, and recruit both motor cortex and cortical areas for dual tasking in addition to the language cortex, making the analysis and interpretation of activation maps much more complicated. Moreover, patient compliance may become very low as task complexity increases. This exemplifies that for some fMRI investigations it is difficult to know with absolute certainty how well the task was performed. It is also important that the subject is able to lie still when solving the task, as movement of the head during scanning gives rise to signal distortions. This is usually solved to a certain extent with physical constraints of the head (e.g., foam pads). The ability to correctly perform the task while remaining still will vary with age, cognitive function and intracranial pathology of the subjects. These factors are therefore important to consider when planning an fMRI investigation in order to ensure that the tasks best suited to delineate the cortical regions close to the lesion are used, with the highest degree of patient compliance.

Task Presentation

The task is usually presented visually (but may be presented auditory) either through MRI-compatible goggles or by using a LCD-screen located behind the scanner opening and viewed via a mirror mounted on the head coil. The task can be of different designs, such as block-, event-related-, mixed block-event related or resting-state-design. For preoperative mapping, block design is most frequently used as it yields strong and robust activation, with minimum duration of fMRI acquisition. In a block design, the task is usually presented in blocks between 15 and 30 s interleaved with equally long or longer blocks of rest, e.g., four blocks of 27 s with finger movement interleaved with five blocks of 27 s of rest (Fig. 23.1). Rest is usually fixation on a cross hair, but can also be presentation of random letters/signs. It is important that the subject performs the task for the full block, i.e., continuously repeats the task, in order to create a steady BOLD effect over time possible to detect with later statistical analysis.

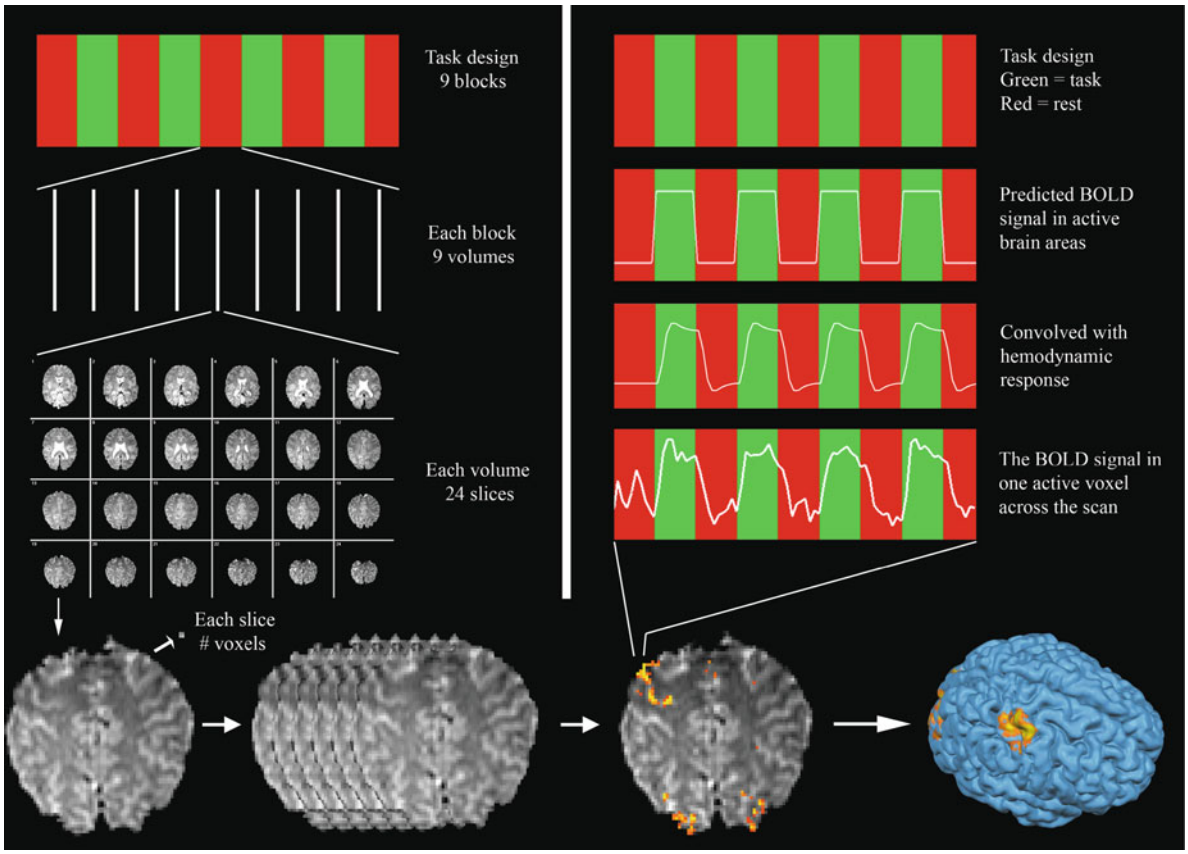

Fig. 23.1 *Left panel*: an example of an fMRI-investigation, with four blocks of activity in *green* (solving the assigned task) and five blocks of rest in *red* (e.g., cross hair fixation). In this example, each block consist of 9 volumes each consisting of 24 slices covering the part of the brain investigated (usually the whole brain is covered). Each slice consists of a given number of voxels (volumetric picture elements). *Right panel*: when analyzing fMRI-data the BOLD signal for active brain areas in the activity blocks is predicted and then convolved with the hemodynamic response, before applying the general linear model to produce statistical activation maps. *Lower panel*: in this example, each part of the brain (represented by a voxel) is mapped 81 times, and then statistical analysis is applied to each voxel separately, to identify those voxels having intensity-variations matching the convolved BOLD signal. Those voxels fitting the model are highlighted in *orange/yellow* colors. In this example, the subject has moved only his left fingers producing significant activation in the primary motor cortex for finger movement in the right hemisphere, but also additionally activation in the visual cortex as it has been active in the same blocks

Scanning Parameters

fMRI for clinical purposes is typically done on a 1.5 or 3 T MRI scanner, using a gradient echo planar imaging (EPI) sequence with a repetition time (TR) of 1500–3000 ms, covering the whole brain (one volume), matrix-size between 64 × 64 and 128 × 128, and slice thickness of 2–5 mm. Each volume consists of between 20 and 40 slices, depending on the slice thickness. These scanning parameters will vary depending on the hardware and the programming of the EPI sequence. A typical block-design experiment with four blocks of task performance interleaved with five blocks of rest where each block consist of 9 volumes, would then consist of 81 whole-brain-volumes, taking 243 s to acquire (Fig. 23.1).

Pre-processing

Directly after image acquisition, while the patient is still in the scanner, it is possible to visually inspect the fMRI data acquired. If quality is low due to motion or artifacts, a new fMRI acquisition should be considered. When image acquisition is completed the fMRI

data has to be pre-processed to correct for head motion during scanning and remove cardio-respiratory artifacts and other cyclical related noise. Thereafter, many choose to perform spatial smoothing ("blurring") of the data, both to increase signal-to-noise ratio but also because some subsequent statistical analysis may require it in order to be valid. This pre-processing can be done using either manufacturer provided software on the MRI-scanner or the fMRI data can be exported and pre-processed offline on a personal computer using software for fMRI analysis (e.g., BrainVoyager, SPM, AFNI, FSL, nordicBrainEx). The pre-processing steps in the different analysis programs are basically similar, but due to differences in the implemented algorithms and optional user defined parameters entered into the analysis, somewhat different results can be obtained. This demonstrates the lack of standardized pre-processing methods for fMRI data. Most motion correction algorithms correct motion by describing six parameters, three for rotation and three for translation along the x, y, and z-axes, and produces line plots of the motion in the different directions that can be inspected. If there has been displacement exceeding 1–2 voxels or more than 5 mm, many choose to reject the datasets as the quality is significantly reduced. Furthermore, the fMRI-data should be visually inspected after motion correction to ensure that it has been successful. This can be done by presenting each EPI-slice, which depicts a cross-section of the same brain area but at different time points, in a rapid movie sequence where any gross uncorrected movement can be detected. The importance of visually inspecting the raw fMRI data cannot be stressed enough. Here one can identify areas with signal dropout, which otherwise is difficult to identify. In our opinion, visual inspection of fMRI data is particularly important in preoperative mapping as it is an easy way to avoid major pitfalls with potentially severe consequences.

Co-registration

In order to localize the eloquent cortex mapped with fMRI in sufficient anatomical detail, the fMRI data has to be co-registered to anatomical/structural images, which have greater anatomical detail. This procedure is usually partial automatic and partial manual and careful co-registration between the fMRI and anatomical T_1 weighted images is essential to ensure correct anatomical localization of the mapped function. Nevertheless, as the functional images and anatomical images are not identical, there will always be some discrepancy between them. The user can, however, ensure as good as possible co-registration within the regions of interest, being the areas with anticipated activations for the function investigated.

Statistical Analysis

After co-registration, statistical analysis has to be applied in order to identify activated brain areas. First the BOLD signal changes co-varying with the task performance are identified by convolving the BOLD signal changes over time with the timing of the task. This is done using assumptions about the temporal properties of the BOLD signal, the so-called canonical hemodynamic response function, which may be modeled according to different functions, for instance by either a single gamma or a double gamma function. For visualization of activity, statistical activation maps is then calculated using the general linear model (Friston et al. 1994) (Fig. 23.1). As previous mentioned the mechanism of the neurovascular coupling and the BOLD signal is not fully understood, thus the models of the hemodynamic response used in the statistical analysis are strictly speaking assumptions of the coupling between the hemodynamic changes and neuronal activity. It has been shown that the hemodynamic response varies across brain regions, an issue rarely considerer in fMRI studies or when used for preoperative mapping (Handwerker et al. 2004). Moreover, it has been indicated that brain pathologies such as glial tumors may reduce the BOLD signal at the edge of the tumor (Schreiber et al. 2000). Both these issues constitute methodological concerns making the inferences about neuronal activity based on changes in local cerebral blood flow, oxygenation and volumes even more difficult.

Statistical Thresholding

The statistical activation maps created represent brain-activity during task performance, but needs to be

statistically thresholded before interpreted (Fig. 23.1). There is no consensus on how to threshold fMRI activation maps for preoperative mapping. In general many choose $p \leq 0.05$ as threshold together with some kind of correction for multiple comparisons, for instance Bonferroni correction, Gaussian random field theory, false discovery rate or Monte Carlo simulations. It is also possible to add a cluster threshold, thus not visualizing clusters of activation smaller than a given value (e.g., a pre-specified number of voxels), based on the assumption that activations have to be of a certain size to consider significant. For preoperative planning a competent investigator (e.g., neuroradiologist) usually decides which clusters of activated voxels that are related to the task performed based on spatial extent of the activations, localization and cluster distribution. Individually thresholded activation maps for each subject and each task is usually used, aiming at producing activation maps unequivocally delineating the cortical area of interest.

Interpretation of Activation(s)

After pre-processing, co-registration, statistical analysis and thresholding, the neuroradiologist, neuroscientist and/or neurosurgeon can interpret the activation maps which usually consist of several activation clusters across the brain. A comprehensive understanding of the steps from image acquisition to activation maps is needed for correct interpretation of fMRI activation maps. Furthermore, each of the preceding steps should be carefully evaluated to determine whether it was successful or not. If not, one can easily be misled to draw erroneous conclusions and thus suggest wrong therapeutic strategies, which in a worst-case-scenario results in removal of functional brain regions. For instance, if a patient with bilateral language lateralization undergoes a reoperation due to regrowth of a frontal tumor, there may be residual metal from the skull drill inducing signal dropouts in the T_2*-weighted fMRI-images of the language areas in this hemisphere. This will produce fMRI-maps with language activations in only the healthy hemisphere and lead to the wrong interpretation that language is fully lateralized to the healthy hemisphere making a resection of the language areas in the hemisphere with the tumor safe. However, if the T_2*-weighted fMRI-images had been visually inspected the areas with signal dropout would have been identified and it would be obvious that conclusions could not made from the available data.

Another pitfall with interpretation of fMRI activations is that fMRI does not necessarily differentiate between essential and participating brain areas, but maps all brain areas active during task performance. With respect to preoperative fMRI this would especially apply to language functions where some areas are considered essential (e.g., Broca's) while others are contributory but non-essential (e.g., dorsolateral prefrontal cortex). Damage to an essential area would certainly result in aphasia while damage to a contributory area could lead to transient language difficulties. In the end, fMRI for preoperative mapping is inherently a user dependent process, heavily dependent on the interpreter's competence, comprehension of functional neuroanatomy and interpretation of the activation maps.

Consensus on Preoperative fMRI

As stated previously, there are no standardized tasks, task instructions, measure of task compliance, scanning procedures, pre-processing algorithms/parameters or interpretation of activations for clinical applications of fMRI. Consensus on these issues need to be obtained in order to produce objective and comparable information between centers engaged in this activity. A more standardized practice is one of the main challenges for clinical fMRI today and for the future. Even though there is no official consensus or guidelines on how to perform clinical fMRI, the American College of Radiology (ACR) and the American Society of Neuroradiology (ASFNR) have developed and published "Practice Guideline for Performance of fMRI of the Brain" as an educational tool (www.asfnr.org). These guidelines give some directions on indication, patient selection, scanning procedure, pre-processing, analysis and interpretation. Furthermore, the ASFNR has collected and published different motor, language, vision and memory-tasks used by their members for dissemination (www.asfnr.org). However, they emphasize that these guidelines are not official recommendations. Nevertheless, both these efforts are important steps in the evolving process of task standardization and creating guidelines for clinical fMRI.

Diffusion Tensor Imaging

The Basis of DTI and DTT

Diffusion tensor imaging (DTI) is developed from diffusion weighted MRI and uses a spin-echo sequence combined with two diffusion gradient pulses that enables detection of the water molecules motion, i.e., Brownian motion. When applying the diffusion gradients, water molecules, which have moved in a direction along the gradient, will give rise to signal loss. By applying the diffusion gradients in the X, Y, and Z direction, diffusion weighted images are created that represent diffusion in a given voxel. DTI is an advanced form of diffusion weighted imaging, where the gradients are applied in at least six directions (combinations of the X, Y, and Z direction), making it possible to create a mathematical model of diffusion in a three-dimensional space, known as the diffusion tensor. From this diffusion tensor it is possible to calculate the direction of maximum diffusivity, which has been shown to coincide with the fiber orientation in the white matter of the brain (Moseley et al. 1990). The more directions the gradients are applied in, the more accurate the estimate of the tensor becomes. Thus, by using DTI it is possible to map the anatomical location of neural tracts in the brain, e.g., the corticospinal tracts, the optic radiations, and the arcuate fasciculus.

Several different parameters can be derived from the DTI images, such as maps of fractional anisotropy (FA) which is a measure of the magnitude of anisotropic diffusion ranging from 0 (isotropic diffusion i.e., non-directional) to 1 (anisotropic diffusion i.e., strongly directional) (Basser and Pierpaoli 1996). Another frequently derived property of DTI is color coded maps, where the direction of maximum diffusivity is modulated with the FA-value, producing maps where the colors represent the direction of the fiber and the intensity represents the anisotropy (Fig. 23.2). The accepted convention for color coding is with blue representing the superior/inferior direction, red the left/right direction, and green the anterior/posterior direction. A third way of presenting the DTI images is through fiber tracking or tractography, which is a visualization technique for neural tracts in three dimensions (Figs. 23.2 and 23.3). These three-dimensional tracts are constructed based on different algorithms such as the TENsor Deflection (TEND) algorithm or the Fiber Assignment by Continuous Tracking (FACT) algorithm (Mori et al. 2002; Lazar et al. 2003). By using such algorithms one is able to calculate which voxels in the different sequential slices that probably are connected with each other based on the diffusion tensor. These algorithms automatically suggest tracts, that according to the mathematical model probably are connected, which then have to be virtually dissected using a region-of-interest tool, used according to anatomical knowledge, to produce plausible tracts. If the corticospinal tracts are to be visualized, region-of-interests have to be defined in regions that these tracts run through, e.g., the posterior limb of the internal capsule and the precentral gyrus. DTI and DTT are the only non-invasive methods of detecting and visualizing white matter tracts in vivo, thus having a great potential for both research and clinical practice. Some of the areas where DTI, and parameters derived from DTI, have been used are in studies of brain development, schizophrenia, Alzheimer's disease, epilepsy and neurosurgical planning.

DTI and DTT in Practice

A DTI investigation consists of several steps, but unlike fMRI the subject being scanned is not required to perform a task and thus only needs to lie still, while the images are being acquired. After scanning the images have to be processed using different algorithms before tractography is performed as a final step.

Methodological Considerations

The MRI-sequence used for DTI is even more sensitive to inhomogeneities of the magnetic field and head-movement than the sequence used for fMRI, causing greater distortions of the signal. Thus the importance of minimizing the head movement becomes even more important and cardiac gated synchronization of scan acquisition has been demonstrated useful in order to minimize brain pulsations following cardiac beats.

A fundamental problem for DTT is the lack of an in vivo gold standard for tractography, thus making it difficult to validate the different algorithms as well as the method itself, however, it has been shown that

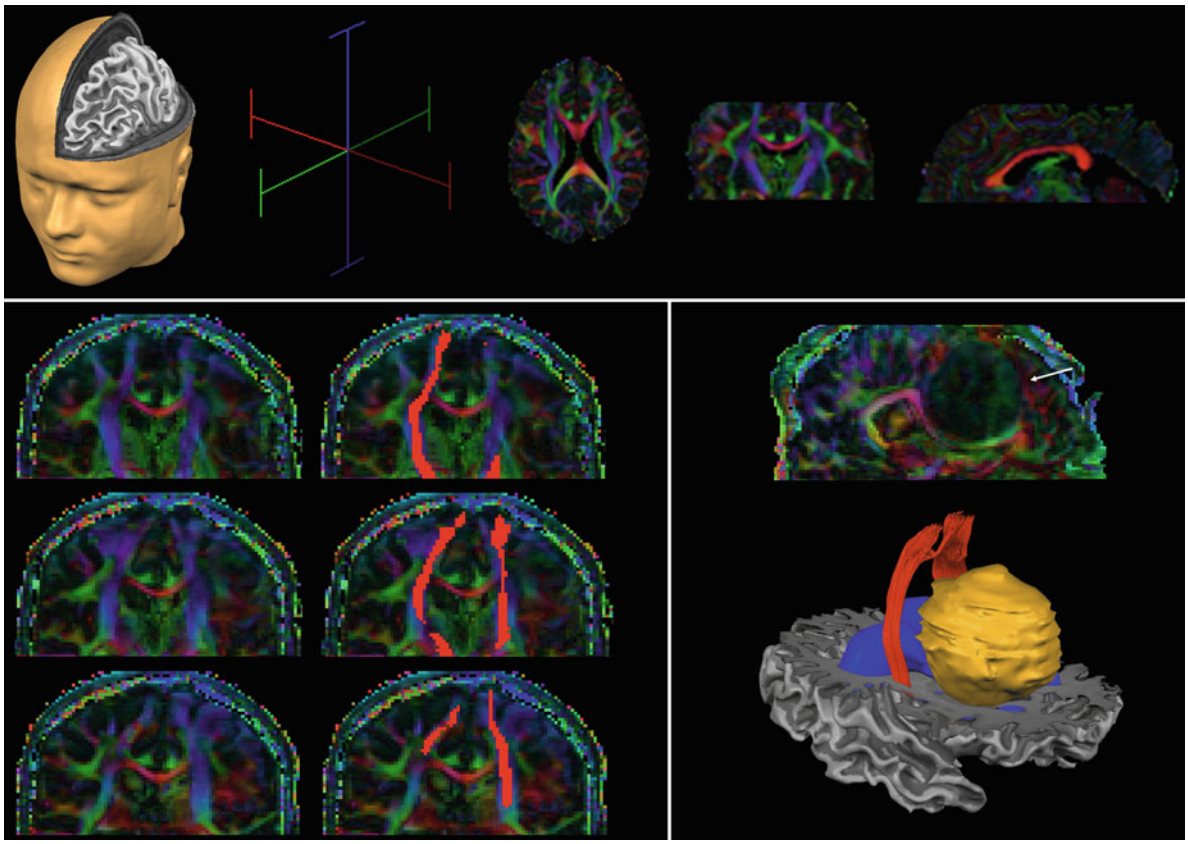

Fig. 23.2 *Top panel*: color coded maps of the white matter, where *blue* represents the superior/inferior direction, *red* the left/right direction, and *green* the anterior/posterior direction. Three slices of the brain in three different planes are shown, first an axial slice, then a coronal slice (where the corticospinal tracts can be seen in *blue*), and last a sagittal slice (where the corpus callosum can be seen in *red*). *Left lower panel*: coronal slices of the brain showing the white matter in color coded maps at the left and the same slices to the right where tractography (fiber tracking) has been performed and the corticospinal tracts are visualized as *red lines*. These tracts can be further visualized in three-dimensional models together with pathology and the rest of the brain, as shown in the *right lower panel*. *Right lower panel*: a sagittal slice of a patient's brain with a lesion (*arrow*) compressing the corpus callosum. By doing tractography of the corticospinal tracts, they can be found posterior to the lesion, as shown in the three-dimensional model at the bottom, with the lesion in orange, the corticospinal tracts as *red tubes* and the ventricular system in *blue*

DTT has good concordance with intraoperative subcortical mapping (Bello et al. 2008). Furthermore, DTT processing consists of several steps with the potential of introducing error(s). For instance, the user has to choose minimum values for FA (e.g., 0.15–0.25) and maximum allowed angulations of tracts (e.g., 40–50°) to be used in the tracking algorithms. White matter regions where there are several fiber bundles with different orientations or where fiber bundles "kiss", cross, merge or diverge are particularly troublesome for the tracking algorithms. In such regions the algorithm can either not track the fiber bundles or will track pathways that do not exist, and similar problems arise in the presence of tumor and edema. Some of these problems might be overcome using novel tracking algorithms or more advanced processing procedures such as probabilistic diffusion tractography. Furthermore, the use of manually drawn regions-of-interests for tracking of white matter bundles makes DTT heavily user dependent. The user performing the tractography should thus have detailed knowledge of neuroanatomy of the white matter of interest and tumor biology.

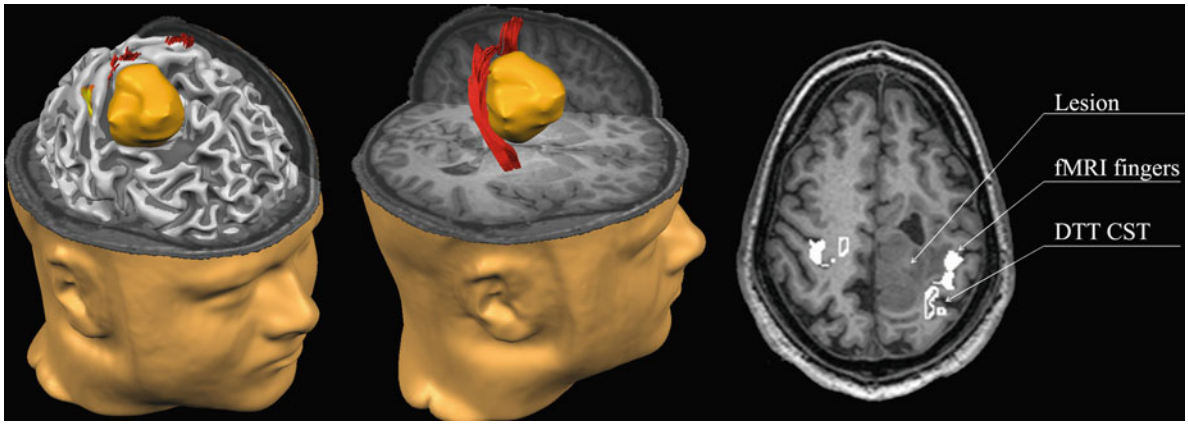

Fig. 23.3 fMRI, functional magnetic resonance imaging; DTT, Diffusion tensor tractography; CST, Corticospinal tract. *Left and middle:* Three-dimensional models of the brain surface in *gray*, a brain lesion in *orange*, the corticospinal tracts as red tubes, and the fMRI activations from finger-movements in *yellow/orange* (on the brain surface in the *left* figure). In the *middle* figure, the brain surface has been removed so one can see how the lesion has dislocated the corticospinal tract laterally and posteriorly. *Right:* An axial T1-weighted slice from the same patient, showing the brain lesion with superimposed fMRI activations as high-intensity white areas and DTT as high-intensity white outlines. This is identical to how the data is imported to the neuronavigation system and used intraoperatively (together with intraoperative ultrasound)

Preoperative Mapping

Recent guidelines from the National Comprehensive Cancer Network has acknowledged the growing evidence that more extensive surgical resection is correlated to prolonged survival for both low- and high-grade gliomas, supporting the goal of maximizing brain tumor resection without inflicting new neurological deficits (Sanai and Berger 2008). This poses a difficult challenge when operating on lesions located near eloquent areas, making accurate localization of eloquent cortices, as well as the white matter tracts connected to these cortical areas, an essential adjunct to successful surgical excision in these patients. To this end, the use of preoperative fMRI and DTI/DTT has grown popular due to their non- invasiveness and little to no additional surgery time required, but also due to the visualization possibilities enabling better understanding of the complicated spatial relationship between the lesion, eloquent cortices and white matter tracts (Fig. 23.3).

Development

One of the first papers reporting the use of fMRI in patients was by Jack et al. (1994), who used both fMRI and invasive cortical mapping to map the motor cortex of two patients with epileptic seizures due to neoplastic brain tumors located in close proximity to the primary motor cortex. They found a correlation between the two techniques, and suggested that preoperative mapping was a potentially useful clinical application of fMRI. This was followed shortly after by Morris et al. (1994) who mapped the language and motor areas of three patients with epilepsy syndromes. Later on Latchaw et al. (1995) demonstrated the same in patients with arteriovenous malformations (AVMs). Following these reports, there was a dramatic increase in the use of fMRI in preoperative mapping before neurosurgical procedures, focusing mostly on motor and language functions.

Clinical use of DTI was demonstrated by Witwer et al. (2002) in nine patients with neoplastic brain tumors and same year Mori et al. (2002) applied DTT to visualize neural fiber tracts in close proximity to neoplastic brain tumors in two patients. These reports have been followed by studies demonstrating the technique in larger number of patients both with neoplastic brain tumors and AVMs.

Combining fMRI and DTI/DTT

Some studies have investigated the combination of fMRI and DTI prior to neurosurgery. It was demonstrated by Ulmer et al. (2004) that twice as many

functional systems were localized within 5 mm of the tumor borders when DTI and fMRI were combined compared to fMRI alone in 28 patients. The functional systems taken into consideration were language, speech, vision, motor and pre-motor functions. Furthermore, only one out of the 24 operated patients (4%) encountered unplanned surgically-induced deficit. A study by Hendler et al. (2003) based on 20 patients with brain lesions investigated with fMRI and DTI/DTT concluded that the combination of fMRI and DTI/DTT provided valuable information that could not be extracted using either method alone. Our own unpublished data supports this, as we reviewed 21 patients with brain lesions (all types of tumors) undergoing both motor fMRI and DTT of the corticospinal tract. In these patients we found a significant decrease in the lesion-to-eloquent-area distance when taking the DTT into account compared to the fMRI alone ($p = 0.001$). Furthermore, the use of DTT seemed crucial and invaluable for visualization and understanding of the complicated spatial relationship between the lesion, gray matter, and white matter fiber bundles (Figs. 23.2 and 23.3).

Mapping of the Primary Motor Cortex

The primary motor cortex controls voluntary movements and is strongly somatotopic organized along the precentral gyrus. Damage to this region during surgery has severe consequences for the patients and has thus been subject to intra-operative mapping since the 1930s. With the advent of fMRI various motor tasks have been used for preoperative mapping, including finger tapping, hand clenching, elbow and shoulder movement, as well as tongue, lip, foot, and toe movement. In our experience, the motor tasks which should be used are movement of the fingers, toes and tongue, as they are robust in identifying their respective motor areas. Furthermore, these motor tasks activate regions at regular intervals along the convexity of the hemisphere making it possible to functionally delineate the primary motor cortex, even in the presence of edema and anatomical distortions. Whether the three tasks should be used alone or in combination depends on how difficult it is to identify the primary motor cortex anatomically, i.e., how gross the anatomy is distorted, the location and size of the tumor with regard to the expected eloquent areas, and the clinical status of the patient. One major constraint with the tongue task, however, is that it is often subject to gross head movement as many patients find it difficult to perform it without moving the head and in such cases movements of the lips may be a better choice. The final decision on choice of tasks should be decided by the neurosurgeon and neuroradiologist in collaboration.

Mapping of Language Areas

Mapping of cortical language areas prior to neurosurgery relies on the classical brain-language model derived from the works of Broca and Wernicke in the 19th century. This model consists of an inferior frontal region for speech production (Broca's area) and a posterior superior temporal region for speech comprehension (Wernicke's area) in the left hemisphere. In modern linguistic and cognitive neuroscience it is uncontroversial that this model is empirically wrong, as it does not explain the range of aphasia syndromes, and linguistically underspecified, as language is not merely production and comprehension. Moreover, this model is anatomically underspecified as also other areas contribute to language processing (Poeppel and Hickok 2004). Recent MRI studies of the preserved brains of two of Broca's patients indicate inconsistencies between what is now called Broca's area and the area originally identified by Broca (Dronkers et al. 2007). Therefore new models for cortical organization of language have been presented and are continuously being developed. However, the classical model is a useful simplification of language distribution for clinical purposes such as preoperative mapping, where the main purpose is to determine hemispheric lateralization and localization of language areas definitively yielding speech disturbances and/or aphasia if damaged. It is therefore important to choose a language task which will activate and unequivocally define the language regions in proximity of the brain lesion with a high degree of reproducibility. In clinical practice, several language tasks are used e.g. word/verb-generation, passive listening, object naming etc. In our experience, a word-generation task should be preferred for mapping of the frontal language area and a responsive naming task (e.g., "what do you call a tall pink bird") for the temporal language region, as these tasks have high spatial consistency across subjects and fair reproducibility of activation size and localization. Future

research should be directed towards developing new language tasks and evaluate which tasks are the most appropriate for preoperative language mapping.

Functional Neuronavigation

During the last two decades several neuronavigation systems for performing frameless stereotactic neurosurgery have been developed, where anatomical data can be used intraoperatively to navigate in the brain during surgery. Thus, the need for integration of functional information from fMRI and DTI into the navigation systems has emerged, in order to take advantage of this functional information also during surgery. Given the functional nature of the information this has been named functional neuronavigation.

Development

Some of the first articles on functional neuronavigation were by Maldjian et al. (1997) and Schulder et al. (1997), where they integrated fMRI into a neuronavigation system, allowing functional identification of eloquent cortex during surgery. This was followed by several other reports in the years to come, either in larger number of patients or combined with other mapping techniques such as direct cortical stimulation. The information from DTI and DTT has also been integrated into such neuronavigation systems, as demonstrated by Nimsky et al. (2006), where fiber tract data from patients with brain lesions were reliably integrated into the navigation system. As a natural consequence, integration of combined fMRI and DTT images into neuronavigation systems has been demonstrated and used for functional neuronavigation in brain lesion patients. There have been a number of clinical papers suggesting that the additional information provided by functional imaging (fMRI and/or DTT) is highly valuable and enables safe resection (Haberg et al. 2004; Yu et al. 2005) especially when incorporated into a neuronavigation system (Krishnan et al. 2004; Nimsky et al. 2006). In previous studies, either integrating fMRI data into neuronavigation systems (Krishnan et al. 2004; Coenen et al., 2005) or based on clinical demonstration of fMRI data and structural pathology (Haberg et al., 2004) a minimal distance between 5 and 15 mm for feasible surgical resection has been suggested. A few papers have also focused on functional navigation using intraoperative 3D ultrasound for intraoperative guidance as well as correction of brain shift (Coenen et al. 2005; Rasmussen et al. 2007).

To our knowledge only one prospective randomized trial examining the clinical impact of DTI-data on degree of tumor resection, clinical outcome and survival has been published. Wu et al. (2007) demonstrated that high-grade glioma patients benefit both in terms of increased tumor resection, improved postoperative outcome and time of survival when DTI-data was used to navigate during surgery, compared to those operated with conventional neuronavigation. This is supported by other non-randomized uncontrolled studies (Haberg et al. 2004; Krishnan et al. 2004; Berntsen et al. 2010).

Brain Shift

A big challenge for navigation based on preoperative images is the deformation of brain tissue during surgery (compared to preoperative images) occuring when the tumor is removed, which is called brain shift. The extent of brain shift for white matter tracts in patients undergoing tumor resection has been shown to vary from an inward shift of 8 mm to an outward shift of 15 mm, and this shift needs to be compensated for throughout the operation (Nimsky et al. 2007). Brain shift correction can be done mentally (i.e., in the surgeons mind), manually (i.e., landmark tracking) or preferably automatically as the shift may be non-uniform and difficult to predict. Several methods have been suggested, such as intraoperative MRI (Nimsky et al. 2007) and 3D ultrasound (Coenen et al. 2005). Our group has previously shown that it is feasible to update MRI data correcting for brain-shift using automatic co-registration of preoperative MRI with intra-operative ultrasound (Rasmussen et al., 2007).

Future Directions

Even though the literature is full of illustrative case reports and studies demonstrating the usefulness of fMRI and DTT before and during neurosurgery, some

issues remains to be resolved. Firstly, there is no consensus as to tasks, task presentation, image acquisition, pre- and post-processing, or interpretation of the activation maps or tractograms produced. Secondly, there is a lack of randomized studies demonstrating significant benefits on final outcome, i.e., improved neurological status and/or survival of the patient, when using fMRI and DTT for preoperative mapping or functional neuronavigation. In spite of this, fMRI and DTT have gained wide popularity, probably due to the promising prospects of further development and intuitive importance of locating eloquent cortices and their white matter tracts. The challenges ahead lie in standardizing clinical fMRI and DTT and carrying out clinical randomized trials or prospective outcome studies showing significant effect on morbidity or mortality in patients with brain lesions.

References

Basser PJ, Pierpaoli C (1996) Microstructural and physiological features of tissues elucidated by quantitative-diffusion-tensor MRI. J Magn Reson Ser B 111:209–219

Bello L, Gambini A, Castellano A, Carrabba G, Acerbi F, Fava E, Giussani C, Cadiolib M, Blasi V, Casarotti A, Papagno C, Gupta AK, Gaini S, Scotti G, Falini A (2008) Motor and language DTI Fiber Tracking combined with intraoperative subcortical mapping for surgical removal of gliomas. Neuroimage 39:369–382

Berntsen EM, Gulati S, Solheim O, Kvistad KA, Torp SH, Selbekk T, Unsgard G, Haberg AK (2010) Functional magnetic resonance imaging and diffusion tensor tractography incorporated into an intraoperative 3-dimensional ultrasound-based neuronavigation system: impact on therapeutic strategies, extent of resection, and clinical outcome. Neurosurgery 67:251–264

Bizzi A, Blasi V, Falini A, Ferroli P, Cadioli M, Danesi U, Aquino D, Marras C, Caldiroli D, Broggi G (2008) Presurgical functional MR imaging of language and motor functions: validation with intraoperative electrocortical mapping. Radiology 248:579–589

Buxton RB, Uludag K, Dubowitz DJ, Liu TT (2004) Modeling the hemodynamic response to brain activation. Neuroimage 23:S220–S233

Coenen VA, Krings T, Weidemann J, Hans FJ, Reinacher P, Gilsbach JM, Rohde V (2005) Sequential visualization of brain and fiber tract deformation during intracranial surgery with three-dimensional ultrasound: an approach to evaluate the effect of brain shift. Neurosurgery 56:133–141; discussion 133–141

Dronkers NF, Plaisant O, Iba-Zizen MT, Cabanis EA (2007) Paul Broca's historic cases: high resolution MR imaging of the brains of Leborgne and Lelong. Brain 130:1432–1441

Friston KJ, Ashburner J, Kiebel SJ, Nichols TE, Penny WD (2007) Statistical parametric mapping: the analysis of functional brain images. Academic Press, Elsevier, London, UK

Friston KJ, Holmes AP, Worsley KJ, Poline JP, Frith CD, Frackowiak RSJ (1994) Statistical parametric maps in functional imaging: a general linear approach. Hum Brain Mapp 2:189–210

Giussani C, Roux FE, Ojemann J, Sganzerla EP, Pirillo D, Papagno C (2010) Is preoperative functional magnetic resonance imaging reliable for language areas mapping in brain tumor surgery? Review of language functional magnetic resonance imaging and direct cortical stimulation correlation studies. Neurosurgery 66:113–120

Haacke EM, Brown RW, Thompson MR, Venkatesan R (1999) Magnetic resonance imaging: physical principles and sequence design. WILEY-LISS, New York, USA

Haberg A, Kvistad KA, Unsgard G, Haraldseth O (2004) Preoperative blood oxygen level-dependent functional magnetic resonance imaging in patients with primary brain tumors: clinical application and outcome. Neurosurgery 54:902–914

Handwerker DA, Ollinger JM, D'Esposito M (2004) Variation of BOLD hemodynamic responses across subjects and brain regions and their effects on statistical analyses. Neuroimage 21:1639–1651

Hashemi RH, Bradley WG Jr, Lisanti CJ (2003) MRI – the basics. Lippincott Williams & Wilkins, Philadelphia, PA.

Hendler T, Pianka P, Sigal M, Kafri M, Ben-Bashat D, Constantini S, Graif M, Fried I, Assaf Y (2003) Delineating gray and white matter involvement in brain lesions: three-dimensional alignment of functional magnetic resonance and diffusion-tensor imaging. J Neurosurg 99:1018–1027

Jack CR, Thompson RM, Butts RK, Sharbrough FW, Kelly PJ, Hanson DP, Riederer SJ, Ehman RL, Hangiandreou NJ, Cascino GD (1994) Sensory-motor cortex – correlation of presurgical mapping with functional MRI and invasive cortical mapping. Radiology 190:85–92

Jezzard P, Matthews PM, Smith SM (2001) Functional MRI – an introduction to methods. Oxford University Press Inc., New York, USA

Krishnan R, Raabe A, Hattingen E, Szelenyi A, Yahya H, Hermann E, Zimmermann M, Seifert V (2004) Functional magnetic resonance imaging integrated neuronavigation: correlation between lesion-to-motor cortex distance and outcome. Neurosurgery 55:904–914

Latchaw RE, Hu XP, Ugurbil K, Hall WA, Madison MT, Heros RC (1995) Functional magnetic-resonance-imaging as a management tool for cerebral arteriovenous-malformations. Neurosurgery 37:619–625

Lazar M, Weinstein DM, Tsuruda JS, Hasan KM, Arfanakis K, Meyerand ME, Badie B, Rowley HA, Haughton V, Field A, Alexander AL (2003) White matter tractography using diffusion tensor deflection. Hum Brain Mapp 18:306–321

Lehericy S, Duffau H, Cornu P, Capelle L, Pidoux B, Carpentier A, Auliac S, Clemenceau S, Sichez JP, Bitar A, Valery CA, Van Effenterre R, Faillot T, Srour A, Fohanno D, Philippon J, Le Bihan D, Marsault C (2000) Correspondence between functional magnetic resonance imaging somatotopy and individual brain anatomy of the central region: comparison with intraoperative stimulation in patients with brain tumors. J. Neurosurg. 92:589–598

Logothetis NK, Pfeuffer J (2004) On the nature of the BOLD fMRI contrast mechanism. Magn Reson Med 22:1517–1531

Maldjian JA, Schulder M, Liu MC, Mun IK, Hirschorn D, Murthy R, Carmel P, Kalnin A (1997) Intraoperative functional MRI using a real-time neurosurgical navigation system. J Comput Assist Tomogr 21:910–912

Matthews PM, Honey GD, Bullmore ET (2006) Applications of fMRI in translational medicine and clinical practice. Nat Rev Neurosci 7:732–744

Mori S, Frederiksen K, Van Zijl PCM, Stieltjes B, Kraut MA, Solaiyappan M, Pomper MG (2002) Brain white matter anatomy of tumor patients evaluated with diffusion tensor imaging. Ann Neurol 51:377–380

Morris GL, Mueller WM, Yetkin FZ, Haughton VM, Hammeke TA, Swanson S, Rao SM, Jesmanowicz A, Estkowski LD, Bandettini PA, Wong EC, Hyde JS (1994) Functional magnetic-resonance-imaging in partial epilepsy. Epilepsia 35:1194–1198

Moseley ME, Cohen Y, Kucharczyk J, Mintorovitch J, Asgari HS, Wendland MF, Tsuruda J, Norman D (1990) Diffusion-weighted MR imaging of anisotropic water diffusin in cat central-nervous-system. Radiology 176:439–445

Nimsky C, Ganslandt O, Fahlbusch R (2006) Implementation of fiber tract navigation. Neurosurgery 58:ONS-292-303; discussion ONS-303–304

Nimsky C, Ganslandt O, Hastreiter P, Wang R, Benner T, Sorensen AG, Fahlbusch R (2007) Preoperative and intraoperative diffusion tensor imaging-based fiber tracking in glioma surgery. Neurosurgery 61:178–185; discussion 186

Ogawa S, Lee TM, Nayak AS, Glynn P (1990) Oxygen-sensitive contrast in magnetic-resonance image of rodent brain at high magnetic-fields. Magn Reson Med 14:68–78

Poeppel D, Hickok G (2004) Towards a new functional anatomy of language. Cognition 92:1–12

Rasmussen IA, Lindseth F, Rygh OM, Berntsen EM, Selbekk T, Xu J, Hernes TAN, Harg E, Haberg A, Unsgaard G (2007) Functional neuronavigation combined with intra-operative 3D ultrasound: initial experiences during surgical resections close to eloquent brain areas and future directions in automatic brain shift compensation of preoperative data. Acta Neurochir 149:365–378

Roux FE, Boulanouar K, Ranjeva JP, Tremoulet M, Henry P, Manelfe C, Sabatier J, Berry I (1999) Usefulness of motor functional MRI correlated to cortical mapping in rolandic low-grade astrocytomas. Acta Neurochir 141:71–79

Sanai N, Berger MS (2008) Glioma extent of resection and its impact on patient outcome. Neurosurgery 62:753–764

Schreiber A, Hubbe U, Ziyeh S, Hennig J (2000) The influence of gliomas and nonglial space-occupying lesions on blood-oxygen-level-dependent contrast enhancement. AJNR Am J Neuroradiol 21:1055–1063

Schulder M, Maldjian JA, Liu WC, Carmel PW, Mun IK, Carmel PW (1997) Functional MRI-guided surgery of intracranial tumors. Stereotact Funct Neurosurg 68:98–105

Ulmer JL, Salvan CV, Mueller WM, Krouwer HG, Stroe GO, Aralasmak A, Prost RW (2004) The role of diffusion tensor imaging in establishing the proximity of tumor borders to functional brain systems: implications for preoperative risk assessments and postoperative outcomes. Technol Cancer Res Treat 3:567–576

Witwer BP, Moftakhar R, Hasan KM, Deshmukh P, Haughton V, Field A, Arfanakis K, Noyes J, Moritz CH, Meyerand ME, Rowley HA, Alexander AL, Badie B (2002) Diffusion-tensor imaging of white matter tracts in patients with cerebral neoplasm. J Neurosurg 97:568–575

Wu JS, Mao Y, Zhou LF, Tang WJ, Hu J, Song YY, Hong XN, Du GH (2007) Clinical evaluation and follow-up outcome of diffusion tensor IMAGING-BASED functional neuronavigation: a prospective, controlled study in patients with gliomas involving pyramidal tracts. Neurosurgery 61:935–948

Yu CS, Li KC, Xuan Y, Ji XM, Qin W (2005) Diffusion tensor tractography in patients with cerebral tumors: a helpful technique for neurosurgical planning and postoperative assessment. Eur J Radiol 56:197–204

Chapter 24

Paradigms in Tumor Bed Radiosurgery Following Resection of Brain Metastases

David Roberge and Luis Souhami

Abstract Radiosurgery offers a mean of delivering prophylactic focused radiation to the periphery of a resection cavity where malignant cells may have been left behind at the time of tumor resection. There is now growing such use of adjuvant radiosurgery following resection of hematogenous brain metastases. Fifteen institutional series have reported on a total of 618 patients treated with radiosurgery to a tumor bed following microsurgery. These cases fall into three paradigms: adjuvant radiosurgery as an alternative to whole-brain radiotherapy (WBRT), radiosurgery as an intensification of adjuvant WBRT and adjuvant radiosurgery for patients having failed prior WBRT. For these paradigms the reported crude local control rates are 83, 95 and 95%, respectively. The procedure appears well tolerated with approximately a 5% risk of late radiation necrosis.

Keywords Radiosurgery · Brain metastases · Whole-brain radiotherapy · Neurological function · Local tumor control · Adult brain tumor

Introduction

Hematogenous metastases are the most common adult brain tumor, representing 100,000–200,000 cases per year in North America (Posner 1992; Johnson and Young 1996). Up to half of these patients will present with a single lesion. In selected patients, local treatment of single metastases has been prospectively shown to improve overall survival. For most small lesions radiosurgery will provide local tumor control comparable to that of microsurgery (Muacevic et al. 2008). However, in many cases, because of diagnostic ambiguity, mass effect or size, surgical resection will be necessary. Even though metastases do not tend to be highly invasive, local failures are common following these operations (Patchell et al. 1998). In addition, the first metastasis is often a harbinger of lesions to come with additional metastases appearing in <50% of patients. Adjuvant whole-brain radiation (WBRT) reduces the incidence of both types of recurrences, decreases the risk of neurological death but does not appear to prolong overall survival (Patchell et al. 1998; Mueller et al. 2009).

In patients treated primarily with stereotactic radiosurgery (SRS), where local control is acceptable without adjuvant treatment, deferring WBRT spares acute toxicity without apparent impact on overall survival (despite more frequent brain recurrences). Although recurrences are known to impair neurological function, a trial looking at neurocognitive function post treatment showed a more frequent decline in Hopkins Verbal Learning Test (HVLT) scores at 4 months (23% vs. 49%, p not available) when WBRT was used upfront vs. deferred (Chang et al. 2009). Treatment with SRS alone is thus increasingly common. Several hundred thousand patients have received SRS for in situ metastatic disease, making this the most common indication for SRS. The specific use of tumor bed SRS is a relatively recent phenomenon. It has been proposed as a means of decreasing the risk of local recurrence (where approximately half of failures occur) while deferring or avoiding the toxicities of WBRT.

D. Roberge (✉)
Department of Radiation Oncology, McGill University Health, Center/Montreal General Hospital, 1650 Cedar Avenue, Montreal, QC H3G 1A4, Canada
e-mail: David.roberge@mcgill.ca

M.A. Hayat (ed.), *Tumors of the Central Nervous System, Volume 4*,
DOI 10.1007/978-94-007-1706-0_24,

Although local recurrences are less frequent with the addition of WBRT, on an actuarial basis local recurrences actually remain common. At 1–2 years, these occur in 20–72% of cases (Patchell et al. 1998; Nieder et al. 2007; Rades et al. 2007, 2008). In our own experience of 69 patients treated from 2000 to 2005, the 2-year actuarial rate (censured at last imaging) of local recurrence after surgeon-reported gross total resection and WBRT was 67% (Alrefae et al. 2009). We thus chose to apply tumor bed SRS *in addition* to WBRT in an attempt to maximize local and in-brain control. The third situation where tumor bed SRS has been used is the scenario where a patient has already been treated with WBRT prior to surgery. In this paradigm, tumor bed SRS is chosen over repeated WBRT or observation.

Radiosurgery is not the only means of irradiating the tumor bed. Alternate published strategies include balloon brachytherapy, seed brachytherapy and conformal radiotherapy. Balloon brachytherapy (Gliasite, Cytyc Surgical Products) has the disadvantages of not being applicable to all surgical cavities, requiring manipulation of a liquid radioactive source, requiring an additional invasive procedure and having potential complications not seen with other types of radiation. Of 71 patients enrolled a Phase II trial for patients with single resected brain metastases, 62 had implants, and only 54 actually received brachytherapy (Rogers et al. 2006). Following brachytherapy, the actuarial 1-year incidence of radiation necrosis without tumor was 23%. One patient each had: CSF leak, hemorrhage and infection. Seed brachytherapy appears to lead to excellent local control but is a complex procedure that requires direct manipulation and placement of 15–66 radioactive sources per patient (Dagnew et al. 2007). Although it may persist as a niche treatment, it is unlikely to see widespread adoption in neurosurgical practice. Conformal radiation is a reasonable means of delivering additional dose to the tumor bed following WBRT. In a retrospective multi-institutional review (Rades et al. 2007), a 10–15 Gy boost (in five fractions) to a 1 cm margin around the pre-operative tumor volume appeared to result in both improved local control and overall survival. Conformal radiotherapy has also been reported as a single adjuvant modality. In a small Phase I/II trial, Coucke et al. reported no local failures after 50.4 Gy in 28 fractions was delivered to the tumor bed with conformal radiotherapy (Coucke et al. 1998). Despite the fact that all patients were initially free of active extra-cranial disease, the median survival was only 7.2 months with death from new brain metastases being common (58%). Such a protracted treatment seems cumbersome and would limit radiotherapy options at progression.

Radiosurgery Experience

Cases series were identified through MEDLINE searches and review of selected proceeding of national and international meetings. For the 13 series of SRS as an alternative to WBRT, patient characteristics and outcomes were averaged across series with weighting for the size of each series. For our own experience, cases were identified in the McGill University Health Centre radiosurgery database. They were retained if patients had a single hematogenous metastasis treated with resection and adjuvant SRS boost in addition to WBRT. Fifteen series were identified reporting on a total of 618 patients (Table 24.1). Of these, 495 were included in 13 series where the aim was to reduce local recurrence whilst deferring WBRT, 44 patients, in a single series, were treated with tumor bed SRS in addition to WBRT and 79 were treated in a series of tumor bed SRS delivered in the context of post-WBRT surgical salvage.

Radiosurgery Without WBRT

Patients in these series were typically somewhat heterogeneous. Non-small cell lung cancer was the most common primary malignancy (42%). A third of patients had one or more additional synchronous brain metastases, in some cases also treated with surgery and tumor bed SRS. In one report (Jagannathan et al. 2009), 6% of patients had had WBRT in addition to SRS but could not be separated out from the rest of the series.

Treatment was delivered using a variety of radiosurgery technologies (54% Gamma Knife). The target volumes ranged from 0.1 to 66.8 cc but the mean/median of each series were rather homogeneous at 8.5–10.7 cc. Dosing was prescribed in a volume and location dependant fashion with mean/median doses ranging from 10 to 19 Gy. In two of the series using

Table 24.1 Reported series of tumor bed radiosurgery

Institution	Year	Patients	% GTR	% Single metastases	Crude LC	1 year LC	Median OS	% New metastases	CNS control	Complications
Series of tumor bed radiosurgery alone										
BNI/UCSF (Kresl et al. 2003)	2003	61	52%	100%	70%	61%	14.9	34%	38% 1 year	2% Necrosis
MSKCC (Narayana et al. 2006)	2006	25	NR	100%	84%	35%	12.0	24%	38% 1 year	4% Necrosis
Osaka (Iwai et al. 2008)	2007	21	100%	76%	76%	82%	20	48%	NR	0%
Stanford (Soltys et al. 2008)	2008	72	85%	65%	86% (per cavity)	79%	15.1	49%	NR	15% Edema, 4% necrosis
UC Irvine (Do et al. 2009)	2008	30	NR	43%	87%	82%	12	63%	22% 1 year	26.6% grade 2
Pittsburgh/Sherbrooke (Mathieu et al. 2008)	2008	40	80%	68%	73%	74%	13	54%	NR	5% Symptomatic T2 changes
Virginia (Jagannathan et al. 2009)	2009	47	100%	28%	94%	NR	10	87%	4% Crude	11% Tumor associated edema
Washington University (Limbrick Jr et al. 2009)	2009	15	80%	80%	73%	77%	20	60%	33% Crude	NR
Allegheny (Karlovits et al. 2009)	2009	52	92%	65%	92%	NR	15	44%	NR	None > grade I
Dartmouth (Hartford et al. 2010)	2010	47	76%	96%	84%	85%	52% at 1 year	74% at 2 year	82% at 2 year	NR
William Beaumont (Dilworth et al. 2010)	2010	47	NR	57%	NR	91%	52% at 1 year	51% at 1 year	NR	NR (one acute grade 3 nausea)
Pittsburgh (Rwigema et al. 2010)	2010	76	82%	NR (85% 1-2)	67%	66%	14.5	39.5%	56% 1 year	One radiation necrosis, two decline in NF
Alabama/UT San Antonio	2010	38	100%	100%	84%	NR	15	42%	NR	8% grade 4
Total		495	83%	70%	83%	75%	14.4	50%		
Tumor bed radiosurgery and whole-brain radiotherapy										
McGill	2010	44	95%	100%	95%	91%	17.1	11%	86% crude, 87% 1 year	7% Symptomatic necrosis
Tumor bed radiosurgery following surgical salvage of whole-brain radiotherapy failures										
Wake Forest (Kim et al. 2006)	2006	79	NR	NR	95%	NR	17	NR	NR	4% necrosis

GTR, gross total resection; LC, local control; NR, not reported; OS, overall survival; NF, neurological function.

linear accelerators, larger tumor cavities were treated in 2–5 sessions to higher total doses (22–30 Gy).

Local control is variably reported and actuarial local progression free survival is not available in three series. When weighted for the number of patients in each series, the overall crude local control is 83% and the estimated 1-year actuarial local control is 75%. Only in two series was it clear that the actuarial calculation censured patients at the time of the last imaging study. The crude averaged incidence of new metastases was 50%. The estimated median overall survival of the patients in the 13 series was 14.4 months. Complications were variably reported – typically in terms of radiation necrosis, symptomatic T2 changes or treatment-related edema. Necrosis rates ranged from 0–6% and, when reported, other complications occurred in 11–27%.

Radiosurgery in Addition to WBRT

Other than our own experience, no additional manuscript was found describing the addition of SRS to post-operative WBRT. A total of 44 patients, operated upon from December 2005 to December 2010, received a planned adjuvant combination of WBRT and single-fraction SRS (Fig. 24.1). The most common primary malignancy was non-small cell lung cancer (66%), followed by breast (14%), melanoma (7%) and colo-rectal (7%). WBRT schedules varied but 84% patients were treated with 30 Gy in 10 daily fractions. Based mainly on scheduling concerns, SRS was delivered before, during or shortly after WBRT. The median interval between SRS and WBRT was 7 days.

Radiosurgery was delivered a median of 42 days after surgery using either fixed non-coplanar beams, dynamic conformal arcs or intensity modulated beams on a modified linear accelerator (BrainLAB, Heimstetten, Germany) or through dose painting with a dedicated robotic linear accelerator (Accuray, Sunnyvale, California). The surgical bed was typically defined with the help of pre-operative MRI images co-registered with the combination of thin-slice contrast-enhanced computed tomography and T1 weighted MRI studies acquired for SRS planning. A 2 mm margin was routinely added to the enhancing border of the tumor bed. The targets ranged in volume from 2 to 61 cc (median 14 cc). The SRS dose was not adjusted for target size and was 10 Gy in all but 1 case. As this is a somewhat counterintuitive application of SRS for which the majority of the target volume is either cerebrospinal fluid or normal brain, an attempt was made to produce more homogeneous treatment plans – the median prescription isodose surface was 83% (77–97%).

The planned follow-up schedule was for patients to have a contrast CT or MRI every 3 months. Cases were censured for local control and occurrence of new metastases at the time of last imaging. Outcomes were measured from the date of surgery. Survival, local control and occurrence of new metastases were calculated actuarially.

In our series, the actuarial 1 and 2-year local control is 91%. The crude rate of new metastases is 11%. At a median follow-up of 10.1 months, 47% of patients

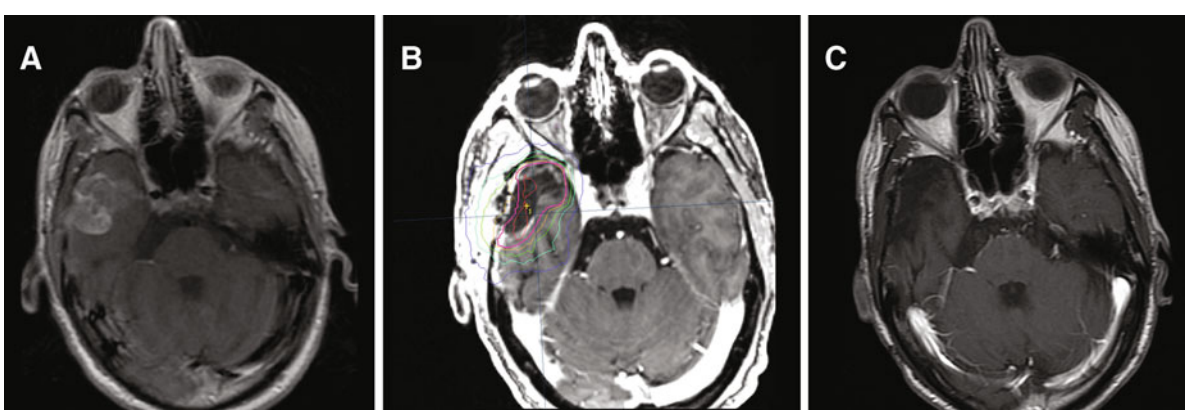

Fig. 24.1 Axial contrast MRI of the brain before (**a**), at the time of (**b**) and years after (**c**) a 10 Gy radiosurgery boost added to surgery and WBRT for metastatic malignant melanoma. The patient is still disease free more than 5 years following treatment of this lesion

have died. The actuarial median overall survival is 17.1 months. At 16 months post-treatment, one patient developed hemiparesis associated with a new enhancing lesion at the surgical bed. This lesion was resected and found to be composed entirely of necrotic tissue without viable tumor cells. A second patient, 4 years after treatment, presented with a seizure and had new enhancement in the tumor bed felt to represent radiation effect. A third patient also presented with seizures and tumor bed enhancement which has been followed for 5 months. Prospective neurocognitive testing has not been performed. The longest survivor – now almost 5 years post resection of a large metastasis from a cutaneous malignant melanoma, reports subjective short-term memory changes (he continues to work full time). A second patient, 4 months following WBRT, required hospital admission for investigation for what is likely symptomatic radiation-induced leukoencephalopathy.

Radiosurgery After Prior WBRT

In a series from Wake Forest University Baptist Medical Center, patients treated after prior WBRT represented 79 of 143 cases of tumor bed SRS. These patients were treated from 2000 to 2005. All patients received a single fraction on a Gamma Knife unit. The median dose was 18 Gy (range 8–24 Gy) prescribed to a modal isodose surface of 50% (range 40–95%). The size of the target volumes was not reported. The crude local recurrence rate was 5.1%. The median overall survival from SRS was 17 months. It is of note that, at the time of SRS, 42% of patients had no other site of metastatic disease. Three patients (3.8%) required surgery for symptomatic radionecrosis following SRS. The mean prescription dose in these patients was 17.3 Gy at the 50% isodose surface. The mean time to the occurrence of symptomatic radionecrosis requiring resection was 6.7 months.

Discussion

As evidenced by the growing number of publications over the past 5 years (Narayana et al. 2006; Quigley et al. 2006; Iwai et al. 2008; Mathieu et al. 2008; Pieper et al. 2008; Soltys et al. 2008; Do et al. 2009; Jagannathan et al. 2009; Limbrick Jr et al. 2009; Roberge et al. 2009), there has been a growing trend for tumor bed radiosurgery. In most cases this has been as an alternative to adjuvant WBRT with isolated reports of its use as an intensification of WBRT or an adjuvant to post-WBRT salvage craniotomy.

The use as an alternative to WBRT is born in the background of growing evidence that the prevention of new metastases does not significantly impact on overall survival and may be associated with acute as well as late neuro-cognitive toxicity (DeAngelis et al. 1989; Chang et al. 2009). As opposed to patients treated with primary SRS, local recurrences are a common problem when patients are observed following surgical resection. These recurrences are often more problematic than new small metastases more readily addressed with salvage SRS. If adjuvant tumor bed SRS provides local control equivalent to adjuvant WBRT, many physicians and patients would be comfortable deferring WBRT on the basis of current prospective data in the post-SRS setting(Aoyama et al. 2006).

As the incidence of local recurrences will depend on patient selection, surgical skill and method of reporting, it is difficult to draw firm conclusions from retrospective data. With these caveats, the 17% crude tumor bed failure rate for the 495 reported cases of tumor bed SRS appears better than the expected 34–46% local failure rate in patients observed after surgical resection(Hagen et al. 1990; Armstrong et al. 1994; Patchell et al. 1998). How much worse (if at all) this is to the local control afforded by WBRT is debatable. The 90% benchmark local control reported by Patchell et al. (1998) has not been consistently reproduced in institutional series(Rades et al. 2008; Roberge et al. 2009) and tumor bed SRS series are contaminated with patients known to have gross residual tumor. On the other hand, the 14.4 month median survival seen with tumor bed SRS is in keeping with published data and reflects the fact that, despite frequent intra-cranial failures, most patients with metastatic brain disease will die of extra-cranial progression.

In contrast to this approach, having dealt with frequent local recurrences despite WBRT, we have chosen an alternative paradigm of adding SRS to WBRT. In addition to its documented efficacy in preventing new metastases, when combined with SRS, WBRT allows for greater dose-intensity at the tumor bed. For example, a 10 Gy SRS boost added to 30 Gy of fractionated radiotherapy is biologically more potent than a single

16 Gy dose of SRS. In addition, WBRT eliminates any risk of marginal miss from difficulties in defining a post-operative target and it addresses the risk of meningeal seeding. Difficult tumor bed definition is an issue highlighted in the Stanford experience where local recurrences occurred less frequently when SRS plans were less conformal (Soltys et al. 2008). As the dose of SRS is reduced when added to WBRT, it opens this option of single fraction SRS to patients with large tumors and lesions approximating critical structures. These patients can be treated without compromising dose-intensity. As the therapy of extra-cranial disease improves, there may be more interest in an approach maximizing intra-cranial control.

There already is debate regarding the two main post-operative approaches tested in prospective trials: WBRT and observation. Despite two randomized trials (Patchell et al. 1998; Mueller et al. 2009), each physician and patient can interpret the facts differently. The trials are underpowered to address the various subgroups of this heterogeneous patient population (such as patients with solitary metastases). In the absence of a documented difference in survival, we are ill equipped to objectively weigh the relative impacts of recurrence and treatment toxicity. Increased adoption of two new approaches will do little to simplify matters as they broaden the therapeutic spectrum. We may now be able to prevent fewer recurrences with less toxicity or prevent more recurrences with more toxicity.

In the patient having failed prior WBRT, the use of tumor bed SRS would appear less controversial. In this setting, the alternatives of brachytherapy, local fractionated radiotherapy, repeat WBRT or observation are all lacking in both appeal and data.

In all three paradigms, the SRS appears well tolerated with risks similar to those of treating in situ brain metastases, i.e., 5% risk of late radiation necrosis.

As the number of patients treated keeps growing, it would seem proper to generate meaningful prospective data for these new treatment paradigms. Anything else than a single arm trial may not be realistic in the setting of WBRT failure but we feel that there is equipoise and interest in investigating the treatment of the radiation naïve patient. For this we begun enrolling patients to a small scale randomized Phase II comparing SRS to WBRT+SRS. In this trial our primary endpoint will be neurocognitive. A larger Phase III trial of WBRT vs. WBRT+SRS, is expected from the North Central Cancer Treatment Group. Although this trial may have overall survival as a primary endpoint in addition to neurocognition, it would seem unlikely that survival would be very different between the two approaches.

Conclusions

In conclusion, the use of tumor bed SRS is reported with increasing frequency. The most common indication is as an alternative to WBRT. Its use is also reported as a local intensification to WBRT or a salvage measure in patients having required surgery after failure of prior WBRT. All three paradigms appear to have merit and we would hope that future prospective trials will help better quantify the pertinent therapeutic ratios.

References

Alrefae MA, Roberge D, Souhami L (2009) Short-course irradiation as adjuvant treatment of surgically resected single brain metastases. ASCO Meeting Abstracts 27:2067

Aoyama H, Shirato H, Tago M, Nakagawa K, Toyoda T, Hatano K, Kenjyo M, Oya N, Hirota S, Shioura H, Kunieda E, Inomata T, Hayakawa K, Katoh N, Kobashi G (2006) Stereotactic radiosurgery plus whole-brain radiation therapy vs stereotactic radiosurgery alone for treatment of brain metastases: a randomized controlled trial. JAMA 295: 2483–2491

Armstrong JG, Wronski M, Galicich J, Arbit E, Leibel SA, Burt M (1994) Postoperative radiation for lung cancer metastatic to the brain. J Clin Oncol 12:2340–2344

Chang EL, Wefel JS, Hess KR, Allen PK, Lang FF, Kornguth DG, Arbuckle RB, Swint JM, Shiu AS, Maor MH, Meyers CA (2009) Neurocognition in patients with brain metastases treated with radiosurgery or radiosurgery plus whole-brain irradiation: a randomised controlled trial. Lancet Oncol 10:1037–1044

Coucke PA, Zouhair A, Ozsahin M, De Tribolet N, Mirimanoff RO (1998) Focalized external radiotherapy for resected solitary brain metastasis: does the dogma stand? Radiotherapy and oncology. J Eur Soc Ther Radiol Oncol 47: 99–101

Dagnew E, Kanski J, McDermott MW, Sneed PK, McPherson C, Breneman JC, Warnick RE (2007) Management of newly diagnosed single brain metastasis using resection and permanent iodine-125 seeds without initial whole-brain radiotherapy: a two institution experience. Neurosurg Focus 22:E3

DeAngelis LM, Mandell LR, Thaler HT, Kimmel DW, Galicich JH, Fuks Z, Posner JB (1989) The role of postoperative radiotherapy after resection of single brain metastases. Neurosurgery 24:798–805

Dilworth JT, Hurst NJ, Chen PY, Shaitelman SF, Baschnagel A, Ye H, Maitz A, Krauss DJ, Pieper D, Grills IS (2010) Outcomes of patients with resected metastatic brain lesions treated with Gamma Knife or whole brain irradiation. ASTRO 52nd Annual Meet, San Diego

Do L, Pezner R, Radany E, Liu A, Staud C, Badie B (2009) Resection followed by stereotactic radiosurgery to resection cavity for intracranial metastases. Int J Radiat Oncol Biol Phys 73:486–491

Hagen NA, Cirrincione C, Thaler HT, DeAngelis LM (1990) The role of radiation therapy following resection of single brain metastasis from melanoma. Neurology 40:158–160

Hartford AC, Paravati A, Spire W, Jarvis L, Erkmen K, Friedman J, Li Z, Hug E, Roberts D, Simmons N (2010) Postoperative stereotactic radiosurgery (srs) without whole-brain radiation therapy (wbrt) for brain metastases: potential role of tumor size. ASTRO 52nd Annual Meet, San Diego

Iwai Y, Yamanaka K, Yasui T (2008) Boost radiosurgery for treatment of brain metastases after surgical resections. Surg Neurol 69:181–186; discussion 186

Jagannathan J, Yen CP, Ray DK, Schlesinger D, Oskouian RJ, Pouratian N, Shaffrey ME, Larner J, Sheehan JP (2009) Gamma Knife radiosurgery to the surgical cavity following resection of brain metastases. J Neurosurg 111:431–438

Johnson JD, Young B (1996) Demographics of brain metastasis. Neurosurg Clin N Am 7:337–344

Karlovits BJ, Quigley MR, Karlovits SM, Miller L, Johnson M, Gayou O, Fuhrer R (2009) Stereotactic radiosurgery boost to the resection bed for oligometastatic brain disease: challenging the tradition of adjuvant whole-brain radiotherapy. Neurosurg Focus 27:E7

Kim PK, Ellis TL, Stieber VW, McMullen KP, Shaw EG, McCoy TP, D'Agostino RB, Bourland JD, DeGuzman AF, Ekstrand KE, Raber MR, Tatter SB (2006) Gamma Knife surgery targeting the resection cavity of brain metastasis that has progressed after whole-brain radiotherapy. J Neurosurg 105 Suppl:75–78

Kresl J, Pueschel J, Porter R, Yan E, McDermott M, Sneed P (2003) Surgical resection and postoperative radiosurgery for single brain metastases [Abstract]. Society for Neuro-Oncology Eighth Annual Meeting: 338A

Limbrick Jr DD, Lusis EA, Chicoine MR, Rich KM, Dacey RG, Dowling JL, Grubb RL, Filiput EA, Drzymala RE, Mansur DB, Simpson JR (2009) Combined surgical resection and stereotactic radiosurgery for treatment of cerebral metastases. Surg Neurol 71:280–288

Mathieu D, Kondziolka D, Flickinger JC, Fortin D, Kenny B, Michaud K, Mongia S, Niranjan A, Lunsford LD (2008) Tumor bed radiosurgery after resection of cerebral metastases. Neurosurgery 62:817–824

Muacevic A, Wowra B, Siefert A, Tonn JC, Steiger HJ, Kreth FW (2008) Microsurgery plus whole brain irradiation versus Gamma Knife surgery alone for treatment of single metastases to the brain: a randomized controlled multicentre phase III trial. J Neurooncol 87:299–307

Mueller RP, Soffietti R, Abacioglu MU, Villa S, Fauchon F, Baumert BG, Fariselli L, Tzuk-Shina T, Collette L, Kocher M (2009) Adjuvant whole-brain radiotherapy versus observation after radiosurgery or surgical resection of 1-3 cerebral metastases: results of the EORTC 22952-26001 study. J Clin Oncol 29:134–141

Narayana A, Chan K, Brennan C, Chang J, Higgins V, Lymberis S, Yamada J, Gutin PH (2006) A phase II trial of stereotactic radiosurgery boost following surgical resection for solitary brain metastases. J Clin Oncol (Meeting Abstracts) 24:1552

Nieder C, Astner ST, Grosu AL, Andratschke NH, Molls M (2007) The role of postoperative radiotherapy after resection of a single brain metastasis. Combined analysis of 643 patients. Strahlenther Onkol 183:576–580

Patchell RA, Tibbs PA, Regine WF, Dempsey RJ, Mohiuddin M, Kryscio RJ, Markesbery WR, Foon KA, Young B (1998) Postoperative radiotherapy in the treatment of single metastases to the brain: a randomized trial. JAMA 280:1485–1489

Pieper D, Suen AW, Grills IS, Nandalur S, Mohammed N, Mitchell C, Maitz A, Kalkanis SN, Martinez AA, Chen PY (2008) Gamma Knife stereotactic radiosurgery for resected brain metastases. Int J Radiat Oncol Biol Phys 72: S227–S228

Posner JB (1992) Management of brain metastases. Rev Neurol (Paris) 148:477–487

Quigley M, Karlovits S, Karlovits B, MacKenzie J, Johnson M, Colonias A, Fuhrer R (2006) 2088: Stereotactic radiosurgery alone and primary resection followed by adjuvant stereotactic radiosurgery in the treatment of limited brain metastases. Int J Radiat Oncol Biol Phys 66:S258–S258

Rades D, Kieckebusch S, Haatanen T, Lohynska R, Dunst J, Schild SE (2008) Surgical resection followed by whole brain radiotherapy versus whole brain radiotherapy alone for single brain metastasis. Int J Radiat Oncol Biol Phys 70:1319–1324

Rades D, Pluemer A, Veninga T, Dunst J, Schild SE (2007) A boost in addition to whole-brain radiotherapy improves patient outcome after resection of 1 or 2 brain metastases in recursive partitioning analysis class 1 and 2 patients. Cancer 110:1551–1559

Roberge D, Petrecca K, El Refae M, Souhami L (2009) Whole-brain radiotherapy and tumor bed radiosurgery following resection of solitary brain metastases. J Neurooncol 95: 95–99

Rogers LR, Rock JP, Sills AK, Vogelbaum MA, Suh JH, Ellis TL, Stieber VW, Asher AL, Fraser RW, Billingsley JS, Lewis P, Schellingerhout D, Shaw EG (2006) Results of a phase II trial of the GliaSite radiation therapy system for the treatment of newly diagnosed, resected single brain metastases. J Neurosurg 105:375–384

Rwigema J-C, Wegner RE, Heron DE, Mintz AH (2010) Stereotactic radiosurgery to the resection cavity of brain metastases. ASTRO 52nd Annual Meeting, San Diego

Soltys SG, Adler JR, Lipani JD, Jackson PS, Choi CY, Puataweepong P, White S, Gibbs IC, Chang SD (2008) Stereotactic radiosurgery of the postoperative resection cavity for brain metastases. Int J Radiat Oncol Biol Phys 70:187–193

Chapter 25

Rat Model of Malignant Brain Tumors: Implantation of Doxorubicin Using Drug Eluting Beads for Delivery

Thomas Brinker and Andrew Lewis

Abstract In this chapter we describe the use of a rat model of malignant glioma for the evaluation of a novel doxorubicin drug eluting bead (DEB) technology. The rationale for locoregional therapy for treatment of glioma is presented in the context of a review of the shortcomings of the currently available therapies. The BT4Ca syngeneic glioma model in BDIX rats is described, together with the intricacies that must be considered when using this model to assess Doxorubicin DEB intratumoral implantation. An overview of the results obtained are presented in the context of other work reported with this drug in the treatment of brain tumors.

Keywords Malignant glioma · Drug eluting bead · BDIX rats · High grade glioma · Carmustine wafers · Brain cancer

Introduction

High grade glioma (HGM) presents severe management challenges: it is difficult to treat, devastating in its progressive and disabling manifestations. Survival time does not exceed 90 weeks in spite of maximum treatment (Affronti et al. 2009).

The standard treatment regimen for patients with *primary* HGM includes tumor surgery as radical as possible followed by radiation therapy. The standard of care is systemic chemotherapy with Temzolomide, which has been shown to be effective in prospective randomized clinical trials. For patients with *recurrent* disease, there is no established chemotherapy regimen available and patients are best treated within investigational clinical protocols (Giglio and Villano 2010; Quant et al. 2010).

Chemotherapeutic treatment of the disease is dogged by the inherent issue of effective delivery of therapeutics across the blood brain barrier and hence, locoregional strategies are being developed to focus drug delivery within the tumor resection cavity. As a prototype, locoregional treatment with Carmustine wafers (Gliadel®) has been approved (Lawson et al. 2007), however demonstrating only modest effect on survival time in primary glioma and none in recurrent disease (Hart et al. 2008). Against this background, search for novel carrier structures and alternate chemotherapeutic agents for locoregional therapy is warranted.

Locoregional Treatment of Gliomas

Around 90% of malignant gliomas recur within 2 cm of the original tumour site, and extra central nervous system (CNS) metastases are exceedingly rare. This strengthens the rationale for strategies aimed at locally controlling this disease. A further factor in favor of local therapies is the lack of systemic toxicity of these treatments, which allow their combination with intravenous or Per Os (orally administered) treatments that have systemic toxicities. Moreover, local therapy offers the possibility of the initiation of

T. Brinker (✉)
International Neuroscience Institute GmbH, D-30625 Hannover, Germany
e-mail: thbrinker@gmail.com

M.A. Hayat (ed.), *Tumors of the Central Nervous System, Volume 4*,
DOI 10.1007/978-94-007-1706-0_25,

an adjuvant therapy immediately after surgical resection, and thus fills the gap between surgery and the beginning of radiotherapy or systemic chemotherapy. Both of these treatment modalities (radiotherapy and systemic chemotherapy) cannot be initiated immediately after surgery due to the associated risk of surgical complications such as infection, cerebral edema, and intracranial hemorrhage. Adjuvant treatments, however, are considered to be most effective in the early stage after surgery, as their effectiveness is very much related to the number of residual tumor cells, which are likely to be at their lowest quantity immediately post-surgery. Due to the high proliferative activity of HGM, even a delay of a few weeks in starting radiation therapy may result in a clinically significant reduction in survival (Irwin et al. 2007). Direct tumor injection of drugs has been practised but has not been adopted as method of treatment for routine clinical practice (Boiardi et al. 2005; Voulgaris et al. 2002). One reason for this has been the rapid wash out of drug from the rapidly proliferating tumors, dose-limiting toxicities in tissues surrounding the tumor, and the invasive nature of the procedure. In an attempt to counter the downsides of direct injection, polymer delivery vehicles have been developed to provide slow sustained release of drug into the tumor, hopefully to eliminate rapid wash out and dose limiting toxicity (Buahin and Brem 1995).

Until today Gliadel, a biodegradable polymer delivering the chemotherapeutic drug carmustine (BCNU), is the only clinically approved chemotherapeutic implant for brain cancer treatment. Gliadel is available as a round cylindric wafer structure with a diameter of 1.45 cm and 1 mm in thickness, containing 7.7 mg of active agent per wafer. It is fabricated from a polyanhydride copolymer, 1,3-bis-(*p*-carboxyphenoxy) propane/poly(sebacic acid) (pCPP20:SA80, known as prolifeprosan 20). In animal models the wafer releases the drug load over a period of approximately 5 days, and the drug has been shown to penetrate several millimetres into the brain parenchyma (reviewed by Weinberg et al. 2008). A number of clinical trials have indicated the safety and efficacy of Gliadel and Food and Drug Administration (FDA) approval was achieved in 1996, representing the first new treatment approved for brain tumors in over 20 years (Lawson et al. 2007). A recent analysis of the published randomized clinical trials with approximately 500 patients in total revealed that Gliadel results in a modest prolongation of survival without an increased incidence of adverse events when used as primary therapy. However, there is no evidence of enhanced progression free survival or quality of life. In recurrent disease, Gliadel does not appear to confer any added benefit (Hart et al. 2008). While Gliadel must be considered as the prototype and proof of principle of locoregional polymer-based chemotherapy, it is obvious that the clinical results are still disappointing. This is the rationale for the ongoing search for improved combinatorial delivery devices, focusing on improved carrier structures and more efficacious chemotherapeutic drugs. Several forms of implants and different chemotherapeutic drugs have been developed, such as compressed discs, cubic phases, fiber discs or sheets, microparticles and nanoparticles (Ranganath et al. 2009). While preclinical studies revealed promising results, so far none of these developments have become successful in the clinical stage.

Among the carriers investigated, microparticulate structures have gained particular attention because microparticles in suspension, due to their size (1–1000 μm), can be easily *injected*, by minimally invasive techniques even in discrete, precise and functional areas of the brain. Only a few microparticulate structures have been clinically investigated, among them 5-Fluouracil-releasing poly(lactic-*co*-glycolic) acid (PLGA) biodegradable microspheres for local treatment of glioblastoma. In a phase 1 study in patients with deep non-operable malignant gliomas 5-FU-microsphere implantation was tolerated well and shown as an efficient system for drug delivery into brain tumors (Menei et al. 2004). However, a randomized phase 2 study in patients with resected tumors revealed only a trend towards improved survival (Menei et al. 2005). Nevertheless, these trials yielded the proof of principle, that microparticulate structures may be used for locoregional delivery of cytostatics in glioma patients.

Drug-Eluting Beads

Drug-eluting beads (DEBs) are microspheres with a diameter in the range of 100–300 μm, produced from a biocompatible polyvinyl alcohol (PVA) hydrogel that has been modified with sulfonate groups for the controlled loading and delivery of chemotherapeutic drugs

(Lewis et al. 2006). DEBs provide the benefit of a controlled and sustained release of chemotherapeutic drugs and precise dosing. DEBs were originally developed for the use in transarterial chemoembolization (TACE) (Lewis et al. 2006), and are successfully used for the local delivery of chemotherapeutics like Doxorubicin (Gonzalez et al. 2008). Doxorubicin is an anthracycline antibiotic that, by inhibiting the topoisomerase II enzyme, causes apoptotic cell death, particularly in exponentially growing cells (Benjamin et al. 1974). A potent antineoplastic activity was proven in vitro for a number of tumor cell lines including glioma cells (Darling and Thomas 2001), and Doxorubicin has been considered as one of the most likely candidates for CNS chemotherapy. However, Doxorubicin lacks the ability to cross the BBB, being a *p*-glycoprotein substrate (Abe et al. 1994) and therefore requires a locoregional application.

Doxorubicin Eluting Beads in Rat Glioma: Considerations of the Model

Here we summarize our findings of the use of a rat glioma model in the evaluation of Doxorubicin eluting DEBs. When selecting a rat brain tumor model, there are several options available as recently reviewed by (Barth and Kaur 2009). Some have arisen naturally (C6 abd T9 for instance) but can sometimes induce immunogenic responses. Others have been chemically induced, such as the BT4C glioma which was formed by administration of ethylnitrosourea to BDIX rats. It has been used to test a variety of novel treatment strategies such as paclitaxel nanoparticles, gene therapy and anti-angiogenic agents. The BT4Ca cell line in BDIX rats was therefore employed in these studies, as it represents a syngeneic glioma model which is similar to human glioblastomas with respect to morphology and biologic behavior such as development of diffuse spread, vascular proliferation and necrosis (Fig. 25.1). The tumor is very rapidly growing, limiting the median survival time of untreated animals to 16 days. The model therefore provides a relatively rapid assessment of the therapeutic benefit of experimental treatments on survival. Prior to the evaluation of DEB in this model, it was necessary to conduct a biocompatibility study implanting polymer beads alone (without drug) in healthy rat brains. After a 2 months implantation period the histological examination demonstrated that the beads were very well-tolerated with no adverse or unexpected tissue reactions, indicating that the drug delivery vehicle was highly biocompatible (Baltes et al. 2010). Thus, any antitumor effect observed in the rat glioma model was likely to be due to the local action of released drug rather than the vehicle itself.

Doxorubicin Eluting Beads in Rat Glioma: Safety and Efficacy Assessment

Experiments to determine the effect of Doxorubicin DEB implantation on tumor size were carried out with a drug dose of 38 μg, which was found to cause no neurological deterioration and only minor local hemorrhagic side effects after cerebral implantation in healthy rats (Baltes et al. 2010). Following the intratumoral injection of Doxorubicin eluting DEBs the median of survival time was 21 days versus 16 days in the untreated animals. Survival statistics revealed a highly significant effect of Doxorubicin (Baltes et al. 2010). This finding corresponds well to the results after transplantation of a pCPP:SA Doxorubicin impregnated wafer in a comparable rat glioma model where a prolonged survival was observed (Lesniak et al. 2005). Histological assessment after the implantation of Doxorubicin DEBs revealed two major findings, a sometimes dramatic decrease of the tumor volume, but in addition the occurrence of largely extended intraparenchymal bleedings surrounding the DEB implantation site (Fig. 25.2). The latter finding must be clearly attributed to the release of Doxorubicin as it was not observed with animals receiving unloaded DEBs (Baltes et al. 2010). Our results are confirmed by the observation of a significant toxicity of doxorubicin in dogs, in which the drug was given i.v. in association with osmotic blood–brain–barrier modification. The neural lesions produced by Doxorubicin were not specific but were manifested as foci of hemorrhagic necrosis and edema. In addition, secondary brainstem hemorrhage was observed in animals that developed even lethal transtentorial herniation (Neuwelt et al. 1983). Similar observations were reported after repetitive administration of doxorubicin containing liposomes in an intracranial glioma model in rats. Up

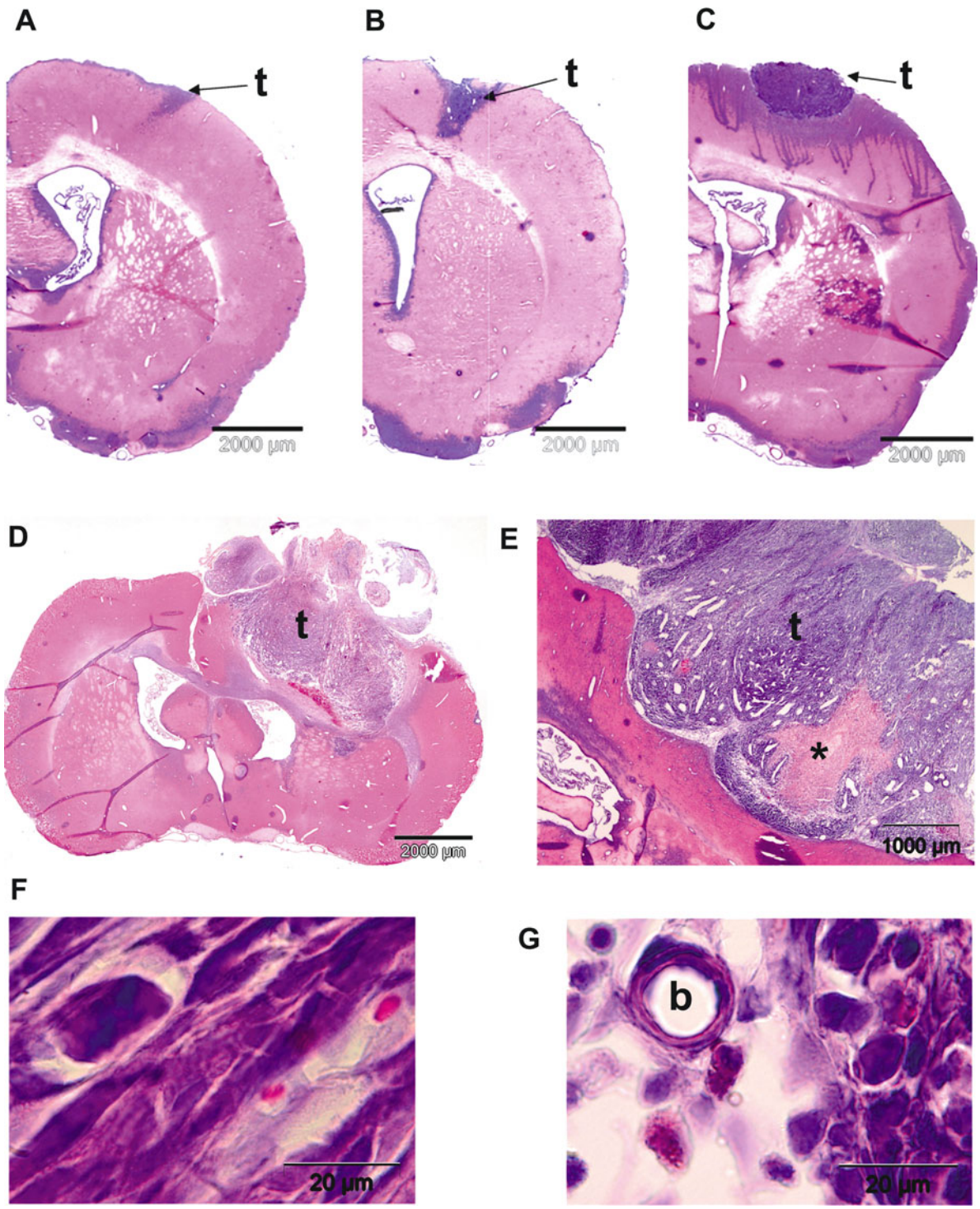

Fig. 25.1 Hematoxylin and eosin (HE) stained tumors (t) 12 days after implantation of 2×10^3 (**a**), 4×10^3 (**b**), 6×10^3 (**c**) or 8×10^3 (**d**–**g**) BT4Ca glioma cells into rat brain parenchyma. 8×10^3 BT4Ca cell mediated tumors matched criteria of grade IV astrocytoma such as high cellularity with nuclear atypia (**e**–**g**), mitoses (**f**), endothelial proliferation (**e**, **g**-b) and necrotic areas (**e**: asterisk). Micrographs represent typical experimental glioma morphology

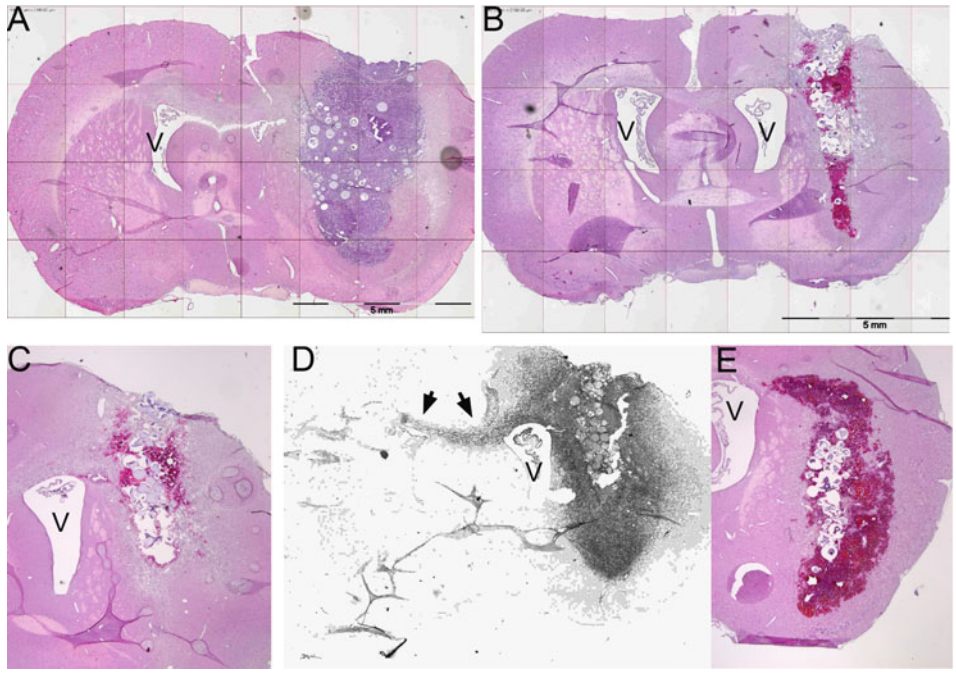

Fig. 25.2 Local histological findings after Implantation of DEB (V: lateral ventricle). (**a**) Tumor growth after implantation of empty DEBs (control group); (**b**) Implantation of Doxorubicin DEBs resulted in a significant shrinkage of the tumor volume, DEBs are surrounded by minor local hemorrhages; (**c** and **d**) local findings after implantation of Doxorubicin DEBs into the tumor. (**c**) H&E staining showing a significant shrinkage of the tumor, only minor bleedings. (**d**) The UV microphotograph of the same specimen. A penetration of Doxorubicin was found of up to 3 mm from the implantation site. A distribution of Doxorubicin was found along the white matter tract via the corpus callosum into the contralateral hemisphere (*arrows*). (**e**) Significant local hemorrhages as result of the implantation of Doxorubicin DEBs

to 75% of the animals developed intratumor hemorrhages which were visible by magnetic resonance (MR) imaging. Histological evaluation showed the putative hemorrhagic regions and revealed necrotic and apoptotic tumor cells surrounding the area of the hemorrhage. A specific cytotoxic effect of Doxorubicin with breakdown of tumor vascular endothelium was suggested (Zhou et al. 2002). However, the antivasculature effects seems to be dose dependent, as we found in healthy animals large areas of cerebral hemorrhages and necrotic brain tissue especially after injection of a volume of 3 μl (114.6 μg total doxorubicin dose), however only to a much lesser extent after 1 and 2 μl (38.2 and 76.4 μg total doxorubicin dose). Implanting healthy rats with 5 μl (191 μg total doxorubicin dose) resulted in the development of significant neurological deficits and mortality with a median survival time of 26.5 days. The histological examination revealed massive intracerebral hemorrhages, sometimes extending through the entire hemisphere. Confirming our findings, the dose dependency of local toxicity was also found after convection-enhanced delivery of polyethylene glycol-coated liposomal doxorubicin in a rat intracranial glioma model (Kikuchi et al. 2008). More recently, Vinchon-Petit et al. investigated total doses of 4 and 40 μg Doxorubicin DEB in combination with whole brain irradiation in a 9L rat glioma model in Fischer F344 rats. They too noticed a strong dose-dependent toxicity but reported that the 4 μg dose was well-tolerated and increased median survival from 28.9 days for DEB alone to 64.4 days for the combination with radiotherapy – a statistically significant increase compared to unloaded beads (Vinchon-Petit et al. 2010).

On the other hand, a local toxicity was not reported from clinical case reports on glioma patients which received intratumoral Doxorubicin via a catheter attached to an implanted reservoir system or an external pump (Voulgaris et al. 2002; Boiardi et al. 2003). However, these clinical observations must be interpreted with caution, as the treatments were performed in only a few selected cases without addressing

dosage issues and systematic assessment of efficacy. Nonetheless, with regard to possible clinical application, the potentially local toxicity of Doxorubicin must be taken seriously, as intratumoral bleeding may cause significant neurological deterioration. Local toxicity is obviously not limited to Doxorubicin, locoregional application of other substances may cause similar side effects. Thus, a clinical trial investigating the application safety of Paclitaxel delivering gel caused a significant brain edema, which required surgical treatment including decompressive craniectomy in 5 of 10 cases (von Eckardstein et al. 2005).

Drug Distribution

Because of its fluorescent properties, Doxorubicin allows for the investigation of its distribution through tumor and brain tissue after locoregional application. Drug penetration is basically limited by the narrow and tortuous extracellular space of the brain and was reported to not exceed distances of a millimeter. Other reports indicate significant larger distances and for Doxorubicin DEB in the liver, drug diffusion has been measured to occur over several hundred microns from the bead surface and to be sustained for several weeks to months (Namur et al. 2010). Our experiments revealed a distinct penetration of doxorubicin into the tumor tissue and the surrounding brain parenchyma passing distances of up to 3 mm from the implantation site. However, Doxorubicin was also found to cover larger distances travelling along the white matter tracts of the brain, even reaching the contralateral hemisphere via the corpus callosum (Fig. 25.2). This finding confirms the observation of others reporting a significant penetration of Doxorubicin through healthy brain and tumor tissue in the rat after its direct infusion via pumps (Khan et al. 2005).

Conclusions

The rat glioma model is a useful experimental representation of brain tumors that can be used to explore the safety and efficacy of novel locoregional treatments. Whilst using direct intratumoral injection in the model best portrays stereotactic administration, it also serves as a good indicator of how a product would perform if administered directly into the tumor resection cavity, as evaluation of drug penetration into the tissue and both antitumoral and toxicity effects on normal brain parenchyma can be evaluated. The studies reported herein for Doxorubicin DEB confirm potential for the treatment of glioma but that there is significant risk of toxicity and in particular from hemorrhaging if the drug dose is too high (i.e. there is a very narrow therapeutic window). From the fluorescent findings, we conclude that DEBs must be basically considered as a suitable carrier structure to achieve a widespread delivery of chemo-therapeutic drugs to intracranial tumor tissue. However, with regard to the side effects of Doxorubicin, alternative chemotherapeutics must be considered. Accordingly we have shown that DEBs releasing Irinotecan do not exhibit the local side effects seen with Doxorubicin DEBs but possess strong antitumor effects in a rat glioma model (Baltes et al. 2010). Alternatively, low dose Doxorubicin DEB may be considered for use in combination with radiotherapy, as the drug is a known radiosensitizer (Vinchon-Petit et al. 2010). While not studied experimentally, one may speculate that as compared with larger polymer wafers, i.e. Gliadel, after intralesional application, microparticulate structures like DEBs should a achieve a better penetration of the drug into the tumor tissue, as closer physical contact between the tumor tissue and the carrier structure is achieved, unlike the wafer which is only applied superficially to the brain/tumor tissue surface. As such, DEB provide a flexible approach to locoregional therapy, allowing the physician to control the volume/dose, the site of injection to avoid eloquent areas of the brain as appropriate; and to use different chemotherapeutic agents depending upon the patient comorbidities, or resistance of the tumor to previous systemic therapy.

References

Abe T, Hasegawa S, Taniguchi K, Yokomizo A, Kuwano T, Ono M, Mori T, Hori S, Kohno K, Kuwano M (1994) Possible involvement of multidrug-resistance-associated protein (MRP) gene expression in spontaneous drug resistance to vincristine, etoposide and adriamycin in human glioma cells. Int J Cancer 58:860–864

Affronti ML, Heery CR, Herndon JE 2nd, Rich JN, Reardon DA, Desjardins A, Vredenburgh JJ, Friedman AH, Bigner DD,

Friedman HS (2009) Overall survival of newly diagnosed glioblastoma patients receiving carmustine wafers followed by radiation and concurrent temozolomide plus rotational multiagent chemotherapy. Cancer 115:3501–3511

Baltes S, Freund I, Lewis AL, Nolte I, Brinker T (2010) Doxorubicin and irinotecan drug-eluting beads for treatment of glioma: a pilot study in a rat model. J Mater Sci Mater Med 21:1393–1402

Barth RF, Kaur B (2009) Rat brain tumor models in experimental neuro-oncology: the C6, 9L, T9, RG2, F98, BT4C, RT-2 and CNS-1 gliomas. J Neurooncol 94:299–312

Benjamin RS, Wiernik PH, Bachur NR (1974) Adriamycin chemotherapy – efficacy, safety, and pharmacologic basis of an intermittent single high-dosage schedule. Cancer 33: 19–27

Boiardi A, Eoli M, Salmaggi A, Lamperti E, Botturi A, Broggi G, Bartolomei M, Silvani A (2003) New approach in delivering chemotherapy: locoregional treatment for recurrent glioblastoma (rGBM). J Exp Clin Cancer Res 22:123–127

Boiardi A, Eoli M, Salmaggi A, Lamperti E, Botturi A, Solari A, Di Meco F, Broggi G, Silvani A (2005) Local drug delivery in recurrent malignant gliomas. Neurol Sci 26(Suppl. 1): S37–39

Buahin KG, Brem H (1995) Interstitial chemotherapy of experimental brain tumors: comparison of intratumoral injection versus polymeric controlled release. J Neurooncol 26: 103–110

Darling JL, Thomas DG (2001) Response of short-term cultures derived from human malignant glioma to aziridinylbenzoquinone, etoposide and doxorubicin: an in vitro phase II trial. Anticancer Drugs 12:753–760

Giglio P, Villano JL (2010) Newly diagnosed high-grade gliomas. Curr TreatOpt Neurol 12:309–320

Gonzalez MV, Tang Y, Phillips GJ, Lloyd AW, Hall B, Stratford PW, Lewis AL (2008) Doxorubicin eluting beads-2: methods for evaluating drug elution and in-vitro:in-vivo correlation. J Mater Sci Mater Med 19:767–775

Hart MG, Grant R, Garside R, Rogers G, Somerville M, Stein K (2008) Chemotherapeutic wafers for High Grade Glioma. Cochrane Database Syst Rev CD007294

Irwin C, Hunn M, Purdie G, Hamilton D (2007) Delay in radiotherapy shortens survival in patients with high grade glioma. J Neurooncol 85:339–343

Khan A, Jallo GI, Liu YJ, Carson BS, Guarnieri M (2005) Infusion rates and drug distribution in brain tumor models in rats. J Neurosurg 102:53–58

Kikuchi T, Saito R, Sugiyama S, Yamashita Y, Kumabe T, Krauze M, Bankiewicz K, Tominaga T (2008) Convection-enhanced delivery of polyethylene glycol-coated liposomal doxorubicin: characterization and efficacy in rat intracranial glioma models. J Neurosurg 109:867–873

Lawson HC, Sampath P, Bohan E, Park MC, Hussain N, Olivi A, Weingart J, Kleinberg L, Brem H (2007) Interstitial chemotherapy for malignant gliomas: the Johns Hopkins experience. J Neurooncol 83:61–70

Lesniak MS, Upadhyay U, Goodwin R, Tyler B, Brem H (2005) Local delivery of doxorubicin for the treatment of malignant brain tumors in rats. Anticancer Res 25: 3825–3831

Lewis AL, Gonzalez MV, Lloyd AW, Hall B, Tang Y, Willis SL, Leppard SW, Wolfenden LC, Palmer RR, Stratford PW (2006) DC bead: in vitro characterization of a drug-delivery device for transarterial chemoembolization. J Vasc Interv Radiol 17:335–342

Menei P, Capelle L, Guyotat J, Fuentes S, Assaker R, Bataille B, Francois P, Dorwling-Carter D, Paquis P, Bauchet L, Parker F, Sabatier J, Faisant N, Benoit JP (2005) Local and sustained delivery of 5-fluorouracil from biodegradable microspheres for the radiosensitization of malignant glioma: a randomized phase II trial. Neurosurgery 56:242–248

Menei P, Jadaud E, Faisant N, Boisdron-Celle M, Michalak S, Fournier D, Delhaye M, Benoit JP (2004) Stereotaxic implantation of 5-fluorouracil-releasing microspheres in malignant glioma. Cancer 100:405–410

Namur J, Wassef M, Millot JM, Lewis AL, Manfait M, Laurent A (2010) Drug-eluting beads for liver embolization: concentration of doxorubicin in tissue and in beads in a pig model. J Vasc Interv Radiol 21:259–267

Neuwelt EA, Glasberg M, Frenkel E, Barnett P (1983) Neurotoxicity of chemotherapeutic agents after blood-brain barrier modification: neuropathological studies. Ann Neurol 14:316–324

Quant EC, Drappatz J, Wen PY, Norden AD (2010) Recurrent high-grade glioma. Curr Treat Opt Neurol 12:321–333

Ranganath SH, Kee I, Krantz WB, Chow PK, Wang CH (2009) Hydrogel matrix entrapping PLGA-paclitaxel microspheres: drug delivery with near zero-order release and implantability advantages for malignant brain tumour chemotherapy. Pharm Res 26:2101–2114

Vinchon-Petit S, Jarnet D, Michalak S, Lewis A, Benoit JP, Menei P (2010) Local implantation of doxorubicin drug eluting beads in rat glioma. Int J Pharm 402:184–189

von Eckardstein KL, Reszka R, Kiwit JC (2005) Intracavitary chemotherapy (paclitaxel/carboplatin liquid crystalline cubic phases) for recurrent glioblastoma – clinical observations. J Neurooncol 74:305–309

Voulgaris S, Partheni M, Karamouzis M, Dimopoulos P, Papadakis N, Kalofonos HP (2002) Intratumoral doxorubicin in patients with malignant brain gliomas. Am J Clin Oncol 25:60–64

Weinberg BD, Blanco E, Gao J (2008) Polymer implants for intratumoral drug delivery and cancer therapy. J Pharm Sci 97:1681–1702

Zhou R, Mazurchuk R, Straubinger RM (2002) Antivasculature effects of doxorubicin-containing liposomes in an intracranial rat brain tumor model. Cancer Res 62:2561–2566

Chapter 26

Electromagnetic Neuronavigation for CNS Tumors

Caroline Hayhurst

Abstract The integration of image guidance into all neurosurgical procedures is fast becoming routine. Most navigation systems are based on optical tracking and therefore require a direct line of sight between camera and tracking probe, interfering with theatre workflow and freedom of movement within the surgical field. Electromagnetic (EM) neuronavigation overcomes many of the obstacles inherent in optical systems and provides rapid, real time, accurate navigation. The advantages of EM navigation are outlined and the potential applications in neuro-oncology, including awake craniotomy and endonasal transphenoidal skull base procedures are highlighted.

Keywords Neurosurgical procedures · Image guidance · Awake craniotomy · Image-guided stereotaxy · Frameless stereotaxy · Subcortical lesions

Introduction

Surgical image guidance based on three-dimensional volumetric data is becoming a routine part of neurosurgical practice. Computer assisted frameless stereotaxy has been available for over two decades With image-guided stereotaxy, smaller cranial and dural openings, minimal exposure of normal brain, accurate localization of subcortical lesions, and assistance with defining the tumor–brain interface are made possible; these factors may account for improved clinical outcomes (Maciunas 1996).

Today, the accuracy of most image-guidance systems, as assessed by target registration error, is well documented with mean values below 2 mm (Walton et al. 1996; Rachinger et al. 2006). The most commonly employed systems use infra-red optical tracking, which requires a direct line of site between camera, tracking device and probe; interfering with theatre and surgical workflow. Electromagnetic (EM) technology for image guidance overcomes many of the obstacles inherent in most navigation systems (Table 26.1). The small size of the reference sensor allows it to be attached directly to the head allowing freedom of movement of the head without loss of accuracy or registration, or interference with the surgical field. A direct line of sight is not required between tracker and probe. Flexible instruments can be tracked at depth in real time and head fixation is not required.

The concept of using an electromagnetic field to provide a frame of reference in which to track anatomy and instruments was introduced in 1991 (Kato et al. 1991) but the need to develop a system that was not susceptible to interference from standard surgical instruments and equipment has meant that only recently has this concept gained widespread acceptance.

Electromagnetic Technology

The StealthStation Axiem navigation system (Medtronic Inc, Louisville, CO) utilizes a transmitter coil array to encompass the head within a cubital low energy magnetic field, to provide a volume

C. Hayhurst (✉)
Department of Neurosurgery, University Hospital of Wales, Heath Park, Cardiff CF14 4XW, UK
e-mail: carolinehayhurst@hotmail.com

M.A. Hayat (ed.), *Tumors of the Central Nervous System, Volume 4*,
DOI 10.1007/978-94-007-1706-0_26,

Table 26.1 Advantages and disadvantages of EM navigation

Advantages	Disadvantages
Direct line of sight not required	Loss of accuracy due to brain shift still occurs
Improved theatre workflow	Loss of navigation due to distortion of magnetic field:
Ideal for endoscopic procedures	– Large retractors
No rigid head fixation	– Cortical stimulation
Head can be moved after registration	Risk of loss of sterility in awake procedures due to head movement
Real time navigation at depth	
Rapid set-up	

in which the location and orientation of a pointer in space can be defined digitally. A scalp applied reference frame identifies the location of anatomy within the frame of reference. By applying a reference frame to the head, the need for rigid fixation of the head relative to the field generator is avoided so the head can be moved at any time during a procedure. The crucial feature of EM technology is that the sensors can be made extremely small, using 1–3 mm copper sensor coils. By contrast an infra-red system, whether active or passive requires several emitters/reflectors separated by several centimetres to achieve comparable accuracy.

Concerns regarding the stability and accuracy of an electromagnetic system in an operating room environment have limited widespread acceptance, as ferromagnetic interference may distort the reference field and limit precision. The accuracy of the Stealth system has been shown in experimental conditions to demonstrate an undistorted reference measurement of 0.1 mm and with ferromagnetic distortion a mean deviation of 0.21–0.56 mm (Schicho et al. 2005). Early concerns regarding application accuracy have not been substantiated, with observed accuracy comparable to optical systems in the order of less than 1–3 mm (Rousu et al. 1998; Benardete et al. 2001; Zaaroor et al. 2001; Mascott 2005). Direct comparison of optical versus electromagnetic tracking shows no difference in application accuracy (Rosenow and Sootsman 2007).

Using optical navigation systems the tracked volume is extracranial and depth is calculated as a derived measure based on probe length, rather than tracking the true probe position within the surgical volume, as is the case with EM navigation. The tracker tools have detector coils at the tip and can be used as instruments, with a high degree of accuracy of the tip position within the surgical volume. A direct line of sight is not required between tracker and transmitter coil, therefore depth is measured in real time and continuous reorientation of instruments toward the transmitter is not required as with optical systems.

Furthermore the small size and cylindrical geometry of the sensor coils means that a stylet can be made carrying coils to within a centimetre of the tip of the catheter. This improves the accuracy of placement as the tip of the stylet is then only approximately 2 cm from the virtual centre of the tracked device. It can therefore be adapted to pass down a biopsy needle or endoscope.

Application for CNS Tumors

Intrinsic Tumors

The integration of neuronavigation techniques into glioma resection allows for planning of optimal craniotomy placement and the trajectory of approach to subcortical lesions. These are paramount when considering a keyhole concept of tumor microsurgery (Teo 2010). By planning the optimal trajectory along the long axis of intrinsic tumors and positioning the head to allow a perpendicular surgical corridor to the tumor, this facilitates microsurgery through very small craniotomies and small incisions (Fig. 26.1). The ability to plan a surgical corridor remote from anatomically eloquent regions and supplement this with integrated imaging identification of functional cortex and tracts has enabled maximal tumor resection in eloquent regions, particularly in insular and thalamic gliomas, where previously a resection would not have been undertaken. As there is increasing evidence that extent of resection correlates with overall survival in both high and low grade glioma (McGirt et al. 2008; Sanai and Berger 2008), any adjuncts that can facilitate maximal resection with minimal morbidity

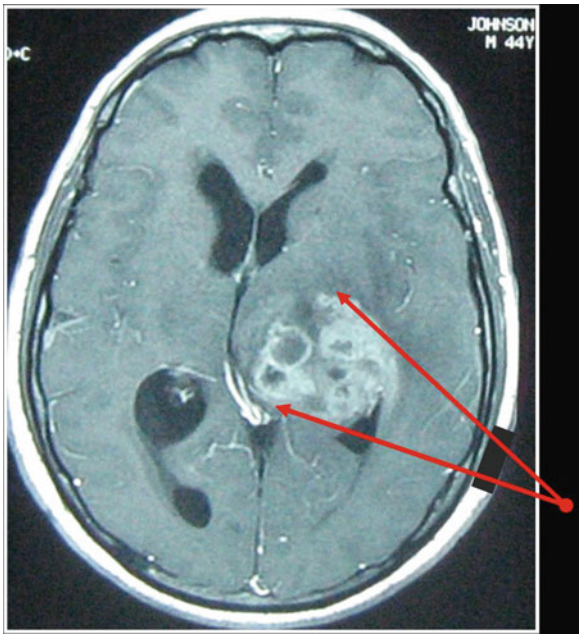

Fig. 26.1 Approach trajectory for deep intrinsic tumor using a mini-craniotomy

should be exploited. Interestingly, there is limited published data on outcome for image-guided tumor resections, although Tan and Mc (2003) demonstrate reduced length of hospital stay and improved postoperative functional status with longer overall survival in a series of image-guided frameless craniotomies for cerebral metastases, when compared to historical cohorts of conventional craniotomies.

In the few selected cases where biopsy only is indicated, the EM stylet can be used within a standard side cutting biopsy needle for frameless, pinless biopsies. Such biopsies can be performed with local anaesthesia and minimal sedation. The majority of patients can then be discharged home on the same day. With advantages in terms of health economics and patient satisfaction, day case surgery is increasing in neuro-oncology (Boulton and Bernstein 2008; Grundy et al. 2008).

Awake Craniotomy

Lesion resection in eloquent areas of the brain using awake craniotomy permits intra-operative functional cortical mapping and facilitates maximal tumour resection. Although some neurophysiological techniques allow motor and sensory mapping under anaesthesia language localisation requires the patient to be awake. Integrating neuronavigation techniques into this procedure has previously required head fixation under local anaesthesia, adding to the ordeal for the patient. Use of a scalp applied reference frame eliminates the need for head fixation without compromising accuracy, enabling greater patient comfort and reducing sedation requirements, which reduces the potential for agitation and loss of compliance with the procedure. The use of EM navigation eliminates the need for any additional skin incisions or direct line of sight between probe and emitters, allowing for greater freedom of movement within the surgical field. All neurophysiological monitoring modalities can be used without interference from the magnetic field. Significant interference does occur during cortical stimulation, preventing simultaneous navigation. However, we have not found that this has impacted on the procedure. The freedom of head movement risks loss of sterility, but we have not experienced this in our small number of cases.

Endonasal Endoscopic Transphenoidal Surgery

Safe exposure of the midline skull base for a range of pathologies via an endonasal approach requires accurate anatomical localization. Traditionally, fluoroscopy was used to identify the boundaries of the sella in the sagittal plane to aid the approach trajectory. However, the combined advances in frameless navigation and endoscopic techniques enable greater exposure of the skull base, with safe exposure of the sella, planum sphenoidale and clivus. Identification of the carotid arteries is critical, particularly in procedures where the working channel is lateral to the carotid, for example exposing the petrous apex or Meckel's cave.

Although the safety of the endonasal approach to the sella and skull base is based on an understanding of the three dimensional anatomy of the paranasal sinuses and parasellar region, both individual anatomic variation and previous surgery can lead to disorientation. Endonasal anatomic variations occur in up to 50% of cases (van Lindert et al. 2010). The sphenoid ostia frequently have a mucosal covering leading

to disorientation in the sagittal plane. The use of image guidance can prevent inadvertent opening of the anterior cranial fossa or clivus with subsequent CSF leak.

For the endonasal transphenoidal approach, we place the head in a 3 pin fixation device and attach the EM reference frame to the forehead using self adhesive tape and secured with an adhesive dressing. The field generator is mounted on the left side of the table via an articulated arm and remains underneath the sterile drapes throughout the procedure. Registration is performed using skin surface matching and confirmed with anatomical bony landmarks such as medial and lateral canthi and nasion. We use a purely endoscopic binostral approach, to allow for a 3 or 4 hand technique. In such a confined, busy surgical field the use of EM navigation is invaluable as there is no need to reorientate or remove instruments from the surgical field

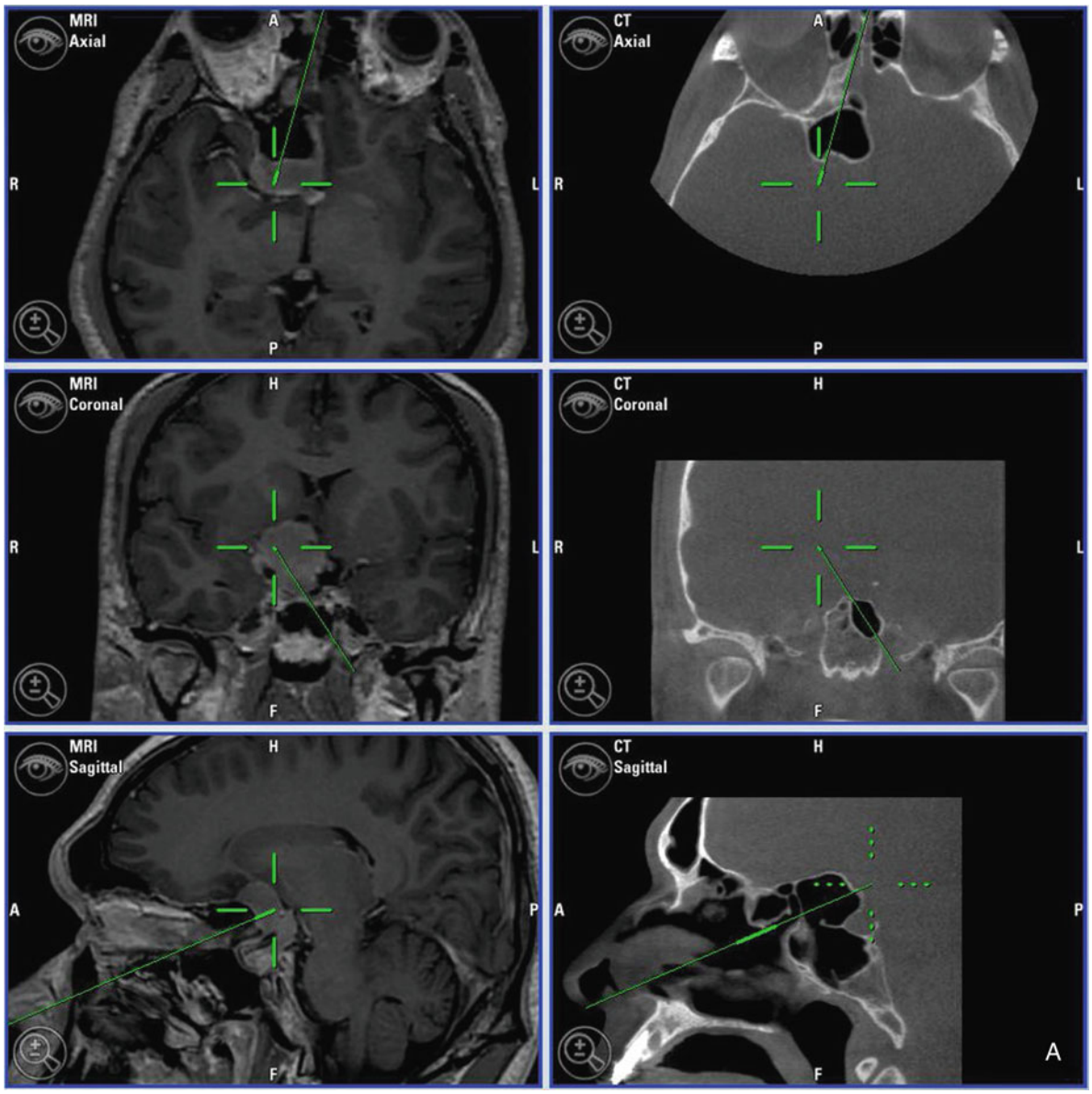

Fig. 26.2 (**a**) Intra-operative snapshot during an expanded endonasal transsphenoidal approach for a large pituitary adenoma. (**b**) Endoscopic view of expanded sella floor and right optico-carotid recess and clival recess

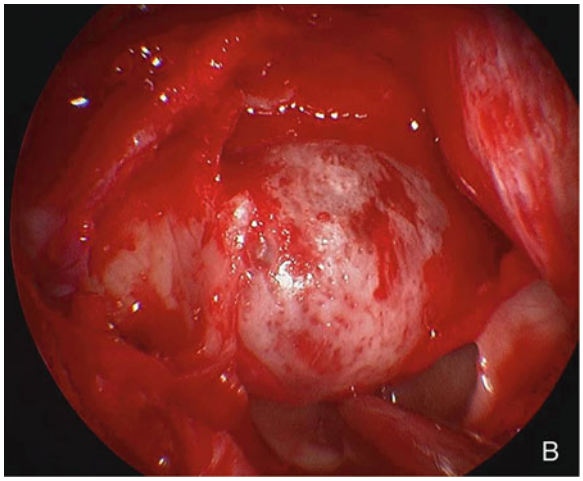

Fig. 26.2 (continued)

in order to gain a line of sight for optical tracking. A sterile 10 cm EM probe is used for intraoperative navigation. We do not use a nasal speculum, so there is no issue with ferro-magnetic interference. The combination of visual and imaging confirmation of the location of vital structures reduces the potential for complications and allows maximal bony exposure, facilitating tumor removal (Fig. 26.2).

EM tracking enables the combination of probe with instruments, such as suction, curette and the endoscope itself (Eboli et al. 2010). In the future, navigation systems will allow virtual images of adjacent anatomical structures, such as the carotid artery and optic nerve, to be superimposed on the live endoscopic images (Thoranaghatte et al. 2009).

Limitations

As with all navigation systems based on a pre-operatively acquired volume imaging dataset, brain shift will occur progressively following durotomy and subsequent tumor resection. Although this is not a significant problem in endoscopic skull base procedures, for intrinsic tumor surgery some form of intra-operative real time imaging update is required to maintain accuracy. Whilst the ultimate real-time imaging is intra-operative high-field MRI, intraoperative ultrasound registered to the pre-operative imaging has been shown to be effective in correcting for brain shift (Berntsen et al. 2010; Ohue et al. 2010).

An electromagnetic field is potentially susceptible to distortion from ferromagnetic materials within the operating room. In our mixed case series we have not experienced interference from equipment outside the surgical field, such as anaesthetic equipment, surgical table or standard Mayfield 3 pin head fixation (Hayhurst et al. 2009). Ferromagnetic instruments moving within the surgical field have not prevented navigation and we have not had to use special instruments. Where large self-retaining retractors are used this may prevent continuous navigation. Removal of the retractor results in restoration of an accurate field.

Conclusion

A neuronavigational tool is a prerequisite for tumor resection and EM technology provides an accurate technique of stereotactic localization without the need for a direct line of sight. The greater freedom of movement that this allows within the surgical field allows for improved workflow in all cases, in particular endonasal approaches. In addition, the lack of need for rigid head fixation or additional incisions for fixation of the reference frame, make the system ideal for awake craniotomies.

References

Benardete EA, Leonard MA, Weiner HL (2001) Comparison of frameless stereotactic systems: accuracy, precision, and applications. Neurosurgery 49(6):1409–1415; discussion 1415–1416

Berntsen EM, Gulati S, Solheim O, Kvistad KA, Torp SH, Selbekk T, Unsgard G, Haberg AK (2010) Functional magnetic resonance imaging and diffusion tensor tractography incorporated into an intraoperative 3-dimensional ultrasound-based neuronavigation system: impact on therapeutic strategies, extent of resection, and clinical outcome. Neurosurgery 67(2):251–564

Boulton M, Bernstein M (2008) Outpatient brain tumor surgery: innovation in surgical neurooncology. J Neurosurg 108(4):649–654

Eboli P, Shafa B, Mayberg M (2010) Intraoperative computed tomography registration and electromagnetic neuronavigation for transsphenoidal pituitary surgery: accuracy and time effectiveness. J Neurosurg 114(2):329–335

Grundy PL, Weidmann C, Bernstein M (2008) Day-case neurosurgery for brain tumours: the early United Kingdom experience. Br J Neurosurg 22(3):360–367

Hayhurst C, Byrne P, Eldridge PR, Mallucci CL (2009) Application of electromagnetic technology to neuronavigation: a revolution in image-guided neurosurgery. J Neurosurg 111(6):1179–1184

Kato A, Yoshimine T, Hayakawa T, Tomita Y, Ikeda T, Mitomo M, Harada K, Mogami H (1991) A frameless, armless navigational system for computer-assisted neurosurgery. Technical note. J Neurosurg 74(5):845–849

Maciunas RJ (1996) Intraoperative cranial navigation. Clin Neurosurg 43:353–381

Mascott CR (2005) Comparison of magnetic tracking and optical tracking by simultaneous use of two independent frameless stereotactic systems. Neurosurgery 57(4 Suppl):295–301; discussion 295–301

McGirt MJ, Chaichana KL, Attenello FJ, Weingart JD, Than K, Burger PC, Olivi A, Brem H, Quinones-Hinojosa A (2008) Extent of surgical resection is independently associated with survival in patients with hemispheric infiltrating low-grade gliomas. Neurosurgery 63(4):700–707; author reply 707–708

Ohue S, Kumon Y, Nagato S, Kohno S, Harada H, Nakagawa K, Kikuchi K, Miki H, Ohnishi T (2010) Evaluation of intraoperative brain shift using an ultrasound-linked navigation system for brain tumor surgery. Neurol Med Chir (Tokyo) 50(4):291–300

Rachinger J, von Keller B, Ganslandt O, Fahlbusch R, Nimsky C (2006) Application accuracy of automatic registration in frameless stereotaxy. Stereotact Funct Neurosurg 84(2–3): 109–117

Rosenow JM, Sootsman WK (2007) Application accuracy of an electromagnetic field-based image-guided navigation system. Stereotact Funct Neurosurg 85(2–3):75–81

Rousu JS, Kohls PE, Kall B, Kelly PJ (1998) Computer-assisted image-guided surgery using the Regulus Navigator. Stud Health Technol Inform 50:103–109

Sanai N, Berger MS (2008) Glioma extent of resection and its impact on patient outcome. Neurosurgery 62(4):753–764; discussion 264–266

Schicho K, Figl M, Donat M, Birkfellner W, Seemann R, Wagner A, Bergmann H, Ewers R (2005) Stability of miniature electromagnetic tracking systems. Phys Med Biol 50(9): 2089–2098

Tan TC, Mc LBP (2003) Image-guided craniotomy for cerebral metastases: techniques and outcomes. Neurosurgery 53(1):82–89; discussion 89–90

Teo C (2010) The concept of minimally invasive neurosurgery. Neurosurg Clin N Am 21(4):583–584, v

Thoranaghatte R, Garcia J, Caversaccio M, Widmer D, Gonzalez Ballester MA, Nolte LP, Zheng G (2009) Landmark-based augmented reality system for paranasal and transnasal endoscopic surgeries. Int J Med Robot 5(4):415–422

van Lindert EJ, Ingels K, Mylanus E, Grotenhuis JA (2010) Variations of endonasal anatomy: relevance for the endoscopic endonasal transsphenoidal approach. Acta Neurochir (Wien) 152(6):1015–1020

Walton L, Hampshire A, Forster DM, Kemeny AA (1996) Accuracy of stereotactic localisation using magnetic resonance imaging: a comparison between two- and three-dimensional studies. Stereotact Funct Neurosurg 66(Suppl 1):49–56

Zaaroor M, Bejerano Y, Weinfeld Z, Ben-Haim S (2001) Novel magnetic technology for intraoperative intracranial frameless navigation: in vivo and in vitro results. Neurosurgery 48(5):1100–1107; discussion 1107–1108

Chapter 27

Stereotactic Radiosurgery for Intracranial Ependymomas

Hideyuki Kano, Ajay Niranjan, Douglas Kondziolka, John C. Flickinger, and L. Dade Lunsford

Abstract To evaluate outcome predictors after stereotactic radiosurgery (SRS) in patients with recurrent or residual intracranial ependymomas, we compared tumor control, survival and complications with tumor grade, volume, age of patients, and imaging characteristics. We retrospectively reviewed records of consecutive 45 ependymoma patients who underwent SRS for 65 tumors. The median patient age was 25 years (range, 2–78 years). Forty-three patients had prior surgical resection of their ependymomas and two patients were diagnosed by stereotactic biopsy. Thirty-seven patients had failed prior fractionated radiation therapy (RT). Fourteen patients had progression despite both RT and chemotherapy. Thirty patients had low-grade ependymomas (40 tumors) and 15 patients had anaplastic ependymomas (25 tumors). The median radiosurgery target volume was 4.9 cc (range, 0.1–36.8 cc) and the median marginal dose was 15.0 Gy (range, 8–22 Gy). At an average of 31 months (range, 4–155 months), 27 patients died from metastases or disease progression. The overall survival after radiosurgery was 65, 41, and 38% at 1, 3 and 5 years, respectively. The progression-free survival after SRS at 1-, 3- and 5 years, respectively were 82, 52 and 52% for all grade ependymomas. Histological tumor grade was not significantly associated with better progression free survival ($p = 0.725$). Factors associated with an improved progression-free survival included smaller tumor volume and homogeneous tumor contrast enhancement. Adjuvant SRS provides another management option for patients with residual or recurrent ependymomas. Predictors of response include older age, smaller volume, lower grade, and homogeneous contrast enhancement.

Keywords Stereotactic radiosurgery · Ependymomas · Neuroepithelial tumors · Intracranial tumors · Posterior fossa · Pseudopalisading necrosis

Introduction

Ependymomas represents 3–9% of all neuroepithelial tumors and 5–12% of all intracranial tumors in children. They are found at a proportionally higher rate in children under 3 years of age, accounting for 30% of all intracranial tumors (Wiestler et al. 2000). In adult patients, infratentorial and spinal ependymomas arise with almost equal frequency, whereas infratentorial ependymomas predominate in young children. They most commonly develop in the posterior fossa followed by the lateral ventricles and the third ventricle (Kudo et al. 1990). Anaplastic ependymomas exhibit high mitotic activity, often accompanied by microvascular proliferation and pseudopalisading necrosis. The diagnosis of anaplastic ependymoma varies considerably in reported series due to uncertainty about the histological criteria for malignancy (Wiestler et al. 2000).

The standard therapeutic approach to manage ependymoma has been surgery followed by external beam fractionated radiation therapy (RT). The presence of gross residual tumor after surgery is a poor prognostic factor (Healey et al. 1991; Horn et al. 1999; Pollack et al. 1995; Rousseau et al. 1994).

H. Kano (✉)
Department of Neurological Surgery, University of Pittsburgh, Pittsburgh, PA 15213, USA
e-mail: kanoh@upmc.edu

M.A. Hayat (ed.), *Tumors of the Central Nervous System, Volume 4*,
DOI 10.1007/978-94-007-1706-0_27,

Unfortunately, complete surgical resection is not always feasible. Recurrent ependymomas are difficult to manage, and multiple recurrences that require further surgery, or chemotherapy are common (Goldwein et al. 1990a).

Stereotactic radiosurgery (SRS) can deliver a single high dose of radiation to the target volume with a rapid fall-off of the radiation dose peripherally and may be applied to treat patients with either incompletely resected or unresectable ependymomas. Stereotactic radiosurgery has been used as an adjunct in the management of intracranial ependymoma and has been used as an effective modality for ependymomas that progress or recur after surgical resection and post operative RT (Aggarwal et al. 1997; Grabb et al. 1996; Hodgson et al. 2001; Jawahar et al. 1999; Kano et al. 2009; Stafford et al. 2000). We reviewed our long-term experience with 45 patients who underwent SRS using the Gamma Knife. We evaluated tumor control, patient survival, adverse radiation effects (ARE), and other variables that affected treatment outcomes.

Methods and Materials

Patient Population

Between December 1989 and August 2006, 45 patients with histologically confirmed ependymomas (WHO grade 2 or 3) underwent primary (two patients) or adjuvant SRS (43 patients) at the University of Pittsburgh (Table 27.1). There were 28 males and 17 females with a median age of 25 years (range, 2–78 years). Forty-three patients had prior surgical resection of their ependymomas and two patients were diagnosed by stereotactic biopsy. Thirty-seven patients had failed RT (average tumor dose = 52 Gy). Fourteen patients had progression despite both RT and chemotherapy (agents included Taxol, Cisplatin, VP-16, Vincristine, Cytoxan, Carboplatin, Etoposide, alone or in combination). Two patients underwent biopsy for deep seated tumors after which they had primary SRS. Twenty-nine patients received SRS at the time of tumor recurrence identified by imaging. The median duration between first surgical removal and progression was 43.2 months (range, 3.9–172 months). Ten patients received boost SRS for residual tumors after initial therapy (two patients had surgical removal, six had surgical removal followed by RT, and two had surgical removal followed by RT and chemotherapy). Tumor progression after initial management was defined as an increase in tumor volume at the time of follow-up magnetic resonance imaging (MRI). Six patients received SRS for intracranial metastases distant from initial tumor location. The median duration between first surgical removal and treatment of the metastatic tumor was 66 months (range, 0.4–127 months).

Pathology review was performed at the referring hospital in 25 patients and at our medical center in 20 patients. All pathological data were reviewed by neuropathologists.

Pathological grading was performed according to the current World Health Organization classification of ependymomas. Thirty patients with 40 lesions had ependymomas which corresponded to WHO grade 2 tumors. Fifteen patients with 25 lesions had anaplastic ependymomas (WHO grade 3).

Radiosurgery Technique

Radiosurgery was performed with the Model U, B, C, or 4-C Leksell Gamma Knife (Elekta Inc, Atlanta, GA). Our radiosurgical technique has been described in detail in previous reports (Kano et al. 2009). The procedure began with application of a model G Leksell stereotactic frame under conscious sedation and local scalp anesthesia except in younger children whose general anesthesia was used. After attaching a fiducial system to the frame, all patients underwent high resolution MRI. A 3-D localizer sequence which included axial, coronal and sagittal images was performed first. The tumor was then imaged using a 3 D gradient recalled sequence images.T2 weighted MRI using Fast Spin Echo technique also was acquired to assess the infiltrative tumor volume. The images were exported to a computer workstation via the hospital Ethernet for dose planning. In 64 tumors the radiosurgery treatment volume was defined by the enhancing tumor volume. In one patient who had a non-enhancing tumor the radiosurgery treatment volume was based on the T2-weighted imaging volume.

The median tumor volume was 3.0 cc (0.1–36.8 cc). The median tumor volume of grade 2 and grade 3 ependymomas was 2.5 and 3.6 cc, respectively

Table 27.1 Patient characteristics in 45 patients with 65 lesions

Characteristics	Grade 2	Grade 3	Entire cases
Number of patients	30	15	45
Number of tumors treated	40	25	65
Median age	26.1	11.9	25.4 (2.7–78.6)
Male	15	13	28
Female	15	2	17
Location: Infratentorial	31	11	16
Supratentorial	9	14	8
Prior surgery (total removal)	29 (8)	14 (7)	43 (15)
Prior biopsy	1	1	2
Prior fractionated radiation therapy	23	14	37
Prior chemotherapy	8	7	15
Prior FRT and chemotherapy	7	7	14
No prior FRT and chemotherapy	5	1	6
SRS for residual lesion	6	4	10
SRS for recurrence lesion	25	14	39
SRS for new lesion (metastases)	9	7	16
mean/median target volume (cc)	5.1/2.5	4.5/3.6	4.9/3.0 (0.1-36.8)
mean/median margin dose (Gy)	13.8/13.0	16.0/16.0	14.6/15.0 (8-22)
mean/median maximum dose (Gy)	27.5/26.0	31.9/32.0	29.2/30.0 (20-40)
mean/median follow-up after SRS (months)	31.4/15.8	30.8/13.4	31.2/14.9 (4.0-155.2)
mean/median follow-up after Dx (months)	96.1/30.8	58.0/27.3	83.4/64.1 (8.7-284.1)

(*t*-test: $p = 0.0003$). A median of 3 isocenters (1–11) were used for dose planning. The median prescription dose delivered to the margins of the tumor was 15 Gy (8–22 Gy). The median marginal dose of grade 2 and grade 3 ependymomas was 13.0 and 16.0 Gy, respectively (*t*-test: $p = 0.6913$). The prescription isodose was 50% in 63 cases. Maximum dose varied from 20 to 40 Gy (median, 30 Gy). All patients received an intravenous dose of 20–40 mg Methylprednisolone after radiosurgery and all were discharged from the hospital within 24 hours.

All patients were evaluated by MR imaging at intervals of 3–6 months after radiosurgery. All living patients had a minimum of 6 months follow-up. Twenty-three patients had follow-up of 24 months or more. The mean follow-up time was 40 months (range, 6.1–155.2 months). The follow-up MRIs were compared to the intraoperative images and tumor dimensions were measured in the axial, sagittal, and coronal planes. A complete response (CR) was defined as the complete disappearance of enhancing or non-enhancing tumor, partial response (PR) was defined as >50% shrinkage of the tumor volume, stable disease (SD) was defined as <25% change in tumor volume and progressive disease (PD) was defined as >25% increase in volume of the enhancing or non-enhancing tumor.

For statistical analysis we constructed Kaplan–Meier plots for survival and progression-free survival using the dates of diagnosis, first surgery, first SRS, follow-up MRIs, and death or last follow-up. Progression-free survival and overall survival time also were calculated from the day of the first SRS using the Kaplan–Meier method. Univariate analysis was performed on the Kaplan–Meier curves using log rank statistic with $p < 0.05$ set as significant. We performed multivariate analysis using the Cox proportional hazards model with $p < 0.10$ set as significant. Standard statistical processing software (SPSS, version 15.0) was used. This retrospective study was approved by the University of Pittsburgh Institutional Review Board.

Results

Tumor Control

Follow-up imaging studies demonstrated tumor control in 48 (74%) of 65 tumors at a median and mean of 15 and 31 months after SRS, respectively. After radiosurgery, complete resolution in tumor volume was identified in seven tumors (five were grade 2

Table 27.2 Tumor grade and imaging response after radiosurgery

Imaging response	Grade 2	Grade 3	Total
Complete resolution	5	2	7
Partial response	8	7	15
Stable disease	16	10	26
Progression disease	11	6	17
Delayed metastasis + outside of SRS treated volume	9	7	16

ependymomas and two were grade 3) and partial response in 15 tumors (eight were grade 2 ependymomas and seven were grade 3). In 26 tumors, the appearance of the tumor remained unchanged after radiosurgery (16 were grade 2 ependymomas and ten were grade 3). Localized in-field tumor progression was seen in 17 patients (six were grade 2 ependymomas and 11 were grade3) (Table 27.2).

Thirteen patients required additional management: two patients underwent surgical debulking alone, two patients had debulking followed by chemotherapy, three patients had debulking followed by RT and chemotherapy, and seven patients had chemotherapy. Three patients underwent repeat SRS. The progression-free survival after SRS was 83, 52 and 52% at 1, 3, 5 years after radiosurgery, respectively.

Patient Survival

At the time of this analysis 18 patients (40%) (12 WHO grade 2, Six WHO grade 3) were alive at an average of 49 months after radiosurgery (range, 6–155 months) and 111 months after initial diagnosis (range, 21–284 months). The overall survival after initial diagnosis was 100, 70, 62 and 42% at 1, 3, 5 and 10 years, respectively. The overall survival after SRS was 65%, 41 and 38% at 1, 3 and 5 years, respectively (Table 27.3, Fig. 27.1). The median survival after initial diagnosis was 104 months and after SRS was 21 months. Of the 45 patients, 16 (36%) patients had neuraxis metastasis after initial diagnosis. Distant metastases occurred in nine (30%) of 30 grade 2 ependymoma patients and seven (47%) of 15 grade 3 patients. Twenty-seven patients (18 WHO grade 2, 9 WHO grade 3 tumors) died at an average of 19.0 months from radiosurgery

Table 27.3 Survival based on tumor grade

	Grade 2 (%)	Grade 3 (%)
Survival rate	60.0	60.0
Actuarial 1-year survival	64.7	66.0
Actuarial 3-year survival	48.7	35.2
Actuarial 5-year survival	44.3	35.2
Recurrence free rate	36.7	40.0
1-Year PFS	82.1	84.0
3-Year PFS	56.1	47.3
5-Year PFS	46.8	47.3

PFS, progression-free survival.

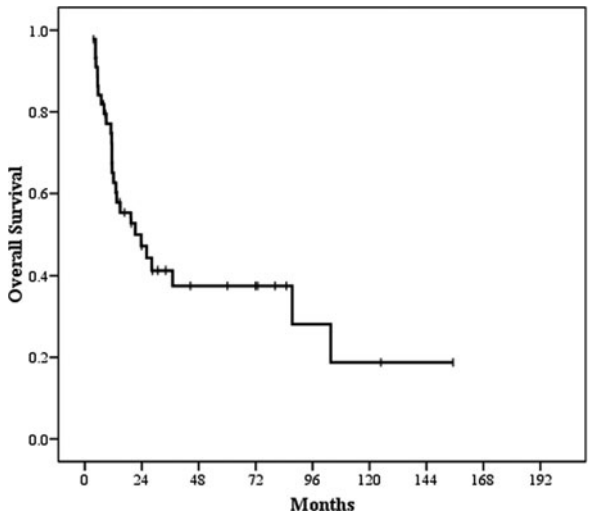

Fig. 27.1 Graph showing Kaplan–Meier estimate of overall survival for ependymoma patients after SRS

(range, 4–104 months) and 68 months from initial diagnosis (range, 12–217 months). Of these thirteen (48%) patients had tumor dissemination and 14 (52%) patients had local tumor progression.

Statistical Analysis

We performed univariate analysis using the log rank test to assess factors that influenced the length of overall and progression free survival. The following variables were assessed: sex (male or female), age (> or <15 years), tumor grade (WHO grade 2, 3), tumor dissemination, initial gross total surgical resection, radiosurgery target volume (> or <5.0 cc), marginal dose

Table 27.4 Results of univariate analysis for 45 patients treated for 65 tumors, with OAS and PFS measured from date of radiosurgery

	OAS	PFS		
	Entire cases	Entire cases	Grade 2	Grade 3
Age (≤15 versus >15 years)	0.022*	0.804	0.928	0.531
Sex (male versus female)	0.400	0.809	0.792	0.996
Tumor grade (2 versus 3)	0.913	0.725	N.A.	N.A.
Tumor location (infratentorial versus supratentorial)	0.602	N.A.	N.A.	N.A.
Delayed of metastases (yes versus no)	0.040*	N.A.	N.A.	N.A.
Gross total surgical resection (total versus partial)	0.268	N.A.	N.A.	N.A.
Prior RT and/or chemotherapy	0.872	N.A.	N.A.	N.A.
Target volume (≤5 cc versus >5 cc)	N.A.	0.019*	0.006*	0.815
Margin dose (≤15 Gy versus >15 Gy)	N.A.	0.368	0.691	0.337
MR feature (homogeneous versus heterogeneous)	N.A.	0.041*	0.005*	0.798
Prior chemotherapy (yes versus no)	N.A.	0.341	0.524	0.279
Adjuvant or boost SRS (yes versus no)	N.A.	0.440	0.935	0.480

* statistical significance; RT, fractionated radiation therapy; OAS, overall survival; PFS, progression-free survival; N.A., not available.

(> or < 15 Gy), prior RT and /or chemotherapy, adjuvant or boost SRS, MR imaging feature (homogeneous or heterogeneous tumor enhancement).

Younger age and existence of dissemination were associated with poor overall survival (Table 27.4). The 5-year overall survival in <15 year-old patients and >15 year-old patients was 26 and 45%, respectively ($p = 0.022$). The median overall survival in <15 year-old patients and >15 year-old patients was 11 months and 37 months, respectively. The 5-year overall survival in patients with tumor dissemination was 18% compared to 48% in patients without dissemination ($p = 0.040$). The median overall survival was 11.4 months in patients with tumor dissemination and 37 months in patients without dissemination.

Smaller radiosurgery target volume and homogeneous tumor enhancement on MRI were associated with improved progression-free survival (Table 27.4). Failed RT was associated with poor progression-free survival in only grade 3 ependymoma. Tumor grade (2 versus 3) was not associated with overall survival ($p = 0.913$, PFS: $p = 0.725$).

Other variables (sex, gross total surgical resection, prior RT and/or chemotherapy) were not significantly associated with better overall survival (Table 27.4).

Tumor Grade

The progression-free survival after SRS at 1-, 3- and 5 years, respectively were 82, 52 and 52% for all grade ependymomas (Fig. 27.2). Eleven of 40 (28%) patients with grade 2 ependymoma showed progression in the SRS volume. Six of 25 (24%) grade 3 ependymoma patients exhibited progression within the SRS volume. Grade 2 ependymoma had a 1-, 3- and 5-year progression free survival of 82, 56 and 47%, respectively. Grade 3 ependymoma had 1-, 3- and 5-year progression free survival of 84, 47 and 47%, respectively (Table 27.3). Histological tumor grade was not significantly associated with progression free survival ($p = 0.725$).

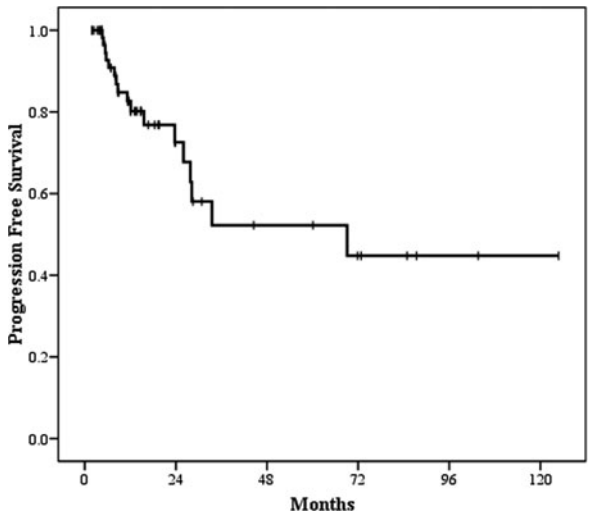

Fig. 27.2 Graph showing Kaplan–Meier estimate of progression-free survival for ependymoma patients treated with SRS

Tumor Volume

In the entire series, six of 41 (15%) lesions with tumor volume of <5.0 cc (mean tumor volume in the total cases) progressed in the SRS volume. The mean time to progression was 83 months. In contrast, 11 of 24 (46%) lesions with tumor volume of >5.0 cc exhibited local progression in the SRS volume. The median time to progression was 28 months. Kaplan–Meier plots, generated for progression free survival showed that lesions with volume of <5.0 cc had a 1- and 5-year progression free survival of 87 and 83%, respectively. Lesions with target volume of >5.0 cc had a 1- and 5-year progression free survival of 76 and 23%, respectively. A target volume of <5.0 cc was significantly associated with better progression free survival ($p = 0.0019$).

In grade 2 ependymoma tumors, a tumor volume of <5.0 cc was significantly associated with better progression free survival ($p = 0.006$). However, for in grade 3 tumors, a tumor volume of <5.0 cc was not significantly associated with better progression free survival ($p = 0.815$).

MRI Feature of Ependymoma

In the entire series, nine of 49 (18.4%) tumors that had homogeneous enhancement on MRI progressed in the SRS volume; the mean time to progression was 78.1 months. In contrast, 8 of 16 (50%) tumors with heterogeneous MRI features including cystic and/or necrotic areas exhibited local progression in the SRS volume; the median time to progression was 28 months. Kaplan–Meier plots, generated for progression free survival showed that tumors with homogeneous features MRI had a 1- and 3-year progression free survival of 92 and 61%, respectively. Tumors with heterogeneous features MRI had a 1- and 3-year progression free survival of 59 and 31%, respectively. Tumors with homogeneous features MRI had better progression free survivals ($p = 0.0041$).

WHO grade 2 ependymomas and homogeneous features MRI had better progression free survivals ($p = 0.005$). Patients with grade 3 ependymomas and homogeneous enhancement features MRI were not significantly associated with better progression free survival ($p = 0.798$). Other variables (age, sex, radiosurgery margin dose, prior SRS chemotherapy, early or late SRS) were not significantly associated with better progression free survival (Table 27.4). An illustrative case of tumor reduction is shown (Fig. 27.3).

Adverse Radiation Effects

Three patients (7%) developed ARE. One grade 2 ependymoma patient who received 13 Gy at the tumor margin showed increased peritumoral T2 signal changes and presumed central necrosis (loss of central

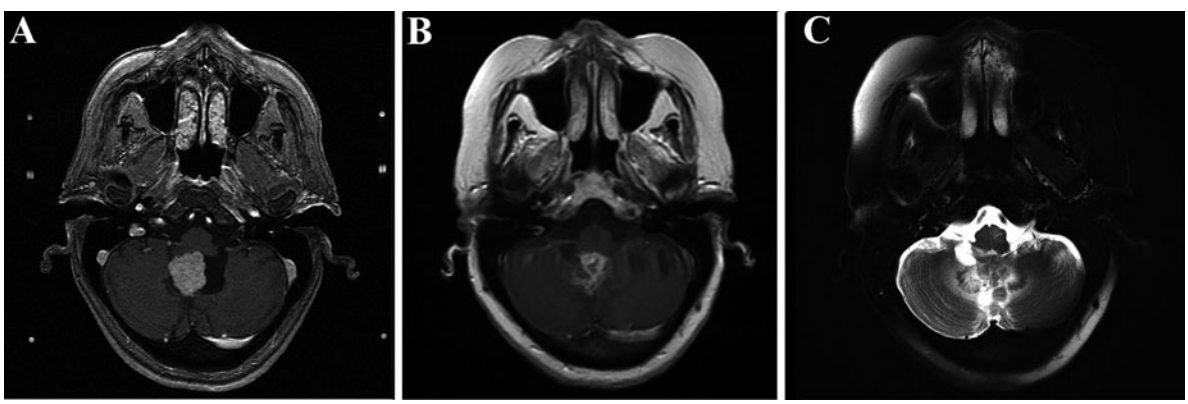

Fig. 27.3 A 57 year-old woman was diagnosed with an ependymoma grade 2 of the fourth ventricle by surgical removal. Axial T1 weighted contrast enhanced MR images showing radiosurgery target at the time of SRS (**a**). Axial T1 weighted contrast enhanced MR images obtained 8 months after SRS (**b**) showing regression of enhancing lesion in the fourth ventricle. Axial T2 weighted MR images obtained 8 months after SRS (**c**) showing no adverse radiation effect

contrast) at 1 year follow-up MRI. This patient was successfully managed with oral corticosteroids. One grade 2 ependymoma patient who received 12 Gy at the tumor margin developed an ipsilateral facial paresis three months after SRS. MRI showed increased peritumoral T2 signal changes. This patient was successfully managed with corticosteroids. One grade 3 ependymoma patient who received 16 Gy at the tumor margin developed increased contrast enhancement with peritumoral T2 signal changes but no symptoms 13 months after SRS. Single Photon Emission Computed Tomography (SPECT) was equivocal. This patient underwent a stereotactic biopsy that confirmed a combination of necrotic tumor with radiation effect. This patient died 28 months after SRS from tumor progression and intratumoral hemorrhage which occurred 2 weeks after reoperation.

Discussion

Primary intracranial ependymomas are typically managed with surgical resection followed by RT. The extent of surgical resection has been shown to influence patient survival and tumor control (Lyons and Kelly 1991; Perilongo et al. 1997; Pollack et al. 1995; Rousseau et al. 1994). Complete or near complete resection emerged as an independent prognostic factor (Jayawickreme et al. 1995; Pollack et al. 1993). The prognosis is better for patients who have complete resection followed by RT. Fractionated dose of 45–54 Gy have been recommended in an effort to improve local control (Goldwein et al. 1990a; Healey et al. 1991).

It was reported by Stafford et al. (2000) that 12 patients (aged 5–56 years) treated with Gamma Knife (12–24 Gy) at the time of disease recurrence. They showed a PFS of 68% at 3 years. There were two in-field failures and one marginal failure. Distant failure occurred in two patients. Two patients had AREs, one of whom received a 24-Gy boost and one who received two overlapping SRS treatments. The median overall survival was 3.4 years, and the median PFS was 18 months. It was reported by Hodgson et al. (2001) that 25 pediatric patients treated with SRS at the time of disease recurrence. They showed the median PFS was 8.5 months and the 3-year PFS was 29%. In the series that include patients of all ages, results are not much better (Hirato et al. 1995; Jawahar et al. 1999; Kano et al. 2009; Stafford et al. 2000). In these series, PFS from local disease is 40–68% over 3 years. However, overall survival is 32–45% at 3 years, due to disseminated disease.

Several studies suggested that younger patients may have a poor survival (Healey et al. 1991; Lyons and Kelly 1991). In our series younger age (<15 years) was associated with worse overall survival ($p = 0.022$). Supratentorial ependymomas are associated with better survival rates compared to posterior fossa neoplasms (Ernestus et al. 1996). However, in our series, tumor location (supratentorial versus infratentorial) was not statistically significant significance ($p = 0.602$).

Anaplastic ependymomas exhibit high mitotic activity, often accompanied by microvascular proliferation and pseudopalisading necrosis. Signs and symptoms are similar to those of grade 2 ependymomas but usually develop more rapidly and may cause increased intracranial pressure at an early stage of the disease. An inconstant relationship between histology and outcome has emerged from the clinical studies published to date (Afra et al. 1983; Ernestus et al. 1996; Figarella-Branger et al. 1991; Kano et al. 2009; Rosenblum 1998; Schiffer et al. 1991). In our series tumor grade was not associated with improved overall survival and progression-free survival (OAS: $p = 0.913$; PFS: $p = 0.725$), although our population is biased for the selection of recurrent tumors. Other authors also note an inconsistent relationship between histology and outcomes (Aggarwal et al. 1997; Grabb et al. 1996; Hodgson et al. 2001; Jawahar et al. 1999; Kano et al. 2009; Stafford et al. 2000). The median marginal dose for grade 3 ependymomas was higher than grade 2 ependymomas (grade 2: 13.0 Gy; grade 3: 16.0 Gy; $p = 0.0003$) even though the median tumor volume of grade 2 and grade 3 ependymomas was similar (grade 2: 2.5 cc; grade 3: 3.6 cc; $p = 0.6913$). Small target volume (<5.0 cc) grade 2 ependymomas had better progression free survival (entire series: $p = 0.019$; grade 2: $p = 0.006$). Small target volume (<5.0 cc) grade 3 ependymomas did not have better progression free survival ($p = 0.815$). In spite of higher margin dose for grade 3 ependymomas, progression free survival was similar to grade 2 ependymomas.

Recurrent ependymomas are difficult to manage, and multiple recurrences despite further surgery, radiation, or chemotherapy are common (Goldwein

et al. 1990a). At recurrence, platinum-, nitrosourea- or temozolomide-based chemotherapies have been administered with very little evidence of efficacy (Reni et al. 2007; Goldwein et al. 1990b). In our series prior chemotherapy was not significantly associated with better overall survival as well as progression free survival.

Dissemination occurs in about 10% of cases of primary intracranial ependymoma (Calvo et al. 1983; Rezai et al. 1996). This data was drawn from primary ependymoma patients who underwent surgical removal and/or RT. In our series dissemination rates were higher than other series because most of the patients had failed prior multimodal therapy. It was reported by Stafford et al. (2000) that distant metastases in two (17%) of 12 patients. In our series dissemination occurred in 16 (36%) of 45 patients. Dissemination was associated with poor overall survival (Table 27.4). The median overall survival in patients with dissemination and without dissemination was 11 and 37 months, respectively. Dissemination occurred in nine (30%) of 30 grade 2 ependymoma patients and seven (47%) of 15 patients. The longer follow-up in our series may be the reason for higher rates of dissemination compared to Stafford's series (Stafford et al. 2000).

Stereotactic radiosurgery has been used as an adjuvant management for ependymomas that progress or recur after prior surgical resection. But there are only a few reported series of SRS as an adjuvant management for ependymomas that progress or recur after prior surgical resection (Grabb et al. 1996; Hirato et al. 1995; Jawahar et al. 1999; Kano et al. 2009; Mansur et al. 2004). It was reported by Mansur et al. (2004) that nine patients (grade 2: seven; grade 3: two) treated with SRS for ependymoma. The 3-year over all survival and 3-year progression free survival were 77 and 56%, respectively. Patients treated with SRS as a boost following RT had an improved progression free survival (100%) compared to those treated with SRS to salvage an RT failure (20%) (Mansur et al. 2004). In our series prior failed RT was not significantly associated with worse progression free survival ($p = 0.256$). It was reported by Lo et al. (2006) that eight ependymoma patients (grade 2: seven patients; grade 3: one patient) were treated with SRS and the 1-, 2- and 3-year progression free survival was 88, 73 and 73%, respectively. The 3-year over all survival was 75%. Two (25%) of the eight patients developed ARE which were treated effectively by corticosteroids. It was reported by Stafford et al. (2000) that they managed 12 ependymoma patients (grade 2: $N = 7$; grade 3: $N = 3$; unknown grade: $N = 2$) with SRS and documented a 3-year progression free survival of 68% at a median follow-up 23 months. Two of 12 (17%) patients developed ARE. Our 1-, 2- and 3-year progression free survivals were 65, 47 and 41, respectively. In our series the median dose of RT was 49.1 Gy prior to 2000 but 53.2 Gy after 2000. Patients who had SRS after 2000 had 1-, 2- and 3-year progression free survivals of 83, 78 and 63%, respectively. Three of 45 patients (7%) developed AREs.

Homogenous enhancement MRI was significantly associated with better progression free survival ($p = 0.041$) especially if it was a grade 2 ependymoma ($p = 0.005$). Homogeneous MRI enhancement in a grade 3 tumor was not significantly associated with better progression free survival ($p = 0.798$). Grade 3 ependymomas often demonstrated heterogeneous MRI enhancement. Our data suggests that homogeneous enhancement MRI of a grade 2 ependymoma predicts a better SRS response.

After failed prior surgery, RT, and chemotherapy, SRS may be the only potentially effective management strategy that remains. Grade 2 ependymoma patients with small volume tumors and homogeneous MRI enhancement will respond best.

References

Afra D, Muller W, Slowik F, Wilcke O, Budka H, Turoczy L (1983) Supratentorial lobar ependymomas: reports on the grading and survival periods in 80 cases, including 46 recurrences. Acta Neurochir (Wien) 69:243–251

Aggarwal R, Yeung D, Kumar P, Muhlbauer M, Kun LE (1997) Efficacy and feasibility of stereotactic radiosurgery in the primary management of unfavorable pediatric ependymoma. Radiother Oncol 43:269–273

Calvo FA, Hornedo J, de la Torre A, Sachetti A, Arellano A, Aramburo P, Aragon G, Otero J (1983) Intracranial tumors with risk of dissemination in neuroaxis. Int J Radiat Oncol Biol Phys 9:1297–1301

Ernestus RI, Schroder R, Stutzer H, Klug N (1996) Prognostic relevance of localization and grading in intracranial ependymomas of childhood. Childs Nerv Syst 12:522–526

Figarella-Branger D, Gambarelli D, Dollo C, Devictor B, Perez-Castillo AM, Genitori L, Lena G, Choux M, Pellissier JF (1991) Infratentorial ependymomas of childhood. Correlation between histological features,

immunohistological phenotype, silver nucleolar organizer region staining values and post-operative survival in 16 cases. Acta Neuropathol 82:208–216

Goldwein JW, Glauser TA, Packer RJ, Finlay JL, Sutton LN, Curran WJ, Laehy JM, Rorke LB, Schut L, D'Angio GJ (1990a) Recurrent intracranial ependymomas in children. Survival, patterns of failure, prognostic factors. Cancer 66:557–563

Goldwein JW, Leahy JM, Packer RJ, Sutton LN, Curran WJ, Rorke LB, Schut L, Littman PS, D'Angio GJ (1990b) Intracranial ependymomas in children. Int J Radiat Oncol Biol Phys 19:1497–1502

Grabb PA, Lunsford LD, Albright AL, Kondziolka D, Flickinger JC (1996) Stereotactic radiosurgery for glial neoplasms of childhood. Neurosurgery 38:696–701; discussion 701–692

Healey EA, Barnes PD, Kupsky WJ, Scott RM, Sallan SE, Black PM, Tarbell NJ (1991) The prognostic significance of postoperative residual tumor in ependymoma. Neurosurgery 28:666–671; discussion 671–662

Hirato M, Nakamura M, Inoue HK, Ohye C, Hirato J, Shibazaki T, Andou Y (1995) Gamma Knife radiosurgery for the treatment of brainstem tumors. Stereotact Funct Neurosurg 64(Suppl 1):32–41

Hodgson DC, Goumnerova LC, Loeffler JS, Dutton S, Black PM, Alexander E 3rd, Xu R, Kooy H, Silver B, Tarbell NJ (2001) Radiosurgery in the management of pediatric brain tumors. Int J Radiat Oncol Biol Phys 50:929–935

Horn B, Heideman R, Geyer R, Pollack I, Packer R, Goldwein J, Tomita T, Schomberg P, Ater J, Luchtman-Jones L, Rivlin K, Lamborn K, Prados M, Bollen A, Berger M, Dahl G, McNeil E, Patterson K, Shaw D, Kubalik M, Russo C (1999) A multi-institutional retrospective study of intracranial ependymoma in children: identification of risk factors. J Pediatr Hematol Oncol 21:203–211

Jawahar A, Kondziolka D, Flickinger JC, Lunsford LD (1999) Adjuvant stereotactic radiosurgery for anaplastic ependymoma. Stereotact Funct Neurosurg 73:23–30

Jayawickreme DP, Hayward RD, Harkness WF (1995) Intracranial ependymomas in childhood: a report of 24 cases followed for 5 years. Childs Nerv Syst 11:409–413

Kano H, Niranjan A, Kondziolka D, Flickinger JC, Lunsford LD (2009) Outcome predictors for intracranial ependymoma radiosurgery. Neurosurgery 64:279–287; discussion 287–278

Kudo H, Oi S, Tamaki N, Nishida Y, Matsumoto S (1990) Ependymoma diagnosed in the first year of life in Japan in collaboration with the International Society for Pediatric Neurosurgery. Childs Nerv Syst 6:375–378

Lo SS, Abdulrahman R, Desrosiers PM, Fakiris AJ, Witt TC, Worth RM, Dittmer PH, Desrosiers CM, Frost S, Timmerman RD (2006) The role of Gamma Knife radiosurgery in the management of unresectable gross disease or gross residual disease after surgery in ependymoma. J Neurooncol 79:51–56

Lyons MK, Kelly PJ (1991) Posterior fossa ependymomas: report of 30 cases and review of the literature. Neurosurgery 28: 659–664; discussion 664–655

Mansur DB, Drzymala RE, Rich KM, Klein EE, Simpson JR (2004) The efficacy of stereotactic radiosurgery in the management of intracranial ependymoma. J Neurooncol 66: 187–190

Perilongo G, Massimino M, Sotti G, Belfontali T, Masiero L, Rigobello L, Garre L, Carli M, Lombardi F, Solero C, Sainati L, Canale V, del Prever AB, Giangaspero F, Andreussi L, Mazza C, Madon E (1997) Analyses of prognostic factors in a retrospective review of 92 children with ependymoma: Italian Pediatric Neuro-oncology Group. Med Pediatr Oncol 29:79–85

Pollack IF, Hoffman HJ, Humphreys RP, Becker L (1993) The long-term outcome after surgical treatment of dorsally exophytic brain-stem gliomas. J Neurosurg 78:859–863

Pollack IF, Gerszten PC, Martinez AJ, Lo KH, Shultz B, Albright AL, Janosky J, Deutsch M (1995) Intracranial ependymomas of childhood: long-term outcome and prognostic factors. Neurosurgery 37:655–666; discussion 666–657

Reni M, Gatta G, Mazza E, Vecht C (2007) Ependymoma. Crit Rev Oncol Hematol 63:81–89

Rezai AR, Woo HH, Lee M, Cohen H, Zagzag D, Epstein FJ (1996) Disseminated ependymomas of the central nervous system. J Neurosurg 85:618–624

Rosenblum MK (1998) Ependymal tumors: a review of their diagnostic surgical pathology. Pediatr Neurosurg 28: 160–165

Rousseau P, Habrand JL, Sarrazin D, Kalifa C, Terrier-Lacombe MJ, Rekacewicz C, Rey A (1994) Treatment of intracranial ependymomas of children: review of a 15-year experience. Int J Radiat Oncol Biol Phys 28:381–386

Schiffer D, Chio A, Cravioto H, Giordana MT, Migheli A, Soffietti R, Vigliani MC (1991) Ependymoma: internal correlations among pathological signs: the anaplastic variant. Neurosurgery 29:206–210

Stafford SL, Pollock BE, Foote RL, Gorman DA, Nelson DF, Schomberg PJ (2000) Stereotactic radiosurgery for recurrent ependymoma. Cancer 88:870–875

Wiestler OD, Schiffer D, Coons SW, Prayson RA, Rosenblum MK (2000) Ependymoma. In: Kleihues P, Cavenee WK (eds) Tumours of the nervous system. IARC, Lyon, pp 72–76

Chapter 28

Is Whole Brain Radiotherapy Beneficial for Patients with Brain Metastases?

Lucyna Kepka and Milena Kolodziejczyk

Abstract Whole-brain radiotherapy (WBRT) has been commonly used since the 1950s in the management of brain metastases. The overall survival rate after WBRT alone is between two and six months and it has not improved over time. The improvement of survival with the use of WBRT has never been demonstrated in the prospective trials. On the other hand, the improvement in the control of the disease within the brain with the use of WBRT has been consistently reported. The potential harms of WBRT in terms of neurocognitive dysfunction and worsening of the quality of life following the treatment should not be disregarded. In particular, the latter harm concerns patients with the worst prognosis as their short life expectancy won't let them recover from WBRT side-effects. Recently, the value of WBRT in terms of symptom palliation seems to have been challenged. The prospective evaluation of this aspect shows much more inferior results in comparison with those reported in the retrospective series. Despite limitations of this method, the WBRT remains apart from steroids, the only method of treatment used in case of multiple brain metastases. In case of oligometastatic brain disease, the omission of WBRT should be cautiously considered given the potential harms of the method, but also the evident benefit of reducing the risk of brain failure.

L. Kepka (✉)
Maria Sklodowska-Curie Memorial Cancer Center and Institute of Oncology, Department of Radiation Oncology, ul. Roentgena 5, 02-781 Warsaw, Poland
e-mail: lucynak@coi.waw.pl

Keywords Whole-brain radiotherapy · Brain metastases · Oligometastatic brain disease · Neurocognitive dysfunction · Peritumoral edema · Steroids therapy

Introduction

The incidence of brain metastases is growing in developed countries. In Sweden, the annual age-adjusted incidence rate of hospitalizations for brain metastases doubled from 7 to 14 patients per 100,000 inhabitants between 1987 and 2006. Within the same period of time, the survival of such patients did not improve. The median survival rate was 2.7 months (Smedby et al. 2009). It shows a little or no improvement in the treatment of brain metastases over the time. Whole brain radiotherapy (WBRT) has been used as the main method of treatment for patients with brain metastases. As the brain metastases cause debilitating neurological symptoms which have a negative impact on the quality of life, the WBRT together with steroids is considered to be a good method of palliation. Indeed, a recent survey has revealed that 95% of physicians referring patients for WBRT thought that such a treatment would not only improve neurologic symptoms and quality of life, but it would also allow doctors to taper the steroids dose (Barnes et al. 2010). However, the palliative value of the WBRT has been recently challenged (Bezjak et al. 2002); especially for patients with poor performance status (Komosinska et al. 2010). Its value for symptom alleviation in comparison with the steroid use, especially in case of poor performance status has not been established. Even, if the improvement of neurological function via better local control in the brain

M.A. Hayat (ed.), *Tumors of the Central Nervous System, Volume 4*,
DOI 10.1007/978-94-007-1706-0_28,

may be obtained, the positive impact of the WBRT on the quality of life may be compromised by worsening of the neurocognitive function related to the treatment toxicity (Chang et al. 2009). Improvement in the control of the disease in the brain that has been demonstrated in most randomized trials has never been translated into the survival advantage (Gaspar et al. 2010). For many opponents of this method, the value of WBRT is compromised by the lack of impact on survival. However, the reasons for this outcome are complex and all the benefits and risks associated with the use of WBRT will be discussed in this chapter.

Symptom Response Rate in WBRT

Retrospective studies report symptom response rate of WBRT for brain metastases in the range of 60–80% (Kepka et al. 2005). Such palliative effect is considered as the main value of this treatment modality. However, when the palliative effect of WBRT was evaluated in the prospective way, only 19% of patients reported symptom improvement (Bezjak et al. 2002). This discrepancy between prospectively collected patient-rated symptoms and retrospective data gathering is related to the obvious weaknesses of the retrospective studies. Additionally, the physicians' overestimation of the treatment effect for WBRT has been recently reported in a study done by Barnes et al. (2010). This study revealed that 87% of physicians thought that WBRT improved quality of life of patients and 78% of them expected neurological impairment reduction following treatment. Some aspects of the quality of life as measured by validated tools may even worsen after WBRT. In the prospective patient-rated symptom assessment by the Edmonton Symptom Assessment Scale, the significant decline from the baseline in the domain of fatigue, drowsiness, appetite was reported in 170 patients after WBRT (Chow et al. 2005). All these items are related to the acute and subacute brain radiation toxicity. Shortly after treatment, its toxicity may negatively impact the quality of life. Thus, the very short survival in some groups of patients carrying the worst prognosis does not allow for disclosure of any symptomatic benefit. It is conceivable that only with improvement of the survival, the potential symptomatic benefit of the WBRT would have been detected. Recent study by Komosinska et al. (2010) confirms this assumption. The study included 91 patients with brain metastases who were referred for WBRT. In addition, they all had poor performance status of less than 70% in Karnofsky performance scale (KPS). They were asked to complete a questionnaire about their symptoms before and one month after WBRT. In 43 (47%) patients who completed both symptom checklists (the remainder died within one month or their condition deteriorated to the point that they were no longer able to answer the questions), the significant worsening of the reported symptom intensity was found. Thus, the palliative value of WBRT, especially for patients with the shortest survival is challenged by the recent data. Its value in terms of symptoms palliation and quality of life for patients who have better prognosis needs further evaluation in prospective studies. The ongoing prospective trials that randomly assign patients to local treatment with or without WBRT are also expected to clarify these issues.

WBRT Versus Steroids

Corticosteroids are used together with WBRT for brain metastases symptom palliation. Steroids treat the peritumoral edema and via this mechanism improve neurological symptoms. However, the use of steroids produces side-effects which have a negative impact on the quality of life. These side-effects include among others: insomnia, mood disorders, weight gain, diabetes, peripheral edema, and myopathy. Thus the goal of WBRT is to taper off the steroids dose. Unfortunately, this outcome of WBRT is largely underreported in the literature. Only in one out of 23 fully published randomized controlled trials with WBRT as treatment intervention, the fixed doses of tapering dexamethasone were reported (Millar et al. 2004). It is crucial to identify patients in whom the efficient tapering of steroids by the WBRT use is not possible due to the very short life expectancy. For such patients, the use of WBRT with its burden of side-effects would not be beneficial. We have no prospective data comparing steroids use with WBRT except for one old trial

from pre-CT era (Horton et al. 1971). In this small trial that included 48 patients, the use of prednisone alone and prednisone plus WBRT was compared. There was no difference in the palliative effect of both treatment modalities (63 and 61% of improvement of performance status for prednisone and prednisone plus WBRT arm, respectively). There was no statistically significant difference in survival; however, the small sample size of the group prevented disclosing such a difference. Supportive care with steroids without WBRT may be an option for patients with short life expectancy. We need prospective trials which may guide us better in the identification of such patient population. In the meantime, we also need more detailed reporting from randomized trials on how WBRT helps in the tapering the steroids dose.

WBRT and Overall Survival

Overall survival of patients with brain metastases treated with WBRT alone is short and typically ranges between 3 and 6 months. The length of the overall survival depends on the presence of three prognostic factors: performance status, presence of extracranial disease and age. Those three prognostic factors were identified in the Radiation Therapy Oncology Group (RTOG) prospective trials on brain metastases and form the basis for Recursive Partitioning Analysis (RPA) RTOG prognostic classes which divide patients into three groups with distinct prognosis (Gaspar et al. 1997). The RPA class 1 carries the best prognosis (median survival about 6 months) and includes patients with no extracranial disease, good performance status (KPS > 70), and age below 65. The RPA class 3 carries the worst prognosis with median survival about 2 months and includes patients with poor performance status (KPS < 70), irrespective of the age and status of extracranial disease. The RPA class 2 carries the intermediate prognosis and includes patients who do not meet class 1 or 3 criteria. Whilst the overall survival after WBRT depends mainly on prognostic factors irrespective of treatment, no one parameter related to the WBRT delivery revealed the influence of the outcome. The pooled analysis of seven randomized trials did not indicate any difference in overall survival for doses superior or lower to dose of 30 Gy given in ten fractions, which is considered as the standard palliative dose. Fractionation schema was also not superior in terms of survival (Gaspar et al. 2010). The potential influence of WBRT on survival would have been demonstrated in the prospective trials comparing local treatment (surgery or stereotactic radiosurgery of brain metastases) alone to the same local treatment combined with WBRT. Only one randomized trial compared surgery alone to surgery and postoperative WBRT (Patchell et al. 1998). The trail included 95 patients with single metastatic lesion in the brain. In this study, the adjunct of WBRT to surgery had significantly improved local control of treated metastasis, it had also prevented the formation of new brain metastases and rate of death from neurological causes was reduced, but the overall survival remained not statistically significantly different unless it was numerically lower in the combined treatment arm. Similar results were reported in the prospective, randomized trials comparing radiosurgery alone to the WBRT with radiosurgery boost. In one study (Aoyama et al. 2006) that included 132 patients with one to four brain metastases, the addition of WBRT to radiosurgery did not improve survival despite better control in the brain in terms of local control of initial lesions and prevention of formation of new brain metastases. In a recent study of 58 patients, that used neurocognitive function as the main endpoint the evaluation, a surprisingly lower overall survival was noted in patients receiving WBRT combined with radiosurgery when compared to patients treated with radiosurgery alone. Such results could be attributed to a statistical hazard, because patients were not stratified according to the burden of extracranial disease and the initial neurocognitive performance. In addition, the study was based on the small sample size (Chang et al. 2009). Recently, the EORTC Radiotherapy and Brain Tumor Group conducted a phase III trial to define the role of adjuvant WBRT after local treatment (surgery or radiosurgery) for brain metastases (Mueller et al. 2009). The results from this study were presented in 2009 at the ASCO Annual Meeting and are in accordance with other available data on the impact of the WBRT on survival. It has been shown that the addition of WBRT to local treatment failed to prolong overall survival, but it reduced the frequency of intracranial relapses and neurologic deaths. Currently, the North Central Cancer Treatment Group (Intergroup N0574) is completing

phase III study (Intergroup N0574). In this study, patients are randomly allocated to stereotactic radiosurgery with or without WBRT. The primary endpoint is overall survival. A total of 528 patients will be accrued for this trial. In summary, the role of WBRT as an adjunct to local treatment of brain metastases should be further validated. Before more data is available, the combination of radiosurgery or surgery with WBRT in patients with brain metastases should be discussed individually.

Addition of Surgery or Radiosurgery to the WBRT

Poor results of WBRT in the management of brain metastases alone led to the attempts of local treatment intensification, via surgery or stereotactic radiosurgery. The theoretical objective of applying surgery prior to radiotherapy in brain metastases patients is the reduction of tumor volume, removal of tumor mass causing life-threatening complications e.g. tumor mass effect, increased intracranial pressure or even brain herniation. On the other hand, the dose from radiotherapy alone is not enough to achieve good local control. There were three randomized trials addressing the role of addition of surgery to WBRT. Two of them (Patchell et al. 1990; Vecht et al. 1993) demonstrated significant improvement in overall survival for patients with good performance status (KPS > 70) and single brain metastasis in whom craniotomy and postoperative WBRT was performed comparing with patients treated with WBRT alone. The third randomized trial (Mintz et al. 1996) failed to demonstrate any survival benefit from surgery. However, this study enrolled patients with poor performance status (KPS > 50). Thus it shows that treatment intensification is not an option for poor performance status patients with brain metastases. Only one sufficiently powered trial was performed to compare WBRT with WBRT combined with radiosurgery boost (Andrews et al. 2004). There were 331 patients with up to three brain metastases and good performance status (KPS $\geq$ 70). The radiosurgery boost led to the improvement of local control of treated lesions in all 331 patients. In the whole cohort of patients, the overall survival did not improve with the use of radiosurgery. The overall survival improved in the subgroup of patients with single metastasis only (4.9 months vs. 6.5 months for WBRT and WBRT plus radiosurgery groups, respectively, $p = 0.01$). The studies comparing WBRT alone with WBRT treatment intensification by radiosurgery or surgery show similar results, irrespective of the type of local treatment used. In summary, the use of surgery or radiosurgery combined with WBRT is beneficial in terms of survival for patients with single brain metastasis and good performance status.

WBRT and Its Impact on Neurocognitive Function

WBRT that is delivered up-front does not prolong survival; therefore, the neurocognition as another important endpoint needs to be considered before making decision on the use of the WBRT. The side-effects of the WBRT represent potential drawbacks of this method. For long term survivors of WBRT, there is potential for developing cognitive injury which intensifies with time and increases with the treatment volume and larger fraction size. In previous studies, both of these parameters were inherently related to the use of WBRT (Lawrence et al. 2010). With short survival of brain metastases patients, the subacute effects of WBRT represent a bigger concern. The transient demyelination of white matter following WBRT causes memory impairment, somnolence syndrome and loss of appetite. Symptoms caused by subacute radiation injury last longer (up to six months) than the expected survival of most patients with brain metastases. On the other hand, WBRT is recognized for its potential to improve control of brain metastases. Thus it should be established whether WBRT or brain tumor progression causes a greater threat of neurocognitive decline. In a randomized study that compared radiosurgery alone and radiosurgery with the use of WBRT no detrimental neurocognitive effect of the WBRT was detected (Aoyama et al. 2006). Recently, a randomized trial (Chang et al. 2009) has addressed the question of the neurocognitive function of patients with one to three metastases undergoing radiosurgery with or without WBRT as a main end-point of the study. The trial was stopped after inclusion of 58 patients on the basis that patients randomized to the

treatment containing WBRT were significantly more likely to have an impairment of learning and memory function as measured by Hopkins Verbal Learning Test-Revised total recall at 4 months. This worsening of neurocognition was disclosed in patients receiving WBRT despite a higher rate of salvage therapies in the group without WBRT (12 craniotomies vs. none in the radiosurgery alone and radiosurgery plus WBRT groups, respectively) related to the significantly worse brain tumor control (73% vs. 27% of 1-year brain tumor recurrence-free survival in the group receiving and not receiving WBRT, $p = 0.0003$). It means that even a lower rate of brain recurrences did not compensate for neurocognitive decline in the WBRT group in comparison with patients without up-front WBRT. This study has been criticized on the basis that patients receiving WBRT had worse baseline of neurocognitive function and a shorter overall survival which may explain worse intellectual performance just before death when the neurocognition was evaluated (Mahmood et al. 2010). Indeed, other data indicates that improvement of local control in the brain leads to the better neurological performance and by this mechanism to better neurocognitive function. In the aforementioned study by Aoyama et al. (2006) comparing radiosurgery and radiosurgery combined with WBRT, the average duration until deterioration of neurocognitive function as measured by Mini-Mental State Examination was 16.5 months in the group receiving up-front WBRT, comparing to 7.6 months in the group withholding WBRT, $p = 0.05$ (Aoyama et al. 2007). It is in line with a finding from another large randomized trial evaluating the use of WBRT with or without a radiosensitizer motexafin gadolinium (MGd) for brain metastases from non-small cell lung cancer. The combined treatment revealed to be more efficient local treatment in this target population leading to improvement of time to neurological improvement and subsequent better neurocognitive function (Mehta et al. 2009). In conclusion, we should be aware of side-effects of the WBRT with regards to a negative impact on neurocognition, however, a possibility of avoidance of debilitating neurological dysfunction by quite efficient local treatment should not be disregarded. Additionally, the omission of up-front WBRT with the use of local treatment only leads to the requirement of very strict follow-up and frequent imaging studies which in practice may be unfeasible due to high costs and compliance issues.

WBRT in Case of Radio-Resistant Histology

The role of WBRT in brain metastases from tumors from so-called "radioresistant histology" remains controversial. It concerns mainly melanoma, renal cancer, and less frequently sarcoma brain metastases. The question of the radioresistance of those tumors is also not unanimously accepted, but it remains beyond the scope of this publication. However, the results reported for WBRT in those indications are particularly obscure, and the term of "radioresistance" is commonly used for such tumors. Indeed, in the prospective trials, evaluating patients with brain metastases from melanoma, the combination of WBRT with chemotherapy either as Temozolomide (Margolin et al. 2002) or Fotemustine (Mornex et al. 2003), the response rate in the brain were lower than 10%. It indicates not only a lack of benefit with the combination treatment, but also a very low therapeutic ratio of the WBRT for melanoma metastases. Such a low efficacy in terms of response in those tumors and the data about no survival benefit with the use of WBRT in general led to the frequent abandonment of the WBRT and the use of local treatment only in radioresistant brain metastases.

A prospective phase II study was conducted by the Eastern Cooperative Oncology Group (ECOG) to test the safety of omission of the WBRT in case of one to three brain metastases from melanoma, renal cancer or sarcoma which would be suitable for radiosurgery. In this study, the brain tumor control rate was particularly low, even lower than in the retrospective studies, with 64.2% of failures in the brain reported at 6 months. Hence the ECOG study concluded that given the high risk of failure within the brain in such brain histologies, the omission of WBRT should be judged very cautiously outside the clinical trials and used only in cases where frequent imaging studies of the brain may be provided (Manon et al. 2005). It also indicates that the results of any therapy for radioresistant brain metastases which include melanoma metastases with especially obscure prognosis remain unsatisfactory. The role of WBRT remains to be established. For now, we should use our clinical judgment in the decision making process. Detailed information about our current knowledge and large room of the uncertainties in this field should be provided to the patient before he or she decides which method of treatment to choose.

Conclusions and Future Directions

Given the paucity of the therapeutic options for multiple brain metastases, the WBRT has been always considered in such patients. In order to answer the question about the benefits of WBRT for brain metastases patients we should formulate a few conclusions. First of all, WBRT has a potential for decreasing brain metastases progression. It is done at the expense of potential radiation toxicity. We apprehend the risk of worsening of neurocognitive function for long-term survivors of brain metastases after irradiation of the whole brain. A worsening of neurocognitive function (Chang et al. 2009) and the quality of life (Komosinska et al. 2010; Chow et al. 2005) as a consequence of acute and subacute radiation side-effects has been recently demonstrated. For symptom response, the value of WBRT may be lower than demonstrated by retrospective studies. We need to continuously educate physicians in this area because a recent study (Barnes et al. 2010) revealed that they were too optimistic about symptomatic effects of WBRT. It urges us to better define the groups of patients in which WBRT may be omitted. For patients with the worst prognosis, the steroids therapy may be sufficient, while for some others a local treatment without WBRT and careful follow-up with repetitive imaging studies may be an option. For omission of the WBRT and the use of the local treatment alone for brain metastases, it is also necessary to evaluate a cost of the approach which requires frequent radiological evaluation. The benefit of prolonging survival with the WBRT has never been demonstrated. We are still waiting for the results from one large phase III study (Intergroup N0574) which is expected to answer this question definitively.

References

Andrews D, Scott C, Sperduto P, Flanders A, Gaspar L, Schell M, Werner-Wasik M, Demas W, Ryu J, Bahary J, Souhami L, Rotman M, Mehta M, Curran W (2004) Whole brain radiation therapy with and without stereotactic radiosurgery boost for patients with one to three brain metastases: phase III results of the RTOG 9508 randomized trial. Lancet 363: 1665–1672

Aoyama H, Shirato H, Tago M, Nakagawa K, Toyoda T, Hatano K, Kenjyo M, Oya N, Hirota S, Shioura H, Kunieda E, Inomata T, Hayakawa K, Katoh N, Kobashi G (2006) Stereotactic radiosurgery plus whole-brain radiation therapy vs. stereotactic radiosurgery alone for treatment of brain metastases. JAMA 295:2483–2491

Aoyama H, Tago M, Kato N, Toyoda T, Kenjyo M, Hirota S, Shioura H, Inomata T, Kunieda E, Hayakawa K, Nakagawa K, Kobashi G, Shirato H (2007) Neurocognitive function of patients with brain metastasis who received either whole brain radiotherapy plus stereotactic radiosurgery or radiosurgery alone. Int J Radiat Oncol Biol Phys 68: 1388–1395

Barnes E, Chow E, Tsao M, Bradley N, Doyle M, Li K, Lam K, Danjoux C (2010) Physician expectations of treatment outcomes for patients with brain metastases referred for whole brain radiotherapy. Int J Radiat Oncol Biol Phys 76: 187–192

Bezjak A, Adam J, Barton R, Panzarella T, Laperriere N, Wong C, Mason W, Buckley C, Levin W, McLean M, Wu J, Sia M, Kirkbride P (2002) Symptom response after palliative radiotherapy for patients with brain metastases. Eur J Cancer 38:487–496

Chang E, Wefel J, Hess K, Allen P, Lang F, Kornguth D, Arbuckle R, Swint J, Shiu A, Maor M, Meyers C (2009) Neurocognition in patients with brain metastases treated with radiosurgery or radiosurgery plus whole-brain irradiation: a randomised controlled trial. Lancet Oncol 10: 1037–1044

Chow E, Davis L, Holden L, Tsao M, Danjoux C (2005) Prospective assessment of patient-rated symptoms following whole brain radiotherapy for brain metastases. J Pain Symptom Manage 30:18–23

Gaspar L, Mehta M, Patchell R, Burri S, Robinson P, Morris R, Ammirati M, Andrews D, Asher A, Cobbs C, Kondziolka D, Linskey M, Loeffler J, McDermott M, Mikkelsen T, Olson J, Paleologos N, Ryken T, Kalkanis S (2010) The role of whole brain radiation therapy in the management of newly diagnosed brain metastases: a systematic review and evidence-based clinical practice guideline. J Neurooncol 96:17–32

Gaspar L, Scott C, Rotman M, Asbell S, Phillips T, Wasserman T, McKenna W, Byrhardt R (1997) Recursive partitioning analysis (RPA) of prognostic factors in three radiation therapy oncology group (RTOG) brain metastases trials. Int J Radiat Oncol Biol Phys 37:745–751

Horton J, Baxter D, Olson K 1971 The management of metastases to the brain by irradiation and corticosteroids. Am J Roent Radiat Ther Nucl Med 3:334–336

Kepka L, Cieslak E, Bujko K, Fijuth J, Wierzchowski M (2005) Results of the whole-brain radiotherapy for patients with brain metastases from lung cancer: the RTOG RPA intraclasses analysis. Acta Oncol 44:389–398

Komosinska K, Kepka L, Niwinska A, Pietrzak L, Wierzchowski M, Tyc-Szczepaniak D, Kaczmarczyk A, Bujko K (2010) Prospective evaluation of the palliative effect of whole-brain radiotherapy in patients with brain metastases and poor performance status. Acta Oncol 49:382–388

Lawrence Y, Li X, El Naqa I, Hahn C, Marks L, Merchant T, Dicker A (2010) Radiation dose-volume effects in the brain. Int J Radiat Oncol Biol Phys 76:S20–27

Mahmood U, Kwok Y, Regine W, Patchell R (2010) Whole-brain irradiation for patients with brain metastases: still the standard of care. Lancet Oncol 11:221–222

Manon R, O'Neil A, Knisely J, Werner-Wasik M, Lazarus H, Wagner H, Gilbert M, Mehta M (2005) Phase II trial of radiosurgery for one to three newly diagnosed brain metastases from renal cell carcinoma, melanoma, and sarcoma: an Eastern Cooperative Oncology Group study (E6397). J Clin Oncol 23:8870–8876

Margolin K, Thompson A, Ernstoff S, Weber J, Flaherty L, Weiss G, Sosman J, Smith W II, Dutcher P, Gollob J, Longmate J, Johnson D (2002) Temozolomide and whole brain irradiation in melanoma metastatic to the brain: a phase II trial of the Cytokine Working Group. J Cancer Res Clin Oncol 128:214–218

Mehta M, Shapiro W, Phan S, Gervais R, Carrie C, Chabot P, Patchell R, Glantz M, Recht L, Langer C, Sur R, Roa W, Mahe M, Fortin A, Nieder C, Meyers C, Smith J, Miller R, Renschler M (2009) Motexafin gadolinium combined with prompt whole brain radiotherapy prolongs time to neurologic progression in non-small cell lung cancer patients with brain metastases: results of a phase III trial. Int J Radiat Oncol Biol Phys 73:1069–1076

Millar B, Bezjak A, Tsao M, Sturdza A, Laperierre N (2004) Defining the impact and contribution of steroids in patients receiving whole-brain irradiation for cerebral metastases. Clin Oncol (R Coll Radiol) 16:339–344

Mintz A, Kestle J, Rathbone M, Gaspar L, Hugenholtz H, Fisher B, Duncan G, Skingley P, Foster G, Levine M (1996) A randomized trial to assess the efficacy of surgery in addition to radiotherapy in patients with a single cerebral metastasis. Cancer 78:1470–1476

Mornex F, Thomas L, Hauschild A, Delaunay M, Lesimple T, Tilgen W, Nguyen B, Guillot B, Ulrich J, Bourdin S, Mousseau M, Cupissol D, Bonneterre J, de Gislain C, Bensadoun J, Clavel M (2003) [Randomized phase III trial of fotemustine versus fotemustine plus whole brain irradiation in cerebral metastases of melanoma.] (Article in French). Cancer Radiother 7:1–8

Mueller P, Soffietti R, Abaciouglu M, Villa F, Fauchon B, Baumert B, Fariselli L, Tzuk-Shina T, Collette L, Kocher M (2009) Adjuvant whole brain radiotherapy versus observation after radiosurgery or surgical resection of 1-3 cerebral metastases: results of the EORTC 22952-26001 study. J Clin Oncol 27(Suppl.):2008

Patchell R, Tibbs P, Regine W, Dempsey R, Mohiuddin M, Kryscio R, Markesbery W, Foon K, Young B (1998) Postoperative radiotherapy in the treatment of single metastases to the brain: a randomized trial. JAMA 280: 1485–1489

Patchell R, Tibbs P, Walsh J, Dempsey R, Maruyama Y, Kryscio R, Markesberry W, Macdonald J, Young B (1990) A randomized trial of surgery in the treatment of single metastases to the brain. N Engl J Med 322:494–500

Smedby K, Brandt L, Backland M, Blomqvist P (2009) Brain metastases admissions in Sweden between 1987 and 2006. Br J Cancer 101:1919–1924

Vecht C, Haaxma-Reiche H, Noordijk E, Padberg G, Voormolen J, Hoekstra F, Tans J, Lambooij N, Metsaars J (1993) Treatment of single brain metastasis: radiotherapy alone or combined with neurosurgery? Ann Neurol 33:583–590

Chapter 29

Triggering Microglia Oncotoxicity: A Bench Utopia or a Therapeutic Approach?

Tim Kees, Rodrigo Mora, Ivana Dokic, Johannes Noack, Anette Abschütz, and Anne Régnier-Vigouroux

Abstract Malignant brain tumors are the third leading cause of cancer death in the 15–34-year group. Due to their infiltrative character and development of resistance to death after therapy, these tumors are very difficult to combat with conventional therapies (surgery, radiation and chemotherapy). Alternative strategies that would efficiently complement the current ones are therefore needed and these include immune therapy. Targeting microglia, the resident immune cells of the brain, and the regulation of their activities represents an interesting approach to novel brain tumor therapies. These phagocytes are endowed with a cytotoxic potential that however seems to be silenced in most cases once the cells have migrated in and populated the tumor. Other data however suggest that in vivo activation of microglia can lead to tumor rejection. This indicates that anti-tumor responses may indeed be raised within the brain with the help of therapeutic settings mimicking these stimuli. Achievement of this goal yet relies on a better characterisation of the oncotoxicity of microglia and its regulation by tumor cells.

Keywords Brain tumors · Microglia · Gliomas · Cytotoxic potential · Tumor rejection · TLR

A. Régnier-Vigouroux (✉)
Program Infection and Cancer, Deutsches Krebsforschungszentrum, D-69120 Heidelberg, Germany
e-mail: regnier@dkfz-heidelberg.de

Introduction

Most cancer therapies aim at targeting the transformed, malignant cells through strategies designed to decrease or stop proliferation, migration and invasion on the one hand side, and to promote killing and elimination of the tumor cells on the other hand side. In solid tumors, such as gliomas, tumor cells are not isolated and co-exist with other non malignant cells. As stated by Condeelis and Pollard (2006), "tumors are complex ecologies of different cell types and (...) the full manifestation of the malignant potential (...) requires an appropriate support structure from the stroma". Whereas this support structure changes with the tumor type, there is one constant: the presence of macrophages, or microglia for brain cancers, that have infiltrated the tumor mass and/or surround it. In gliomas, tumor-infiltrating microglia, together with blood–borne macrophages, can account for roughly 30–40% of the tumor mass. Similar to macrophages, their peripheral relatives, microglia are endowed with immune competences that make them potential players in innate and adaptive immune response (Kreutzberg 1996). Anti-tumor activities could thus be expected from such cells. This is not, or very rarely, the case. Most experimental and clinical observations indeed indicate that tumor-associated macrophages, as well as tumor-infiltrating microglia, support, or even promote tumor growth and migration, as if tumor cells would educate them to perform these tasks (Condeelis and Pollard 2006; Yang et al. 2010). A positive contribution of macrophages to tumor regression has been reported in very few studies performed in the human or rodent models (Forssell et al. 2007; Galarneau et al. 2007). Several tumor-derived factors like the transforming

M.A. Hayat (ed.), *Tumors of the Central Nervous System, Volume 4*,
DOI 10.1007/978-94-007-1706-0_29,

growth factor (TGF)-β or the interleukin (IL)-10 can lead to an inhibition of microglial functions and even to a reprogramming of these cells as they trigger the microglial release of tumor supporting substances like growth factors, angiogenic substances or matrix metalloproteases that enhance tumor cell invasion. The regulation of macrophages and microglia functions by glioma cells is therefore of high relevance for the design of efficient (immuno)therapies. These cells constitute potential new drug targets that are worth exploring, namely in the case of gliomas for which alternative therapies or therapies complementary to the existing ones are urgently needed.

As attractive and legitimate as it first appears, targeting microglia is far from an easy task. One has to reckon with the uniqueness of the brain milieu that shapes these cells and their interactions with the various other neural cells. Stimulating anti-tumor activities of microglia may be deleterious not only to tumor cells but also to neurons, unless one designs a way to restrict these activities or the microglia stimulation to the tumor mass only. The neurotoxicity of microglia has been and still is a break in the conception of strategies aiming at the induction or increase of microglia cytotoxic activities. This is however the path we followed in the last years as we tried to answer a simple question: can we re-program microglial cells to become efficient and specific killers of glioma cells? In the following discussion, we will strive to convey the message that this task is not a utopia but a path to alternative therapies.

Cytotoxic Functions of Microglia and Their Regulation by Brain Cells

The nature and functions of microglia in the healthy, neurodegenerative or tumor-bearing brain have recently been extensively discussed in excellent reviews to which we refer the reader (Block et al. 2007; Streit 2002; von Bernhardi 2007; Yang et al. 2010). We will focus in this section on microglia functions most relevant to the purpose of this review.

Microglia, also called the brain resident macrophages, are of hematopoietic origin and populate the parenchyma as well as the perivascular spaces. In a healthy brain, these cells behave as highly dynamic patrollers acting as housekeepers. They are extremely sensitive to immune and non-immune events and the motility of these so-called "resting" microglia most likely facilitates their prompt reaction to any type of brain injury. This extreme sensitivity of microglia to changes in the composition of the brain milieu and their faculty to quickly respond to central nervous system (CNS) specific signalling substances or invading pathogens fully justifies their nickname as "sensors" of the brain (Kreutzberg 1996). From a sentinel status, microglia will switch to the so-called "activated" status that shall support neuroprotective or immune functions which aim at restoring the previous homeostasis. Activation of microglia proceeds according to steps which have been well characterised. The resting state, characteristic for a cell in a healthy brain environment, is defined by a ramified morphology, an absence of voltage-gated currents and a high motility. Disturbance of brain homeostasis leads to an activated state that translates in a temporal sequence of morphological changes from a ramified to rod-like and amoeboid structures, acquisition of distinct patterns of K+ channels and neurotransmitter receptors (Pocock and Kettenmann 2007), migratory and proliferative behaviour, release of various reactive oxygen species (ROS), reactive nitrogen species (RNS), cytokines and growth factors and phagocytic activity. These changes are not irreversible, demonstrating a very important feature of microglia that is their plasticity (Schwartz et al. 2006). The cytotoxic activities of microglia mainly rely on their release of ROS and RNS that can cause irreversible damage to neurons (Block et al. 2007), on their induction of programmed cell death through the secretion of tumor necrosis factor (TNF)-α and activation of the CD95/CD95L system (Pocock and Kettenmann 2007), or on the release of proteases such as cathepsins. Neuronal death is desirable at certain steps of development or as a kind of death-blow in case of irreversible neuronal damage. This event however certainly must be a rare one which implies a strict in situ regulation of the microglia neurotoxic activities, and more generally of microglia activation, by constitutive or induced mechanisms.

Regulation by Neurons

The regulation of microglia activation by its neighbouring neural cells, especially astrocytes and neurons, is not yet fully understood. The active involvement of

neurons in this regulation has recently been reviewed (Biber et al. 2007). In a healthy brain, interactions between the neuronal CD200 or CD22 molecules and their respective microglial receptors (CD200R, CD45) have been shown to be crucial for the regulation of the toxic and inflammatory activities of microglia. Recently the Notch signalling pathway has emerged as an important actor in the control of microglia activation as it modulates the transcription of pro-inflammatory cytokines and the production of nitric oxide (NO) (Grandbarbe et al. 2007). According to their in vitro observations, the authors hypothesize that in physiological conditions, Notch ligands, which are secreted by neurons, would stimulate the Notch receptor present on microglia, maintaining these cells in a resting, quiescent state. In an inflammatory milieu, these interactions would decrease or inhibit microglial over-activation. The toxic and inflammatory activities of microglia are contained as well by most neurotransmitters (Pocock and Kettenmann 2007). These so-called "off" signals however are taken over by "on" signals in the situation of brain injury (Biber et al. 2007). Purines, such as ATP or UTP, that are released by damaged or overactive neurons, have been shown to trigger either a protective or a destructive response from microglia. The same holds true for glutamate. An excessive release of glutamate by neurons can activate the metabotropic glutamate receptors of the group II expressed by microglia, leading to a TNF-α and CD95L-induced neuronal apoptosis. On the contrary, activation of the group III receptors leads to neuroprotection (Pocock and Kettenmann 2007). These few examples illustrate the complexity of the regulation of microglia activities that depends on a fine tuning between levels of triggers, patterns of responding molecules in microglia and cellular interactions.

Regulation by Astrocytes

Astrocytes can modulate the cytotoxicity of microglia as well as their immune status. TGF-β released by these cells plays a key role in this modulation. TGF-β is involved in the deactivation of the microglial immune status as well as in the regulation of their ROS- and NO-mediated cytotoxicity. Astrocytes modulate microglia reactivity to β-amyloid that is a threat to neurons (Smits et al. 2001). They release gliotransmitters that comprise purines and glutamate which most likely contribute to the regulation of microglia activity to the same extent as their neuronal counterparts do. ATP-mediated Ca^{++} signalling between astrocytes and microglia can even lead to microglial cell death. This rather definitive way to silence microglia function may serve the purpose of regulating the amount of activated microglia in pathological conditions.

Oncotoxicity of Microglia

Microglia present in the tumor mass show no obvious sign of toxic activities although they clearly exhibit an activation phenotype, as they promote growth and migration of the tumor cells. These latter can exert most of the tolerogenic effects triggered by astrocytes on microglia, monocytes or macrophages. Brain tumor cells may thus have kept and even amplified these microglial regulatory features during the transformation process (Kostianovsky et al. 2008). Does the same hold true for the regulation of microglia cytotoxicity? How is this activity controlled by tumor cells? Can microglia be released from this control and switch on again their cytotoxic activities?

The Rodent Model

Frei and colleagues were the first in 1987 to report on the induction of microglial cytotoxicity toward the mastocytoma cell line P815, in the mouse model (Frei et al. 1987). Upon treatment with the pro-inflammatory cocktail composed of the bacterial lipopolysaccharide (LPS) and of interferon (IFN)-γ, they observed that microglia released TNF-α which induced cell death. Since this first characterisation, few studies have been reported and little progress has been made in understanding the molecular basis of this toxicity. NO was later confirmed to be an important factor in the microglia-mediated death of tumor cells. Rosales and Roques reported in 1997 their investigation of toxic, anti-tumor factors secreted by the retinal microglia (Rosales and Roque 1997). These authors took an original approach based on the observation that tumors very rarely develop in an adult retina. They hypothesized that microglia may be the source of anti-tumor

factors. They indeed could show a toxic activity of retinal microglia supernatant that both impaired proliferation and induced death of the C6 rat glioblastoma cell line. Their attempt to purify and identify these factors unfortunately was not crowned with success as judged by the absence of further report by these authors on that issue.

We started our own quest with a rather simple question and approach. Can we trigger a microglial cytotoxic activity *specific* for tumor cells, i.e. an *oncotoxicity*, upon treatment with the pro-inflammatory cocktail used by Frei and colleagues? This cocktail represents the standard activation cocktail that triggers the bactericidal and tumoricidal activities of macrophages. LPS and IFN-γ activation of their respective receptors leads typically to activation of the nicotinamide adenine dinucleotide phosphate (NADPH) oxidase, induction of the inducible nitric oxide synthase (iNOS) expression and triggering of the nuclear factor kappa-light-chain-enhancer of activated B cells (NF-κB) signalling, which result in ROS, NO and release of pro-inflammatory cytokines such as TNF-α. There was yet no report about the specificity of action of microglia activated by LPS and IFN-γ. One of our first concerns was therefore to assess whether murine microglia treated for 48 h with LPS and IFN-γ killed tumor cells, and only tumor cells. Positive detection of ROS (our unpublished data), NO and TNF-α (Abschuetz et al. 2006; Mora et al. 2009) in the supernatant of the treated microglia indicated their successful activation under these conditions. Co-culture of the murine glioma cell lines with treated microglia or with the supernatant of these cells led to tumor cell death within 3–4 days of incubation (our unpublished data; (Mora et al. 2009)). Since the killing activity of microglia was present in their supernatant, we further used this supernatant rather than the cells in the hope of identifying possible (new) toxic soluble factors. Were these factors acting specifically on tumor cells? They were. Primary cultures of astrocytes or neurons incubated with the supernatant showed no sign of death, despite the presence of potentially harmful molecules such as TNF-α and the remnants of LPS and IFN-γ. We even observed a neuroprotective and neurotrophic effect of the supernatants from activated microglia. We did not investigate the nature of this effect but one explanation may lie in the presence of neurotrophins, for instance the brain-derived neurotrophic factor (BDNF) that can be released by microglia upon LPS treatment, or in the neuroprotective nature of low doses of IFN-γ (Schwartz et al. 2006). Whatever the explanation might be, the observed oncotoxicity of such a supernatant was the proof that microglia, in culture, can be appropriately stimulated to specifically kill tumor cells. The low doses of LPS (0.1 μg/ml) and IFN-γ (33 ng/ml) we used might have guaranteed the right balance between protective and killing activities borne by the soluble factors. The killing activities obviously are induced by the treatment, as shown by the lack of toxicity exhibited by the supernatant of untreated microglia. The protective activities however are present in both untreated and treated microglia supernatants. Further investigation will be necessary to reveal the nature of these protective activities in both cases and hence, the effects exerted by the LPS/IFN-γ stimulation on the production and pattern of (neuro)protective molecules.

The Human Model

What happens in the human model? Studies similar to those performed with rodent microglia are scarce due to the difficulties in isolating and keeping adult microglia in culture. Hussain and colleagues were the first to report a successful isolation of glioma-infiltrating microglia/macrophages (GIM) that they characterised ex vivo for their innate immune functions and anti-tumor activities (Hussain et al. 2006). Using flow cytometry analysis, they could demonstrate that GIM express various toll-like receptors (TLR) that are essential molecules in the activation of the innate immune potential of these cells. The authors could not detect intracellular expression of pro-inflammatory cytokines in GIM and therefore suggested that the TLR may not be fully functional in these cells. However, they observed that freshly isolated GIM incubated for 24 h with the human U-87 MG glioma cell line killed the tumor cells in absence of any added stimulus. According to their report, the efficacy of this killing was similar to that exerted by peripheral blood mononuclear cells (PBMC) but lower than that of microglia they isolated from a healthy, tumor-free brain. This level of cytotoxicity is unexpected in absence of exogenous stimulus. This latter might have been provided during the isolation procedure, resulting in a mild state of microglia activation. Although these observations await further confirmation from

independent laboratories, they emphasize the extreme plasticity of the microglia and their capacity to regain functions that tumor cells suppress or keep at a low level.

Searching for Oncotoxic Factors

The characterisation of each of the components of the untreated ("basal" status) and of the treated ("activated" status) microglia supernatants would provide invaluable information. This is a colossal work that Hwang and colleagues have recently undertaken in the rat model (Hwang et al. 2009). In their set up, both untreated and treated microglia preparation were found oncotoxic. Rat microglia may differ from mouse microglia in their basal level of toxic activities, which were found to be enhanced by the treatment. Proteomic analysis of the secreted microglia proteins indicated a role for the cysteine protease Cathepsin B in tumor cell death mediated by microglia, through mechanisms that still have to be unravelled (Hwang et al. 2009). Further developments and results of this proteomic approach will be very interesting to closely follow up. Our attempts to identify and purify a toxic factor from mouse microglia unfortunately failed. Our efforts to track it down however taught us that microglia oncotoxicity was not mediated by one factor but by a combination of factors. This may explain the success of the supernatant in killing tumor cells that are resistant to TNF-α and to the TNF-related apoptosis-inducing ligand (TRAIL). The combination of factors present in the supernatant helped to overcome the resistance of the two murine glioma cell lines we used towards these two death inducers. Actually, the death signals sent by the microglia supernatant turned the basal autophagy observed in the cell lines from a survival pathway into a deadly one. This combination of factors may also explain the efficacy of the supernatant in killing cell lines which exhibit differences in their morphology, phenotype, sensitivity to NO (Mora et al. 2009) or p53 status, which appears to be mutated in the SMA-560 but not in the MT539MG cell lines (our unpublished data).

This supernatant may therefore be compared to an optimal combinatorial therapy: neuroprotective and oncotoxic activities are present in amounts that ensure efficacy, specificity and safety. This encourages the search for proper ways to stimulate microglia in situ, since, through their nature, they are the best equipped to secrete the right combination of protective and oncotoxic factors. However, this search is paved with obstacles. How to reach microglia and only microglia in the tumor mass? How to ensure this "proper activation"? Can the microglia be at all activated in the tumor mass, given the immunosuppressive environment created by the tumor cells and the regulation these cells exert on microglia functions?

Targeting Microglia: Wishes and Reality

Activation of Microglia In Situ

According to our observations, we could activate microglia to exert oncotoxicity, in the mouse model. These experiments were done with cells isolated from healthy brains that had lost the contact with other types of brain cells during the culture and that had never been in contact before with tumor cells or tumor infiltrating cells. Would microglia present in the tumor mass still be responsive to stimulating molecules? Would the toxic factors still be effective in the tumor mass? In order to answer these questions, we took advantage of a culture model in which cells are grown in spheroids. This reconstitutes a three dimensional environment that mimics to a certain extent the physiological condition. Mixed spheroids composed of tumor cells and microglia were exposed to the medium of culture or to the LPS and IFN-γ cocktail. Microglial cells that had been exposed in the spheroid to factors secreted by glioma cells and to a direct contact with these cells showed two distinct phenotypes. In absence of any exogenous stimulus, they supported the growth and migration of tumor cells out of the spheroids. When the spheroids were treated with the pro-inflammatory cocktail, microglia mediated glioma cell death (Mora et al. 2009). Different conclusions can be drawn. First, microglia in monolayer or spheroid culture, in absence of the pro-inflammatory LPS/IFN-γ treatment, support tumor growth and migration. Second, microglia present in the tumor mass indeed respond to the LPS/IFN-γ stimulus. Third, the toxic factors indeed effectively kill the tumor cells in the tumor mass. This last point was further confirmed in experiments in

which explants of tumors grown in the mouse brain were embedded in a collagen matrix and exposed to microglia supernatant.

These observations support the idea that in situ activation of microglia in the tumor is feasible and can lead to microglia oncotoxicity. However we still have to validate these results in vivo, as well as in the human model. We also have to define the best and safest stimulus/stimuli of the innate oncotoxic response of microglia for therapeutic purposes. Human microglia express most of the TLR known up to now. TLR3 agonists (such as poly(I:C)), and not the TLR4 agonists (such as LPS), seem to mediate the strongest pro-inflammatory response in these cells and activate their immune competence (Jack et al. 2007). The effects of TLR3 agonist on microglia activation and the induced anti-tumor activities have still to be assessed in an experimental glioma model. On the one hand side, poly(I:C) concentrations have to be chosen carefully in vivo due to severe side effects in case of overdoses (Okada et al. 2005). On the other hand side, it may be inefficient as indicated by the results of a phase II clinical study. In this study, poly(I:C) was administrated to patients suffering from anaplastic glioma. Although the treatment was well tolerated, it did not lead to an improvement in the 6-month progression free survival (Butowski et al. 2009).

More successful though contradictory were the attempts to target the TLR9 on microglia. We shall expect that the TLR9 agonist, CpG oligodeoxynucleotide, activates the innate and adaptive immune potential of microglia. Following treatment of glioma-bearing animals with CpG, rat or mice microglia were shown to exhibit morphological changes, expression of activation markers (Carpentier et al. 2000; Schluesener et al. 2001) and an antigen presenting cell profile (El Andaloussi et al. 2006; Ginzkey et al. 2010). However these activation profiles not always correlated with anti-tumor effects. Whereas some studies indicate a beneficial effect, as CpG treatment led to an increased survival and tumor eradication (Carpentier et al. 2000; El Andaloussi et al. 2006) and induction of glioma cell apoptosis (El Andaloussi et al. 2006), other studies failed to demonstrate effects on tumor growth or on animal survival (Ginzkey et al. 2010). These discrepancies may be explained by differences in the injection route (intra-venous versus intra-tumoral), in the oligodeoxynucleotides used, or in the glioma cell lines used (Gl261 by El Andaloussi and colleagues; 9L by Ginzkey and colleagues; CNS-1 by Carpentier and colleagues).

Whatever the explanations may be, these studies illustrate two major obstacles one has to overcome in the design of in situ activation. The first one consists in the specificity of action of the drug. Tumor cells express a wide range of TLR and therefore may be activated through their own TLR in a way that might lead to an increased suppression of microglia anti-tumor activities. Stimulation of microglial TLR9 may be toxic not only for glioma cells but for other types of brain cells, for instance neurons (Iliev et al. 2004). The second obstacle relates to the efficient delivery in the CNS parenchyma, that is the crossing of the blood brain barrier. There are only a few small molecules that can cross the blood-brain barrier. They typically have an average molecular mass of 0.36 kDa and cross either via a lipid mediation or a carrier transportation system. A novel small molecule that inhibits STAT3, an important mediator in the IFN-γ signalling cascade, has been described to efficiently reach the CNS and activate the immune potential of microglia, both in ex vivo isolated human brain tumor cells and in mouse experimental subcutaneous model with glioma cells (Hussain et al. 2007). Upregulation of STAT3 had been observed in the macrophage/microglia population isolated from human glioblastoma as well as in human monocytes that had been co-cultured with glioma cells. This upregulation correlated with the secretion of the anti-inflammatory cytokine IL-10 (Kostianovsky et al. 2008). A recent study performed in a mouse experimental glioma model strengthens the very promising use of the small molecule inhibitor of STAT3. Treatment of glioma-bearing mice with a STAT3 specific silencing RNA led to microglia activation and inhibition of tumor growth. Silencing of STAT3 in microglia in vitro counteracted the immunosuppressive activity of glioma cells (Zhang et al. 2009). These studies convincingly demonstrated the efficiency of a treatment based on the delivery of the compound via intra peritoneal and intra tumoral injections. They however did not address in detail the specificity of the cellular targeting of the silencing RNA or of the small molecule inhibitor, an issue that may be critical for the fate of cells (tumor or brain cells) other than the target cells, hence for the clinical relevance of this treatment.

An interesting though still speculative approach would consist in designing a tumor-specific killer that

induces the immunogenicity of the dying tumor cells. Such an immunogenic cell death has been shown to be critical for the development of anti-tumor responses (Kepp et al. 2009). Activation of the pro-inflammatory profile and of the antigen presenting cell profile of microglia upon phagocytosis of dying cells could be extremely beneficial in the context of a tumor-harbouring brain. Most chemotoxic drugs, such as anthracyclins that are known for their capacity to induce immunogenic cell death (Kepp et al. 2009), unfortunately lack cell-specificity of action. The use of oncotropic, oncolytic viruses, like the parvovirus, may prove very promising in that regard (Cornelis et al. 2004). Parvoviruses are non pathogenic for adult human beings. They are innocuous towards normal, healthy astrocytes and microglia but readily kill murine and human glioma cell lines (Abschuetz et al. 2006) through a mechanism that differs from a classical apoptosis (Di Piazza et al. 2007). They may therefore provide an excellent tool for a tumor cell-specific killing that may trigger the immune potential of phagocytosing microglia.

Activation of Microglia Ex Vivo

As we have seen, microglia isolated from brain tumors or from healthy brain can easily be activated. Could such cells be injected in the body, reach the CNS and exert their anti-tumor activities therein? Protocols for ex vivo activation of T cells or macrophages isolated from patients have shown little side effects and promising results in clinical trials for glioma treatment (Plautz and Shu 2001; Sutton et al. 2008). Circulating monocytes can engraft in the brain and differentiate into microglia. In the case of CNS infection, it seems that they could contribute during the resolution of the inflammation and tissue repair through their phagocytosis of dead cells (Djukic et al. 2006) and through the anti-inflammatory response driven by that uptake (Magnus et al. 2002). Hematopoietic progenitors cells migrate efficiently towards intra-cerebral gliomas but are absent from the tumor-free hemisphere, illustrating the specificity of this tropism (Tabatabai et al. 2005). In a rat spinal cord injury model, microglia activated in vitro with LPS and transplanted at the injury site promoted the recovery of hind limb motor function (Yu et al. 2009). These few examples illustrate that strategies based on ex vivo activation of microglia isolated from the tumor and re-injected in the patient either in the blood circulation or intrathecally bear promises for future therapies.

Conclusion

A certain conception of the "immune privilege" of the brain and the scarecrow of microglia neurotoxic activities have impeded the exploration of alternative therapeutic ways in which microglia could be essential and effective death effectors and immune actors. The continuous investigation and hence a better understanding of the nature and function of microglia, of their interactions with tumor and neural cells, as well as of the interactions between the nervous and the immune systems shall open the door to innovative, complementary therapeutic strategies involving these highly dynamic and sensitive cells.

Acknowledgments We gratefully acknowledge the continuous support of Prof. Jean Rommelaere. We apologize to all authors whose work could not be cited due to space restriction.

References

Abschuetz A, Kehl T, Geibig R, Leuchs B, Rommelaere J, Régnier-Vigouroux A (2006) Oncolytic murine autonomous parvovirus, a candidate vector for glioma gene therapy, is innocuous to normal and immunocompetent mouse glial cells. Cell Tissue Res 325:423–436

Biber K, Neumann H, Inoue K, Boddeke HW (2007) Neuronal 'On' and 'Off' signals control microglia. Trends Neurosci 30:596–602

Block ML, Zecca L, Hong JS (2007) Microglia-mediated neurotoxicity: uncovering the molecular mechanisms. Nat Rev Neurosci 8:57–69

Butowski N, Lamborn KR, Lee BL, Prados MD, Cloughesy T, DeAngelis LM, Abrey L, Fink K, Lieberman F, Mehta M, Ian Robins H, Junck L, Salazar AM, Chang SM (2009) A North American brain tumor consortium phase II study of poly-ICLC for adult patients with recurrent anaplastic gliomas. J Neurooncol 91:183–189

Carpentier AF, Xie J, Mokhtari K, Delattre JY (2000) Successful treatment of intracranial gliomas in rat by oligodeoxynucleotides containing CpG motifs. Clin Cancer Res 6: 2469–2473

Condeelis J, Pollard JW (2006) Macrophages: obligate partners for tumor cell migration, invasion, and metastasis. Cell 124:263–266

Cornelis JJ, Lang SI, Stroh-Dege AY, Balboni G, Dinsart C, Rommelaere J (2004) Cancer gene therapy through autonomous parvovirus – mediated gene transfer. Curr Gene Ther 4:249–261

Di Piazza M, Mader C, Geletneky K, Herrero YCM., Weber E, Schlehofer J, Deleu L, Rommelaere J (2007) Cytosolic activation of cathepsins mediates parvovirus H-1-induced killing of cisplatin and TRAIL-resistant glioma cells. J Virol 81:4186–4198

Djukic M, Mildner A, Schmidt H, Czesnik D, Bruck W, Priller J, Nau R, Prinz M (2006) Circulating monocytes engraft in the brain, differentiate into microglia and contribute to the pathology following meningitis in mice. Brain 129: 2394–2403

El Andaloussi A, Sonabend AM, Han Y, Lesniak MS (2006) Stimulation of TLR9 with CpG ODN enhances apoptosis of glioma and prolongs the survival of mice with experimental brain tumors. Glia 54:526–535

Forssell J, Oberg A, Henriksson ML, Stenling R, Jung A, Palmqvist R (2007) High macrophage infiltration along the tumor front correlates with improved survival in colon cancer. Clin Cancer Res 13:1472–1479

Frei K, Siepl C, Groscurth P, Bodmer S, Schwerdel C, Fontana A (1987) Antigen presentation and tumor cytotoxicity by interferon-gamma-treated microglial cells. Eur J Immunol 17:1271–1278

Galarneau H, Villeneuve J, Gowing G, Julien JP, Vallieres L (2007) Increased glioma growth in mice depleted of macrophages. Cancer Res 67:8874–8881

Ginzkey C, Eicker SO, Marget M, Krause J, Brecht S, Westphal M, Hugo HH, Mehdorn HM, Steinmann J, Hamel W (2010) Increase in tumor size following intratumoral injection of immunostimulatory CpG-containing oligonucleotides in a rat glioma model. Cancer Immunol Immunother 59:541–551

Grandbarbe L, Michelucci A, Heurtaux T, Hemmer K, Morga E, Heuschling P (2007) Notch signaling modulates the activation of microglial cells. Glia 55:1519–1530

Hussain SF, Kong LY, Jordan J, Conrad C, Madden T, Fokt I, Priebe W, Heimberger AB (2007) A novel small molecule inhibitor of signal transducers and activators of transcription 3 reverses immune tolerance in malignant glioma patients. Cancer Res 67:9630–9636

Hussain SF, Yang D, Suki D, Aldape K, Grimm E, Heimberger AB (2006) The role of human glioma-infiltrating microglia/macrophages in mediating antitumor immune responses. Neuro-oncology 8:261–279

Hwang SY, Yoo BC, Jung JW, Oh ES, Hwang JS, Shin JA, Kim SY, Cha SH, Han IO (2009) Induction of glioma apoptosis by microglia-secreted molecules: The role of nitric oxide and cathepsin B. Biochim Biophys Acta 1793:1656–1668

Iliev AI, Stringaris AK, Nau R, Neumann H (2004) Neuronal injury mediated via stimulation of microglial toll-like receptor-9 (TLR9). FASEB J 18:412–414

Jack CS, Arbour N, Blain M, Meier UC, Prat A, Antel JP (2007) Th1 polarization of CD4+ T cells by Toll-like receptor 3-activated human microglia. J Neuropathol Exp Neurol 66:848–859

Kepp O, Tesniere A, Schlemmer F, Michaud M, Senovilla L, Zitvogel L, Kroemer G (2009) Immunogenic cell death modalities and their impact on cancer treatment. Apoptosis 14:364–375

Kostianovsky AM, Maier LM, Anderson RC, Bruce JN, Anderson DE (2008) Astrocytic regulation of human monocytic/microglial activation. J Immunol 181:5425–5432

Kreutzberg GW (1996) Microglia: a sensor for pathological events in the CNS. Trends Neurosci 19:312–318

Magnus T, Chan A, Savill J, Toyka KV, Gold R (2002) Phagocytotic removal of apoptotic, inflammatory lymphocytes in the central nervous system by microglia and its functional implications. J Neuroimmunol 130:1–9

Mora R, Abschuetz A, Kees T, Dokic I, Joschko N, Kleber S, Geibig R, Mosconi E, Zentgraf H, Martin-Villalba A, Régnier-Vigouroux A (2009) TNF-alpha- and TRAIL-resistant glioma cells undergo autophagy-dependent cell death induced by activated microglia. Glia 57:561–581

Okada C, Akbar SM, Horiike N, Onji M (2005) Early development of primary biliary cirrhosis in female C57BL/6 mice because of poly I:C administration. Liver Int 25:595–603

Plautz GE, Shu S (2001) Adoptive immunotherapy of CNS malignancies. Cancer Chemother Biol Response Modif 19:327–338

Pocock JM, Kettenmann H (2007) Neurotransmitter receptors on microglia. Trends Neurosci 30:527–535

Rosales AA, Roque RS (1997) Microglia-derived cytotoxic factors. Part I: inhibition of tumor cell growth in vitro. Brain Res 748:195–204

Schluesener HJ, Seid K, Deininger M, Schwab J (2001) Transient in vivo activation of rat brain macrophages/microglial cells and astrocytes by immunostimulatory multiple CpG oligonucleotides. J Neuroimmunol 113:89–94

Schwartz M, Butovsky O, Bruck W, Hanisch UK (2006) Microglial phenotype: is the commitment reversible? Trends Neurosci 29:68–74

Smits HA, van Beelen AJ, de Vos NM, Rijsmus A, van der Bruggen T, Verhoef J, van Muiswinkel FL, Nottet HS (2001) Activation of human macrophages by amyloid-beta is attenuated by astrocytes. J Immunol 166:6869–6876

Streit WJ (2002) Microglia as neuroprotective, immunocompetent cells of the CNS. Glia 40:133–139

Sutton L, Chaoui D, Cazin B, Azar N, Chokri M, Romet-Lemonne JL, Maloum K (2008) Autologous activated macrophages (MAK) coated ex vivo with humanized anti-CD20 monoclonal antibodies can eradicate minimal residual disease in chronic lymphocytic leukaemia in clinical response. Br J Haematol 142:996–998

Tabatabai G, Bahr O, Mohle R, Eyupoglu IY, Boehmler AM, Wischhusen J, Rieger J, Blumcke I, Weller M, Wick W (2005) Lessons from the bone marrow: how malignant glioma cells attract adult haematopoietic progenitor cells. Brain 128:2200–2211

von Bernhardi R (2007) Glial cell dysregulation: a new perspective on Alzheimer disease. Neurotox Res 12:215–232

Yang I, Han SJ, Kaur G, Crane C, Parsa AT (2010) The role of microglia in central nervous system immunity and glioma immunology. J Clin Neurosci 17:6–10

Yu TB, Cheng YS, Zhao P, Kou DW, Sun K, Chen BH, Wang AM (2009) Immune therapy with cultured microglia grafting into the injured spinal cord promoting the recovery of rat's hind limb motor function. Chin J Traumatol 12: 291–295

Zhang L, Alizadeh D, Van Handel M, Kortylewski M, Yu H, Badie B (2009) Stat3 inhibition activates tumor macrophages and abrogates glioma growth in mice. Glia 57:1458–1467

Chapter 30

Preoperative Motor Mapping

Thomas Picht and Ayçe Atalay

Abstract Neurosurgery must always carefully balance the benefit of surgical therapy against the risk of causing or increasing neurological symptoms. Preoperative risk assessment on the basis of standard anatomical imaging alone is often insufficient because of inherent variations in motor representation from one patient to the next and because pathology can obscure or alter the anatomy. Several sophisticated new technologies have been developed in the past 30 years: PET, fMRI, MEG, TMS, DTI, which substantially improve the capabilities of the neurosurgical team to assess cortical function and improve their surgical planning. Neurosurgeons need to understand and use this modern technology to create patient-specific cortical maps and management plans, in order to improve therapeutic effectiveness and reduce morbidity. This chapter presents the current technologies in use for preoperative mapping of the motor system.

Keywords Neurosurgery · Brain tumors · Brain tissue · Functional motor topography · Cortical function · fMRI

Introduction

The benefit of surgical removal of brain tumors must be weighed against the risk of causing or increasing neurological symptoms by damaging functional brain tissue. Preoperative risk assessment cannot rely only on standard anatomical imaging because the relation between anatomy and function can be somewhat variable between different patients and because tumors can distort, obscure, or even reorganize the anatomy of the motor system. Five main technologies are in current use for preoperative mapping of the functional motor topography: PET, fMRI, MEG, TMS and DTI, and each has its own advantages, limitations, and uses.

The classic indication for preoperative mapping of the cortico-spinal system is a case where the exact spatial relationship between the tumor and the essential motor areas remains unclear after anatomical imaging. The tumor's infiltration or mass effect is the usual reason for this lack of clarity after anatomical imaging. But preoperative mapping is also indicated if there is a discrepancy between the imaging results and the clinical findings (e.g., a large tumor within M1 but no noticeable motor deficits). In such case, the functional anatomy may have changed due to tumor-induced plasticity. Lack of awareness of plastic changes of functional anatomy can lead to unexpected new neurological deficits after standard operative procedures. Because of that risk, preoperative functional mapping must be regarded as mandatory whenever a neurosurgical procedure is planned in areas that are or may be eloquent (i.e., carry essential function).

The main aim of preoperative motor mapping is to identify the areas that cannot be removed or damaged without causing a permanent neurological deficit ("eloquent" areas). Historically, the primary motor cortex (which is part of the precentral gyrus and has a strict somatotopic order) has been considered the only eloquent structure at the cortical level. Although this view has been modified by findings on overlapping motor representations within the precentral gyrus

T. Picht (✉)
Department of Neurosurgery, Charité - Universitaetsmedizin Berlin, Berlin, Germany
e-mail: Thomas.picht@charite.de

M.A. Hayat (ed.), *Tumors of the Central Nervous System, Volume 4*,
DOI 10.1007/978-94-007-1706-0_30,

and direct corticospinal tracts originating from the superior frontal gyrus, the precentral gyrus and its descending tracts still remains the main area for assessing the risk of morbidity in rolandic tumor surgery. Studies on brain connectivity and intraoperative stimulation studies have proven that the motor system is a dynamic network that is organized hierarchically around the cortical epicenter, i.e., the precentral gyrus, yet also includes other structures (Mesulam et al. 2000). The various brain mapping technologies have different ways of representing this complex network, and, therefore, they have various advantages and drawbacks.

Evolution and Classification of the Technologies

The functional organization of the brain has been a topic of interest for a long time, and some of the basic science used in current mapping technologies long preexisted its use in a routine clinical setting. Even before scientific methodology became well established, there were prescientific efforts to map the brain and define areas related to specific functions. During the late 19th century, investigators sought to correlate postmortem examinations with functional data in patients who had undergone neurologic testing during life, usually including patients with neurologic diseases (Potchen and Potchen 1991). Thus by the end of the 19th century, medical researchers had a basically correct understanding of the functional organization of the brain. Much of the fundamental science in physiology, chemistry, and physics (that is used as the basis of brain mapping technologies today) was, in fact, already available by the middle of the 20th century.

Although the underlying basic science has often been available and tinkered with in a few hospital laboratories since the early 20th century, preoperative motor mapping really did not begin entering widespread clinical usage until the 1980s. For example, although there are studies from the 19th century demonstrating that brain glucose and oxygen requirements are coupled to cerebral blood flow, this basic knowledge only reached the clinical setting in fMRIs in the 1990s. Similarly, the scientific background for electrophysiology-based techniques, such as MEG and TMS, dates back to the 1920s, when Berger (1929) demonstrated that electrical activity over the occipital cortex disappears when the subject's eyes are closed, thus illustrating that mental activity is accompanied by a change in the electroencephalogram. The reason for the long delay in making use of all the basic science is that until recent decades, television monitors and computer processors remained too crude and too rare for clinical medicine to harness the available basic science knowledge into devices that were clinically serviceable. Now, with the development of powerful and sophisticated computers and monitors, the past three decades have seen an almost miraculous development in our technological ability to see the functions of specific parts of the brain without opening the patient's skull. Although many further improvements are still needed and can certainly be expected, it is worth considering that the technologies available today for mapping the motor cortex would surely seem like science fiction to our predecessors of 80 years ago. These preoperative mapping technologies have enabled enormous advances in our ability to treat brain tumors surgically. Yet in order to be able to intelligently use the results from any of these mapping technologies, it is essential that the clinician has a thorough understanding of each technology's mode of functioning, degree of accuracy, and inherent methodological limitations.

The technologies for motor mapping can be divided into three major categories: (1) imaging of motor cortex activity (e.g., fMRI, PET, MEG), (2) stimulation mapping (e.g., TMS), and (3) projective computer modeling (e.g., DTI). All preoperative mapping modalities that have been used in recent years (fMRI, MEG, PET) record "brain activity" after the patient has performed certain tasks and then use biomathematical models to reconstruct the recorded data into functional information. This information has been successfully implemented into surgical planning. Nevertheless, these observational methods suffer from the limitation that their biomathematical models can be inadequate to reliably determine which areas produce essential function in the vicinity of a tumor, especially when complex networks are activated during motor paradigms. There is a risk of false-negatives, which can increase the surgical morbidity, and there is also the risk of false-positives, which can leave tumors inadequately resected. The reason for the false-positives is that these observational

methods also identify areas as "essential" that are merely involved in the task in inessential ways, and, therefore, could be safely resected without causing any lasting deficit (Krainik et al. 2004). The imaging techniques for human brain mapping can be further divided into two subgroups: hemodynamic/metabolic (e.g., fMRI, PET) and electrophysiological (e.g., MEG). Electrophysiological imaging methods (such as MEG) provide direct measurement of the brain's neural activity, while hemodynamic/metabolic methods measure neural activity indirectly by measuring their blood flow and metabolism. Experimental studies suggest that the hemodynamic response and neuronal activity are closely coupled to each other ("neurovascular coupling"), especially for local field potential (synaptic activity) rather than spiking activity. Yet, hemodynamic response tends to be more widespread in space and lasts longer in time as compared with the neural activity (Shibasaki 2008). In contrast to those methods, TMS is the only technology available using noninvasive *stimulation* for brain mapping. Like intraoperative direct electrical stimulation (DES), TMS stimulates points on the brain and then records motor output, rather than asking the patient to make a movement and then recording brain activity, like the imaging technologies mentioned above. Finally, projective computer modeling (currently only DTI) generates 3D visual computer models of the location of neural structures, based upon the analysis of imaging data (e.g., the direction of water diffusion on an MRI is used by DTI to generate models of the location of white matter tracts). This classification system should help to explain and organize the differences in the advantages and limitations of these five technologies.

The Current Technologies for Preoperative Motor Mapping

Positron Emission Tomography (PET)

The Fick principle postulates that the quantity of any substance taken up in a given time by an organ from the blood is equal to the total amount of the substance carried to the organ by arterial flow minus the amount removed by the venous drainage during the same period. This principle serves as the basis for the noninvasive measurement of cerebral functions by injecting a tracer into the blood circulation and then measuring the quantity of that tracer in different parts of the brain. Total brain blood flow was measured in the 1940s using nitrous oxide as the tracer (Kety and Schmidt 1948), while later studies used other tracers, such as xenon-133, and other administration routes such as intracarotid injection or inhalation. A major advance was reported in 1966, when Ter-Pogossian and Wagner (1998) introduced the use of the cyclotron accelerator to produce a variety of short-lived positron radionuclides that were unavailable from other sources such as radioisotopes of oxygen, carbon, nitrogen, and glucose. The use of these new tracers has enabled improvements in the quality of PET imaging and has also enhanced its range of applications. In addition to measuring merely the regional blood flow, the metabolic state of circumscribed brain areas has become measurable by new tracers such as glucose derivatives. Despite the early development of PET technology, the location and behavior of cerebral structures that participate in the generation of voluntary movements was only studied using PET starting from the 1980s onward (Fox et al. 1985).

In PET imaging, a radioactive tracer compound labeled with a positron-emitting isotope is administered to the patient's bloodstream and the patient is then imaged in a scanner containing rings of scintillation detectors that determine the position of the isotopes within the body (Tharin and Golby 2007). The most commonly employed PET tracer today is ^{18}F-FDG, which is a positron-emitting sugar-derivative that is actively transported across the blood-brain barrier into the neurons. It is distributed in the brain according to local metabolic activity. PET with ^{18}F-FDG has been compared with intraoperative cortical electrostimulation for the localization of motor areas in brain tumor patients (Schreckenberger et al. 2001), and was shown to have 94% sensitivity and 95% specificity for identifying the primary motor cortex. Cerebral blood flow can also be measured with 15O H_2O. The areas of PET activation using 15O H_2O during the performance of motor, visual, and language tasks have been compared to the results of intraoperative cortical stimulation in a sample of 12 patients and was concordant for cortical levels in all cases (Vinas et al. 1997). When tumors cause swelling and deformation of cortical structure, functional mapping with 15O H_2O allows for reliable identification of the

motor cortex (Nariai et al. 1997). One study has suggested that PET scans with 11-C methionine can be used to visualize tumor infiltration and to plan resection in cases of gliomas (Nariai et al. 1997), but this has never been confirmed elsewhere or become part of clinical practice. One advantage of PET is its ability to study a wide range of functions. Any brain function that can be called upon with a behavioral task can be studied by PET (Tharin and Golby 2007); but due to its complexity and costs, the method is available for motor mapping only at highly specialized centers.

Functional Magnetic Resonance Imaging (fMRI)

Routine structural MRIs can accurately show brain tumor location, but they do not provide information about the involvement and integrity of functional areas surrounding the tumor. The unprecedented accuracy of MRI in anatomical imaging led to the suggestion that multiplanar MRIs might serve as a useful preoperative planning aid, also for functional topography (Berger et al. 1990). The realization that the deoxyhemoglobin of the blood could be used as an endogenous contrast-enhancing agent opened up the possibility of identifying structures involved in specific functions, because brain activity involves increase blood flow to those structures. fMRI has been shown to be a reliable tool for preoperative identification of motor areas (Kwong et al. 1992) and can help to determine the feasibility of surgical planning in tumor patients (Lee et al. 1999).

Patient performance of specific behavioral tasks leads to regionally increased neuronal activity and localized hemodynamic changes that produce a signal response on the fMRI. The activation of neural cell populations can increase regional cerebral blood flow by as much as 50% (Tieleman et al. 2009). The deoxyhemoglobin in the blood is paramagnetic and therefore appears on T2 weighted MRI sequences. The fMRI signal response is based on the relative decrease of deoxyhemoglobin in activated brain tissue. For each voxel, the change in T2 signal is calculated between rest and activation. This change in signal is very small, so the signal is averaged over multiple trials to obtain an acceptable signal-to-noise ratio before it is subjected to further statistical analysis.

fMRI measurements include motor mapping using voluntary motor paradigms, language mapping, and various other cognitive tasks. Voluntary motor paradigms may need to be adjusted according to the functional level of the patients. For use with paretic patients, it has been suggested that the primary motor cortex is activated when thinking only regarding motor output, and it has been demonstrated that even imagining movement can produce activation in the primary motor cortex (Stippich et al. 2002). Additionally, passive fMRI paradigms have also been described where electrical stimulation of median and tibial nerves is used for activation analysis of the somatosensory cortex (Gasser et al. 2004).

The distance between the tumor margin and critical motor areas is the determining factor for the surgical resection and outcome. It has been proposed that the safety margins between the tumor border and fMRI motor areas should be between 1 and 2 cm to minimize morbidity (Tieleman et al. 2009; Gasser et al. 2004). Yet, the area of motor representation identified by fMRI differs noticeably depending on the statistics used for analyzing the BOLD data (Fig. 30.1) (Picht et al. 2009).

fMRI is currently the most commonly used method for preoperative motor mapping, in large part because of the widespread availability of MR units. Nonetheless, it has been suggested that tumor-induced changes of cerebral vasculature and neurovascular coupling can compromise the validity of this method. Current research with fMRI focuses mainly on its capacity to analyze complex networks. Its use for establishing a detailed cartography of cortical function has been decreasing.

Magnetoencephalography (MEG)

The electrical activity of the brain has been frequently measured with a commonplace electroencephalogram (EEG) for over a century now. As simple and useful as it is for other applications, the EEG has never entered into modern usage in preoperative mapping of the motor cortex, despite recurrent periods of interest in the 20th century. However, the electrical activity of the brain (as measured by a commonplace EEG) is

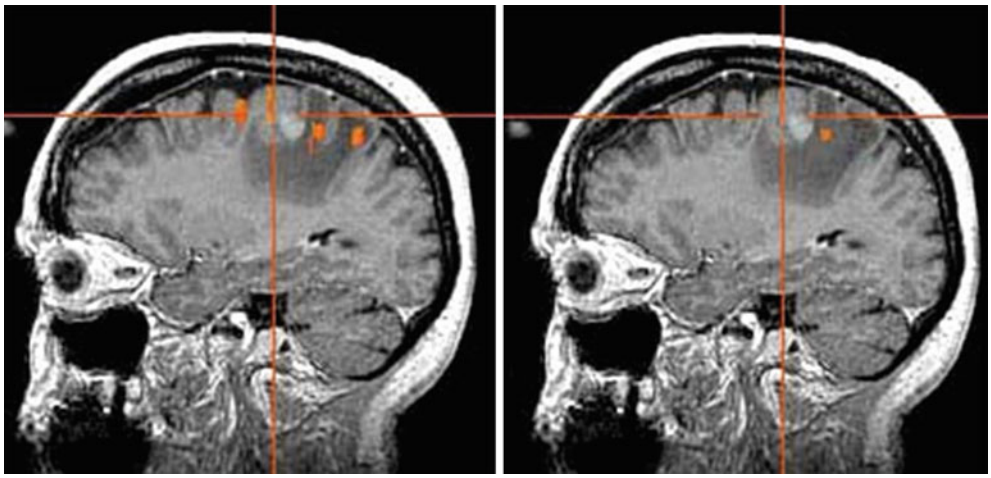

Fig. 30.1 Gadolinium-enhanced sagittal T1-weighted MRI: white area = centrally located metastasis, orange area = fMRI activation (finger tapping). *Left panel*: fMRI result at analysis threshold of $p < 0.0001$ (activations within the premotor, the sensory and the primary motor cortex). *Right panel*: fMRI result at analysis threshold $p < 0.000001$ (activation only within the primary motor cortex)

naturally accompanied by magnetic field changes. This has led relatively recently to the development of the most highly sophisticated and powerful imaging technology available: magnetoencephalography (MEG).

MEG uses a few hundred superconducting quantum interference detectors (arranged in a helmet placed over the patient's head) to measure magnetic flux from a few hundred points above the patient's scalp. In its raw form, MEG provides signal traces of brain activity (like an EEG) from the few hundred sensors, arranged in a topographic layout. This raw MEG data are then normally combined with anatomical data from a standard structural MRI to produce activation maps of the brain with the functional information overlaid on the corresponding anatomy.

MEG is capable of measuring electromagnetic changes from neuronal activity with an exceptionally high temporal resolution of mere milliseconds. For voluntary movements, these electromagnetic changes are detected immediately before the onset of movement. The primary somatosensory cortex can be located by stimulating various body parts tactilely or by stimulating peripheral nerves electrically. MEG has demonstrated its ability to reliably identify the precentral gyrus in healthy subjects and also in tumor patients (Nagarajan et al. 2008). Preoperative functional imaging using MEG has been compared with intraoperative direct cortical stimulation, and the accuracy was found to be sufficient to define the motor and somatosensory strips (Roberts et al. 1995). Schiffbauer et al. (2003) compared preoperative MEG recordings integrated into a neuronavigation system to intraoperative electrophysiological cortical mapping and concluded that the two modalities demonstrated a favorable degree of quantitative correlation. According to their findings, the distance between two corresponding points determined using magnetic source imaging and electrophysiological cortical mapping was 19 ± 1.3 mm for motor comparisons.

Because MEG measures magnetic fields, artifacts can easily arise. MEG must be conducted in a special shielded room to minimize interference from external magnetic sources, including other electrical equipment, radio signals, and even the Earth's own magnetic field. Nonetheless, artifacts can still arise from the patient (from dental fillings, cardiac pacemakers, spinal implants, etc.) and may interfere with the recordings. In order to improve the signal-to-noise ratio, it is often necessary to average tens or hundreds of event-related responses. New signal processing techniques are being studied to optimize MEG recordings. One such technique is the Signal Space Separation (SSS) method, which can efficiently remove several types of artifacts often seen in clinical practice (Taulu et al. 2004). MEG is uniquely capable of observing brain activities, due to MEG's near-real-time temporal resolution. Regrettably, the high cost of MEG systems restricts its usage to a very limited

number of highly specialized centers. Currently, it is best suited for research studies, especially those requiring extremely high temporal resolution to study the sequence of cortical brain events.

Transcranial Magnetic Stimulation (TMS)

TMS delivers magnetic stimulation to points on the brain, and then records the motor output by EMG. More specifically, an electric current passes through a coil placed above the patient's skull, and this generates a magnetic field, which then creates electric countercurrents inside the patient's skull. This then causes depolarization of the neurons, which, if they are responsible for controlling motor output, leads to a muscle response that can be recorded on a standard EMG. By moving the coil and stimulating multiple spots on the brain, the functional topography of essential areas of the motor cortex can be precisely mapped. The predominant application of TMS is planning surgery in the area of the primary motor cortex, but it can also be used to map secondary or supplemental motor cortices or language cortices (by disrupting speech).

TMS was introduced into clinical practice as early as 1985 for other applications (Barker et al. 1985), but the first articles on the use of TMS for the preoperative work-up of motor cortex surgery only appeared a decade later (Krings et al. 1997). Even then, TMS remained an obscure technology not widely used or known among neurosurgeons, because the early TMS systems were more demanding to use and less informative than TMS systems of today. Since then, both the hardware and the software of TMS systems have been substantially improved. The two main improvements of the hardware have been the refinement of the stimulation coils to make them more precisely focused (thus, increasing the accuracy of the results), and the development of more versatile navigation systems to guide the stimulation (rather then relying on conjunctures from anatomical landmarks on the skull). The two main improvements of the software have been that it now takes into account all known physical factors that have an influence on the stimulation (thus, better calculating the true location and intensity of stimulation) and also that it now has a much more intuitive user-interface, so the examiner can concentrate on the mapping rather than on deciphering the TMS system itself.

These recent improvements enable more reliable and practical use of TMS, and thus have led to TMS being enthusiastically rediscovered by the neurosurgery community. TMS is the only painless noninvasive method that allows for examination by stimulation of the brain, like the gold standard of intraoperative DES. The magnetic stimulation of a precise cortical spot enables assessment without the complex biomathematical modeling involved in some of the other methods. Points of the brain where TMS evokes MEPs can be considered as "essential" with the same reliability as intraoperative stimulation mapping. For visualization of the TMS results, all positive responses close to the tumor are displayed, and identification of M1 should be self-evident. Negative spots located within the tumor or immediately adjacent to it can also be shown, in order to document the lack of function within the tumor or close to the planned resection margin (Fig. 30.2).

TMS is easy to use and provides immediate results. The method does not involve any post-processing, which allows its interpretation straight forward and intuitive. The synthesis of the patient's clinical status, MRI findings, and TMS somatotopy in primary and nonprimary motor areas can improve the surgical team's ability to better plan the surgical strategy (Picht et al. 2011). TMS is evolving as a powerful probe for preoperative analysis of motor topography.

Diffusion Tensor Imaging (DTI)

Whereas the functional imaging methods and noninvasive stimulation mapping are restricted to the gray matter, diffusion tensor imaging (DTI) enables the noninvasive visualization of the white matter fiber tracts. DTI is a specific application of MRI technology, which projectively models the descending motor pathways, based upon analysis of the random motion of water molecules, as detected on the MRI. Water diffusion is less restricted parallel to the white matter tracts than perpendicular to them (Witwer et al. 2002), so by analyzing the direction of water diffusion on an MRI, the pathway and volume of the white motor tracts can be modeled. It has been suggested that imaging of the pyramidal tract with DTI can also reflect the functional

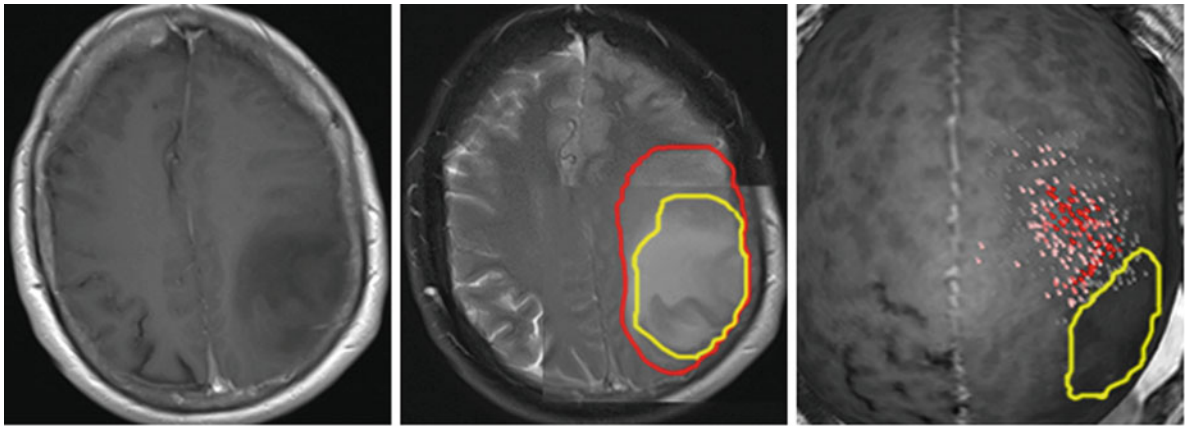

Fig. 30.2 *Left panel*: gadolinium-enhanced axial T1-weighted MRI of a right fronto-parietal low-grade glioma. *Middle panel*: overlay of T1 and FLAIR MRIs with the tumor border according to T1 MRI outlined in yellow and the tumor border according to FLAIR MRI outlined in red. *Right panel*: preoperative TMS with the tumor border according to T1 MRI outlined in *yellow*, nonresponsive TMS stimulation spots shown in *gray*, and responsive TMS stimulation spots shown in *color* (no motor function within the T1 hypointense area; motor function within the FLAIR area beyond the T1 hypointense area)

condition of the fibers, but this interpretation remains controversial (Yamada et al. 2003).

In neurosurgery, DTI is currently used to model the spatial location of the white matter tracts relative to the tumor. The effect of a brain tumor on the white matter tracts, as analyzed by DTI, can be categorized into four groups: displacement, invasion, edema and destruction; but the exact effect of the tumor on the tract can only be elucidated together with the standard MRI images and the clinical findings and may nevertheless remain unclear. When integrating the DTI data into the neuronavigation for intraoperative use, one must remain aware that the white matter tracts are at risk usually only after debulking of the tumor and occurrence of relevant amounts of brainshift. Thus, the location of white matter tracts as indicated by DTI may no longer be accurate when they are encountered, even if it was exactly accurate before the operation began.

DTI has two major advantages. First, DTI is currently the only method available that allows for visualization of white matter tracts. Second, the raw data for DTI can be acquired from every MRI scanner without much extra scan time. Yet, running DTI software depends heavily on the examiner's expertise, especially for determining the thresholds used to analyze the diffusion of the water. These thresholds strongly influence the volume and direction of the fibers that are computer-modeled on the MRI. Although DTI is a promising technology which would add the unique capability of visualizing white matter tracts, the actual benefits of DTI for treatment planning still remain to be seen.

Comparative Evaluation of the Technologies

Comparative Advantages and Limitations of PET

PET offers some advantages such as higher signal-to-noise ratio, less susceptibility to artifacts (from motion, draining veins, etc.), and a unique ability to evaluate tumor metabolism (which is useful for distinguishing recurrent tumor from radiotherapy-induced necrosis). However, PET has disadvantages in terms of exam duration, personnel requirements, and expense, due to the complexity of both the examination set-up and the raw data evaluation. Currently, only specialized centers use PET for preoperative functional mapping because PET has high costs for both initial acquisition and ongoing maintenance.

Several studies have compared PET and fMRI. Results of PET scanning using the tracer 15O H_2O have been compared with fMRI in 11 patients (Bittar et al. 1999). It was found that 96% of the activation peaks obtained by each of the two techniques were

located on either the same or the adjacent sulci and gyri; overlapping of voxels activated by each modality occurred in 92% of the cases. Another study compared fMRI and 15O H_2O PET in 25 patients with tumors of various etiologies near the central region (Reinges et al. 2004). The mean (SD) localization difference between fMRI and PET was 8.1 (4.6) mm, so the investigators concluded that both techniques demonstrate comparable results and are sensitive, reliable tools to map the central region. In a study comparing ^{18}F-FDG PET, fMRI, and direct cortical stimulation, 12 patients had overlapping results, 6 patients had neighboring results of PET and fMRI (between 1 and 2 cm distance), and 1 patient demonstrated discordance between fMRI and PET with direct cortical stimulation, speaking in favor of fMRI (Krings et al. 2002). Those investigators concluded that neurosurgeons must decide on a case-by-case basis which imaging modality to use. Although both PET and fMRI are commonly accepted modalities with widespread availability, the lower cost and greater technical ease of fMRI has led to its greater usage.

Comparative Advantages and Limitations of fMRI

The first obvious advantage of fMRI is that it is already widely available at many hospitals and also that there is a vast scientific literature regarding its use and interpretation. A sufficient spatial correlation between fMRI and other mapping techniques seems to exist for the motor areas. fMRI enables analysis of the whole brain over a period of time. Although the temporal resolution is low, it is sufficient to enable the medical team to distinguish between areas that are activated almost simultaneously versus areas that are activated separately. So, fMRI can provide rough information on the temporal sequence of all the neural areas involved in a task. Thus, one may draw conclusions regarding distinct networks and their interconnections. Additionally, longitudinal fMRI data make it possible to visualize any long-term brain plasticity after a tumor resection, which can have important implications on the further therapeutic strategy.

fMRI has various methodological shortcomings, including tumor-induced neurovascular uncoupling and artifacts from electromagnetic interference or patient head motion (Tieleman et al. 2009). Also, there are no standardized, user-independent protocols. It has been reported that slight changes in task design, task performance, or data analysis can have substantial impact on the activation maps one obtains (McGonigle et al. 2000). Successful identification of the precentral gyrus depends upon the quality of the data, which is influenced by many factors: the signal-to-noise ratio, artifacts, the motor task selected, the subject's ability to perform the task, and an intact neurovascular coupling. All these factors can be compromised in tumor patients and negatively affect the accuracy of the fMRI mapping result. Even when the data are of good quality, the biomathematical analysis of the data requires an expert examiner who knows by experience which analysis threshold best reflects reality and still there is a real risk of false-negatives, especially if there is impaired neurovascular coupling around the tumor. There is also a risk of false-positives, primarily due to activation of non-motor areas, because it is very difficult to selectively activate only the primary motor cortex (Rutten and Ramsey 2010). For all these reasons, the use of fMRI has been declining recently.

Comparative Advantages and Limitations of MEG

The main advantage of MEG is that it has superior temporal resolution compared to all other methods. MEG measures electromagnetic changes from neuronal activity on a timescale of milliseconds immediately before the onset of voluntary movement. By contrast, fMRI is based on the measurement of hemodynamic responses to neuronal activation, which are much longer than the underlying neuronal activity, lasting up to 15 s after a stimulus; and TMS cannot analyze the temporal activation pattern of distinct cortical areas at all, because it measures EMG motor output, not brain activity. MEG's superior temporal resolution enables the medical team to analyze each step of motor planning and performance in millisecond slices (Mäkelä et al. 2006). This ultrafine temporal analysis of the motor network is not possible with any other mapping modality. But like fMRI and PET, MEG involves biomathematical analysis of the raw data that is time consuming and requires expert knowledge.

A few studies have compared the accuracy of MEG and other mapping technologies. In one study,

somatosensory-evoked fields were measured after median nerve stimulation and compared with fMRI in 12 normal volunteers and 11 patients with intracranial tumors (Inoue et al. 1999). The fMRI-defined central sulcus coincided with the MEG-defined central sulcus in 82% of the affected hemispheres. In another study, MEG was compared with fMRI and intraoperative cortical mapping in 15 patients with a lesion near the primary sensorimotor cortex (Korvenoja et al. 2006). MEG depicted the central sulcus correctly in all patients as verified by intraoperative mapping, but fMRI agreed with intraoperative mappings in only 11 patients. So far, there have been no studies comparing MEG and TMS, undoubtedly because neither technology is widespread yet and only a few centers in the world have them both. Unfortunately, MEG has a very high cost – for both initial acquisition and ongoing maintenance. Therefore, it is available only at highly specialized centers. Furthermore, the procedure is also long and requires more personnel than for other methods.

Comparative Advantages and Limitations of TMS

Intraoperative direct electrical stimulation (DES) is the gold standard for functional mapping of the primary motor cortex, and DES has 100% sensitivity for detection of eloquent structures, according to a recent review of the literature (Mandonnet et al. 2010). In comparison to functional neuroimaging methods, TMS has the benefit of being the only painless preoperative method that establishes a causal link between the stimulation of an area and the observed motor output, in a fashion analogous to DES. The advantage of TMS over DES is that the former is conducted preoperatively. Clearly, this allows a more timely and thorough examination of motor topography with TMS, especially if the operation is challenging (e.g., due to a severe tumor mass effect). Moreover, if intraoperative complications are encountered, these can lead to aborting DES mapping altogether.

Currently available results suggest that navigated TMS motor mapping has an accuracy similar to that of DES. In a recent study the mean ± SEM distance between the APB hotspots of nTMS and DES was 7.83 ± 1.18 mm (Picht et al. 2011). Two earlier articles also reported a good correspondence between TMS and DES (Kantelhardt et al. 2010; Krings et al. 1997), although each paper's comparison of TMS and DES was based on only two patient cases each, so the findings cannot be taken as conclusive. In a previous report, exactly the same spots were stimulated with TMS and DES in a 5 mm raster (Picht et al. 2009). The median (range) distance between TMS and DES hotspots in that study was 5 (0–7) mm. It should be stressed that for both TMS and DES, the exact extent of the stimulated cortical area still remains unclear. So we do not know exactly where the depolarization of pyramidal cells takes place, and we do not know how large the area of suprathreshold stimulation is. Despite this uncertainty, it is still safe to assume that points of the brain where TMS (like DES) does *not* elicit an MEP, are not essential for function and can be safely resected.

TMS and fMRI findings would not necessarily agree completely because they activate the motor system quite differently and measure different outputs. So far, only one small ($n = 15$) study from the gray literature has compared fMRI and TMS to DES in the same patients (Forster and Szelényi 2010). They found a mean (SD) distance of 10.5 (5.7) mm between the TMS and DES hotspots and 15.0 (7.6) mm between the fMRI and DES hotspots. Further peer-reviewed comparisons of the topographic precision of fMRI vs. TMS are still needed, but regardless, the strong point of fMRI is the visualization of complex networks and the possible changes in brain activation patterns due to tumor-induced plasticity. In contrast, TMS is especially well-suited for clarifying the peritumoral functional anatomy, and it can be conducted on patients who are not able to perform movement tasks for functional imaging. Thus, TMS and fMRI are complementary methods, each best suited for answering different kinds of questions.

Comparative Advantages and Limitations of DTI

DTI is the only imaging method that allows visualization of subcortical motor pathways. All other modalities discussed here are limited to the cortex. For this reason, DTI is never an alternative to the other modalities. Instead, it serves as an important compliment

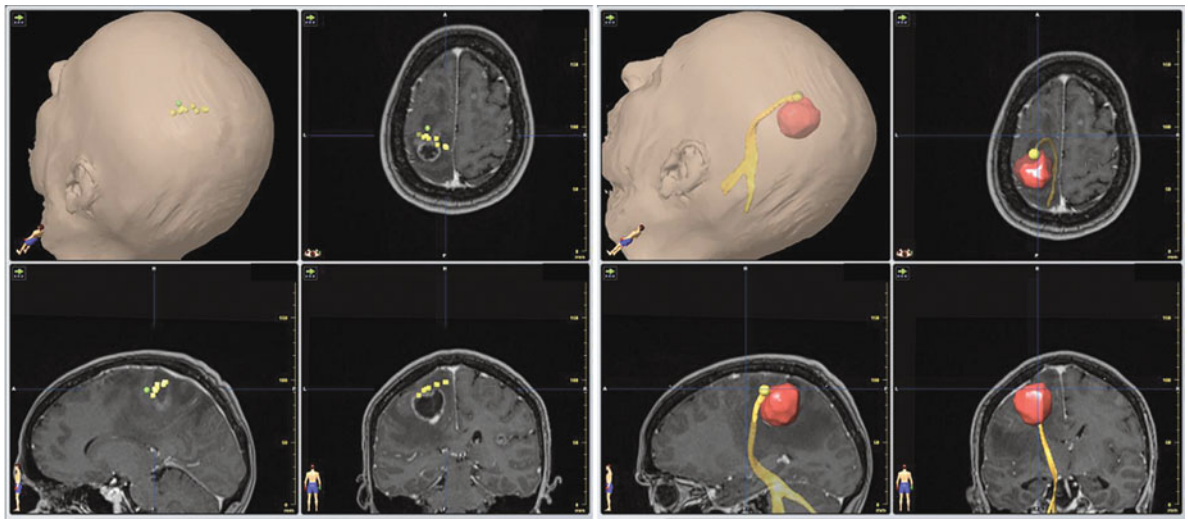

Fig. 30.3 *Left panel*: results from TMS motor cortex mapping in a patient with a postcentral metastasis transferred to the DTI tracking software (*yellow* spots represent TMS stimulation spots which evoked a MEP in the hand (abductor pollicis brevis muscle) and leg (tibial anterior muscle) with the *green* spot depicting the strongest MEP response. *Right panel*: DTI fiber tracking image. The strongest MEP response from the TMS study (*green dot*) has been used to start the fiber-tracking algorithm. This physiologically-based fiber-tracking shows that the pyramidal tract is located immediately anteriorly to the tumor

when the tumor may be compromising essential white matter tracts. In such cases, DTI enables a more complete preoperative risk assessment. Results of cortical mapping (from fMRI or TMS for example) can be used to facilitate DTI (Kleiser et al. 2010) (Fig. 30.3). Although DTI is difficult to validate in terms of spatial accuracy, it has already found its way into the presurgical work-up, due to its unique capability to visualize white matter tracts.

The Multimodal Approach to Preoperative Surgical Planning

Because each of the five technologies discussed has its unique advantages and limitations, their usage can and should be combined as needed on a case-by-case basis to improve the overall preoperative assessment of surgery candidates with a tumor in or near the motor cortex. Having different methods for preoperative analysis of motor topography at hand, the surgical team must decide which one or which combination of methods would be the most useful, i.e., which technologies are needed to optimize the therapeutic effectiveness and patient safety. Generally, the combination of similar methods (e.g., two measurements both relying on changes in the cerebral blood flow) is less beneficial than the combination of methods using different means of analyzing the motor system. For example, in the case of a centrally located subcortical tumor with unclear cortical anatomy due to mass effect of the tumor and edema, various questions must be addressed. First, the precentral gyrus must be identified, which is especially important if a transcortical approach is being planned. Here, a method which allows for a targeted analysis of cortical topography would be advisable, e.g., by TMS or MEG. Next, the possible displacement of the pyramidal tract should be clarified preoperatively. This can be achieved by applying a DTI fiber-tracking algorithm to the diffusion-weighted MRI dataset. If there is a discrepancy between the imaging results and the clinical findings (for example, a large tumor within M1 but no noticeable motor deficits), analysis of the cortical motor network to check for possible plastic changes would be beneficial. For example, this could be done by fMRI or PET. Of course, economic considerations must be taken into account and usually only 2 or 3 of these methods would be available at any one hospital; but the surgical team should be aware of all possible methods and their capabilities and their limitations in order to perform the optimal preoperative work-up or to refer patients to specialized centers with

the capability to provide additional examinations as needed.

Conclusion

In brain tumor surgery, the dilemma has always been the trade-off between maximizing the extent of resection versus minimizing the risk of causing new neurological deficits. The prerequisite for counseling the patient about balancing maximal resection and minimal morbidity is detailed knowledge of the functional topography. Because functional eloquence cannot be reliably predicted from the anatomical features alone, neurosurgeons need to take advantage of modern technology and mapping techniques to create individualized maps and management plans. Outside of research environments, the methods of preoperative mapping must be precise and reliable, easy to integrate into the surgical workflow, and cost-effective over the years.

fMRI is a powerful and readily available way to investigate the motor network and detect plastic changes induced by the tumor or the surgery. But its poor test-retest reliability due to the complex statistical analysis involved has decreased its use in clarifying the functional anatomy and planning neurosurgical procedures. MEG provides unsurpassed temporal resolution enabling the examiner not only to visualize the spatial pattern of network activation but even more so the temporal pattern. Only PET can detect metabolic changes with the cortex, though this information is only rarely needed. Despite their unique capabilities, the use of MEG and PET for motor mapping is restricted to specialized centers, due to their high costs. Navigated TMS it is a new method in neurosurgery which has demonstrated its usefulness in routine neurosurgical planning (Picht et al. 2011). It is introducing the gold standard of electrocortical stimulation mapping to the preoperative setting, thereby allowing for a reliable targeted analysis of peritumoral motor topography. Since subcortical tumor resection is often the step of the procedure defining the morbidity, DTI fiber tracking is a valuable emerging supplement to these technologies.

Functional mapping should be regarded as mandatory whenever an operation is planned in or near the motor cortex. The sophisticated technologies that have become available in recent decades are substantially improving our ability to surgically resect tumors with less patient morbidity. Reliable interpretation and use of the results of any of these technologies requires both a clear understanding of the methodology that produced the results and thorough knowledge of functional brain anatomy.

References

Barker AT, Jalinous R, Freeston IL (1985) Non-invasive magnetic stimulation of human motor cortex. Lancet 1:1106–1107

Berger H (1929) Uber das Elektrenkephalogramm des Menschen. Arch Psychiatr Nervenkr 87:527–570

Berger MS, Cohen WA, Ojemann GA (1990) Correlation of motor cortex brain mapping data with magnetic resonance imaging. J Neurosurg 72:383–387

Bittar RG, Olivier A, Sadikot AF, Andermann F, Pike GB, Reutens DC (1999) Presurgical motor and somatosensory cortex mapping with functional magnetic resonance imaging and positron emission tomography. J Neurosurg 91:915–921

Forster MT, Szelényi A (2010) Integration neuronavigierter transkranieller Manetstimulation in die Resektionsplanung zentral gelegener Tumore. 17. Tagung der Sektion Neurophysiologie der Deutschen Gesellschaft für Neurochirurgie 19. 20.02.2010 Frankfurt

Fox PT, Fox JM, Raichle ME, Burde RM (1985) The role of cerebral cortex in the generation of voluntary saccades: a positron emission tomographic study. J Neurophysiol 54:348–369

Gasser TG, Sandalcioglu EI, Wiedemayer H, Hans V, Gizewski E, Forsting M, Stolke D (2004) A novel passive functional MRI paradigm for preoperative identification of the somatosensory cortex. Neursurg Rev 27:106–112

Inoue T, Shimizu H, Nakasato N, Kumabe T, Yoshimoto T (1999) Accuracy and limitation of functional magnetic resonance imaging for identification of the central sulcus: comparison with magnetoencephalography in patients with brain tumors. Neuroimage 10:738–748

Kantelhardt SR, Fadini T, Finke M, Kallenberg K, Siemerkus J, Bockermann V, Matthaeus L, Paulus W, Schweikard A, Rohde V, Giese A (2010) Robot-assisted image-guided transcranial magnetic stimulation for somatotopic mapping of the motor cortex: a clinical pilot study. Acta Neurochir 152:333–343

Kety SS, Schmidt CF (1948) The nitrous oxide method for the quantitative determination of cerebral blood flow in man: theory, procedure and normal values. J Clin Invest 27:476–483

Kleiser R, Staempfli P, Valavanis A, Boesiger P, Kollias S (2010) Impact of fMRI-guided advanced DTI fiber tracking techniques on their clinical applications in patients with brain tumors. Neuroradiology 52:37–46

Korvenoja A, Kirveskari E, Aronen HJ, Avikainen S, Brander A, Huttunen J, Ilmoniemi RJ, Jaaskelainen JE, Kovala T, Makela JP, Salli E, Seppa M (2006) Sensorimotor cortex

localization: comparison of magnetoencephalography, functional MRI imaging, and intraoperative cortical mapping. Radiology 241:213–222

Krainik A, Duffau H, Capelle L, Cornu P, Boch AL, Mangin JF, Le Bihan D, Marsault C, Chiras J, Lehéricy S (2004) Role of the healthy hemisphere in recovery after resection of the supplementary motor area. Neurology 27: 1323–1332

Krings T, Buchbinder BR, Butler WE, Chiappa KH, Jiang HJ, Rosen BR, Cosgrove GR (1997) Stereotactic transcranial magnetic stimulation: correlation with direct electrical cortical stimulation. Neurosurgery 41:1319–1325

Krings T, Schreckenberger M, Rohde V, Spetzger U, Sabri O, Reinges MH, Hans FJ, Meyer PT, Möller-Hartmann W, Gilsbach JM, Buell U, Thron A (2002) Functional MRI and !8F FDG-positron emmission tomography for presurgical planning: comparison with electrical cortical stimulation. Acta Neurochir 144(9):889–899

Kwong KK, Belliveau JW, Chesler DA, Goldberg IE, Weiskoff RM, Poncelet BP, Kennedy DN, Hoppel BE, Cohen MS, Turner R, Cheng HM, Brady TJ, Rosen BR (1992) Dynamic magnetic resonance imaging of human brain activity during primary sensory stimulation. Proc Natl Acad Sci USA 89:5675–5679

Lee CC, Ward HA, Sharbrough FW, Meyer FB, Marsch WR, Raffel C, So EL, Cascino GD, Shin C, Xu Y, Riederer SJ, Jack CR (1999) Assessment of functional MR imaging in neurosurgical planning. Am J Neuroradiol 20:1511–1519

Mäkelä JP, Forss N, Jääskeläinen J, Kirveskari E, Korvenoja A, Paetau R (2006) Magnetoencephalography in neurosurgery. Neurosurgery 59:493–510

Mandonnet E, Winkler PA, Duffau H (2010) Direct electrical stimulation as an input gate into brain functional networks: principles, advantages, and limitations. Acta Neurochir (Wien) 152:185–193

McGonigle DJ, Howseman AM, Athwal BS, Friston KJ, Frackowiak RS, Holmes AP (2000) Variability in fMRI: an examination of intersession differences. NeuroImage 11:708–734

Mesulam MM (2000) Principles of behavioral and cognitive neurology. Oxford University Press, New York

Nagarajan S, Kirsch H, Lin P, Findlay A, Honma S, Berger MS (2008) Preoperative localization of hand motor cortex by adaptive spatial filtering of magnetoencephalography data. J Neurosurg 109:228–237

Nariai T, Senda M, Ishii K, Maehara T, Wakabayashi S, Toyama H, Ishiwata K, Hirakawa K (1997) Three-dimensional imaging of cortical structure, function and glioma for tumor resection. J Nucl Med 38:1563–1568

Picht T, Mularski S, Kuehn B, Vajkoczy P, Kombos T, Suess O (2009) Navigated transcranial magnetic stimulation for preoperative functional diagnostics in brain tumor surgery. Neurosurgery 65 (6 Suppl):93–99

Picht T, Schmidt S, Brandt S, Frey D, Hannula H, Neuvonen T, Karhu J, Vajkoczy P, Suess O (2011) Preoperative functional mapping for rolandic brain tumor surgery: comparison of navigated transcranial magnetic stimulation to direct cortical stimulation. Neurosurgery 2011 Mar 23. [Epub ahead of print]

Potchen SE, Potchen MJ (1991) The imaging of brain function. Positron emission tomography, single-photon emission computed tomography, and some prospects for magnetic resonance. Invest Radiol 26:258–265

Reinges MH, Krings T, Meyer PT, Schreckenberger M, Rohde V, Weidemann J, Sabri O, Mulders EJ, Buell U, Thron A, Gilsbach JM (2004) Preoperative mapping of the cortical motor function: prospective comparison of functional magnetic resonance imaging and [15O]-H2O-positron emission tomography in the same co-ordinate system. Nucl Med Commun 25:987–997

Roberts TP, Zusman E, McDermott M, Barbaro N, Rowley HA (1995) Correlation of functional magnetic source imaging with intraoperative cortical stimulation in neurosurgical patients. J Image Guid Surg 1:339–347

Rutten GJ, Ramsey NF (2010) The role of functional magnetic resonance imaging in brain surgery. Neurosurg Focus 28:E4

Schiffbauer H, Berger MS, Ferrrari P, Freudenstein D, Rowley HA, Roberts TP (2003) Preoperative magnetic source imaging for brain tumor surgery: a quantitative comparison with intraoperative sensory and motor mapping. Neurosurg Focus 15:E7

Schreckenberger M, Spetzger U, Sabri O, Meyer PT, Zeggel T, Zimny M, Gilsbach J, Buell U (2001) Localisation of motor areas in brain tumour patients: a comparison of preoperative [18F] FDG-PET and intraoperative cortical electrostimulation. Eur J Nucl Med 28:1394–1403

Shibasaki H (2008) Human brain mapping: hemodynamic response and electrophysiology. Clin Neurophysiol 119: 731–743

Stippich C, Ochmann H, Sartor K (2002) Somatotopic mapping of the human primary sensorimotor cortex during motor imagery and motor execution by functional magnetic resonance imaging. Neurosci Lett 331:50–54

Taulu S, Simola J, Kajola M (2004) MEG recordings of DC fields using the signal separation method (SSS). Neurol Clin Neurophysiol 30:35

Ter-Pogossian MM, Wagner HN (1998) A new look at the cyclotron for making short-lived isotopes. 1966-classical article. Semin Nucl Med 28:202–212

Tharin S, Golby A (2007) Functional brain mapping and its applications to neurosurgery. Neurosurgery 60(4 Suppl 2):185–201

Tieleman A, Deblaere K, Van Roost DV, Van Damme OV, Achten E (2009) Preoperative fMRI in tumour surgery. Eur Radiol 19:2523–2534

Vinas FC, Zamorano L, Mueller RA, Jiang Z, Chugani H, Fuerst D, Muzik O, Mangner TJ, Diaz FG (1997) [15O]-water PET and intraoperative brain mapping: a comparison in the localization of eloquent cortex. Neurol Res 19:601–608

Witwer BP, Moftakhar R, Hasan KM, Deshmukh P, Haughton V, Field A, Arfanakis K, Noyes J, Moritz CH, Meyerand ME, Rowley HA, Alexander AL, Badie B (2002) Diffusion-tensor imaging of white matter tracts in patients with cerebral neoplasm. J Neurosurg 97:568–575

Yamada K, Kizu O, Mori S, Ito H, Nakamura H, Yuen S, Kubota T, Tanaka O, Akada W, Sasajima H, Mineura K, Nishimura T (2003) Brain fiber tracking with clinically feasible diffusion-tensor MR imaging: initial experience. Radiology 227: 295–301

Chapter 31

Intraoperative Monitoring for Cranial Base Tumors

Ryojo Akagami, Charles Dong, and Henrik Huttunen

Abstract Intraoperative neurophysiological monitoring is used to guide surgery and predict the postoperative neurological function of patients. Surgery for basal neurosurgical tumors is fraught with difficulties due to the important neurovascular anatomy at risk. During these often long surgical cases, the function of the nerves and long tracts at risk can be monitored, giving the surgeon near real time feedback on how the patient is doing and what functions if any are being affected. This information is useful in trying to reduce and prevent injuries for quality control and improve patient outcomes. With the advent and effectiveness of alternative treatment strategies for many of these tumors, such as focused stereotactic radiation as primary treatment or surgery plus radiation (for planned subtotal resections), surgical outcomes need to be looked at critically; it becomes necessary to be able to perform these operations with minimal morbidity. Intraoperative monitoring is an adjunct to surgery that aids the surgeon in procedures for patients with these difficult tumors.

Keywords Neurophysiological monitoring · Neurosurgical tumors · Stereotactic radiation · Neurovascular anatomy · Cranial base tumors · Auditory evoked potentials

R. Akagami (✉)
Division of Neurosurgery, Gordon and Leslie Diamond Health Care Center, Vancouver General Hospital, Vancouver, BC V521M9, Canada
e-mail: Ryojo.akagami@vch.ca

Introduction

Every neurosurgery trainee learns that neurosurgery is unique amongst the surgical specialties in that the surgeon does not know how the patient is doing (neurologically) until the patient wakes up in the postoperative unit. Even when a procedure is preformed without any incident, there is a certain amount of anxiety that is lifted when a patient wakes up and is able to perform the neurological tests. By their nature, more difficult or longer cases may cause more concern for the neurosurgeon; surgery for cranial base tumors are such cases. Intraoperative monitoring is an attempt to monitor how the patient is doing neurologically during the operation, information sometimes useful in changing what is being done, and relieving some of the inherent anxiety related to these procedures by reassuring the surgeons that certain select neurological pathways are still intact. Neurosurgeons are experts at surgical anatomy, but unfortunately, when operating on tumors, the anatomy is distorted and predictions of the location of certain structures can often be incorrect. Monitoring can help localize certain important structures; for example in the oculomotor nerve can be difficult to find in en plaque medial sphenoid wing meningiomas, and in our experience the facial nerve can be stimulated on the posterior wall of an acoustic neuroma in approximately 1/100 cases. Like many techniques or technology in surgery, there are no randomized control trials looking at these techniques. At best there are only case series and before and after studies with historical controls, often with small numbers. Surgeons who use these techniques feel strongly that they are beneficial. Despite the lack of class 1 data, intraoperative monitoring

M.A. Hayat (ed.), *Tumors of the Central Nervous System, Volume 4*,
DOI 10.1007/978-94-007-1706-0_31,

techniques have become routine and almost standard of care for a number of procedures. The lack of class 1 data is not unique to intraoperative monitoring, and is true of surgical data in general, particularly relating to surgical technique. Neurosurgeons have learned that 'Anatomical' preservation (for example nerves) does not imply 'functional' preservation and newer monitoring techniques are able to predict functional preservation of neurological structures during surgery.

Indications

The indications for the use of monitoring are quite straightforward. If a particular neurological structure is at risk and being discussed with a patient as surgical risk, monitoring its function should be considered. In the case of skull base tumors, these refer to specific cranial nerves, as well as the motor and sensory pathways. A number of techniques are available as outlined in the overview that follows. Monitoring is resource intensive. It takes valuable operating time to set-up and requires a dedicated team to do the monitoring since the more demanding technique requires expertise to set-up, perform, and interpret. Surgeons have to have enough confidence in the monitoring and experience to know what to do with the information that the monitoring provides. Changes encountered during monitoring have to be correlated to what is being done and manipulated; they need to be addressed and not ignored. Like anything, some practice and experience is required and these techniques should be used often and not just in the most complex cases. One needs to know their own monitoring machine, its unique warning noises and be familiar with the technician or neurophysiologist who you are working with and helping to alert you to any changes.

Overview of Monitoring Techniques

Several electrophysiological techniques are commonly used to monitor the function of neural structures at risk during cranial base surgeries. These techniques include auditory evoked potentials (AEPs), electromyography (EMG), somatosensory evoked potentials (SSEPs) and transcranial electrical stimulation (TcES) myogenic motor evoked potentials (mMEPs).

Auditory Evoked Potentials

Auditory evoked potentials (AEPs) are electric signals generated along the auditory pathway in response to transient sound stimulation and include brainstem auditory evoked potentials (BAEPs), cochlear nerve action potentials (CNAPs) and electrocochleogram (ECochG). Since ECochG evaluates the most distal portion of the auditory pathway (i.e. the cochlea and the distal end of the auditory nerve), damage to the proximal portion of the nerve or the brainstem will not be detected by this modality. Therefore, its utility in monitoring cranial base procedures is limited. The following discussion will focus on BAEPs and CNAPs only.

Brainstem Auditory Evoked Potentials

The BAEP is one of the most commonly used monitoring modalities in posterior fossa surgeries. It provides functional assessment of the auditory pathways from the distal to the proximal eighth cranial nerve (CN) and to the brainstem up to the level of the caudal midbrain. It is usually recorded from the vertex and earlobe electrodes and normally contains five waves I–V within 10 ms from the onset of stimulus (Jewett and Williston 1971).

Waves I, III, and V are the most consistently present and easily identifiable waves and thus are usually followed intraoperatively. Although there is lack of a one-to-one relationship between the neural generators and individual BAEP waves, for monitoring purposes it is generally accepted that wave I is generated from the most peripheral portion of the auditory nerve near the cochlea, wave III in the lower pons around the region of the cochlear nucleus and wave V in the caudal midbrain near the area of the inferior colliculus (Legatt 1999).

Insert foam or miniature stereo earphones are placed in the external ear canal for stimulation. Each ear is stimulated independently, one ear at a time. Stimuli consist of broadband clicks with either a rarefaction or an alternating polarity, driven by 100-μs rectangular

electrical pulses. In the cases where stimulus artifact is excessive, clicks of alternating polarity are preferred to cancel out those unwanted activities with opposite phases during averaging. Relatively high stimulus intensities (70–100 dB HL or 105–135 dB peSPL) are utilized to compensate for ambient noises in the operating room and any pre-existing conductive hearing loss. Despite a mild detrimental effect on BAEP amplitude, fast repetition rates (11.3–33.7 stimuli per second) are used to obtain BAEP responses as quickly as possible.

Standard EEG cup electrodes applied with collodion to the vertex and earlobes are used to record BAEPs. An adhesive surface electrode is placed on the forehead or the shoulder as the ground electrode. With careful skin preparation, impedances at all electrodes are kept below 5 k Ohms. Sterile subdermal needle electrodes can be used as an alternative for recording as they can be quickly applied and provide consistent, stable impedances. However, care should be taken to secure the needle electrodes and prevent them from being dislodged during the operation.

The montage most commonly employed during BAEP monitoring includes the vertex (Cz) to the ipsilateral earlobe (Ai) and the vertex (Cz) to the contralateral earlobe (Ac). A time base of 15–20 ms is needed to demonstrate the delayed responses in certain pathologic conditions and provide a suitable display for easy peak identification and measurement. Although a bandpass filter of 30–3000 Hz is routinely used in the outpatient clinical laboratory, a more restrictive filter setting of 100–1500 Hz is often employed to facilitate rapid BAEP acquisition during surgery. Because BAEPs are in the sub-microvolt range and embedded in larger background noise, averaging of 800–1500 individual trials is required to obtain an interpretable BAEP waveform.

Interpretation of intraoperative BAEP changes is primarily based on the measurement of the absolute latencies and amplitudes of waves I, III and V if present, and on the comparison of these measures with baseline obtained after the induction of anesthesia and opening the dura. Measurement of interpeak latencies of I–III, III–V and I–V is helpful, but practically one may obtain the information of changes in interpeak latencies by visual inspection and comparison of the BAEP waveform with baseline. On the basis of our current understanding of the neural generators of BAEP components and the pattern of BAEP changes, the locus or loci of dysfunction in the auditory pathway may be roughly inferred. If wave I becomes delayed and attenuated or disappears with parallel changes in the subsequent waves, damage to the cochlea or the distal auditory nerve is likely the cause. If wave I is largely unchanged while waves III and V are prolonged and decreased in amplitude with little change in the IPL III–V or these late waves are completely obliterated, there is strong evidence that the function of the auditory nerve proximal to its cochlear end has been affected or damaged by surgical manipulations. In the case that there is a delay and a decrease in amplitude of wave V but waves I and III remain relatively stable, changes in the function of the brainstem should be suspected.

Currently, there is no consensus on the warning criterion of intraoperative BAEP changes. In practice, wave V has often been selected as the most important indicator of neural conduction along the auditory pathway (Hatayama and Moller 1998). Greater than 50% amplitude decrease and/or greater then 1.0 ms latency prolongation of wave V are usually considered significant. However, since BAEPs are very robust in the face of changes in anesthesia and/or fluctuations of the blood pressure, even smaller, but consistent, changes in the BAEP are noteworthy.

Cochlear Nerve Action Potentials

The CNAP represents the temporal and spatial summation of conduction of action potentials in the eighth nerve in response to sound stimuli. It is recorded with an electrode placed directly on or in the vicinity of the exposed proximal eighth nerve near the brainstem referenced to a distant electrode, usually a needle electrode inserted in a muscle flap of the surgical field or a cup electrode on the scalp (Moller and Jannetta 1983).

The CNAP is usually biphasic or triphasic. The initial small positive wave is generated by neural depolarization approaching the recording electrode and the large negative wave N1 produced when depolarization passes under the recording electrode. Because of the short distance between the neural generator and the recording electrode, this near field potential has relatively high amplitude in the range of 5–50 μV. Thus, a reliable CNAP response can be obtained very quickly with averaging of only a few to 100 individual trials and changes in neural conduction in the eighth

nerve due to surgical manipulation can be detected promptly.

Several types of electrodes are suitable for recording CNAPs from the exposed eighth nerve. One is a fine, Teflon-insulated wire electrode with a 2 mm bare tip sutured with a cotton wick (Moller and Jannetta 1983). A single contact disc electrode with a delicate lead wire can also be used for this purpose. Another type of these electrodes is a C-shaped self-retaining electrode (Cueva et al. 1998), which is about 6 mm in diameter and can be attached to the proximal eighth nerve using an applicator. Stimulus and recording parameters are the same as those for BAEPs, except that a time base of 10–15 ms is appropriate for the CNAP because its latency usually falls between 3 and 4 ms.

Intraoperatively, the amplitude and latency of the major negative wave N1 in the CNAP are measured. A 50% decrease in amplitude and/or >1 ms delay in latency has been used to alert the surgeon of impending injury to the eighth nerve if not tended. These criteria are useful but have not been proven to correlate with postoperative hearing. Because the CNAP is very resistant to alterations in anesthesia, any consistent changes in the response that exceed baseline variability can be significant. The primary drawback of this technique is that it is only applicable during removal of small cerebellopontine (CP) angle tumors and requires stabilizing the recording electrode on the eighth nerve to obtain reliable responses.

Electromyography

EMG records the electrical potentials of muscle fibers with electrodes in or on the surface of the muscle and is commonly used to monitor the motor components of cranial nerves III, IV, VI, V, VII, IX, X, XI and XII. Although intraoperative EMG monitoring utilizes different muscles for different cranial nerves (e.g. the medial, and/or superior rectus muscles for CN III, the lateral rectus for CN VI, the masseter for motor CN V, the orbicularis oculi and oris for CN VII, the cricothyroid or vocalis muscle for CN X), the basic principles for monitoring each of motor cranial nerves are the same. Standard EMG monitoring techniques include spontaneous EMG, also known as free-running EMG and stimulus triggered compound muscle action potentials (CMAPs) or triggered EMG.

Spontaneous Electromyography

Spontaneous EMG involves continuous recording of motor unit potential activity from the muscle(s) innervated by a nerve. Among several different types of EMG activities that can be recorded during surgery, the neurotonic discharge is of the major interest (Daube and Harper 1989), which is defined as bursts (<200 ms in duration) or trains (>200 ms) of motor unit potentials that fire in a rapid (30–100 Hz) and irregular manner in response to mechanical or metabolic stimulation of the nerve innervating the muscle. The burst activity is usually associated with inadvertent mechanical irritation of the nerve during dissection and can alert the surgeon of the close proximity of the nerve, but does not necessarily indicate neural injury. Train activities, on the other hand, are produced by mechanical manipulation, compression and ischemia of the nerve and may signify potential injury of the nerve. However, these long trains of neurotonic discharges can also be induced by saline irrigation due to the change of the metabolic environment around the nerve without adverse sequelae. In addition, acute transection of a nerve is less likely to produce neurotonic discharges. Therefore, there is only a rough correlation between neurotonic discharges and postoperative outcome.

Two types of electrodes are commonly used for recording spontaneous EMG activities during surgery: one is the subdermal needle electrode and the other the hook wire electrode. The subdermal needle electrodes can be easily placed subcutaneously or directly in the muscle. However, they need to be secured in place with adhesive tapes to prevent possible dislodgement during surgery and may be too bulky for some deep, small muscles (e.g., extraocular muscles). Alternatively, a pair of hook wire electrodes can be inserted into the muscle with a small needle (e.g., 26-gauge). Their 2–3 mm bared hooked tips provide the recording surface and help keep the wires in place when the needle is removed. They require special adapters for amplifier connection and may take longer to set up. In general, both types of these electrodes provide reliable and good-quality recordings.

Spontaneous EMG recordings are usually obtained with an amplifier gain of 100–200 μV per division, a bandpass filter of 30–10,000 Hz and a time base of 1000–5000 ms. These EMG activities are made audible through a loudspeaker and visible on the screen of the monitoring machine for quick feedback.

Compound Muscle Action Potentials

CMAPs represent the temporal and spatial summation of individual muscle fiber action potentials in response to direct electrical stimulation of the nerve innervating a muscle. They can be used to locate and identify the nerve and provide the assessment of nerve function along the course of surgery. Two types of hand-held stimulators, i.e. monopolar and bipolar stimulators, are commonly in use. A monopolar stimulator utilizes the cathode to stimulate in the surgical field and the anode is placed some distance away from the nerve (>4 cm), either a needle electrode in a muscle flap of the surgical field or a surface electrode on the shoulder or knee. When used to search for a nerve, a monopolar stimulator is very sensitive, but can be unspecific due to current spread to nearby nerves. With a bipolar stimulator, on the other hand, the cathode and anode are only several millimeters apart and provide very focal stimulation. However, current shunting may occur between the cathode and anode of the bipolar stimulator if there is excessive fluid in the surgical field, preventing effective stimulation of the nerve.

Both constant current and constant voltage stimulation can be used. Stimuli consist of electrical pulses with 0.05–0.1 ms duration delivered at a rate of 2–5 per second. For the purpose of searching, a stimulus intensity of 1–1.5 mA is usually adequate. Higher intensities may be required for damaged nerves, but intensities >2 mA should be avoided to prevent current spread to adjacent nerves. Recording parameters are the same as for spontaneous EMG except for a shorter time base (i.e. 20–40 ms). Additional surface electrodes placed on the muscle may be helpful for accurate quantitative measurement.

Two principal criteria are used to determine the functional status of a cranial nerve during surgery. One is the change in threshold for stimulation and the other is the proximal to distal CMAP amplitude ratio obtained with supramaximal stimulation. If the stimulation threshold of a nerve is markedly increased, there is a strong indication that the nerve is injured to some degree along the course of surgical dissection. If the nerve can be stimulated well at the site distal but not proximal to that of surgical manipulation making the CMAP ratio very small, significant damage to the nerve should be expected. On the other hand, maintaining CMAP amplitude with proximal stimulation reassures the surgeon the functional integrity of the nerve. In the case of CN VII monitoring, it has been found that a >0.3 proximal to distal facial CMAP ratio and a proximal stimulation threshold $\leq$0.3 mA predict good postoperative facial function (Silverman et al. 1994; personal experience). The major disadvantage with this technique includes that it is unavailable before identifying the nerve on the brainstem, which is usually late in the procedure, especially for large tumors.

Somatosensory Evoked Potentials

SSEPs are electrical signals recorded along the somatosensory pathways in response to electrical stimulation to the peripheral nerves and can be used intraoperatively to assess the functional integrity of these pathways during surgical procedures in/around the spinal cord, brainstem and cerebral cortex. SSEPs to median nerve stimulation alone or to both median and tibial nerve stimulation are monitored for various types of surgery. The techniques described here tend to be more relevant to monitoring of cranial base procedures.

Median Somatosensory Evoked Potentials

The median nerve is stimulated with a pair of adhesive surface ("stick-on") or subdermal needle electrodes at the wrist between the tendons of the palmaris longus and flexor carpi radialis muscles, with the cathode approximately 2–3 cm proximal to the wrist crease and the anode 2–3 cm distal to the cathode. Although they can be quickly applied, needle electrodes carry risks of bleeding and infection and need to be well secured in place. Constant current stimulation is commonly used to compensate for variations in electrode impedance and provide consistent effective stimulation. Stimuli consist of monophasic rectangular pulses of 200–300 μs duration delivered at a rate of 4.3–6.9 per second. Supramaximal stimulus intensities, usually between 15–25 mA for surface electrodes and 5–10 mA for needle electrodes, are used to ensure adequate activation of the nerve and repeatable responses recorded at central locations. Each of the median nerves (i.e. left and right) is stimulated alternately.

SSEP responses are recorded with EEG cup, adhesive surface or subdermal needle electrodes. Skin preparation is needed to keep the electrode impedance below 5 kΩ. A minimum of two-channel recording is required. A peripheral channel, with adhesive surface or subdermal needle electrodes placed at the ipsilateral (active) and contralateral (reference) Erb's points or on the medial surface of the arm at the mid-humeral level, registers passage of the afferent volley past the recording sites and confirms the delivery of stimulation. A cortical channel, consisting of EEG cup or subdermal needle electrodes at CPc (active, 2 cm posterior to C3 or C4 scalp site of the International 10–20 System *contralateral* to the stimulated limb) and CPi (reference, 2 cm posterior to C3 or C4 scalp site of the 10–20 System *ipsilateral* to the stimulated limb), records N20, a near-field negative potential with a latency of about 20 ms generated in the sensorimotor cortex contralateral to the stimulated limb (Desmedt and Cheron 1981). A third channel consisting of electrodes at CPi (active) and a non-cephalic site (e.g. Erb's point, reference) may be added to record subcortical far-field potentials of brainstem and/or thalamus origin including P14 and N18 (Desmedt and Cheron 1981, 1982). However, inclusion of this channel into monitoring is sometimes discouraged because its low signal-to-noise ratio increases averaging time, resulting in a significant delay in surgical feedback.

The bandpass filter settings are generally 30–500 Hz for cortical and subcortical SSEPs and 100–1000 Hz for peripheral responses. A time base of 40–50 ms is appropriate. The number of trials to be averaged is determined by the signal-to-noise ratio at the time of recording, but is usually 150–300 for cortical and peripheral responses and 1000–1500 for subcortical responses.

Tibial Somatosensory Evoked Potentials

The posterior tibial nerve is usually stimulated with a pair of adhesive surface ("stick-on") or subdermal needle electrodes at the ankle, with the cathode placed between the medial malleolus and the Achilles tendon just proximal to the malleolus and the anode 2–3 cm distal to the cathode. The same considerations for median nerve stimulation towards the type and parameters of stimulus apply to tibial nerve stimulation, except that higher stimulus intensities (35–50 mA with surface "stick-on" electrodes and 10–15 mA with subdermal needle electrodes) and lower repetition rates (3.7–5.1 per second) are required.

Electroencephalography cup, adhesive surface or subdermal needle electrodes can be used to record tibial SSEPs. A minimal montage includes a peripheral and a cortical channel with a possible addition of a subcortical channel. The peripheral channel registers the afferent volley at the popliteal fossa with a pair of adhesive surface or needle electrodes placed in the midline, 2 cm (active) and 5 cm (reference) respectively above the popliteal crease, and verifies the delivery of stimulus. The cortical channel, consisting of a pair of EEG cup or subdermal needle electrodes placed at the designated scalp sites (see below), records P40, a near-field positive potential of about 40 ms latency generated in the primary cortical somatosensory receiving area (Allison and Hume 1981; Desmedt and Cheron 1981). Because there is considerable variability in the scalp topography of the P40 response, mapping its scalp distribution is needed to determine the optimal derivations to record this potential (MacDonald 2001). Commonly used derivations include CPz (2 cm posterior to Cz of the 10–20 system)–CPc, CPi–Fpz and CPz–Fpz. The subcortical channel records the far-field P31 and N34 potentials of brainstem and/or thalamus origin with EEG cup or needle electrodes at Fpz (active) and C5S (reference). Similar to median SSEPs, the usage of this channel is limited because of its low signal-to-noise ratio causing delayed surgical feedback. Except for a longer time base (75–80 ms), other recoding parameters are the same as for median SSEPs.

Although a warning criterion for spinal cord monitoring has been put forth, which includes 50% amplitude reduction and/or 10% latency prolongation of cortical SSEP responses (Brown et al. 1984; Nuwer 1999), there is no consensus on warning criteria of SSEP changes for cranial base surgeries. However, it is advisable that, after technical factors are excluded and anesthetic alterations taken into account, any sudden, consistent changes beyond the normal variability in cortical responses should be immediately brought to the surgeon's attention to allow the underlying causes to be treated as early as possible.

Transcranial Electrical Stimulation Myogenic Motor Evoked Potentials

TcES mMEPs are EMG responses recorded from limb or cranial muscles following transcranial electrical stimulation of cerebral cortex. They can be used to monitor the function of the corticospinal and corticobulbar tracts as well as the spinal and motor cranial nerves during different types of surgical procedures where these neural structures are at risk of iatrogenic injury. The techniques presented here are more applicable to monitoring of cranial base surgeries.

Limb Myogenic Motor Evoked Potentials

Limb mMEPs can be elicited with multipulse TcES delivered through a pair of electrodes placed at C1 and C2 or 1 cm anterior to these scalp sites, with the anode contralateral to the limb from which MEP responses are recorded. Although stimulating electrodes can also be placed at C3 and C4 or 1 cm anterior to produce limb mMEPs, stimulating at these scalp sites is not recommended for cranial base procedures because of potential deeper penetration of current to the site caudal to the neural structures at risk resulting in false negative findings and larger stimulus-evoked muscle movement interfering with surgical manipulation. Several different types of electrodes can be used for TcES, which include EEG cup, subdermal needle and corkscrew needle electrodes. Among them, corkscrew electrodes are preferred by many users because they can be easily applied, are well secured in place and provide stable contact resistance. Constant voltage or current stimulation is commonly used which consists of trains of 3–6 electrical pulses of 50–500 μs duration and 2–4 ms interstimulus interval (ISI). Supra-threshold stimulus intensities are applied to obtain reliable limb muscle responses. For upper extremities, 150–250 V or 50–80 mA is normally sufficient, while for lower extremities, higher stimulation intensities, usually in the range of 250–450 V or 80–150 mA, are needed.

MEP responses are recorded with needle or surface electrodes from the thenar or the first dorsal interosseous muscle and forearm flexors in the upper limb and the tibialis anterior and abductor hallucis muscles of the lower extremity. The bandpass filter settings are usually between 30 and 5000 Hz. A time base of 75–100 ms is appropriate. Because these limb muscle responses have large amplitude, averaging is not required and thus they can be obtained instantaneously. The primary disadvantage of this technique is the stimulus-induced muscle twitches that may interfere with surgery. Therefore, the stimulus intensity should be kept as low as possible to minimize muscle movement but high enough to allow reliable MEP recordings.

Due to the large inherent variability of limb mMEPs, the presence or absence of these MEP responses has been used as a warning criterion during spinal cord monitoring (Dong et al. 2002). However, there is no enough data to suggest that this criterion can be safely extended to monitoring of cranial base surgeries. Until more experience is obtained, it is advisable to report to the surgeon any consistent significant reduction (50–75%) in mMEP amplitude after other confounding factors are excluded.

Cranial Myogenic Motor Evoked Potentials

Cranial mMEPs are recorded from muscles innervated by motor cranial nerves following multipulse TcES. Because most of our experience with cranial mMEPs is attained with facial nerve monitoring during CP angle surgery, only facial mMEP techniques will be elaborated here. These techniques, however, can be easily extended to other cranial nerves or muscles (e.g. vocal muscle MEPs for CN X).

To obtain facial mMEPs, TcES is applied through a pair of corkscrew needle or EEG cup electrodes fixed at the sites 1 cm anterior to C3 or C4 and Cz, with the anode contralateral to the operative side and the cathode at the midline. Advantages of this stimulating montage include that the lateral anode is close to the facial motor cortex, permitting lower stimulus intensity to minimize current spread, movement and stimulus artifact and the midline cathode is far from the targeted facial nerve to avoid direct distal activation. Constant voltage or current stimuli are employed, consisting of trains of 4–6 electrical pulses of 50–500 μs duration. A short ISI (i.e. 1–2 ms) is used to limit the duration of stimulus artifact and prevent it from overriding short-latency facial mMEPs. Stimulus intensity is adjusted individually, usually between 150 and 300 V or 50 and 100 mA, to obtain supra-threshold facial mMEPs while

preventing excessive stimulus-evoked movement. In order to exclude the possibility of direct facial nerve stimulation at a site distal to that of potential injury due to current spread, the absence of facial muscle responses to single pulse stimulation needs to be confirmed for the stimulus intensity used and the onset latency of the responses consistent with the central origin.

Facial mMEPs are recorded from the same needle electrodes in the ipsilateral orbicularis oris muscle for EMG monitoring, with the responses obtained from the needle electrodes in the thenar or the first dorsal interosseous as a systemic control. The bandpass filters are usually set between 30 and 5000 Hz. However, it is often necessary to raise the low frequency filter to 100 Hz to minimize the stimulus artifact. A time base of 50–75 ms is required to properly display facial mMEPs.

Facial mMEPs tend to be polyphasic with an onset latency of 12–16 ms. Similar to limb mMEPs, they exhibit large intra-subject trial-to-trial and inter-subject amplitude variability. Interpretation of intraoperative facial mMEP changes has to be put in the context of surgical events and anesthetic alterations. A retrospective study conducted by our group has shown a strong correlation between facial mMEP changes and postoperative facial outcome (Akagami et al. 2005; Dong et al. 2005). Based on our analysis, it is recommended that, after technical and anesthetic factors are taken into account, any consistent >50% amplitude decrements of facial mMEPs be reported to the surgeon to minimize the risk of permanent severe facial nerve injury.

Anesthetic Considerations

An anesthetic technique to facilitate accurate, reliable and reproducible conditions for intraoperative monitoring requires an understanding of the monitoring techniques, knowledge of the effects of various anesthetics on intraoperative monitoring and communication between anesthesiologists, surgeons and neurophysiologists. The most commonly used intraoperative monitoring techniques during cranial base tumor surgery are: brainstem auditory evoked potentials (BAEPs), electromyography (EMG), somatosensory evoked potentials (SSEPs), and motor evoked potentials (MEPs). Effects of various anesthetics on these monitoring modalities will be further described in this section. The most common clinical decision in anesthetic drug choices involves the decision between maintenance of anesthesia with volatile or intravenous based anesthesia, as well as whether neuromuscular blockade will be required for surgery. Regardless of the intraoperative monitoring techniques used or the anesthetic regimen employed, once baseline neurophysiologic signals have been recorded, it is important to avoid bolus doses or rapid changes in anesthetic depth during key portions of surgical resection to avoid confounding influences on signal integrity at a time when the monitoring modality is most useful.

Brainstem Auditory Evoked Potentials

BAEPs are much less sensitive to anesthetic effects than other types of IOM. High anesthetic concentrations can obliterate most cortically recorded evoked potentials, yet BAEPs remain robust even during isoelectric EEG conditions. Inhalational anesthetics can statistically but not clinically significantly increase latency of wave V, as these latency changes are less than 0.75 ms (Legatt 2002). Nitrous oxide causes no change in either amplitude or latency of signals (Manninen et al. 1985). Continuous infusions of intravenous anesthetics or narcotics have minimal effects of BAEP latency or amplitude. Yet, high dose or bolus administration of propofol has been reported to decrease amplitude and increase latency. Neuromuscular blocking drugs commonly used to facilitate tracheal intubation or for maintenance of paralysis have no effect on BAEPs as these drugs act at neuromuscular junctions which are not involved in the signal transduction pathway of BAEPs.

Electromyography

Facial nerve EMG is frequently recorded in addition to BAEPs during cranial base tumor surgery particularly during resection of cerebellopontine angle tumors. Both free running EMG as well as stimulated EMG (CMAP) is used. EMG signals are easily recorded under both volatile and intravenous anesthetic

maintenance regimens. Since EMG monitoring records the compound muscle action potential, neuromuscular blocking drugs will depress EMG signals in a dose-dependent fashion, as these agents act at suppressing neural transmission at the neuromuscular junction. If neuromuscular blockade (NMB) is required to facilitate safe surgical resection, NMB should be maintained at less than 50% to ensure recordable facial nerve EMG signals (Cai et al. 2009). In addition to localizing nerve structures to minimize iatrogenic injury at time of tumor resection, facial nerve EMG has also been used to determine anesthetic depth and predict patient movement under anesthesia (Jellish et al. 2009).

Somatosensory Evoked Potentials

While SSEPs are not degraded to the same extent as motor evoked potentials by inhalational anesthetics, they exhibit a dose-related increase in latency and decrease in amplitude under volatile anesthesia. When volatiles are used, they are commonly dosed below one MAC (minimum alveolar concentration) to maintain SSEP signal quality. This is often facilitated by the co-administration of potent opiates, which do not affect signal quality. The addition of nitrous oxide is typically avoided, as it results in further degradation of the signal.

The use of intravenous anesthetics such as propofol, thiopental, or midazolam infusion results in superior signal quality compared to volatile agents. Ketamine and etomidate have been reported to increase the amplitude of SSEPs, though the effect that this has on their sensitivity and utility remains a matter of speculation. Neuromuscular blocking agents have no effect on SSEPs (Banoub et al. 2003).

Motor Evoked Potentials

MEPs are the most sensitive to anesthetics of the monitoring techniques described for cranial base surgery; therefore, a tailored approach is required when selecting the most appropriate anesthetic regimen. Transcranial magnetic stimulation generated MEPs are much more sensitive to anesthetics than transcranial electrical stimulation (TcE), as a result, transcranial electrical stimulation is almost exclusively used as the stimulation technique during intraoperative monitoring. Preliminary work with TcE MEPs showed that single pulse signals were extremely sensitive to anesthetics even at subclinical doses (Lotto et al. 2004). Subsequently, multi-pulse stimulation techniques have been shown to improve both low amplitude baseline signals as well as anesthetic depressed MEP signals. Anesthetics also cause a time dependent decrease in MEP signal amplitude, proportionate to the length of surgery regardless of the anesthetic regimen (Lyon et al. 2005). This phenomenon is referred to as "anesthetic fade". Anesthetic fade can be overcome by increasing stimulation energy, but may lead to false-positive signal changes.

Volatile anesthetics are commonly used for the maintenance of anesthesia. Unfortunately, all currently used halogenated ethers cause significant dose-dependent depression of myogenic MEP signals. With desflurane or sevoflurane at 0.5 MAC (minimum alveolar concentration) with either nitrous oxide or a narcotic infusion, MEPs are recordable in 100% of patients (Lo et al. 2006; Reinacher et al. 2006), yet there is sparse evidence to date to show adequate clinical recording conditions with a volatile anesthetic as compared with total intravenous anesthetic options (Lo et al. 2006).

Propofol is currently the most popular anesthetic agent for the maintenance of anesthesia during MEP monitoring since it is easily titratable and has a favourable pharmacokinetic profile. Titrating propofol intraoperatively among clinically relevant concentrations does not significantly affect MEP responses (Scheufler et al. 2005). Bolus administration of propofol can lead to loss of MEP signals; yet, due to its rapid redistribution and metabolism, signals return within minutes (Kalkman et al. 1992). Other intravenous anesthetics including, midazolam, ketamine, and etomidate do not clinically significantly suppress MEPs. Opioids are commonly administered in conjunction with other anesthetic agents. Opioids are frequently used when MEP monitoring is required as they have minimal effects. At target controlled plasma concentrations, remifentanil has the least effect (Scheufler and Zentner 2002).

Neuromuscular blockade is frequently desired to facilitate tracheal intubation. However, boluses of muscle relaxants lead to loss of MEPs, as they block signal transduction at the level of the neuromuscular junction.

Careful infusions of neuromuscular blockers with 20–50% maintenance of single twitch height have been shown to allow reliable MEP recordings when used in conjunction with a minimally suppressant anesthetic and multi-pulse TcE (van Dongen et al. 1999). Caution should be used in patients with preoperative neurologic deficits as they appear to be more sensitive to the depressant effects of neuromuscular blocking drugs (Lang et al. 1996). It is generally acceptable for a single dose of a short acting neuromuscular blocking agent to be used at the time of induction of anesthesia, however, maintenance of neuromuscular blockade or re-bolusing can pose considerable challenges to the interpretation of MEPs.

Use of Monitoring During Surgery/Benefits

As mentioned previously, there are no randomized control trials of studies looking at the benefits of intraoperative monitoring. Like any tool used in surgery, surgeons who use it swear by it while those who either did not use it in their training, do not have access to it, or do not use it (or use it only intermittently) may not be as enthusiastic (Cabraja et al. 2009). We have learned that relying just on preserving anatomy does not always correlate to useful function (Samii and Matthies 1997; Nielsen 1942), and anatomic preservation of certain structures such as facial or vestibulocochlear nerve does not always correlate with functional outcome. Intraoperative monitoring looking at function, as in motor evoked potentials of cranial nerves is predictive of functional integrity during surgery and able to predict very well how nerves will work postoperatively (Akagami et al. 2005). Use of intraoperative monitoring (in addition to careful microsurgical technique) has increased the functional preservation of nerves during these types of procedures (Delgado et al. 1979; Sekhar et al. 1995). Of course the simple act of using monitoring will not allow for better outcomes and surgeons need to have experience to know what to do with the information. As a rule of thumb, any change approaching 50% of baseline in SSEP's, limb/cranial nerve MEP's, or wave 5 of BSAER are clinically significant. With anything persistently lower that 50% of baseline, premature termination of surgery should be considered if you want a patient to wake up without a significant corresponding deficit. Changes need to be correlated with what is being done at that moment and adjustments to the technique need to be made. Often changes are not all or none and recovery can occur; surgeons may need to work in other areas or simply pause to wait for any recovery prior to proceeding. If using a monopolar stimulator, care must be exercised particularly with non-insulated stimulators that what you are looking at is actually being stimulated and not a proximal structure that the instrument is resting on. When using a monopolar stimulator, surgeons need to know that stimulators only stimulate a small point of contact and not an 'area'. It is also important to check and make sure there are no technical problems with the monitoring. Baseline recordings are often done preoperatively. At the beginning of an operation when using a stimulator, check for the stimulus artifact, and check that the stimulator working on an easily identifiable motor nerve (such as the accessory nerve in posterior fossa surgery).

Conclusion

Intraoperative monitoring is a relatively new technology, which like many technologies, have now been incorporated into regular practice of many surgeons. It maybe considered standard of care in certain procedures (Sekhar et al. 1995; Cabraja et al. 2009). It is a benefit to the surgeon, by relieving anxiety, and providing reassurance that critical functions are still intact during surgery. Subtle changes may lead the surgeon to change what he is doing in an attempt to preserve these functions. It allows for good quality control; the surgeon being able to correlate changes to certain maneuvers, or in the case where multiple surgeons are involved in a complex case, isolating when any injury occurred. If a conservative operation is being planned, being able to stop surgery before damage occurs is preferable; this can be predicted by changes in monitoring. The worst-case scenario is doing a conservative operation but finding out postoperatively that the patient already has the deficit that one was trying to avoid (and the patient not being 'cured', with residual tumor left behind). In the case of acoustic neuromas, the advent of monitoring techniques for cranial nerves have changed the preservation rates of facial nerve function by significant magnitude, and despite lack

of ‘evidence’, no neurosurgeon would have their own tumor operated on without adequate monitoring. Over the last decade it has become rare to have facial nerve palsies for these tumors. These techniques have made surgery safer for patients and helps reassure surgeons during complex long cases.

References

Akagami R, Dong CC, Westerberg BD (2005) Localized transcranial electrical motor evoked potentials for monitoring cranial nerves in cranial base surgery. Neurosurgery 57(1 Suppl):78–85

Allison T, Hume AL (1981) A comparative analysis of short-latency somatosensory evoked potentials in man, monkey, cat, and rat. Exp Neurol 72(3):592–611

Banoub M, Tetzlaff JE, Schubert A (2003) Pharmacologic and physiologic influences affecting sensory evoked potentials: implications for perioperative monitoring. Anesthesiology 99(3):716–737

Brown RH, Nash CL, Berilla JA, Amaddio MD (1984) Cortical evoked potential monitoring. A system for intraoperative monitoring of spinal cord function. Spine 9:256–261

Cabraja M, Stockhammer F, Mularski S, Suess O, Kombos T, Vajkoczy P (2009) Neurophysiological intraoperative monitoring in neurosurgery: aid or handicap? An international survey E2. Neurosurg Focus 27(No. 4):E2

Cai YR, Xu J, Chen LH, Chi FL (2009) Electromyographic monitoring of facial nerve under different levels of neuromuscular blockade during middle ear microsurgery. Chin Med J 122(3):311–314

Cueva RA, Morris GF, Prioleau GR (1998) Direct cochlear nerve monitoring: first report on a new atraumatic, self-retaining electrode. Am J Otol 19(2):202–207

Daube JR, Harper CM (1989) Surgical monitoring of cranial and peripheral nerves. In: Desmedt JE (ed) Neuromonitoring in surgery. Elsevier, Amsterdam, pp 15–151

Delgado TE, Buchheit WA, Rosenholtz HR, Chrissian S (1979) Intraoperative monitoring of facial muscle evoked responses obtained by intracranial stimulation of the facial nerve: a more accurate technique for facial nerve dissection. Neurosurgery 4:418–420

Desmedt JE, Cheron G (1981) Non-cephalic reference recording of early somatosensory potentials to finger stimulation in adult or aging normal man: differentiation of widespread N18 and contralateral N20 from the prerolandic P22 and N30 components. Electroencephalogr Clin Neurophysiol 52(6):553–570

Desmedt JE, Cheron G (1982) Somatosensory evoked potentials in man: subcortical and cortical components and their neural basis. Ann N Y Acad Sci 388:388–411

Dong CC, MacDonald DB, Akagami R, Westerberg B, Alkhani A, Kanaan I, Hassounah M (2005) Intraoperative facial motor evoked potential monitoring with transcranial electrical stimulation during skull base surgery. Clin Neurophysiol 116(3):588–596

Dong C, MacDonald DB, Janusz MT (2002) Intraoperative spinal cord monitoring during descending thoracic and thoracoabdominal aneurysm surgery. Ann Thorac Surg 74: S1873–1876

van Dongen EP, ter Beek HT, Schepens MA, Morshuis WJ, Langemeijer HJ, de Boer A, Boezeman EH (1999) Within-patient variability of myogenic motor-evoked potentials to multipulse transcranial electrical stimulation during two levels of partial neuromuscular blockade in aortic surgery. Anesthes Analges 88(1):22–27

Hatayama T, Moller AR (1998) Correlation between latency and amplitude of peak V in the brainstem auditory evoked potentials: intraoperative recordings in microvascular decompression operations. Acta Neurochir 140(7): 681–687

Jellish WS, Leonetti JP, Buoy CM, Sincacore JM, Sawicki KJ, Macken MP (2009) Facial nerve electromyographic monitoring to predict movement in patients titrated to a standard anesthetic depth. Anesthes Analges 109(2): 551–558

Jewett DL, Williston JS (1971) Auditory-evoked far fields averaged from the scalp of humans. Brain 94(4):681–696

Kalkman CJ, Drummon JC, Ribberink AA, Patel PM, Sano T, Bickford RG (1992) Effects of propofol, etomidate, midazolam, and fentanyl on motor evoked responses to transcranial electrical or magnetic stimulation in humans. Anesthesiology 76(4):502–509

Lang EW, Beutler AS, Chesnut RM, Patel PM, Kennelly NA, Kalman CJ, Drummnd JC, Garfin SR (1996) Myogenic motor-evoked potential monitoring using partial neuromuscular blockade in surgery of the spine. Spine 21(14): 1676–1686

Legatt AD (1999) Brainstem auditory evoked potentials: methodology, interpretation, and clinical application. In: Aminoff MJ (ed) Electrodiagnosis in clinical neurology, 4th edn. Churchill Livingstone, New York, pp 451–484

Legatt AD (2002) Mechanisms of intraoperative brainstem auditory evoked potential changes. J Clin Neurophys 19(5): 396–408

Lo YL, Dan YF, Tan YE, Nurjannah S, Tan SB, Tan CT, Raman S (2006) Intraoperative motor-evoked potential monitoring in scoliosis surgery: comparison of desflurane/nitrous oxide with propofol total intravenous anesthetic regimens. J Neurosurg Anesthesiol 18(3):211–214

Lotto ML, Banoub M, Schubert A (2004) Effects of anesthetic agents and physiologic changes on intraoperative motor evoked potentials. J Neurosurg Anesthesiol 16(1):32–42

Lyon R, Feiner J, Lieberman JA (2005) Progressive suppression of motor evoked potentials during general anesthesia: the phenomenon of “anesthetic fade”. J Neurosurg Anesthesiol 17(1):13–19

MacDonald DB (2001) Individually optimizing posterior tibial somatosensory evoked potential P37 scalp derivations for intraoperative monitoring. J Clin Neurophysiol 18(4): 364–371

Manninen PH, Lam AM, Nicholas JF (1985) The effects of isoflurane and isoflurane-nitrous oxide anesthesia on brainstem auditory evoked potentials in humans. Anesthes Analges 64(1):43–47

Moller AR, Jannetta PJ (1983) Monitoring auditory functions during cranial nerve microvascular decompression

operations by direct recording from the eighth nerve. J Neurosurg 59(3):493–499

Nielsen A (1942) Acoustic tumors: with special reference to end-results and sparing of the facial nerve. Ann Surg 115: 849–863

Nuwer MR (1999) Spinal cord monitoring. Muscle Nerve 22:1620–1630

Reinacher PC, Priebe H, Blumrich W, Zentner J, Scheufler KM (2006) The effects of stimulation pattern and sevoflurane concentration on intraoperative motor-evoked potentials. Anesthes Analges 102(3):888–895

Samii M, Matthies C (1997) Management of 1000 Vestibular Schwannomas (Acoustic Neuromas): surgical management and results with an emphasis on complications and how to avoid them. Neurosurgery 40(1):11–23

Scheufler KM, Reinacher PC, Blumrich W, Zentner J, Priebe H (2005) The modifying effects of stimulation pattern and propofol plasma concentration on motor-evoked potentials. Anesthes Analges 100(2):440–447

Scheufler KM, Zentner J (2002) Total intravenous anesthesia for intraoperative monitoring of the motor pathways: an integral view combining clinical and experimental data. J Neurosurg 96(3):571–579

Sekhar LN, Bejjani G, Nora P, Vera PL (1995) Neurophysiologic monitoring during cranial base surgery: is it necessary? Clin Neurosurg 42:180–202

Silverman H, Willcox TO, Rosenberg SI, Seidman MD (1994) Prediction of facial nerve function following acoustic neuroma resection using intraoperative facial nerve stimulation. Laryngoscope 104:539–544

Chapter 32

Brain Tumours: Pre-clinical Assessment of Targeted, Site Specific Therapy Exploiting Ultrasound and Cancer Chemotherapeutic Drugs

Anthony P. McHale and Nikolitsa Nomikou

Abstract Although recent advances in developing drug carriers and targeting systems to facilitate site-directed, cancer chemotherapy-based treatment modalities for solid tumours in general have indicated very significant patient benefit, tumours occurring in the brain have presented significant challenges. The purpose of this chapter will be to review existing therapeutic applications of transcranial ultrasound and to examine current experimental approaches based on the use of ultrasound to non-invasively enhance the action of cancer chemotherapeutics in a site-specific manner. Benefits afforded by such therapeutic strategies in the treatment of localised intracranial solid tumours will be highlighted.

Keywords Transcranial ultrasound · Site-directed · Chemotherapy-based · Cancer chemotherapeutics · Localised brain tumours · Malignant gliomas

Introduction

Despite modern medicine affording ever-increasing post-treatment survival rates following diagnosis of brain cancer, the prognoses for a wide variety of tumours in the brain remain relatively poor. The principle modes of treatment for relatively localised brain tumours include surgical resection, treatment with radiation, chemotherapeutic drugs or combinations of these approaches. Poor therapeutic outcome derives from a number of challenges including the pernicious infiltrative nature of tumours such as malignant gliomas that precludes accurate pre-surgical mapping and subsequent complete surgical resection (Neuwelt 2004). Although advances in modern diagnostic approaches are addressing the former (Vincenzini et al. 2008), the latter remains a significant challenge and usually necessitates subsequent follow up with some form of adjuvant therapy (Moustakas and Kreisl 2010). Amongst the therapeutic options currently available for the treatment of brain tumours, chemotherapy plays only a limited role either as a concurrent or follow-up adjuvant therapy (Nishikawa 2010). The limited role for cancer chemotherapeutics in the treatment of brain tumours essentially derives from the existence of the blood–brain barrier (BBB). This relatively impermeable barrier results from a sophisticated vascular architecture comprised of endothelial cell tight junctions reinforced by an endothelial cell basement membrane. This structure is surrounded in turn by perivascular cells, an astrocyte basement membrane and finally the flattened protrusions of astrocytes. Essentially this barrier precludes the movement of ionised, water-soluble substances with molecular weights >180 Da (Daltons) into the brain unless those substances exploit endogenous transporter mechanisms. Since many currently used cancer chemotherapeutic agents range in size from 2000 to 12,000 Da, they are effectively precluded from entry into the brain. The situation is further complicated by the heterogeneous nature of the blood-tumour barrier (BTB) in brain lesions, with that barrier somewhat leakier towards the centre and much less so at the actively growing regions in the tumour periphery. Unfortunately, the amount of chemotherapeutic drug accessing the latter regions can be negligible. Although

A.P. McHale (✉)
School of Pharmacy, University of Ulster, Coleraine, Co. Derry BT51 1SA, UK
e-mail: ap.mchale@ulster.ac.uk

M.A. Hayat (ed.), *Tumors of the Central Nervous System, Volume 4*,
DOI 10.1007/978-94-007-1706-0_32,

the above challenges present a considerable obstacle to the successful application of chemotherapeutics in the treatment of brain tumours, the search for improved means of exploiting this therapeutic option has led to approaches that seek to either deliver drugs directly to the brain or to disrupt the blood brain barrier. In experimental settings, directly introducing drugs to the brain has been accomplished via intracerebral implantation, intracerebroventricular infusion or convection enhanced diffusion (Vykhodtseva et al. 2008). Because these strategies are based on diffusion, limited penetration into the brain still compromises these approaches and this is further exacerbated by rapid elimination of drugs from the brain by active drug efflux transport mechanisms. More recent advances in drug delivery systems have sought to exploit nanoparticulate and liposomal formulations of systemically administered cancer chemotherapeutic agents to circumvent the BBB, however, non-localised uptake presents a challenge even with strategies such as these (Orive et al. 2010). Alternatives approaches have involved transient disruption of the BBB including the use of intracarotid arterial infusion of hyperosmotic solutions and alternative suggested experimental strategies using disruptive agents such as dimethylsulphoxide and vasoactive agents (Patel et al. 2009). Despite some exciting recent advances, the major limitation with these approaches however derives from the lack of control over anatomical positional deposition of these BBB-disrupting agents, resulting in non-localised uptake of the therapeutic agent and consequential collateral damage at non-target sites.

An ideal therapeutic regime might involve the use of some form of extracorporeal stimulus that could stimulate controlled, site-specific, transient compromise of the BBB in order to facilitate passage of a therapeutic agent across the BBB at an identified target site. Such an approach would very positively enhance the uptake of systemically-administered chemotherapeutic agents and preclude the negative aspects associated with the above-mentioned alternative modulators of the BBB. In addition, this approach would enhance the capabilities offered by recent developments in the design of drug carriers and strategies based on molecular targeting. In this chapter we will review recent advances in exploiting ultrasound to enhance the action of cancer chemotherapeutics and suggest how such approaches could provide mainstream therapeutic modalities for the treatment of brain tumours.

Ultrasound, Sonoporation and Cancer Chemotherapeutics

Ultrasound may be defined as an oscillating pressure wave propagating through a gas, liquid or solid at frequencies in excess of 20 kHz. Propagation velocity through living tissues is dependant on the nature of the tissue and this has had a profound influence on the development of ultrasound for medical applications. In medicine the historical development of ultrasound has primarily been related to diagnostics although the suggestion that it may play a role in therapeutics is certainly not a new one. It has been suggested that the first report by Wood and Loomis in 1927, describing the effects of ultrasound on tissues, led to the development of ultrasound as a therapeutic tool (ter Haar 2007). Indeed since then, many reports relating to the use of ultrasound in the treatment of cancer have culminated in the development of what is now known as HIFU treatment or high intensity focused ultrasound treatment. Such an approach is based on exploiting the ability to non-invasively focus ultrasound to a single point in three dimensions in order to stimulate a localised increase in temperature thereby delivering a hyperthermic ablative capability. More recent developments in this area have centred on coupling MR imaging capabilities with the HIFU approach and such devices are currently being trialled in a number of clinical settings (Jolesz 2009; McDannold et al. 2010). Some of these therapeutic applications will be discussed in more detail below in the context of transmitting ultrasound into the brain.

Although all current clinical treatments for cancer using ultrasound exploit site-specific hyperthermic ablation, it has also been recognised that ultrasound, at somewhat lower intensities, can induce transient changes in living cells and tissues that could lead to the development of new treatment strategies. Here it is perhaps worth taking time out to describe some of the parameters by which ultrasound is characterised when using it as a therapeutic tool. For therapeutic applications of ultrasound, exposures may be characterised by frequency, intensity (acoustic pressure/power density), the manner in which the ultrasound is delivered to the target (pulsed or continuous wave) and finally the duration of exposure. In addition, ultrasound may be delivered to a target as a columnar or focused beam.

The advantages associated with the latter relate to delivery of ultrasound at therapeutic levels to deeper sites within the organism without exposing the intervening tissues to ultrasound at those therapeutic doses. For hyperthermic treatments based on the use of HIFU, which obviously uses a focused beam configuration, the intensity or power density is usually greater than 5 W/cm^2 at the focal point/therapeutic site. In practice, it is usually much higher than this and treatment duration will be relatively short. For more subtle responses ultrasound power densities usually range from 1 to 5 W/cm^2 and it is these types of responses we will primarily be dealing with here. In addition, although frequencies ranging from 3 to 10 MHz are commonly employed in diagnostic ultrasound imaging, frequencies at or below 1 MHz are normally exploited for therapeutic or cell/tissue-modifying applications because tissue attenuation of ultrasound increases with increasing frequency. Essentially, lowering the ultrasound frequency ensures enhanced tissue transmission/penetration and permits greater access to target sites deep within the body. In any case, as mentioned above, ultrasound at intensities of 1–5 W/cm^2 has been reported to elicit effects on living cells and tissues that can not be entirely attributed to increases in temperature. Using both in vitro and in vivo model systems it has been shown that exposure to ultrasound at specific intensities and frequencies can induce a transient breakdown in the semi-permeable nature of cell membranes and this has become known as sonoporation (reviewed by Nomikou and McHale 2010). Discovery of this phenomenon has proven exciting from a therapeutic perspective because it can be induced non-invasively and in a site-specific manner, is a reversible phenomenon and can be exploited to enhance passage of therapeutic materials into target cells. Many reports have appeared in the literature describing the combined use of cancer chemotherapeutic agents together with ultrasound (Feril et al. 2002; Li et al. 2008; Nomikou et al. 2010) and they describe the exciting potential offered by such an approach in delivering site-specific, enhanced action of cancer chemotherapeutic drugs using an external, non-invasive physical stimulus. In many of these studies, particularly those employing cell culture-based model systems, it has been suggested that enhanced action of the chemotherapeutic agent is facilitated, at least in part, by sonoporation events induced by the ultrasonic stimulus. In our own studies we have confirmed this using in vitro test systems, although we have further suggested, based on data using in vivo models, that the ultrasound-induced enhancement may also be due to increased tissues dispersion of the chemotherapeutic agent following exposure to ultrasound (Nomikou et al. 2010). Regardless of the precise mechanism by which exposure of tissue to ultrasound renders them more susceptible to chemotherapeutic agents, it is difficult to ignore the significant therapeutic potential suggested by the wealth of reports in the literature.

In further exploring sonoporation and its therapeutic potential, researchers have found that this phenomenon is greatly enhanced in the presence of microbubble-based ultrasound contrast agents (reviewed by Nomikou and McHale 2010). Microbubbles are usually comprised of a shell surrounding some form of inert gas and gases commonly exploited for these purposes include air, sodium hexafluoride or a range of perfluorocarbon gases. The shells of these microbubbles, which serve to stabilise the overall entity, may be composed of denatured albumin, polymers or lipids and can further include surface modifications including polyethylene glycol (PEG) coatings to enhance stability (reviewed by Nomikou and McHale 2010). As mentioned above these microbubbles are exploited clinically to enhance ultrasound-mediated imaging by providing increased echogenicity and are routinely employed in echocardiography and in the determination of gross vascular integrity. Essentially, because ultrasound does not travel very effectively through a gas, these agents yield an enhanced echo as a result of reflection from the tissue–gas interface. It has also been found that at specific ultrasound intensities these microbubbles can give rise to either stable or inertial cavitation. At a microscopic level, if a microbubble is proximal to a target cell membrane, stable ultrasound-induced cavitation (or oscillation) can give rise to disturbances such as microstreaming in that micro-environment. If the ultrasound intensity is increased (usually to intensities greater than those used in diagnostic ultrasound imaging) so that inertial cavitation or catastrophic collapse of the microbubble occurs, then these violent effects can have a significant impact on a cell membrane that is proximal to those effects. It is believed that these violent effects underpin the mechanism by which microbubbles

enhance sonoporation or transient compromise in the permeability of cell membranes thereby facilitating entry of extracellular materials to intracellular spaces. Because these microbubbles respond in such a manner to ultrasonic fields and because their shells can also accommodate therapeutic payloads, it has been suggested that they may represent a convenient, stimulus-responsive drug delivery vehicle for use with cancer chemotherapeutic agents (Nomikou and McHale 2010). Essentially, the drug trapped on the microbubble would be administered systemically. During exposure of the target site (tumour) to ultrasound at intensities that would result in inertial cavitation, microbubbles passing through capillaries in the exposed tissues would disintegrate resulting in deposition and accumulation of the cancer chemotherapeutic payload at that pre-determined target site. Because such a strategy would facilitate accumulation of the cancer chemotherapeutic agent at the target site, the approach would permit administration of a reduced overall dose thereby impacting positively on therapeutic indices of relevant cancer chemotherapeutic agents.

One other aspect of ultrasound that indicates its exciting potential in site-specific delivery of drugs, particularly for the treatment of cancer, is suggested by relatively recent reports indicating that ultrasound can stimulate site-specific extravasation. It has been shown that treatment with ultrasound at specific intensities can result in extravasation of circulating marker dyes (e.g. Evans blue) with clear demonstration of the dye in extravascular tissues at the treatment site. Since dyes like Evan's blue interact very strongly with plasma proteins such as albumin, the data indicate compromise of the microvasculature at the ultrasound-treated target site (Bohmer et al. 2010). In our own laboratories we have also observed this phenomenon in the presence or absence of microbubbles although the presence of microbubbles enables the phenomenon to be observed at lower ultrasound intensities. Observations such as these present the exciting possibility that ultrasound can play a role in facilitating (i) site-specific deposition of drugs from a microbubble-based vehicle (ii) extravasation of those drugs from the microvasculature to extravascular target tissues, (iii) dispersion of drugs through those extravascular tissues and finally (iv) entry into target cells via sonoporation events. Since the above aspects are facilitated using a non-invasive, extracorporeal stimulus (namely ultrasound), exciting potential therapeutic options become possible, particularly for the non-invasive treatment of brain lesions. Of course realising such options would be dependant on being able to non-invasively deposit ultrasonic energy at a single, pre-determined point in 3-dimensions in the brain and the following section will review current developments in this area.

Transcranial Ultrasound

The suggestion that ultrasound might be exploited from a neurological perspective is not novel. In the 1940s, the Austrian neurologist, Karl Dussik together with his brother Friedrich working at the University of Vienna, experimented with transcranial ultrasound to locate brain lesions and cerebral ventricles (reviewed by Baker 2005). Since then many of the developments in the use of ultrasound relating to the brain have centred on brain ultrasonography, primarily in assessing brain vasculature (Seidel et al. 2004). It has long since been recognised that the skull and in particular the manner in which ultrasound passes through the bones of the skull represents perhaps the most serious challenge to the development of ultrasound as either a transcranial diagnostic or therapeutic tool. Because of the unpredictable nature of ultrasound transmission through many of the bones that constitute the skull, technology for ultrasonography was primarily developed to exploit what is known as the 'temporal window' and this was chosen because the temporal bones of the skull are relatively thin. Indeed exploiting the temporal window, led to developments in ultrasound imaging strategies including its use in assessing cerebral artery integrity and cerebral artery infarction (Seidel et al. 2004). Following on from the recognition that ultrasound could transit this temporal window with some degree of predictability, a therapeutic application for ultrasound was suggested that involved using ultrasound to enhance tPA (tissue plasminogen activator)-mediated thrombolysis in the treatment of brain ischemia resulting from stroke. Others have shown that inclusion of microbubble preparations in such strategies can further enhance t-PA-mediated thrombolysis in a manner that significantly limits adverse post-treatment haemorrhagic events (Hitchcock and Holland 2010). Although this transcranial therapeutic application of ultrasound

has encountered a number of setbacks in translation to the clinic, the considerable literature describing pre-clinical and clinical outcomes does emphasise that it is possible to deliver ultrasound transcranially, with considerable spatial control for therapeutic purposes. Taken in concert with the above listed potential attributes associated with ultrasound in terms of enhancing the action of cancer chemotherapeutics, a role for ultrasound in facilitating site-specific deposition of cancer chemotherapeutics for the treatment of brain lesions seems possible.

As mentioned above, delivery of ultrasound through the bones of the skull can present a significant challenge to its exploitation in facilitating treatment of intracranial lesions. Looking at this in more depth, the challenge basically relates to the unpredictable nature of ultrasound as a result of strong scattering and attenuation by the bones of the skull. In order to understand this behaviour and in an attempt to predict the nature of ultrasound on passage into the brain, a large number of studies have described the behaviour of ultrasound as it passes through the skull bones. Studies such as these have described direct effects of ultrasound on the bones through which the ultrasound is transmitted and particularly on tissues overlaying and underlying the bone at the point of transmission. It has been shown that even at relatively low frequencies (which are normally chosen as a result of the relationship between ultrasound attenuation and frequency) significant thermal accumulation can occur at tissue-bone interfaces (Hynynen et al. 2006). Some of these studies were performed in order to ascertain whether or not HIFU-based approaches could be exploited in developing thermal ablative treatments for tumours in the brain. In this approach the objective was to deposit ultrasound at a sufficient energy density to facilitate thermal ablation at a precisely targeted focal point without destruction of tissues between the emitting surface of the transducer and that focal point. In those studies it was clear that ultrasound could be transmitted from focused transducers with sufficient accuracy and precision to enable hyperthermic treatments of tumours with a diameter of 10 mm. In a more recent clinical study, aimed at achieving hyperthermic ablation, McDannold et al. (2010) confirmed localised deposition of ultrasonic energy in three glioblastoma patients with an extremely high degree of precision. As mentioned above, deposition of ultrasonic energy at densities to facilitate tissue ablation caused adverse thermal accumulation at the scalp–skull and skull–brain interfaces. However, in applying ultrasound to enhance or target the action of cancer chemotherapeutics, the ultrasonic energy required would be much lower than that required for HIFU-based thermal ablation and the above mentioned challenges would therefore be significantly reduced. In addition, because the application of ultrasound to the brain for enhancing cancer chemotherapeutics at a precise point in three dimensions necessitates the use of focused transducers, geometric configurations with relatively large curvatures could be exploited, thereby minimising the energy striking these interfaces and this would further serve to circumvent thermal accumulation at the bone–tissue interfaces.

In terms of non-invasively delivering ultrasound through the skull to a single point in three dimensions in the brain and because of the potential for significant distortion as the ultrasound passes through the bones of the skull, an elegant approach involving the use of a time reversal mirror can be exploited in order to enhance targeting to that single point. This involves the use of an array of transducers that emit an acoustic wave front towards a target, receive and analyse the return signal from the target and re-emit a subsequent wave front that is corrected for distortion and focused on the target. Using this approach Pernot et al. (2007) demonstrated that the use of HIFU to facilitate non-invasive brain surgery with a high degree of geometric precision was feasible. The approach also suggested that patient-specific distortions (as a result of variations in skull geometry) with respect to transcranial ultrasound transmission could be addressed. It is clear from the above, that ultrasound can be delivered through the skull with a degree of precision and at acoustic pressures (ultrasound intensities) that facilitate either enhanced thrombolysis for the treatment of ischemia in stroke patients or for thermal ablation of tissues in the treatment of brain tumours. Since ultrasound can be transmitted to specific sites in the brain for the above listed therapeutic applications and since the ultrasound power densities required for bioeffects that enhance the action of cancer chemotherapeutic agents (sonoporation, drug dispersion, extravasation) are much lower, a therapeutic approach that involves the combined use of ultrasound and cancer chemotherapeutic drugs in the treatment of brain lesions seems extremely feasible.

Ultrasound, the Blood Brain Barrier and Cancer Chemotherapeutic Drugs

As mentioned in the Introduction, the blood-brain barrier poses one of the most significant challenges to successful treatment of brain tumours using chemotherapeutic drugs. Treatment of tumours in the brain by systemic administration of cancer chemotherapeutics, either as a front-line or adjuvant therapy is hindered by this barrier and achieving a dose that can result in a therapeutic effect necessitates alternatives to conventional systemic administration. Recognition of this has led to the development of alternative strategies which have involved circumventing the BBB using invasive procedures or compromising the BBB in a relatively non-specific manner. Many of these approaches, although certainly providing therapeutic benefit over and above that provided by direct systemic administration, can lead to complications such as brain toxicity resulting from compromise to the BBB at non-target regions and/or toxicity resulting from prolonged compromise to the BBB. In an ideal therapeutic regime involving the use of cancer chemotherapeutic agents for the treatment of brain lesions, non-invasive stimulation of site-specific transient compromise of the BBB to enable uptake of systemically administered low dose cancer chemotherapeutic drug would be highly desirable. In addition, as a result of brain tumour architecture and atypical vasculature, a means of non-invasively stimulating site-specific tissue dispersion of the drug, once delivered, would also be expected to provide significant therapeutic advantage. Finally, a means of non-invasively stimulating entry of the cancer chemotherapeutic drug into target cells would again provide therapeutic advantage since many cancer chemotherapeutic drugs have intracellular targets. This aspect would also be highly relevant where drug resistance by cellular drug export mechanisms may be evident.

The realisation that ultrasound can induce extravasation of dyes from the microvasculature in general has led to a number of studies that have investigated its effects on the BBB. Indeed in some of the studies related to intracranial ultrasound-enhanced thrombolysis and HIFU applications for ablation, it was noted that the blood-brain barrier was compromised at the treatment site. It was subsequently noted that exposure of rat brain to ultrasound together with a microbubble-based ultrasound contrast agent led to an enhanced degree of compromise of the BBB and this compromise was dose dependant with respect to the microbubbles (Mychaskiw et al. 2000). It was subsequently demonstrated using this approach that compromise to the BBB could also be related to the ultrasound dose and depending on the dose delivered; compromise appeared to be self-healing (Hynynen et al. 2006). The latter study was performed using contrast enhanced MRI to monitor compromise of the BBB and it was found that self-healing occurred within 6 h when an appropriate dose of ultrasound was delivered. More recent studies using the mouse as a model supported earlier studied in determining that the net effect of inclusion of microbubbles in treatment regimes served to reduce the acoustic pressure (ultrasound intensity) required to facilitate transient BBB disruption without collateral tissue damage (Tung et al. 2010). In addition to the above studies using relatively small animal models, Xie et al. (2008) demonstrated BBB compromise in larger animal models (porcine) showing ultrasound-induced, site-specific uptake of MRI contrast agents at pre-defined sites in the brain. In these studies it was also confirmed that the effects were more apparent when ultrasound was administered through the temporal bone.

In attempts to exploit ultrasound-induced compromise of the BBB in chemotherapy-based treatment of brain tumours, Mei et al. (2009) compared ultrasound-mediated compromise of the BBB to direct internal carotid artery injection for delivery of methotrexate to chosen areas of the brain. In that study, the authors were able to demonstrate that ultrasound treatment resulted in a 10-fold increase in the amount of methotrexate at the targeted regions of the brain following systemic administration of the drug. When compared with the best results achieved by direct carotid artery injection, concentrations of methotrexate in the treated regions were 3.7-fold higher in the ultrasound treated subjects. In an approach that involved the use of microbubbles, Treat et al. (2007) explored the possibility of delivering doxorubicin to precise locations in the brain using focused ultrasound. The objective was to determine whether or not ultrasound could stimulate site-specific deposition of therapeutic concentrations (in humans) of the drug at pre-defined regions of the rat brain. When compared with the level of drug in the brain following systemic administration and depending on the acoustic pressure

(ultrasound intensity) employed, up to a 23-fold increase in doxorubicin concentration was detected at ultrasound-treated sites. Although in this work the authors did not premeditatedly attach the doxorubicin to the microbubble preparation, it has previously been demonstrated that microbubbles can serve as carriers for this drug with appropriate design of the microbubble (Nomikou and McHale 2010). The latter raises the interesting possibility of employing the microbubbles as an ultrasound-responsive chemotherapeutic carrier for delivery to lesions in the brain and from a therapeutic perspective this would be expected to provide benefit by facilitating a reduction in the amount of drug administered to the patient. In terms of targeting cancer chemotherapeutic agents to tumour tissues in the brain, Liu et al. (2010a) examined the effect of ultrasound in modifying the BBB to enhance delivery of systemically administered BCNU [1,3-bis(chloroethyl)-1-nitrosourea] to a glioblastoma model in rats. They were able to show that ultrasound treatment enhanced penetration of intravenously-administered BCNU across the blood brain barrier and demonstrated that drug uptake at the treated sites was enhanced by 200%. They were also able to demonstrate that while administration of BCNU in the absence of ultrasound was only transiently capable of controlling glioblastoma growth, treatment with ultrasound prior to administration of the BCNU led to very significant reductions in tumour growth and enhanced animal survival. The enhanced therapeutic effects were attributed to opening of the BBB by ultrasound and subsequent enhanced uptake of the drug at that site. In addition to the above, it has also been demonstrated that focused ultrasound can be exploited to enhance uptake of the chemotherapeutic epirubicin attached to a nanoparticulate carrier by glioma tumours in the rat brain (Liu et al. 2010b). In that study it was found that treatment of tumours with ultrasound in the presence of the drug-nanoparticle carrier reduced tumour growth and significantly enhanced survival. In addition to clearly providing pre-clinical evidence demonstrating that ultrasound can be exploited in enhancing uptake of a cancer chemotherapeutic drug to facilitate a site-directed therapeutic response in the brain, this report further demonstrated the versatility of the approach in enabling enhanced uptake of a nanoparticulate entity. The latter is important in the context of characterising the nature of ultrasound-induced compromise to the BBB and indicates that the approach can be employed to enable large entities to bypass the BBB. This has positive consequences where entry by macromolecular biotherapeutics may be a necessity. Although it has already been demonstrated that ultrasound-induced compromise of the BBB can facilitate entry of antibody molecules into the brain, these molecules are much smaller than entities such as plasmid DNA which may, in the future, be exploited in gene-based therapies for the treatment of localised brain lesions. Indeed it has been demonstrated some time ago that ultrasound can be exploited to facilitate gene transfer into target cells in the brain in a site-specific manner (Shimamura et al. 2004) although the DNA was administered intracranially and it remains to be seen whether or not ultrasound-induced compromise of the BBB could facilitate uptake of therapeutic DNA constructs following systemic administration. From a cancer chemotherapy perspective, advances in gene targeting to lesions in the brain could be exploited using strategies such as gene-directed prodrug therapy thereby further enhancing the specificity of treatment. A typical example of this approach is illustrated by the insertion of a transgene encoding Herpes simplex thymidine kinase (HSVtk) into target cells. When the target cells are exposed to the prodrug, ganciclovir, the HSVtk catalyses its phosphorylation and the resulting activated drug then competitively inhibits incorporation of dGTP into nucleic acid in the target cell which then results in cell death (reviewed by Nomikou and McHale 2010). Using such an approach, the degree of specificity incorporated into the therapeutic regime may, in the future, provide a particular advantage in treating highly metastatic brain lesions.

In all of the above approaches, the ability of ultrasound to non-invasively stimulate BBB by-pass combined with cell membrane permeabilisation at the target site underpins the enormous therapeutic potential offered by such strategies. Understanding the mechanism by which ultrasound facilitates BBB compromise is key to further developing the approach and its translation into the clinic. Although we have discussed ultrasound transmission through the skull to facilitate site-directed deposition of energy sufficient to facilitate opening of the BBB, the mechanism by which this occurs at tissue and molecular level needs to be explored further. In a study involving the use of a mouse model system with systemic administration (IV and IP) of a BBB impermeable gadolinium-based MRI contrast agent and fluorogenic tracer dyes to assess

BBB compromise post-ultrasound treatment, Baseri et al. (2010) demonstrated that observed effects at a histological level were dependant on acoustic pressure (ultrasound intensity). They found that effects ranged from intense tissue disruption to mildly diffuse opening across the brain parenchyma with minimal tissue damage and they concluded that ultrasound parameters could be chosen to select for the latter. In this study microbubbles were employed to enhance the effects and on that basis one can conclude that the observed bioeffects resulted from ultrasound-induced inertial cavitation, particularly at the acoustic pressures exploited. In another study a rat glioma model was employed to examine the effects of ultrasound in combination with microbubbles on the blood-tumour barrier (BTB) (Shang et al. 2010). This study involved the use of Evan's blue to assess compromise of the barrier and further sought to examine the effects of ultrasound treatment at a molecular level by examining mRNA expression levels of tight junction-related proteins. They found that following exposure of tissues to ultrasound, compromise of the BTB was afforded and when expression levels of tight junction-related proteins were examined at various times post treatment, those levels dropped significantly at 3 h post treatment and subsequently recovered at 12 h post treatment. The authors suggested that reduced expression of these proteins in the post treatment period could be related to compromise of the BTB. From these studies, it is clear that ultrasound together with microbubbles are exerting a significant disruptive effect on the microvasculature at treatment sites and this results in a weakening of the tight junction architecture that subsequently permits release of the tracer dyes into the surrounding tissues. Although this can explain enhanced deposition of a chemotherapeutic agent into a target region in the brain, it is perhaps worth noting that it may not fully explain the observed potentiation of chemotherapeutic drugs in the brain. As already mentioned ultrasound-induced bioeffects can also involve enhanced diffusion of chemotherapeutic agents through relatively impermeable tissues and this can provide significant therapeutic benefit particularly in the treatment of solid tumours where the vasculature and tissue architecture can be extremely atypical (Nomikou et al. 2010). In addition, sonoporative effects on cells at the tumour site, where transient permeabilisation of the target cell membrane can be achieved, could also play a significant role, particularly since many cancer chemotherapeutic drugs exploit intracellular targets (Li et al. 2008). In any event and regardless of the precise mechanisms involved, it is clear from the above that ultrasound can play a major role in facilitating compromise of the BBB/BTB and the non-invasive nature of this potentiating stimulus suggests some very exciting possibilities in terms of delivering site-directed chemotherapy for the treatment of brain lesions.

Conclusions

In the above chapter we have sought to relate studies describing the translation of transcranial ultrasound for therapeutic purposes into the clinic to pre-clinical studies describing the benefits afforded by exploiting ultrasound to enhance or potentiate the action of cancer chemotherapeutic drugs. Recent advances relating to clinical therapeutic applications of ultrasound have demonstrated site-specific deposition of ultrasonic energy to facilitate hyperthermic tissue ablation and the precision and predictability with respect to targeting without collateral tissue damage along the ultrasound transmission path is extremely impressive. From those and other studies, it was realised that ultrasound, at specific frequencies and acoustic pressures (intensities) could be exploited to facilitate site-selective opening of the BBB/BTB. On the other hand a significant body of pre-clinical data has been accumulated over the years demonstrating significant benefit associated with the use of ultrasound to potentiate the action of cancer chemotherapeutics in a site-specific manner. Essentially ultrasound, together with microbubble-based ultrasound contrast agents, can facilitate entry of cancer chemotherapeutic drugs into target cells by promoting transient, cell membrane permeabilisation. In addition, ultrasound can promote dispersion of drugs through the relatively impermeable tissues of solid tumours. If one takes the latter two observations in concert with ultrasound-induced transient opening of the BBB/BTB, the therapeutic potential offered by combining this non-invasive stimulus with systemically-administered cancer chemotherapeutics for the treatment of brain lesions is staggering. Essentially, the approach suggested primarily involves ultrasound-mediated opening of the BBB/BTB in the vicinity of the lesion. In doing so ultrasound will also serve to 'hyper-sensitise' the relevant lesion, by

(i) facilitating dispersion of the cancer chemotherapeutic drug through impermeable tumour tissues and (ii) facilitating entry of the cancer chemotherapeutic drug into target cells via sonoporation. Based on some of the data presented here, there is strong evidence to support a move towards translation of this overall approach into the clinic. Indeed there is also sufficient evidence to indicate very significant patient benefit in being able to provide non-invasive, site-specific chemotherapy in the treatment of brain lesions since the approach would permit a reduction in the overall dose of chemotherapeutic administered to the patient. This would be expected to provide a positive impact on apparent therapeutic indices of cancer chemotherapeutic drugs. In addition, this approach would also enable the use of highly effective chemotherapeutic agents that are currently not indicated for the treatment of brain lesions on the basis that they are incapable of crossing the BBB. Significant patient benefit using this approach would also derive from minimising the invasive nature of existing therapeutic alternatives. We believe that existing technological developments in site-specific delivery of transcranial ultrasound, the wealth of preclinical data relating to ultrasound potentiated cancer chemotherapy and perceived patient benefit, provide compelling evidence for translation of this approach to the clinic, particularly for the treatment of focal brain lesions.

References

Baker JP (2005) The history of sonographers. J Ultrasound Med 24:1–14

Baseri B, Choi JJ, Tung YS, Konofaguo EE (2010) Multimodality safety assessment of blood-brain barrier opening using focused ultrasound and Definity microbubbles: a short-term study. Ultrasound Med Biol 36:1445–1459

Bohmer MR, Chlon CHT, Raju BI, Chin CT, Shevchenko T, Klibanov AL (2010) Focused ultrasound and microbubbles for enhanced extravasation. J Control Release 148:18–24

Feril LB, Kondo T, Umemura S, Tachibana K, Manalo AH, Riesz P (2002) Sound waves and antineoplastic drugs: the possibility of an enhanced combined anticancer therapy. J Med Ultrasonics 29:173–187

Hitchcock KE, Holland CK (2010) Ultrasound-assisted thrombolysis for stroke therapy: better thrombus break-up with bubbles. Stroke 41:S50–S53

Hynynen K, McDannold N, Clement G, Jolesz FA, Zadicario E, Killiany R, Moore T, Rosen D (2006) Pre-clinical testing of a phased array ultrasound system for MRI-guided noninvasive surgery of the brain – a primate study. Eur J Radiol 59: 149–156

Jolesz PA (2009) MRI-guided focused ultrasound surgery. Ann Rev Med 60:417–430

Li YS, Reid CN, McHale AP (2008) Enhanced ultrasound-mediated cell membrane permeabilisation (sonoporation) using a high frequency pulse regime and implications for ultrasound-aided cancer chemotherapy. Cancer Lett 266:156–162

Liu HL, Hua MY, Chen PY, Chu PC, Pan CH, Yang HW, Huang CY, Wang JJ, Yen TC, Wei KC (2010a) Blood-brain barrier disruption with focused ultrasound enhances delivery of chemotherapeutic drugs for glioblastoma treatment. Radiology 255:415–425

Liu HL, Hua MY, Yang HW, Huang CY, Chu PC, Wu JS, Tseng IC, Wang JJ, Yen TC, Chen PY, Wei KC (2010b) Magnetic resonance monitoring of focused ultrasound/magnetic nanoparticle targeting delivery of therapeutic agents to the brain. Proc Natl Acad Sci USA 107: 15205–15210

McDannold N, Clement GT, Black P, Jolesz F, Hynynen K (2010) Transcranial magnetic resonance imaging-guided focused ultrasound surgery of brain tumors: initial findings in 3 patients. Neurosurgery 66:323–332

Mei J, Cheng Y, Song Y, Yang Y, Wang F, Liu Y, Wang Z (2009) Experimental study on targeted methotrexate delivery to the rabbit brain via magnetic resonance imaging-guided focused ultrasound. J Ultrasound Med 28:871–880

Moustakas A, Kreisl TN (2010) New treatment options in the management of glioblastoma multiforme: a focus on bevacizumab. Onco Targets Ther 10:27–38

Mychaskiw G, Badr AE, Tibbs R, Clower BR, Zhang JH (2000) Optison (FS069) disrupts the blood-brain barrier in rats. Anesth Analg 91:798–803

Neuwelt EA (2004) Mechanisms of disease: the blood-brain barrier. Neurosurgery 54:141–142

Nishikawa R (2010) Standard therapy for glioblastoma – a review of where we are. Neurol Med Chir (Tokyo) 50: 713–719

Nomikou N, Li YS, McHale AP (2010) Ultrasound-enhanced drug dispersion through solid tumours and its possible role in aiding ultrasound-targeted cancer chemotherapy. Cancer Lett 288:94–98

Nomikou N, McHale AP (2010) Exploiting ultrasound-mediated effects in delivery targeted, site-specific cancer therapy. Cancer Lett 296:133–143

Orive G, Ali OA, Anitua E, Pedraz JL, Emerich DF (2010) Biomaterials-based technologies for brain anti-cancer therapeutics and imaging. Biochim Biophys Acta 1806: 96–107

Patel MM, Goyal BR, Bhadada SV, Bhatt JS, Amin AF (2009) Getting into the brain: approaches to enhance brain drug delivery. CNS Drugs 23:35–58

Pernot MA, Aubry JF, Tanter M, Boch AL, Marquet F, Kujas M, Seilhean D, Fink M (2007) *In vivo* transcranial brain surgery with an ultrasonic time reversal mirror. J Neurosurg 106:1061–1066

Seidel G, Meyer-Wiethe K, Berdien G, Hollstein D, Toth D, Aach T (2004) Ultrasound perfusion imaging in acute middle cerebral artery infarction predicts outcome. Stroke 35: 1107–1111

Shang X, Wang P, Liu Y, Zhang Z, Xue Y (2010) Mechanism of low-frequency ultrasound in opening blood-tumour barrier by tight junction. J Mol Neurosci 43:364–369

Shimamura M, Sato N, Taniyama Y, Yamamoto S, Endoh M, Kurinami H, Aoki M, Ogihara T, Kaneda Y, Morishita R (2004) Development of efficient plasmid DNA transfer into adult rat central nervous system using microbubble-enhanced ultrasound. Gene Ther 11: 1532–1539

ter Haar G (2007) Therapeutic applications of ultrasound. Prog Biophys Mol Biol 93:111–129

Treat LH, McDannold N, Vykhodtseva N, Zhang Y, Tam K, Hynynen K (2007) Targeted delivery of doxorubicin to the rat brain at therapeutic levels using MRI-guided focused ultrasound. Int J Cancer 121:901–907

Tung YS, Vlachos F, Choi JJ, Defieux T, Selert K, Konofagou EE (2010) In vivo transcranial cavitation threshold detection during ultrasound-induced blood-brain barrier opening in mice. Phys Med Biol 55:6141–6155

Vincenzini E, Delfini R, Magri F, Puccinelli F, Altieri M, Santoro A, Giannoni MF, Bozzao L, Di Piero V, Lenzi GL (2008) Semiquantitative human cerebral perfusion assessment with ultrasound in brain space-occupying lesions: preliminary data. J Ultrasound Med 27:685–692

Vykhodtseva N, McDannold N, Hynynen K (2008) Progress and problems in the application of focused ultrasound for blood-brain barrier disruption. Ultrasonics 48:279–296

Xie F, Boska MD, Lof J, Uberti, G, Tsutsui JM, Porter TM (2008) Effects of transcranial ultrasound and intravenous microbubbles on blood-brain barrier permeability in a large animal model. Ultrasound Med Biol 34:2028–2034

Part VI
Quality of Life

Chapter 33

Headaches in Patients with Brain Tumors

David Fortin and Philippe Goffaux

Abstract Although most people who suffer from headache do not present with an underlying mass lesion, a large number of patients with brain tumors do complain of headache (as many as 60% in our institution). The problem for clinicians is that the tumor-headache association is not universal, as evidenced by anecdotal reports of patients with large tumors, elevated intracranial pressure but a complete absence of headache. In this chapter, we examine over 80 years of research on brain tumor headaches, delineating the link between tumor location, laterality, growth-rate, and pain. Most importantly, we position our review within the context of current aetiological theories and propose new models involving the peripheral and central sensitization of nociresponsive neurons. A brief examination of headaches as a result of surgery and adjuvant chemo-radiation therapy is also provided.

Keywords Headache · Brain tumors · Intracranial pressure · Migraine-like · Tension type · Cluster headaches

Headache as a General Symptom

Headache is an extremely prevalent and often non specific symptom. Prevalence estimates indicate that 35–90% of us will experience headaches at least once in our lives (Dousset et al. 2000). The most common type of headache is by far tension type headache (69–88%) followed by migraine (6–25%) and cluster headaches (0.006–0.24%) (Dousset et al. 2000). In some cases, headaches do not readily fit into the classification categories established by the International Headache Society, and are thus considered atypical. Prevalence estimates for atypical headaches are scarce, but a relatively recent study conducted to test the utility of magnetic resonance (MR) imaging in the evaluation of chronic headache revealed that 15.9% of referred cases were atypical, whereas 40% of cases were migraine-like and 17.6% were tension type headaches (Wang et al. 2001). One must interpret these numbers with caution, as they were likely biased toward higher representation of atypical cases, since these cases are more likely to be considered for neuroimaging. Nevertheless, it is important to properly investigate atypical headaches since major abnormalities are found following MR imaging in 14.1% of cases, as opposed to 0.6% for migraine and 1.4% for tension type headache (Wang et al. 2001).

Headache as a Symptom of a Brain Tumor

So when does a headache signal the presence of an intracranial neoplasm? As is often the case in medical sciences, there is no straightforward answer to that question. Headaches often are early indicator of central nervous system tumors. However, headaches are also present in a wide variety of other conditions, and are sometimes (surprisingly) absent in patients with primary neoplasms or metastatic tumors. This thus prevents the formulation of a generalized statement linking headache to the presence of an intracranial

D. Fortin (✉)
Department of Neurosurgery and Neuro-Oncology, Faculty of Medicine, Sherbrooke University, Sherbrooke, QC, Canada
e-mail: David.fortin@usherbrooke.ca

M.A. Hayat (ed.), *Tumors of the Central Nervous System, Volume 4*,
DOI 10.1007/978-94-007-1706-0_33,

Table 33.1 Signs warranting the need for further investigation

Red Flags
Sudden onset headache or persistent headache associated with an absent family history of migraine
Headaches that have changed in character/quality
Headaches not resembling any of the primary headaches
Headaches associated with nausea/vomiting in nonmigraineur patients
Persistent headaches associated with substantial episodes of confusion, disorientation, or emisis
Rapid onset of headache following strenuous exercise
Papilledema, diplopia, blurred vision
Headaches that awaken the patient repeatedly from sleep or occur immediately on waking
Focal neurological symptoms other than visual or sensory aura and/or hemicrania associated with contralateral neurological symptoms

neoplasm. Let us thus examine the data available on this interesting topic, with the purpose of drawing some generalizations.

Headaches are rarely the result of a brain tumor; however brain tumors are frequently associated with headaches. As a general rule, approximately 50% of patients bearing a brain tumor will complain of headache pain. Studies addressing the question specifically have reported estimates varying from 33 to 71%. Interestingly, Schankin et al. (2007) reported that when headaches are presents, they rarely occur in isolation, presenting as such in only 10% of case. Loghin and Levin (2006) reported that brain tumor headaches are typically accompanied by varied symptoms, including nausea, emesis, papilledema and blurred vision (in the context of intracranial hypertension), personality changes, seizures, and/or other focal neurological signs. These companion symptoms are considered "red flags", and call for immediate imaging investigations (brain MRI or scan), lest the presence of a lesion be missed (Table 33.1). More so, according to Forsyth and Posner (1993) a change in a pre-existing headache can also be indicative of a newly expending mass lesion and should definitely be investigate.

The character of the headache per se can be of some diagnostic value. Most brain tumor headaches are expressed as dull, aching pain, and are rarely described as throbbing or pulsating, as described by Schankin et al. (2007). According to Forsyth and Posner (1993), the general consensus seems to be that brain tumor headaches mostly mimic tension type headaches. On some occasions, however, Pfund et al. (1999) reported that brain tumor headaches will be described as similar to migraine-like headaches (in approximately 10% of cases). Nevertheless, drawing parallels between brain tumor headaches and idiopathic or primary headaches (e.g., tension type or migraine – see description and comparison in Table 33.2) can be useful, especially given the sometimes complex mechanisms underlying the development of brain tumor headaches.

Does Headache Localization Echo Tumor Location?

Historically, it was thought that the topographic distribution of headaches could have some predictive value in determining the location of underlying mass lesions. The tremendous advancements in neuro-imaging have largely rendered the pursuit of this relation obsolete.

However, over 80 years of research on this issue have provided valuable data allowing certain generalizations. Thus, Dalessio (1978) reported that infratentorial lesions are more frequently associated with occipital than frontal or temporal headaches. Infratentorial tumors can also be accompanied by nuchal pain and cervical muscle spasms. Supratentorial tumors, on the other hand are more frequently associated with vertex and frontal pain according to Suwanwela et al. (1994). Kunkle et al. concluded on the fact that frontal headache per se has poor localizing value since it can be produced by tumors in remote locations. In addition, published prevalence estimates pairing supratentorial tumors to frontal headaches indicate that this association happens in less than 50% of cases, according to Forsyth and Posner (1993), thus emphasizing the looseness of this association.

Despite the limited utility of precise localization attempts, correspondence between headache laterality and tumor location is much higher. Headaches, it seems, occur more frequently on the ipsilateral side

Table 33.2 Clinical characteristics underlying migraine, tension type headache, cluster headache, and brain tumor headache

Migraine	Tension type headache	Cluster headache	Brain tumor headache
Headache attacks last anywhere from 4 to 72 h	Headaches last anywhere from 30 min to 7 days	Frequency can vary from one every other day to as many as eight per day and last from 15 to 180 min	Headaches may be intermittent and are often relieved by simple analgesics
Headaches are typically unilateral and pulsating	Headaches are bilateral and typically described as pressing/tightening (non-pulsating)	Headaches are associated with sever unilateralorbital, supraorbital, and/or temporal pain	Headaches can be unilateral or bilateral (depending on the location of the tumor and on the presence of elevated intracranial pressure), and are more frequently described as dull, deep aching pain
Headaches are moderate to severe and limit daily activities	Headaches are mild to moderate and do not prohibit daily activities	Cluster headache attacks are debilitating and patients often become agitated	Headaches are usually mild to moderate but can be fulminatory if the tumor grows rapidly. Elevation of intracranial pressure is not necessary for its occurrence
Accompanied by photo- or phono-phobia, and by nausea/vomiting. Sometimes accompanied by one or more fully reversible aura symptoms indicating focal cerebral, cortical, or brainstem functions	Photo- or phono-phobia are usually absent and headaches are not accompanied by nausea/vomiting	Associated with conjunctival injection, lacrimation, nasal congestion, rhinorrhoea, forehead and facial sweating, miosis, ptosis, eyelid oedema	Typically associated with the classic triggers of worsening in the morning, coughing, or Valsalva manoeuvre when accompanied by elevated intracranial pressure and/or when the tumor is located along midline structures
Headaches are not better explained by an underlying physical or neurological disorder	Headaches are not better explained by an underlying physical or neurological disorder	Headaches are not accompanied by gastrointestinal disturbances and are not associated with trigger points (as in trigeminal neuralgia)	Often include the presentation of neurological symptoms related to the growth of a mass lesion within brain parenchyma

of unilateral tumor(s), particularly in the absence of elevated intracranial pressure. In fact, in the absence of high intracranial pressure, Suwanwela et al. (1994) found that headaches correctly predict the lateralization of supratentorial lesions in 100% of cases. According to Dalessio (1978), this is likely due to the absence of extensive brain displacement and ventricular obstruction, both of which tend to produce distal rather than proximal traction on pain-sensitive structures such as veins and meningeal arteries. In the absence of distal traction, headaches occur regionally, and are thus more predictive of tumor location. It was reported by Forsyth and Posner (1993) that for similar reasons, dural-based tumors produce localized headaches of predictive value, which develop in close proximity to the tumor site.

As the tumor grow and produce an increase in intracranial pressure, however, headache pain looses its localizing/lateralizing value, as the distal traction produced by elevated pressure activates pain sensitive structures in widespread areas and away from the tumor.

It thus becomes relevant to pay attention and understand the pathogenesis of brain tumor headaches. The next section deals specifically with this issue.

Headaches associated with a mass lesion are often worse in the morning, since brain edema increases overnight from the effects of gravity in the reclining position. When associated with projectile vomiting and an abrupt worsening in mental state, such headaches are always a cause for concern and call for immediate investigation.

Pathogenesis of Brain Tumor Headache

Traction Hypothesis

Being devoid of pain receptors, the brain parenchyma, is insensitive to pain per se. Thus, headache pain has to be triggered by surrounding structures. Intra- and extra-cranial pain-sensitive structures potentially involved in the genesis of headache include venous sinuses, dural and cerebral arteries, dura, skin, subcutaneous and muscle tissue, and the periosteum of the skull. The most frequently cited cause of brain tumor headache is the presence of traction on intra- and extra-cranial pain-sensitive structures. In brain cancer, traction results from the expansion of tumoral tissue, oedema, and, secondary hemorrhages, as reported by Kunkle et al. (1942).

A number of tumor-associated features tend to validate the traction hypothesis of brain tumor headaches. For example, tumor-associated peritumoral edema, papilledema, and supratentorial midline shift (Fig. 33.1) are all key markers of increased intracranial pressure, and can be paired to the presence of diffuse, poorly localized headaches, as reported by Pfund et al. (1999). Pressure-induced traction is the most likely explanation in the genesis of these diffuse headaches.

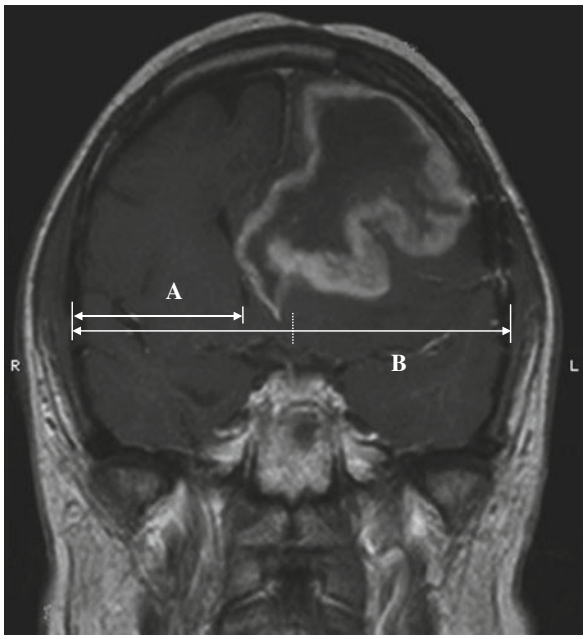

Fig. 33.1 Coronal brain section (gadolinium-enhanced T_1 magnetic resonance slice) showing the presence of a significant tumor-induced horizontal shift of the third ventricle. Measurements for horizontal shift typically involve subtracting the measured distance from the inner table of the skull to the midpoint of the third ventricle (**a**) from one-half the distance between the inner tables of the skull (**b**)

According to Loghin and Levin (2006), the growth-rate of space occupying lesions also plays an important role in predicting the occurrence of traction and headache pain. Tumors that increase rapidly in size can cause sharp, intense pain because the intracranial space does not have a chance to adapt to the increased pressure. As described above, this is thought to result from the sudden irritation of pain-sensitive structures. Slow growing tumors, on the other hand, produce headaches that are transitory and occur only later in the course of disease, principally because protracted mechanical adaptation to the expanding tumor is possible.

A final clinical feature which tends to validate the traction hypothesis is tumor location. Although tumor location does not always predict *where* headaches will occur, it adequately predicts *if* headaches will occur. Suwanwela et al. (1994) concluded that tumors that typically provoke headaches include intraventricular, midline, and posterior fossa lesions. Here, CSF flow obstruction, followed by internal hydrocephalus and local or distal traction is the most likely explanation.

Traction Hypothesis in Intracranial Hypertension: The CSF Dynamics

It is common knowledge that intracranial hypertension will most commonly be accompanied diffuse dull headaches.

However, it is important to point out that increased intracranial pressure can also lead to transitory but intense headaches. One possible explanation for the development of such acute pain is a periodic obstruction of the ventricular system (e.g., ball-valving of a mass *within* the ventricular system or intermittent compression of a pedunculated mass *upon* the system). A change in posture, exertion, coughing, or the Valsalva manoeuvre can all lead to such periodic obstruction. Acute onset headaches can also occur as a result of abnormal pressure waves or "plateau" waves. These waves, originally described by Lundberg (1960), are due to a vasodilatatory cascade consisting of: (i) a rise in blood volume as a result of vasodilatation, (ii) a decrease in cerebral perfusion pressure,

and (iii) a sharp elevation in intracranial pressure, as reported by Rosner and Becker (1984). According to Castellani et al. (2009), the normal autoregulatory response which would otherwise induce vasoconstriction is lost (or at least delayed) during plateau waves. Pressure waves can last anywhere from 5 to 30 min, which coincides with the rapid-onset, short-duration headache described by patients who have documented plateau waves.

Despite the value of intracranial pressure in forecasting brain tumor headaches, an important limitation must be addressed. Markers of intracranial pressure (e.g., papilledema, ventricular shifts or compression) do not systematically predict headache pain in patients with brain tumors. This may result from the lack of specificity provided by these clinical and radiological markers. In other words, papilledema or ventricular shifts may be good markers of increased intracranial pressure, but they are not specifically tied to the appearance of headaches. Obtaining more direct measures of brain, blood, or cerebrospinal fluid (CSF) parameters may help establish a closer link between intracranial pressure and distal traction on pain sensitive structures. Along these lines, Loghin and Levin (2006) recently argued that we should turn our attention to the measurement of CSF dynamics, since changes here may be important in helping to predict when increased intracranial pressure is associated with brain tumor headaches. Interestingly, neurosurgeons have known for quite a while (since the 1940s) that a progressive distension of the lateral ventricle with a balloon during surgery provokes homolateral headache pain. This is thought to occur because of an ensuing irritation of adjacent pain sensitive structures/vessels. In the same manner, saline injections into the ventriculo-subarachnoid system stretches arteriovascular networks, activating nociceptive afferents which can provoke pain along venous and arterial branches, as originally reported by Fay (1940) – see Fig. 33.2 for a depiction of tumor growth effects on trigemino-vascular free-nerve endings).

Unfortunately, researchers have not capitalized on these original findings, and so there is currently a remarkable lack of data describing the role played by

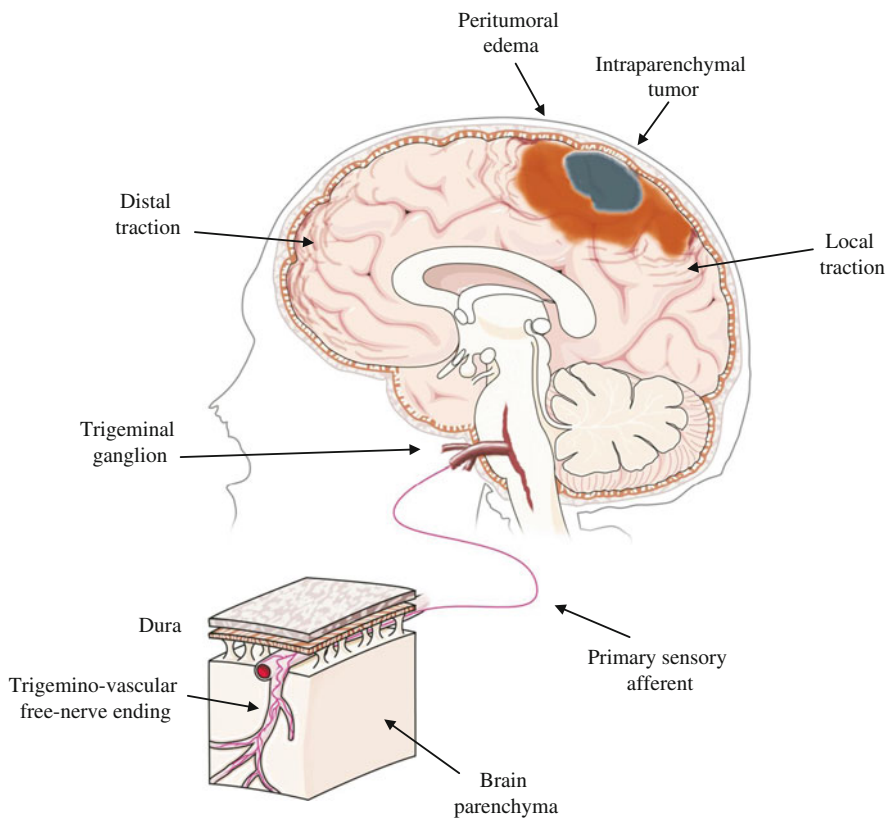

Fig. 33.2 Innervations of dura and blood vessels by branches of the trigeminal nerve terminate within the trigeminocervical complex extending from the brainstem to the dorsal horns of C1 and C2. According to the traction hypothesis, expanding tumor tissue and peri-tumoral edema produces a progressive irritation of intracranial pain-sensitive structures. Depending on the presence or absence of raised intracranial pressure, traction-effects can be either far removed or located close to the presenting lesion, resulting in headaches that are, respectively, described as either diffuse or well circumscribed in nature

CSF circulatory dynamics in brain tumor headaches. To address this limitation, future studies should obtain explicit measures of CSF pressure and flow using non-invasive techniques to measure CSF flow through the cerebral aqueduct, foramen of Monro, or the prepontine cistern using MR imaging with phase-contrast. With this technology, McGirt et al. (2006) found that occipital headaches were strongly associated with hindbrain CSF flow abnormalities, even in the absence of visible compression on MR imaging. Measuring CSF flow, therefore, may help detect subtle pathological changes (e.g., arachnoid scarring and minor occlusions of the ventricular system) missed by conventional MR scans. CSF obstruction may also explain why some patients continue to report headaches even after successful surgical debulking. Actually, as reported by Pfund et al. (1999) approximately 15% of patients with pre-treatment headaches report persistent post-treatment headaches. Despite the possibility that such patients present with idiopathic rather than symptomatic headaches, the prospect of continued CSF flow obstruction remains. Future research in this field is needed to illuminate this possibility.

Cranial or Cervical Nerve Compression

While direct compression of cranial (e.g., trigeminal) and cervical (C1 and C2) nerve roots is a possible cause of brain tumor headaches, a large number of neuro-oncology patients present no direct evidence of nerve compression or entrapment, despite reporting headache pain. Vazquez-Barquero et al. (1994) reported that nerve compression, in fact, is very rarely suspected as a cause of brain tumor headache. According to McGirt et al. (2006), even in patients with Chiari I malformations, nerve compression resulting from the downward displacement of posterior fossa structures into the foramen magnum does not always cause headaches. Furthermore, the pain described by patients suffering from brain tumor headaches is very different from the intense, paroxystic pain felt when sensory afferents are stretched or compressed, as in the case of trigeminal neuralgia, as summarized by Kunkle et al. (1942).

When cervical nerve compression does occur, the associated headache may be accompanied by muscle tenderness and the presence of myofascial trigger points. In this situation, headaches would probably be aggravated by neck movements and external pressure over the upper cervical or occipital region on the symptomatic side.

In cases where the tumor is located near the cervicomedullary junction, Hashiguchi et al. (2007) reported that entrapment of the occipital nerve can cause symptoms which mimic occipital neuralgia (a condition characterized by chronic pain in the upper neck, back of the head and behind the eyes. Pain localized in the back of the head and up to or behind the eye, therefore, suggests a posterior fossa localization, and indicates a possible, albeit rarely occurring, compression of the greater occipital nerve, as reported by Garza (2007). More frequently, infratentorial lesions produce pain which can be referred to one or more regions of the head or face. Since this type of presentation is also true of cervicogenic headaches, it is important to consider the set of characteristics which generally indicate the presence of a cervicogenic, as opposed to neoplastic headaches. Symptoms more closely tied to cervicogenic headaches include: (i) pain which begins in the occipital region *and then* progressively spreads upwards into the head, (ii) pain which can be made worse (or actually initiated) by head or neck movements, and (iii) the presence of marked tenderness in the suboccipital region.

Peripheral Sensitization

In cases where intracranial pressure produces a prolonged irritation of pain sensitive structures, afferent branches innervating cerebral, venous, and pial vessels may eventually release pro-inflammatory neuropeptides at the site of inflammation, further enhancing vascular oedema and the consequent infiltration of immune cells. Welch (2003) discussed the fact that this focal, antidromic, reaction is known as neurogenic inflammation, a phenomenon which predominantly involves the release of substance P and calcitonin gene-related peptide (CGRP), and which is thought to underlie some forms of refractory headache pain. Substance P and CGRP facilitate plasma protein extravasation, vascular permeability, and mast cell degranulation, each of which contribute to the peripheral sensitization of nociceptive fibers (Goadsby 2009). If prolonged, neurogenic inflammation can lead to

structural changes in dura matter which will maintain headache pain well beyond the resorption of intracranial pressure according to Bendtsen (2000). Although neurogenic inflammation plays a key role in the development of idiopathic headache, it is not yet clear what percentage of intractable headache pain in brain tumor patients is attributable to this prolonged inflammatory response. Addressing this question is particularly relevant since brain tumors normally release pro-inflammatory agents as reported by Nitta et al. (1994), adding to the *chemical soup* already present as a result of mechanical irritation.

Central Sensitization and Impaired Brainstem Inhibition

Over the last few decades, the basic neuroscience of brain tumor headache has focused on the irritation of pain sensitive pericranial structures. More recently, however, Bartsch et al. (2003) have studied in greater detail the central sensitization of second-order trigeminovascular neurons and the impaired response of mesencephalic modulatory neurons; these are now considered as key players in the development and maintenance of prolonged headache pain. Thus, in predisposed individuals, prolonged irritation from pericranial structures can lead to the sensitization of trigeminal convergent neurons. This induces: (i) a reduction in the activation threshold of nociceptors, (ii) an increased response to afferent stimulation, and (iii) an enlargement of peripheral receptive fields. These mechanisms are consistent with the development of prolonged, refractory headache pain in patients presenting with primary supratentorial lesions, and offer an explanation for why surgical decrease in mass effect does not systematically eradicate all pain in all patients.

Strassman et al. (1996) reported that sensory afferents originating from meninges and cranial vessels terminate within the medullary dorsal horn of the caudal trigeminal nucleus whereupon they synapse onto convergent neurons. Prolonged stimulation from primary afferents provokes local hypersensitivity to painful drives. Local segmental hypersensitivity is considered a hallmark of central sensitization and has, historically, been very difficult to control. This underscores the importance of quickly addressing initial complaints of pain. It is important to point out, however, that increased excitability to converging synaptic inputs may additionally result from a decrease in local segmental inhibition. Nociceptive drives entering spinal and trigemino-cervical neurons are subject to modulation by descending inhibitory efferents arising from brainstem nuclei, including the periaqueductal grey (PAG), the locus coeruleus, and the nucleus raphe magnus, as reported by Behbehani (1995). Under normal conditions, endogenous inhibitory responses produce profound antinociception even on trigeminovascular inputs (Leonard et al. 2008). Interestingly, dysfunctional pain-modulating circuits in the brainstem have recently been found in patients suffering from migraine (Sandrini et al. 2006) and tension type headache (Pielsticker et al. 2005), suggesting a pathogenic contribution of inhibitory systems in headache pain. The possibility of deficient brainstem inhibition and/or segmental hypersensitivity resulting from prolonged pericranial irritation as a cause of refractory headache pain in neuro-oncology patients remains to be tested. Doing so could explain why some patients remit from neoplastic headache pain, while others do not.

Veiling Headache Pain Because of Tumor-Induced Sensorial Defects

Although the growth of a mass lesion can produce headache pain, it can also lead to significant sensory deficits, thus interfering with the proper processing of pain intensity and/or unpleasantness. This possibility was originally raised by Kunkle et al. (1942) who noticed that some of their neuro-oncology patients showed apathy, especially when the tumor was located near the frontocallosal region. This affliction can lead to a deficiency in the proper processing and the articulation of pain. Thus, when patients suffer from apathy, headache pain might be under-reported, possibly biasing overall prevalence estimates.

Despite the importance of paying attention to the possibility of tumor-induced sensorial deficits, very little research has been carried out on this issue. One exception is the work carried out by Greenspan et al. (1999), who showed that neoplastic lesions involving the parietal operculum, either alone or with the adjacent posterior insula, lead to elevated heat and pin-prick pain thresholds. Interestingly, the authors

also found that cold-pain tolerance was greater on the hand contralateral to the lesion, especially when the tumor involved a large part of the insula. Since cold-pain tolerance involves more affective/motivational aspects of pain than threshold tests, this confirms recent suggestions by Apkarian et al. (2005) which propose that the insula is involved in both affective and sensory/discriminative processes. Finally, it is important to point out that lesions which spared the parietal operculum were associated with normal threshold values. These findings suggest that the functional integrity of nociresponsive neurons located within the parietal operculum are essential to the proper processing of painful signals and may alter the perception of headache pain when compromised by a nearby lesion.

Distinguishing Surgical from Brain Tumor Headaches

In most instances, patients with primary or metastatic brain tumors will require some form of surgical intervention. This means that surgery-induced pain (i.e., cranial or headache pain) is a likely prospect. Important to clinicians is the fact that neurosurgery-induced headaches display a different set of characteristics and a more predictable evolution than tumor-induced headaches. For example, surgical pain is somatic in nature and usually remains confined to the affected dermatome. This is not the case for brain tumor headaches. Furthermore, surgical headaches are typically characterized as pulsating or pounding, much like migraine headaches but unlike brain tumor headaches, as described by de Gray and Matta (2005). Finally, post-craniotomy headaches appear within the first 48 h of surgery, and rapidly wane thereafter. Such fleeting pain is not a common presentation for brain tumor headaches.

Interestingly, patients who suffer from neoplastic headaches commonly report an alleviation of their symptoms following surgery. This improvement strongly suggests that patients must have suffered from a variant of hypertension headache, and indicates that debulking surgery must have decreased the ill-effects of prolonged traction on pain sensitive structures. It appears, therefore, that alleviating intracranial hypertension, by any means, including surgery, will help to reduce the tension-type pain which develops contemporaneously with elevated pressure. The clinical price to be paid for neurosurgery is the possible appearance of temporary post-craniotomy pain. Despite this possibility, such pain-for-pain substitutions are warranted since post-operative pain is much less severe than hypertensive headache pain, not to mention clinically defensible.

Although post-craniotomy pain is common, it is not ubiquitous, and appears to be closely tied to the surgical approach chosen and to the cranial region involved. Skull base surgeries such as sub-occipital or sub-temporal craniotomies are particularly prone to the development of severe post operative pain, as observed by Vijayan (1995). Standard pterional craniotomies must also be included among the group of usual suspects since they often provoke intense post-surgical pain. In view of the fact that skull base and pterional surgeries produce significant pain, one can presume that pain sensitive structures are significantly more compromised during these interventions, as opposed to high convexity surgeries. This is consistent with anatomical data – and our own clinical experience – showing that soft tissues, dura matter, and pericranial muscles found near the skull base (all proven pain sensitive structures) are massively violated during sub-occipital, sub-temporal, and pterional craniotomies. In further support of this explanation, Rocha-Filho et al. (2007) recently confirmed that post-craniotomy patients suffering from headache pain have greater masticatory muscle tenderness and greater joint limitations than patients without headaches, thus highlighting the importance of preserving muscle integrity if post-craniotomy pain is to be minimized.

Finally, it is important to note that, compared to other types of surgery, craniotomies are usually considered at the lower end of the pain intensity spectrum. This may explain why post-operative pain is not regarded as a clinical priority in the neurosurgical context. We must also remember that there is a constant need for the neurosurgery staff to preserve and assess the wakefulness of patients. Thus, aggressive analgesic treatments, along with their accompanying side-effects, may be ill-advised. Nevertheless, it is estimated that at least 60% of patients will complain of post-craniotomy pain. This estimate advocates for the expenditure of adequate analgesic use in these patients. Interestingly, a study conducted by Stoneham and Walters (1995) revealed that opiophobia among neuroanesthetists constitutes a continuing

barrier to the ultimate resolution of post-operative pain. The authors found that even if 97% of consultant members of the Neuroanaesthesia Society of Great Britain used intramuscular codeine for post-operative analgesia, and even if most members thought it provided inadequate analgesia, only 3% of those surveyed would ever consider using stronger opioids during the post-operative period. The remaining 97% would not consider stronger opioids because of prevailing fears regarding cardio-respiratory depression and altered consciousness (i.e., traditional prejudices against opioids). Clearly, more work is needed to address these (nevertheless) legitimate fears, while also encouraging the proper control of post-operative pain.

Adjuvant Therapies as Pain Inducers

Following the surgical resection of a mass lesion, adjuvant chemotherapy and/or ionizing radiotherapy is often necessary. These additional treatments do not systematically cause pain in neuro-oncology patients, but have been known to do so in a small percentage of cases. For example, Cross and Glantz (2003) reported that acute radiotherapy-induce encephalopathy can occur within two weeks of radiation treatment onset, and can cause headache pain because of white matter edema (secondary to diffuse myelin sheath damage) and an ensuing rise in intracranial pressure. Treatment with corticosteroid therapy is recommended to alleviate this type of headache pain.

Chemotherapeutic agents can also cause temporary headaches in neuro-oncology patients. For example, temozolomide, one of the most commonly used drugs to treat malignant gliomas, can cause headaches in up to 25% of patients. Plotkin and Wen (2003) reported that thalidomide, methotrexate, cisplatin, etoposide, imatinib, and hydroxyurea may also cause headaches. Unfortunately, the underlying neurobiology of chemotherapy-induced headache pain is still poorly understood. One possible explanation is that chemotherapeutic agents produce oxidative stress, alter cytokine regulation and/or induce deficits in neuronal repair, all of which can lead to decreased central nervous system function, inflammation, and increased pain. This hypothesis is also consistent with a growing amount of research showing that the chemotherapy agents most closely associated with inflammatory cytokine release are also the most likely to cause neuropathic pain. Additional research is necessary to identify patients most at risk of developing neuropathic or vascular pain following the use of chemotherapeutic agents to treat their malignancy. Prospective studies that evaluate inter-individual differences in circulating and central nervous system cytokine concentrations are also needed to clearly establish the putative link between chemotherapy, inflammation, and pain.

Conclusion

Despite historical attempts to establish headache pain as a pathognomonic marker of brain tumor, the prevalence of headache pain in neuro-oncology patients is insufficiently high, and its presentation too diverse to justify using this symptom as a diagnostic hallmark. Among neuro-oncology patients, intracranial pressure and traction upon pain sensitive structures remains the most likely cause of headache pain. However, it is clear that for some patients, peripheral and central sensitization contributes to the pain felt during *and following* the removal of their tumor. Finally, it is important to point out that despite the absence of pain receptors in brain parenchyma, neurosurgery and adjuvant chemo-radiation therapy can be a source of pain and discomfort to patients. This is often overlooked in our desire to treat the underlying malignancy, but deserves our full attention if we are to help patients maintain elevated quality of life levels for as long as possible.

References

Apkarian AV, Bushnell MC, Treede RD, Zubieta JK (2005) Human brain mechanisms of pain perception and regulation in health and disease. Eur J Pain 9:463–484

Bartsch T, Goadsby PJ (2003) Increased responses in trigeminocervical nociceptive neurons to cervical input after stimulation of the dura mater. Brain 126:1801–1813

Behbehani MM (1995) Functional characteristics of the midbrain periaqueductal gray. Prog Neurobiol 46:575–605

Bendtsen L (2000) Central sensitization in tension-type headache--possible pathophysiological mechanisms. Cephalalgia 20:486–508

Castellani G, Zweifel C, Kim DJ, Carrera E, Radolovich DK, Smielewski P, Hutchinson PJ, Pickard JD, Czosnyka M

(2009) Plateau waves in head injured patients requiring neurocritical care. Neurocrit Care 11:143–150
Cross NE, Glantz MJ (2003) Neurologic complications of radiation therapy. Neurol Clin 21:249–277
Dalessio DJ (1978) Mechanisms of headache. Med Clin North Am 62:429–442
de Gray LC, Matta BF (2005) Acute and chronic pain following craniotomy: a review. Anaesthesia 60:693–704
Dousset V, Henry P, Michel P (2000) Epidemiology of headache. Rev Neurol (Paris) 156(Suppl 4):4S24–4S29
Fay T (1940) A new test for the diagnosis of certain headaches: the cephalalgiogram. Dis Nerv Syst 1:312–315
Forsyth PA, Posner JB (1993) Headaches in patients with brain tumors: a study of 111 patients. Neurology 43:1678–1683
Garza I (2007) Craniocervical junction schwannoma mimicking occipital neuralgia. Headache 47:1204–1205
Goadsby PJ (2009) Migraine – a disorder involving trigeminal brainstem mechanisms. In: Basbaum A, Bushnell MC (eds) Science of pain. Elsevier, Oxford, pp 461–468
Greenspan JD, Lee RR, Lenz FA (1999) Pain sensitivity alterations as a function of lesion location in the parasylvian cortex. Pain 81:273–282
Hashiguchi A, Mimata C, Ichimura H, Kuratsu J (2007) Occipital neuralgia as a presenting symptom of cervicomedullary dural arteriovenous fistula. Headache 47: 1095–1097
Kunkle EC, Ray BS, Wolff HG (1942) Studies on headache: the mechanisms and significance of the headache associated with brain tumor. Bull N Y Acad Med 18:400–422
Leonard G, Mathieu D, Kenny B, Blanchard J, Goffaux P, Marchand S (2008) Evidence of descending inhibition deficits in atypical trigeminal neuralgia. Pain Res Manage 13:11(abstr)
Loghin M, Levin VA (2006) Headache related to brain tumors. Curr Treat Options Neurol 8:21–32
Lundberg N (1960) Continuous recording and control of ventricular fluid pressure in neurosurgical practice. Acta Psychiatr Scand Suppl 36:1–193
McGirt MJ, Nimjee SM, Fuchs HE, George TM (2006) Relationship of cine phase-contrast magnetic resonance imaging with outcome after decompression for Chiari I malformations. Neurosurgery 59:140–146
Nitta T, Ebato M, Sato K, Okumura K (1994) Expression of tumour necrosis factor-alpha, -beta and interferon-gamma genes within human neuroglial tumour cells and brain specimens. Cytokine 6:171–180
Pfund Z, Szapary L, Jaszberenyi O, Nagy F, Czopf J (1999) Headache in intracranial tumors. Cephalalgia 19:787–790
Pielsticker A, Haag G, Zaudig M, Lautenbacher S (2005) Impairment of pain inhibition in chronic tension-type headache. Pain 118:215–223
Plotkin SR, Wen PY (2003) Neurologic complications of cancer therapy. Neurol Clin 21:279–318
Rocha-Filho PA, Fujarra FJ, Gherpelli JL, Rabello GD, de Siqueira JT (2007) The long-term effect of craniotomy on temporalis muscle function. Oral Surg Oral Med Oral Pathol Oral Radiol Endod 104:e17–e21
Rosner MJ, Becker DP (1984) Origin and evolution of plateau waves. Experimental observations and a theoretical model. J Neurosurg 60:312–324
Sandrini G, Rossi P, Milanov I, Serrao M, Cecchini A, Nappi G (2006) Abnormal modulatory influence of diffuse noxious inhibitory controls in migraine and chronic tension-type headache patients. Cephalalgia 26:782–789
Schankin CJ, Ferrari U, Reinisch VM, Birnbaum T, Goldbrunner R, Straube A (2007) Characteristics of brain tumour-associated headache. Cephalalgia 27:904–911
Stoneham MD, Walters FJ (1995) Post-operative analgesia for craniotomy patients: current attitudes among neuroanaesthetists. Eur J Anaesthesiol 12:571–575
Strassman AM, Raymond SA, Burstein R (1996) Sensitization of meningeal sensory neurons and the origin of headaches. Nature 384:560–564
Suwanwela N, Phanthumchinda K, Kaoropthum S (1994) Headache in brain tumor: a cross-sectional study. Headache 34:435–438
Vazquez-Barquero A, Ibanez FJ, Herrera S, Izquierdo JM, Berciano J, Pascual J (1994) Isolated headache as the presenting clinical manifestation of intracranial tumors: a prospective study. Cephalalgia 14:270–272
Vijayan N (1995) Postoperative headache in acoustic neuroma. Headache 35:98–100
Wang HZ, Simonson TM, Greco WR, Yuh WT (2001) Brain MR imaging in the evaluation of chronic headache in patients without other neurologic symptoms. Acad Radiol 8: 405–408
Welch KM (2003) Contemporary concepts of migraine pathogenesis. Neurology 61:S2–S8

Chapter 34

Headache Associated with Intracranial Tumors

Luca Valentinis and Antonio Palmieri

Abstract A secondary headache in patients with a brain tumor is defined in the International Classification of Headache Disorders (ICHD-II) in subchapter 7.4. Headache can be attributed to a brain tumor if it develops in close temporal relation to the neoplasm and improves after effective treatment. Despite the fact that headache is known as a cardinal sign of intracranial tumor, special analysis of this complaint is relatively rare in the literature. The studies performed after the advent of modern neurodiagnostic techniques have pointed out that the "classic" brain tumor headache (i.e., severe, worse in the morning, with nausea and vomiting) is uncommon. Although there are no absolute indications that the headache is related to a brain tumor, a few predictive factors for an intracranial mass (the so called "red flags") can guide the physician in establishing an accurate diagnosis.

Keywords Secondary headache · Brain tumor · Neurodiagnostic techniques · Nausea · Papilledema · Vomiting

Introduction

Headache is one of the most frequent complaints of patients seeking medical care. Headaches secondary to organic brain diseases, including those caused by brain tumors, constitute less than 10% of all recorded headaches (Loghin and Levin 2006). Despite this relatively rare incidence, however, patients with headaches are often concerned that they may have a brain tumor. The prevalence of headache in patients with intracranial tumors varies in different epidemiological studies. Considering only the studies performed after the advent of modern neurodiagnostic techniques, it ranges between 32.2% (Vazquez-Barquero et al. 1994) and 71% (Suwanwela et al. 1994) in unselected series. Although headache may be the patient's first complaint in a quarter of cases (Pfund et al. 1999), it very seldom occurs as the sole presenting symptom (Vazquez-Barquero et al. 1994). More frequently, brain tumor headaches are accompanied by nausea, emesis, papilledema, blurred vision (in the context of intracranial hypertension), personality changes, seizures, and/or other focal neurological signs (Goffaux and Fortin 2010).

Clinical Features of Headache Associated with Intracranial Tumors

Special analysis of headache associated with intracranial tumors is relatively rare in the literature. Moreover, data regarding its characteristics are often discordant. These discrepancies are most likely due to differences in patients' samples, in study methodology and in the definition of intracranial tumor headache. The "classic" brain tumor headache is mild at onset, begins when the patient awakens in the morning, disappears shortly after he or she arises, and recurs the following morning (De Angelis and Posner 2009). Changes in position, coughing, straining and Valsalva's maneuver may exacerbate headache (Giglio and Gilbert 2004).

L. Valentinis (✉)
Neurology Unit, San Tommaso Dei Battuti Hospital,
30026 Portogruaro, Italy
e-mail: luca.valentinis@tin.it

M.A. Hayat (ed.), *Tumors of the Central Nervous System, Volume 4*,
DOI 10.1007/978-94-007-1706-0_34,

The headaches gradually increase in frequency, duration, and severity until, in their later stages, they are almost constant and they are associated with vomiting (Ropper and Brown 2005; De Angelis and Posner 2009). However, the "classic" brain tumor headache is uncommon, occurring in less than 20% of cases (Forsyth and Posner 1993; Valentinis et al. 2010). On the contrary, the general consensus seems to be that brain tumor headaches usually have no specific features (Goffaux and Fortin 2010). Pain is usually located bilaterally over the frontal region (Forsyth and Posner 1993; Valentinis et al. 2010), non-throbbing in quality (Suwanwela et al. 1994; Schankin et al. 2007) and of moderate intensity, requiring common analgesics for sufficient control (Suwanwela et al. 1994; Schankin et al. 2007; Valentinis et al. 2010); it is rarely associated with nausea or vomiting (Valentinis et al. 2010). The headaches are usually intermittent, they last for few hours and present no typical daily distribution (Suwanwela et al. 1994; Pfund et al. 1999; Valentinis et al. 2010). Nocturnal awakening because of pain occurs in only a small proportion of patients and is by no means diagnostic (Forsyth and Posner 1993; Ropper and Brown 2005). To complicate matters, brain tumor headache may mimic a variety of primary headache types, such as migraine, tension-type or cluster headache (Suwanwela et al. 1994). Furthermore, brain tumors may only increase a patient's pre-existing chronic headaches (De Angelis and Posner 2009).

Risk Factors for Brain Tumor-Related Headache

It was reported by De Angelis (2001) that the malignant astrocytomas (anaplastic astrocytoma and glioblastoma multiforme) are the tumors most commonly associated with headache. Beside tumor type, other factors may be associated with an increased risk of headache. Forsyth and Posner (1993) reported a link between tumor area and the presence of headache, but their findings have not been confirmed in later studies (Pfund et al. 1999; Schankin et al. 2007). As documented in many studies (Suwanwela et al. 1994; Pfund et al. 1999, Valentinis et al. 2010), headache seems to be much more common in tumors situated below the tentorium cerebelli than in those above. As stated by Loghin and Levin (2006), the role of increased intracranial pressure (ICP) in generating headache remains controversial in tumor cases. Nevertheless, several authors (Forsyth and Posner 1993; Suwanwela et al. 1994; Valentinis et al. 2010) found a trend towards an increased prevalence of tumor-related headache in association with increased ICP. Furthermore, the ICHD-II distinguished between headache in brain tumor patients with and without increased ICP (Headache Classification Committee of the International Headache Society 2004). In addition to tumor-related factors, a history of prior headaches seems to be associated with a higher risk to develop a headache secondary to an intracranial tumor (Forsyth and Posner 1993; Schankin et al. 2007; Valentinis et al. 2010).

Headache in Children with Brain Tumors

Headache frequently heralds the development of a brain tumor in a child. Headache, however, is suffered by 5–30% of elementary school children (Linet and Stewart 1984), whereas the annual incidence of brain tumor in this age group approximates only three per hundred thousand (0.003%) (Young and Miller 1975; Schoenberg et al. 1976). Uncritical imaging would result in a large number of normal neuroimaging studies (Dobrovoljac et al. 2002). In a large retrospective study of the Childhood Brain Tumor Consortium (1991), analysing 3291 patients, more than 60% of the children with brain tumors experienced headache prior to their first hospitalization. This symptom was more common in infratentorial tumors (70%) than in supratentorial ones (58%). However, regardless of tumor location, at diagnosis the duration of headache was less than 1 year in most cases and less than 1% of children with headache had no other recorded symptom. Furthermore, fewer than 3% of children with headache and a brain tumor had no abnormality on neurological examination. These data are consistent with the recent study of Wilne et al. (2006), who reported that the majority of 82 children with brain tumor and headache as initial manifestation will have abnormal neurological findings (above all papilledema, cranial nerve signs or cerebellar signs) at the moment of diagnosis. The authors stated that among children who present with a single symptom (other than seizures) and have a normal neurological

examination and normal growth very few will have an underlying brain tumor.

Headache in Cancer Patients

About 15% of cancer patients complain of headache (Clouston et al. 1992). In one-third of cases the cause is intracranial metastases (Clouston et al. 1992; Christiaans et al. 2002). Christiaans et al. (2002), using multivariate logistic regression analysis, found that headache duration of less than 10 weeks, emesis and headache pain not of tension type were independent predictors of intracranial metastasis. Despite these predictors, few patients could be excluded from undergoing MRI study, because of a low specificity. Therefore the general consensus is that MRI of the brain is warranted in every cancer patient with new or changed headache of recent onset (Loghin and Levin 2006; Kirby and Purdy 2007).

Uncommon Headaches in Patients with Intracranial Tumors

Headache associated with brain tumors has no specific features and may mimic a variety of primary headache types, especially tension-type headache and migraine. However, it is not unusual that its phenotype resembles less common primary headache syndromes. This latter occurrence is relatively frequent in the case of pituitary tumors: Levy et al. (2005) reported a series of 84 patients with pituitary micro- and macroadenomas and troublesome headache and found that 5% had short-lasting unilateral neuralgiform headache attacks with conjunctival injection and tearing (SUNCT), 4% had cluster headache and 1% had hemicrania continua. On the contrary, paroxysmal headache is associated with colloid cyst of the third ventricle or other pedunculated tumors that block the flow of cerebrospinal fluid (CSF). The headache occurs suddenly and has a brief duration (several minutes to a few hours) and is characterized by severe and bi-frontal pain, precipitated by changes in position. It may be associated sometimes with loss of consciousness, sudden "drop attacks", vertigo, nausea, vomiting, and even sudden death (Loghin and Levin 2006; Kirby and Purdy 2007).

Pathogenesis of Brain Tumor-Related Headache

The brain parenchyma is insensitive to pain as well as are the ependyma, the choroid plexus, the skull, the pia mater, the arachnoid, and the dura mater at the vertex. The pain is the result of the stimulation of nociceptive terminals located in intra- and extracranial structures, including: skull base cerebral arteries; intracranial venous sinuses; dura mater at the skull base; dural, arachnoid, and pial vessels; eyes, ears, nasal cavity, and sinuses; the Vth, IXth, and X cranial nerve as well as the first three cervical nerves; skin, subcutaneous tissue, muscles, vessels, and periosteum in the skull (Boiardi et al. 2004). The tumor can cause headache by traction on the intra- and extracranial pain-sensitive structures or, in rare cases, compression and entrapment of cranial (e.g., trigeminal, glossopharyngeal, or vagus) and cervical (C1 and C2) nerve roots. Alternatively, the mass can determine an obstruction to the CSF efflux leading to intracranial hypertension. The headaches can present different clinical manifestations even in the presence of tumors sharing similar anatomic site and histologic characteristics. The disease duration as well as the tumor growth speed are thought to play a key role in the development of the headache. According to most authors, in the slowly growing tumors (e.g., meningiomas), the headaches are less frequent and would appear in the late stages, since the nociceptive structures could adapt to the modification induced by the tumor. On the other hand, the headache would be more frequent and early in onset in fast growing tumors such as high grade astrocytomas and methastases, in which the brain compensative mechanism would be prevented by the rapid and aggressive development of the neoplasm. An increase in ICP might play an important role in the development of the headache in patients with brain tumor. The headache associated with obstructive hydrocephalus is presumed to be determined by the traction and/or dislocation of the periventricular nociceptive structures. In the other cases of raised ICP the underlying mechanisms causing headache are still being debated. However, the speed of ICP increase appears to be critical: a tumor constricting the foramen of Monroe or the aqueduct can provoke a sudden raise in ICP, usually resulting in paroxysmal headache. On the other hand, gradual

increase of the ICP may be associated with mild or no headache. The pituitary adenomas constitute a separated chapter. It has long been thought that headaches associated with pituitary adenomas may be caused by the traction on the dura mater operated by the tumor growing within the sella turcica and, at least in part, to the compression of the ophthalmic branch of the trigeminal nerve and the internal carotid artery following the infiltration of the cavernous sinus in which these structures are located. Nevertheless, these mechanisms have not been confirmed in a recent study by Levy et al. (2004). The authors examined 63 individuals affected by hypophyseal tumor in which a headache was reported by 70% of the sample. However, the "Clinical Headache Score" – an index of headache severity – was not correlated neither with the size of adenoma nor with the extent of the cavernous sinus invasion. On the basis of those findings, the authors have hypothesized that the headache associated with pituitary tumors could be secondary to biochemical and neuroendocrine rather than mechanical factors, also taking into account that headache is particularly frequent in patients with secreting adenomas – first of all prolactinomas – and it is usually dramatically improved by endocrine therapies, including bromocriptine and octreotide. However, it cannot be excluded that mechanical factors play a key role in a minority of cases, particularly when headache is accompanied by ipsilateral trigeminal autonomic symptoms (e.g., cluster headache, SUNCT).

Neuroimaging Studies in the Evaluation of Headache

Neuroimaging studies must be considered as part of the work up in every patient with headache and an unexplained abnormal finding on the neurological examination (Loghin and Levin 2006). Otherwise, their value is controversial. As reported by Frishberg (1994) and Evans (1996), the chance of a brain tumor as the cause of headache in a patient with normal neurological examination is exceedingly low (about 1%), but that chance is never zero (Kirby and Purdy 2007). Therefore, neuroimaging is not usually warranted in headache patients with normal neurological examination, but it should be considered in the presence of the following clinical parameters (the so-called "red flags"): headaches of new onset in an adult aged >40; significant change in previous headache pattern; headaches subacute and progressive in nature (over a period of days/weeks); headaches not resembling any of the primary headaches; headaches that awaken the patient repeatedly from sleep or occur immediately on waking; headaches precipitated or exacerbated by exertion; headaches associated with episodes of confusion, seizures, change in personality; headaches that do not respond to reasonable therapy (Loghin and Levin 2006; Goffaux and Fortin 2010).

Treatment of Headache Associated with Intracranial Tumors

In most cases, headache associated with brain tumors disappears after surgery (Pfund et al. 1999; Valentinis et al. 2010). Before the operation and when surgery is not recommended, the therapy may vary according to the severity of the disease, to the type of tumor and to the patient's functional status. For patients presenting with headache and evidence of cerebral edema, corticosteroids are the mainstay of treatment. Their anti-edema effect is probably due to the decrease of the capillary permeability of the blood-brain barrier as a result of decreased expression of vascular endothelial growth factor (Loghin and Levin 2006). The optimal dose and best preparation of corticosteroids are not established: the dosage should probably vary with the nature of the problem and its severity (De Angelis and Posner 2009). Dexamethasone is the most potent corticosteroid (nearly six times as potent as prednisone) and it may be preferred to other synthetic glucocorticoids because of its relatively long half-life, limited mineral corticoid effect and diminished inhibition of leukocyte migration (Loghin and Levin 2006; De Angelis and Posner 2009). In patients with brain tumors the effective dose of dexamethasone is usually 2–4 mg twice daily, although an initial dose of 10 mg delivered intravenously, followed by 4 mg every 6 h, may be used for brief periods (Froehler 2008). Beside corticosteroids, medical management of cerebral edema includes osmotic therapy and diuretics. Hypothermia, fluid restriction, and elevation of the head of the bed at 30° to increase jugular venous

outflow are additional general measures that should be initiated when signs of severe ICP are present (Loghin and Levin 2006; Froehler 2008). In the case of ICP secondary to hydrocephalus, patients may get some headache relief in response to oral acetazolamide; however, in the long term, these patients will require ventricular drainage and/or ventricular shunting of CSF (Loghin and Levin 2006; Froehler 2008). If no edema is present, or if headache persists despite corticosteroids, conventional analgesics and adjuvant therapies including antidepressants or anticonvulsants are appropriate. Non-steroidal anti-inflammatory drugs (NSAIDs) should constitute the first choice for patients with mild headache. Opioids are commonly prescribed for the relief of moderate to severe pain (Loghin and Levin 2006). Metastatic disease is treated symptomatically with corticosteroids and whole brain radiation, and in patients with limited numbers of metastases and a reasonable performance status, stereotactic radiosurgery or surgical resection. Palliative radiotherapy relieved headache in 82% of patients with brain metastases (Kirby and Purdy 2007).

References

Boiardi A, Salmaggi A, Eoli M, Lamperti E,and Silvani A (2004) Headache in brain tumours: a symptom to reappraise critically. Neurol Sci 25:S143–S147

Childhood Brain Tumor Consortium (1991) The epidemiology of headache among children with brain tumor: headache in children with brain tumors. J Neurooncol 10:31–46

Christiaans MH, Kelder JC, Arnoldus EPJ, Tijssen CC (2002) Prediction of intracranial metastases in cancer patients with headache. Cancer 94:2063–2068

Clouston PD, De Angelis LM, Posner JB (1992) The spectrum of neurological disease in patients with systemic cancer. Ann Neurol 31:268–273

De Angelis LM (2001) Brain tumors. N Engl J Med344:114–123

De Angelis LM, Posner JB (2009) Intracranial metastases. In: De Angelis LM, Posner JB (eds) Neurologic complications of cancer, 2nd edn. Oxford University Press, New York, pp 141–193

Dobrovoljac M, Hengartner H, Boltshauser E, Grotzer MA (2002) Delay in the diagnosis of paediatric brain tumours. Eur J Pediatr 161:663–667

Evans RW (1996) Diagnostic testing for the evaluation of headaches. Neurol Clin 14:1–26

Forsyth PA, Posner JB (1993) Headaches in patients with brain tumors: a study of 111 patients. Neurology 43:1678–1683

Frishberg BM (1994) The utility of neuroimaging in the evaluation of headache in patients with normal neurologic examinations. Neurology 44:1191–1197

Froehler MT (2008) Management of elevated intracranial pressure. In: Johnston MV, Gross RA (eds) Principles of drug therapy in neurology, 2nd edn. Oxford University Press, New York, pp 204–233

Giglio P, Gilbert MR (2004) Cancer and the nervous system: clinical features and complications. In: Bradley WG, Daroff RB, Fenichel GM, Jankovic J (eds) Neurology in clinical practice, 4th edn. Butterworth Heinemann, Philadelphia, pp 1363–1369

Goffaux P, Fortin D (2010) Brain tumor headaches: from bedside to bench. Neurosurgery 67:459–466

Headache Classification Committee of the International Headache Society (2004) The International Classification of Headache Disorders, 2nd edn. Cephalalgia 24(Suppl. 1):1–160

Kirby S, Purdy RA (2007) Headache and brain tumors. Curr Neurol Neurosci Rep 7:110–116

Levy MJ, Jager R, Powell M, Matharu MS, Meeran K, Goadsby PJ (2004) Pituitary volume and headache: size is not everything. Arch Neurol 61:721–725

Levy MJ, Matharu MS, Meeran K, Powell M, Goadsby PJ (2005) The clinical characteristics of headache in patients with pituitary tumours. Brain 128:1921–1930

Linet MS, Stewart WF (1984) Migraine headache: epidemiological perspectives. Epidemiol Rev 6:107–139

Loghin M, Levin VA (2006) Headache related to brain tumors. Curr Treat Options Neurol 8:21–32

Pfund Z, Szapary L, Jaszberenyi O, Nagy F, Czopf J (1999) Headache in intracranial tumors. Cephalalgia 19:787–790

Ropper AH, Brown RH (2005) Intracranial neoplasms and paraneoplastic disorder. In: Ropper AH, Brown RH (eds) Adams and Victor's principles of neurology, 8th edn. McGraw-Hill, New York, pp 144–167

Schankin CJ, Ferrari U, Reinisch VM, Birnbaum T, Goldbrunner R, Straube A (2007) Characteristics of brain tumour-associated headache. Cephalalgia 27:904–911

Schoenberg BS, Schoenberg DG, Christine BW (1976) The epidemiology of primary intracranial neoplasms of childhood: a population study. Mayo Clin Proc 51:51–56

Suwanwela N, Phanthumchinda K, Kaoropthum S (1994) Headache in brain tumor: a cross-sectional study. Headache 34:435–438

Valentinis L, Tuniz F, Valent F, Mucchiut M, Little D, Skrap M, Bergonzi P, Zanchin G (2010) Headache attributed to intracranial tumours: a prospective cohort study. Cephalalgia 30:387–388

Vazquez-Barquero A, Ibanez FJ, Herrera S, Izquierdo JM, Berciano J, Pascual J (1994) Isolated headache as the presenting clinical manifestation of intracranial tumors: a prospective study. Cephalalgia 14:270–272

Wilne SH, Ferris RC, Nathwani A, Kennedy CR (2006) The presenting features of brain tumours: a review of 200 cases. Arch Dis Child 91:502–506

Young JL, Miller RW (1975) Incidence of malignant tumors in U.S. children. J Pediatr 86:254–258

Chapter 35

Patients with Brain Cancer: Health Related Quality of Life

Philippe Goffaux, Kathya Daigle, and David Fortin

Abstract The last few decades have seen an increase in the amount of research dedicated to the quality of life (QOL) of cancer survivors, especially for breast and lung cancers. Unfortunately, relatively little attention has been paid to the QOL of neuro-oncology patients. Moreover, reports on the QOL of brain cancer patients are often qualitative and/or converge on a single dimension of well-being. Future QOL studies will have to focus on multiple dimensions of QOL, establishing prospective evaluations of baseline and serial parameters. Research objectives should also include the concomitant exploration of radiological, histopathological, and patient-related factors as potential predictors of QOL. Comprehensive models are particularly useful because they can help account for the reciprocal connections often observed between baseline variables, and because they promise to shed light on some of the contradictory results observed in the field, such as the presumed long-term benefits of resection. Empirical QOL data obtained within a biopsychosocial framework may guide the development of new treatment avenues and may help promote the application of focused, patient-centered support programs.

Keywords Brain tumor · Health related quality of life (HRQOL) · Neuro-oncology · QLQ-C15 · FACT-G · QLQ-C30

P. Goffaux (✉)
Department of Neurosurgery and Neuro-Oncology, Faculty of Medicine, Sherbrooke University, Sherbrooke, QC, Canada
e-mail: Philippe.goffaux@usherbrooke.ca

Introduction

For brain tumor patients, health related quality of life (HRQOL) is an important issue. This is understandable if we consider that patients are regularly confronted with serious challenges to their health. Given these challenges, understanding what defines quality of life is essential, especially if the provision of professional, compassionate care is to be encouraged. Although long neglected, HRQOL has received increased attention in the last few years.

Unfortunately, there is still no accepted standard for the definition, and measurement of HRQOL. Moreover, the concept is still evolving. In fact, we now know that HRQOL is culturally biased, varies as a function of age, and represents a multidimensional construct.

Thus, it may be unwise to seek a single, monotonic description of HRQOL. Many authors, in fact, suggest that several key concepts contribute to HRQOL, including, the subjective appreciation of physical, psychological, and emotional function, the ability to perform everyday activities, and the enjoyment of social or personal relations (Aaronson 1988; Cella and Tulsky 1990). Recognizing the multidimensional nature of HRQOL in clinical research is paramount, but potentially problematic if researchers keep using different definitions of HRQOL and different instruments to measure it. The pernicious effect of measuring HRQOL in different ways is that inter-study comparisons become nearly impossible to make.

Circumscribing a unique but comprehensive definition of HRQOL in neuro-oncology, therefore, will certainly help the field move forward.

M.A. Hayat (ed.), *Tumors of the Central Nervous System, Volume 4*,
DOI 10.1007/978-94-007-1706-0_35,

Assessing HRQOL in Neuro-oncology

Measurement of patient-rated well being has improved dramatically over the past few years, and there are now excellent HRQOL tools available in oncology and neuro-oncology. In fact, the field has progressed so much that it is no longer considers the use of physician-rated functional scores, such as the Karnofsky Performance Scale (KPS), as a valid way to measure HRQOL. Today, generic instruments exist which have gone through years of development and which have strong psychometric properties. Excellent examples include the European Organization for Research and Treatment of Cancer (EORTC) QLQ-C30, the Functional Assessment of Cancer Therapy – General (FACT-G), and, the Short Form 36 Health Survey (SF-36). The EORTC QLQ-C30 contains 30 items regrouping five functional domains (physical, role, cognitive, emotional, and social), three symptom domains (fatigue, pain, and nausea and vomiting), six single-items, and two global HRQOL scores (Aaronson et al. 1993). The QLQ-C30 must be combined with the EORTC Brain Cancer Module (BN20) in order to capture both core and disease-specific concerns (Osoba et al. 1996). The FACT-G is also a widely used instrument (Cella et al. 1993). It contains 26 items and covers physical, family, social, emotional, and functional well-being domains. Like the EORTC QLQ-C30, it has to be administered in conjunction with a brain tumor module (Br). The Br module contains 23 items and taps into symptoms which are clinically relevant to brain cancer patients (Weitzner et al. 1995; Cella et al. 2003). As a rule, the FACT-Br is more frequently used in the United States, whereas the EORTC-BN20 is more frequently used in Europe and Canada (Conroy et al. 2004). Despite being two of the most popular HRQOL instruments, the EORTC QLQ-C30 and the FACT-G have rarely been compared directly.

Studies which have tried to equate these questionnaires confirm the presence of comparable scores on physical, emotional and functional/role domains. Scores obtained on the social domain, however, remain extremely discrepant (see an excellent recent example from Holzner et al. 2006). Despite considerable overlap in structure between the QLQ-C30 and the FACT-G, complete replacement of scores from questionnaire-to-questionnaire is not possible, and the direct comparison of results from study-to-study is probably ill-advised.

The SF-36 (Ware and Sherbourne 1992) is also frequently used to assess HRQOL in neurooncology. This 36-item self-report questionnaire provides eight scale-scores reflecting physical functioning, role limitations caused by physical health problems, bodily pain, general health perception, vitality, social functioning, role limitations caused by emotional problems, and general mental health. The SF-36 was designed for use in clinical practice, health policy evaluations, and general population surveys. It was not designed for use among neuro-oncology patients and so tends to underrepresent social, psychological, and neurocognitive functions (Farace and Shaffrey 2005). Here again, the use of a module specific to patients with brain tumors should be employed to supplement the SF-36 in neurooncological settings.

A potential problem associated with the use of separate questionnaires to capture general and disease-specific effects is that long testing sessions are required. Long sessions burden patients who already have to deal with increased fatigue and concentration difficulties. To prevent this problem, a single, concise instrument should be used. The importance of brevity during testing has even pushed the EORTC quality of life group to develop a new shorter version of their widely-used core HRQOL questionnaire (i.e., their original QLQ-C30). The EORTC's new, shorter instrument, the QLQ-C15, is an extremely promising tool and its conception demonstrates that even a short questionnaire (i.e., 15 questions) can adequately measure global quality of life issues (Groenvold et al. 2006). The QLQ-C15, however, is not sensitive to disease-specific concerns (nor was it intended to be) and must be supplemented by items or modules measuring missing issues. To our knowledge, the only questionnaire currently available that measures both core and disease-specific concerns germane to neurooncology patients is the Sherbrooke Neuro-Oncology Assessment Scale (SNAS, see Goffaux et al. 2009). This instrument was recently developed in our lab and is composed of 30 items which cover seven multi-item scales. These scales include functional well-being, symptom severity/fear of death, social support/acceptance of disease, autonomy in personal care, digestive symptomatology, neurocognitive function, and pain. The SNAS is highly consistent (Cronbach alphas for all scales $\geq$0.65), and reflects the known

multidimensional nature of HRQOL (Aaronson et al. 1993; Cella et al. 1993; Groenvold et al. 2006). In addition to the questionnaire's elevated internal consistency, it adequately discriminates between patients with varying degrees of functional performance (KPS scores) and clinical status (exposure to neurosurgery, radiotherapy, and use of chemotherapy and anticonvulsants). The SNAS, therefore, demonstrates that it is possible to properly assess HRQOL while avoiding the pitfalls associated with modular testing approaches.

HRQOL in Brain Cancer Patients

A review of the literature on HRQOL in neuro-oncology confirms that high-grade glioma patients have significantly lower HRQOL scores than healthy age- and sex-matched adults (Taphoorn et al. 2005; Bosma et al. 2009). Unfortunately this information is not very informative if we cannot distinguish between general and disease-specific effects.

Regrettably, very few studies have directly compared the HRQOL scores of brain tumor patients with the HRQOL scores of patients suffering from another medical condition. One notable exception is a study conducted by Klein et al. (2001) who tested newly diagnosed glioma patients and compared their HRQOL scores to those of patients suffering from lung cancer. The authors found that brain and lung cancer patients showed much poorer overall HRQOL than healthy adults. However, compared to lung cancer patients, glioma patients reported significantly more neurological symptoms, including visual problems, motor dysfunctions, communication deficits, headaches, and epileptic seizures. Moreover, glioma patients presented with greater objectively-assessed (and subjectively-experienced) cognitive deficits. This means that malignancies affecting the brain produce condition-specific effects that are neurological and neuropsychological in nature. This agrees with logical considerations regarding brain function and with the results obtained by other studies interested in this issue (Osoba et al. 2000a; Giovagnoli et al. 2005). Interestingly, when high-grade glioma patients are compared to patients suffering from another central nervous system condition, such as multiple sclerosis or polyneuropathy, the former tend to show more problems with attentional function (Giovagnoli et al. 2005). It is important to point out, however, that the presence of greater cognitive deficits among brain cancer patients is not ubiquitous. For example, Anderson et al. (1990) showed that patients with lesions caused by tumors were significantly less affected than patients with similarly located lesions caused by stroke. In fact, cognitive impairments caused by brain tumors were generally quite mild.

This finding is likely attributable to the infiltrating nature of brain tumors which displace, rather than destroy neural tissue. Stroke, on the other hand is closely associated with neuronal death and with long-lasting loss of function. The diffuse, infiltrative growth pattern of tumor cells is a key characteristic of gliomas, and explains why neurosurgeons and neurooncologists often find extensive tumors that fail to provoke extensive deficits. This neurobiological fact must always be kept in mind when studying (and treating) neurooncology patients. Together, these findings indicate that generalities regarding HRQOL in neuro-oncology are hard to formulate. This is because too many factors (including clinical, demographic, and social variables) influence patient welfare for sweeping statements to be made. The next section, therefore, pays particular attention to the specific factors which affect HRQOL in neuro-oncology.

Biomedical Attributes as Predictors of HRQOL

As expected, factors directly associated with disease severity have a significant impact on patient well-being. For example, tumor grade (or histotype) is known to predict HRQOL, such that patients with high grade tumors report poorer HRQOL scores than patients with low grade tumors. Domains most affected by tumor grade appear to include functional status, cognitive functioning, and fear of death (Giovagnoli et al. 2005; Osoba et al. 2000a; Veilleux et al. 2010). This finding, however, must be viewed cautiously since Kayl and Meyers (2003) found that the effects of histology on patient well-being (especially cognitive function) disappear when tumor volume and tumor location are controlled for. Thus, it is possible to conclude that tumor cell proliferation/aggressiveness is not, on its own, causally related to quality of life in

brain tumor patients – although it is undeniably related to survival.

Interestingly, the results obtained by Kayl and Meyers (2003) indicate that tumor location may have an important impact on patient well-being. Unfortunately, the influence of tumor location on HRQOL and adjustment is currently inconclusive, and probably attributable to the far-reaching effects of disease which can disrupt functional circuits well beyond the site of the tumor. In spite of a tenuous link between tumor location and the appearance of circumscribed deficits, current studies indicate a tendency whereby left-sided tumors are associated with greater depressive symptoms, more memory problems, and poorer verbal abilities, while right-sided tumors are associated with greater anxiety and the presence of prosopagnosia (Hahn et al. 2003; Mainio et al. 2003). The use of adapted neuropsychological testing batteries should help validate these preliminary findings.

Treatment-related factors are another important contributor to HRQOL in neuro-oncology. Treatment in neuro-oncology typically involves surgery, radiotherapy, chemotherapy, and the use of concomitant medication. If we first consider the effects of surgery, it is clear that extent of resection positively predicts survival. However, it is still a matter of debate whether extent of resection benefits HRQOL. Part of the reason why equivocal results persist is because extent of resection is poorly quantified. Volumetric measurements are considered the accepted standard, however, many centers still rely on the surgeon's report or on the two dimensional measurement of post-operative MRI sequences. Two-dimensional measurements are a rudimentary way of calculating tumor volume. This approach involves calculating the largest cross-sectional area of the enhancing tumor. It continues to be used in clinical settings to track the progression of brain tumors and to facilitate the comparison of results between patients. Using this approach, a patient's cancer may be considered clinically progressive when, on follow-up MRI scans, the product of the largest perpendicular diameters of his/her contrast enhancing tumor is $\geq$25% (worsening of neurological status is also indicative of progression). However, when a precise quantification of the tumor is required, volume measurements are preferred. Volume measurements are obtained by calculating individual axial areas on each MRI slice, multiplying each by the appropriate slice thickness (typically 1 mm), and summing the subvolumes. Volume measurements provide the precision necessary for researchers to conduct reliable investigations of the effects of surgery and tumor volume. Unfortunately this approach is rarely used to study the link between tumor volume and HRQOL.

Another reason why it is difficult to provide strong conclusions regarding the benefits of cytoreduction by surgery is because surgery is not an option for all patients. In fact, the reasons which preclude surgery (such as a patient frailty or tumors with multiple-foci) are also included among the factors which negatively predict HRQOL. As a result of this shared association, surgery tends to be an option only for those who have the best (or at least better) HRQOL. This means that any study which attempts to define the relationship between resection and HRQOL is necessarily biased. Along the same lines, peri-tumoral edema may also prejudice the association between tumor size and HRQOL. This is because peri-tumoral edema has profound effects in terms of focal neurological deficits such as motor weakness, epilepsy, visual field defects, aphasia, and pain. From the point of view of HRQOL, therefore, the control of peritumoral edema may be as important as the control of the tumor itself. This issue has recently been explored by Pan et al. (2008) who investigated the impact of peri-tumoral edema on the HRQOL of brain cancer survivors. The authors found that decreased edema volumes were associated with better HRQOL but not with prolonged survival. Not surprisingly, the authors also found that the use of dexamethasone, a corticosteroid drug prescribed to reduce inflammation, promoted better HRQOL. Long-term corticosteroid use, however, may not be a good idea since it can lead to important side-effects such as swelling, muscle weakness, and irritability. This means that a balanced approach must be used when prescribing corticosteroids, and that the effects of corticosteroids on HRQOL will depend on time-on-drug. It is important to point out that in addition to peritumoral edema, seizures are also a common problem. The incidence of seizures may even be as high as 5% for neuro-oncology patients who undergo a supratentorial craniotomy (Warnick and Petr 2008). To prevent the appearance of seizures, antiepileptic drugs are prescribed. Unfortunately, these drugs lead to important adverse effects, mostly with respect to cognition. Our experience with patients who receive antiepileptic medication is that despite the possibility of adverse effects, the benefits of proper seizure control

largely outweigh the costs. When it comes to assessing HRQOL, therefore, researchers and clinicians must be aware of the adverse effects provoked by antiepileptic drugs, and must be careful to note and statistically controlled for these effects.

In contrast to the relatively short-term and reversible side effects produced by antiepileptic medication and corticosteroid drug use, radiation therapy can have irreversible neuro-toxic effects. Indeed, when prolonged whole-brain, high-fraction doses are used to treat neurooncology patients, late-delayed radiation encephalopathy can develop. Late-delayed encephalopathy is a serious disorder characterized by local radionecrosis, diffuse leucoencephalopathy and cerebral atrophy (Taphoorn and Klein 2004). Cognitive disturbances are always present (usually mental slowing, impaired attention, and decreased memory). Luckily, clinicians are very aware of these delayed negative effects and thus radiotherapy is now carefully delivered. In fact, when focal, low fraction doses (less than 2 Gy) are used, very little side effects are observed, at least in the short-term. It is important to note that a set of companion papers on low grade glioma survivors confirmed that radiotherapy is never completely safe (see Klein et al. 2002; Douw et al. 2009). The authors of these papers found that despite minor changes in cognitive status at 6 years followup, patients who received radiotherapy (even less than 2 Gy) showed a progressive decline in attentional functioning, executive control, and information processing at 12 years follow-up. These deficits were closely associated with radiological abnormalities but independent of fraction dose, tumor lateralization, extent of resection, age, and antiepileptic drug use. The authors conclude that long-term risks, including the possibility of cognitive dysfunction and cortical damage, should be carefully considered when contemplating radiotherapy for low grade gliomas.

Although standard care for high grade tumors includes surgical resection with subsequent radiotherapy, chemotherapy is also frequently prescribed. In fact, increased efforts have been made in the last decade to develop new chemotherapy agents. These efforts have led to the introduction, and widespread use, of temozolomide (TMZ), an oral alkylating agent which is now used for the treatment of high grade tumors, and which has largely replaced Procarbazine-Lomustine-Vincristine (PCV) chemotherapy. The effect of TMZ treatment has, of course, been measured by looking at its effects on survival (including progression-free survival), but, it has also been measured by looking at its effects on HRQOL. Thus, we now know that TMZ therapy for glioblastoma multiform promotes survival/delays relapse and improves HRQOL when compared to traditional procarbazine treatment (Osoba et al. 2000b). Moreover, when TMZ is given during ionizing radiotherapy, its effects on survival are even stronger (Stupp et al. 2005). This has favoured the endorsement of chemoradiation therapy with concomitant TMZ as the new standard of care for the treatment of glioblastoma. However before radiotherapy plus adjuvant TMZ could be considered as the new standard of care, it had to be demonstrated that HRQOL was not negatively affected – or at least not for long. This, in fact, is exactly what was shown. The research team investigating this issue noted that during treatment, patients receiving both radiotherapy and TMZ reported more side effects (nausea, vomiting, appetite loss, constipation, and fatigue) than patient receiving radiotherapy only (Taphoorn et al. 2005). However, these negative effects were rather mild and short lived (recovering by 1 year follow-up). The conclusion drawn was that chemoradiation therapy with TMZ prolonged survival without producing significant and long-lasting negative effects on HRQOL. This example is highlighted here because it is arguably one of the best clinical/drug validation studies in our field. Considering both survival and HRQOL as critical determinants of therapeutic success demonstrates a good understanding of the importance placed on both the quantity and quality of survival.

A final factor which is known to affect HRQOL in neuro-oncology is chronological age. Using a developmental life-stage perspective to assess and interpret the impact of age, our research team recently showed that younger and older adults were differently affected by the presence of a supratentorial tumor (Veilleux et al. 2010). Even after having controlled for disease and treatment-related effects, younger adults maintained higher functional well-being and better neurocognitive scores than older adults. More importantly, we found that the factors which predicted HRQOL differed depending on age. Thus, support from friends and the presence of physical pain were strongly related to general well-being for younger adults, whereas concentration difficulties and the capacity to enjoy life were strongly related to general well-being for older

adults. Interestingly, the ability to continue working was closely related to well-being at all ages. This suggests that work-related productivity and the impact access to work has on financial standing, financial independence, housing, etc., are important at all ages. Together, these findings indicate that developmental life-stage, indexed by chronological age, affects biological, social and personal life-goals. These goals are not static, but instead evolve through time – changing as we do.

The Importance of Longitudinal Designs

While the effects of disease, treatment, and sociodemographic variables are important, and have been the focus of a growing amount of research, existing studies are largely retrospective. This makes it very difficult to identify how HRQOL changes over time. It also makes it difficult to know which of concurrent or sequential treatments are affecting HRQOL, and which of patient-, tumor-, or treatment-related factors are having the greatest impact. Longitudinal designs, although rare, offer an opportunity to answer these questions. One good example is a study published by Liu et al. (2009), which compared the HRQOL scores of low grade glioma patients to those of healthy controls and found lower well-being scores for patients than controls. Their analyses also confirmed that patients maintain baseline HRQOL levels throughout the course of their treatment. Most importantly, the authors did not limit their analyses to a comparison between inter- and intra-group variability (computed as the *F*-ratio), but instead regressed their independent variables onto different intra-individual change parameters using hierarchical linear modeling (HLM). HLM, or growth curve modeling, is increasingly used to analyze HRQOL data in cancer research, but is still rarely used in the field of neuro-oncology (Liu et al. 2009). This is regrettable since individual growth models allow researchers to define the shape and direction of change for individual patients, and to identify the tumor- or treatment-related variables which are associated with individual differences in HRQOL trajectory. Future longitudinal studies interested in exploring the HRQOL of brain cancer patients should use both standard general linear models and HLM if they wish to take full advantage of complex outcome data. Examples of questions that can be answered, by using this approach include: Does HRQOL change significantly as patients progress from baseline to follow-up? What are the change parameters which best describe within patient variations in HRQOL over time? What treatment- or tumor-related factors predict variations in the trajectory of change between patients?, etc. Although the study published by Liu et al. (2009) was well conducted, it focused exclusively on low grade glioma patients. Prospectively studying high grade glioma patients is also of interest since high grade gliomas evolve rapidly and since the maintenance of HRQOL may be a primary objective for patients with this type of tumor. In an attempt to address this issue, Bosma et al. (2007) studied the course of neurocognitive functioning in high grade glioma patients and found marked deterioration in cognitive functioning from baseline to 8 month follow-up. Of course, this was less pronounced when tumor recurrence was absent. In fact, when the authors completed a second study focusing specifically on long-term high grade glioma survivors, they found that long-term survivors had normal HRQOL scores (i.e., comparable to those of healthy controls, see Bosma et al. 2009). Interestingly, short-term and long-term survivors did not differ with respect to their baseline HRQOL scores, suggesting that HRQOL, although important, has little prognostic value (also see Mauer et al. 2007). One exception to the poor prognostic value of patient related factors seems to be the predictive value afforded by cognitive test scores. In a detailed study of patients with recurrent brain tumors, Meyers and Hess (2003) found that brain function began to worsen well before MRI evidence of tumor progression – by as much a 6 weeks! This early decline was particularly obvious for verbal memory and fine motor control. Tests of cognitive function, therefore, may be especially useful when seeking to predict tumor evolution and patient well-being. The prospective exploration of HRQOL data and neurocognitive function among patients with high-grade gliomas demands consideration of patient fatigue, loss of communication skills, and impaired comprehension. Indeed, given the cognitive deficits that high grade gliomas can produce, especially in the late stages of disease, substantial amounts of missing data are to be expected when testing patients. The best approach developed so far to remedy this problem has been to use proxy reports by partners or health care providers (Sneeuw et al. 2002; Giesinger

et al. 2009). This approach, however, has met with mixed results, and can only be recommended tentatively. Nonetheless, a provisional conclusion regarding the use of proxy ratings might be that there is a fairly good agreement between patient- and proxy ratings when it comes to judging tangible dimensions of well-being such as physical functioning, sleep disturbances, or appetite loss, but that the correlation weakens when it comes to measuring subjective or ethereal dimensions such as social and emotional functioning, the presence of fatigue, or the disability provoked by pain (Giesinger et al. 2009). Despite what the literature may suggest, it is important to remember that HRQOL will always constitute a subjective measure and that the personal parameters against which HRQOL is judged can change over time. This phenomenon is known as response shift, and reflects the change in personal standards adopted by patients when judging HRQOL in the face of a life-threatening disease. As a result of response shift, patients may gradually consider mild decline in HRQOL as a gain when significant decline is both possible and probable. Response shift is hard to appreciate for proxies, and usually leads to an underestimation of patient HRQOL scores. For this reason, missing data and the substitution of scores by proxies will always have to be considered carefully in neuro-oncology research.

Conclusion

Despite general recognition that HRQOL is an important end-point in neuro-oncology, it remains largely understudied. Longitudinal studies, in particular, are needed to better understand the trajectory of change experienced by patients. It is no longer useful to merely quantify the presence of change, but rather, it is important to know why change occurs and what can slow the progression of disease and the decline of patient well-being. Brief and focused questionnaires that respect patient fatigue and frailty are also needed. This includes the use of short cognitive test-batteries for studies interested in obtaining objective measures of cognitive function. Moreover, the inclusion of baseline scores, healthy controls, and proxy ratings may be useful additions to consider when conducting longitudinal studies. Finally, although HRQOL may have little prognostic power when compared to host-, tumor- or treatment-related attributes, it remains an important part of what defines therapeutic success. Including it as a variable of interest in clinical trials is now considered as good practice and good clinical science.

References

Aaronson NK (1988) Quality of life: what is it? How should it be measured? Oncology (Williston Park) 2:69–76, 64

Aaronson NK, Ahmedzai S, Bergman B, Bullinger M, Cull A, Duez NJ, A Filiberti, H Flechtner, Fleishman SB, de Haes JC (1993) The European Organization for Research and Treatment of Cancer QLQ-C30: a quality-of-life instrument for use in international clinical trials in oncology. J Natl Cancer Inst 85:365–376

Anderson SW, Damasio H, Tranel D (1990) Neuropsychological impairments associated with lesions caused by tumor or stroke. Arch Neurol 47:397–405

Bosma I, Reijneveld JC, Douw L, Vos MJ, Postma TJ, Aaronson NK, Muller M, Vandertop WP, Slotman BJ, Taphoorn MJ, Heimans JJ, Klein M (2009) Health-related quality of life of long-term high-grade glioma survivors. Neuro-oncology 11:51–58

Bosma I, Vos MJ, Heimans JJ, Taphoorn MJ, Aaronson NK, Postma TJ, van der Ploeg HM, Muller M, Vandertop WP, Slotman BJ, Klein M (2007) The course of neurocognitive functioning in high-grade glioma patients. Neuro-oncology 9:53–62

Cella D, Paul D, Yount S, Winn R, Chang CH, Banik D, Weeks J (2003) What are the most important symptom targets when treating advanced cancer? A survey of providers in the National Comprehensive Cancer Network (NCCN). Cancer Invest 21:526–535

Cella DF, Tulsky DS (1990) Measuring quality of life today: methodological aspects. Oncology (Williston Park) 4:29–38

Cella DF, Tulsky DS, Gray G, Sarafian B, Linn E, Bonomi A, Silberman M, Yellen SB, Winicour P, Brannon J (1993) The Functional Assessment of Cancer Therapy scale: development and validation of the general measure. J Clin Oncol 11:570–579

Conroy T, Mercier M, Bonneterre J et al (2004) French version of FACT-G: validation and comparison with other cancer-specific instruments. Eur J Cancer 40(15):2243–2252

Douw L, Klein M, Fagel SS, van den HJ, Taphoorn MJ, Aaronson NK, Postma TJ, Vandertop WP, Mooij JJ, Boerman RH, Beute GN, Sluimer JD, Slotman BJ, Reijneveld JC, Heimans JJ (2009) Cognitive and radiological effects of radiotherapy in patients with low-grade glioma: long-term follow-up. Lancet Neurol 8:810–818

Farace E, Shaffrey ME (2005) . In: Schiff D, O'Neill BP (eds) Principles of neuro-oncology. McGraw-Hill, New York, p 201

Giesinger JM, Golser M, Erharter A, Kemmler G, Schauer-Maurer G, Stockhammer G, Muigg A, Hutterer M, Rumpold G, Holzner B (2009) Do neurooncological patients and their significant others agree on quality of life ratings? Health Qual Life Outcomes 7:87

Giovagnoli AR, Silvani A, Colombo E, Boiardi A (2005) Facets and determinants of quality of life in patients with recurrent high grade glioma. J Neurol Neurosurg Psychiatry 76: 562–568

Goffaux P, Boudrias M, Mathieu D, Charpentier C, Veilleux N, Fortin D (2009) Development of a concise QOL questionnaire for brain tumor patients. Can J Neurol Sci 36: 340–348

Groenvold M, Petersen MA, Aaronson NK, Arraras JI, Blazeby JM, Bottomley A, Fayers PM, de Graeff A, Hammerlid E, Kaasa S, Sprangers MA, Bjorner JB (2006) The development of the EORTC QLQ-C15-PAL: a shortened questionnaire for cancer patients in palliative care. Eur J Cancer 42:55–64

Hahn CA, Dunn RH, Logue PE, King JH, Edwards CL, Halperin EC (2003) Prospective study of neuropsychologic testing and quality-of-life assessment of adults with primary malignant brain tumors. Int J Radiat Oncol Biol Phys 55: 992–999

Holzner B, Bode RK, Hahn EA, Cella D, Kopp M, Sperner-Unterweger B, Kemmler G (2006) Equating EORTC QLQ-C30 and FACT-G scores and its use in oncological research. Eur J Cancer 42:3169–3177

Kayl AE, Meyers CA (2003) Does brain tumor histology influence cognitive function? Neuro-oncology 5:255–260

Klein M, Heimans JJ, Aaronson NK, van der Ploeg HM, Grit J, Muller M, Postma TJ, Mooij JJ, Boerman RH, Beute GN, Ossenkoppele GJ, van Imhoff GW, Dekker AW, Jolles J, Slotman BJ, Struikmans H, Taphoorn MJ (2002) Effect of radiotherapy and other treatment-related factors on mid-term to longterm cognitive sequelae in low-grade gliomas: a comparative study. Lancet 360:1361–1368

Klein M, Taphoorn MJ, Heimans JJ, van der Ploeg HM, Vandertop WP, Smit EF, Leenstra S, Tulleken CA, Boogerd W, Belderbos JS, Cleijne W, Aaronson NK (2001) Neurobehavioral status and health-related quality of life in newly diagnosed high-grade glioma patients. J Clin Oncol 19:4037–4047

Liu R, Solheim K, Polley MY, Lamborn KR, Page M, Fedoroff A, Rabbitt J, Butowski N, Prados M, Chang SM (2009) Quality of life in low-grade glioma patients receiving temozolomide. Neuro-oncology 11:59–68

Mainio A, Hakko H, Niemela A, Tuurinkoski T, Koivukangas J, Rasanen P (2003) The effect of brain tumour laterality on anxiety levels among neurosurgical patients. J Neurol Neurosurg Psychiatry 74:1278–1282

Mauer ME, Taphoorn MJ, Bottomley A, Coens C, Efficace F, Sanson M, Brandes AA, van der Rijt CC, Bernsen HJ, Frenay M, Tijssen CC, Lacombe D, van den Bent MJ (2007). Prognostic value of health-related quality-of-life data in predicting survival in patients with anaplastic oligodendrogliomas, from a phase III EORTC brain cancer group study. J Clin Oncol 25:57315737

Meyers CA, Hess KR (2003) Multifaceted end points in brain tumor clinical trials: cognitive deterioration precedes MRI progression. Neuro-oncology 5:89–95

Osoba D, Aaronson NK, Muller M, Sneeuw K, Hsu MA, Yung WK, Brada M, Newlands E (1996) The development and psychometric validation of a brain cancer quality-of-life questionnaire for use in combination with general cancer-specific questionnaires. Qual Life Res 5:139–150

Osoba D, Brada M, Prados MD, Yung WK (2000a) Effect of disease burden on health-related quality of life in patients with malignant gliomas. Neuro-oncology 2:221–228

Osoba D, Brada M, Yung WK, Prados M (2000b) Health-related quality of life in patients treated with temozolomide versus procarbazine for recurrent glioblastoma multiforme. J Clin Oncol 18:1481–1491

Pan HC, Sun MH, Chen CC, Chen CJ, Lee CH, Sheehan J (2008) Neuroimaging and quality-of-life outcomes in patients with brain metastasis and peritumoral edema who undergo Gamma Knife surgery. J Neurosurg 109(Suppl): 90–98

Sneeuw KC, Sprangers MA, Aaronson NK (2002) The role of health care providers and significant others in evaluating the quality of life of patients with chronic disease. J Clin Epidemiol 55:1130–1143

Stupp R, Mason WP, van den Bent MJ, Weller M, Fisher B, Taphoorn MJ, Belanger K, Brandes AA, Marosi C, Bogdahn U, Curschmann J, Janzer RC, Ludwin SK, Gorlia T, Allgeier A, Lacombe D, Cairncross JG, Eisenhauer E, Mirimanoff RO (2005) Radiotherapy plus concomitant and adjuvant temozolomide for glioblastoma. N Engl J Med 352: 987–996

Taphoorn MJ, Klein M (2004) Cognitive deficits in adult patients with brain tumours. Lancet Neurol 3:159–168

Taphoorn MJ, Stupp R, Coens C, Osoba D, Kortmann R, van den Bent MJ, Mason W, Mirimanoff RO, Baumert BG, Eisenhauer E, Forsyth P, Bottomley A (2005) Health-related quality of life in patients with glioblastoma: a randomised controlled trial. Lancet Oncol 6:937–944

Veilleux N, Goffaux P, Boudrias M, Mathieu D, Daigle K, Fortin D (2010) Quality of life in neurooncology – age matters. J Neurosurg 113:325–332

Ware JE Jr, Sherbourne CD (1992) The MOS 36-item short-form health survey (SF-36). I. Conceptual framework and item selection. Med Care 30:473–483

Warnick RE, Petr MJ (2008) Neuro-oncology: the essentials. In: Bernstein M, Berger MS (eds). Thieme Medical Publishers, Inc., New York, p 132

Weitzner MA, Meyers CA, Gelke CK, Byrne KS, Cella DF, Levin VA (1995) The Functional Assessment of Cancer Therapy (FACT) scale. Development of a brain subscale and revalidation of the general version (FACT-G) in patients with primary brain tumors. Cancer 75:1151–1161

Chapter 36

Emerging Role of Brain Metastases in the Prognosis of Breast Cancer Patients

Amanda Hambrecht, Rahul Jandial, and Josh Neman

Abstract An estimated 40,000 women die each year from breast cancer, the vast majority due to complications from metastases (Jemal et al. 2011, CA Cancer J Clin). Paradoxically, the incidence of brain metastases has increased dramatically in subsets of breast cancer patients, possibly as an indirect result of improved systemic and targeted therapies that are effective at controlling extracranial disease. Once diagnosed with a brain metastasis, patients have a dismal 20% probability of surviving more than 1 year (Gril et al. 2010, Eur J Cancer 46:1204–1210; Lin and Winer 2007, Clin Cancer Res 13:1648–1655). Other than radiotherapy and neurological surgery, no standard treatment options exist, underscoring the significant need to investigate the biology of these clinically recalcitrant tumors.

Keywords Breast cancer · Brain metastasis · Recalcitrant tumor · Triple-negative · Basal-like · Melanoma

Introduction

The brain has increasingly become the site of untreatable relapse (Neman et al. 2010). Moreover, breast cancer is the most common malignancy in women in the United States (Cheng and Hung 2007). An estimated 40,000 women die each year from breast cancer, the vast majority due to complications from metastases (Jemal et al. 2011). Autopsy studies have shown that up to 25% of patients who die from cancer develop brain metastases (Deeken and Loscher 2007). The top five primary tumors that lead to brain metastasis are lung, breast, melanoma, renal and colorectal (Lin et al. 2010). Brain metastases have a 5-year cumulative incidence rate in 16% of lung cancer patients, 7% of breast cancer patients and 5% of colon cancer patients (Deeken and Loscher 2007). The incidence rate in melanoma patients has been reported as high as 55% (Deeken and Loscher 2007). More than 25% of tumors found in the brain are metastatic lesions derived from melanoma, lung cancer and breast cancer (Fidler et al. 2002). However, each type of cancer has a variable period of dormancy prior to relapse in the brain (Neman et al. 2010). In the United States, up to 40% of cancer patients develop brain metastasis (Lin et al. 2010). The median survival of untreated patients is 1–2 months (Lin et al. 2010). Once diagnosed with a brain metastasis, patients have a dismal 20% probability of surviving more than 1 year (Gril et al. 2010; Lin and Winer 2007). But, chemotherapy, in conjunction with surgery and radiation therapy, can extend survival to 4–6 months (Lin et al. 2010). Poor prognosis is primarily due to chemoresistance, as brain metastases are highly resistant to chemotherapy (Lin et al. 2010). Given the emerging role of brain metastases in the prognosis of breast cancer patients, a better understanding and more research studies need to be conducted in order to come up with therapies and trial that will allow eligibility of brain metastatic patients to participate in them.

J. Neman (✉)
Department of Neurosurgery, Beckman Research Institute, City of Hope National Cancer Center, CA, USA
e-mail: jneman@coh.org

M.A. Hayat (ed.), *Tumors of the Central Nervous System, Volume 4*,
DOI 10.1007/978-94-007-1706-0_36,

Primary Breast Cancer Subtypes

There are several subtypes of breast cancer, two of which are triple-negative and basal-like breast cancers. Triple-negative breast cancers are defined as tumors that lack expression of estrogen receptor (ER), progesterone receptor (PR) and Her2 (Foulkes et al. 2010). Basal-like breast cancers are characterized by the absence or low levels of ER expression, absence of Her2 overexpression and the expression of many genes usually found in basal or myoepithelial cells of the normal breast (Foulkes et al. 2010). Even though a majority of basal-like cancers are also triple-negative breast cancers and about 80% of triple-negative breast cancers are also basal-like, they are not synonymous (Foulkes et al. 2010). Up to 20% of basal-like cancers express ER or overexpress Her2 (Foulkes et al. 2010). Triple-negative breast cancers encompass other molecular subtypes of breast cancer including: claudin-low tumors enriched with cells that have properties similar to stem cells and features of epithelial-mesenchymal transition (EMT) as well as interferon-rich tumors associated with considerably better prognosis than other triple-negative breast cancers (Foulkes et al. 2010). 12–17% of women with breast cancer have triple-negative breast cancer and as a group, these patients have a relatively poor outcome (Foulkes et al. 2010). They cannot be treated with endocrine therapy or therapies targeted against Her2 (Foulkes et al. 2010). When Her2 is overexpressed, it is a target for Trastuzumab, the humanized monoclonal antibody (Foulkes et al. 2010). Both triple-negative and basal-like breast cancers are more likely to metastasize to viscera, such as the lungs and brain, and are less likely to metastasize to bone (Foulkes et al. 2010).

Triple-negative and basal-like cancers are very heterogeneous at the genetic level (Foulkes et al. 2010). They account for almost 15% of all invasive breast cancers and usually have a high histologic grade (Foulkes et al. 2010). Both types occur more frequently in young black and Hispanic women than in young women of other racial or ethnic groups (Foulkes et al. 2010). Women who develop a basal-like breast cancer had certain features not shared by women without cancer (Foulkes et al. 2010). They reached menarche at an earlier age, they had a higher body mass index during premenopausal years, had higher parity and lower lifetime duration of breast-feeding (Foulkes et al. 2010). The risk of basal-like breast cancer rises with increasing parity and an increasing ratio of waist-to-hip circumference, indicating a complex interplay of genetic and societal factors (Foulkes et al. 2010). Basal-like breast cancer cells possess some phenotypic characteristics that are consistent with those of breast stem cells and display gene-expression patterns consistent with cells undergoing an EMT (Foulkes et al. 2010). Cancer stem cells are ultimately responsible for the maintenance of a population of malignant cells with metastatic potential (Foulkes et al. 2010). They do not necessarily have to arise from the tissue stem cells, but can come from other differentiated cancer cells that have acquired the property of self-renewal (Foulkes et al. 2010). Cancer cells from triple-negative and basal-like breast cancers display a profile of cell-surface markers that is similar to that of breast cancer stem cells, such as the phenotype $CD44^{+}CD24^{-}$ and the expression of aldehyde dehydrogenase (Foulkes et al. 2010). It is currently unclear if all basal-like cancers are enriched with cancer stem cells or if they have a disproportionately high content of cells undergoing EMTs (Foulkes et al. 2010).

There is a link between the BRCA1 pathway, basal-like breast cancers and triple-negative breast cancers (Foulkes et al. 2010). More than 75% of tumors in women with a BRCA1 mutation also have a triple-negative phenotype, a basal-like phenotype, or both (Foulkes et al. 2010). Basal-like breast cancers and tumors with a BRCA1 mutation have many characteristics in common as compared with nonhereditary breast cancers or BRCA2-related tumors (Foulkes et al. 2010). They both rarely have amplifications of the cyclin D1 gene (CCND1), they both express lower levels of p27 and they both express higher levels of S-phase kinase associated protein 2 (SKP2), cyclin E, fascin, caveolins 1 and 2, osteonectin and caspase 3 (Foulkes et al. 2010). One study found that both basal-like breast cancer and BRCA1-related breast cancer have a defect in the maintenance of normal chromosome X inactivation (Foulkes et al. 2010). This suggests that similarity between the two tumor types could lie in chromatin remodeling (Foulkes et al. 2010). In other studies, a subgroup of basal-like breast cancers with low levels of BRCA1 expression had high levels of inhibitor of DNA binding 4 (ID4) expression, a BRCA1 silencer (Foulkes et al. 2010). Recent experiments have found that levels of BRCA1 protein

may be lower in grade 3 tumors that do not express ER or PR and possess a basal-like phenotype than in other types of breast cancer (Foulkes et al. 2010). This downregulation could be mediated by epigenetic changes (Foulkes et al. 2010). Mice deficient in both Brca1 and p53, a tumor suppressor gene, in mammary epithelial cells develop tumors that are both triple-negative and basal-like (Foulkes et al. 2010). The resulting tumors are very similar to those that occur in humans with a BRCA1 mutation (Foulkes et al. 2010). This suggests that BRCA1 plays a permissive role in the transition of undifferentiated breast cells to their more mature counterparts (Foulkes et al. 2010).

Triple-negative and basal-like breast cancers show aggressive clinical behavior (Foulkes et al. 2010). The survival curve for patients with either type of breast cancer has a sharp decrease during the first 3–5 years after diagnosis (Foulkes et al. 2010). However, a distant relapse is much less common after this time (Foulkes, et al. 2010). After 10 years, ER-positive cancer patients are more likely to relapse than are those with ER-negative tumors (Foulkes et al. 2010). There is some hope for a small subgroup of patients with either triple-negative or basal-like breast cancer. This population is markedly sensitive to chemotherapy and is associated with a good prognosis when treated with conventional chemotherapy agents (Foulkes et al. 2010). Some triple-negative and basal-like breast cancers have a dysfunctional BRCA1 pathway, which may make them sensitive to certain agents (Foulkes et al. 2010).

Many studies have shown that angiogenesis is involved in breast cancer metastases to the brain (Cheng and Hung 2007). Brain metastatic tumors showed more angiogenesis but a lower vascular permeability than did the primary breast cancer, suggesting that the cranial environment is leakage resistant but proangiogenic (Cheng and Hung 2007). Several essential factors for breast cancer metastasis are vascular endothelial growth factor (VEGF), matrix metalloproteinases (MMPs) and the chemokine receptor CXCR4 (Cheng and Hung 2007). VEGF is expressed nearly four times higher in primary breast cancer patients with brain metastases than in those without (Cheng and Hung 2007). It was speculated that VEGF might enhance the transendothelial migration of tumor cells through the downregulation of endothelial integrity (Cheng and Hung 2007). This was confirmed in several studies in which increased VEGF expression was marked by an increase in the adhesion of tumor cells on the HMBEC monolayer (Cheng and Hung 2007). Brain metastatic lesions of several variants showed a higher vascular density and released significantly more VEGF and IL-8 when compared with the original cell line (Cheng and Hung 2007). A VEGF receptor specific tyrosine kinase inhibitor that targeted endothelial cells reduced angiogenesis and restricted the growth of brain metastases (Cheng and Hung 2007). Matrix metalloproteinases are zinc-dependent proteinases that play a key role in extracellular matrix degradation (Cheng and Hung 2007). In a breast cancer brain metastasis rat model, a micrometastasis showed a significantly higher expression of MMP2, 3 and 9 as well as an increase in MMP2 and three activities as compared to the normal brain (Cheng and Hung 2007). The development of a brain metastasis was significantly decreased with treatment of a selective synthetic MMP inhibitor (Cheng and Hung 2007). Another study confirmed that in human breast cancer cells overexpressing MMP2, there was a higher incidence of metastasis to the brain (Cheng and Hung 2007). An in vitro study showed that brain-seeking breast cancer cells had a higher total and active amount of MMP1 and 9, which provide the cells with a greater migration and invasion capacity (Cheng and Hung 2007). These capacities, as well as the amount, could be decreased with the application of a MMP1 and/or nine inhibitors (Cheng and Hung 2007).

It is known that malignant breast cancer cells express the chemokine receptor CXCR4. The expression of CXCR4 is consistently higher in primary breast tumor cells than in normal breast epithelial cells (Cheng and Hung 2007). When these cells invade the ECM and circulate in the blood and lymphatic vessels, they are attracted to SDF-1α (Cheng and Hung 2007). The malignant cells then leave the circulation and migrate into organs with large amounts of chemokines (Cheng and Hung 2007). Once there, the cancer cells proliferate, induce angiogenesis and form metastatic tumors (Cheng and Hung 2007). In vitro studies showed that SDF-1α could induce blood vessel instability by increasing vascular permeability, resulting in the penetration of breast tumor cells through the HMBECs (Cheng and Hung 2007). In another study, anti-CXCR4 antibodies decreased transendothelial breast cancer migration as well as vascular permeability (Cheng and Hung 2007). It has been shown that ErbB2 could induce CXCR4 expression and may

interact with the chemokine in order to contribute to brain metastasis (Cheng and Hung 2007).

Other chemokines and their receptors play an important role in brain metastases. The results from a recent study that analyzed a set of 142 auxillary node positive breast cancer patients suggested the chemokine receptor, CX3CR1, and its ligand, fraktalkine, are significantly associated with brain metastases (Cheng and Hung 2007). Another chemokine and receptor pair that may be involved in breast cancer metastases is Slit and Robo (Cheng and Hung 2007). The Slit family of secreted proteins are Slit1, 2 and 3 and their corresponding Robo receptors are Robo1, 2, 3 and 4 (Cheng and Hung 2007). They play an integral role in neuronal development as Slit proteins guide the directional migration of neurons in the brain and olfactory system (Cheng and Hung 2007). Slit1 is predominantly expressed in the nervous system (Cheng and Hung 2007). Studies have suggested that Slit/Robo1 signaling may be involved in the metastasis of breast cancer to the brain (Cheng and Hung 2007). An in vitro study showed that Slit2/Robo1 signaling was capable of inducing directed migration (Cheng and Hung 2007). Slit2 acted as a potent attractor for breast cancer cells expressing Robo1 (Cheng and Hung 2007). Attracted by Slit, circulating Robo expressing tumor cells will attach to the vascular endothelial cells in the brain (Cheng and Hung 2007). The increased activities of MMP9 and VEGF facilitate their penetration of the blood-brain barrier (BBB) (Cheng and Hung 2007).

Store-operated Ca^{2+} influx is also known to be involved in cancer cell migration (McCarthy 2009; Yang et al. 2009). Yang et al. (2009) determined that the function of two known regulators of Ca^{2+} influx was essential for breast cancer metastasis (McCarthy 2009). The two regulators, ORAI1 and stromal interaction molecule 1 (STIM1), have different roles in maintaining store-operated Ca^{2+} influx in non-excitable cells; STIM1 is a Ca^{2+} sensor and ORAI1 is part of a pore that enables store-operated Ca^{2+} entry (McCarthy 2009; Yang et al. 2009). Studies have shown that inhibition of store-operated channels suppressed serum-induced cell migration (McCarthy 2009; Yang et al. 2009). Small interfering RNAs against STIM1 or ORAI1 indicated that these proteins are required for the migration of MDA-MB 231 human breast tumors cell in vitro (McCarthy 2009; Yang et al. 2009). Cells with reduced levels of ORAI1 and STIM1 had impaired migration because the assembly and disassembly of focal adhesions are crucial for cellular migration (McCarthy 2009; Yang et al. 2009). MDA-MB 231 cells with reduced expression levels of either STIM1 or ORAI1 showed significantly lower levels of metastatic growth (McCarthy 2009; Yang et al. 2009). A pharmacological inhibitor of store-operated Ca^{2+} channels, SKF96365, reduced growth of 4T1 mouse breast cancer cells after orthotopic injections (McCarthy 2009; Yang et al. 2009). Thus, STIM1 and ORAI1 are potential new targets for the inhibition of breast cancer cell migration and metastasis (McCarthy 2009; Yang et al. 2009).

There are several conventional treatments such as corticosteroids, whole brain radiation therapy, surgical resection, stereotactic radiosurgery and chemotherapy, as well as new techniques available for the treatment of brain metastases. Corticosteroids relieve symptoms by decreasing cerebral edema surrounding brain metastases, but have not shown large improvements in overall patient survival (Cheng and Hung 2007). Whole brain radiation therapy (WBRT) is the most common choice for patients with multiple brain metastases (Cheng and Hung 2007). It is also a popular choice for patients that have a solitary brain metastasis that does not qualify for either surgical resection or stereotactic radiosurgery (Cheng and Hung 2007). This treatment is able to control neurologic symptoms and has been shown to improve the quality of life in about 75–85% of patients (Cheng and Hung 2007). It can also prolong the mean survival of patients compared with corticosteroids alone (Cheng and Hung 2007). An advantage of surgical resection is that it allows for pathologic diagnosis (Cheng and Hung 2007). By decompressing the effect of the tumor mass, it may improve neurologic symptoms as well and increase the quality of life (Cheng and Hung 2007). It improves the overall median survival compared to supportive care alone (Cheng and Hung 2007). However, unless there is an obvious symptomatic lesion, surgical resection in patients with multiple brain metastases has limited use (Cheng and Hung 2007). Stereotactic radiosurgery uses a linear accelerator or multiple cobalt-60 sources to deliver focal radiation to areas smaller than 3.5 cm, minimizing radiation exposure (Cheng and Hung 2007). It is less invasive than surgical resection and is given to patients who cannot tolerate surgery or have surgically inaccessible lesions (Cheng and Hung 2007). A study showed that the combination

of stereotactic radiosurgery and WBRT significantly improved the overall survival of patients with a single brain metastasis, but provided no survival advantage for patients with multiple brain metastases (Cheng and Hung 2007). Chemotherapy is not a very useful treatment for brain metastases because the tight junctions of the blood–brain barrier prevent the entry of most chemotherapeutic agents into the CNS as previously discussed (Cheng and Hung 2007). Some drugs, however, have shown promise when used in combination with radiation therapy (Cheng and Hung 2007). For example, Efaproxiral can increase tumor oxidation and therefore, increase radiation sensitivity (Cheng and Hung 2007). Studies have also shown an improvement in median survival when chemotherapy was used in combination with WBRT compared to WBRT alone (Cheng and Hung 2007). Several strategies for new delivery techniques are currently being tested in animal models. The placement of carmustine (BCNU), an impregnated polymer wafer that protects hydroxylasing and allows for the slow release of chemotherapeutic agents, in the resection cavity has shown success in primary brain tumors (Cheng and Hung 2007). It is now being tested in metastasis cancers (Cheng and Hung, 2007). Intracerebral microinfusion has shown effectiveness in animal studies but has not yet been tested in humans (Cheng and Hung 2007).

Therapies can, however, indirectly influence the course and pattern of metastasis by delaying systemic disease and favoring the emergence of recurrences in specific organs (Nguyen et al. 2009). Several studies observed a rising incidence of brain metastasis in ErbB2-positive breast cancer patients when they were treated with the ErbB2 antibody Trastuzumab (or Herceptin) (Nguyen et al. 2009). The FDA approved Herceptin as an anti-cancer treatment in 1998 (Cheng and Hung 2007). It has shown an improved disease-free and overall survival when delivered with cytotoxic chemotherapy to patients with ErbB2 overexpressing metastatic breast cancer cells (Cheng and Hung 2007). However, patients frequently developed brain metastases, with an incidence of 25–50%, while responding to Herceptin (Cheng and Hung 2007). The development of brain metastases varied from 4 to 24 months (Cheng and Hung 2007). ErbB2 overexpression is now known to be a predictive factor for CNS relapse in breast cancer patients treated with Herceptin (Cheng and Hung 2007).

Chemotherapy is the current treatment available for women with triple-negative breast cancer (Foulkes et al. 2010). As a group, they have a worse outcome after chemotherapy than patients with breast cancer of other subtypes (Foulkes et al. 2010). Neoadjuvant studies have suggested that treatment is very effective in the minority of women with triple-negative breast cancer whose tumors are extremely sensitive to chemotherapy (Foulkes et al. 2010). These patients show a complete pathological response and thus, have an excellent outcome (Foulkes et al. 2010). The use of cisplatin and carboplatin to treat triple-negative breast cancers is currently being assessed in clinical trials (Foulkes et al. 2010). Initial findings suggest that neoadjuvant use of cisplatin results in high rates of complete pathological response in patients with breast cancer who have BRCA1 mutations and maybe in patients who triple-negative cancer (Foulkes et al. 2010). Overexpression of EGFR is more common in triple-negative breast cancer than in other subtypes (Foulkes et al. 2010). The use of the monoclonal antibody Cetuximab, targeted against EGFR, is currently being studied in combination with carboplatin (Foulkes et al. 2010). However, triple-negative and basal-like breast cancers often display abnormalities in PTEN, which is frequently associated with resistance to anti-EGFR therapies (Foulkes et al. 2010). A recent clinical target in triple-negative breast cancer is the enzyme PARP [poly(adenosine diphosphate-ribose) polymerase] (Foulkes et al. 2010). It is involved in base-excision repair after DNA damage (Foulkes et al. 2010). Inhibitors of PARP have shown very encouraging clinical activity in early trials with BRCA mutation tumors and sporadic triple-negative cancers (Foulkes et al. 2010). In a recent randomized phase II trial, a PARP inhibitor was used in combination with chemotherapy and resulted in statistically significant improvements in the rate of tumor regression, median progression-free survival and median overall survival (Foulkes et al. 2010).

Breast to Brain Metastases

Breast to brain metastases appear in either the parenchyma or along the leptomeninges (Cheng and Hung 2007). The majorities of tumors occur in

the parenchyma and follow a vascular distribution mainly through hematogeneous spread (Cheng and Hung 2007). Clinical symptoms of parenchymal brain metastases include headache, mental status change, cognitive disturbances and other manifestations that could reflect the location of the lesion (Cheng and Hung 2007). Leptomeningeal tumors are less common but can arise through multiple pathways including: hematogeneous spread, infiltration from vertebral metastases via the venous plexus and extension along nerves or perineural lymphatics (Cheng and Hung 2007). Clinical symptoms of leptomeningeal metastases tend to be nonlocalizing, such as pain, headache and cranial neuropathies (Cheng and Hung 2007). Two types of neuroimaging are popular for detecting brain metastases: gadolinium-enhanced MRI and contrast-enhanced CT (Cheng and Hung 2007). MRI is preferred over CT because it is more sensitive for identifying parenchymal and leptomeningeal metastases (Cheng and Hung 2007). CSF cytology has a higher specificity than that of MRI and can be used to detect leptomeningeal metastases as well (Cheng and Hung 2007).

Studies have revealed that directly or indirectly, an individual's genetic background can determine metastasis susceptibility in breast cancer (Nguyen and Massague 2007). Population-genetic studies have revealed inherited tendencies to develop cancer and have suggested the existence of alleles that predispose breast cancer metastasis (Nguyen and Massague 2007). A study combining gene expression analysis and population genetics revealed that tumors from pre-menopausal African-American patients expressed a gene signature that typifies the basal subtype of breast cancer with higher prevalence than those from Caucasian patients (Nguyen and Massague 2007). This polygenic signature correlates with aggressive metastatic relapse (Nguyen and Massague 2007). Using a QTL analysis and multiple cross-mapping study researchers identified a single nucleotide polymorphism (SNP) in SIPA1, a GTPase-activating protein (GAP) that inhibits RAP1 and RAP2 activity, which determined metastatic susceptibility (Nguyen and Massague 2007). This SNP resulted in an amino-acid substitution that hindered RAP-GAP function, attenuating pulmonary metastasis (Nguyen and Massague 2007). Polymorphisms of this kind have been reported in human breast cancer samples and correlate with poor prognosis (Nguyen and Massague 2007). Recent research has pointed to complex sets of genes engaged in various mechanisms that play a role in mediating metastasis (Nguyen and Massague 2007). In a lobular breast cancer model, overexpression of TWIST and SNAI1, promoted EMT and intravasation (Nguyen and Massague 2007). The pleiotropic effects of these developmental and lineage-determining factors might contribute to multiple steps in malignant progression, from the aggressiveness of local tumor cells to their dissemination and the onset of distant organ metastasis (Nguyen and Massague 2007).

A member of the epidermal growth factor receptor (EGFR) family, ErbB2/Her2/neu, plays an essential role in breast cancer to brain metastasis and overall patient survival (Cheng and Hung 2007). The ErbB2 gene encodes a transmembrane receptor tyrosine kinase that is elevated in 20–30% of human breast cancers (Cheng and Hung 2007). The elevation results from genomic amplification of the ErbB2 proto-oncogene and transcriptional upregulation of the ErbB2 promoter (Cheng and Hung 2007). Patients with overexpression of ErbB2 had a worse overall survival as it predicts Tamoxifen resistance in the primary tumor (Cheng and Hung 2007). Furthermore, ErbB2 overexpression has been shown to be associated with the brain metastatic phenotype (Cheng and Hung, 2007). ErbB2 amplification is an important risk factor for brain metastasis (Cheng and Hung 2007). The correlation between ErbB2 overexpression in primary breast cancers and subsequent brain metastases is 97% (Cheng and Hung 2007).

Upon activation, ErbB2 phosphorylates many downstream molecules that activate a variety of signaling cascades (Cheng and Hung 2007). By activating different pathways, ErbB2 causes alterations in a variety of gene expressions at different levels such as transcription, translation and protein stability that are implicated in cell growth, survival and metastases (Cheng and Hung 2007). Overexpression of ErbB2 has been found to increase membrane degradation by activating the transcription of and enhancing the secretion of MMP9 (Cheng and Hung 2007). It also increases the invasiveness of breast cancer cells by upregulating the chemokine receptor CXCR4 (Cheng and Hung 2007). Breast cancer cells that express high levels of CXCR4 increase the permeability of brain endothelial cells, facilitating their invasion into the brain (Cheng and Hung 2007). If a therapeutic drug can penetrate the blood–brain barrier, ErbB2 directed therapy could

be targeted against ErbB2 overexpressing breast cancer cells growing in the brain (Cheng and Hung 2007). Lapatinib is an irreversible inhibitor of the ErbB2 tyrosine kinase that can cross the BBB (Cheng and Hung 2007). In a study to determine its effects, responses were observed in 2 out of 39 patients (Cheng and Hung 2007).

In order to improve prognosis for patients, early therapeutic targeting of both the disseminating seed and the evolving metastatic soil is essential (Psaila and Lyden 2009). These therapies may need to be tailored to specific stages of the metastatic cascade (Psaila and Lyden 2009). When metastasis suppressor genes are re-expressed in malignant cells, they prevent metastasis without affecting growth at the primary tumor site (Psaila and Lyden 2009). They may alter the ability of cells to respond to survival signals received from the local microenvironment (Psaila and Lyden 2009). This determines whether a certain microenvironment is permissive or inhibitory for the establishment of metastasis (Psaila and Lyden 2009). Thus, it may be beneficial for systemic therapies targeted to the metastatic microenvironment to be used early (Psaila and Lyden 2009). Immunological features of the pre-metastatic niche can be used to identity a propensity to develop metastatic disease earlier than prognostic techniques are able (Psaila and Lyden 2009). By examining the destination sites for metastasis, patients who present with a seemingly localized disease, but have evidence of pre-metastatic niche formation, can be helped (Psaila and Lyden 2009).

Epithelial-Mesenchymal Transition

During embryonic development, mesenchymal cells form from a primitive epithelium and acquire a morphology that is appropriate for migration in an extracellular environment and settlement in areas involved in organ function (Thiery 2002). An epithelial-mesenchymal transition (EMT) is essential to this process. It is characterized by the conversion of polarized epithelial cells into motile cells (Thiery 2002). Epithelial cells shed their differentiated characteristics such as cell adhesion, polar and apical-basal polarity and lack of motility and acquire mesenchymal features including motility, invasiveness and a heightened response to apoptosis (Polyak and Weinberg 2009). The same regulatory mechanisms that convert epithelial cells to migratory mesenchymal cells, which are crucial to the formation of organs during embryonic development, become abnormally activated in cancer and contribute to invasion and metastasis (Polyak and Weinberg 2009). An essential difference between the embryonic and tumorigenic process is that the latter involves genetically abnormal cells that progressively lose their responsiveness to normal growth-regulatory signals (Polyak and Weinberg 2009). Epithelial-mesenchymal transitions contribute to invasion, metastatic dissemination and the acquisition of therapeutic resistance (Polyak and Weinberg 2009). This process generates cancer cells with stem cell-like characteristics (Polyak and Weinberg 2009). These cells possess the ability to evolve, which is derived from the inherent genetic and epigenetic instability in most neoplastic cell types (Polyak and Weinberg 2009). This instability generates multiple distinct subpopulations of cancer cells within larger tumors, constituting a source of phenotypic heterogeneity within tumors (Polyak and Weinberg 2009). There is evidence that an EMT gives rise to the dissemination of single cancer cells from primary tumor sites (Thiery 2002). The initiation of an EMT can occur from multiple extracellular signals and significant crosstalk, in the form of multiple positive feedback loops, among downstream intracellular signaling pathways and transcription factors (Polyak and Weinberg 2009). This network of interactions leads to increased stability of the acquired mesenchymal cell phenotype (Polyak and Weinberg 2009). Recent data have shown that sustained activation of an EMT leads to progressive epigenetic changes in cells (Polyak and Weinberg 2009). These alterations induce heritable effects that maintain the mesenchymal state even after EMT-initiating signals are no longer present (Polyak and Weinberg 2009).

Mesenchymal-Epithelial Transition

Distant metastases derived from primary cancers are largely composed of cancer cells with an epithelial phenotype that closely resembles that of cancer cells in the primary tumor (Polyak and Weinberg 2009). In order to disseminate, cancer cells must pass through an EMT and acquire mesenchymal features, but the

resulting metastases look like the primary cancers at the histopathological level (Polyak and Weinberg 2009). Following metastatic spread and colonization, a mesenchymal-epithelial transition (MET) usually coverts the disseminated mesenchymal cancer cells back to a more differentiated, epithelial cell state (Polyak and Weinberg 2009). In the absence of signals that actively promote the induction and continued expression of an EMT, many normal and neoplastic cells will revert back to the epithelial state because of a transcriptional default mechanism (Polyak and Weinberg 2009). For example, several studies have shown that the DNA methylation status of the CDH1 promoter varies at different stages of the metastatic process (Polyak and Weinberg 2009). In primary breast cancers, the tumor cells that undergo transient hypermethylation and silencing of CDH1 expression are more invasive and metastatic (Polyak and Weinberg 2009). However, E-cadherin expression is re-induced in metastases and is accompanied by the demethylation of the CDH1 promoter (Polyak and Weinberg 2009). Epithelial-mesenchymal transitions and their converses, mesenchymal-epithelial transitions, are central regulators of cellular plasticity in cancers (Polyak and Weinberg 2009). They have important roles in therapeutic resistance, tumor recurrence and metastatic progression (Polyak and Weinberg 2009).

The Role of the Blood Brain Barrier in Metastasis

Of all the central nervous system (CNS) barriers, the blood-brain barrier (BBB) exerts the greatest control over the immediate microenvironment of brain cells (Abbott et al. 2006). The BBB is a selective barrier formed by the endothelial cells that line cerebral microvessels (Abbott et al. 2006). The tight junctions between adjacent endothelial cells force most molecular traffic to take a transcellular route rather than a paracellular one (Abbott et al. 2006). The luminal and abluminal membranes have specific transport systems that regulate the transcellular traffic across the BBB (Abbott et al. 2006). The BBB protects the brain from exposure to toxins, both endogenous and exogenous (Deeken and Loscher 2007). It functions as a physiologic obstruction to the delivery of systemic chemotherapy and newer drugs to the brain parenchyma and CNS (Deeken and Loscher 2007). Mahar Doan et al. (2002) analyzed 18 different physiochemical properties of drugs used to treat CNS and non-CNS disease to determine which molecules have the greatest efficacy in treating the brain (Deeken and Loscher 2007). They found that transcellular passive diffusion is restricted to small, nonpolar and lipophilic compounds, while water-soluble or polar compounds can only penetrate via active transport across the BBB (Deeken and Loscher 2007).

The blood–brain barrier has several important roles in brain homeostasis, such as supplying the brain with essential nutrients, mediating the efflux of many waste products, restricting ionic and fluid movements between the blood and the brain and protecting the brain from fluctuations in ionic composition after a meal or exercise (Abbott et al. 2006). The BBB also helps keep separate the pools of neurotransmitters and neuroactive agents that act centrally and peripherally (Abbott et al. 2006). In addition to the endothelial BBB, the homeostasis of the brain also depends on the epithelial blood-cerebrospinal fluid (CSF) barrier located at the choroid plexus and outer arachnoid membrane (Deeken and Loscher 2007). The surface area of the BBB, however, is about 5000 fold larger than that of the blood–CSF barrier (Deeken and Loscher 2007).

Early histological studies have shown that brain capillaries are surrounded by or closely associated with several cell types, including the perivascular endfeet of astrocytic glia, pericytes, microglia and neuronal processes (Abbott et al. 2006). Recently, pericytes, perivascular macrophages and neurons have been shown to contribute to induction of the blood–brain barrier (Abbott et al. 2006). The blood–brain barrier also consists of capillary endothelial cells and a basement membrane (Cheng and Hung 2007). The astrocytes have tight junctions between each other, enclosing the capillary on all sides (Cheng and Hung 2007). Astrocytes can regulate many features of the BBB, such as expression and polarized location of transporters and specialized enzyme systems, resulting in tighter tight junctions (Abbott et al. 2006). Astrocyte endfeet cover over 90% of the endothelial cell surface (Deeken and Loscher 2007). They tightly ensheath the vessel wall and seem to be critical for the induction and maintenance of the endothelial barrier (Deeken and Loscher 2007). Astrocytes can secrete a

range of chemical agents, such as TGF-β, glial-derived neurotrophic factor (GDNF), bFGF and angiopoietin 1 (ANG1), which induce aspects of the BBB phenotype in endothelial cells in vivo (Abbott et al. 2006). The endothelial cells within the BBB are nearly leak-proof (Cheng and Hung 2007). They are equipped with selective substance permeability and only allow in particles less than 20 nm in diameter (Cheng and Hung 2007). The brain capillary network is extensive (Deeken and Loscher 2007). The surface area of the capillary endothelium is about 20 m^2 and it is thought that 100 billion capillaries measuring 650 km in length comprise the brain vasculature (Deeken and Loscher 2007). Every neuron is likely perfused by its own blood vessel (Deeken and Loscher 2007). Therefore, substrates are delivered directly to each neuron if, of course, they can cross the BBB (Deeken and Loscher 2007).

Characteristics of the brain endothelium differentiate these cells from those found in endothelial beds in other organs of the periphery (Deeken and Loscher 2007). In endothelial cells forming peripheral capillary beds, there are intercellular clefts maintained by relatively loose attachments (Deeken and Loscher 2007). Endothelial cells can form fenestrae with invaginations that increase the surface area over which substrates can diffuse (Deeken and Loscher 2007). Also, plasmalemmal or pinocytic vesicles can be formed at the cell surface (Deeken and Loscher 2007). Brain endothelial cells, on the other hand, have continuous tight junctions, no fenestrations and exhibit very low pinocytic activity (Deeken and Loscher 2007). A basal membrane and ECM, as well as pericytes and astrocyte foot processes surround the brain endothelial cells (Deeken and Loscher 2007). These all form the BBB and mediate its permeability (Deeken and Loscher 2007). Pericytes embrace the capillaries and contribute to the development, maintenance and regulation of the BBB (Deeken and Loscher 2007). Brain capillaries have greater numbers and volumes of mitochondria than peripheral tissue capillaries (Deeken and Loscher 2007). Brain capillaries have a high transendothelial electrical resistance (TEER), measured between 1000 and 2000 Ohm cm^2, while that of peripheral capillaries is typically measured at 10 Ohm cm^2 (Deeken and Loscher 2007). The cause of the high electrical resistance is thought to be due to differences in protein composition, such as high occludin and claudin expression (Deeken and Loscher 2007). Expression of claudin 3, claudin 5 and possibly claudin 12 appear to contribute to the high TEER in brain endothelial cells (Abbott et al. 2006). The transmembrane proteins occludin and the claudins are also important contributors to the tight junction structure (Abbott et al. 2006). The junctional adhesion molecules (JAM), such as JAM-A, JAM-B and JAM-C, are present in brain endothelial cells and are involved in tight junction function and maintenance (Abbott et al. 2006).

Many features of the BBB phenotype are subject to change or modulation (Abbott et al. 2006). Astroglia can release chemical factors and signals that modulate the permeability of the brain endothelium (Deeken and Loscher 2007). The transcription factor NF-κB can alter tight junction protein expression and therefore, regulate BBB permeability (Abbott et al. 2006). Traditionally, resistance of brain metastasis to chemotherapy has been attributed to the blood-brain barrier (Lin et al. 2010). However, recent studies have revealed that the BBB is not intact in larger metastases because the metastatic tumor cells release VEGF, a vascular permeability factor (Lin et al. 2010). The blood-brain barrier remains intact in and around experimental brain metastases smaller than 0.25 mm in diameter (Fidler et al. 2002). More than 70% of brain metastasis cases exhibit enhanced lesions on magnetic resonance imaging due to leakage of contrast agents from blood vessels, indicating BBB permeability (Lin et al. 2010). With larger tumors, the tight junctions between the endothelial cells become stretched out (Cheng and Hung 2007). Primary and metastatic cancerous tumors involve alterations in brain endothelial cells (Deeken and Loscher 2007). There is a compromised tight junction structure and an increase in the perivascular space (Deeken and Loscher 2007). Blood vessels within the tumors have fenestrations that mirror those found in the peripheral vasculature (Deeken and Loscher 2007). There is also an increase in the number and activity of pinocytic vesicles present (Deeken and Loscher 2007). The blood brain barrier is an obstacle to tumor cells with its tight layer of endothelial cells and astrocyte foot processes (Nguyen et al. 2009). Brain metastasis might involve an active crosstalk between the cancer and stromal cells, as suggested by the range of unique cell types that constitute the brain parenchyma and their anatomical organization (Nguyen et al. 2009).

Astrocytes are the predominant cells in the brain and maintain homeostasis of the brain microenvironment (Lin et al. 2010). They transport various nutrients from the circulation to the neurons, participate in neural signal transduction and buffer the ionic balance or the extracellular matrix (Lin et al. 2010). Under pathological conditions, such as trauma, ischemia and neurodegenerative disease, astrocytes become activated, as indicated by the upregulation of glial fibrillary acidic protein (GFAP) (Lin et al. 2010). These reactive astrocytes have been shown to protect neurons from injury-induced apoptosis (Lin et al. 2010). Reactive astrocytes can also protect melanoma cells in brain metastases from cytotoxicity due to chemotherapeutic drugs (Lin et al. 2010). An experiment by Lin et al. (2010) studied the sensitivity of melanoma cells to chemotherapeutic agents when co-cultured with mouse astrocytes or fibroblasts. Their results revealed that astrocytes, not fibroblasts, reduced apoptosis in human melanoma cells treated with various chemotherapeutic drugs (Lin et al. 2010). The chemotherapeutic effect was dependent on physical contact and gap junctional communication (GJC) between astrocytes and tumor cells (Lin et al. 2010). Gap junctional communication channels directly connect the cytoplasm between adjacent cells (Lin et al. 2010). The channels have been shown to be involved in the transmission of survival and apoptotic signals between neighboring cells (Lin et al. 2010). Gap junctions between astrocyte processes allow them to communicate with each other (Lin et al. 2010). The results from Lin et al.'s experiments showed that the astrocytes sequestered calcium from the cytoplasm of tumor cells (Lin et al. 2010). Calcium is one of the most important second messengers transmitted through GJC channels (Lin et al. 2010). It has been shown to play a causal role in cell death (Lin et al. 2010). Melanoma cells incubated with chemotherapeutic agents showed an increase in cytoplasmic calcium followed by an appearance of fragmented DNA, a hallmark of apoptosis (Lin et al. 2010). An analysis of cytoplasmic Ca^{2+} in paclitaxel-treated tumor cells by flow cytometry revealed that co-culture with astrocytes significantly reduced cytoplasmic calcium levels when compared with tumor cells incubated with paclitaxel in the absence of astrocytes (Lin et al. 2010). Their data implicate calcium sequestration through GJC channels as a key mechanism by which astrocytes protect the tumor cells from chemotherapy (Lin et al. 2010). Brain tumors can harness the neuroprotective effects of reactive astrocytes for their own survival (Lin et al. 2010). Successful treatment of brain metastasis will require chemotherapy in combination with agents that selectively interfere with the GJC channels (Lin et al. 2010). Targeted therapies could include GFAP antibodies to tumor-associated astrocytes or short nucleotide sequences complementary to GFAP mRNA (Lin et al. 2010). The results from Lin et al. delineate a previously unrecognized mechanism for resistance in brain metastases that might be of relevance to the clinic (Lin et al. 2010).

The blood–brain barrier is composed of xenobiotic transporters that extrude substrates from the brain into the CSF and systemic circulation (Deeken and Loscher 2007). These transporters also extrude drugs and toxins if they gain entry into the cytoplasm of brain endothelial cells (Deeken and Loscher 2007). It is expected that lipid-soluble drugs would readily cross the BBB, but studies have found that many of them have a lower permeability than predicted by their lipid solubility (Deeken and Loscher 2007). These drugs happen to be substrates for the drug efflux transporters, which are also present in the blood–CSF barrier (Deeken and Loscher 2007). The activity of these transporters very efficiently removes the drugs from the CNS and thus, limits brain uptake (Deeken and Loscher 2007). Studies have identified numerous efflux transporters that comprise the BBB, such as P-glycoprotein, members of the multidrug resistance protein family (MRP) as well as members of the organic cation and anion transporter families (OCT and OAT, respectively) (Deeken and Loscher 2007).

P-glycoprotein (or ABCB1) is encoded by the multidrug resistance gene MDR1 (Deeken and Loscher 2007). It was initially discovered as a highly expressed protein in multidrug resistant tumor cell lines (Deeken and Loscher 2007). Its expression in the brain has been found in many species including humans, rats and primates (Deeken and Loscher 2007). In the blood–CSF barrier, P-glycoprotein is mostly expressed in the proximity of the apical membrane in the choroid plexus (Deeken and Loscher 2007). Its likely role is to transport substrates into the CSF from the endothelium and brain parenchyma (Deeken and Loscher 2007). The exact location of P-glycoprotein in the blood–CSF barrier has been debated, however, as one study found it to be expressed in vesicles adjacent to the apical membrane of the choroid epithelium rather than in the membrane itself (Deeken and Loscher 2007).

There it may serve as a transporter which effluxes drugs into vesicles, which in turn, are inserted into the apical membrane for substrate exocytosis into the CSF (Deeken and Loscher 2007). In the brain capillary, P-glycoprotein is principally expressed at the luminal membrane where it serves as an efflux pump to extrude substrates back into the circulation, restricting or preventing entry into the brain parenchyma (Deeken and Loscher 2007). Interestingly, many of the chemotherapeutic agents used in clinical practice have been discovered to be substrates for P-glycoprotein (Deeken and Loscher 2007). In Mdr1 knockout mice, researchers observed an increase in the brain of P-glycoprotein substrates from the circulation as compared with wild-type mice (Deeken and Loscher 2007). Similarly, animals treated with inhibitors of P-glycoprotein have increased amounts of P-glycoprotein substrates in the CNS (Deeken and Loscher 2007). Mice with a xenograft glioblastoma tumor were given paclitaxel and a P-glycoprotein inhibitor and showed an increased brain concentration of paclitaxel and improved tumor response as compared to animals given paclitaxel alone (Deeken and Loscher 2007). This increased penetration of drugs after P-glycoprotein inhibition has been confirmed in a human study (Deeken and Loscher 2007).

There are other important transporters involved in forming the BBB (Deeken and Loscher 2007). Multidrug resistance protein 1 (MRP1) through MRP9 are all members of the ABCC family of transporters (Deeken and Loscher 2007). Recent studies have reported a predominantly apical plasma membrane distribution for MRP1, MRP2 and MRP5 and an almost equal distribution for MRP4 on the apical and basolateral membranes (Deeken and Loscher 2007). The transporter ABCG2 (or BCRP) was initially named the breast cancer-resistant protein as it was first discovered in a chemotherapy-resistant breast cancer cell line (Deeken and Loscher 2007). It has been detected in the capillary endothelial cells of the brain in humans as well as in other species, and is mainly expressed on the luminal surface (Deeken and Loscher 2007). Based on mRNA expression levels, ABCG2 may be even more strongly expressed than either P-glycoprotein or MRP1 (Deeken and Loscher 2007). In one study, Bcrp1 knockout mice had a 2.5-fold increase in brain concentration of a substrate for ABCG2 as compared with wild-type mice (Deeken and Loscher 2007). Similarly, another study found that co-administration of an ABCG2 substrate and inhibitor resulted in a 4.2-fold increase in bran penetration (Deeken and Loscher 2007). Organic anion and cation transporter families have also been found in the brain endothelium (Deeken and Loscher 2007). They typically exchange anions and cations, respectively, across concentration gradients from the blood to the brain or vice versa (Deeken and Loscher 2007). Therefore, drug transport into and out of the brain will depend on ionic or drug gradients (Deeken and Loscher 2007). The exact location of transporters from the OAT and OCT families as well as those from the organic anion-transporting polypeptide (OATP) family is unclear (Deeken and Loscher 2007). Organic cation transporter 2 (OCT2) is expressed in the choroid plexus and is localized in cytosolic vesicles or in the apical membrane (Deeken and Loscher 2007). In rats, OATP2 is expressed in the apical and basolateral membranes, while in humans OAT3 is predominantly expressed at the basolateral membrane (Deeken and Loscher 2007). Organic anion transport 1 (OAT1) has been found in the brush border of the choroid plexus (Deeken and Loscher 2007). Studies determining the role of OATs and OATPs in forming the BBB are difficult to perform given the overlapping substrate specificity of OATs and OATPs with ABC transporters (Deeken and Loscher 2007). However, in a mouse model, OATP3 has been shown to play a significant role in forming the blood-brain barrier (Deeken and Loscher 2007).

Primary and metastatic cancerous tumors involve alterations in the expression of transporters (Deeken and Loscher 2007). The expression level of P-glycoprotein in blood vessels supplying melanoma CNS metastases was only 5% of that seen in normal brain tissue (Deeken and Loscher 2007). Similarly, the vasculature around CNS lung metastases had just 40% of the P-glycoprotein expression found in normal brain vasculature (Deeken and Loscher 2007). Two different studies found conflicting levels of P-glycoprotein expression in the vasculature of malignant gliomas (Deeken and Loscher 2007). Becker et al. (1991) found diminished expression as compared with normal brain vasculature, while Toth et al. (1996) found no difference between tumor vasculature and normal tissue (Deeken and Loscher 2007). Haga et al. (2001) also found no difference in the expression level of P-glycoprotein and MRP2 between normal brain and malignant glioma cells (Deeken and Loscher 2007). However, they did find increased expression of MRP1 and MRP3 in the endothelial cells forming the vasculature around tumor sites (Deeken and Loscher 2007).

Difficulty with Treatment

Primary brain malignancies are intrinsically resistant to most chemotherapies and metastatic releases are often associated with resistance to treatment (Deeken and Loscher 2007; Nguyen et al. 2009). This might be due to cell-intrinsic mechanisms, such as genetic alterations, that confer drug resistance after a period of therapeutic response (Nguyen et al. 2009). Resistance to therapy can also be coupled with the potential acquisition of pro-metastatic functions in tumors (Nguyen et al. 2009). Cancer cells in the CNS could be shielded by the blood-brain barrier from drug delivery or protected with survival signals from the host microenvironment (Nguyen et al. 2009). The unique structure of the BBB limits the effectiveness of current treatments (Cheng and Hung 2007). In brain tumors, there is a breakdown of the BBB, however (Abbott et al. 2006). Studies have observed a downregulation of the tight junction proteins claudin 1 and 3 (Abbott et al. 2006). During inflammation, certain released agents have the ability to increase the permeability of the brain endothelium (Abbott et al. 2006). Bradykinin acts on endothelial bradykinin B_2 receptors to raise intracellular Ca^{2+} concentrations and open tight junctions (Abbott et al. 2006). It also activates NF-κB in astrocytes, resulting in the release of IL-6, which can amplify the effect by acting back on the endothelium (Abbott et al. 2006). TNF-α can further increase BBB permeability by directly acting on the endothelium and by indirectly involving the production of endothelin 1, which is present on the endothelium, and IL-1β release from astrocytes via an immunoregulatory loop (Abbott et al. 2006). The BBB disrupted at the site of significant brain disease has been termed the "tumor–blood barrier" (Deeken and Loscher 2007). But, only in larger tumors is it greatly impaired in terms of transporter expression and function as well as in terms of the permeability of the endothelium (Deeken and Loscher 2007). This allows a sufficient amount of systemically delivered chemotherapy to reach the tumor and affect a response (Deeken and Loscher 2007). A number of studies performed in the 1980s investigated levels of chemotherapy agents in brain tissues and found higher levels at sites of larger tumors than in neighboring tissues (Deeken and Loscher 2007). In smaller aggregates of metastatic tumor cells, the disruption of the BBB is less significant (Deeken and Loscher 2007). Since a smaller amount of drug reaches these micrometastases, they can grow, develop neovasculature structures and ultimately, reach a clinically significant size (Deeken and Loscher 2007).

There are three general methods in use to increase drug delivery to the brain (Deeken and Loscher 2007). The first is the administration of chemotherapy agents directly into the CNS with the use of Ommaya reservoirs, intrathecal injections, intra-arterial injections or high-dose systemic therapy (Deeken and Loscher 2007). Although this approach has found success, toxicities can be significant (Deeken and Loscher 2007). The second method is to disrupt the BBB followed by administration of chemotherapy (Deeken and Loscher 2007). In order to increase the CNS penetration of chemotherapy agents, the BBB is often disrupted with hypertonic solutions such as mannitol (Deeken and Loscher 2007). Another agent that disrupts the BBB is RMP-7, a synthetic analogue of the peptide bradykinin (Deeken and Loscher 2007). It is specific for the bradykinin-P2 receptor, which participates in the modulation of tight junctions in brain endothelial cells (Deeken and Loscher 2007). In preclinical models, RMP-7 has been found to increase the brain concentration of a chemotherapy agent using intracarotid or intravenous administration (Deeken and Loscher 2007). Unfortunately, this activity was not observed in two phase II trials (Deeken and Loscher 2007). The third approach is to deliver chemotherapy drugs with an agent that inhibits the drug transporters of the BBB (Deeken and Loscher 2007). Inhibition of ABCG2 has been tested preclinically (Deeken and Loscher 2007). Researchers have found a higher CNS penetrance of chemotherapy agents (Deeken and Loscher 2007). Nonselective inhibitors of MRP1 have also been tested in preclinical models (Deeken and Loscher 2007). A neuroblastoma cell line has been shown to have an increased cellular sensitivity to chemotherapy (Deeken and Loscher 2007). Over the past two decades, researchers have been looking to develop agents that inhibit P-glycoprotein at the cellular level and thus, increase intracellular concentrations of toxic chemotherapy agents in resistant tumors (Deeken and Loscher 2007). However, clinical trials have been disappointing (Deeken and Loscher 2007). Promising phase II trials were followed by negative phase III trials (Deeken and Loscher 2007). But, all hope is not lost.

In animal models, the administration of P-glycoprotein inhibitors has been found to increase intracranial concentrations of chemotherapy agents (Deeken and Loscher 2007).

There are several creative strategies to deliver drugs across the blood-brain barrier currently being tested in both in vitro and in vivo models. The human brain microvascular endothelial cell (HBMEC) is a widely used in vitro model system that mimics the in vivo human blood-brain barrier (Cheng and Hung 2007). With this model, researchers have used nanoparticles to facilitate the entry of drugs into the brain parenchyma (Deeken and Loscher 2007). They encapsulated chemotherapy agents and other drugs in 250-nm diameter nanoparticles using poly(butyl)cyanoacrylate (PBCA) (Deeken and Loscher 2007). The nanoparticles were then endocytosed by the BBB endothelium and the drug was free to diffuse into the brain parenchyma (Deeken and Loscher 2007). Researchers using animal models tested the delivery of drugs across the BBB by tagging or attaching liposome-containing drugs to an antibody that recognizes receptors along the endothelium (Deeken and Loscher 2007). Endogenous large-molecule peptides, such as transferrin, insulin and leptin cross the BBB via receptor-mediated transport by attaching to such receptors (Deeken and Loscher 2007). The monoclonal antibody OX26, which recognizes the transferrin receptor, was attached to a liposome-containing digoxin, allowing digoxin to cross the BBB (Deeken and Loscher 2007). Huwyler et al. (1996) used the OX26 immunoliposome to transport daunorubicin using an animal in vivo model and found increased brain delivery and higher concentrations of the drug by a factor of 4 log values when compared to delivery without this vehicle (Deeken and Loscher 2007). Another approach is to deliver chemotherapy drugs with an agent that selectively utilizes the influx transporters on the BBB (Deeken and Loscher 2007). Influx transporters move substances from the circulation into the brain parenchyma (Deeken and Loscher 2007). They line the endothelium, both on the luminal and basolateral surfaces (Deeken and Loscher 2007). This is an important strategy to not only circumvent the efflux capacity of the blood–brain barrier but also increase drug delivery to brain tumors (Deeken and Loscher 2007).

Potential Therapeutic Interventions

Micrometastases often remain after conventional surgery, radiotherapy and/or chemotherapy (Thiery 2002). By targeting the signal transduction pathways that contribute to the invasive and metastatic properties of cancer cells, therapeutic interventions have the potential to block tumor progression and prevent metastasis (Thiery 2002). Several receptor tyrosine kinases (RTKs) are mutated and constitutively active in many cancer types (Polyak and Weinberg 2009). Obvious targets include Met, Igfr1 and those of the ErbB family (Thiery 2002). Approved by the FDA in 1998 and currently on the market is Trastuzumab (Herceptin), a monoclonal antibody directed against ErbB2 (Thiery 2002). Given that EMTs are associated with a poor clinical outcome in multiple tumor types, it is essential to understand the processes that trigger EMTs in order to prevent them (Polyak and Weinberg 2009; Thiery 2002). In several studies, an EMT has been shown to result in cancer cells with stem cell-like characteristics, such as invasion of the parenchyma and resistance to certain therapeutic interventions (Polyak and Weinberg 2009). Cancer cells with stem cell characteristics are enriched in the residual tumors remaining after standard chemotherapeutic treatments (Polyak and Weinberg 2009). Thus, inhibition of EMTs is an attractive therapeutic approach (Polyak and Weinberg 2009). However, the complexity of the signaling networks involved that regulate the induction of EMTs and the reversibility of the acquired mesenchymal phenotype pose significant challenges to researchers (Polyak and Weinberg 2009). So it is not known when therapies that could inhibit this transition should be initiated (Polyak and Weinberg 2009). It is also unknown which pathways should be inhibited to be most effective while causing minimal toxicity in normal tissues (Polyak and Weinberg 2009). The process is further complicated by the similarities between EMT and normal stem cell programs (Polyak and Weinberg 2009).

Previous studies have shown that to produce brain metastasis, tumor cells must reach the vasculature of the brain, attach to the endothelial cells of the microvasculature, extravasate into the parenchyma, proliferate in response to growth factors and induce the formation of new blood vessels (Fidler et al. 2002).

Vascular endothelial growth factor (VEGF) stimulates the proliferation and migration of endothelial cells and induces the expression of MMPs and plasminogen activity (Fidler et al. 2002). Overexpression of VEGF in tumor cells enhances tumor growth and metastasis by stimulating vascularization and increasing microvessel density (Fidler et al. 2002). Studies outlining the important role of VEGF in the progressive growth of brain metastases showed that VEGF expression is necessary, but not sufficient, for the production of brain metastases (Fidler et al. 2002).

Given the important role of VEGF in cancer progression and neo-angiogenesis, several VEGF antagonists have been approved by the FDA (Joyce and Pollard 2009). They increase survival in patients with metastatic breast and colorectal cancers when combined with chemotherapy (Joyce and Pollard 2009). Despite its positive effects on established localized tumors, inhibition of angiogenesis can result in increased tumor invasion and metastasis (Paez-Ribes et al. 2009). In a glioblastoma multiforme (GBM) mouse model, treatment with sunitinib (a VEGFR and PDGFR kinase inhibitor) or SU10944 (a VEGFR-selective kinase inhibitor) increased invasion (Paez-Ribes et al. 2009). The data suggest that VEGFR inhibitors might precondition the host microenvironment, making it favorable for metastasis (Paez-Ribes et al. 2009). The proper timing of anti-angiogenic therapy needs to be determined (Paez-Ribes et al. 2009). It is also unclear whether combining these agents with chemotherapy or other treatments can counteract the unfavorable effects (Paez-Ribes et al. 2009).

Three strategies have been developed for reconstituting protein function in metastasis suppressor genes (Smith and Theodorescu 2009). One approach is the reconstitution of metastasis suppressor expression by induction of the endogenous locus through gene therapy (Smith and Theodorescu 2009). Another approach is to target essential downstream pathways that are activated by loss of suppressor function (Smith and Theodorescu 2009). The third technique is direct administration of the suppressor protein itself (Smith and Theodorescu 2009). Restoring endogenous expression is one potential advantage of targeting metastasis suppressors over the related tumor suppressor genes (Smith and Theodorescu 2009). Tumor suppressors are often inactivated by mutation early in the development of cancer and are not amenable to re-induction at the endogenous locus (Smith and Theodorescu 2009). In recent years, researchers have created a massive repository of gene expression data from several cell lines after treatment with over 1000 bioactive compounds, termed the Connectivity Map (Smith and Theodorescu 2009). It provides the signatures of gene expression profiles induced by such materials (Smith and Theodorescu 2009). This results in a systemic framework for the potential discovery of drugs that target an entire signature (Smith and Theodorescu 2009).

Conclusion

It is currently unknown whether metastasis emerges from a progenitor pool that is present in early seeding or from later dissemination of cells that acquired their aggressiveness in the primary tumor (Nguyen and Massague 2007).

The need to understand the biology of metastasis becomes increasingly important as clinical oncology moves toward personalized medicine (Nguyen et al. 2009). This may be enhanced by the better classification of tumors on the basis of molecular markers for metastatic potential and therapeutic intervention for both latent and active tumors (Nguyen et al. 2009). However, recapitulating the metastatic niche within in vitro studies is difficult, as it has a highly complex cellular and molecular architecture (Psaila and Lyden 2009). It is naïve to think that individual cell types function in isolation in such a complex system (Joyce and Pollard 2009). Advancements in the treatment of both primary and metastatic cancers will require an understanding, through a systems biology approach, of the role wielded by the microenvironment in order to model these complex interactions and their evolution over time (Joyce and Pollard 2009).

References

Abbott NJ, Ronnback L, Hansson E (2006) Astrocyte-endothelial interactions at the blood-brain barrier. Nat Rev Neurosci 7:41–53

Becker I, Becker KF, Meyemann R, Hollt V (1991) The multidrug-resistance gene MDR1 is expressed in human glial tumors. Acta Neuropathol (Berl) 82:516–519

Cheng X, Hung MC (2007) Breast cancer brain metastases. Cancer Metastasis Rev 26:635–643

Deeken JF, Loscher W (2007) The blood-brain barrier and cancer: transporters, treatment, and Trojan horses. Clin Cancer Res 13:1663–1674

Fidler IJ, Yano S, Zhang R, Fujimaki T, Bucana CD (2002) The seed and soil hypothesis: vascularisation and brain metastases. Lancet Oncol 3:53–57

Foulkes WD, Smith IE, Reis-Filho JS (2010) Triple-negative breast cancer. N Engl J Med 363:1938–1948

Gril B, Evans L, Palmieri D, Steeg PS (2010) Translational research in metastasis is identifying molecular pathways that may lead to the development of new brain therapeutic strategies. Eur J Cancer 46:1204–1210

Haga S, Hinoshita E, Ikezaki K, Fukui M, Scheffer GL, Uchiumi T, Kuwano M (2001) Involvement of the multidrug resistance protein 3 in drug sensitivity and its expression in human glioma. Jpn J Cancer Res 92:211–219

Huwyler J, Wu D, Pardridge WM (1996) Brain drug delivery of small molecules using immunoliposomes. Proc Natl Acad Sci USA 93:14164–14169

Jemal A, Bray F, Center MM, Ferlay J, Ward E, Forman D (2011) Global cancer statistics. CA Cancer J Clin (61):67–68

Joyce JA, Pollard JW (2009) Microenvironmental regulation of metastasis. Nat Rev Cancer 9:239–252

Lin Q, Balasubramanian K, Fan D, Kim S, Guo L, Wang H, Bar-Eli M, Aldape KD, Fidler IJ (2010) Reactive astrocytes protect melanoma cells from chemotherapy by sequestering intracellular calcium through gap junction communication channels. Neoplasia 12:748–754

Lin NU, Winer EP (2007) Brain metastases: the HER2 paradigm. Clin Cancer Res 13:1648–1655

Mahar Doan KM, Humphreys JE, Webster LO, Wring SA, Shampine LJ, Serabjit-Singh CJ, Adkison KK, Polli JW (2002) Passive permeability of P-glycoprotein – mediated efflux differentiate central nervous system (CNS) and non-CNS marketed drugs. J Pharmacol Exp Ther 303:1029–1037

McCarthy N. (2009) Calcium influx is moving. Nat Rev Cancer 9:230–231

Neman J, Somlo G, Jandial R (2010) Classification of genomic changes in breast cancer brain metastasis. Neurosurgery 67:N18–19

Nguyen DX, Bos PD, Massague J (2009) Metastasis: from dissemination to organ-specific colonization. Nat Rev Cancer 9:274–284

Nguyen DX, Massague J (2007) Genetic determinants of cancer metastasis. Nat Rev Genet 8:341–352

Paez-Ribes M, Allen E, Hudock J, Takeda T, Okuyama H, Vinals F, Inuoue M, Bergers G, Hanahan D, Casanovas O (2009) Antiangiogenic therapy elicits malignant progression of tumors to increased local invasion and distant metastasis. Cancer Cell 15:220–231

Polyak K, Weinberg RA (2009) Transitions between epithelial and mesenchymal states: acquisition of malignant and stem cell traits. Nat Rev Cancer 9:265–273

Psaila B, Lyden D (2009) The metastatic niche: adapting the foreign soil. Nat Rev Cancer 9:285–293

Smith SC, Theodorescu D (2009) Learning therapeutic lessons from metastasis suppressor proteins. Nat Rev Cancer 9: 253–264

Thiery JP (2002) Epithelial-mesenchymal transitions in tumour progression. Nat Rev Cancer 2:442–454

Toth K, Vaughan MM, Peress NS, Slocum HK, Rustum YM (1996) MDR1 P-glycoprotein is expressed by endothelial cells of newly formed capillaries in human gliomas but is not expressed in the neovasculature of other primary tumors. Am J Pathol 149:853–858

Yang S, Zhang JJ, Huang XY (2009) Orai1 and STIM1 are critical for breast tumor cell migration and metastasis. Cancer Cell 15:124–134

Index

M.A. Hayat (ed.), *Tumors of the Central Nervous System, Volume 4*,
DOI 10.1007/978-94-007-1706-0, © Springer Science+Business Media B.V. 2012

D

E

I

T